Investigation into the effects of viral-mediated Ang-(1-9) delivery on cardiac function and remodelling in a mouse model of myocardial infarction

Caroline Fattah BSc (Hons), MRes

Submitted in fulfilment of the requirements for the degree of Doctor of Philosophy to the Institute of Cardiovascular and Medical Sciences, University of Glasgow.

Research conducted at the British Heart Foundation Glasgow Cardiovascular Research Centre, Institute of Cardiovascular and Medical Sciences, College of Medical, Veterinary and Life Sciences, University of Glasgow, U.K.

2015

Author's declaration

I declare that this thesis has been written entirely by myself and is a record of work performed solely by me at the University of Glasgow Cardiovascular Research Centre in the Institute of Cardiovascular and Medical Sciences under the supervision of Dr. Stuart A. Nicklin and Dr. Christopher M. Loughrey. This thesis has not been submitted previously for a higher degree. The adenoviral vectors were generated previously by Dr. Monica Flores-Munoz and the AAV vectors were kindly provided as a gift from Professor Mauro Giacca.

Caroline Fattah

2015

Acknowledgements

First a foremost I would like to thank my two fantastic supervisors Stu and Chris. Their doors have always been open to me whenever I have needed them and they have provided me with their knowledge, time, patience and understanding throughout. They have somehow managed to put up with me through all the tears and tantrums, and have helped me develop not only as a scientist, but also as a person and I cannot thank them enough for that. A massive thank you also has to go to the BHF, as without their financial support none of this would have been possible.

A huge thank you goes to all the staff at the GCRC, who essentially taught me everything I know. This applies especially to Nic and Gregor, who know everything there is to know in the level 4 lab, and to all the post-docs and my fellow students who helped me out over the years. Thanks to Kirsty, who dedicated a lot of time to teaching me my *in vivo* skills, and to Charlotte whose help with the single cell experiments I could not have been without ("I don't know what button I pressed but now it won't work!"), and who always had time for a weekend bottle of wine after a hard week! Also a big thanks goes to the biological services staff whose help was invaluable. Sometimes on my busy days they were my only source of human contact, which helped keep me sane! A special mention has to go to David whose dulcet tones ringing down the corridor always helped brighten even the gloomiest of days!

Thank you to my office buddies Clare, Liz, Hannah and Josie. It really makes all the difference to have some fantastic people to share the PhD experience with and who can truly appreciate the highs and the lows with you. I'll really miss our office gossips and the morning cups of tea! A big thanks also to my fellow BHF-ers Annabel, Andy, Craig and Chris for all your support and for making the past few years so much fun- our BHF away days will be something I'll never forget! Thanks also to my besties Maddy, Jennifer and Laura for always being there to lend an ear and share a cocktail!

Thanks to all my siblings (in chronological order: Layla, Haitham, Hyder, Sharif, Sammy and Lisa) for all your support throughout, even though you may not have always known exactly what it is I do! (Microbiology? Biochemistry? Something

with viruses?). A huge thank you has to go to my mum for her love and support, and to my dad as without his constant encouragement for me to aim high and believe in my own abilities I definitely would not be where I am today. One of the biggest thanks has to go to my partner in crime, Allan, whose support (both emotionally and financially) has been unwavering throughout my PhD, and especially while writing this thesis. He has always been my rock, my shoulder to cry on and my biggest source of motivation throughout. His patience and understanding is unrivalled and I owe him everything. Without him I don't think I would ever have finished writing!

My final thanks goes to someone who perhaps had the biggest influence on my life and who helped make me the person I am today- my Grandma. She was able to see me set out on this journey but sadly is not with us to see the end. Although she is no longer here, I know she has been 'in my pocket' throughout, and I know that she would be so proud to see me achieve something I have worked so hard for. This thesis is dedicated to her.

Table of contents

List of figures

List of tables

List of publications, presentations and awards

Publications

McKinney, C.A., **Fattah C.**, Loughrey C.M., Milligan G. and Nicklin, S.A (2014). Angiotensin-(1-7) and angiotensin-(1-9): function in cardiac and vascular remodelling. Clin Sci, 126, 815-827.

Presentations

Fattah C., Loughrey C.M., Nicklin S.A (2012). Targeting the counter-regulatory renin-angiotensin system in myocardial infarction. Joint Edinburgh and Glasgow BHF 4-Year PhD Meeting, University of Edinburgh. [Oral communication].

Fattah C., Loughrey C.M., Nicklin S.A (2013). The effect of angiotensin-(1-9) on isolated mouse cardiomyocyte calcium handling. BHF Fellows Meeting, University of Oxford. [Poster communication].

Fattah C., Loughrey C.M., Nicklin S.A (2014). Adenoviral delivery of angiotensin-(1-9) improves cardiac function in a murine model of myocardial infarction (MI). BHF 4-Year PhD Cardiovascular Science Annual Meeting, University of Manchester. [Poster communication].

Fattah C., Loughrey C.M., Nicklin S.A (2014). Adenoviral delivery of angiotensin-(1-9) improves cardiac remodelling and function in a murine model of myocardial infarction (MI). BSGCT annual conference, University College London. [Poster communication].

Awards

British Society for Gene and Cell Therapy annual conference poster prize winner, April 2014.

List of abbreviations and definitions

AA	Arachidonic acid
AAV	Adeno-associated virus
ABC	Avidin biotinylated enzyme complex
ACE	Angiotensin-converting enzyme
ACE2	Angiotensin-converting enzyme 2
Ad	Adenovirus
ADAM	A disintigrin and metalloproteinase
Ang II	Angiotensin II
Ang-(1-7)	Angiotensin 1-7
Ang-(1-9)	Angiotensin 1-9
ANP	Atrial natriuretic peptide
AT_1R	Angiotensin type 1 receptor
AT_2R	Angiotensin type 2 receptor
ANOVA	Analysis of variance
ANP	Atrial natriuretic peptides
AP	Action potential
AP-1	Activator protein 1
ARB	Angiotensin type 1 receptor blocker
ARD	Acute respiratory distress
AVU	Adeno-associated virus Vector-Unit
BCA	Bicinchoninic acid
ß-gal	ß-galactosidase
ß-MyHC	ß-myosin heavy chain
BNP	Brain natriuretic peptide
BP	Blood pressure
BK	Bradykinin
BK_2R	Bradykinin type 2 receptor
BPM	Beats per min
BSA	Bovine serum albumin
Ca^{2+}	Calcium ion
CAL	Coronary artery ligation
CaM	Calmodulin
CaMKII	Calcium calmodulin kinase II
cAMP	3’-5’-cyclic adenosine monophosphate
CAR	Coxsackie adenovirus receptor
CCD	Charged-coupled device

cDNA	Complementary deoxyribonucleic acid
cGMP	Cyclic guanosine monophosphate
CHD	Coronary heart disease
CICR	Calcium-induced calcium-release
CNS	Central nervous system
CO	Cardiac output
CO_2	Carbon dioxide
CpA	Cathepsin A
C_t	Cycle threshold
CTGF	Connective tissue growth factor
CVD	Cardiovascular disease
CUPID	Calcium upregulation by percutaneous administration of gene therapy in cardiac disease
Cxp	Carboxypeptidase
DAD	Delayed after-depolarisations
DAPI	4',6'-diamidino-2-phenylindole
DMSO	Dimethyl sulphoxide
DNA	Deoxyribonucleic acid
dP/dt_{max}	Maximum rate of rise of pressure
dp/dt_{min}	Minimum rate of fall of pressure
E/A	Early/after
EAD	Early after-depolarisations
EC	Endothelial cells
ECC	Excitation-contraction coupling
ECL	Enhanced chemiluminsecent
EDP	End diastolic pressure
EDPVR	End-diastolic pressure-volume relationship
EDV	End diastolic volume
EF	Ejection fraction
EGF	Endothelial growth factor
EGFR	Epidermal growth factor receptor
eNOS	Endothelial nitric oxide synthase
ERK	Extracellular-signal-related-kinase
ESP	End systolic pressure
ET-1	Endothelin-1
ET_AR	Endothelin type A receptor
FGF	Fibroblast growth factor
FS	Fractional shortening
GATA-4	GATA binding protein 4

GFP	Green fluorescent protein
Gp-130	Glycoprotein 130
HB-EGF	Heparin binding-epidermal growth factor
HEPES	2-[4-(2-hydroxyethyl)piperazin-1-yl]ethanesulfonic acid
HF	Heart failure
H_2O_2	Hydrogen peroxide
HRP	Horseradish peroxidase
HR	Heart rate
hr	Hour
HSV	Herpes simplex virus
HW	Heart weight
IgG	Immunoglobulin G
IHC	Immunohistochemistry
IL	Interleukin
ILK	Integrin-linked kinase
im	Intramuscular
iNOS	Inducible nitric oxide synthase
ip	Intraperitoneal
IP_3	Inositol triphosphate
I/R	Ischaemia/reperfusion
ITR	Inverted terminal repeat
iv	Intravenous
JAK	Janus kinase
JG	Juxtaglomerular
JNK	c-Jun kinase
KAT	Kuopio angiogenesis trial
kDa	Kilodalton
K/s	Thousand units per second
L	Litre
LAD	Left anterior descending
LB	Luria broth
LiW	Liver weight
LuW	Lung weight
LV	Left ventricle
LVEDD	Left ventricular end diastolic dimension
LVESD	Left ventricular end systolic dimension
M	Molar
mM	Millimolar

MAPK	Mitogen activated protein kinases
MCP-1	Monocyte chemoattractant protein 1
MEF-2	Myocyte enhancer factor-2
MEK	Mitogen-activated protein kinase kinase
MEM	Minimal essential media
MI	Myocardial infarction
min	Minute
mL	Millilitre
mM	Millilmolar
mmHg	Millimeters of mercury
MMP	Matrix-metalloprotease
MOI	Multiplicity of infection
mRNA	Messenger ribonucleic acid
ms	Millisecond
NAD(P)H	Nicotinamide adenine dinucleotide phosphate
NCX	Sodium-calcium exchanger
NE	Norepinephrine
NFAT	Nuclear factor of activated T-cells
NF-κß	Nuclear factor κß
nM	Nanomolar
nm	Nanometer
NOAEL	Non-observable adverse effect level
NOS	Nitric oxide synthase
Nox	NAD(P)H oxidase subunit
ORF	Open reading frames
PAGE	Polyacrylamide gel electrophoresis
PCR	Polymerase chain reaction
PA	Phosphatidic acid
PAI	Plasminigen activator inhibitor
PARP-1	Poly(ADP-ribose) polymerase-1
PBS	Phosphate-buffered saline
PD	Proportionate distance
PVDF	Polyvinylidene difluoride
PE	Phenylephrine
PF	Pulmonary fibrosis
PFA	Paraformaldehyde
PH	Pulmonary hypertension
PKA	Protein kinase A

PKC	Protein kinase C
PLA_2	Phospholipase A_2
PLB	Phospholamban
PLC	Phospholipase C
PLZF	Promyelocytic zinc finger protein
POP	Prolyl endopeptidase
PV	Pressure-volume
qPCR	Quantitative real-time polymerase chain reaction
RAAS	Renin-angiotensin-aldosterone system
rAAV	Recombinant adeno-associated virus
Rac-1	Ras-related C3 botulinum toxin substrate 1
rAd	Recombinant adenovirus
RAS	Renin-angiotensin system
RGB	Red-green-blue
RGS	Regulators of G-protein signalling
RLU	Relative light units
RNA	Ribonucleic acid
ROS	Reactive oxygen sepcies
RPE	Retinal pigment epithelial
RQ	Relative quantification
RT	Reverse transcription
RyR	Ryanodine receptor
RV	Right ventricle
SCD	Sudden cardiac death
SDS	Sodium dodecyl sulphate
s	Second
SEM	Standard error of the mean
SERCA	Sarcoplasmic reticulum calcium transport ATPase
SHRSP	Stroke-prone spontaneously hypertensive rat
SR	Sarcoplasmic reticulum
STAT	Signal transducer and activator of transcription
SV	Stroke volume
TBS	Tris-buffered saline
TE	Tris-EDTA
TGF-ß	Transforming growth factor ß
TIMI	Thrombolysis in myocardial infarction
TIMP	Tissue inhibitors of metalloproteases
TL	Tibia length

TNF-α	Tumor necrosis factor α
TOP	Thimet endopeptidase
TRP	Transient Receptor Potential
TRPC	Transient receptor potential canonical
T-tubule	Transverse tubule
μM	Mircomolar
μm	Micrometer
UV	Ultraviolet
VEGF	Vascular endothelial growth factor
VP	Viral particle
VR	Variable regions
VSMC	Vascular smooth muscle cells
VT	Ventricular tachycardia
WGA	Wheat germ agglutinin
WHO	World Health Organisation
wk	Week

Summary

Coronary heart disease (CHD) leading to myocardial infarction (MI) is the primary cause of morbidity and mortality globally. Following an MI, a number of structural and functional changes to the myocardium occur, known as cardiac remodelling. Initially, these changes are adaptive. Inflammation and deposition of extracellular matrix (ECM) components and collagen occurs in order to form the scar tissue, and in response to the rise in wall stress cardiomyocytes undergo adaptive hypertrophy in order to maintain contractile performance of the heart. There are also alterations in the electrical properties of the heart, including dysregulation of a variety of Ca^{2+}-handling proteins. In the long term these processes become maladaptive. Reactive fibrosis stiffens the ventricular wall, eccentric hypertrophy contributes to expansion of the left ventricle (LV) and the electrical changes lead to reduced contraction and increased propensity to arrhythmia, all of which can contribute to the development of heart failure (HF) and the possibility of sudden cardiac death (SCD). Dysregulation of the renin-angiotensin system (RAS) is one of the factors responsible for driving these adaptive and maladaptive remodelling processes. The main effector peptide of the RAS, Angiotensin II (Ang II), acting *via* the Angiotensin type 1 receptor (AT_1R) mediates the majority of the maladaptive changes which occur post-MI. The counter-regulatory axis of the RAS has been found to counteract many of deleterious effects associated with Ang II signalling. The peptide Ang-(1-7), signalling *via* Mas, has been found to exert anti-fibrotic and anti-hypertrophic effects and improve LV function post-MI. Less is known about the peptide Ang-(1-9), however there is evidence that it too is able to exert anti-hypertrophic and anti-fibrotic effects post-MI, however improvements on cardiac function have not been previously demonstrated. Therefore, the main aim of this thesis was to investigate the therapeutic potential of Ang-(1-9) *via* a gene transfer approach on adverse remodelling in a mouse model of MI, with a focus on cardiac functional parameters.

First, the mouse model of MI was established and characterised for adverse structural and functional remodelling parameters. Haemodynamic and functional measurements using echocardiography and pressure-volume (PV) loops demonstrated a reduction in contractility and ejection fraction (EF) following MI. This was also associated with an increase in concentric cardiomyocyte

hypertrophy, fibrosis and collagen deposition. Moreover, alterations in expression of cardiac AT_1R, Angiotensin type 2 receptor (AT_2R), Angiotensin converting enzyme (ACE) and Angiotensin converting enzyme 2 (ACE2) were detected. Following characterisation, this model was utilised to assess the effects of viral-mediated Ang-(1-9) delivery.

Initially, an adenoviral vector (Ad) expressing a biological peptide pump enabling the synthetic production of Ang-(1-9) [RAdAng-(1-9)] was utilised in order to assess the effects of the peptide following MI. Efficient transduction of the healthy myocardium following MI was demonstrated using direct intramyocardial Ad injection. Initially, it was found that administration of RAdAng-(1-9) reduced the mortality rate associated with the MI procedure, with a reduction in deaths from unknown causes and cardiac rupture. Functional cardiac parameters were monitored using echocardiography for a 4 week period, with RAdAng-(1-9) administration found to be associated with increased LV fractional shortening (FS) compared to MI controls from 1 to 4 wks. PV loop measurements confirmed this improved function, with increased end systolic pressure (ESP) and normalised EF found in RAdAng-(1-9) administered animals. Post-mortem analysis and histology demonstrated an anti-hypertrophic effect of RAdAng-(1-9) delivery, with reduced heart weight and cardiomyocyte thickness in MI animals over-expressing Ang-(1-9). An anti-fibrotic effects was also evident, with a reduction in total LV fibrosis demonstrated, primarily due to reduced collagen I expression.

Next, an adeno-associated virus serotype 9 (AAV9) vector expressing the Ang-(1-9) fusion protein expression cassette [AAVAng-(1-9)] was utilised in the same mouse MI model in order to assess the effects of Ang-(1-9) 8 wks post-MI. Global transduction of the healthy myocardium in MI hearts using a single tail vein injection of AAV9 was demonstrated, with transgene expression detectable as early as 1 wk post-MI. Similarly to the previous study, AAVAng-(1-9) delivery demonstrated a reduction in the incidence of cardiac rupture following MI. Echocardiography also demonstrated improvements in cardiac contractility, with increased FS evident from 1 to 8 wks post-MI in AAVAng-(1-9) transduced animals. Again, PV loop measurements found that AAVAng-(1-9) increased ESP and normalised EF. Moreover, CO was significantly elevated in Ang-(1-9) expressing animals. Due to the more advanced 8 wk time-point, a reduction in

LV stiffness was detectable in AAVAng-(1-9) animals compared to controls as measured by the end diastolic pressure-volume relationship (EDPVR). In contrast to RAdAng-(1-9) administration at 4 wks post-MI, no anti-hypertrophic effect was detectable, with an increase in heart weight and cardiomyocyte thickness found in AAVAng-(1-9) animals equivalent to control MI groups. However, AAVAng-(1-9) administration was associated with a reduction in total fibrosis in MI animals, which was attributable to reduced collagen I expression. Moreover, gene expression analysis in MI animals found AT_2R expression was elevated in the myocardium of AAVAng-(1-9) administered animals, which had not previously been identified.

Finally, in order to attempt to elucidate the mechanism of action of Ang-(1-9), single cardiomyocyte Ca^{2+}-handling measurements were utilised in order to assess its effects on Ca^{2+}-handling protein function. Pre-treatment of isolated mouse cardiomyocytes with 1 μM Ang-(1-9) increased cardiomyocyte Ca^{2+}-transient amplitude and shortening compared to control, equivalent to the effects seen using 1 μM of Ang II. However, only Ang II induced an increase in spontaneous rises in intracellular Ca^{2+}. Ang-(1-9) pre-treatment was also associated with increased sarcoplasmic reticulum (SR) Ca^{2+} content.

Overall the findings from this thesis have demonstrated for the first time that Ang-(1-9) exerts beneficial effects on cardiac function post-MI, which may in part be due to modulation of cardiomyocyte Ca^{2+}-handling. These findings provide the impetus to further investigate the potential of Ang-(1-9) as a possible therapeutic agent to prevent progression of adverse cardiac remodelling and HF post-MI.

Chapter 1: General introduction

1.1 The heart

The mammalian heart can be thought of as two muscular pumps that function by operating in series in order to pump blood from the systemic veins into the pulmonary circulation *via* contraction of the right atrial and ventricular chambers, and deliver this oxygenated blood to the systemic circulation from the pulmonary veins *via* the contraction of the left atrial and ventricular chambers (Katz, 2010). The contraction of the heart is initiated and controlled by electrical impulses generated and conducted by specialised myocardial cells. The muscle is composed of working contractile cardiomyocytes of the atria and ventricles, which, combined with the conduction system cardiomyocytes, account for 70 % of the heart's overall cellular mass, with non-cardiomyocyte cells such as vascular smooth muscle cells (VSMCs), endothelial cells (ECs) and cardiac fibroblasts accounting for the remainder (Katz, 2010). Fibroblasts secrete and maintain the fibres required for the hearts framework and contribute to stiffness and tensile strength (Katz, 2010). SMCs and ECs form the network of coronary vessels (Irani, 2000). The contraction of the heart and the maintenance of blood flow is one of the most essential mammalian physiological processes. As such, understanding the physiological processes and mechanisms underlying the regulation of normal heart function, and determining the pathophysiological changes that occur during disease, has proved essential in the development of treatment for contractile dysfunction and HF.

1.2 Normal function of the heart

1.2.1 Excitation-contraction coupling

Excitation-contraction coupling (ECC) is the process by which electrical signals are translated into mechanical movement of the heart *via* the utilisation of the second messenger molecule calcium (Ca^{2+}) in order to enable the cardiac chambers to contract and relax (Maier and Bers, 2007). Central to this is the concept of Ca^{2+}-induced Ca^{2+}-release (CICR) brought about by depolarisation of the cardiomyocyte cell membrane (Bers, 2002; Fabiato, 1983).

1.2.1.1 The ventricular cardiomyocyte action potential

The fast-response cardiomyocyte action potential (AP) is the mechanism by which extracellular Ca^{2+} enters ventricular cardiomyocytes *via* activation of the depolarization-activated Ca^{2+} channels (Bers, 2002). It begins with generation of an electrical signal at the sinoatrial (SA) node which is propagated through the atrial conduction system to the atrioventricular (AV) node. The AV node slowly conducts the electrical signal before it is rapidly passed through the *His-Purkinje* system to the cardiomyocytes where it coordinates ventricular contraction (Downey, 2003). The cardiomyocyte AP varies between species but can generally be divided into 5 main stages:

- Phase 0- Rapid upstroke or depolarization
- Phase 1- Early rapid repolarization
- Phase 2- Plateau
- Phase 3- Late repolarization
- Phase 4- Resting membrane potential/diastolic depolarization

The rapid depolarization of the cell is initiated by the electrical current delivered by the *Purkinje* system. This stimulus opens the voltage-gated sodium (Na^+) channels, generating the inward Na^+ current (I_{Na}) which dramatically alters membrane potential from a resting state at approximately -90 mV to approximately +20 mV (Bers, 2002). The early repolarization in phase 1 is brought about by inactivation of the Na^+ channels and activation of the rapid I_{Kto} current [outward potassium (K^+) channels]. The plateau phase is brought about by the balance between delaying repolarization *via* the inward movement of Ca^{2+} (I_{CaL}) through the L-type Ca^{2+} channels and the outward movement of K^+ through the delayed rectifier currents (I_{ks}). Acceleration of repolarization occurs in phase 3 where the L-type Ca^{2+} channels are closed but the rectifying K^+ currents remain active. The resting membrane potential is then restored in phase 4 and equilibrium is maintained mainly by the inward rectifying K^+ currents (I_{k1}) (Bers, 2002) (Figure 1.1)

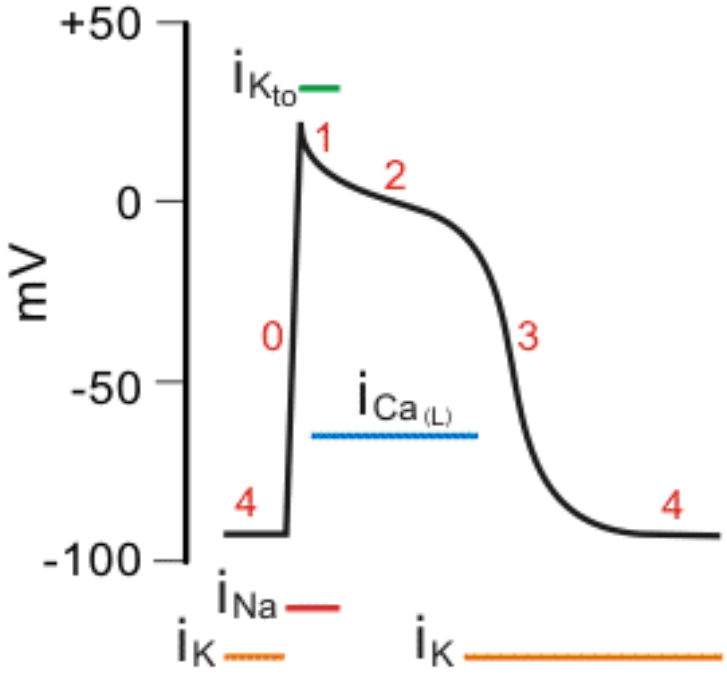

Figure 1.1 The ventricular cardiomyocyte action potential.
Depolarization of membrane (phase 0) stimulated *via* I_{Na+}, which is deactivated in phase 1 upon activation of I_{Kto}. Ca^{2+} enters *via* I_{CaL} during plateau/phase 2. Deactivation of I_{CaL} in phase 3 induces repolarization while I_K remains active. Resting membrane potential (phase 4) maintained by I_K. I_{Na}= inward Na^+ current, I_{Kto}= outward K^+ current, I_{CaL}= L-type Ca^{2+} channel current, I_K= rectifying K^+ currents (Klabunde, 2011).

1.2.1.2 Cardiomyocyte Ca^{2+}-handling

Entry of Ca^{2+} into the cell *via* the L-type Ca^{2+} channel, increasing cytosolic [Ca^{2+}], triggers CICR. The L-type Ca^{2+} channels are located in the cardiomyocyte T-tubules, co-localized with the ryanodine receptor (RyR) situated on the cell's intracellular store of Ca^{2+}, the sarcoplasmic reticulum (SR) (Sah et al., 2003). The RyR is the SR Ca^{2+} release complex. When $[Ca^{2+}]_i$ is raised *via* entry through the L-type Ca^{2+} channel, it stimulates the opening of the SR *via* the RyR, resulting in a synchronous release of Ca^{2+}, further raising $[Ca^{2+}]_i$. It is thought that 2-4 Ca^{2+} ions binding per RyR is enough to stimulate release (Bers, 2001). Neighbouring RyRs are then stimulated either by the increase in local $[Ca^{2+}]_i$ or by coupled-gating between RyRs (Bers, 2002). The increase in local $[Ca^{2+}]_i$ also turns off the L-type Ca^{2+} channels *via* a positive-feedback loop. The amount of Ca^{2+} release upon stimulation of the RyR depends on its sensitivity, which is reliant on SR [Ca^{2+}]. If Ca^{2+} is high, the RyR has increased Ca^{2+} sensitivity as there is increased availability of SR Ca^{2+}. Conversely, if SR Ca^{2+} content is low, the RyR may become so desensitized to Ca^{2+} that it may fail to be triggered by Ca^{2+} entry *via* the L-type Ca^{2+} channel. In response to depleted SR [Ca^{2+}] other Ca^{2+}-handling protein functions are altered to address the imbalance. L-type activity is increased to promote entry of Ca^{2+} into the cell, the sodium-calcium exchanger (NCX) which extrudes Ca^{2+} is down-regulated and Ca^{2+} uptake into the SR is enhanced *via* the phosphorylation of phospholamban (PLB) by cyclic AMP (cAMP), protein kinase A (PKA) or calcium/calmodulin-dependent protein kinase II (CaMKII), which relieves inhibition of the SR Ca^{2+}-ATPase (SERCA), promoting influx of Ca^{2+} into the SR (Bers, 2002; Brittsan and Kranias, 2000).

After release of Ca^{2+} from the SR, CICR is switched off by inactivation of the RyR. Ca^{2+} then binds to troponin C found on the cardiomyocyte myofilaments, activating cellular contraction which produces rapid shortening in order to facilitate ventricular contraction and ejection of blood from the chamber (Bers, 2002). The force of cellular contraction is directly related to the $[Ca^{2+}]_i$ and the sensitivity of the myofilaments to Ca^{2+}. Following contraction, $[Ca^{2+}]_i$ must be reduced in order to facilitate dissociation of Ca^{2+} from the myofilaments to allow for relaxation. This requires extrusion of Ca^{2+} from the cytoplasm, achieved *via* two mechanisms; extrusion from the cell *via* the NCX, or back into the SR *via* SERCA, with the majority returned to the SR from where it originated (Sah et

al., 2003). The exact proportions of Ca^{2+} extrusion by each channel varies between species, with SERCA responsible for removal of 70 % of $[Ca^{2+}]_i$ in rabbit and human cardiomyocytes compared to 92 % in rat and mouse (Bers, 2002; Hove-Madsen and Bers, 1993). The slow Ca^{2+} extrusion systems of the sarcolemmal Ca^{2+}-ATPase and mitochondrial Ca^{2+} uniporter account for only 1 % of extrusion in each case (Bers, 2002). An equivalent amount of Ca^{2+} is required to be extruded from the cell as entered at each contraction to maintain a steady state (Bers, 2002; Eisner et al., 2000), with $[Ca^{2+}]_i$ rising from a diastolic resting concentration of approximately 0.1 μM up to approximately 1 μM with each contraction (Sah et al., 2003) (Figure 1.2).

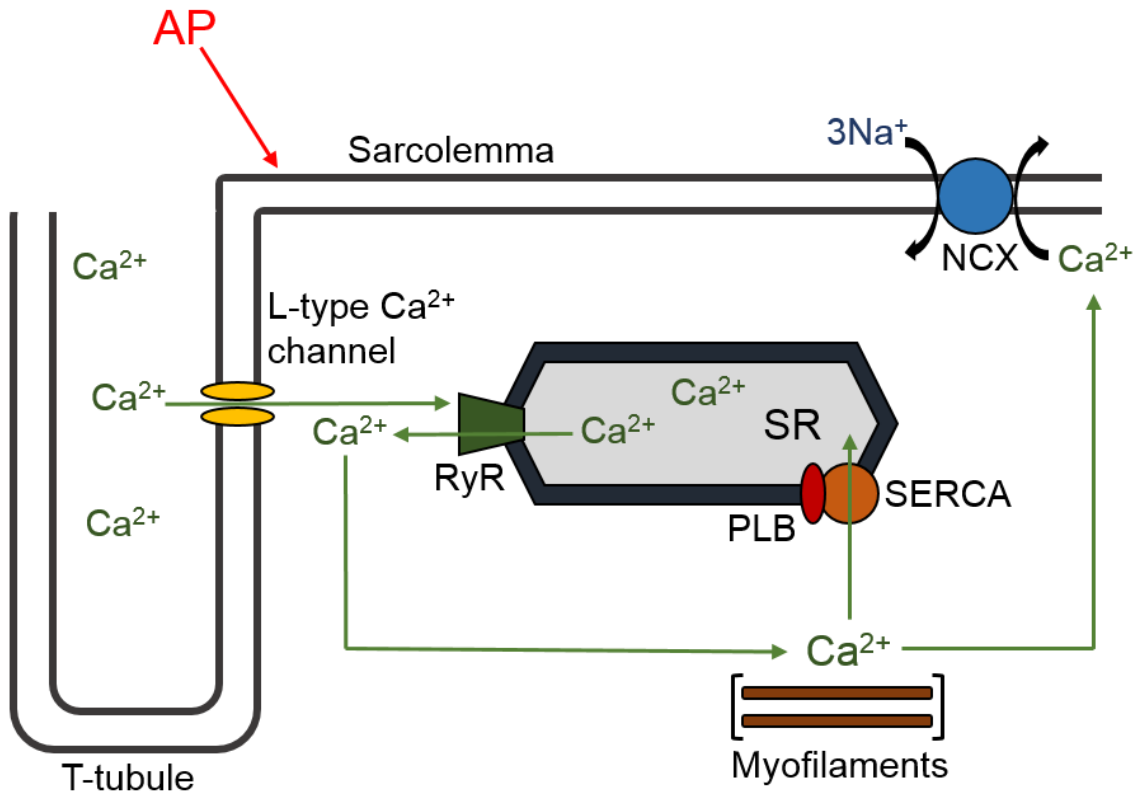

Figure 1.2 Cardiomyocyte Ca^{2+}-handling.
The process of cardiomyocyte Ca^{2+}-handling that occurs during ECC to facilitate cardiomyocyte contraction. Ca^{2+}= calcium, RyR= ryanodine receptor, PLB= phospholamban, SERCA= sarcoplasmic reticulum Ca^{2+}-ATPase, NCX= sodium-calcium exchanger, AP= action potential.

1.3 The diseased heart

According to the World Health Organisation (WHO), cardiovascular disease (CVD) is the primary cause of death globally, with 17.5 million people dying as a result of CVD complications in 2012, accounting for 31 % of all deaths. Of these, 7.4 million were attributable to CHD (WHO, 2015). CHD occurs through the development of a myocardial ischemia, or MI, formed as a result of a stenosis, or narrowing, of the coronary artery, reducing or blocking blood flow to a region of the myocardial tissue itself (Libby and Theroux, 2005). Although the overall mortality rate of CHD has shown a decline since 1998, the burden of the disease remains high due to the increased survival rates following MI leading to increased development of HF (Roger et al., 2012).

1.3.1 Structural remodelling processes post-MI

Following infarction and loss of myocardium there is an abrupt increase in wall stress triggering a number of LV structural changes in an attempt to normalise increased wall stress and maintain LV contraction (Sutton and Sharpe, 2000). These processes following MI, termed adaptive remodelling, can be divided into 2 phases; the early phase (<72 hr following infarction) where scar expansion and potential cardiac rupture can occur (Erlebacher et al., 1984), and the late phase (>72 hr following infarction) where global alterations in cardiac architecture occur including LV dilation, distortion of the LV shape, cardiomyocyte hypertrophy and collagen scar formation (Pfeffer and Braunwald, 1990). Failure of these alterations to normalise wall stress results in further LV expansion and deterioration of contractile function (Pfeffer and Braunwald, 1990).

1.3.1.1 Early remodelling and scar formation

Immediately following infarction and cardiomyocyte necrosis there is an influx of macrophages, monocytes and neutrophils into the infarcted region, followed by the appearance of myofibroblasts within the scar. Macrophages facilitate the removal of necrotised cardiomyocytes and cellular debris, and the rapid degradation of cardiomyocyte collagen struts occurs through the activation of collagenases, serine proteases and matrix metalloproteases (MMPs) released from infiltrating neutrophils, with the normal collagen structure of the infarcted myocardium completely removed by 1 week post-MI (Cleutjens et al., 1995b; Ertl

and Frantz, 2005). MMPs are crucial in the regulation of the cardiac extracellular matrix (ECM) during this process as they are the only enzymes capable of breaking down the proteolytic-resistant helical structure of collagens (Mann and Spinale, 1998). MMP1 cleaves the collagens into fragments which are then unfolded and degraded by MMP2, MMP3 and MMP9 (Mann and Spinale, 1998). This degradation process results in infarct expansion, which occurs within 24 hr of injury and elevates diastolic and systolic wall stress (Warren et al., 1988). Scar expansion is a permanent and disproportionate regional thinning, dilation and elongation of the infarct zone which occurs prior to collagen scar formation and causes a distortion in the LV shape (Weisman and Healy, 1987). Following the degradation of the collagen network and prior to the formation of a stable scar, a reduction in the number of cardiomyocytes across the infarcted region as a result of slippage between muscle bundles can occur and also contributes to expansion (Pfeffer and Braunwald, 1990). This extreme wall-thinning during expansion can result in cardiac rupture and mortality in 5-30 % of MI cases (Anzai et al., 1997). The extent of expansion appears to be directly related to infarct size, with larger expansion indicating poor prognosis due to the further increase in LV cavity exerting increased wall stress and work-load on the non-infarcted myocardium (Pfeffer et al., 1991; Weisman and Healy, 1987).

The final early remodelling stage of scar formation is facilitated by the myofibroblasts, which are modified fibroblasts with SMC-like features, including the presence of functional gap junctions and the expression of α-SM actin, and are characterised by the presence of contractile apparatus consisting of actin myofilament bundles (Tomasek et al., 2002). The myofibroblasts construct a new collagen network, requiring several weeks to form a solid, stable collagen scar interspersed with some remaining myofibroblasts which contribute to collagen turnover and scar contraction (van den Borne et al., 2010; Willems et al., 1994). Myofibroblasts do not exist in healthy myocardium (Porter and Turner, 2009), and only following myocardial injury are normal cardiac fibroblasts stimulated to differentiate into myofibroblasts in response to a change in the mechanical microenvironment. Migration of the myofibroblasts to the site of injury is then facilitated by chemotactic factors such as transforming growth factor β (TGF-β) (Porter and Turner, 2009; van den Borne et al., 2010). Myofibroblast proliferation, migration and secretion of ECM components is regulated by various

stimuli including mechanical stretch, vasoactive peptides such as Ang II, autocrine/paracrine factors and pro-inflammatory cytokines (Porter and Turner, 2009). At the site of infarction myofibroblasts deposit new ECM proteins, first in the border zone between the infarcted and non-infarcted myocardium before expanding into the central region of the scar (van den Borne et al., 2010). The myofibroblasts produce interstitial collagens. Initially collagen III is produced, with levels found to be elevated as early as 3 days post-MI in the rat MI model (Cleutjens et al., 1995a), with collagen I deposition occurring more slowly and to lower levels than that of collagen III. Cross-linking of multiple collagen I fibres confers tensile strength to the scar (Cleutjens et al., 1999) (Figure 1.3).

1.3.1.2 Cardiac hypertrophy

Adaptive eccentric and concentric cardiomyocyte hypertrophy occurs in response to increased wall stress and myocardial loss following scar formation (Janssens et al., 2004). In response to pro-hypertrophic signals, cardiomyocytes can increase in size by up to 70 % (Sutton and Sharpe, 2000) as a result of increased contractile protein synthesis (Carabello, 2002). Where eccentric and concentric hypertrophy differ is in what arrangement the contractile proteins are assembled. Eccentric hypertrophy occurs primarily in response to volume overload and involves the assembly of sarcomeric proteins in a series, resulting in cell lengthening, whereas concentric hypertrophy results from pressure overload and results in the parallel assembly of sarcomeric proteins, resulting in an increase in cardiomyocyte width (Kehat et al., 2011). Pressure overload results from the heart having to contract while experiencing excessive afterload, or stress, on the LV wall, whereas volume overload occurs when the LV has an excessive blood volume, adversely affecting function due to increased myocardial stretch (Gotzmann et al., 2012; Pang and Levy, 2010; Peterson, 2002). As there is a combined increase in volume and pressure overload post-MI as a result of increased strain on the surviving myocardium, scar expansion and increased wall stress, both concentric and eccentric hypertrophy have been shown to occur (Force and Molkentin, 2006; Opie et al., 2006; Runge and Patterson, 2007).

Hypertrophy is triggered by a range of factors post-MI, including increased myocardial stretch, activation of the local tissue RAS, and paracrine/autocrine

factors (Sutton and Sharpe, 2000). Ca^{2+} signalling can also trigger hypertrophy, with it demonstrated in animal models that increased L-type Ca^{2+} channel, NFAT and calcineurin expression and decreased Ca^{2+} release from the SR induce cardiomyocyte hypertrophy (Berridge et al., 2003). Increased norepinephrine (NE) release stimulates a hypertrophic response directly and indirectly by raising plasma Ang II and endothelin-1 (ET-1) levels (Ju et al., 1998). Local Ang II and ET-1 release stimulates the synthesis of sarcomeric contractile proteins (Sadoshima et al., 1992). The activation of the G-protein-coupled receptor AT_1R by Ang II activates multiple signalling pathways including tyrosine kinases, protein kinase C (PKC), mitogen activated protein kinases (MAPKs) and S6 kinase (Ju et al., 1998), which stimulates further Ang II release and activation of foetal gene expression such as α-actin, ß-myosin heavy chain (ß-MyHC), and ANP (Yamazaki et al., 1995). Cardiomyocyte hypertrophy is initially a cardio-protective response, attenuating progressive LV dilation and stabilising contraction (Garza et al., 2015). However, over time the chronic neurohormonal activation, myocardial stretch, RAS activation and presence of autocrine/paracrine factors promotes eccentric, pathological hypertrophy over concentric hypertrophy (Garza et al., 2015). Transition from concentric to eccentric hypertrophy is a marker of transition from compensatory to pathological remodelling. It causes severe chamber dilation, a reduction in ventricular contraction and progression to HF (Lemmens et al., 2007) (Figure 1.3).

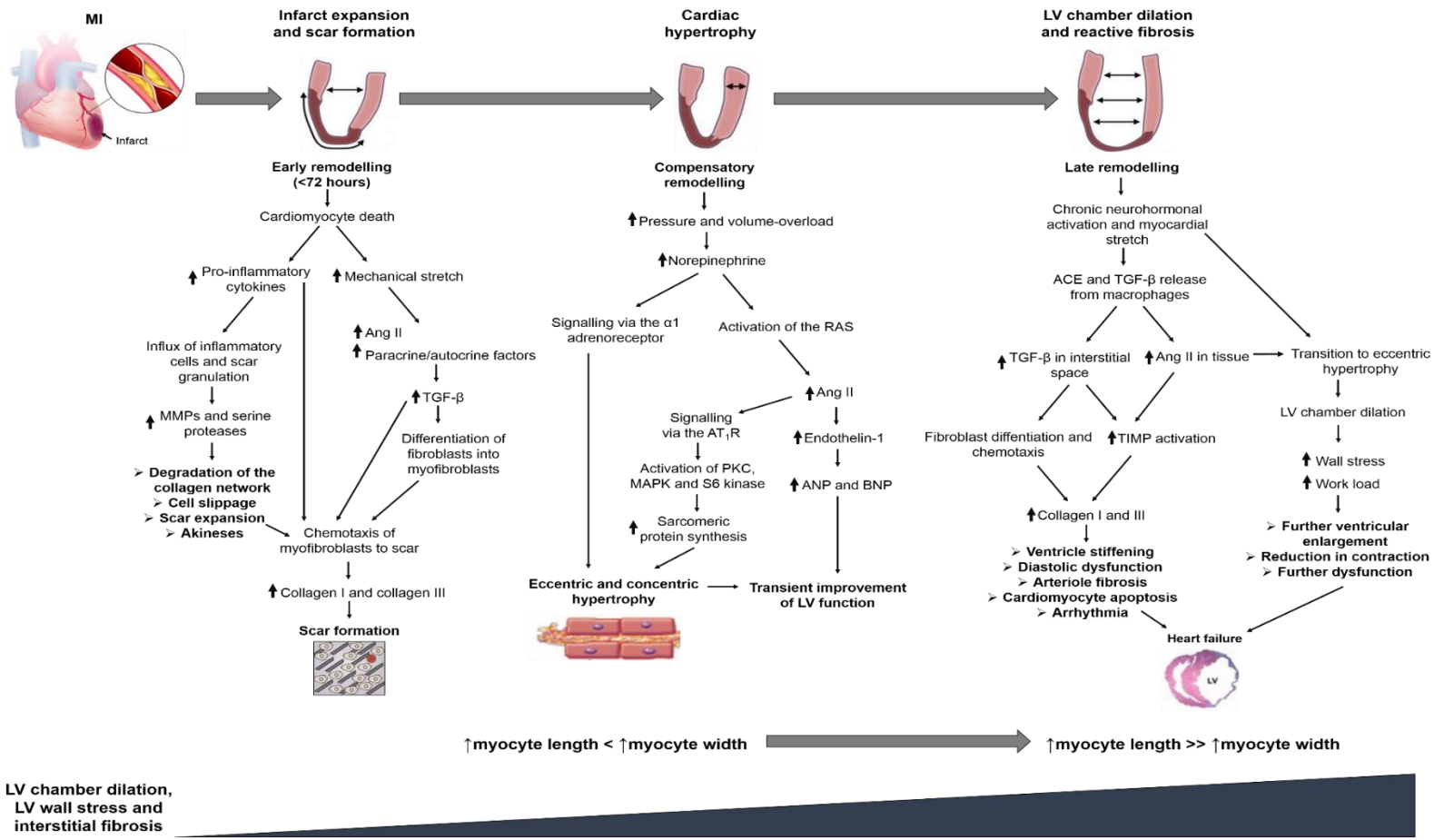

Figure 1.3 Phases and mechanisms of structural remodelling post-MI.
Signalling pathways activated during the early, adaptive and maladaptive phases of myocardial remodelling post-MI. MMP= matrix metalloprotease, TGF-β= transforming growth factor-β, PKC- protein kinase-C, AT_1R= angiotensin type 1 receptor, ANP= atrial natriuretic peptide, BNP= brain natriuretic peptide, MAPK= mitogen activated protein kinase, ACE= angiotensin converting enzyme, LV= left ventricle, TIMP= tissue inhibitors of metalloproteases. Figure adapted from (Seropian et al., 2014; Takemura et al., 2009; van den Borne et al., 2010).

1.3.1.3 Cardiac fibrosis and collagen deposition

While collagen deposition and a high percentage of ECM components in the scar is essential for effective healing, collagen deposition and fibrosis in the non-infarcted myocardium is detrimental to cardiac function (Cleutjens et al., 1999). This reactive fibrosis involving collagen deposition within the interstitial space of the non-infarcted myocardium is a result of sustained elevation of Ang II-induced TGF-β release (Sun et al., 2002). TGF-β is primarily involved in the regulation of myofibroblast collagen secretion and is able to diffuse into the interstitial spaces of the myocardium, remote from the infarct region. In doing so it promotes the chemotaxis of myofibroblasts and collagen deposition within the interstitial space (Sun et al., 2002). This increased ECM has adverse effects on cardiac function, with a 2- to 3- fold increase in collagen content of the non-infarcted myocardium being sufficient for the development of myocardial stiffness and dysfunction (Covell, 1990). Not only does this progressive increase in collagen deposition exaggerate mechanical stiffness and promote diastolic dysfunction, it also disrupts electrical conductivity between cardiomyocytes, increasing the possibility of re-entrant arrhythmias (Brown et al., 2005). Perivascular fibrosis around cardiac arterioles also occurs, which can impair cardiomyocyte oxygen availability, promoting further cardiomyocyte apoptosis (Brown et al., 2005) (Figure 1.3).

1.3.1.4 Late remodelling and systolic HF

HF is a complication of MI owing to adverse cardiac remodelling processes which occurs in 22 % of males and 46 % of females within 6 years of the initial infarction (Lloyd-Jones et al., 2009). HF is an end-stage heart disease where the heart no longer compensates for the loss of myocardium and as a result cardiac performance is so impaired that it is no longer able to meet systemic energy requirements (Chiariello and Perrone-Filardi, 1998; Kannel and Belanger, 1991). The structural alterations which the heart undergoes during the compensatory phase are the very mechanisms which contribute to eventual development of HF (van den Borne et al., 2010). The initial compensatory hypertrophic response become progressively more eccentric (Lemmens et al., 2007). The cardiomyocytes lengthen and the LV chamber becomes progressively more dilated, exerting further wall-stress on the myocardium. This effect may be

initially compensatory in an effort to maintain stroke volume (SV), however this eventually promotes further ventricular enlargement and dysfunction (van den Borne et al., 2010). HF hearts are often associated with a reduced number of myofibroblasts in the scar region, which is indicative of poor ECM maintenance and also allows further expansion of the scar (van den Borne et al., 2010). This combined with accumulation of collagen in the non-infarcted myocardium, stiffening the muscle wall, promoting diastolic dysfunction and resulting in cardiomyocyte apoptosis all contribute to the HF phenotype (Figure 1.3).

1.3.2 Electrical remodelling processes post-MI

ECC in ventricular cardiomyocytes isolated from hearts of HF patients is dramatically altered, with abnormal Ca^{2+}-handling (Gwathmey et al., 1987) and a prolongation of the AP (Gwathmey et al., 1990). It has been further postulated that the haemodynamic and contractile dysfunction observed in diseased myocardium is associated with a common pattern of electrophysiological changes within ventricular cardiomyocytes. This has been studied extensively in both failing human hearts and animal models of cardiac dysfunction, with specific proteins that contribute to this altered state identified (O'Rourke et al., 1999). Abnormal Ca^{2+}-handling features associated with the ventricular cardiomyocytes of diseased hearts include increased diastolic $[Ca^{2+}]_i$, a slower decline of the Ca^{2+}-transient, a reduced Ca^{2+}-transient amplitude and reduced cellular contractility, as observed in HF patients and animal models of HF (Beuckelmann et al., 1992; Beuckelmann et al., 1995; Gomez et al., 2001; Houser et al., 2000; O'Rourke et al., 1999; Piacentino et al., 2003).

Dysregulation of SERCA is a main contributor to Ca^{2+}-handling abnormalities, with decreased SERCA expression or activity coupled with reduced SR $[Ca^{2+}]$ being a feature found in animal and human cardiomyocytes from failing hearts (Beuckelmann et al., 1995; del Monte et al., 2001; Frank et al., 2002; Hobai and O'Rourke, 2001; Levitsky et al., 1991; Piacentino et al., 2003). Reduced SERCA activity may explain the reduced SR $[Ca^{2+}]$, a common feature in cardiac contractile dysfunction, and reduced release of Ca^{2+} from the SR during CICR, reducing the amplitude of the Ca^{2+}-transient (Bers, 2002; Gomez et al., 2001; Piacentino et al., 2003). Expression of the regulator of SERCA, PLB (which has an inhibitory effect on SERCA), appear to remain unchanged in diseased hearts

(Frank et al., 1998; Hasenfuss et al., 1994; Huang et al., 1999; Schwinger et al., 1995), however its phosphorylation does change, with a decrease in phosphorylation at Ser16 and Thr17 (Huang et al., 1999; MacLennan and Kranias, 2003; Schwinger et al., 1999), leading to increased inhibition of SERCA and a decrease in Ca^{2+} uptake into the SR (Kadambi et al., 1996).

Another characteristic of cardiomyocytes from diseased hearts is the increased incidence of spontaneous diastolic Ca^{2+} release, or Ca^{2+} sparks, from the SR as a result of increased RyR sensitisation (Litwin et al., 2000; Shannon et al., 2003). As well as increasing the loss of Ca^{2+} from the SR, further depleting its concentration, the production of Ca^{2+} sparks can spread through the cell causing abnormal Ca^{2+} wave propagation, resulting in delayed afterdepolarizations (DADs). These DADs have been associated with development of ventricular arrhythmias and increased incidence of SCD, which accounts for 50 % of all CV-related mortality (Chen et al., 2009; Gilmour and Moïse, 1996; Lehnart et al., 2006; Pogwizd and Bers, 2002; Wang et al., 2014b).

Identifying the mechanisms and pathways driving adverse structural and functional remodelling changes post-MI is crucial in the development of novel therapeutic strategies that can attenuate the decline in cardiac function and prevent progression to HF. One such pathway is the RAS.

1.4 The classical RAS

A central pathway crucial in the regulation of cardiovascular function and many other basic physiological processes is the RAS. Traditionally, the ‘classical RAS’ axis was described in the 1940’s as a sequential, endocrine system revolving around the main RAS effector molecule Ang II, which was identified as a vasoactive peptide whose primary role was thought to be blood pressure regulation (Braun-Menendez et al., 1940; Bumpus et al., 1954). Our understanding of the RAS has evolved considerably since, with it now also appreciated as a local system in individual tissues whose components have been identified in every organ, and consequentially the signalling and function of the RAS is far more complex than the basic sequential pathway (Paul et al., 2006). Moreover, an alternative ‘non-classical’ or counter-regulatory RAS axis has also been identified, which blocks many actions of the classical axis (Chappell et al.,

1989). The RAS is now implicated in the regulation of a variety of physiological processes including those in renal, neuronal, cardiac, pancreatic, vascular, adrenal, pituitary, cognitive, aging, inflammatory and reproductive functions (Paul et al., 2006).

The classical axis of the RAS begins with angiotensinogen; a 453 amino acid protein that is the source of all RAS peptides (Chappell, 2012b). It is primarily synthesised by the liver and secreted into the circulation (Navar, 2014), where it is hydrolysed between residues 10 and 11 by the aspartyl protease renin to produce the inactive peptides Ang I [or angiotensin-(1-10)] and (des-Ang I)-angiotensinogen (Chappell, 2012b). Renin was the first RAS component identified in 1898 when it was isolated from rabbit renal cortex lysates (Tigerstedt and Bergman, 1898). It is produced in the kidney by the juxtaglomerular (JG) cells that line the arterioles of the afferent renal glomerulus in response to changes in renal perfusion pressure, tubular sodium chloride concentration, activation of the sympathetic nervous system and negative feedback of Ang II on the JG cells (Atlas, 2007; Persson, 2003). Angiotensinogen is renin's only known substrate, however other proteases including chymase, tonin, kallikrein and cathepsin D hydrolyse angiotensinogen within tissues (Chappell, 2012b; Ihara et al., 1999). The conversion of angiotensinogen to Ang I is the rate-limiting step of the RAS and is primarily dependent on renin activity as plasma angiotensinogen levels remains relatively constant (Morgan et al., 1996). The inactive decapeptide Ang I is further hydrolysed by the metallopeptidase ACE, which cleaves Ang I between residues 8 and 9 to form the active effector peptide Ang II and the dipeptide His-Leu (Chappell, 2012b) (Figure 1.5). ACE is a membrane-bound dipeptidyl carboxy-peptidase located on the endothelial surface of pulmonary vessels and on renal, intestinal and choroid epithelial cells (Bruneval et al., 1986).

1.5 Ang II

Ang II has an important function in renal physiology and blood pressure homeostasis through regulation of sodium and blood volume (Hall, 1986), including effects on haemodynamics and peripheral vascular tone, stimulation of sodium reabsorption in the kidney, stimulation of the adrenal glands for the production of aldosterone, inhibition of renin release from the kidneys and activation of the sympathetic nervous system (Ito et al., 1995; Phillips et al.,

1993). Through the promotion of vasoconstriction and sodium reabsorption by the nephron, Ang II increases blood pressure and volume thus restoring renal perfusion, which in turn reduces renin release, maintaining homeostasis (Atlas, 2007). Within tissues Ang II also has roles in the regulation of cell growth, proliferation and apoptosis, the inflammatory response and oxidative stress (Ferrario, 2006). Ang II has a very short circulating half-life of approximately 30 s (van Kats et al., 1997), therefore it is thought that the ubiquitous endothelial cell membrane-bound nature of ACE makes it possible for Ang II to be synthesised close to its site of action (Atlas, 2007). Local synthesis of Ang II within tissues is thought to occur through uptake of renin and/or angiotensinogen from the circulation into the tissue (Carey and Siragy, 2003). Ang II signals *via* two receptor subtypes; the AT_1R and the AT_2R, with the former mediating the majority of the physiological and pathophysiological effects of Ang II (Carey and Siragy, 2003). Both receptors belong to the seven-transmembrane G protein-coupled receptor superfamily (Mehta and Griendling, 2007) (Figure 1.5).

1.5.1 AT_1R

The AT_1R is a 40 KDa protein composed of 349 amino acids and is found widely distributed throughout the body (Mehta and Griendling, 2007). Four cysteine residues on the extracellular binding domain form disulphide bridges crucial in Ang II signalling (Ohyama et al., 1995). G-protein coupling occurs at the NH_2 terminus of the transmembrane portion of the receptor and the first and third extracellular loops (Bumpus, 1991). The cytoplasmic tail of the receptor contains serine and threonine residues which can be phosphorylated by G-protein receptor kinases (Mehta and Griendling, 2007). It is these phosphorylation sites which are believed to play a role in receptor desensitisation (Du et al., 2004). Following stimulation by Ang II, AT_1Rs are endocytosed within approximately 10 min, with 25 % of these recycled back to the cell surface and the remainder degraded (Griendling et al., 1987). Regulation of the AT_1R is under the control of a tight negative feedback loop with Ang II, with an acute increase in Ang II increasing the expression of the AT_1R, but chronic Ang II activation leading to receptor down-regulation (Lassegue et al., 1995). Its expression is also regulated by a variety of other factors including glucocorticoids and mineralocorticoids, insulin, nitric oxide, LDL and epidermal growth factor (Kaschina and Unger,

2003). Its regulation also changes under pathophysiological conditions, including in MI and HF (Nio et al., 1995; Yamamoto et al., 2000; Zhu et al., 1999).

Ang II signalling *via* the AT_1R mediates the majority of its physiological actions. The 'classical' actions mediated through the stimulation of the AT_1R include generalised vasoconstriction (Unger, 2000). Activation of the AT_1R on VSMCs by Ang II promotes vasoconstriction which is further enhanced by the release of noradrenaline and ET-1 (Hahn et al., 1993). AT_1R-induced vasoconstriction is strongest in the kidney, where it also facilitates reabsorption of sodium ions in the kidney proximal tubes (Unger, 2000) and also modulates renal glomerular filtration and cellular growth and differentiation (Kaschina and Unger, 2003). AT_1R stimulation promotes the release of aldosterone from the adrenal cortex and in the heart it stimulates cell growth in the LV and exerts a positive inotropic effect by increasing the rate and force of contraction by initiating noradrenaline release from the sympathetic nerve terminals (Unger, 2000). The AT_1R is also deemed to exert the detrimental effects of Ang II in pathophysiological cardiac remodelling and HF, including roles in cardiac hypertrophy, fibrosis, inotropy and arrhythmogenisis, which will be discussed later (Opie and Sack, 2001).

1.5.1.1 AT_1R signalling

Following Ang II binding to the AT_1R, a number of signalling cascades are activated which can be divided into G-protein and non-G-protein pathways (Mehta and Griendling, 2007). The primary signalling pathways activated and the physiological effects resulting from AT_1R stimulation are summarised in Table 1.1.

Table 1.1 AT_1R signalling pathways

Pathway	Downstream effector	Signalling molecules	Factors/pathways regulated	Effect	References
G-protein coupled (Gαq11, Gα12/13 and Gßy subunits)	PLC	IP_3, PKC and DAG	VSMC MyHC phosphorylation; aldosterone release; phosphorylation of Na^+/H^+ pump; Ras, Raf, MEK and ERK activation	Vasoconstriction and cell growth	Yan et al., 2003; Yasunari et al., 1999
	PLD	DAG and PKC	Hydrolysis of phosphatidly choline and PA production	Cell contraction and growth	Touyz and Schiffrin, 2000
	PLA_2	AA production and NADPH oxidation	AA metabolites (e.g. hydroxyeicosatetraenoic acids) and ROS	Pro-hypertensive, regulation of vascular tone, vasoconstriction	Griendling et al., 2000; Sarkis et al., 2004
Non-G-protein coupled	ROS	Nox-1 and Nox-4 membrane NADPH, superoxide, H_2O_2	p38MAPK, Akt, Src and EGFR, and transcription factors NF-κB, AP-1 and NRF	Development of vascular injury and atherosclerosis	Lassègue et al., 2001; Papaiahgari et al., 2006; Pueyo et al., 2000
	Tyrosine-kinase cross-talk	EGFR, PDGF, insulin receptor, c-Src, Pyk-2 and FAK	Ras/Raf/MAPK cascade activation and MAPK translocation to the nucleus	Cell growth, apoptosis, contraction and differentiation	Bucher et al., 2001; Kaschina and Unger, 2003
		JAK-STAT	Induction of early response genes *c-fos*, *c-jun* and *c-myc*	Activated in MI and hypertrophy; cell growth, adhesion, migration and ECM secretion; adaptive and maladaptive changes in heart and vasculature during injury	Mascareno and Siddiqui, 2000; Omura et al., 2001

PLC= Phospholipase C, PLD= Phospholipase D, PLA_2= Phospholipase A_2, IP_3= Inositol trisphosphate, PKC= Protein kinase C, DAG= 2,3-diamino-2,3-dideoxyglucose, VSMC= Vascular smooth muscle cells, MyHC= Myosin heavy chain, MEK/MAPK= Mitogen-activated protein kinase kinase, ERK= Extracellular-signal-related-kinase, PA= Phosphatidic acid, AA= Arachidonic acid, NADPH= Nicotinamide adenine dinucleotide phosphate, ROS= Reactive oxygen species, Akt= Protein kinase B, Src= Proto-oncogene tyrosine-protein kinase Src, EGFR= Epidermal growth factor receptor, NF-κβ= Nuclear factor κβ, AP-1= Activator protein 1, NRF= Nuclear respiratory factor, PDGF= Platelet-derived growth factor, FAK= Focal Adhesion Kinase, JAK-STAT= Janus kinase-signal transducer and activator of transcription.

1.5.2 AT_2R

The AT_2R is a 41 KDa protein consisting of 363 amino acids, which only shares 34 % homology with the AT_1R (Mukoyama et al., 1993). Despite the lack of similarity between the two receptors, Ang II has a similar affinity for both (Steckelings et al., 2011). Unlike the AT_1R, the AT_2R is expressed only at very low levels in adult tissues, in contrast it is widely expressed in foetal tissues, with expression dropping dramatically after birth, suggesting it plays a crucial role in foetal development (Shanmugam et al., 1996). After birth AT_2R expression is restricted to a few organs including the brain, adrenal glands, heart, kidney, myometrium and ovary, with expression predominantly in mesenchymal tissues, suggesting the receptor may be involved in developmental and differentiation processes (Kaschina and Unger, 2003; Shanmugam et al., 1995).

Regulation of AT_2R expression occurs in response to a variety of factors. It is down-regulated in response to Ang II, norepinephrine and growth factors including endothelial growth factor (EGF) and fibroblast growth factor (FGF) and glucocorticoids (Kijima et al., 1996; Matsubara and Inada, 1998). It is stimulated by insulin, interferon regulatory factors and interleukin-1β, however the majority of this has been observed *in vitro* (Unger, 1999). Limited *in vivo* evidence has suggested it is increased in certain cell types in response to oestrogen and decreased in response to aldosterone and NO (Bucher et al., 2001; Mancina et al., 1996; Wang et al., 1998). The most well documented change in expression of the AT_2R has been shown to occur during pathological conditions (Mehta and Griendling, 2007). Its expression is significantly increased following MI, and in CHF there is significant down-regulation of the AT_1R in relation to the normal expression levels of the AT_2R (Tsutsumi et al., 1998). Normal receptor expression on rat cardiomyocytes has been reported to consist of 10 % of total ventricular cardiomyocytes expressing AT_2R and 40 % of total ventricular cardiomyocytes expressing the AT_1R. Following MI, the percentage of cardiomyocytes expressing the AT_2R increases to 60 % (Busche et al., 2000).

The AT_2R regulates a variety of processes which generally counteract the effects exerted through Ang II-AT_1R signalling (Nouet and Nahmias, 2000). Disruption of the *Atrg2* gene encoding for the AT_2R has demonstrated its role in negatively regulating blood pressure (Ichiki et al., 1995), with its over-expression exerting

anti-pressor activity and a strong negative inotropic effect (Masaki et al., 1998). It is also the first G-protein coupled receptor to be identified as a receptor-specific antagonist, capable of inhibiting AT_1R-mediated responses *via* heterodimerisation *in vitro* (AbdAlla et al., 2001). Like the AT_1R, the AT_2R is able to form a stable heterodimer with the BK_2R which is functional and thought to possibly promote vasodilation through NO and cGMP release (Abadir et al., 2006).

AT_2R stimulation is also associated with anti-proliferative and pro-apoptotic effects (Nouet and Nahmias, 2000). It has been demonstrated to mediate apoptosis and broad anti-growth effects in a variety of cultured cell models (Dimmeler et al., 1997; Li et al., 1998) (Meffert et al., 1996; Tsuzuki et al., 1996), and is pro-apoptotic in VSMCs and in the cerebral cortex following stroke *in vivo* (Zhu et al., 2000). Unlike Ang II-AT_1R signalling, the AT_2R is thought to be anti-proliferative but able to promote cellular differentiation (Kaschina and Unger, 2003). Although its exact mechanism of action is unclear, one study in endothelial cells suggested it is able to inhibit growth *via* the up-regulation of thrombospondin-1, a modulator of endothelial cell adhesion, motility and growth (Fischer et al., 2001). *In vivo* the AT_2R has been demonstrated to inhibit angiogenesis and promote vasodilation, counter-acting the effects associated with the AT_1R (Munzenmaier and Greene, 1996).

However, some of the established effects of the AT_2R in the heart have been disputed due to publication of varying results. Studies in adult cardiomyocytes *in vivo* have produced conflicting evidence for the role the AT_2R in hypertrophy. Loss-of-function studies using the AT_2R-deficient mouse have shown there is no hypertrophic response observed in AT_2R KO mice in response to pressure overload or Ang II infusion, suggesting the receptor is required for the hypertrophic response and protein synthesis (Akishita et al., 2000; Ichihara et al., 2001; Senbonmatsu et al., 2000). However, gain-of-function studies utilising overexpression of the AT_2R have reported results which dispute this. Lentiviral over-expression of the AT_2R in the rat has been demonstrated to exert an anti-hypertrophic response to Ang II infusion (Falcón et al., 2004). Similarly, transgenic mice selectively over-expressing the AT_2R in ventricular cardiomyocytes show an attenuated hypertrophic response following aortic banding compared to WT controls (Yan et al., 2008). Moreover, in cultured adult

rat cardiomyocytes there is no evidence for a pro-apoptotic effect of the AT_2R, but rather apoptosis appears to be mediated by the AT_1R (Cigola et al., 1997; Kajstura et al., 1997). Therefore, due to conflicting results produced by these studies the precise role of the AT_2R in the heart remains controversial (Avila et al., 2011). Moreover, despite its evident up-regulation in pathological conditions, the exact role the AT_2R plays in this setting is unclear (Mehta and Griendling, 2007). Following MI in the rat, an increase in numbers of progenitor cells characterised as c-kit$^+$$AT_2R^+$ have been identified, suggesting a role for the receptor in regeneration and tissue repair (Ludwig et al., 2012). AT_2R expression in human HF appears to be primarily in interstitial fibroblasts (Tsutsumi et al., 1998), however the exact physiological effects of the receptor following MI remain to be elucidated.

Despite this, the AT_2R remains a promising therapeutic target. It is thought to mediate the cardio-protective effects of AT_1R blockers (Oishi et al., 2006) and the synthetic AT_2R agonist C21 has been found to exert potent cardio-protective effects post-MI through anti-inflammatory and anti-oxidant mechanisms (Kaschina et al., 2008). Moreover, C21 has recently been identified as exerting cerebro-protective effects following ischaemic stroke in the rat and therefore is being pursued as a potential novel therapeutic for CVD (Joseph et al., 2014).

1.5.2.1 AT_2R signalling

Unlike Ang II stimulation of the AT_1R, the signalling cascades involved in AT_2R stimulation are far less characterised (AbdAlla et al., 2001). Although classed as a G-protein coupled receptor, the AT_2R has atypical signal transduction and G-protein coupling, with initial studies failing to show it was G-coupled (Nahmias and Strosberg, 1995; Porrello et al., 2008). It has since been shown that coupling of the AT_2R to $G_{i\alpha 2/3}$ or an unknown G-protein does occur (Buisson et al., 1995; Horiuchi et al., 1997; Jones et al., 2008; Zhu et al., 1998). There is also evidence to suggest the AT_2R can signal in the absence of Ang II due to its constitutively active nature (Porrello et al., 2008). The primary signalling pathways activated and physiological effects of AT_2R stimulation that have been characterised are summarised in Table 1.2.

Table 1.2 AT_2R signalling pathways

Pathway	Downstream effector	Signalling molecules	Factors/pathways regulated	Effect	References
G-protein coupled (Giα2/3 or unknown subunit)	Protein phosphatases	MKP-1, SHP-1 and PP2A activation	MAPK and ERK inactivation; dephosphorylation of Bcl-1 and activation of the JNK pathway	Anti-growth and anti-proliferation, pro-apoptotic	Bedecs et al., 1997; Horiuchi et al., 1997; Kaschina and Unger, 2003; Shenoy et al., 1999
	Kinin/NO/cGMP	Increased cGMP and PKA activation	eNOS phosphorylation, bradykinin activation	Vasodilation, sodium excretion and anti-proliferation	Gohlke et al., 1998; Liu et al., 1997; Siragy et al., 1996; Yayama et al., 2006
	PLA_2	AA and PP2A	MAPK and ERK activation	Myocyte pH regulation, proximal tubule sodium excretion and neuronal cell current regulation	Dulin et al., 1998; Haithcock et al., 1999; Kohout and Rogers, 1995; Zhu et al., 1998
Constitutive activation	unknown	unknown	p38MAPK and caspase 3	Cell growth and apoptosis	D'Amore et al., 2005; Miura and Karnik, 2000; Porrello et al., 2008

MKP-1= Mitogen-activated protein kinase phosphatase-1, PP2A= Protein phosphatase 2, MAPK= Mitogen activated protein kinase, ERK= Extracellular-signal-related-kinase, JNK= c-Jun kinase, NO= Nitric oxide, cGMP= Cyclic guanosine monophosphate, PKA= Protein kinase A, eNOS= Endothelial nitric oxide synthase, PLA_2= Phospholiapse A_2, AA= Arachidonic acid.

1.6 The RAS in cardiac remodelling

1.6.1 Ang II in structural remodelling

Using animal models it has been demonstrated that immediately following MI there are dramatic changes in the levels of RAS hormones, enzymes and receptors which correlate with the dramatic changes that occur in the cardiac architecture (Sun, 2010). In the infarcted rat myocardium, renin, which is not found in the healthy rat heart, is significantly up-regulated along with ACE and AT_1R expression, which are both usually expressed at low levels under normal conditions (Passier et al., 1996; Sun and Weber, 1996; Yamagishi et al., 1993). Renin, ACE and AT_1R are expressed by macrophages, myofibroblasts and vascular cells, which locally produce the high levels of Ang II also found in the infarct region, further promoting the early inflammatory response and influx of inflammatory cells (Falkenhahn et al., 1995; Sun and Weber, 1996). During this acute phase post-MI, circulating RAS effector molecule expression has been shown to be unaltered in the rat, suggesting local cardiac RAS activation promotes early remodelling independent of the systemic RAS (Hodsman et al., 1988). Chronic RAS activation also contributes significantly to the pathogenesis of HF. Within the myocardium of animals with experimental HF, increased levels of renin have been identified in the myocardium along with increased expression of ACE and AT_1R (Pieruzzi et al., 1995). Similarly, in human HF, uptake of renin from the circulation into the myocardium is enhanced, as is expression of ACE from both endothelial cells and other cells types within the heart (Wollert and Drexler, 1999). An inverse correlation between renin levels and angiotensinogen has also been identified in failing hearts, indicating enhanced cleavage of angiotensinogen and an increase in local Ang II production (Danser et al., 1997).

Elevated local Ang II expression regulates macrophages, endothelial cells and myofibroblasts during the acute post-MI phase (Sun, 2010). Ang II activates macrophages in an autocrine manner, promoting the removal of necrotic cardiomyocytes and facilitating the inflammatory response *via* inducing expression of NF-κB through ROS generation, thus promoting the activation of monocyte chemoattractant protein 1 (MCP-1) which further recruits macrophages and monocytes to the infarct region (Takahashi et al., 2008). ROS, produced primarily by NADPH oxidase in the heart, can be produced through Ang

II/AT_1R signalling through up-regulation of several components of NADPH, which has been found to be most elevated 2 weeks post-MI (Wolf, 2000). Following MI, vascular endothelial cell expression of ACE and AT_1R increases, with it proposed that Ang II facilitates angiogenesis in the scar region through increased expression of VEGF (Skaletz-Rorowski et al., 2004). Although Ang II has been shown to promote neovascularisation post-MI in mice (Toko et al., 2004), it has also been shown to inhibit neovascularisation post-MI in transgenic rats over-expressing the AT_1R in a cardiac-specific manner (de Boer et al., 2003). Ang II is also locally released by myofibroblasts (Sun and Weber, 1996). Myofibroblast-released Ang II regulates the myofibroblasts in an autocrine manner, signalling *via* the AT_1R and significantly increasing TGF-β expression, which as previously described is required for myofibroblast differentiation, chemotaxis towards the infarct region and collagen secretion for synthesis of the scar (Sun et al., 1998). Ang II also activates tissue inhibitors of metalloproteinases (TIMPs), thus inhibiting MMP activity to stop collagen degradation at the infarct (Lijnen et al., 2000). This demonstrates that Ang II is integral in facilitating inflammation and scar healing in the acute remodelling phase post-MI.

1.6.1.1 Ang II signalling in hypertrophy

Ang II is the primary regulatory of the pro-hypertrophic response of the myocardium post-MI (Lijnen and Petrov, 1999). Although associated with pro-hypertrophic effects, studies *in vitro* suggest that Ang II does not promote cardiomyocyte hypertrophy directly in adult cardiomyocytes as it only produces a small hypertrophic response through AT_1R-mediated ERK activation (Ruf et al., 2002). Therefore it has been proposed that Ang II promotes hypertrophy *in vivo* through the activation of various growth factors which then act locally *via* paracrine/autocrine mechanisms in order to promote cardiomyocyte hypertrophy (Sadoshima and Izumo, 1993). Growth factor expression has been demonstrated to occur through the activation of various second messenger pathways including phospholipases C, D, and A2, PKC, tyrosine kinases, $p21^{Ras}$, MAPKs, S6 kinase, c-Jun NH_2-terminal kinase, ERKs and Raf-1 kinase (Kudoh et al., 1997; Sadoshima et al., 1993; Zou et al., 1996) which are thought to be activated through either Ang II-induced G-coupling of the AT_1R or ROS signalling (Frey et al., 2004; Mehta and Griendling, 2007).

One of the factors thought to be crucial in the pro-hypertrophic effects exerted by Ang II is TGF-ß. Ang II can induce TGF-ß release from myofibroblasts in an autocrine manner (Sun et al., 1998). *In vitro* experiments on rat cardiomyocytes have also demonstrated that Ang II signalling *via* the AT_1R can induce TGF-ß activation, however whether its release occurs from myofibroblasts, cardiomyocytes or both *in vivo* is yet to be clarified (Gray et al., 1998). Another factor crucial in the regulation of Ang II-induced hypertrophy is ET-1. *In vitro* experiments have shown that exposing cardiomyocytes to Ang II increases prepro-ET-1 mRNA expression in a PKC-dependent manner (Ito et al., 1993). Increased expression has also been demonstrated in cardiomyocytes subjected to mechanical stretch (Yamazaki et al., 1996). ET-1 itself has been shown to be a potent pro-hypertrophic factor for cardiomyocytes *via* signalling of the ET_A receptor and activation of the Raf-1 kinase and MAPK second messenger pathways and a resulting increase in protein synthesis and expression of the proto-oncogenes *c-fos* and ANP, which in turn regulate cell growth and gene expression (van Wamel et al., 2001).

Studies performed in AT_1R over-expressing transgenic animals and *in vitro* have demonstrated that Ang II is able to directly induce cardiomyocyte hypertrophy *via* the transactivation of the epidermal growth factor receptor (EGFR) and subsequent activation of MAPKs, independent of growth factor activation (Shah and Catt, 2003). Ang II signalling has been shown to cause AT_1R-EGFR association in lipid rafts on VSMC membranes and promotion of the tyrosine phosphorylation of the EGFR (Ushio-Fukai et al., 2001). Activation of the AT_1R by Ang II stimulates PLC and subsequent signalling molecules including PKC, Ca^{2+}, ROS and tyrosine kinase (Eguchi et al., 2001). This activates the MMP-a disintegrin and metalloprotease domain (ADAM) which converts pro-heparin binding EGF to its active form which subsequently binds, phosphorylates and activates the EGFR (Asakura et al., 2002). This activates the MAPK signalling cascade and promotes cardiomyocyte hypertrophy through activation of Raf, ERK 1/2 and JAK-STAT (Saito and Berk, 2001; Thomas et al., 2002) (Figure 1.4).

1.6.1.2 Ang II signalling in fibrosis

Ang II signalling is crucial in orchestrating pro-fibrotic pathways in the heart following MI through driving differentiation of cardiac fibroblasts to

myofibroblasts and promoting synthesis of collagen I and collagen III. Activation of the AT_1R on cardiac fibroblasts has been shown to activate the PKC-NADPH-oxidase pathway, promoting production of ROS and inducing fibroblast differentiation and collagen I and III production *in vitro* (Bai et al., 2013). Interstitial cardiac fibrosis is also induced through ROS-dependent Ang II signalling. Ang II infusion in mice induces severe interstitial fibrosis through activation of Nox-2-containing NADPH oxidase which increases cardiac fibronectin and pro-collagen I expression and increases MMP-2 and NF-κB activity (Johar et al., 2006). Activation of NF-κB has been found to be associated with increased expression of collagen I and connective tissue growth factor (CTGF) genes in response to Ang II through cross-talk with integrin-linked kinase (ILK) (Thakur et al., 2014).

Ang II also promotes the proliferation of cardiac fibroblasts through AT_1R-dependent activation of MAPK, MEK and ERK1/2 (Stockand and Meszaros, 2003), as well as inducing autocrine production of TGF-β in cardiac fibroblasts (Lee et al., 1995; Olson et al., 2005). MAPK regulation by Ang II in cardiac fibroblasts is thought to be through modulation of Ca^{2+}-calmodulin activated phosphatase, or calcineurin, and its downstream transcriptional effector nuclear factor of activated T-cells (NFAT) (White et al., 2012). Ang II activation of this pathway increases fibroblast proliferation, fibronectin and pro-collagen expression and inducible nitric oxide synthase production (iNOS) (White et al., 2012). AP-1-dependent activation of the immediate-early genes *c-jun* and *c-fos* was previously described as being important in Ang II-mediated pro-hypertrophic signalling, however it is also important in the pro-fibrotic response to Ang II (Huang et al., 2009).

Treatment of cardiac fibroblasts with Ang II promotes DNA binding of AP-1, *c-jun* and *c-fos* through the activation of JNK in a poly(ADP-ribose) polymerase-1 (PARP-1)-dependent manner which in turn promotes expression of pro-collagen, MMPs, TGF-β and other ECM proteins (Chen and Mehta, 2006; Huang et al., 2009). Infusion of rats with Ang II induces perivascular fibrosis through promotion of adventitial and interstitial fibroblast proliferation within intramyocardial coronary arterioles in an AT_1R-depdendent manner (McEwan et al., 1998). TGF-β is is responsible for enhancing ECM synthesis by myofibroblasts, increasing the secretion of collagens, fibronectin and proteoglycans, and preventing ECM

breakdown through the inhibition of MMP activity and induction of Plasminogen Activator Inhibitor (PAI)-1 and TIMP synthesis (Schiller et al., 2004). Many of these functions are mediated by the activation of the Smad3 signalling pathway (Verrecchia and Mauviel, 2002). As well as activation of TGF-β, Ang II also induces the phosphorylation of Smad3 in fibroblasts through promoting production of IL-6, thus promoting the pro-fibrotic effects of TGF-β (Ma et al., 2012) (Figure 1.4).

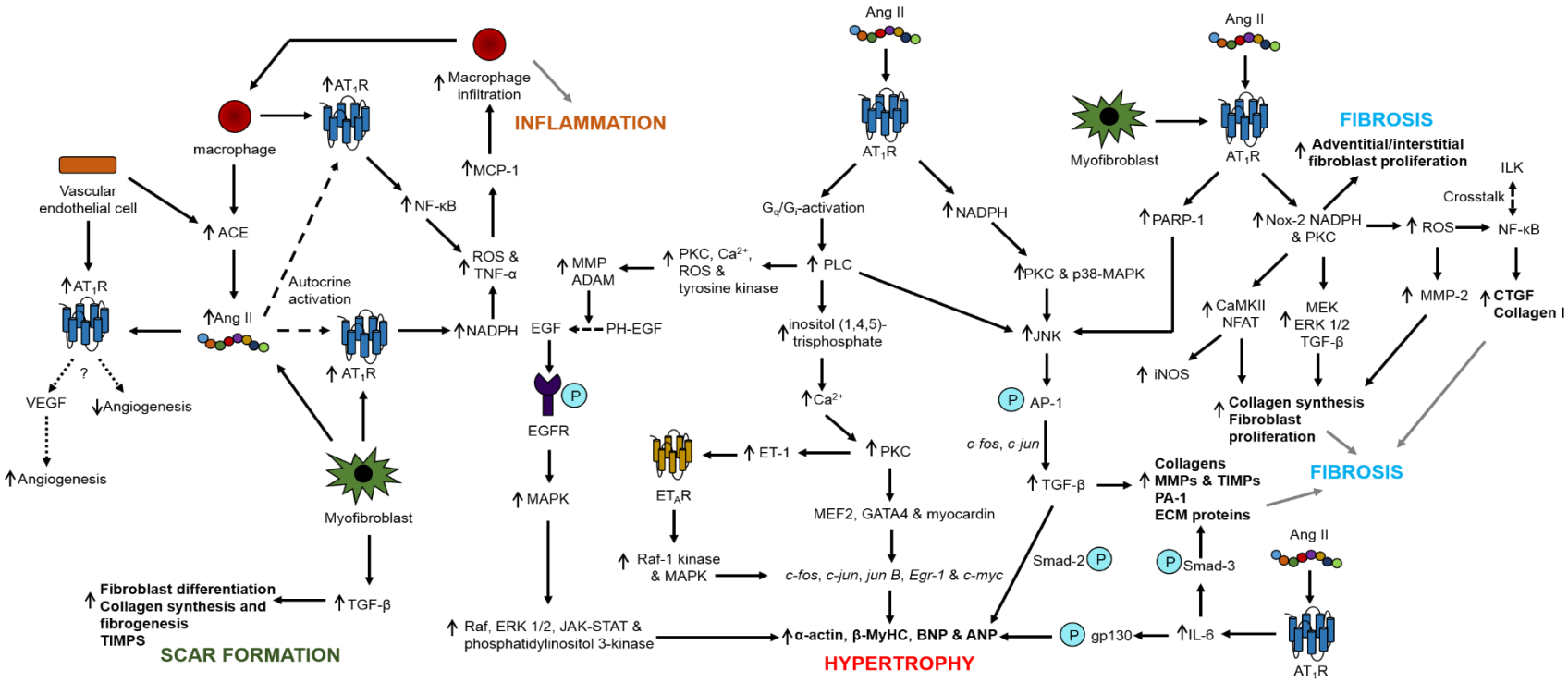

Figure 1.4 Ang II signalling in structural remodelling post-MI.
Signalling pathways involved in Ang II-induced myocardial remodelling post-MI. P= phosphorylated, AT_1R= angiotensin type 1 receptor, MCP-1= monocyte chemoattractant protein 1, VEGF= vascular endothelial growth factor, ACE= angiotensin converting enzyme, ROS= reactive oxygen species, TNF- α= tumor necrosis factor-α, NADPH= nicotinamide adenine dinucleotide phosphate-oxidase, TGF-β= transforming growth factor-β, TIMP= tissue inhibitors of metalloproteases, MMP= matrix metalloprotease, NF-κB= nuclear factor κB, EGF= endothelial growth factor, EGFR= endothelial growth factor receptor, PH-EGF= pro-heparin binding endothelia growth factor, ET-1= endothelin 1, ET_AR= endothelin type A receptor, PKC= protein kinase C, MAPK= mitogen-activated protein kinases, JNK= c-Jun N-terminal kinases, PA-I= plasminogen activator inhibitor, CTGF= connective tissue growth factor, NFAT= nuclear factor of activated T-cells, ERK= extracellular signal-regulated kinases, IL-6= interleukin 6, ECM= extracellular matrix, PLC= phospholipase C, BNP= brain natriuretic peptide, ANP= atrial natriuretic peptide, gp130= glycoprotein 130, AP-1= activator protein-1, PARP-1= poly(ADP-ribose) polymerase-1, CaMKII= Ca^{2+}/calmodulin-dependent protein kinase, ILK= integrin-linked kinase, iNOS= inducible nitric oxide synthase, ADAM= a disintegrin and metalloprotease domain, JAK-STAT= janus kinase/signal transducers and activators of transcription, β-MyHC= β-myosin heavy chain.

1.6.2 Ang II in electrical remodelling

Ang II activation has also been linked directly to dysfunctional regulation of Ca^{2+}-handling proteins in various animals models of cardiac dysfunction and in isolated cardiomyocytes (Mehta and Griendling, 2007). *In vivo* this has been demonstrated in the TG1306/1R transgenic mouse model of cardiac-specific Ang II over-expression. These animals develop progressive cardiac hypertrophy as a result of chronic cardiac Ang II overexpression, which was shown to be accompanied by the dysregulation of Ca^{2+}-handling proteins. Initially an up-regulation of NCX was observed, which was thought to be an adaptive change in response to the pro-hypertrophic signals. However, in older animals with a chronic form of the disease, a maladaptive reduction in SR [Ca^{2+}] and sensitisation of the RyR was seen in response to the shift towards NCX Ca^{2+} extrusion, resulting in reduced cardiomyocyte function (Gusev et al., 2009). Transgenic mice over-expressing the human AT_1R in a cardiac-specific manner also develop cardiac hypertrophy and contractile dysfunction. This was again associated with abnormal Ca^{2+}-handling, with cardiomyocytes showing decreased Ca^{2+}-transient amplitude, reduced SR [Ca^{2+}] and a prolongation in transient decay as well as reduced ICaL and reduced Cav1.2 and SERCA expression (Rivard et al., 2011). Inhibition of the RAS in the rat MI model of CHF shows normalisation of sarcolemmal NCX and Na^+-K^+-ATPase exchanger activity and expression, combined with an improvement in cardiac function, suggesting a role of the RAS in modulating the expression and activity of ion channels in the normal Ca^{2+}-handling and function of cardiomyocytes (Shao et al., 2005).

In vitro Ang II-AT_1R signalling is also associated with an increased Cl^- current and increased inward rectifying K^+ current in rabbit ventricular cardiomyocytes, resulting in a biphasic modulation of the AP, with an initial reduction and then an increase in AP duration (Morita et al., 1995). ATP-sensitive K^+ channels, which regulate AP duration and cardiac contractility, close in response to Ang II signalling in isolated guinea pig ventricular cardiomyocytes as a result of AT_1R-mediated adenylate cyclase inhibition which increases subsarcolemmal ATP concentration. This can have the detrimental effect of prolonging the AP and can lead to larger infarct sizes in animal models of MI (Tsuchiya et al., 1997). Ang II also mediates the AP in isolated rat cardiomyocytes through a reduction in the outward rectifying K^+ current (I_{to}). Interestingly, this was found to be

mediated by the AT_2R rather than the AT_1R, which activated serine/threonine phosphatase type 2A (PP2A) resulting in a decrease in the current (Caballero et al., 2004). I_{to} is also modulated by Ang II in isolated canine cardiomyocytes, where it shows a slower recovery from inactivation in an AT_1R-dependent manner, thus prolonging the AP (Yu et al., 2000). In isolated rabbit cardiomyocytes, Ang II increases the L-type Ca^{2+}-current *via* modulation of the Na^+-H^+ antiporter in a AT_1R-dependent manner (Kaibara et al., 1994). In cardiomyocytes isolated from cardiomyopathic hamsters, AP prolongation by Ang II is also associated with increased L-type Ca^{2+} activity *via* PKC activation (De Mello and Monterrubio, 2004).

Various studies have demonstrated a pro-arrhythmogenic effect of Ang II, with RAS blockade shown to significantly reduce the incidence of ischemia-induced ventricular arrhythmia (Lee et al., 1997). Transgenic mice with cardiac-specific over-expression of ACE succumb to sudden cardiac death as a result of arrhythmia, with no associated structural cardiac remodelling due to atrial arrhythmia and cardiac block (Xiao et al., 2004). In isolated rat cardiomyocytes, Ang II induces cellular arrhythmia through a Nox-2 mediated increase in RyR Ca^{2+}-leak *via* CaMKII activation (Wagner et al., 2014) and Ang II-induced cardiac hypertrophy in mice is associated with a high incidence of arrhythmia-induced SCD (Wang et al., 2014b). Perturbation of electrical synchronisation between cardiomyocytes by Ang II through modulation of gap junctions has also been demonstrated. Ang II has been shown to reduce junctional conductance between rat ventricular cardiomyocyte pairs in a PKC-dependent manner (De Mello and Altieri, 1992). A similar effect is also seen in cells from failing hamster hearts, where junctional conductance is reduced by Ang II in an AT_1R-dependent manner (De Mello, 1996). Connexin 43 (Cx43) is a major component of the mammalian gap junction, with its reduction shown to be a major contributor to ventricular tachycardia (VT) (Efimov, 2006; Iravanian and Dudley, 2008). Cardiomyocyte-specific over-expression of ACE in mouse hearts and a resulting increase in Ang II caused a significant loss of total Cx43 and elevated levels of dephosphorylation, thus deactivation, of the protein, with the result of elevated incidence of VT and sudden death in these animals (Kasi et al., 2007). Rats expressing humanized RAS genes also showed a high incidence of sudden death which was attributable to significantly reduced Cx43 expression and increased susceptibility to VT

(Fischer et al., 2007). Interestingly, mice with a cardiac-specific over-expression of ACE2, which is usually associated with cardio-protective effects, were found to die suddenly also as a result of VT, presumed to be a result of down-regulation of both Cx43 and Cx40 (Donoghue et al., 2003).

Ang II signalling is able to modify the properties and function of various Ca^{2+}-handling proteins through redox modification *via* increasing cardiac ROS in a Nox-2-dependent manner (Akki et al., 2009; Garrido and Griendling, 2009; Hingtgen et al., 2006). In HF, Ang II levels are high while SERCA is generally found to be suppressed through modulation of NADPH oxidase-activation and ROS (Li et al., 2006a) (Hasenfuss, 1998). Chronic Ang II treatment of H9c2 cells mediates a reduction in Na^+ channel current associated with a decrease in expression of the Na^+ channel scn5a (Shang et al., 2008). Ang II also increases L-type Ca^{2+} channel activity through up-regulation of the α1c subunit in HL-1 cells in a NADPH-oxidase-dependent manner (Tsai et al., 2007). Ang II-induced modulation of K^+ channel current and expression and Cl^- current in rat and rabbit cardiomyocytes has also been demonstrated (Ren et al., 2008; Shimoni et al., 2005; Zhou et al., 2006). Other studies have identified a role for PKC and MAPK in the effects of Ang II, with these pathways implicated in the negative inotropic effects observed in isolated rat cardiomyocytes in response to Ang II (Palomeque et al., 2006) and the Ang II-induced increase seen in the L-type Ca^{2+} channel (De Mello and Monterrubio, 2004).

Overall these studies show the complex regulatory relationship between the RAS and modulators of cardiac function and how activation of the RAS can be a primary stimulus driving the development of contractile dysfunction and progression to HF post-MI.

1.7 The counter-regulatory RAS

The counter-regulatory axis of the RAS revolves around a homologue of the ACE enzyme known as ACE-related cardoxypeptidase, or ACE2 (Donoghue et al., 2000). Initially, ACE2 was identified as having the primary role of facilitating the hydrolysis of Ang I to the peptide Ang-(1-9) through the removal of a C-terminal leucine residue (Donoghue et al., 2000), however it was later demonstrated that the preferred substrate of ACE2 is Ang II, to which it has a 400 times greater

affinity than Ang I, facilitating the conversion of Ang II to the peptide Ang-(1-7) (Tipnis et al., 2000; Vickers et al., 2002). Prior to the identification of ACE2, a variety of other enzymes were identified as being capable of generating Ang-(1-7) *via* the hydrolysis of Ang I or Ang II. Prolyl-endopeptidase (PEP), neutral-endopeptidase (NEP) and thimet oligopeptidase (TOP) are all capable of producing Ang-(1-7) in an ACE2-independent manner (Chappell et al., 1994; Greene et al., 1982; Yamamoto et al., 1992). Moreover, Ang-(1-7) can be formed from the hydrolysis of Ang-(1-9) by ACE, which cleaves a phenylalanine and a histidine residue from the N-terminus of the peptide, and which can also occur through the activity of NEP (Vickers et al., 2002). Ang-(1-9) formation has also been demonstrated to occur from Ang I through the activity of carboxypeptidase A or cathepsin A in human heart extracts (Jackman et al., 2002; Kokkonen et al., 1997). In cytosolic extracts of the rat kidney and lung, Ang-(1-9) has been shown be converted into Ang II in an ACE-independent manner by aminopeptidase and N-like carboxypeptidase activity (Drumme et al., 1988). Ang-(1-7) and Ang-(1-9) both facilitate the actions of the counter-regulatory axis of the RAS by signalling *via* the Mas and AT_2R, respectively, counter-acting Ang II signalling *via* the AT_1R (McKinney et al., 2014) (Figure 1.5).

1.7.1 ACE2

Unlike ACE, ACE2 has only one active enzymatic site that shares 42 % homology with ACE, therefore it functions as a carboxypeptidase rather than a dipeptidyl carboxypeptidase (Burrell et al., 2004). Its high affinity for Ang II suggests it plays a role in limiting the vasoconstrictor function of Ang II through its inactivation and counteracting its effects through the production of Ang-(1-7) (Burrell et al., 2004). ACE2 has a far more restricted distribution throughout the body compared to ACE, with it primarily identified in the heart, kidneys and testis of humans on vascular and proximal tubule epithelial cells, as well as in the brain, GI tract and lung (Donoghue et al., 2000; Harmer et al., 2002; Tipnis et al., 2000).

ACE2 has been shown to be an important regulator in the heart. Studies in ACE2 knockout mice have suggested an essential regulatory role for the enzyme, as ACE2 deficient mice have abnormal heart function with impaired contractility, combined with increased Ang II levels, enhanced cardiac hypertrophy and

elevated hypoxia marker expression such as PAI-1 and hypoxia-inducible factor 1 (HIF-1) (Crackower et al., 2002). ACE2 deletion also enhances pathological remodelling in the TAC model of cardiac pressure-overload, with the development of more pronounced hypertrophy, dilation and decreased contractility (Yamamoto et al., 2006). ACE2 is also found up-regulated following MI in rats and humans, and it is thought to play a role in negatively regulating the RAS to degrade Ang II following injury (Burrell et al., 2005). However, despite the evidence for a potent cardio-protective effect of ACE2, the production of a transgenic mouse over-expressing ACE2 revealed that it induced a high rate of SCD due to the increased risk of ventricular tachycardia as a result of connexin down-regulation (Donoghue et al., 2003). Moreover, ACE2 expression is significantly increased in the LV of patients with idiopathic and ischemic cardiomyopathic HF, however the functional consequence of this remains to be identified (Goulter et al., 2004). However, the dual benefits of ACE2 of both degrading Ang II and producing Ang-(1-7) means it remains a promising therapeutic target for CVD (Ferreira et al., 2012).

1.7.2 Ang-(1-7)

Upon its identification, the heptapeptide Ang-(1-7) was initially thought to be an inactive peptide product of RAS metabolism (Greene et al., 1982; Santos et al., 1988). However, in 1988 a study assessing its effects on neurohypophysial explants found it was as potent as Ang II for promoting the release of vasopressin (Schiavone et al., 1988). The biological activity of Ang-(1-7) was further confirmed when it was found to decrease arterial pressure following injection into the nucleus of the solitary tract (Campagnole-Santos et al., 1989). Since then there has been an abundant body of work produced detailing the physiological effects and signalling mechanisms of Ang-(1-7). A major step in deciphering the physiological mechanism by which Ang-(1-7) exerts its effects was upon the identification of its receptor. Early studies demonstrated that the potent pressor and diuretic effects elicited by Ang-(1-7) treatment were blocked using a specific angiotensin antagonist A-779, but its effects were still observed upon AT_1R or AT_2R antagonism, suggesting a specific receptor was facilitating its actions (Fontes et al., 1994; Santos et al., 1994). The receptor was identified using radioligand binding assays and transgenic mice and found to be the ‘orphan’ seven transmembrane G-protein coupled receptor Mas (Santos et al.,

2003). Although much is known regarding the functional effects of Mas stimulation by Ang-(1-7), the signalling mechanisms still remain poorly understood. There is evidence to suggest Akt activation and eNOS are involved in Mas signalling following Ang-(1-7) stimulation in the heart. In the rat, Ang-(1-7)-mediated stimulation of Mas has been demonstrated to phosphorylate JAK2 and Akt specifically at threonine 308 and serine 473 in a PI3K-dependent manner (Giani et al., 2007; Muñoz et al., 2010). Mas activation in the heart has also been shown to inhibit the NF-κB signalling pathway, with a reduction in inflammatory marker expression (Al-Maghrebi et al., 2009) and inhibition of growth promoting pathways induced by Ang II through inhibition of the phosphorylation of ERK1/2 and Rho kinase (Giani et al., 2008).

The physiological effects of Ang-(1-7) have been demonstrated to counteract those exerted by Ang II signalling *via* the AT_1R, including promoting vasodilation, exerting anti-thrombotic effects, increasing sodium excretion in the kidney and inhibiting cell proliferation and angiogenesis (Santos et al., 2008). Moreover, it has been found to counteract the adverse cardiac remodelling processes exerting by Ang II, especially fibrosis and hypertrophy, in a variety of disease models, making it a promising alternative therapeutic for adverse cardiac remodelling post-MI.

1.7.2.1 Ang-(1-7) in structural remodelling

The anti-hypertrophic and anti-fibrotis effects of Ang-(1-7) have been demonstrated in transgenic [TGR(A1–7)3292] rats, which over-express a fusion protein form of Ang-(1-7) in the heart resulting in a doubling of circulating Ang-(1-7), and [TG(hA-1-7)L7301] rats, which over-expresses a cardiac-specific Ang-(1-7) fusion protein, and both demonstrated resistance to isoproterenol-induced stress, with reductions in cardiac hypertrophy and cardiac fibronectin and collagen III deposition (Ferreira et al., 2010a; Santos et al., 2004). In adult rat cardiac fibroblasts, Ang-(1-7) inhibits collagen synthesis and fibroblast growth in response to growth factors, (Iwata et al., 2005) and in the Ang-(1-7) cardiac over-expressing transgenic mouse, cardiac hypertrophy and fibrosis was significantly attenuated in response to hypertensive challenge, as was impaired cardiac contractility (Mercure et al., 2008). This was found to be mediated *via*

Mas activation which modulated TGF-β expression through inhibition of p38 MAPK phosphorylation (Mercure et al., 2008).

In models of MI and HF, Ang-(1-7) has been demonstrated to exert therapeutic effects. Minipump infusion of Ang-(1-7) in the rat MI model was found to preserve cardiac function through increased LVEDP and LVESP, thus preventing progression to HF (Loot et al., 2002a). Increased circulating levels of Ang-(1-7) in MI animals was also found to prevent cardiac hypertrophy, which was associated with the stimulation of bone-marrow derived progenitor cells which increased the level of c-kit and VEGF-positive cells in the infarcted hearts (Wang et al., 2010b). In the mouse ACE2-null model of pressure-overload induced HF, Ang-(1-7) infusion was able to recover systolic function, suppress NADPH oxidase activation and normalise pathological signalling pathways similar to the effects exerted by the ARB irbesartan (Patel et al., 2012). An oral formulation of Ang-(1-7), HPβCD/Ang-(1–7), administered to infarcted rats improved cardiac FS and EF and exerted an anti-fibrotic effect *via* downregulation of TGF-β and collagen I, thus further confirming the therapeutic potential of the peptide (Marques et al., 2012). Moreover, using the Mas receptor blocker A-779, Ang-(1-7) signalling following MI in the rat was observed to be crucial in facilitating the healing process in the heart *via* the promotion of angiogenesis in the infarcted region through stimulating the expression of VEGF-D and MMP-9 (Zhao et al., 2013). Ventricular function was also impaired in animals treated with the Mas receptor blocker (Zhao et al., 2013). Therefore Ang-(1-7) can not only be utilised in a therapeutic capacity, but also appears to be essential for the normal healing process of the heart following MI.

1.7.2.2 Ang-(1-7) in electrical remodelling

There is an accumulation of evidence in the isolated rat heart I/R model that Ang-(1-7) exerts cardio-protective effects including improved post-ischemic cardiac function, reduced incidence and duration of arrhythmias and activation of the Na^+ pump, with its effects demonstrated to be exerted in a Mas-dependent manner and associated with increases in prostaglandin and bradykinin release. This was shown to result in re-established impulse propagation through Na^+ pump activation, with prostaglandin and bradykinin release facilitating cardio-protective and vasodilatory effects as well as activation of EP3 receptors

which activates repolarising currents (De Mello, 2004; Ferreira et al., 2001; Santos and Almeida, 2002). These effects were further demonstrated in I/R injury of hearts isolated from transgenic TGR(A1–7)3292 rats over-expressing circulating Ang-(1-7), which also showed improved function and reduced duration of arrhythmias (Santos et al., 2004), and in hearts from Mas knock-out mice which demonstrated worse post-I/R function compared to WT animals (Castro et al., 2006). As I/R injury-induced arrhythmias and contractile dysfunction are related to a disturbance in Ca^{2+} homeostasis, this suggests Ang-(1-7) may regulate intracellular Ca^{2+}-handling directly. This was demonstrated in a recent study which utilised an isolated rat ventricular cardiomyocyte model of I/R to show that Ang-(1-7) attenuated the increase in cytosolic Ca^{2+} during reperfusion, restored the decrease in peak systolic Ca^{2+} and reversed the decrease in Ca^{2+}-transient amplitude, which was combined with decreased ROS production during ischemia (Wang et al., 2014a).

Similar to the effects seen in I/R injury, in the dog pacing model of atrial tachycardia Ang-(1-7) significantly reduced incidence of atrial fibrillation which was associated with decreased atrial interstitial fibrosis as a result of ERK modulation (Liu et al., 2010a). In this model, Ang-(1-7) also attenuated the decrease in AP duration, characteristically observed in atrial cardiomyocytes during AF, as well as prevented the decrease in expression of the L-type Ca^{2+} channel and outward K^{+} channel observed in the model (Liu et al., 2010a). A later study demonstrated in the same AF model that this improvement was also associated with increased density of the Na^{+} current which improved atrial conductance, similar to the effects Ang-(1-7) exerts in the ventricle during I/R injury (Wang and Li, 2014). A recent *in vitro* study utilising dye-coupling experiments between rat cardiomyocyte cell pairs demonstrated that Ang-(1-7) was able to re-establish dye-coupling following a decrease in gap junction permeability induced by hypertonic saline treatment, suggesting that during instances such as myocardial ischemia, Ang-(1-7) may be able to prevent impairment of cell communication and impulse propagation, therefore reduce the incidence of re-entrant arrhythmias (De Mello, 2014). These studies suggest the protective effects of Ang-(1-7) are multi-faceted, with beneficial effects on cardiac structural, electrical and functional remodelling all having been demonstrated.

1.7.3 Ang-(1-9)

Similarly to Ang-(1-7), Ang-(1-9) was originally thought to be an inactive product of RAS metabolism, with any biological actions observed thought to be as a result of conversion to Ang-(1-7) (Greene et al., 1982; Ocaranza and Jalil, 2012). In human heart tissue, the main products of Ang I degradation are Ang-(1-9) and Ang II (Jackman et al., 2002). However, although Ang-(1-9) can be produced from Ang I *via* ACE2 activity, this is extremely inefficient compared to Ang-(1-7) production from Ang II (Rice et al., 2004). Therefore it is more likely that the activity of carboxypeptidases enzymes such as CxA and CpA have a more prominent role in Ang-(1-9) production (Jackman et al., 2002; Kokkonen et al., 1997). The peptide is found in the plasma of healthy humans and rats at concentrations of 2 to 6 fmol/mL (Campbell et al., 1993), with levels in the kidney found to be at higher concentrations than Ang II (Campbell et al., 1991). Its levels are also found increased in some pathological conditions, such as following MI (Ocaranza et al., 2006), and in animals treated with ACEIs and ARBs (Johnson et al., 1989; Ocaranza et al., 2006; Ocaranza and Jalil, 2012). The plasma half-life of Ang-(1-9) is also thought to be longer than other RAS peptides, with its hydrolysis shown to occur 18 times slower *in vitro* compared to Ang I (Chen et al., 2005).

Much more recently than for Ang-(1-7), Ang-(1-9) has now been identified as a biologically active molecule. The first study to indicate the potential activity of Ang-(1-9) was performed as recently as 2005, where RAS peptide metabolism was studied in CHO cells transfected with human ACE and the BK_2R (Chen et al., 2005). This study suggested Ang-(1-9) was able to enhance bradykinin activity, which is associated with cardio-protective effects, through competitive inhibition of ACE and re-sensitisation of the BK_2R (Chen et al., 2005). A later study found that at 1 week post-MI, levels of Ang II, ACE, ACE2 and Ang-(1-9) were found to be up-regulated compared to controls, however at 8 weeks only Ang II and ACE remained high, with circulating levels of ACE2 and Ang-(1-9) dropping lower than the control group, with Ang-(1-7) levels remaining unchanged (Ocaranza et al., 2006). Treatment with the ACE inhibitor Enalapril exerted cardio-protective effects, associated with the inhibition of the down-regulation of circulating ACE2 and Ang-(1-9) 8 weeks post-MI, suggesting ACE2

acting *via* Ang-(1-9) was potentially able to counter-regulate the actions of Ang II signalling (Ocaranza et al., 2006).

1.7.3.1 Signalling and effects in the heart

One of the most notable studies performed for Ang-(1-9) to date was that which identified the receptor for Ang-(1-9). Using radioligand binding studies, Flores-Muñoz *et al.*, demonstrated that Ang-(1-9) was able to bind the AT_2R, albeit with lower affinity than that reported for Ang II (Flores-Muñoz et al., 2011). Moreover, using H9c2 cells and primary rabbit cardiomyocytes they demonstrated that the peptide exerted anti-hypertrophic effects, shown *via* reduction of hypertrophy marker expression (ANP, BNP, ß-MHC and MLC), in response to Ang II and vasopressin and that this could be attenuated using the AT_2R blocker PD123319 (Flores-Muñoz et al., 2011). The importance of this, and other similar studies, was the separation of the actions of Ang-(1-9) from those of Ang-(1-7). Although demonstrated to exert similar anti-hypertrophic and anti-fibrotic effects, their actions are blocked by completely different receptor antagonists; PD123319 for Ang-(1-9) and A-779 for Ang-(1-7), with no effect of Mas antagonism on the function of Ang-(1-9), suggesting it mediates its effects independently of Ang-(1-7) conversion (Flores-Muñoz et al., 2012; Flores-Muñoz et al., 2011; Flores-Munoz et al., 2012; Ocaranza et al., 2014).

Similarly to Ang-(1-7), the actions of Ang-(1-9) appear to counter-act those of Ang II signalling *via* the AT_1R. The physiological effects primarily reported for Ang-(1-9) have been anti-hypertrophic and anti-fibrotic effects it exerts on cultured cardiomyocytes and in the hearts of hypertensive animal models of cardiac remodelling. The first of these studies demonstrated that Ang-(1-9) was able to counter-act norepinephrine and insulin-like growth factor-1 induced cardiomyocyte hypertrophy in an Ang-(1-7)-independent manner (Ocaranza et al., 2010). This *in vitro* evidence for an anti-hypertrophic effect of the peptide led to further *in vivo* studies using the rat MI model, where Ang-(1-9) infusion *via* minipump was again found to attenuate cardiac hypertrophy, an effect which correlated with decreased plasma Ang II levels (Ocaranza et al., 2010). Moreover, treatment of MI animals with enalapril or candesartan, which also attenuated LV hypertrophy, was associated with increased plasma Ang-(1-9) levels (Ocaranza et al., 2010). However, no beneficial effects of cardiac

contraction was observed in MI through the infusion of Ang-(1-9) (Ocaranza et al., 2010).

Despite the identification of its receptor the signalling mechanisms for Ang-(1-9) remain elusive. The identification of the AT_2R as the primary receptor for Ang-(1-9) suggests it may trigger the signalling pathways associated with this receptor, thus exerting counter-regulatory effects to Ang II-AT_1R signalling. Experiments using aortic wire myography revealed that Ang-(1-9) was able to improve endothelial cell function, demonstrated by decreased vascular resistance, in an AT_2R-dependent manner through increasing NO bioavailability, possibly *via* increased expression of Nox-4 (Flores-Munoz et al., 2012). Ang-(1-9) minipump infusion was also associated with beneficial anti-fibrotic effects in the SHRSP model of hypertensive cardiac fibrosis, with it found to significantly reduce cardiac fibrosis by 50 % through inhibition of cardiac collagen I deposition (Flores-Munoz et al., 2012). Moreover, Ang-(1-9) was demonstrated to improve function in small mesenteric arteries of the SHRSP in an AT_2R-dependent manner through up-regulation of endothelial NO-synthase with associated decreases in oxidative stress and TGF-ß expression (Ocaranza et al., 2014). It is possible this occurs through stimulation of the bradykinin NO/cGMP pathway and/or a direct increase in NO release triggered by Ang-(1-9)-AT_2R signalling (Jackman et al., 2002). Incubation of CHO cells with Ang-(1-9) triggers the release of AA, increases intracellular Ca^{2+} and re-sensitises the BK_2R (Erdös et al., 2002). It has also been demonstrated in CHO cells and human primary endothelial cells that Ang-(1-9) is more active than Ang-(1-7) and is able to enhance the effects of a BK analogue, also promoting the release of NO and AA by kinins (Jackman et al., 2002). This increased AA release is most likely a result of increased PLA_2 activity triggered by Ang-(1-9), which also appears to be able to act as an ACE-BK_2R complex allosteric modifier (Chen et al., 2005). *In vivo* studies using the DOCA salt model of hypertension has also suggested that modulation of the Rho kinase signalling pathway may be involved in the improved vascular function and increased NO release seen using Ang-(1-9) (Ocaranza et al., 2011). The use of a ROCK inhibitor in this experimental model of hypertension was associated with increased plasma Ang-(1-9) levels as a result of increased ACE2 activity (Ocaranza et al., 2011). Moreover, as well as increasing vascular eNOS expression, ROCK inhibition was associated with normalisation of vascular TGF-ß,

MCP-1 and PAI-1 expression (Ocaranza et al., 2011). Another recent study found that Ang-(1-9) increases ANP secretion in isolated atria subjected to stretch, without affecting contraction *in vivo via* an AT_2R dependent mechanism (Cha et al., 2013). Stimulation of the AT_2R was found to activate PI_3K, Akt and stimulate the NO/cGMP signalling pathway, leading to increasing ANP secretion which may play a role in the beneficial effects it exerts on the heart (Cha et al., 2013).

To date, only one study has demonstrated protective functional effects of Ang-(1-9) on the heart. Minipump infusion of Ang-(1-9) was shown to exert cardio-protective effects, including anti-hypertrophic and anti-fibrotic effects and decreased expression of cardiac pro-hypertrophic markers, TGF-ß and collagen I in the STZ-induced mouse model of diabetic cardiomyopathy (Zheng et al., 2015). Moreover, Ang-(1-9) was shown to exert beneficial functional effects, with Ang-(1-9) treated animals showing improved EF (Zheng et al., 2015). There was also reduced cardiac ROS and an anti-inflammatory effect of the peptide (Zheng et al., 2015). Mechanistically Ang-(1-9) was found to suppress cardiac NADPH oxidase activity, reduce NF-κB and MPO activation and decrease expression of TGF-ß and IL-1ß. These effects were associated with suppressed ACE activity and decreased cardiac Ang II levels, further affirming the counter-regulatory effects of Ang-(1-9) (Zheng et al., 2015).

One particular group has performed studies which suggest caution is needed with regards to the therapeutic potential of the Ang-(1-9). In experiments assessing the effects of Ang-(1-9) they found that it was pro-thrombotic in models of electrically stimulated arterial thrombosis and stasis-induced venous thrombosis *via* increased expression of PAI-1 (Kramkowski et al., 2010; Mogielnicki et al., 2013). However, this was found to occur in a AT_1R-dependent manner without the direct interaction of Ang-(1-9) with the AT_1R receptor, suggesting it was acting through conversion to Ang II (Kramkowski et al., 2010; Mogielnicki et al., 2013). This highlights the importance of further research into the dynamics and physiological effects of the counter-regulatory axis of the RAS. Overall the effects that Ang-(1-9) has been shown to exert *in vitro* and *in vivo* suggests it would make an ideal alternative therapeutic for adverse cardiac remodelling post-MI.

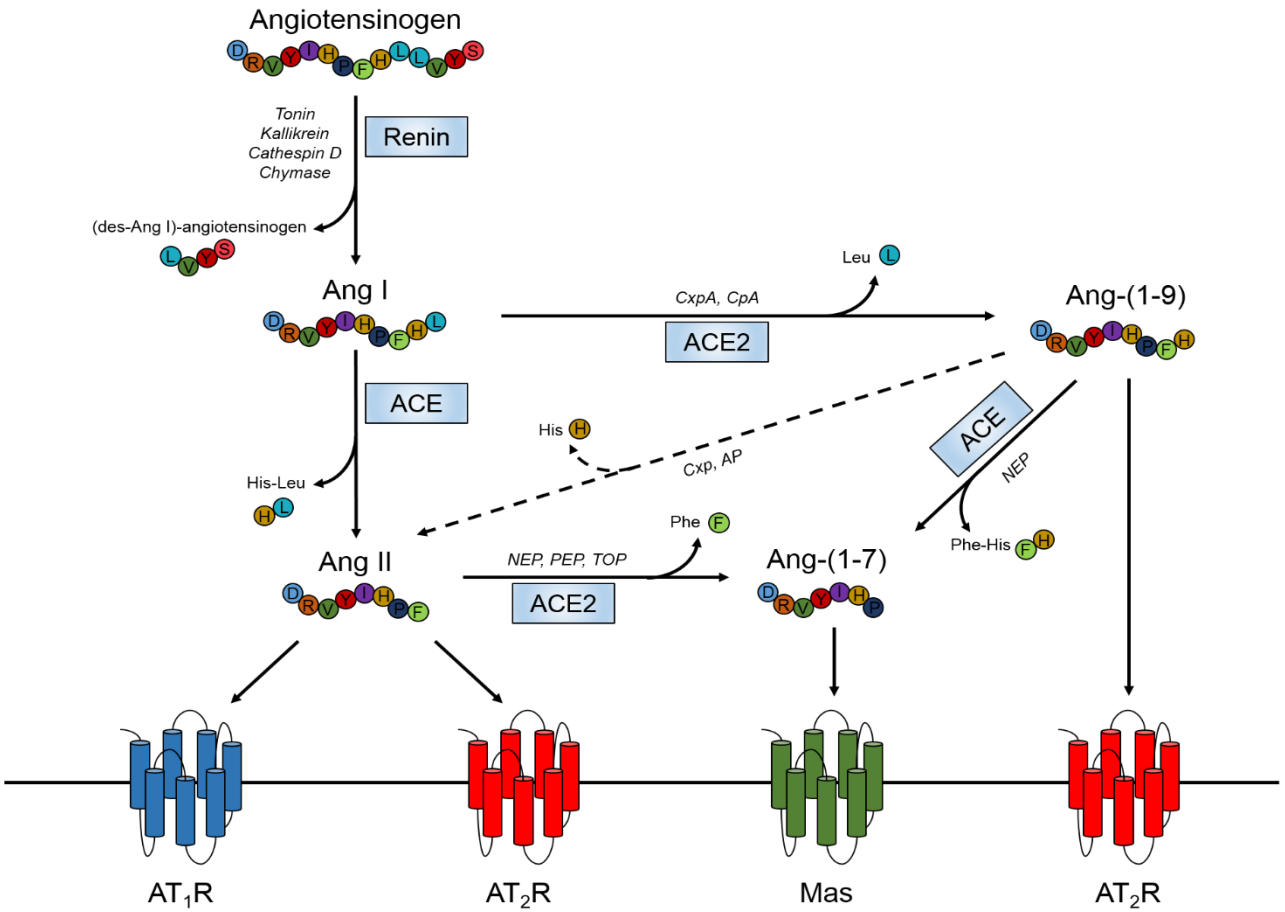

Figure 1.5 The classical and counter-regulatory axis of the RAS.
The classical axis of the RAS requires the production of Ang II from the precursor molecules Angiotensinogen and Ang I by the action of renin and ACE, respectively. Ang II signals *via* the AT_1R and the AT_2R. The counter-regulatory axis revolves around ACE2 which converts Ang I and Ang II into Ang-(1-9) and Ang-(1-7), respectively. Ang-(1-7) signals *via* the Mas receptor, whereas Ang-(1-9) signals *via* the AT_2R. ACE= angiotensin converting enzyme, AT_1R= angiotensin type I receptor, AT_2R= angiotensin type 2 receptor, CxpA= carboxypeptidase A, CpA= cathepsin A, AP= aminopeptidase, NEP= neutral-endopeptidase, PEP= Prolyl-endopeptidase, TOP= thimet oligopeptida

1.7.4 Other peptide metabolites

As well as the primary counter-regulatory RAS effector peptides, other peptide cleavage products of the RAS have been identified, some of which appear to exert biological functions (Atlas, 2007), including Ang-(1-12), Ang-(2-10), Ang III, Ang IV, Ang-(3-7), Ang A and Alamandine, the details of which are summarised in Table 1.3.

Table 1.3 RAS peptide metabolites

Peptide	Formation	Receptor	Role/effect	References
Ang-(1-12)	2 extra aa on C-terminus of Ang I. Possibly formed from angiotensinogen.	none	Alternative non-renin dependent precursor for RAS peptides. Any effects facilitated via conversion to Ang II.	Ahmad et al., 2013; Nagata et al., 2010
Ang-(2-10)	Hydrolysis of Ang I by aminopeptidase A.	AT_1R	Anti-hyperplasic and anti-hypertrophic effects in VSMCs. Protective vascular effects in SHRSP	Min et al., 2000; Mustafa et al., 2004; Velez et al., 2009
Ang III [Ang-(2-8)]	Removal of N-terminus aa of Ang II via aminopeptidase A.	AT_4R	Acts in CNS regulating BP. Stimulates PAI-1 secretion from endothelium.	Reudelhuber, 2005; Stanton, 2003
Ang VI [Ang-(3-8)]	Removal of N-terminus aa of Ang III via aminopeptidase N and hydrolysis of Ang II via dipeptidyl aminopeptidase IV.	AT_4R and AT_1R	Co-operative role in Ang II signalling. Stimulates PAI-1 secretion from endothelium.	Chappell, 2012a; Reudelhuber, 2005; Stanton, 2003
Ang-(3-7)	Derived from Ang II, Ang-(1-7) or Ang IV through the activity of aminopeptidases and carboxypeptidases.	AT_4R	Regulatory role in sympathetic drive and BP in CNS.	Ferreira et al., 2007; Handa, 2000; Welches et al., 1991
Ang A	Decarboxylation of the first aspartate residue of Ang II to form an alanine through the activity of a leukocyte-derived aspartate decarboxylase	AT_1R and AT_2R	Pressor effects.	Coutinho et al., 2014; Jankowski et al., 2007; Yang et al., 2011
Alamandine	ACE2 conversion of Ang A or carboxylase action of Ang-(1-7)	MrgD	Regulates eNOS dependent vasodilation. Exerts anti-fibrotic and anti-hypertensive effects.	Dell'Italia and Ferrario, 2013; Habiyakare et al., 2014; Lautner et al., 2013

AA= archadonic acid, aa= amino acid, RAS= renin angiotensin system, VSMC= vascular smooth muscle cell, SHRSP= spontaneously hypertensive stroke-prone rat, CNS= central nervous system, BP= blood pressure, eNOS= endothelial nitric oxide synthase, PAI-1= plasminogen activator inhibitor 1.

1.8 CVD therapeutics

The development of surgical intervention and pharmacological management of patients following an acute MI has dramatically reduced the mortality associated with the initial infarction (Sarmento-Leite et al., 2001). This however has the potential to increase the number of patients developing HF, which despite optimised medical therapy has a high mortality and morbidity rate (DiGiorgi et al., 2005). Therefore more effective therapies are required to prevent the progression to HF following MI.

1.8.1 Coronary reperfusion

It was in the 1970s that the idea of reperfusion of the infarcted region of the myocardium through removal of the blockage was a successful way of salvaging the myocardium and improving survival rates post-MI (Chazov et al., 1976). This was initially achieved pharmacologically, using intravenous infusion of streptokinase, a thrombolytic agent (Markis et al., 1981). Following this, more potent thrombolytic agents, tissue plasminogen activators, were developed as were ways to surgically clear the blockage (Ganz, 1985). These included percutaneous coronary angioplasty which was combined with deployment of a stent later, and thrombus aspiration which is carried out prior to stent deployment (Keeley et al., 2003; Svilaas et al., 2008; Zhu et al., 2001). These interventions have proved successful in halving mortality rates following acute MI, from 15 to 7.5 % (Braunwald, 2012). However, myocardial reperfusion is not 100% effective as whilst it minimises ischaemic death, it also injures the surviving myocardium in a process known as reperfusion injury (Braunwald and Kloner, 1985; Yellon and Hausenloy, 2007). This is thought to result from 3 main phenomena: the Ca^{2+} paradox where there is an intracellular influx of Ca^{2+}; the oxygen paradox where myocardial ROS is increased, and the pH paradox where the pH is suddenly increased to normal following acidosis in the ischaemic zone, all of which is thought to damage the myocardial mitochondria leading to cardiomyocyte death (Braunwald, 2012; Yellon and Hausenloy, 2007). Although research into minimising reperfusion injury, such as myocardial pre-conditioning, is in progress it is not currently used clinically (Longacre et al., 2011). Moreover, revascularisation using stenting has the added complications of stent thrombosis and restenosis (Serruys et al., 2006).

1.8.2 RAS-targeted therapeutics

To date, the most successful treatments for CVD have involved the inhibition or blockade of the RAS. The idea of ACE inhibitors (ACE-I) was triggered in the 1960's when peptides found in snake venom were shown to reduce blood pressure and produce beneficial haemodynamic effects in HF patients through degradation of ACE (Ferrario, 2006). Captopril, the first orally active ACE-I, was designed based on carboxypeptidase A (Brown and Hall, 2005; Wong et al., 2004). However, unwanted side-effects led to the development of a range of drugs such as lisinopril, benazepril, quinapril, ramipril, perindopril, cilazapril, trandolapril and fosinopril (Brown and Hall, 2005; Wong et al., 2004). ACE-I competitively blocks ACE activity thus reduce Ang II levels by preventing the conversion of Ang I (Lopez-Sendon et al., 2004). Short term use of ACE-I induces a dose-dependent reduction in cardiac pre-load and after-load and lowers blood pressure (Lopez-Sendon et al., 2004). Early trials in patients who had suffered an MI demonstrated that ACE-I attenuated LV remodelling and progression to HF and alleviated the symptoms of developed HF, including pulmonary congestion, and prolonged life (Investigators, 2003; Lopez-Sendon et al., 2004; Yusuf et al., 2000). Although generally well tolerated and effective, there are some disadvantages and side-effects associated with ACE-I treatment (Wong et al., 2004). Prolonged use of ACE-I leads to elevated Ang I levels and renin activity that can potentially overcome the blockade (Atlas et al., 1984). Kininase II, which has an identical structure to that of ACE, is also inhibited and can lead to accumulation of substance P which leads to dry cough (Wong et al., 2004). This can also lead to the more serious side-effects of angioedema and foetal developmental abnormalities (Wong et al., 2004). Other side-effects include hypotension, deterioration of renal function, hyperkalemia, hepatic toxicity and proteinuria (Wong et al., 2004).

The development of selective AT_1R inhibitors (ARBs) began in the 1990s in the hope they would be more specific than ACE-I by blocking Ang II signalling *via* its primary receptor rather than one of its synthesis pathways (Ferrario, 2006). Losartan was the first of these, with others including valsartan, irbesartan, candesartan, eprosartan, telmisartan, and olmesartan developed thereafter (Ferrario, 2006). ARB usage results in an increase in Ang II levels due to the negative feedback loop of the RAS (Hernandez-Hernandez et al., 2002), with it

postulated that increased Ang II binding to the AT_2R may mediate further beneficial effects (Atlas, 2007). Although there is no clinical data to suggest this is the case, evidence produced using valsartan in the mouse model of MI and AT_2R knock-out transgenic animals suggests the AT_2R does mediate some of the protective effects exerted by ARBs, including reduction in LV dimensions, reduced LV hypertrophy and alleviated pulmonary congestion (Carey and Siragy, 2003; Oishi et al., 2006). ARB therapy has been shown in clinical trials to confer benefits to hypertensive patients as well as reducing the inflammatory response in patients with atherosclerosis (Ibrahim, 2006; Koh et al., 2003; Navalkar et al., 2001). It has also been shown to confer reduced cardiovascular risk, with a reduced likelihood of suffering from cardiovascular death, stroke and MI (Dahlöf et al., 2002). In HF, ARB treatment reduces incidence of mortality (Maggioni et al., 2002; Pfeffer et al., 2003) and following MI it reduces risk of recurrent MI, SCD, and all-cause mortality (Dickstein et al., 2002). ARBs are generally better tolerated than ACE-I, however their use is also associated with abnormal foetal development during pregnancy and instances of hypotension, hyperkalemia and deteriorating renal function as with ACE-I (Atlas, 2007).

Despite the successes of the various established treatments for CVD, the overall mortality rate as a result of MI and HF remain high (WHO, 2015) and therefore new, more effective therapies are needed.

1.9 Gene therapy

Advances in molecular cardiology have made it possible to identify a number of novel cardiac gene therapy targets which are promising for the treatment of acute MI and HF (Müller et al., 2007). However, the implementation of this has required the development and optimisation of gene delivery vectors (Müller et al., 2007). Viral-vector based gene delivery is one such approach which utilises the natural viral infection pathway in order to gain access to human tissue cells in order to express therapeutic genes (Thomas et al., 2003). This requires the deletion of enough of the viral genome in order to insert the gene of interest while maintaining the ability of the particles to infect target cells (Thomas et al., 2003). There are currently 5 main viral vectors in development for therapeutic use; oncoretroviruses, lentiviruses, herpes simplex-1 viruses (HSV-

1s), Ad and AAVs; with Ad and AAV being the most commonly used (Thomas et al., 2003).

1.9.1 Adenoviral gene transfer vectors

In 2012 over 1800 gene therapy clinical trials had been completed, were ongoing or had been approved worldwide. Of these, the vast majority (23.3 %) were utilising Ad vectors (Ginn et al., 2013). Ad gene therapy has also been utilised for the treatment of a variety of diseases such as cancer, cystic fibrosis (Bellon et al., 1997), muscular dystrophy (Cerletti et al., 2003) and macular degeneration (Campochiaro et al., 2006).

After cancer and monogenic disease, the third most popular disease for gene therapy research is cardiovascular disease (Ginn et al., 2013). To date, the most common form of cardiovascular gene therapy has been aimed at promoting therapeutic myocardial angiogenesis in ischemic heart disease. Intramyocardial delivery of an E1/ E3 deleted Ad expressing the pro-angiogenic factor VEGF121 (AdVEGF121) has been utilised in clinical trials for the treatment of ischemic heart disease, and so far has demonstrated improvements in exercise tolerance and angina class in treated patients (Rosengart et al., 1999; Stewart et al., 2006). VEGF165 has also been utilised in the KAT (Kuopio angiogenesis trial) clinical trial which utilised an Ad (VEGF-AdV) delivered *via* catheter to the heart during a standard angioplasty and stenting procedure. Six month follow-ups of patients receiving the virus showed no change in restenosis compared to placebo, however myocardial perfusion rates were significantly increased in the treated patient group (Hedman et al., 2003). The AGENT phase I-II clinical trials investigated the effects of an E1 deleted Ad5 vector expressing FGF-4 (Ad5FGF-4) on the perfusion of ischemic myocardium in patients with stable angina and reversible ischemia. Similarly to the VEGF121 studies, patients demonstrated a higher tolerance for exercise testing, which was combined with evidence for increased perfusion of the ischemic tissue with smaller infarct size reported (Grines et al., 2002; Grines et al., 2003). However, when this was expanded into phase III clinical trials neither of these improvements were noted (Henry et al., 2007). What all these trials have demonstrated, regardless of outcome, is that delivery of an Ad vector to the heart is safe and shows sufficient transgene expression.

1.9.2 AAV

AAVs suitability as a gene therapy vector means it is currently in use in clinical trials for a variety of diseases, with its use accounting for 5 % of all gene therapy clinical trials in 2012 (Ginn et al., 2013). Their potential use in the treatment of metabolic diseases has received a lot of attention in recent years (Alexander et al., 2008), with the very first licencing of an AAV1-based gene therapy vector, alipogene tiparvovec (or Glybera ©), in Europe in 2012 for treatment of lipoprotein lipase deficiency (LPLD), a rare genetic disorder (Flemming, 2012). Other diseases for which AAV vectors are being pursued as potential treatments include cystic fibrosis (Moss et al., 2007), haemophilia B (Manno et al., 2006), muscular dystrophy (Bowles et al., 2011), rheumatoid arthritis (Evans et al., 2005), ophthalmic diseases (Buch et al., 2008) and disease of the CNS including Alzheimer's (Mandel, 2010) and Parkinson's disease (Carter et al., 2008; LeWitt et al., 2011).

Similarly to Ad vectors, pre-clinical studies have looked at the potential of AAVs to promote angiogenesis in ischemic hearts through the delivery of transgenes carrying pro-angiogenic factors. An AAV vector expressing human VEGF165 injected directly into the infarcted mouse heart has been shown to promote neoangiogenesis without the induction of an inflammatory response (Su et al., 2000). Moreover, transgene expression was demonstrated to be able to be controlled through the use of a cardiac-specific, hypoxia-inducible promotor cardiac myosin light chain 2v (MLC-2v) and the hypoxic-response element, which restricted VEGF transgene expression to ischemic mouse hearts, showing greater vascularisation, smaller infarcts and improved cardiac function (Su et al., 2004). Direct myocardial delivery of an AAV2 vector expressing a p53-inducible human VEGF-A transgene in the rat TAC-model of pressure-overload promoted neovascularisation, significantly improved cardiac function and decreased fibrosis. As p53 is induced in the heart during chronic hypoxia and is associated with the transition to de-compensatory cardiac hypertrophy, the gene therapy restricted transgene expression to the target tissue and stimulated VEGF-A expression in the heart when it was required (Bajgelman et al., 2015). Genes other than pro-angiogenic factors have also been targeted for AAV gene therapy. AAV-mediated delivery of microdystrophin to the hearts of the mdx mouse muscular dystrophy model has been shown to restore cardiac dystrophin-

glycoprotein complex levels thus stabilising the sarcolemmal integrity of the heart, which demonstrated therapeutic potential for cardiomyopathy in patients with Duchenne's muscular dystrophy (Yue et al., 2003). The long-term expression properties of AAV have been exploited as a potential therapy for hypertension. AAV-mediated systemic delivery of the serine protease kallikrein has been shown to ameliorate hypertension in the SHRSP model. This was associated with confirmation of long-term expression of the protein in various tissues and reduced renal damage and collagen deposition in the heart (Wang et al., 2004).

The direct targeting of Ca^{2+} handling proteins for the treatment of cardiac contractile dysfunction has also received great interest. S100A1, a positive inotropic regulator of cardiac function, was delivered *via* a rAAV6 vector under the control of a cardiac-selective promotor through catheter-mediated delivery into the aortic root of HF rats (Pleger et al., 2007). It was shown to have chronic HF-rescuing properties, mediated by improved SR Ca^{2+} handling, improved cardiac contraction and ameliorated LV remodelling, with improved beneficial effect over ß-adrenergic blockade (Pleger et al., 2007). Administration of the same vector in a large animal pre-clinical pig model of HF resulted in a reversal of adverse structural and functional myocardial changes and a complete normalisation of cardiomyocyte and SR Ca^{2+}-handling (Pleger et al., 2011). Transcoronary delivery of a rAAV vector expressing a pseudo-phosphorylated PLB mutant (S16EPLN) has also been shown to attenuate contractile dysfunction in a hamster model of dilated cardiomyopathy and the rat MI HF model through chronic PLB inhibition resulting in increased LV EF, lower EDP and a reduction in cardiac hypertrophy (Hoshijima et al., 2002; Iwanaga et al., 2004). An AAV9 vector has also recently been utilised to investigate the possibility of inhibiting protein phosphatase 1 (PP1) ß, a catalytic subunit involved in inhibition of Ca^{2+} uptake into the SR, by expressing a short hairpin RNA molecule of PP1ß under control of a HF-inducible BNP promotor. This approach was shown to have beneficial effects on LV diastolic function and remodelling, with reduction in BNP expression and cardiac interstitial fibrosis deposition in a mouse model of cardiac dysfunction (Miyazaki et al., 2012).

1.9.3 SERCA gene therapy

Of all the Ca^{2+}-handling proteins targeted for viral-mediated gene therapy, SERCA2a has perhaps generated the most interest, with its effects in small animal CVD models first assessed in 2000. A gene therapy approach using catheter-based delivery of an Ad vector expressing the SERCA2a gene directly to the heart of the aortic banding HF rat model (del Monte et al., 2001; Miyamoto et al., 2000) and the senescent rat heart (Schmidt et al., 2000) was used to assess the effects of SERCA2a overexpression on contractile dysfunction and diastolic function *in vivo*. In the rat HF model, overexpression of SERCA was associated with improved SR pump function and normalisation of LV systolic pressure indices and an increased rate of isovolumetric relaxation back to near sham levels compared to animals receiving control virus (Miyamoto et al., 2000). As well as improved haemodynamic parameters, restoration of SERCA in the failing rat heart was also shown to produce an improved phosphocreatine/ATP ratio which is found reduced in failing hearts. As phosphocreatine is the heart's major energy reserve molecule, this showed that SERCA overexpression maintained the energy potential of the heart, with resulting metabolomic and functional effects (del Monte et al., 2001). The senescent rat heart shows unaltered systolic functional parameters, however it shows severe diastolic dysfunction with significantly increased EDP and decreased isovolumetric relaxation. Restoration of SERCA expression has also been shown to significantly improve these parameters in comparison to control vector administered animals (Schmidt et al., 2000). Despite these successes, overexpression of SERCA *in vivo* was shown to have some disadvantages, with it being demonstrated in the rat MI model that in transgenic rats overexpressing SERCA, although enhanced myocardial function post-MI was evident in the transgenic animals, there was also an increased incidence of ventricular arrhythmia (Chen et al., 2004). This may indicate that overexpression of SERCA in every cardiomyocyte from birth may have detrimental side effects later in life following cardiac insult.

More recently, studies utilising large animal models have produced convincing pre-clinical trial data demonstrating similar benefits to what was observed in the small animal models. In sheep with pacing-induced HF, delivery of an AAV serotype 1 (AAV2/1) vector overexpressing SERCA demonstrated a dose-dependent improvement on cardiac contractility as assessed by left ventricular

pressure measurements and echocardiography when administered *via* a cardiac-directed recirculating delivery approach (Byrne et al., 2008). Pigs with volume-overload induced HF administered with a rAAV1 vector overexpressing SERCA *via* intracoronary infusion again demonstrated improved left ventricular function combined with positive effects on left ventricular remodelling (Kawase et al., 2008). In both cases, levels of BNP expression remained stable or reduced compared to control animals (Byrne et al., 2008; Kawase et al., 2008).

These data paved the way for AAV-mediated gene delivery of SERCA2a in human clinical trials for the treatment of HF. The 'Calcium Up-Regulation by Percutaneous Administration of Gene Therapy in Cardiac Disease', or CUPID, multicentre phase I/II clinical trial was launched in the US in 2007 (Hajjar et al., 2008; Jaski et al., 2009). The study recruited 9 patients with advanced HF who underwent intracoronary infusion of an AAV1 vector expressing the SERCA2a protein, with patients receiving the highest dose demonstrating improvement from baseline symptomatic and functional parameters at 6 month follow-up (Jaski et al., 2009). Phase II trials involving 39 patients further demonstrated the efficacy and safety of the virus as well as its beneficial effects, with decreased frequency of cardiovascular events compared to placebo group at 12 month follow-up (Jessup et al., 2011). Three year follow up of these 39 patients demonstrated long-term transgene expression and an 82 % reduction in recurrent cardiovascular events in the group receiving the high dose (Zsebo et al., 2014). This initial success of the CUPID inspired 2 further trials utilising AAV delivery of SERCA2a; the 'AAV-CMV-Serca2a GENe Therapy Trial in Heart Failure' (AGENT-HF) in the UK and a parallel study in the UK and France in patients using LV assist devices, both of which were recruiting patients for phase I/II trials as of 2011 (Kawase et al., 2011). Following the success of the initial trial, the CUPID2 Phase 2b 243-patient intention-to-treat population trial was undertaken which was a randomized, double-blind, placebo-controlled, multinational trial evaluating a single intracoronary infusion of the SERCA2a gene using the AAV vector which is now termed 'MYDICAR®' on primary and secondary outcomes in HF patients (Celladon, 2015). The most recent data from this trial as of April 2015 reported no adverse effect of vector delivery, however the vector itself failed to show any difference in endpoint comparison with the placebo groups with no differences in heart failure-related hospitalizations, ambulatory

treatment for worsening heart failure, all-cause death, need for a mechanical circulatory support device or heart transplant (Celladon, 2015).

1.9.4 Gene therapy approaches for targeting the counter-regulatory RAS

RAS gene therapy for CVD has primarily utilised over-expression of ACE2 or Ang-(1-7). Huentelman *et al* (2005) were the first to develop an ACE2-expressing lentiviral vector (Huentelman et al., 2005). Administration of this vector directly into the LV cavity of 5 day old rats demonstrated that ACE2 over-expression could attenuate cardiac hypertrophy and fibrosis following Ang II minipump infusion 10 weeks post-lentiviral delivery (Huentelman et al., 2005). This same vector utilised in the SHR was shown to significantly reduce BP, LV wall thickness and perivascular fibrosis 4 months following transduction (Díez-Freire et al., 2006). More recently, an Ad vector over-expressing ACE2 was developed and utilised in the Streptozocin (STZ) rat model of diabetic cardiomyopathy (Dong et al., 2012). Animals administered with the Ad showed increased cardiac MMP-2 activity, increased LV EF, decreased LV EDV and ESV, reduced LV fibrosis and reduced expression of cardiac ACE, Ang II and collagens (Dong et al., 2012). Lentiviral vectors have also been utilised for the delivery of Ang-(1-7) in rat models of pulmonary fibrosis (PF) and pulmonary hypertension (PH) (Shenoy et al., 2010). Intra-tracheal delivery of this vector was demonstrated to reduce ACE and AT_1R expression, decrease collagen deposition and attenuate expression of pro-inflammatory cytokine and TGF-ß in the lungs of PF animals and reduce RV hypertrophy, fibrosis and systolic pressure in PH animals, all of which was mediated *via* the Mas receptor (Shenoy et al., 2010).

Intracardiac injection of a lentiviral vector expressing ACE2 in the rat model of MI exerts cardio-protective effects, including increased EF and cardiac contractility and reduced wall-thinning (Der Sarkissian et al., 2008). Cardiac ACE2 over-expression using intracardiac injection of an Ad vector also shows cardio-protective effects in the rat MI model, with reduced LV dilation, increased EF, attenuated LV fibrosis and decreased expression of ACE, Ang II and collagen I all associated with Ad-administered animals (Zhao et al., 2010). The effects of Ang-(1-7) following MI have also been characterised in the rat using lentiviral-mediated cardiac overexpression (Qi et al., 2011). Lentiviral

administration ameliorated a variety of MI associated pathologies, including improved EF, improved LVEDP, reduced LV hypertrophy, decreased ACE expression, increased ACE2 and BK_2R expression, decreased wall-thinning and decreased pro-inflammatory cytokine expression (Qi et al., 2011). These studies demonstrate how viral-vector mediated gene therapy can be an effective, translational method by which to harness the cardio-protective potential of the counter-regulatory RAS for the treatment of CVD.

1.10 Hypothesis and aims

Ang-(1-9) is emerging as a potential novel therapeutic peptide for adverse cardiac remodelling. Little is known about its mechanism of action and there is currently only one study to suggest it confers a beneficial effect functionally in the heart. All *in vivo* studies performed have also only utilised minipump infusion as the method of Ang-(1-9) delivery. The beneficial structural remodelling effects of the peptide combined with the evidence of a functional effect through counteracting Ang II signalling in the heart *via* activation of the counter-regulatory RAS axis suggest Ang-(1-9) may confer cardio-protective effects in an animal model of acute cardiac dysfunction such as in MI. Therefore we hypothesised that viral vector-mediated over-expression of Ang-(1-9) in the mouse MI model would attenuate adverse structural and functional cardiac remodelling.

The principle aim of this thesis was to assess the effects of cardiac over-expression of Ang-(1-9) on structural and functional cardiac parameters following MI. This was achieved through the following experimental aims:

- Develop a technique for the successful cardiac over-expression of Ang-(1-9) in the mouse MI model using viral vector-mediated gene transfer.

- Assess changes in functional and structural cardiac parameters post-MI in Ang-(1-9) over-expressing animals compared to controls.

- Investigate the effect of Ang-(1-9) on the Ca^{2+}-transient in isolated adult cardiomyocytes.

Chapter 2: Materials and methods

2.1 Materials

All chemicals for mouse cardiomyocyte studies, histological and biochemical applications were purchased from Sigma-Aldrich (Poole, UK) unless otherwise stated. Chemicals used for cardiomyocyte isolation were dissolved in double distilled water (ddH_2O, 18 MΩ/cm) filtered *via* a Purelab Option-R 15 purification system (Cole-Parmer, London, UK) to ensure solutions were nominally calcium-free. Angiotensin peptides were purchased from Phoenix Pharmaceuticals (Karlsrhue, Germany) or Sigma-Aldrich (Poole, UK) and Losartan and PD123319 were purchased from Sigma-Aldrich, all of which were also re-suspended in sterile ddH_2O. DNA mini- and maxi-prep kits, RNA extraction kits, DNA gel extraction kits and DNase were purchased from Qiagen (Manchester, UK). Reverse transcription and quantitative real-time polymerase chain reaction (qRT-PCR) reagents were purchased from Invitrogen (Paisley, UK). Restriction endonucleases were purchased from New England Biolabs (NEB) (Hertfordshire, UK) or Promega (Southampton, UK). Luria broth (LB) and LB-agar were purchased from Sigma-Aldrich. All western immunoblot reagents, buffers and gels were also purchased from Invitrogen. Normal goat serum and rabbit IgG for immunohistochemistry (IHC) were purchased from Dako (Cambridge, UK).

2.1.1 Solutions

- 1 x Krebs-Henseleit solution (in mmol/L): NaCl 130.0, KCl 5.4, 4-(2-hydroxyethyl)-1-piperazineethanesulfonic acid (HEPES) 25.0, NaH_2PO_4 0.4, $MgCl_2$ 0.5, glucose 22.0. pH 7.4 at 37 °C with NaOH.

- 10 x HEPES buffered perfusate (in mmol/L): NaCl 140.0, KCl 4, $MgCl_2$ 1.0, HEPES 5.0, glucose 11.1, $CaCl_2$ 1.8. pH 7.4 at 37 °C with NaOH.

- 10 x Tris-buffered saline (TBS) (in mmol/L): Tris-HCL 162.6, Tris-base 46.0, NaCl 1505.0. pH 7.6 at room temperature.

- 10 x Phosphate-buffered saline (PBS) (in mmol/L): NaCl 1370.0, KCl 27.0, Na_2HPO_4 100.0, KH_2PO_4 18.0. pH 7.4 at room temperature.

- 50 mM Tris-buffered tween (Tbt) (in mmol/L): Tris-HCl 40.3, Tris-base 9.7, NaCl 150.0. pH 7.5 at room temperature. 0.5 mL Tween-20/L.

- 10 mM Sodium citrate (in mmol/L): Trisodium citrate 11.4. pH 6 at room temperature. 0.5 mL Tween-20/L.

- 10 x Citric saline (in mmol/L): KCl 13.4, sodium citrate 1.7.

- 10 x Tris-EDTA (TE) buffer (in mmol/L): Tris-base 100.0, EDTA 1.3. pH 8 with HCl at room temperature.

- 1 x Tris density (TD) buffer (in mmol/L): NaCl 750.0, KCl 50.0, Tris-HCl 250.0, Na_2HPO_4 10.0. pH 7.4 at room temperature.

- 1 x Protein lysis buffer (in mmol/L): Tris-HCl 50.0, NaCl 150.0, EDTA 2.5, EGTA 2, Triton X-100 200 µL/L, PMSF 0.2, NaF 100.0. 1 x complete mini protein inhibitor cocktail tablet (Roche, Welwyn, UK).

2.2 Cell culture

2.2.1 Cell lines and maintenance

Both H9c2 (immortalised rat heart myoblast cell line) and HeLa (immortalised human cervical epithelial carcinoma cell line) cells were purchased from the European Collection of Animal Cell Cultures (Wiltshire, UK). 293 cells are a human embryonic kidney cell line transformed with the left-hand fragment of the adenovirus serotype 5 (Ad-5) genome which transcomplements the E1 Ad-5 genomic region to allow propagation of replicant-deficient rAd vectors *in vitro* (Mahmood and Yang, 2012). They were purchased from Microbix Biosystems (Toronto, Canada). All cell culture work was performed in a sterile class II microbiological safety cabinet under laminar flow (Thermo Scientific, Basingstoke, UK). Tissue culture plastics were purchased from Corning, Fisher Scientific (Loughborough, UK). Cells were maintained in minimal essential media (MEM, Gibco, Paisley, UK) supplemented with 10 % foetal bovine serum (FBS), 2 mM L-Glutamine, 1 IU/ mL Penicillin, 100 µg/µL Streptomycin and 100 mM Sodium Pyruvate in a humidified incubator at 37 °C and 5 % CO_2. Cells were

grown in a monolayer and passaging (or sub-culturing) was performed when cells reached 60-70 %, 90-100 % and 80-90 % confluency for H9c2, HeLa and 293 cell lines, respectively (Section 2.2.2).

Frozen cell stocks of all cell lines were stored long term in liquid nitrogen and replenished from live stocks as needed. Briefly, a confluent 150 cm^2 vented-lid flask (T150) of cells were passaged as described in Section 2.2.2. Media was removed from the cell pellet and discarded. Cells were re-suspended in 4-6 mL of supplemented MEM containing 5 % (v/v) dimethyl sulfoxide (DMSO). Cells were divided into 1 mL aliquots into cryovials and frozen gradually in order to avoid cellular rupture by submerging tubes in 100 % isopropanol and placing in a -80 °C freezer for 24 hr before transfer to liquid nitrogen. To recover cells from frozen stocks an aliquot was thawed rapidly at 37 °C in a water bath and transferred to a sterile tube which was centrifuged at 500 x g for 10 min at room temperature. DMSO contaminated media was removed and discarded and the cell pellet re-suspended in fresh MEM and placed in a T150 cm^2 flask to recover.

2.2.2 Cell passaging and plating

Cells (in T150 cm^2 flasks) were passaged by washing twice with sterile PBS before 5 mL of pre-warmed trypsin-ethylenediamine tetra-acetic acid (trypsin-EDTA, for HeLa and H9c2 cells) or 5 mL 1 x citric saline (293) was added to the flask, followed by incubation at 37 °C for approximately 5 min or until cells detached from the flask. Approximately 10 mL of pre-warmed 10 % FCS-supplemented MEM was added to the flask in order to avoid over-digestion of the cells. The entire contents of the flask were transferred to a sterile tube and centrifuged for 10 min at 500 x g. The media was decanted and the cell pellet re-suspended in 4-8 mL of fresh MEM, depending on the density to be seeded. Finally, 1 mL of the cell suspension was added to a new T150 cm^2 flask and the total volume adjusted to 25 mL using MEM.

In order to plate cells at a specific density for experimentation, they were counted following re-suspension in fresh MEM. This was performed by loading 12 µL of cell suspension into a haemocytometer, the number of cells in each of the four quadrants counted and an average number of cells per quadrant determined. The number of cells per mL equalled the average number of cells

per quadrant x 10^4. In order to calculate the volume of cell suspension required to plate a specific density the following calculation was used:

$$\text{volume required} = \frac{\text{cell density required}}{\text{number of cells per mL}} \times 1000 = \text{volume in µL per well}$$

The appropriate volume of cell suspension was then added to each well and MEM added to adjust the volume to 2 mL, 1 mL, 0.5 mL or 200 µL for a 6-, 12-, 24- or 96-well plate, respectively.

2.2.3 Transfections

Transfections were performed using Xfect transfection reagent (Clontech, California, USA) as per the manufacturer's instructions. Cells were seeded in 6 well plates at a density of 3 x 10^5 cells/well (HeLa) or 6 x 10^4 cells/well (H9c2) 24 hr prior to transfection. Plasmid DNA was diluted in Xfect reaction buffer to achieve 2.5, 5 or 7.5 µg of DNA in a total volume of 100 µL. An equivalent volume of Xfect polymer was diluted in the same reaction buffer with 0.3 µL of polymer added per µg of DNA. Tubes were vortexed well before the DNA and polymer was mixed and vortexed again. A polymer-only mix was prepared as a control for toxicity. Samples were incubated at room temperature for 10 min to allow biodegradable DNA-polymer nanoparticles to form. Media was removed from cells and 1 mL of fresh MEM added to each well before the entire 200 µL of nanoparticle preparation was added to the well drop-wise in triplicate. A set of triplicate wells remained un-transfected as a control. Plates were incubated at 37°C for 4 hr before media and nanoparticles were removed *via* aspiration and replaced by 2 mL of fresh media. Media was changed again at 24 hr and cells harvested 48 hr post-transfection.

2.3 Adenovirus purification

The method for preparation of high-titre recombinant adenoviral (RAd) stocks is described in detail elsewhere *(*Nicklin and Baker, 1999*)*. First, 25 x T150 cm^2 flasks of 293 cells at 80-90 % confluence were infected with an in-house viral seed stock (a gift from SA Nicklin) at a multiplicity of infection (MOI) of between 0.1-10 per flask. Cells were incubated for 3-4 days until cytopathic effect became apparent. Next, media and cells were collected and cells harvested *via*

centrifugation at 2000 x g for 10 min at 4°C. Media was discarded and the cell pellet re-suspended in ~6 mL of sterile PBS. An equivalent volume of trichlorotrifluoroethane (Arklone P, ICI Ltd., Cheshire, UK) was added, followed by inversion for approximately 10 s and then shaking for 5 s. These steps were repeated to release the viral particles and the preparation was centrifuged at 3000 x g for 10 min. The upper aqueous layer containing the virus was transferred to a fresh sterile tube and either immediately underwent purification or was stored at -80°C.

2.3.1 Double caesium chloride gradient purification

Double caesium chloride (CsCl) gradient ultracentrifugation is used in order to remove cellular contaminants from viral preparations. CsCl solutions were prepared *via* dissolving the required mass of CsCl in 50 mL of TD buffer in order to achieve the correct density solutions; 1.25 g/mL (18.08 g), 1.34 g/mL (31.1 g) and 1.4 g/mL (25.6 g). Solutions were then filter sterilised and all subsequent steps of the extraction performed under sterile conditions in a class II microbiological safety cabinet under laminar flow (Thermo Scientific, Basingstoke, UK). A sterilised thin-walled 14 mL 14 x 95 mm centrifuge tube (Beckman Coulter, High Wycombe, UK) suitable for use in an SW40 centrifuge rotor was filled with 2.5 mL of the 1.4 g/mL CsCl solution. A further 2.5 mL of the 1.25 g/mL CsCl solution was carefully layered on top followed by the crude virus preparation. Tubes were carefully sealed in a SW40 rotor tube and centrifuged at 90000 x g for 1.5 hr at 18 °C in an Optima L-80 XP ultracentrifuge (Beckman Coulter, High Wycombe, UK). Tubes were then carefully removed from the rotor tube and mounted in a clamp stand (Figure 2.1 A). The lower virus particle band was extracted using a 21 gauge needle and a 5 mL syringe. The needle was inserted through the tube wall and the virus band withdrawn into the syringe. The viral preparation then underwent a second round of purification using another density gradient. A sterilised centrifuge tube was filled with 5 mL of the 1.34 g/mL CsCl solution. The extracted virus was carefully layered on top and the tube filled with sterile PBS. The preparation was centrifuged at 90000 x g at 18 °C for 18 hr. The single virus band (Figure 2.1 B) was extracted in an identical manner as described previously.

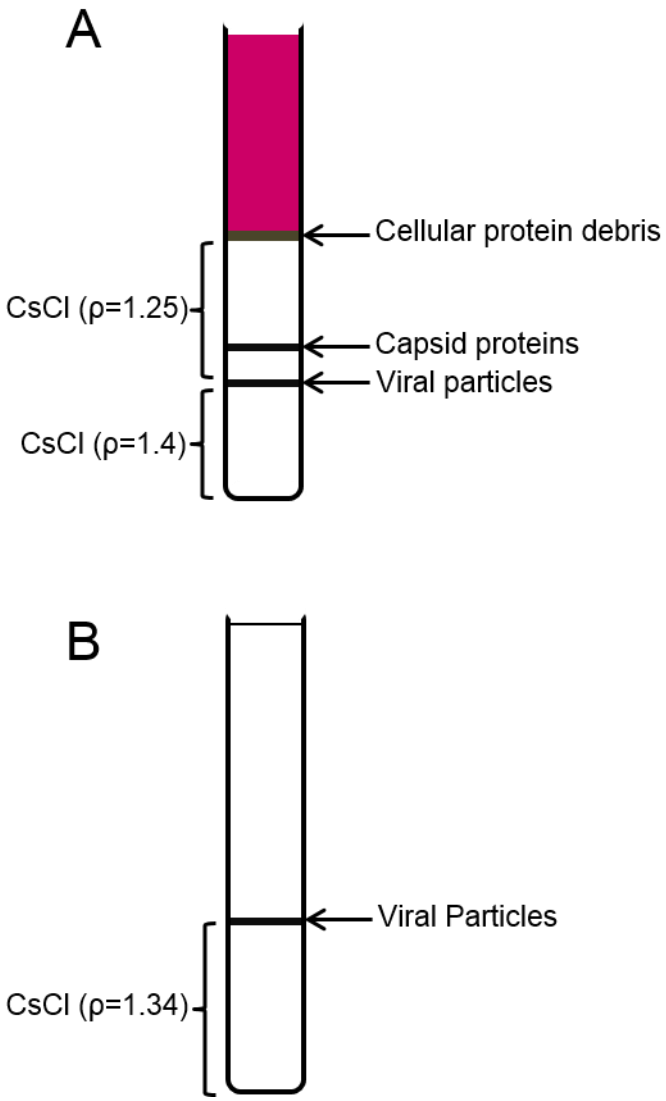

Figure 2.1 Separation of viral particles after CsCl density gradient ultracentrifugation. Schematic of polypropylene centrifuge tubes showing separation of fractions after CsCl density gradient ultracentrifuge. (A) Separation after spin at 90000 x g for 1.5 hr using 1.25 g/mL and 1.4 g/mL density CsCl solutions. Viral capsid layer forms between 1.25 g/mL and 1.4 g/mL CsCl solutions, with viral capsid proteins forming a second band slightly above. Cellular protein debris and PBS form the upper layer (Nicklin and Baker, 1999). (B) Separation after second 90000 x g spin for 18 hr showing formation of viral particle layer directly on top of 1.34 g/mL CsCl solution (Alba et al., 2012).

2.3.2 Dialysis

In order to remove any CsCl contamination from the preparation, the virus was loaded into a Slide-A-Lyser dialysis cassette (Perbio Science, Northumberland, UK) with a molecular weight cut off of 10 000 kDa. The preparation was dialysed in 2 L of sterile 1 x TE buffer for 2 hr, the buffer replaced and the dialysis continued for a further 2 hr. Finally the preparation was dialysed overnight in 1 x TE supplemented with 10 % glycerol. The virus was then removed, aliquoted and stored at -80 °C.

2.3.3 Recombinant adenoviral vector titration

Infectious viral particle titres were assessed *via* end point dilution, and total viral particles *via* micro-Bicinchoninic Acid (BCA) assay, allowing a ratio of infectious virions: total particles to be determined.

2.3.3.1 Titration by end-point dilution assay

One x T150 cm^2 flask of 293 cells were passaged as described in Section 2.2.2 and re-suspended in 25 mL MEM. Three mL of the cell solution was then diluted into a final volume of 20 mL MEM and 200 µL of this added to each well of a 96 well plate to achieve 50-60% confluence. 24h later viral dilutions were prepared in media with dilutions ranged from 10^{-2} to 10^{-12}. Media was removed from each well and replaced starting at the bottom of the plate where 100 µL of media was added to each well as a negative control. Each subsequent row was replaced with 100 µL of increasing viral concentrations. This process was also repeated identically using a 96-well plate containing HeLa cells in order to assess whether there was replication competent adenovirus present in the preparation. Media was replaced on the cells after 24 hr and then every 2 days for 8 days. When viral plaques became apparent, the wells were marked and the media was no longer replaced. In order to calculate titre accurately, one dilution must present with no plaques, one with less than 50 % of wells presenting with plaques and one with greater than 50 %. Plaque forming units (pfu)/mL was then calculated using the equations as follows:

The proportionate distance (PD) from the 50 % end-point =

$$\frac{\%\text{ positive above 50 \% - 50 \%}}{\%\text{ positive above 50 \% - \% positive below 50 \%}}$$

and $\log ID_{50}$ (infectivity dose) = log dilution above 50 % + (PD x -1) x dilution

For example; for a plate with 7 positive wells out of 10 (70 %) at 10^{-10} dilution and 1 positive well out of 10 (10 %) at 10^{-11} dilution, the calculation would be as follows:

$$PD = \frac{70 - 50}{70 - 10} = 0.33$$

$$\log ID_{50} = -10 + (0.33 \times -1) = -10.33$$

$ID_{50} = 10^{-10.33}$ therefore, $TCID_{50} = \frac{1}{10^{-10.33}} = 10^{10.33}$ x by dilution factor (10)

$= TCID_{50}/mL = 10^{11.33} = 2.14 \times 10^{11}$

Where ID_{50} = infectivity dose 50 and $TCID_{50}$ = tissue culture infectivity dose 50. As 1 $TCID_{50}$/mL is equivalent to 0.7 pfu, multiply by 0.7 to get the final titre,

$2.14 \times 10^{11} \times 0.7 =$ **1.5×10^{11} pfu/mL**

Viral tires ranged from 1.88×10^{10}- 5.176×10^{11} pfu/mL.

2.3.3.2 Particle titration by micro-BCA assay

Micro-BCA was performed using a micro-BCA protein assay kit (Thermo Scientific, Basingstoke, UK) as per the manufacturer's instructions. First, a 2000 µg/mL BSA stock was serially diluted in 1 x PBS to produce a set of standards ranging from 0.5 µg/mL to 200 µg/mL of protein. Next, 150 µL of each standard was added in duplicate to a well of a clear, flat-bottomed 96-well plate (Corning, Loughborough, UK) with 150 µl of 1 x PBS also added in duplicate to act as a negative control. Next, 1, 3 and 5 µL of adenoviral vectors was added in duplicate to the 96-well plate and the total volume adjusted to 150 µL with PBS.

The BCA working solution was prepared *via* mixing reagents MA, MB and MC in the ratio 25: 24: 1, respectively. Next, 150 µL of working solution was added to each well using a multi-channel pipette and the plate incubated in the dark at 37°C for 2 hr. Absorbance at 562 nm was then determined using a Wallac VICTOR$_2$ plate reader (PerkinElmer, Wallac, Finland). The total number of virus particles per mL was then calculated by identifying the protein standard with the closest absorbance to that of the sample and using the following formula:

$$\left(\frac{\text{Total protein in BSA standard well (µg)}}{\text{Absorbance of standard}} \times \frac{\text{Absorbance of sample well}}{\text{Virus volume in µL}}\right) \times \left(4 \times 10^9\right)$$

= particle titre in µg/mL

This was performed for each volume of virus and the values averaged to give the final viral particle titre (VP)/mL.

2.3.4 Virus infections

Cells were seeded in 6 well plates as described in Sections 2.2.2 and 2.2.3 24 hr prior to viral transduction. Adenovirus aliquots were thawed on ice, diluted in MEM where required and added directly to each well to achieve the desired multiplicity of infection (MOI). MOI is the ratio of infectious viral particles per cell. The volume of virus required to achieve a specific MOI is calculated based on both cell density and virus pfu titre (Section 2.3.3.1), and is determined using the following formula:

$$\text{Volume of virus} = \left\{\left(\frac{\text{Cell density}}{\text{Desired MOI}}\right) \div \text{virus pfu}\right\} \times 1000 = \text{volume in µL}$$

Cells were harvested 48 hr post-virus transduction.

2.4 AAV production

AAV9-Ang-(1-9) and AAV9-eGFP vectors were prepared at the AAV Vector-Unit (AVU) Core facility at the International Centre for Genetic Engineering and Biotechnology (ICGEB) in Trieste, Italy and were provided as a gift by Professor Mauro Giacca.

2.5 Nucleic acid extraction

2.5.1 DNA extraction

2.5.1.1 Mini-preparation

A small-scale plasmid preparation was utilised to isolate up to 20 µg plasmid DNA from 1-10 mL of bacterial preparation. Prior to purification, 5 mL of the selected bacterial colony was produced *via* incubation in liquid growth media over-night (Section 2.6). Next, 4 mL of the bacterial culture was harvested at 6800 x g in a table-top centrifuge for 3 min at room temperature. The bacterial pellet was re-suspended in buffer P1 containing 0.1 mg/mL RNase A, followed by addition of 250 µL of cell lysis buffer P2. The tubes were inverted to mix. Next, 350 µL of precipitation buffer N3 was added to the tube followed by mixing. The sample was subjected to centrifugation in a table-top micro-centrifuge at 17900 x g for 10 min at room temperature. The resulting supernatant was transferred to the spin column, avoiding the pellet of cellular debris. The spin columns were subjected to centrifugation at maximum speed for 1 min to bind the DNA to the silica membrane, and the flow-through discarded. The membrane was washed using 0.5 mL of buffer PB followed by a further wash using 0.75 mL of ethanol-containing wash buffer PE and centrifugation for a further min to dry the membrane. The column was transferred to a collection tube and the DNA eluted from the column *via* the addition of 50 µL nuclease-free H_2O followed by incubation at room temperature for 1 min and a subsequent 1 min centrifugation at 17900 x g. DNA concentration was determined *via* nanodrop (Section 2.5.3) and DNA was stored at -20 °C.

2.5.1.2 Maxi-preparation

Large-scale maxi preparations allow purification of up to 100-500 µg of plasmid DNA from 100-500 mL of bacterial culture. Overnight-incubation of 500 mL of bacterial culture was carried out (Section 2.6) and harvested the following day *via* centrifugation at 6000 x g for 15 min at 4 °C. The bacterial pellet was re-suspended in 10 mL of RNase A containing buffer P1 followed by the addition of 10 mL of lysis buffer P2. After a 5 min incubation at room temperature, 10 mL of pre-chilled neutralisation buffer P3 was added, followed by vigorous inversion of the tube to ensure thorough mixing and incubated on ice for 20 min before

centrifugation at 20000 x g for 30 min at 4 °C. The cleared supernatant containing the DNA was removed from the tube immediately, avoiding the cell debris pellet, and loaded onto a QIAGEN-tip 500 which had been equilibrated previously using 10 mL of QBT buffer. The supernatant was allowed to enter the column resin by gravity flow. The bound DNA was then washed twice using 30 mL of medium-salt concentration QC buffer, again under gravity flow. Elution was performed under gravity flow *via* addition of 15 mL of buffer QF to the column which was collected in a centrifuge tube. DNA was precipitated *via* the addition of 10.5 mL of room-temperature isopropanol followed by immediate centrifugation at 15000 x g for 30 min at 4 °C. The isopropanol was then discarded and the DNA pellet washed in 5 mL of 70 % ethanol before a final centrifugation step for 10 min at 15000 x g. Finally the pellet was air-dried and re-suspended in an appropriate volume of nuclease-free H_2O. DNA concentration was determined by Nanodrop (Section 2.5.3) and DNA was stored at -20 °C and thawed on ice as needed.

2.5.2 RNA extraction

Filter pipette tips and RNase-free plastics were used throughout the RNA purification protocol.

2.5.2.1 Cell and tissue lysis

Tissue samples (10-20 mg), preserved in liquid nitrogen and stored at -80 °C (Section 2.10.5), were placed in 2 mL Eppendorfs on dry ice and a 5 mm stainless steel bead added to each tube. The tubes were placed at room temperature and 700 µL of QIAzol reagent added immediately to each tube. Tubes were placed in a Tissue Lyser (Qiagen, Manchester, UK) 2 x 24 Adaptor Set and lysed at 30 Hz for 2 x 2 min in order to rupture the cell membranes of the tissue. RNA extraction was performed immediately following lysis (Section 2.5.2.2).

Cells were washed twice with PBS, followed by the addition of 700 µL of QIAzol directly to each well. Cell lysis was facilitated *via* physical removal of cells from the plate surface using a 2 mL syringe plunger. The entire contents of each well was aspirated and placed in a 1.5 mL Eppendorf. Tubes were vortexed to ensure

complete homogenisation and samples were either stored at -80 °C until required or RNA extracted immediately following lysis (Section 2.5.2.2).

2.5.2.2 Purification

QIAzol homogenates had 140 µL of chloroform added to each tube before vigorous shaking for 15 s. The tubes were incubated at room temperature for 2-3 min before centrifugation for 15 min at 12000 x g at 4 °C. The upper aqueous phase was removed to a fresh tube and 525 µL of 100 % ethanol was added in order to facilitate RNA binding to the mini column membrane. RNA was bound to the column *via* centrifugation at 8000 x g for 15 s. At this stage the on-column DNase digest was performed (Section 2.5.2.3). Following DNase treatment, the membrane was washed with 2 x 500 µL of the ethanol-based RPE wash buffer. The column was then subjected to centrifugation at 16000 x g for 1 min to dry the membrane. The spin column was placed in a collection tube and RNA eluted using 30 µL of nuclease free water and centrifugation at 8000 x g for 1 min. RNA concentration was determined using Nanodrop (Section 2.5.3) and was stored at -80 °C and thawed on ice as needed.

2.5.2.3 DNase treatment

The spin column membrane was washed with 350 µL of the ethanol-based wash buffer RWT. DNase I was prepared as per the manufacturer's instructions (10 µL of DNase I diluted in 70 µL of buffer RDD). The entire 80 µL was then added directly to the mini spin column membrane and incubated for at least 15 min at room temperature. The DNase I was then removed by a further wash with 350 µL of RWT buffer. The RNA extraction procedure was then completed as described (Section 2.5.2.2).

2.5.3 Nucleic acid quantification

DNA and RNA concentrations were determined using a ND-1000 Nanodrop full-spectrum (220-750 nm) spectrophotometer (Thermo Scientific, Loughborough, UK). The Nanodrop is operated by 1-2 µL of sample being placed on the fibre optic cable and a second cable lowered down on an arm so the sample forms a column between the two. A near-monochromatic pulse of light is then produced from a xenon flash lamp at 260 nm which passes through the sample. The light

that passes through the sample is analysed by a linear charged-coupled device (CCD) array and the absorbance at 260 nm used to correlate the absorbance with nucleic acid concentration using the Beer-Lambert equation which is as follows:

$$c=A/(E\times b)$$

Where, c= nucleic acid concentration (mol/L), A= absorbance ($\log_{10} P_0/P$) , E= extinction coefficient (L/mol/cm) and b= path length of sample (cm).

The extinction coefficients for nucleic acids are as follows: dsDNA= 50, ssDNA= 33, RNA= 40. The absorbance ratio at 260/280 was used to assess nucleic acid purity, with a ratio of ≥ 1.8 considered pure.

2.6 Molecular cloning

2.6.1 Bacterial culture and antibiotic selection

Escherichia Coli (*E.coli*) Top10 cells were produced in-house and with efficiency >1 x 10^8 cfu/mL. Following transformation (Section 2.6.6), bacteria were grown on solid antibiotic containing-Luria Broth (LB) agar plates. As the density of bacterial growth cannot always be anticipated, 20 and 200 µL of bacterial culture were plated on 2 individual plates per transformation and distributed evenly across the plate's surface using a sterile spreader. Plates were incubated at 37 °C overnight to allow bacterial colonies to form.

2.6.1.1 Cryopreservation of bacterial stocks

1 mL of bacterial culture carrying the plasmid of interest was placed in a 2 mL cryovial and mixed *via* pipetting with 200 µL of sterile 100 % glycerol to achieve a 20 % final glycerol content (v/v). The vial was stored at -80 °C. In order to expand a clone from a glycerol stock for DNA extraction, the vial was thawed on ice and 20 µL spread onto an agar plate containing the appropriate antibiotic and the plate incubated as described. A single colony was picked and cultured as described (Section 2.6).

2.6.2 Restriction endonuclease digestion

All restriction endonuclease reactions were performed as per manufacturer's instructions. Multiple 20 µL restriction digest reactions containing 1 µg of plasmid DNA were performed in order to confirm plasmid integrity and for screening clones. 50 µg plasmid DNA was utilised in restriction endonuclease reactions to purify fragments for sub-cloning. DNA was mixed with the appropriate volume of enzyme and buffer diluted to 1 x using sterile water in a 1.5 mL Eppendorf and incubated at 37 °C in a water bath for 1-4 hr (20 µL reaction) or overnight (100 µL reaction). Fragments could then be visualised using gel electrophoresis (Section 2.6.3).

2.6.3 Agarose gel electrophoresis

A 0.8 % agarose gel (w/v) was made by dissolving the required weight of agarose in 1 x TE buffer by heating. The liquid agarose was allowed to cool for 5 min before the addition of 0.01 µL/mL of ethidium bromide. The agarose was poured into a gel mould and a comb put in place to form the sample wells. The gel was allowed to set at room temperature for 1 hr. Samples were prepared by the addition of 6 x gel loading dye (New England Biolabs, Hertfordshire, UK) directly to the restriction endonuclease reaction to achieve a final concentration of 1 x (e.g. 3.33 µL in a 20 µL reaction). Each sample (and 1kb Ladder) was loaded and the gel electrophoresed at 100 volts for 45 min (or until the loading dye approached the bottom of the gel). DNA bands were visualised and photographed using a Bio-Rad ChemiDoc XRS ultra violet (UV) transilluminator and accompanying software (Bio-Rad, Hertfordshire, UK).

2.6.4 DNA gel purification

The DNA bands were visualised using UV light and excised using a clean, sharp scalpel blade. Bands were weighed and placed in a 2 mL Eppendorf tube and 3 volumes of buffer QG added to 1 volume of gel (100 mg of gel ~ 100 µL of buffer). The tubes were heated on a heat block at 50°C for 10 min, or until the gel slices had completely dissolved, with frequent vortexing. One gel volume of isopropanol was added to the tubes and the contents immediately loaded onto spin columns. The tubes were centrifuged for 1 min at 17900 x g. The membrane was washed with a further 0.5 mL of buffer QG to ensure removal of salt

contamination followed by 0.75 mL of buffer PE. The membrane was then dried *via* centrifugation for 1 min before DNA elution using 50 µL of nuclease free H_2O. The H_2O was incubated on the membrane for 4 min at room temperature prior to centrifugation of the columns in a collection tube *via* centrifugation for 1 min at 17900 x g.

2.6.5 Ligation of DNA fragments into plasmid vectors

T4 DNA ligase (New England Biolabs, Hertfordshire, UK) was used as per manufacturer's instructions. The amount of backbone DNA was kept constant at 50 ng per reaction, with the amount of DNA insert varied at 25, 50, 100 and 150 ng per reaction. A backbone only reaction was performed as a negative control. Components were mixed as follows in a well of a 96-well plate: 1 µL insert DNA, 1 µL 10 x T4 DNA ligase buffer, 1 µL vector DNA, 6 µL sterile H_2O and 1 µL T4 DNA ligase. The plate was sealed and incubated on a PCR heat block at 16 °C for 16 hr.

2.6.6 DNA transformation and clone screening

Following ligation DNA was transformed into bacteria. Top10 cells were defrosted slowly on ice, with all steps carried out on ice unless otherwise specified and 50 µL of cells used per reaction. 5 µL of each chilled ligation reaction was added to the cells which were mixed gently and incubated on ice for 30 min. Sterile H_2O was used as a negative control and an intact plasmid carrying the same antibiotic resistance gene used as a positive control. Tubes were placed in a water bath at 42 °C for exactly 30 s and immediately placed back on ice for 2 min. Next, 250 µL of sterile SOC media was added to each reaction and tubes were incubated at 37 °C and shaken at 200 rpm for 1 hr. Cells were then plated on selective growth media overnight as described in Section 2.6. Following transformation and culture, clone screening was performed to identify those which carry the successfully ligated plasmid.

2.6.7 Polymerase chain reaction

PCR reactions were prepared on ice in a 96-well plate using *Taq* DNA polymerase with a Thermopol buffer (New England Biolabs, Hertfordshire, UK) following the manufacturer's instructions for 25 µL reactions. For each reaction 100 ng of

cDNA was used. The sequences of the forward and reverse primers used are shown in Table 2.1. Reverse transcription (RT) reactions performed without the addition of reverse transcriptase were used as a negative control and also to check for genomic DNA contamination. PCR reactions were also established using 100 ng of intact original pBluescript plasmid DNA to act as a positive control. Reaction components were as follows: 2.5 µL 10x reaction buffer, 0.5 µL 10 mM dNTPs, 0.5 µL of each primer (of 10 µM stocks, forward and reverse), 0.125 µL of 5 units/µL *Taq* polymerase and nuclease free H_2O to make the final reaction volume up to 25 µL. The plate was sealed well and placed on a PCR heat block set at the cycling temperatures shown in Table 2.2. PCR reactions were resolved on an agarose gel as described in Section 2.6.3.

2.6.8 DNA sequencing

Sequencing was performed using the BigDye Terminator v3.1 Cycle Sequencing Kit (Invitrogen, Paisley, UK) which performs fluorescence-based cycle sequencing reactions for double-stranded DNA. The sequencing protocol was performed in 2 steps. First a PCR reaction was carried out which was then loaded onto an ABI Prism 377 laser DNA sequencer (Invitrogen, Paisley, UK) which determines the base sequence.

The sequencing protocol was carried out as per the manufacturer's instructions. For the PCR step, 100 ng of plasmid DNA in a total volume of 1-2 µL was mixed in a total reaction volume of 20 µL. Sequencing of the original pBluescript plasmid was performed as a positive control. Multiple reactions were set up for each plasmid to be sequenced; one for each sequencing primer. Each reaction contained the following components: 4 µL BigDye sequencing buffer, 1 µL BigDye ready reaction mix, 2 µM of sequencing primer (1 µL of a 10 µM stock) and the template DNA, with the total reaction volume made up to 20 µL with Millipore filtered H_2O. The plate was sealed and heated on a PCR block at the cycling temperatures shown in Table 2.3. Prior to sequencing, the PCR reaction underwent a clean-up to remove any remaining enzyme and other reagents. This was performed by the addition of 10 µL of room-temperature, well-agitated Agencourt CleanSEQ (Beckman-Coulter, High Wycombe, UK) to each reaction well. Next, 62 µL of 85 % ethanol was added to each well before the plate was re-sealed and carefully vortexed to mix. The plate was centrifuged briefly

before being placed on an Agencourt 96-well magnet plate (Beckman-Coulter, High Wycombe, UK) for 2 min. The DNA, now attached to the beads, remained in the plate as long as it was placed on the magnet. The plate, still on the magnet, was then blotted upside down to remove the ethanol. The DNA was washed by the addition of 150 µL of 85 % ethanol to each well and the magnet-blot process repeated. The plate, still in the magnet block and upside down, was subjected to centrifugation briefly to remove excess ethanol. The plate was left to air dry for 10 min at room temperature. The beads were then re-suspended in 40 µL of Millipore filtered H_2O (with the plate now removed from the magnet block). With the DNA now removed from the beads and in solution, the plate was placed on the magnet block one last time and the DNA carefully removed, avoiding any of the beads. The DNA was either transferred directly onto a sequencing plate or into a sterile Eppendorf tube to be stored at -20 °C prior to sequencing. For sequencing, 20 µL of purified PCR product was added to a well of a 96-well ABI sequencing plate (Invitrogen, Paisley, UK) which was subsequently loaded onto the ABI Prism 377 laser DNA sequencer. Electropherograms were imported into CLC Genomics Workbench 7.0 software and analysed compared to a reference sequence.

Table 2.1 Primer sequences for PCR and sequencing of expression cassette.

Primer	Direction	Sequence (5'-> 3')
Expression cassette sequencing	Forward 1	TGGGTAACGCCAGGGTTT
Expression cassette sequencing	Forward 2	TGGCATGGATCAATTCCG
Expression cassette sequencing	Reverse 1	TCATGTGGTCGGGGTAGC
Expression cassette sequencing	Reverse 2	GGGCTGCAGGAATTCTCA
Expression cassette sequencing	Reverse 3	AGCGGATAACAATTTCACAC
pAAV-MCS PCR	Forward	CCCATAGAGAGGATTACAAC
pAAV-MCS PCR	Reverse	TTTAGTGCGTACGCGAGAT
pAAV-MCS sequencing	Forward 1	CATCGAGAGAACCATCTCAA
pAAV-MCS sequencing	Forward 2	CTGGCCCATCACTTTGGC
pAAV-MCS sequencing	Forward 3	GACAGCCTTCCACTTCGG
pAAV-MCS sequencing	Reverse 1	TCAGGCTTTCTCGGATTGA
pAAV-MCS sequencing	Reverse 2	GAAACCCCGTCTCTACCA
pAAV-MCS sequencing	Reverse 3	CTGCAGGTCGACTCTAGA

Table 2.2 PCR cycling conditions.

Step	Temperature (°C)	Time (s)	Purpose	
1	95	30	Initial melting	
2	95	30	Melting	Steps 2-4 repeated for 30 cycles.
3	55	60	Primer annealing	
4	68	60/kb	Strand expansion	
6	68	300	Final strand expansion	

Table 2.3 BigDye sequencing PCR cycling temperatures.

Step	Temperature (°C)	Time	
1	95	5 min	
2	95	30 s	Steps 2-4 repeated for 30 cycles.
3	55	10 s	
4	60	4 min	

2.7 Protein extraction

2.7.1 Cell lysis

Cell lines cultured in 6-well plates as described in section 2.2.2 and transfected as described in Section 2.2.3 were washed twice with sterile PBS and trypsinised as described in section 2.2.2. The cells were aspirated from the wells and placed in a 1.5 mL Eppendorf tube before being pelleted *via* centrifugation at 16000 x g for 5 min. The supernatant was discarded and the cell pellet re-suspended in 200 µL of protein lysis buffer. Cell lysis was encouraged *via* repeated aspiration using a 28 G needle and 1 mL syringe. The samples were shaken on ice for 1 hr to allow for complete cell lysis and protease inhibition before any remaining debris was removed *via* centrifugation at 16000 x g for 10 min at 4 °C. The protein sample was transferred to a fresh 1.5 mL Eppendorf and stored at -80 °C, being thawed on ice as needed.

2.7.2 Bicinchoninic acid (BCA) assay

The BCA assay was performed using the Pierce BCA assay kit (Thermo Scientific, Loughborough, UK) as per the manufacturer's instructions. Briefly, a set of protein standards were prepared *via* serial dilution of a bovine serum albumin (BSA) stock solution (2000 µg of protein per mL) in protein lysis buffer to produce a range of protein concentrations. Once prepared, 25 µL of each standard was pipetted in duplicate into wells of a clear, flat-bottomed 96-well plate. Protein lysis buffer only was used as a negative control. Next, 1, 5 and 10 µL of each protein sample, prepared as described in section 2.7.1, was pipetted into wells of the same plate in duplicate. Each sample well was adjusted to a final total volume of 25 µL *via* the addition of the appropriate volume of protein lysis buffer (24, 20 and 15 µL, respectively). The working BCA solution was then prepared by mixing reagents A and B in a ratio of 49:1. Next, 25 µL of this working solution was added to each sample and standard well using a multichannel pipette before incubation of the plate in the dark at 37 °C for 30 min. The colour intensity of the plate was then determined *via* absorbance measurement at 562 nm using a Wallac VICTOR$_2$ plate reader (PerkinElmer, Wallac, Finland).

Protein concentration of each sample was then determined by first averaging the duplicates for each value and plotting the standard curve using the absorbance reading from the standards against the total protein in each well of the standard (Figure 2.2). The equation of the line was then used to determine protein concentration of each sample by solving for X, using the absorbance of each sample as Y and correcting for the volume of the sample in the well (divide by the volume in µL). Concentration determined for each lysate volume (1, 5 and 10 µL) were then averaged to calculate the final protein concentration.

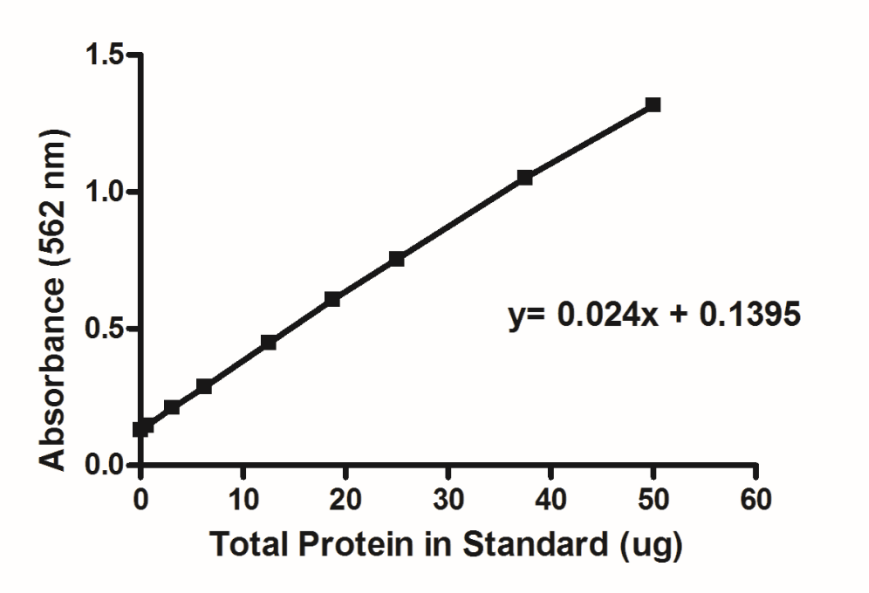

Figure 2.2 Linear relationship of protein concentration and absorbance at 562 nm in a BCA assay.
Absorbance readings from a set of protein standards in a BCA assay plotted as total protein per well (X) against absorbance at 562 nm (Y) producing a strong linear correlation. The equation of the line can be used to determine protein concentration in other samples.

2.8 Western immunoblotting

Protein samples, prepared and quantified as described in Sections 2.7.1 and 2.7.2, were first diluted to equivalent concentrations in protein lysis buffer, with samples kept on ice throughout. Samples were then reduced by mixing 30 µL of protein sample buffer with 10 µL of 4 x NuPAGE LDS sample buffer and 4 µL of NuPAGE reducing agent in a 1.5 mL Eppendorf tube. Reduction was achieved by heating the sample mixture for 10 min at 70 °C on a heat block. Next, 800 mL of 1 x NuPAGE MOPS SDS running buffer was prepared by dilution of the 20 x stock in H_2O. The pre-cast 12-sample 4/12 % bis-tris NuPAGE gel was then prepared by removal of the sample comb and was assembled in a gel tank (Invitrogen, Paisley, UK) which was then filled with the running buffer. Once prepared, 20 µL of each prepared sample was loaded into the gel using gel-loading pipette tips, with 5 µL of Seeblue protein ladder (Invitrogen, Paisley, UK) loaded into one well as a molecular weight reference. The gel was electrophoresed for 1 hr at 200 volts.

2.8.1 Transfer

During the electrophoresis step, the transfer buffer was prepared by diluting the 20 x stock of NuPAGE transfer buffer to 1 x in 20 % methanol in H_2O and a Novex polyvinylidene difluoride (PVDF) pre-cut blotting membranes with 0.45 µm pore-size (Invitrogen, Paisley, UK) and 2 pre-cut filter papers were pre-soaked in the transfer buffer as were 7 sponges. Once the electrophoresis was complete, the gel was carefully removed from the cassette and place on top of 3 pre-soaked sponges and one piece of filter paper which had been stacked into the transfer cassette. The PVDF membrane was place on top followed by the second filter paper and remaining 4 sponges. The cassette was then closed, ensuring no air bubbles remained between any of the layers, and locked into the transfer tank, ensuring the current would be running perpendicular to the gel and such that the positive electrode was on the membrane side of the cassette, ensuring transfer would take place in the correct direction. The tank was then filled with the transfer buffer and a current applied at 40 volts for 1 hr.

2.8.2 Protein detection

Two-stage protein detection was performed by first probing for the protein using an un-tagged antibody against the protein of interest and then probing for the primary antibody using a horseradish peroxidase (HRP) conjugated secondary antibody, making for more specific detection. After transfer, the membrane was removed from the cassette and a corner cut off to mark the top and protein side of the membrane. The membrane was blocked in 10 % milk (Marvel, Premier Foods, Hertfordshire) in TBS-T (0.1 % tween) for 1 hr at room temperature with shaking to prevent non-specific antibody binding. The primary rat anti-mouse IgG2b antibody [1 mg/mL stock, Abcam (ab167476), Cambridge, UK] was then prepared by dilution 1 in 250 in 10 % milk in TBS-T and was incubated on the membrane for 2 hr at room temperature with shaking. The membrane was then washed for 3 x 10 min in TBS-T before incubation with the secondary rabbit anti-rat IgG HRP antibody [Dako (P0450), Cambridge, UK] diluted 1 in 1000 in 10 % milk in TBS-T for 2 hr at room temperature. The membrane was washed again for 3 x 10 min in TBS-T. The membrane was incubated with Amersham ECL prime solution (GE Healthcare, Buckinghamshire, UK), prepared by mixing reagents 1 and 2 in equal volumes as per the manufacturer's instructions, for 1 min. The membrane was immediately transferred to an X-ray film cassette for development with photographic film.

2.9 Real-time quantitative reverse transcription PCR

2.9.1 Reverse transcription

Reverse transcription of RNA was performed using a reverse transcription kit (Invitrogen, Paisley, UK) as per the manufacturer's instructions for a 40 µL reaction using 500 ng of RNA per reaction. Reactions were set up in a 96-well plate on ice with components per reaction as follows: 4 µL of 10x reaction buffer, 8.8 µL of $MgCl_2$, 8 µL of dNTPs (2.5 mM each dNTP), 2 µL of 50 µM random hexamers, 0.8 µL of 20 U/µL RNAse inhibitor and 1 µL of 50 U/µL reverse transcriptase (multiscribe) enzyme with the total reaction volume made up to 40 µL with the addition of nuclease-free H_2O. The 96-well plate was sealed and centrifuged briefly to mix. The plate was placed on a PCR heat block and set for

the cycling conditions for the reverse transcriptase reaction as shown in Table 2.5. Once complete, the plate was stored at -20 °C until needed.

2.9.2 Quantitative PCR

QPCR reactions were set up in a 384-well MicroAmp optical PCR plate (Invitrogen, Paisley, UK) with a total reaction volume of 10 µL on ice. Reactions were performed in duplicate using 1.5 µL of each RT product per reaction (Section 2.9.1). H_2O was used as a negative control. 5 µL of TaqMan Universal Master Mix II (Invitrogen, Paisley, UK), containing ultra-pure AmpliTaq Gold DNA Polymerase, dNTPs and buffer components, was added to each well with 0.5 µL of the TaqMan assay containing the primer-probe combination for the specific gene of interest (see Table 2.4) and the total reaction volume made up to 10 µL with nuclease-free H_2O. The plate was sealed with an optical adhesive film and centrifuged briefly to mix the components. QPCR was performed on a 7900HT Fast Real-Time PCR System (Invitrogen, Paisley, UK). Cycle threshold values (Ct) for each gene was normalised to that of a house-keeper gene for each sample. Data was expressed as fold change compared to a reference sample determined using the $2^{-\Delta\Delta Ct}$ method (Schmittgen and Livak, 2008), where $\Delta\Delta Ct$= (Ct of sample)-(Ct of reference sample), with the fold change represented arbitrarily as relative quantification (RQ).

Table 2.4 TaqMan gene expression assay details

Gene	Assay ID	RefSeq Gene ID	Label
Agtr1a (AT_1R)	Mm01957722_s1	NM_177322.3	FAM
Agtr2 (AT_2R)	Mm01341373_m1	NM_007429.5	FAM
Mas 1	Mm00434823_s1	NM_008552.4	FAM
ACE	Mm00802048_m1	NP_001268748.1	FAM
ACE2	Mm01159003_m1	NP_001123985.1	FAM
B2m	Mm00437762_m1	NM_009735.3	FAM
GAPDH	4352339E	NM_008084.2	VIC
18S	4319413E	X03205.1	VIC

Table 2.5 Reverse-transcription cycling temperatures

Step	Temperature (°C)	Time (min)
1	25	10
2	48	30
3	95	5

2.10 *In vivo* models and physiological measurements

2.10.1 The mouse model of myocardial infarction

All surgical procedures were performed in accordance with the Animals Scientific Procedures Act (1986) and were approved by the University of Glasgow Ethical Review Panel and the UK Home Office. Animals were male C57BL/6 mice obtained from Harlan (UK) at 8 weeks of age and housed under controlled environmental conditions (12 hr light/dark cycle at ambient temperature and humidity) and maintained on a standard chow diet. Animals were allowed at least a 1 week acclimatisation period before being used for procedure between 9-11 weeks of age (body weight 23-28 g).

2.10.1.1 Theatre set-up, animal preparation and intubation

The MI procedure was performed using sterile technique. Pre- and post-operative analgesia was prepared and administered prior to surgery in order to give adequate time for the drugs to take effect. Each animal received an intra-peritoneal injection of 0.6 µg Buprenorphrine and 0.1 mg Carprofen in 0.4 mL of sterile 5 % NaCl saline. Post-surgery animals received 25 µg of Temegesic (Buprenorphrine) delivered in soft food daily for 3 days following surgery. The surgical area was set up under a surgical microscope with a heat mat and ventilator (Figure 2.3).

The induction box was filled with 4 % isofluorane in oxygen at a flow rate of 1 L/min and animals placed in the box for induction. Animals were then placed on a facemask on the same isofluorane-oxygen mix in the preparation area and the hair removed from the chest. The shaven area was cleaned thoroughly using Hibiscrub surgical disinfectant after which the animal was transferred to a facemask in the surgical area. Prior to intubation, analgesia and fluids were administered and a sterile ocular lubricant (Lacrilube, Allergen Inc., USA) used to cover the eyes to prevent drying during surgery. The intubation apparatus, comprised of a plastic support with a suture loop attached, was prepared under the dissecting microscope. Animals were then intubated using a custom-made 0.8 mm diameter, 25 mm long intra-tracheal cannula (Harvard Apparatus, Kent, UK, Figure 2.3) covered with a silicone cuff to prevent air leakage (Figure 2.3). The Y-piece of the cannula was attached to the inspiration and expiration tubes

of a Minivent Mouse Ventilator Type 845 (Hugo Sachs Elektronik- Harvard Apparatus, Germany) set at 25 µL SV and 25 strokes/min, with the flow rate reduced to 0.6 L/min. Correct placing of the cannula was assessed by noticeable synchronous rise and fall of the chest with the ventilator. After successful intubation, the animal was positioned on a pre-warmed heat mat (Figure 2.3), on their back, slightly on their right hand side with right fore- and hind-limbs taped to the heat mat. The left arm was suspended using a piece of tubing to make the left-hand side chest accessible. The remaining left hind-limb remained free for regular flexor withdrawal monitoring and the ventilator tubes taped down securely to prevent movement.

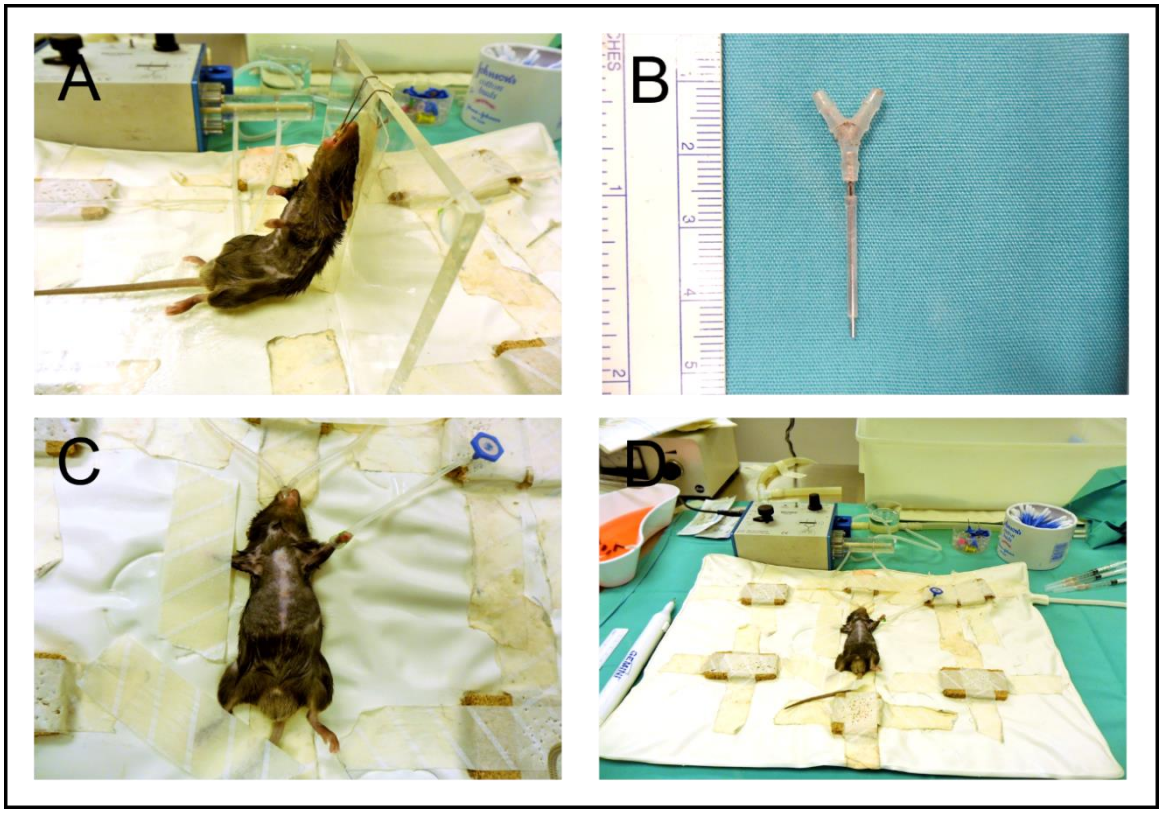

Figure 2.3 Animal preparation and intubation for the MI surgical procedure.
(A) Positioning of the animal for intubation, allowing visualisation of the throat under the microscope for accurate insertion of the cannula. (B) The custom-made intubation cannula. (C) Positioning of the animal prior to surgery. (D) Positioning of equipment with ventilator proximal to the heat mat and the surgical surface covered in sterile drapes.

2.10.1.2 Thoracotomy, left anterior descending coronary artery ligation and recovery

Isofluorane concentration was gradually and incrementally reduced as the surgical procedure progressed to 0 % by the end of the surgery. Once positioned, a diagonal incision was made in the skin using sharp dissection scissors running upward at an angle left to right. The skin was retracted using elastic blunt hook retractors (Harvard Apparatus, UK) which were secured in place using pin-tacks inserted though the retractor into cork underlying the surgical drape. Blunt dissection of the muscles was performed which were secured clear of the rib cage using the retractors. Entry into the chest was made *via* the fourth intercostal rib space by first perforating the muscle by carefully inserting the tip of a pair of sharp angled forceps. Full entry was made using a battery-operated cauterising pen (Harvard Apparatus, UK), in order to avoid substantial blood loss, and the ribs retracted in order to visualise the left ventricle, with care taken not to damage the lung.

For sham procedures the surgery was identical, however the left anterior descending (LAD) coronary artery ligation was not performed and the surgery progressed to closing of the chest and recovery. For animals undergoing MI, visualisation of the LAD was achieved by increasing the magnification and light intensity of the microscope. The vessel was ligated using 9-0 ethilon suture (Ethicon, Livingston, UK) to achieve an approximately 40 % infarct of the left ventricle, with the suture placed as close to the vessel as possible to avoid any other major vessel ligation. Correct placing of the suture was immediately obvious due to the blanching observed in the myocardial tissue below the suture (Figure 2.5).

Following ligation, the ribs were released from the retractor hooks and 3 pieces of non-absorbable 6-0 Prolene sutures (Ethicon, UK) placed between the 3rd and 5th intercostal muscles. The left most suture was used to gently raise the rib cage while the lung was re-inflated *via* occlusion of the ventilator expiration tube by pinching until the lung reached the surgical marker points made earlier in the surgery. The expiration tube was placed in a beaker of tap water to maintain lung re-inflation by creating positive end-expiratory pressure. The sutures were then tied firmly to close the excision. Muscles were released from

the retractors and replaced before the skin was replaced and the incision closed using 5-6 individual stitches with absorbable 6-0 Vicryl suture (Ethicon, Livingston, UK) (Figure 2.4). At this stage, isofluorane level was reduced to 0 % and the wound cleaned well with Hibiscrub disinfectant. The animal remained on the ventilator at 100 % oxygen for 5 min following surgery and remained on the ventilator on room air thereafter until signs of consciousness became apparent. Upon recovery, animals were placed in a pre-heated cage lined with soft bedding. Animals received analgesia as described, were weighed daily for one week check for any substantial weight loss and were checked 3 times daily for 3 days to assess activity levels and ensure the wound remained closed and showed no signs of infection.

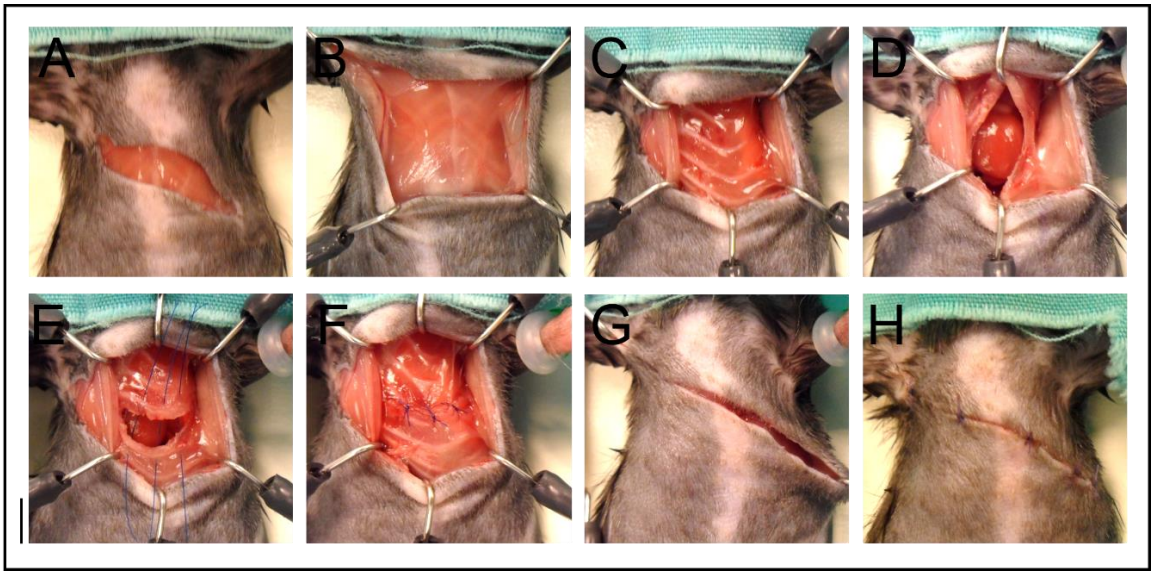

Figure 2.4 Images of MI surgical procedure.
Images of the stages of thoracotomy and closing for the MI procedure in the order performed (A-H) as described in the text. Scale bar= 5 mm.

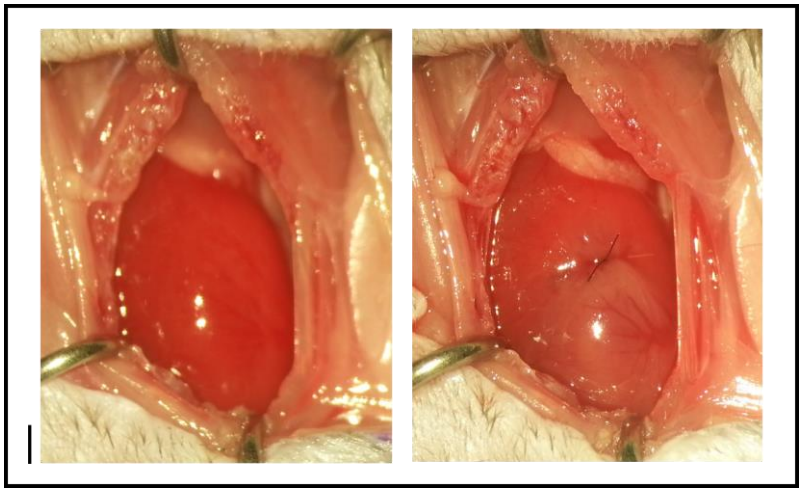

Figure 2.5 LAD ligation.
Images showing exposed mouse heart before and after LAD ligation. Blanched myocardium visible below the suture indicates successful ligation of the vessel. Scale bar= 1 mm

2.10.2 *In vivo* viral vector delivery in the mouse MI model

2.10.2.1 Adenoviral vectors

Ad vectors were delivered directly to the myocardium during the MI procedure. A viral dose of 1 x 10^9 pfu per animal was chosen based on the literature (Moilanen et al., 2011; Ruixing et al., 2007; Toivonen et al., 2012). This dose was confirmed in initial experiments utilising RAdCMV-LacZ, a reporter gene expressing adenoviral vector which enabled direct visualisation of gene transfer efficiency in the myocardium (see Chapter 4).

RAdAng-(1-9) or empty control virus (RAd60) were defrosted on ice and diluted to 1 x 10^9 pfu in a 50 µL volume using sterile PBS in a class II microbiological safety cabinet. The animals were prepared for surgery and the MI procedure carried out up until the LAD ligation (Section 2.10.1). Following LAD ligation, the sterile adenoviral vector preparation was warmed briefly to room temperature and loaded into a sterilised 50 µL Hamilton syringe (Hamilton Company, Nevada, USA) with a 30 G needle. The total volume was delivered in 5 x 10 µL injections distributed evenly across the border zone LV proximal to the blanched region of the heart. The animal was then closed and monitored post-operatively (Section 2.10.1).

2.10.2.2 Adeno-associated viral vectors

AAV9 vectors were delivered to MI animals *via* intra-venous tail vein injection following MI surgery. The viral dose per animal of 1 x 10^{11} viral geneomes (vg) was chosen based on the literature (Denegri et al., 2014; Inagaki et al., 2006) and preliminary experiments performed using an enhanced green fluorescent protein (eGFP)-expressing AAV9 control virus (see Chapter 5).

AAV was prepared and transported to the surgical theatre as described for adenovirus (Section 2.10.2.1), with 1 x 10^{11} vg prepared in a total volume of 100 µL. The MI surgery was performed up until before recovery of the animal as described (Section 2.10.1). The animal's tail was then swabbed with 70 % ethanol and heated using a heat lamp in order to visualise a tail vein. The AAV was heated briefly to room temperature and loaded into a 100 µL Hamilton syringe (Hamilton Company, Nevada, USA) with a 30 G needle. The needle was

carefully inserted into the vein and the entire volume injected. Pressure was immediately placed on the injection site using a sterile swab to prevent any leakage of the injection until no more bleeding was evident. Animals were then recovered and monitored post-operatively.

2.10.3 Echocardiography

Echocardiography was used as a means of making serial measurements of cardiac function in MI animals for longitudinal study. Both M-mode and Doppler measurements were recorded for each animal. Echocardiographic images of the mouse heart were obtained using a Siemens Acuson Sequoia 512 ultrasound unit with an 18LS probe set at a frequency of 14 MHz. Animals were anesthetised in 4 % isofluorane mixed with oxygen. They were placed on a nose cone on a heat mat where the isofluorane was reduced to 1.5 % at a flow rate of 1 L/min for the duration of the measurements. Temperature was monitored throughout using a precision thermometer with flexible probe (Harvard Apparatus, Kent, UK) with excess heat provided using a heat lamp where required. Animals were placed on their back with the forelimbs retracted slightly to open the chest but so as not to inhibit breathing. Ultrasound gel was placed on the animal's chest and on the probe and M-mode images captured in both the longitudinal and transverse axis. Imaging was kept consistent between animals by measurements being made just above where the papillary muscles could be visualised. Doppler measurements were made by placing the probe below the animal's diaphragm pointed up towards the heart to achieve a 4 chamber view. The mitral valve was located using colour-flow mapping, where blood flow toward the probe appeared as red.

Analysis was performed using ImageJ software, with measurements taken as an average between analyses of four separate images. Fractional shortening (FS) was calculated as follows:

$$FS = 100 - \left(\frac{LVESD}{LVEDD} \times 100\right)$$

Where LVEDD = Left ventricular end diastolic chamber dimension, LVESD = Left ventricular end systolic chamber dimension and FS = Fractional shortening (Figure 2.6).

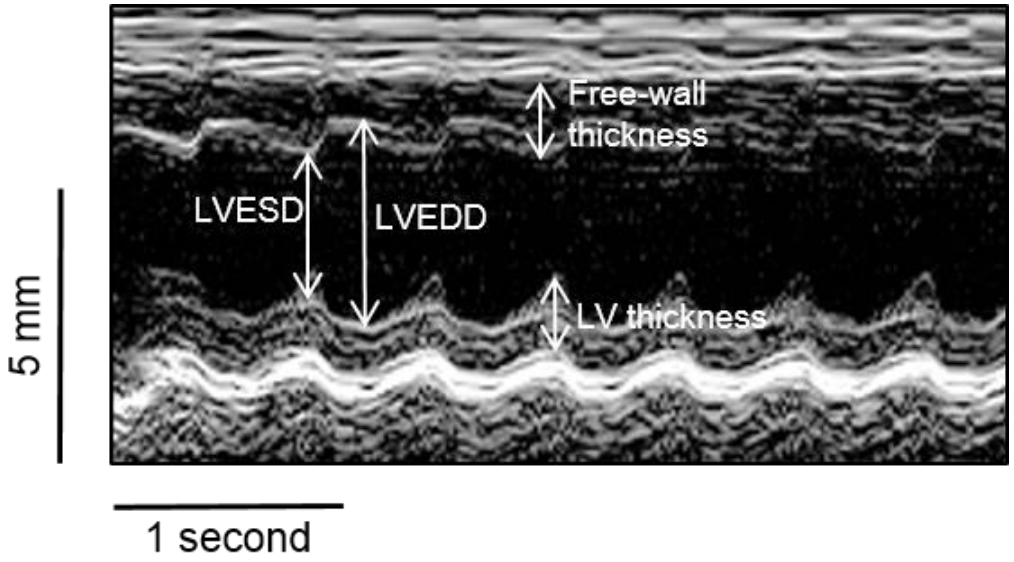

Figure 2.6 Echocardiography M-mode image analysis.
Transverse M-mode image taken in a 4-week sham animal demonstrating the measurements performed for each images to asses functional parameters and cardiac remodelling. LVEDD = Left ventricular end diastolic chamber dimension, LVESD = Left ventricular end systolic chamber dimension.

2.10.4 Pressure-volume loop measurements

Pressure-volume loop measurements are widely regarded as the gold-standard in assessing intact heart function in real-time. It is an invasive method involving the insertion of a miniature sensor catheter into the left ventricle of the heart which is able to determine ventricular pressure and true blood volume independent from loading conditions (Pacher et al., 2008).

2.10.4.1 The ADVantage PV-loop system

The ADVantage AD500 PV-loop system (Transonic Systems Inc., The Netherlands) is a small animal PV-loop system that uses admittance catheter-based technology to measure true-blood volume in real time without the need for a hypertonic saline bolus injection offset (see Section 2.10.4.5). Traditional conductance-based PV loop systems use a tetra-polar catheter placed inside the LV which stimulates an electrical field and measures conductance of both the blood pool and myocardium, over-estimating true blood volume and measuring only resistivity of the blood and myocardium, and not the capacitive properties of the cardiac tissue. Where the admittance system varies is that it is able to measure both conductive and capacitive properties of blood and tissue. When this is performed at a frequency of 20 kHz, blood has resistivity only. This allows separation of blood and muscle admittance by the system by modelling blood as only resistive and the muscle as both resistive and capacitive. Admittance technology uses production of an alternating electrical current which is phase-shifted by the charge of the cardiomyocytes themselves, causing a time-delay in the current received by the catheter compared to the emission signal. This phase-shift is used to determine muscle conductance and remove it completely from the total measured conductance. Real-time calculations are then used to determine true blood volume independent from muscle. These calculations utilise the mathematical algorithm known as Wei's equation (Wei et al., 2005) which relies on several measurements made by the catheter itself in real-time and some constants which are determined by other means (see Sections 2.10.4.4 and 2.10.4.5). The catheter itself comprises 4 platinum electrode rings which generate the current, an electrical sensing window and a membrane pressure sensor (Figure 2.7). When placed in the ventricle, 4 separate parameters are measured: pressure (mmHg), volume (μL), phase (degrees) and magnitude (μS).

Phase corresponds to the muscle-derived conductance only and admittance magnitude corresponds to both blood and muscle-derived conductance. Both phase and magnitude are calculated in real time and are dependent upon in-put information about the myocardial permitivity and conductivity properties (see Section 2.10.4.5). This information is then used to calculate true blood volume using Wei's equation (Scisence PV Technical Note) as follows:

$$Vol = \frac{1}{\left(1 - \frac{G_b}{\gamma}\right)} \rho L^2 (G_b)$$

Where ρ = blood resistivity, L = measuring electrode distance, G_b = measured blood conductance (separated from muscle conductance using admittance phase measurements) and γ is the equation as follows:

$$\gamma = \frac{-b \pm \sqrt{(b^2 - 4ac)}}{2a}$$

Where:

$$a = SV - \rho L^2 (G_{b-ED} - G_{b-ES})$$

$$b = -SV \cdot (G_{b-ED} + G_{b-ES})$$

$$c = SV \cdot G_{b-ED} \cdot G_{b-ES}$$

Where SV = stroke volume, $G_{b\text{-}ES}$ = blood conductance at end-systole and $G_{b\text{-}ED}$ = blood conductance at end-diastole.

SV is a constant determined independently and input into the system (see Section 2.10.4.4).

2.10.4.2 PV-loop surgery

Prior to surgery, the ADV500 system (Transonic Systems Inc., The Netherlands) was set up on the surgical table connected to a laptop *via* a 4-channel analogue to digital converter with Labscribe2 software (iWorx, New Hampshire, USA) open. Channels were connected in the correct order (1-4 for pressure, volume,

phase and magnitude, respectively). The 1.2 F 4.5 mm spaced PV admittance catheter (FTH-1212B-4517, Transonic Systems Inc., The Netherlands, Figure 2.7) was connected to the ADV500 box and carefully secured in a clamp stand above a pre-heated tissue bath set at 37 °C and soaked in warmed 5 % NaCl saline for 1 hr prior to use so that calibration could be performed at physiological temperature. Upon first use, a 2 point in-built calibration specific for mouse was performed (Table 2.6) and recorded for each channel and the Labscribe2 file saved to be used for each subsequent recording. Prior to each insertion of the catheter into the carotid, a fine adjustment was performed to balance the pressure signal.

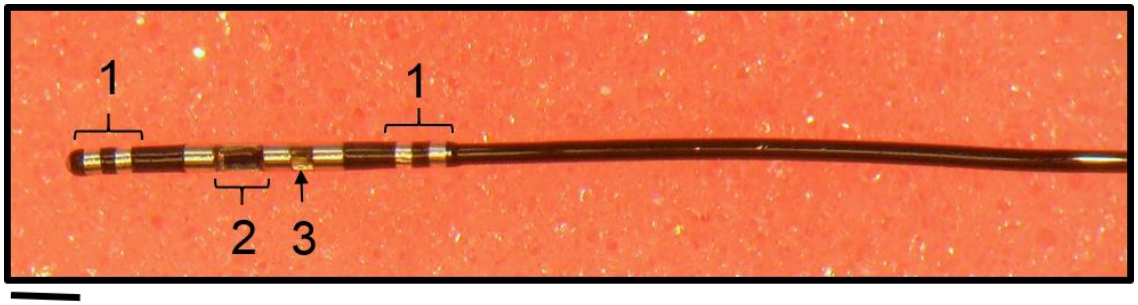

Figure 2.7 ADVantage PV-loop mouse admittance catheter.
Image of the 1.2 F, 4.5 mm spaced mouse ADVantage PV-loop system catheter. 1= four platinum ring electrodes for absolute volume measurements, 2= Pressure membrane sensor and 3= electrical sensor window. Scale= 1 mm.

Table 2.6 Two point calibration values for mouse using ADVantage PV-loop system.

	Calibration value	
Output	**Low**	**High**
Pressure (mmHg)	0	100
Volume (μL)	0	150
Phase (degrees)	0	20
Magnitude (μS)	0	5000

Mice were induced and intubated as described in Section 2.10.1.1. The mouse was positioned upside down with its cranial end towards the surgeon (Figure 2.8) and placed on a homeothermic monitoring system (Harvard Apparatus, Kent, UK) which was used to keep body temperature at 37 °C for the duration of the procedure, with a heat lamp used for extra heat where required. The animal was laid on its back and its fore-limbs retracted gently and taped to the heat mat. One hind-limb was left free in order to monitor the flexor withdrawal response. Isofluorane concentration was reduced gradually throughout the procedure and measurements were taken at 1.5 %. A vertical incision was made in the skin of the neck which was retracted using elastic blunt hook retractors (Harvard Apparatus, Kent, UK). Underlying muscle was blunt dissected and retracted in the same manner, with care taken not to disturb the trachea. Further blunt dissection was performed to free the right carotid artery of surrounding tissue. The vessel was kept moist using warmed 5 % NaCl saline throughout the remainder of the procedure. The vessel was permanently occluded at the cranial end using a length of 6-0 silk braided suture (Pearsalls, Somerset, UK) sutured tightly around the vessel. The length of the suture was used to anchor the vessel and raise it slightly to simplify the remainder of the procedure. Two pre-tied single-throw sutures were positioned around the vessel and the blood flow at the dorsal end temporarily occluded using a weighted length of suture wrapped around the vessel (Figure 2.9). The prepared catheter was then moved to the surgical table and the receiver taped down securely. Ensuring blood flow in the vessel had been suspended, a small incision was made using micro-dissection scissors in the cranial end of the carotid artery. A small amount of blood loss confirmed successful perforation. The catheter was then inserted into the vessel and the two pre-tied sutures tightening to hold it in place, avoiding the electrodes and sensing windows. The temporary dorsal occlusion was then removed and blood flow returned to the vessel (Figure 2.10). Data recording was established on the ADV500 box and Labscribe2 software. The catheter was advanced down into the left ventricle, with successful entry confirmed with a drop in the end diastolic pressure reading to near 0 mmHg. Optimal positioning of the catheter into the centre of the ventricle was achieved initially using a real time pressure *vs.* magnitude plot and positioning the catheter so that the phase value read as low as possible (typically <5°) and the loop was as large as it could be. Once optimal placement was achieved, a baseline scan was performed

on the ADV500 box. This calculates blood and myocardial electrical parameters and applies them to Wei's equation to generate true blood volume which appears as an additional channel to phase and magnitude. At this stage the loop can be viewed as pressure *vs.* volume channels and the animals temperature was adjusted to 37 °C and the isofluorane concentration reduced to 1.5 %. A 5 min acclimatisation period was then allowed before a further baseline scan followed by a 10 min steady state recording period.

Following steady state, a vena cava occlusion was performed in order to assess left ventricular stiffness and diastolic dysfunction. An incision was made just below the xiphoid process through the skin and muscle, with care taken not to cause any excessive bleeding. The liver was depressed slightly using a clean cotton bud in order to visualise the vena cava behind it next to the diaphragm (Figure 2.11). Slow, gradual occlusion of the vessel was achieved while still recording the PV-loop data by gently depressing the vessel using a clean cotton bud, resulting in a 'family of loops' cause by gradual reduction of both pressure and volume parameters due to decreased cardiac loading. Finally, the animals underwent Schedule 1 *via* cervical dislocation.

Figure 2.8 PV-loop surgical set up and animal positioning.
Images showing positioning of animal as described in the text and the positioning of the ventilator and recording equipment in relation to the surgical area.

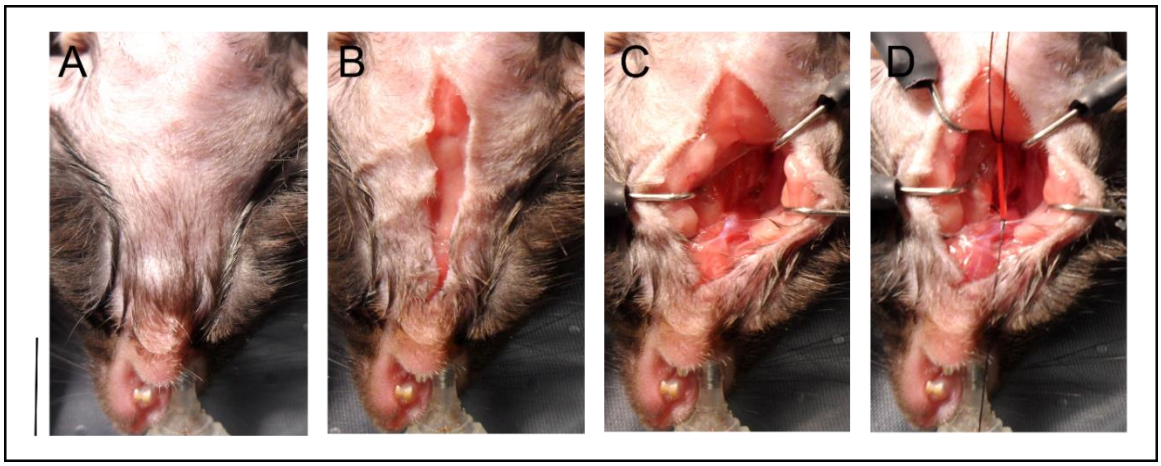

Figure 2.9 PV loop surgical carotid artery dissection.
Sequential images showing the stages of carotid dissection for insertion of the PV-loop cathter. (A) Visualisation of the animal neck area. (B) Vertical incision made in the skin. (C) Blunt dissection and retraction of the surrounding tissue and muscle. (D) Cranial permanent occlusion and dorsal temporary occlusion and re-positioning of the carotid artery. Scale bar= 1 cm.

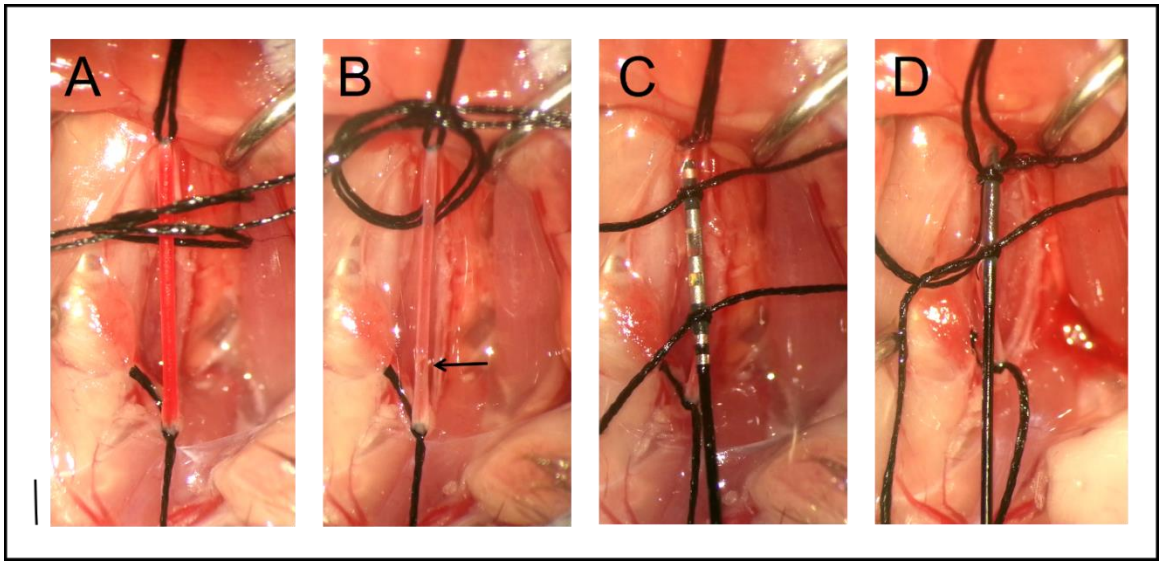

Figure 2.10 PV-loop carotid catheter cannulation.
Sequential images showing carotid cannulation and insertion of the PV-loop catheter. (A) Pre-tied suture positioned around vessel. (B) Incision made into the cranial end of the carotid (indicated by the arrow). (C) Insertion of the catheter through the incision and securing it in place by tightening sutures. (D) Advancement of catheter into the vessel down into the left ventricle. Scale bar= 1 mm.

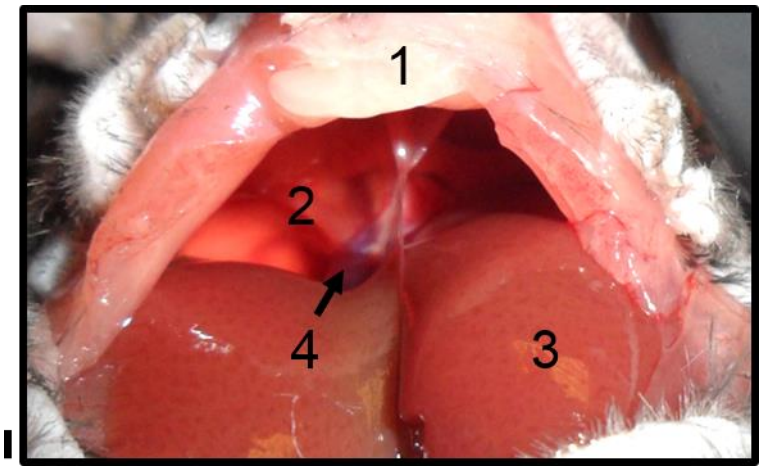

Figure 2.11 PV-loop vena cava occlusion.
Image showing visualisation of the vena cava prior to occlusion.1= Xiphoid process, 2= Diaphragm, 3= Liver and 4= vena cava. Scale bar= 1 mm.

2.10.4.3 PV-loop analysis

PV-loop data was analysed offline in Labscribe2 software by generation of an average loop from analysis of 2 min steady-state recording and determination of multiple haemodynamic and contractile parameters based on this average loop. Stiffness was determined using the end-diastolic pressure-volume relationship (EDPVR) by fitting a non-linear exponential equation to the end-diastolic pressure and volume points generated from the family of loops produced through vena cava occlusion. The equation is as follows:

$$EDP=Cexp^{(\beta*EDV)}$$

Where EDP= end-diastolic pressure, EDV= end-diastolic volume, C= a curve fitting constant and ß= the diastolic stiffness coefficient (Burkhoff et al., 2005).

2.10.4.4 Aortic flow-probe surgery

Aortic flow probe measurements were performed using a Transonic MA1.5PSL mouse flowprobe and T5420 transit-time perivascular flow meter (Transonic Systems Inc., The Netherlands). Theatre was prepared for surgery as described in Section 2.10.4.2. The perivascular flow meter was positioned on the surgical table and connected to a laptop *via* an analogue to digital converter and Labscribe2 (iWorx, New Hampshire, USA) software opened. The flow probe was connected to the flow meter and soaked in clean 5 % NaCl saline warmed to 37 °C for 1 hr prior to surgery. A 2 point calibration of the probe was then performed using two in-built values (0 V= 0 mL/min and 1 V= 5 mL/min). Animals were induced, intubated and positioned as described (Section 2.10.4.2). Temperature was monitored throughout using a homeothermic monitoring system (Harvard Apparatus, Kent, UK) and isofluorane reduced gradually throughout the procedure. A right-thoracotomy was performed in a similar fashion to the left-thoracotomy carried out for the MI procedure (Section 2.10.1.2), however entry into the chest was made *via* the 2nd intercostal rib space. Upon entry and retraction of the ribs, the aorta became immediately obvious (Figure 2.12). Very careful blunt dissection around the aorta was performed to allow placement of the probe around the vessel, with care taken not to rupture any vessels or disturb the right atria. A piece of 6-0 silk braided

suture (Pearsalls, Somerset, UK) was looped under the vessel to aid positioning of the flow probe. The flow probe was prepared by drying on a clean swab and insertion of surgical lubricant (Savage Labs, New York, USA) into the sensing window to ensure no air pockets interfered with the signal. The probe body was then inserted into the surgical cavity and the suture loop used to gently lift the vessel and place it into the sensing window (Figure 2.12). More surgical gel was inserted around the probe once placed. Cardiac output (CO) was measured in Labscribe2 software and a micro-manipulator arm used to achieve optimum flow readings. Isofluorane concentration was reduced to 1.5 % for the duration of the measurements. A 5 min acclimatisation period was allowed before steady state measurements were taken for 5 min. Following surgery, the probe was carefully removed and soaked in a 1 % solution of biological enzyme (Tergazyme, Alconex, New York, USA) for 1 hr, rinsed thoroughly with distilled water and air-dried prior to storage. Data was analysed offline using Labscribe2 software. The average SV calculated from average CO values from a group of animals was used to determine true blood volume as part of Wei's equation for PV-loop measurements. Flow probe measurements carried out in adult male C57BL/6 mice demonstrated an average CO of 9± 1.29 mL/min, an average HR of 466± 11.4 bpm and an average SV of 20± 3 µL (*n*= 3, Figure 2.13). Individual animal measurements are shown in Table 2.7. Therefore, SV was set at 20 µL for subsequent PV-loop measurements. This was within the normal SV range (17-30 µL) reported elsewhere for mice anaesthetized with isofluorane (Pacher et al., 2008).

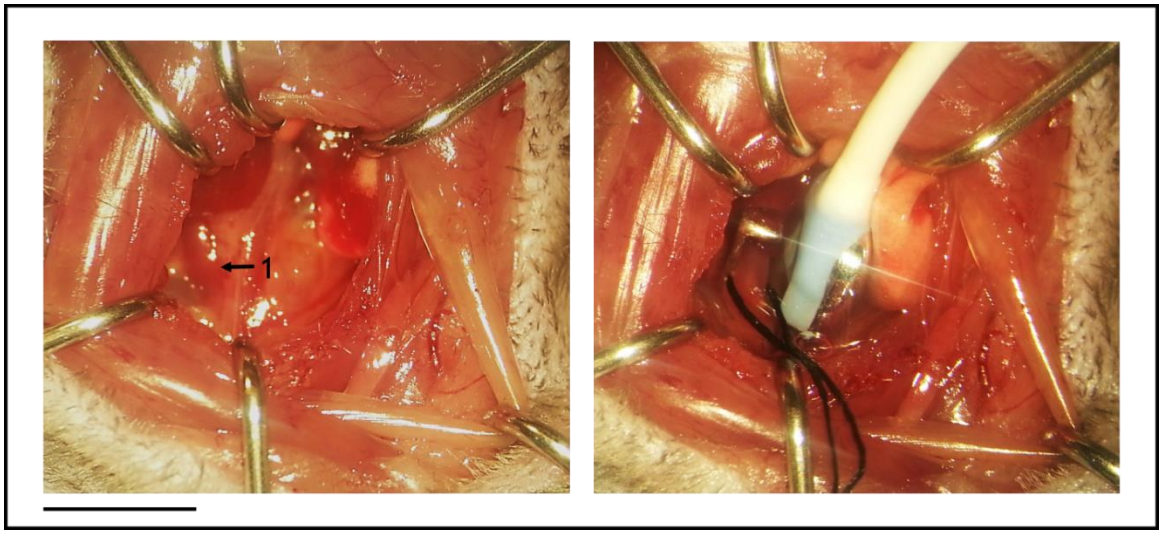

Figure 2.12 Aortic flow-probe placement.
Images demonstrating the view upon entry into the chest cavity with immediate visualisation of the aorta (1) and placement of the vessel into the flow probe. Scale bar= 5 mm.

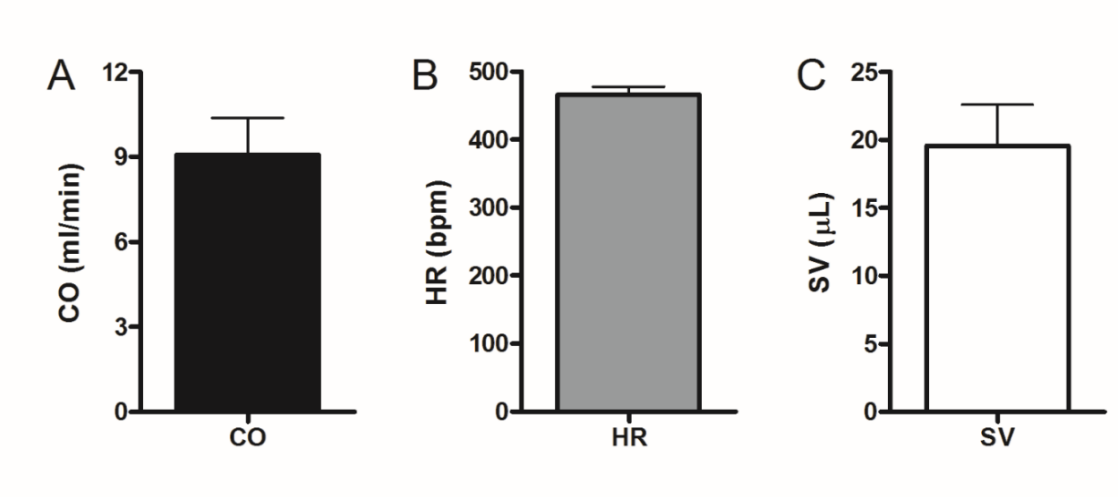

Figure 2.13 Flow probe measurements.
Flow probe analysis of adult C57BL/6 mice for determination of CO (A), HR (B) and SV (C), *n*= 3. Data presented as mean± SEM. CO= cardiac output, HR= heart rate, SV= stroke volume.

Table 2.7 Individual animal flow probe measurement indices.

Animal	CO (mL/min)	HR (bpm)	SV (µL)
1	11.59	459.36	25.23
2	7.31	488.06	14.97
3	8.35	450.35	18.53

2.10.4.5 Murine myocardial permittivity and conductivity measurements

Traditional conductance-based catheter systems for the measurement of left-ventricular blood volume rely on hypertonic saline bolus offset to differentiate the contribution of the parallel admittance of the myocardium to the conductance measurements of the blood (Raghavan et al., 2009). However, due to the small size of mice, the bolus significantly alters haemodynamic properties of the heart, making it a less than optimal approach for assessing true blood volume in this setting (Raghavan et al., 2009). The admittance-based catheter technology used here utilises an in-built offset for myocardial interference, i.e. contribution of the cardiac muscle conductivity to the calculation of blood volume, with reading of true blood volume by utilising pre-determined myocardial conductance properties of the murine myocardium which is used as part of Wei's equation (Section 2.10.4.1) in determining blood volume. Previous studies (Porterfield et al., 2009) have determined conductivity: permittivity (σ: ε) ratios in normal and aortic-banded C57BL/6 mouse hearts using epicardial surface probe measurements, determining a ratio of 800 thousand units/s (K/s) for normal mice (Porterfield et al., 2009). It was reported that in a diseased state, the myocardial electrical properties are altered, with a decrease in ratio to 700 K/s in the hypertrophied myocardium of the aortic banded mice. In the ADVantage system, the 'heart type' or σ: ε ratio is pre-set at 800 K/s, however this can be modified on the system. In order to establish the heart type that should be used in the MI model, an epicardial surface calibration probe (FM-1987-1H, Transonic Systems Inc., The Netherlands) was used.

Animals were prepared for surgery, intubated and positioned as described (Section 2.10.4.2). Temperature was monitored throughout using a homeothermic monitoring system (Harvard Apparatus, UK). A left thoracotomy was performed identical to that described (Section 2.10.1.2). In MI animals any adhesive tissue was carefully dissected away to expose the left ventricular wall. The surface probe was connected to the ADVantage system control box and measurements recorded in Labscribe2 software (iWorx, New Hampshire, USA). To take measurements, the probes electrodes were placed on the moist epicardial surface of the non-infarcted LV, avoiding any major blood vessels. A micromanipulator was used to hold the probe in place and a steady state flow recording was taken. The probe was then removed, rinsed well and air dried

before storage. Recordings were analysed offline by averaging the steady state measurement in Labscribe2 software. Average ‘heart-type’ values were determined by averaging α:ε ratios for each group of animals. The heart type was determined in both 8 week sham and MI animals using permittivity probe measurements of the myocardium (Figure 2.14). Both sham and MI α:ε ratios were determined to be approximately 800 K/s with no significant differences between the two groups (n= 5 per group, $p>0.05$). Therefore, heart type remained at the system default setting of 800 K/s for both sham and MI animals.

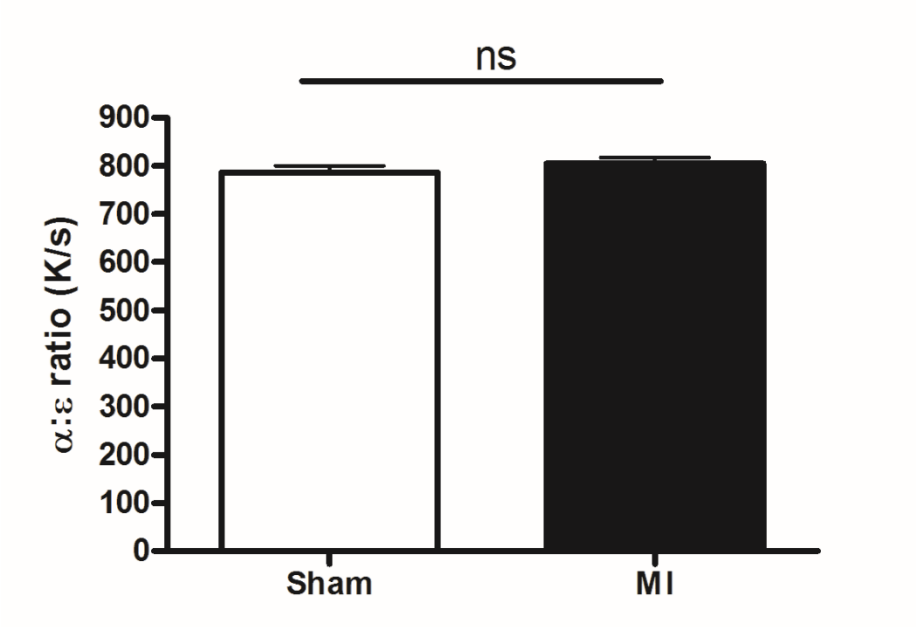

Figure 2.14 Cardiac permittivity measurements.
Cardiac permittivity measurements for 8 week sham and MI animals, *n*= 5 per group. Data presented as mean± SEM.

2.10.5 Animal post-mortem and tissue harvest

Mice were euthanized rapidly *via* cervical dislocation. Organ weights were taken as a measure of cardiac hypertrophy and dysfunction. Hearts were rapidly excised and immediately washed in a beaker of ice-cold 5 % NaCl saline before being cannulated and perfused with the same solution. Hearts were photographed and dabbed dry on a swab before being weighed. All lobes of the lung and liver were excised, washed and dabbed dry before being weighed. All organ weights were normalised to tibia length. Cardiac tissue was preserved in paraformaldehyde for histology and snap frozen for gene expression analysis. For hearts taken for both uses, a longitudinal section of the heart was snap frozen in liquid nitrogen and stored at -80 °C, with the remainder placed in 10 % neutral buffered saline with 4 % paraformaldehyde (Cellstore, UK) overnight before being stored in 1 x PBS prior to processing. For whole hearts taken only for gene expression analysis, dissection was first performed to separate the hearts into the following regions: scar, border (peri-infarct), remainder LV, remote LV, septum and RV. The paleness of the scar tissue made it easily distinguished from non-infarcted myocardium and was removed first. A 1 mm region of tissue proximal to the scar region was then removed as the border region. The RV and septum were then separated from the LV, which was subsequently divided into two sections: the remote LV proximal to the atria and the remainder LV proximal to the border region. The remote LV was utilised for gene expression analysis. Dissection was performed accurately using micro dissection instruments and a dissection microscope.

2.11 Histology

2.11.1 Tissue processing

Following fixation, tissue sample were processed on a Shandon Excelsior tissue processor (Thermo Scientific, Basingstoke, UK, Table 2.8) and embedded in paraffin wax the following day for histological use. Hearts were mounted longitudinally in order to visualise all cardiac structures. Tissue sections were prepared for IHC and histology by first chilling the paraffin blocks on a cold plate before using a microtome to cut sections at a thickness of 4 μm which were then dried on Tissue-Tek adhesion microscope slides (Sakura, Thatcham, UK)

overnight at 50 °C and stored at room temperature until use. For heart tissue blocks, serial sections were taken every 100 µm until the chambers of both ventricles became evident. Sections for staining were taken at this point in an effort to keep the tissue depth consistent between animals. Prior to histological staining or IHC, sections were de-paraffinised and re-hydrated using Histoclear and decreasing concentration gradients of ethanol.

Table 2.8 Processing sequence for paraffin embedding of tissue samples.

Solution	Incubation Time (min)
70 % Ethanol	30
95 % Ethanol	30
100 % Ethanol	30
100 % Ethanol	30
100 % Ethanol	45
100 % Ethanol	45
100 % Ethanol	60
Xylene	30
Xylene	30
Xylene	30
Paraffin Wax	30
Paraffin Wax	45
Paraffin Wax	45

2.11.2 Immunohistochemistry

Tissue sections were cut and rehydrated as described in Section 2.11.1. Endogenous peroxidase activity was quenched using incubation in 3 % H_2O_2 in distilled H_2O for 30 min at room temperature followed by a 5 min wash in distilled H_2O. Sodium citrate antigen retrieval was then performed (for all primary antibodies apart from anti-ß-galactosidase). 10 mM sodium citrate solution was heated until boiling. Sections were placed in a plastic rack, submerged in the hot solution and heated for 15 min, slides were then cooled for 30 min to ensure correct re-folding of the antigen. Slides were washed in running tap water for 5 min. Blocking was performed to prevent non-specific antibody binding using incubation with the appropriate blocking solution (Table 2.9) for 30 min at room temperature. Blocking solution was removed and slides incubated with primary antibody diluted in a reduced concentration blocking solution for the appropriate length of time (Table 2.9). Rabbit IgG diluted to the same final concentration was used as a negative control. Following primary antibody incubation, slides were washed for 3 x 5 min using the appropriate wash buffer before incubation with the appropriate secondary antibody diluted in reduced concentration blocking solution for the specified time (Table 2.10). Sections were washed for 3 x 5 min using wash buffer. For secondary antibodies conjugated directly to HRP, 3,3'-Diaminobenzidine (DAB) staining could be performed directly. For biotinylated antibodies an extra step was performed to attach a HRP-labelled avidin-biotin or streptavidin-biotin complex to the secondary antibody. Avidin and streptavidin molecules have a very high affinity for biotin and as such will bind to the biotinylated antibody, amplifying the signal. For anti-collagen III, the VECTASTAIN standard ABC reagent kit was used (Vector Laboratories, Peterborough, UK) as per the manufacturer's instructions. Two drops of each reagent A and B were mixed in 5 mL of PBS and incubated at room temperature for 30 min to allow avidin-biotin complexes to form. Sections were then incubated with the ABC for 30 min before being washed well for 3 x 5 min in PBS and DAB staining performed. For anti-eGFP and ß-galactosidase, Streptavidin peroxidase (Sigma-Aldrich, Poole, UK) was used. Streptavidin was diluted 1: 200 in PBS/TBS and incubated on the slides for 30 min at room temperature before the slides were washed for 3 x 5 min and DAB staining performed.

The Vector DAB substrate kit (Vector Laboratories, Peterborough, UK) was prepared as per the manufacturer's instructions (2 drops of buffer, 4 drops of DAB chromagen, 2 drops of H_2O_2 and 2 drops of nickel (optional) per 5 mL of distilled H_2O). The prepared substrate was added to one slide and a stopwatch started. The slide was monitored under a microscope to look for colour development. As soon as the dark-brown staining became apparent the slide was placed in distilled H_2O to stop the reaction and the time of incubation noted. All slides were then developed for this length of time to keep staining intensity consistent. This was typically between 1-5 min. Slides were washed in running tap water for 5 min before counter-staining of the nuclei for 30 s in Harris haematoxylin (Sigma-Aldrich, Poole, UK). Slides were washed for 5 min in running tap water before being dehydrated using the reverse of the re-hydration procedure. Slides were then mounted using DPX histological mounting medium (Merck Chemicals Ltd., Nottingham, UK) and dried overnight at room temperature.

Table 2.9 Primary IHC antibodies and reaction conditions.

Protein	Concentration	Company & Clone number	Host Species	Dilution	Blocking Solution	Incubation Time
eGFP	0.5 mg/mL	Abcam (ab6556)	Rabbit	1:200	15 % normal goat serum in TBS-T	Overnight at 4 °C
ß-galactosidase	2.5 mg/mL	MP-Biomedicals (8559762)	Rabbit	1:350	20 % normal goat serum in PBS	1 hr at room temperature
Mouse collagen I	1 mg/mL	Abcam (ab34710)	Rabbit	1:200	6 % normal goat serum in 1% BSA/PBS	Overnight at 4 °C
Mouse collagen III	1 mg/mL	Abcam (ab7778)	Rabbit	1:1000	2 % normal goat serum in PBS-T	Overnight at 4 °C

Table 2.10 Secondary IHC antibodies and reaction conditions.

Protein	Secondary Antibody	Concentration	Company & Clone number	Host Species	Dilution	Incubation Time
eGFP	Anti-rabbit IgG biotinylated	1.5 mg/mL	Vector (BA-1000)	Goat	1:200	2 hr at room temperature
ß-galactosidase	Anti-rabbit IgG biotinylated	1.5 mg/mL	Vector (BA-1000)	Goat	1:200	30 min at room temperature
Mouse collagen I	Anti-rabbit IgG HRP	0.25 mg/mL	Dako (P0448)	Goat	1:100	45 min at room temperature
Mouse collagen III	Anti-rabbit IgG biotinylated	1.5 mg/mL	Vector (BA-1000)	Goat	1:500	30 min at room temperature

2.11.3 Picrosirius red staining

Tissue sections were re-hydrated and incubated in a 1 mg/mL solution of Sirius red (Sigma-Aldrich, Poole, UK) in saturated picric acid (picrosirius red stain) in the dark at room temperature for 90 min. Sections were washed 2 x 3 min in 0.01 N HCl acidified water followed by dehydration in 2 x 3 min washes in 100 % ethanol and 2 x 7 min washes in Histoclear. Sections were mounted using DPX histological mounting medium (Merck Chemicals Ltd., Nottingham, UK) and dried overnight at room temperature.

2.11.4 Imaging and analysis

Once dry, IHC and picrosirius red sections were imaged on an EVOS FL colour imaging system (Life Technologies, Paisley, UK). Whole sections were imaged and captured as 8-bit TIFF files which were exported directly to an external memory source. Staining quantification was performed using ImageJ software. For whole heart sections, quantification was performed per region of the heart (scar, LV, RV and septum) with an equivalent apical section taken as a scar region in non-MI animals. For analysis, images were split into a red-green-blue (RGB) image stack. For DAB staining, quantification was performed on the blue image and for picrosirius red the green image was used. In each case a colour-intensity threshold was set to include all positive-stained pixels in the image and staining quantified as the % of total pixels within the intensity threshold of a selected area of interest. For vessel-associated staining quantification, images were analysed in the same way with the region of interest limited to any vessels visible in the image. Scar sizing in MI animals was performed using measurements in picrosirius red stained sections using the following equation:

$$\text{Infarct size } (\%) = \frac{\text{EPI infarct ratio} + \text{ENDO infarct ratio}}{2} \times 100$$

Where EPI ratio= epicardial infarct length/epicardial circumference and ENDO ratio= endocardial infarct length/ endocardial circumference. Measurements were performed on two sections approximately 200 μm apart per heart. The infarcted area was defined as where >50 % of the thickness of the myocardium was fibrotic tissue.

2.11.5 Wheat germ agglutinin staining

Tissue sections were re-hydrated and underwent sodium citrate antigen retrieval as described in Section 2.11.2. Sections were blocked for 1 hr at room temperature with 1 % BSA in PBS and 5 % goat serum. Next, sections were incubated with 10 µg/mL of WGA conjugated with Alexa Fluor 555 (Life Technologies, Paisley, UK) diluted in the blocking solution for 1 hr at room temperature in the dark. Slides were washed in PBS for 2 x 5 min before being dabbed dry and mounted with Prolong Gold anti-fade reagent + 4',6-diamidino-2-phenylindole (DAPI) to stain nuclei (Life Technolgies, Paisley, UK). Slides were dried at room temperature overnight and stored in the dark at 4 °C prior to imaging.

2.11.5.1 Confocal imaging and image analysis

Confocal images of WGA stained sections were taken using a LCI Plan-Neofluar 25x/0.8 1 mm Korr Ph2 confocal water-immersion objective lens on a Zeiss laser scanning confocal microscope (LSM 510 Meta, Carl Zeiss Ltd., Cambridge, UK) and accompanying software. Line-scan images were obtained using Diode 405-30 (excitation of DAPI) and HeNe 543 (excitation of WGA) lasers with a total exposure time of 1 min and 40 s. Images of cellular cross-sections of cardiomyocytes in both transverse and longitudinal axis of the LV were captured for each heart section and exported as 8-bit TIFF files.

Images were exported into ImageJ where a macro setting a scale for each image was applied. Cell length (longitudinal images) and cell diameter (transverse images) was measured for each image. Two sections and two images per cellular orientation of the LV were analysed per animal. Cells were chosen at random using placement of a grid pattern overlying the image with cells selected where grid lines intersected. Cell length and diameter was determined for each animal by averaging all cell measurements. Exclusion criteria were applied for minimum cell length of <70 µm to account for not being able to observed the whole cell given the optical sectioning of the confocal microscope.

2.12 β-Galactosidase staining

In order to stain for ß-galactosidase activity in intact tissue samples preserved in paraformaldehyde, 5-bromo-4-chloro-3-indolyl-ß-D-galactosidase (X-GAL) staining was used. X-GAL (Melford Laboratories, Ipswich, UK) was re-suspended in dimethylformamide (DMF) to achieve a final stock concentration of 20 mg/mL and stored at -20 °C and defrosted to make up the stain as needed. The X-GAL stain was made fresh and stored at 4 °C for a maximum of 7 days. The composition was as follows (final concentrations): Na_2HPO_4 1.54 mM, NaH_2PO_4 0.46 mM, $MgCl_2$ 26.00 µM, $H_3Fe(CN_6)_6$ 60.00 µM, $H_4Fe(CN_6)_6$ 60.00 µM and 1.00 mg/mL X-GAL. After fixation, tissue samples were washed well 2 x in PBS and submerged in X-GAL stain. Samples were incubated in the stain in the dark overnight at 37 °C and then washed 2 x in PBS. Areas of positive ß-galactosidase expression appeared dark blue after staining. Tissue samples were photographed and were processed and wax-embedded as described (Section 2.11.1).

2.13 eGFP assay

An eGFP assay was used in order to assess transgene expression within cell lysates using the eGFP fluorescence intensity of a lysed tissue sample in relation to protein concentration. First, 25-30 mg of frozen tissue harvested in liquid nitrogen as described in Section 2.10.5 was placed on dry ice in a 2 mL Eppendorf tube. A 5 mm stainless steel bead (Qiagen, Manchester, UK) and 300 µL of 1 x reporter lysis buffer (5 x stock diluted to 1 x in PBS, Promega, Southampton, UK) was added to each tube. Tissue was lysed on a Qiagen Tissue Lyser (Qiagen, Macnchester, UK) at 20 Hz for 3 x 90 s. Samples were shaken on ice for 10 min to ensure total lysis of all the tissue before remaining debris was removed from the samples *via* centrifugation in a table top centrifuge at full speed for 5 min. The supernatant was removed to a fresh tube and placed on ice and the debris and bead discarded. Next, 20 µL of each sample was pipetted into a well of a black 96-well plate (BD Biosciences, Oxford, UK) in duplicate and made up to a total volume of 100 µL by addition of 80 µL of 1 x reporter lysis buffer. As a negative control, 100 µL of 1 x reporter lysis buffer was used. The plate was incubated in the dark at room temperature for 10 min before fluorescence was determined on a Wallac VICTOR2 plate reader (PerkinElmer, Wallac, Finland) *via* excitation at 488 nm and emission recorded at 509 nm.

Fluorescence was normalised to protein concentration of each sample determined *via* BCA assay (Section 2.7.2). Fluorescence was expressed as relative light units (RLU) per mg of protein.

2.14 Mouse cardiomyocyte isolation

Single mouse ventricular cardiomyocytes were isolated from the hearts of adult C57BL/6 mice *via* constant-flow Langendorff retrograde perfusion with collagenase type I enzyme (Figure 2.15). This method involves cannulation of the aorta resulting in perfusion through the coronary system of the enzymatic solution which digests extracellular matrix and connective tissue, yielding single cardiomyocytes in the solution.

Adult C57BL/6 mice were euthanized *via* cervical dislocation and the heart and lungs rapidly excised *via* thoracotomy and washed in a beaker of ice cold Krebs-Heinseleit solution (Figure 2.15). The lungs and surrounding tissue were dissected in order to free and identify the aorta. The heart was cannulated using a 1 mm diameter catheter and secured using 6-0 silk braided suture (Pearsalls, Somerset, UK). The peristaltic pump was switched on in order to begin constant perfusion of the heart at a rate of 4 mL/min with 37 °C Krebs-Heinseleit solution. Blood clearing from visible vasculature on the surface of the heart was used as confirmation of successful cannulation. The heart was placed vertically in a clamp stand and perfused until the perfusate ran clear (1-2 min) before the addition of collagenase I (Worthington Chemicals, USA) and protease type XIV (Sigma-Aldrich, Poole, UK) directly to the Krebs-Heiseleit reservoir at final concentrations of 0.7 mg/mL and 0.07 mg/mL, respectively. Digestion times varied between preparations, but on average were performed for 6 min, with adequate digestion observed as a paling of the cardiac tissue and loss of obvious vessel architecture. As the digestion progressed, noticeable paling of the heart was observed (Figure 2.16 A and B). After adequate digestion time a 3-way tap was used to change the source of the perfusate to a second reservoir containing pre-warmed 0.5 % BSA in Krebs-Heiseleit solution. Perfusion of the BSA solution was continued for a further 4 min in order to deactivate the enzyme and prevent over-digestion. The heart was then cut down from the cannula and the atria, vessels and RV removed (Figure 2.16 C). The remaining LV and septal tissue was cut into small pieces and placed in a 15 mL Falcon tube with 5 mL of BSA

solution. Trituration using a flame-blunted Pasteur pipette was used to agitate the tissue and release the individual cells from any remaining tissue into suspension (Figure 2.16 D and E). Any remaining tissue was allowed to settle to the bottom of the tube and the cell suspension aspirated off and placed in a new tube. This process was repeated twice more with the remaining tissue to achieve a total volume of 15 mL. This was concentrated gently using a hand-operated centrifuge to pellet the cells. The supernatant was removed and discarded and the cells re-suspended in 5 mL of fresh BSA solution. The calcium concentration of the cellular suspension was raised gradually from 0 to 1 mM by the addition of 1 µL/mL of 100 mM $CaCl_2$ solution to the suspension every 5 min to prevent cellular hyper-contraction as a result of the calcium paradox (Chapman and Tunstall, 1987). This is a manifestation which occurs when cardiomyocytes are in a nominally Ca^{2+}-free surrounding. The re-introduction of physiological Ca^{2+} levels immediately results in an influx of Ca^{2+} which binds the myofilaments and causes hyper-contraction and balling of the cell. Re-introducing Ca^{2+} gradually minimises this. The final cellular suspensions compromises recognisable rod-shaped cardiomyocytes with visible striations and hyper-contracted ball-shaped cells which occur as a result of damage of the sarcolemma, either as a result of enzymatic activity or physical damage, allowing influx of Ca^{2+} into the cell (Figure 2.16 F and G).

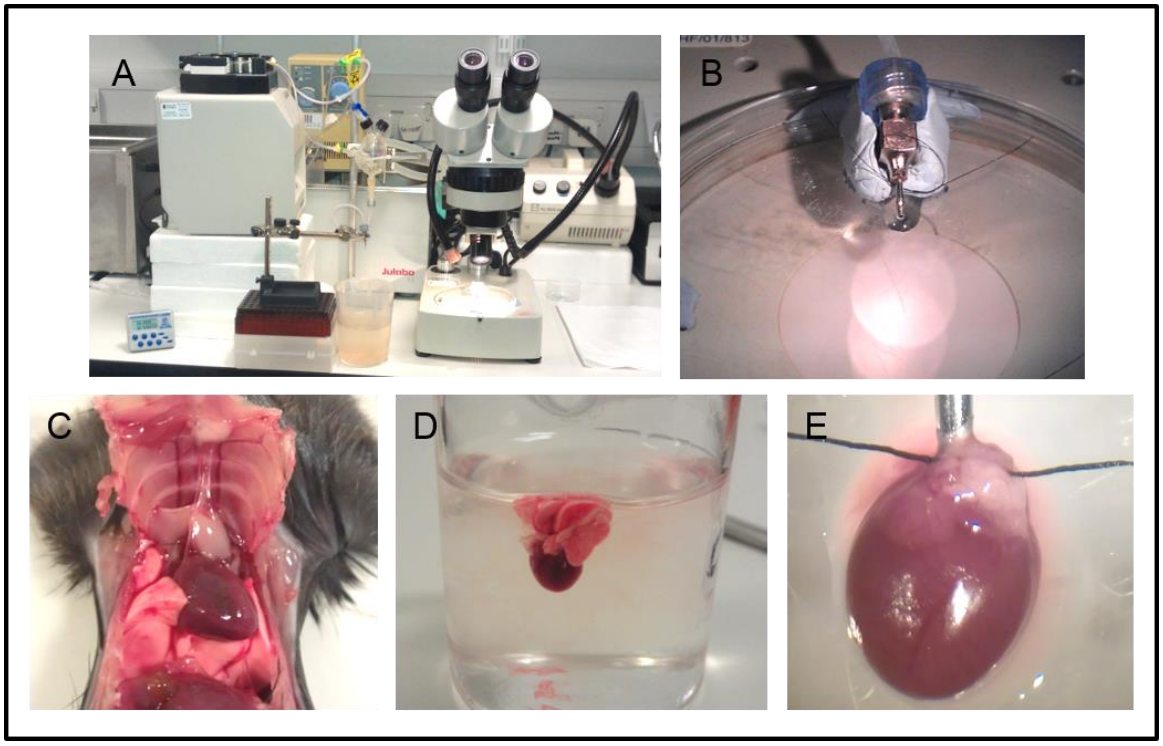

Figure 2.15 Mouse cardiomyocyte isolation Langendorff set-up, heart excision and cannulation.
Images showing Langendorff rig set-up (A), cannula positioned under dissection microscope with pre-tied suture (B) and dissection, washing and cannulation of the heart (C-E).

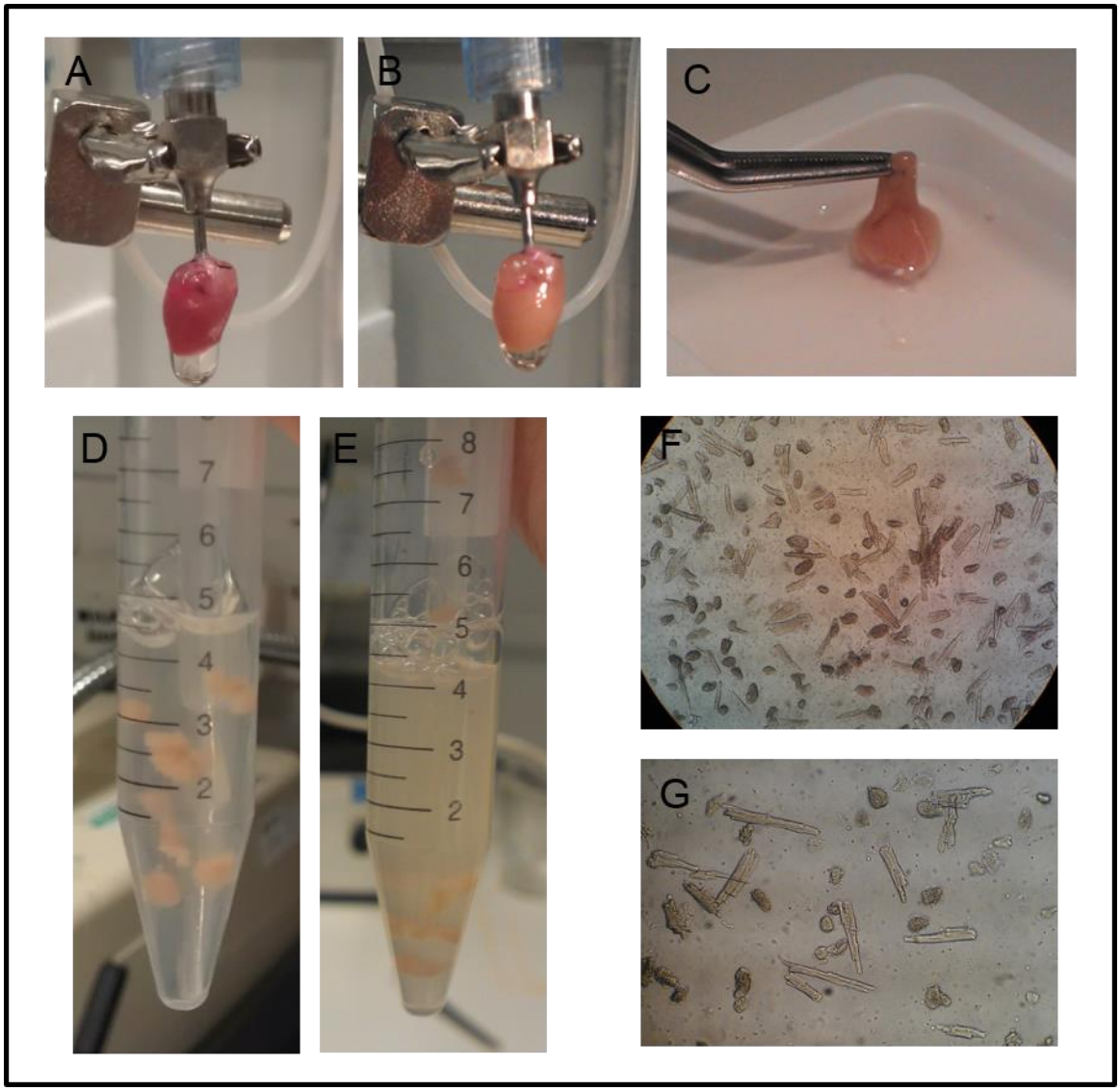

Figure 2.16 Mouse cardiomyocyte isolation collagenase I digestion.
Images showing collagenase I digestion of the mouse heart to yield single cells. Enzyme perfusion of the heart results in noticeable paling of the cardiac tissue (A & B). After digestion the RV, atria and vessels are discarded (C) and the remaining tissue agitated to dissociate the cells (D & E). Rod and ball-shaped myocytes are visible in the preparation (F & G).

2.15 Single cardiomyocyte Ca^{2+}-handling measurements

2.15.1 Epifluorescence microscopy

The use of epifluorescence microscopy to image Ca^{2+} in isolated cardiomyocytes requires the use of a Ca^{2+}-sensitive fluorescent probe, or fluorophore. Ratiometric fluorophores are particularly appropriate for this purpose as they correct for differential dye-loading and path-lengths which may cause misleading [Ca^{2+}] measurements. Differential path length and dye loading stems from heterogeneity in cellular morphology, meaning photons from different parts of the cell travel to the detector *via* different paths. For measurements in static cells this can be accounted for by normalisation to a baseline measurement, however as cardiomyocytes are contractile this cannot be done. Here the ratiometric Ca^{2+}-sensitive fluorophore Fura-4F, with excitation at 340 and 380 nm when bound and unbound to Ca^{2+}, respectively, and emission at 510 nm was used. The dye associates and dissociates from the Ca^{2+} in the cytoplasm of the cardiomyocyte as it is released and taken back up by the SR during ECC. When bound, it is excited at 340 nm and when unbound at 380 nm, so as emission from excitation at one wavelength increases, it decreases from the other and vice-versa. When the ratio of emission at 340 and 380 nm is calculated, the trace rises and falls with Ca^{2+} release and re-uptake (Wokosin et al., 2004).

2.15.2 Experimental protocols

Calcium imaging was performed on an inverted epifluorescence microscope positioned in a Faraday cage in a darkened room. All experiments were carried out at 37 °C under constant pressure perfusion with the use of a heated perfusion pen (Cell Microcontrols, Virginia, USA) and a peristaltic pump outflow. Cell stimulation was at a rate of 1 Hz and cells were loaded with Fura-4F AM ester ratiometric dye (Life Technologies, Paisley, UK). Experiments were carried out at physiological [Ca^{2+}] (1.8 mM) and pH (7.48) with the use of a HEPES buffered superfusate in which all other components were diluted. SR Ca^{2+} content was determined using a 10 mM caffeine solution. Instantaneous solution changes were achieved by priming the system with up to 7 different solutions which were interchangeable *via* an automated pinch-valve system.

For all Ca^{2+} imaging experiments, isolated cardiomyocytes were pelleted using a hand-operated centrifuge and re-suspended in 5 mL of HEPES buffered superfusate. Cells were then loaded by the addition of 5 µL of Fura-4F to 1 mL of cells and followed by incubation in the dark at room temperature for 10 min, after which time a further 3 mL of superfusate was added to the cells to de-esterificate the fluorophore. Cells were loaded onto a cell bath (Cell Microcontrols, Virginia, USA) connected to a stimulator set at 1 Hz with 2 ms duration voltage pulses delivered *via* parallel platinum wires. Cell stimulation simulates sarcolemmal depolarization in response to an AP. Cells were visualised using a 40 x oil immersion objective lens and perfusion and outflow started. Prior to each experimental protocol, a 20 second steady state recording of quiescent cell fluorescence was recorded to determine the resting cell $[Ca^{2+}]$, or R_{min}. At the end of each experimental protocol, stimulation was terminated simultaneously with the application of the 10 mM caffeine bolus. This empties the SR of Ca^{2+} producing a caffeine-induced Ca^{2+}-transient which can be used to determine SR calcium content. In a group of cells the R_{max} was determined by perforation of the cell using a pulled glass micropipette positioned using a micromanipulator arm.

2.15.3 Data acquisition and analysis

For Ca^{2+} imaging, the fluorescence signal was sampled at 5000 Hz and data recorded in Clampex 10.3 software using an analogue to digital convertor (Axon Instruments, California, USA). Data was imported into Origin 6.1 software (Originlab, Massachusetts, USA) and the 340/380 ratio (fluorescence corrected for artefact) determined for the trace. A timing signal was generated based on the sampling frequency and a steady-state recording of 12 transients used to calculate an average transient using a macro written by Prof. Godfrey Smith, University of Glasgow. Exponential decay functions were calculated using the software's own programmes. Fluorescence ratio could be converted into $[Ca^{2+}]_i$ using the following equation:

$$[Ca^{2+}] = K_d \times \beta (R - R_{min}) / (R_{max} - R)$$

Where K_d= the dissociation constant of the dye (0.77 µM for Fura-4F)(Wokosin et al., 2004), ß= the relative change in fluorescence between 0 and saturating

$[Ca^{2+}]$ at 380 nm, R= the ratio signal, R_{min}= the minimum ratio before stimulation (0 $[Ca^{2+}]$) and R_{max}= is the maximum signal (saturating $[Ca^{2+}]$). β was measured by Dr. Chris Loughrey during system set-up and calibration, with $K_d\beta = 2.8 \times 10^{-6}$ for Fura-4F.

2.15.4 Fractional shortening measurements

Cell shortening was measured simultaneously with Ca^{2+} imaging using edge-detection imaging equipment (IonOptix, Dublin, Ireland) and accompanying software (Ionwizard 6.0) which measured the change in cell length during stimulation. Data was sampled at 2000 Hz and traces were exported as text files to be analysed in Origin 6.1 software. An equivalent length of trace to Ca^{2+} transient analysis was averaged (12 contractions) and a timing signal generated using a macro. Diastolic cell length was taken immediately before stimulation (L_0) and used to calculate fractional shortening as the average % reduction from L_0.

2.16 Statistical analysis

Data are represented as mean values ± the standard error of the mean (SEM) unless otherwise stated. qRT-PCR data was expressed as relative quantification (RQ) with each sample normalised to a control. qRT-PCR error was expressed as rq_{max}, which is calculated based on the maximum expression level that represents a 95 % confidence interval of the mean RQ value according to Students T-test and represents the standard error of the mean expression level. Paired student's T-test was performed for direct comparisons and one-way analysis of variance (ANOVA) with Tukey's post-test was performed for multiple comparison, with a *P* value <0.05 considered statistically significant.

For animal groups in *in vivo* studies, *n*-numbers are indicated for each figure. Data for echocardiography was analysed using repeated measures ANOVA with Tukey's post-test. A *P* value <0.05 was considered statistically significant. All statistical analysis was carried out using Graphpad Prism 4 software (GraphPad Software Inc., California, USA).

Chapter 3: Characterisation of a mouse MI model

3.1 Introduction

3.1.1 The mouse model of coronary artery ligation

Two-thirds of human patients who develop HF do so as a result of myocardial infarction caused by coronary artery disease (Ho et al., 1993; Klocke et al., 2007). Therefore a desirable animal model for the development of potential therapeutics for cardiac contractile dysfunction post-MI is one which mimics the same injury and disease processes, such as in the mouse MI model. Mouse models in general are extremely popular in biological research for a variety of reasons. They share 99 % of their genes with humans and have similarities in all major organ systems; they are small, docile, cheap and easy to maintain and breed; they are easy to genetically manipulate and a variety of 'humanising' experimental procedures have been developed to mimic human conditions (Rosenthal and Brown, 2007). Although the MI procedure is performed in large animal models such as dog or pig there can be a high incidence of ventricular tachycardia and ventricular fibrillation (Hood et al., 1967; Iwanaga et al., 2004) as well as incurring significantly higher maintenance, infrastructure and purchase costs. Mice are also extremely well suited to adenoviral-vector administration for the assessment of gene therapy based therapeutics as they can be administered with high viral doses without an apparent toxicity response (Curiel and Douglas, 2002). C57BL/6 mice have a non-observable adverse effect level (NOAEL) dose of 2.4×10^9 pfu/m^2 for Ad vectors compared to that of 1.7×10^9 pfu/m^2 for hamsters and 1.2×10^7 pfu/m^2 for humans which is advantageous for experimental purposes but may be problematic from a translational aspect (Curiel and Douglas, 2002). Due to their small size lower vector load is required per animal compared to that of a pig or dog. This makes mice a more economical choice in terms of vector production for the use of viral gene therapy and allows assessment of gene therapy approaches for the treatment of remodelling post-MI.

The CAL MI model was selected for the present study as it matches the aetiology of the disease by mimicking acute occlusion of the coronary artery in acute MI, resulting in ischemia of the myocardium while also permitting control over the time and site of the occlusion allowing for reproducibility (Klocke et al., 2007). The CAL MI model was first described in mice in 1977 (Zolotareva and Kogan,

1978) and has since been increasingly used to investigate underlying mechanisms contributing to cardiac dysfunction in MI in both wild type and transgenic mice. Small animals are suited to determination of cardiac functional parameters and infarct sizes using techniques such as echocardiography, as well as for electrophysiological characterisation using *ex vivo* preparations on Langendorff apparatus (Kuhlmann et al., 2006). Cardiac haemodynamic parameters have also been well characterised in the model at various time points and remodelling severities using pressure-volume relationships (Patten et al., 1998; Shioura et al., 2007). This has been made possible due to the popularity of the mouse as an experimental model leading to the development of advanced technologies which are able to make accurate measurements on such a small scale.

3.1.2 Study of the RAS in the mouse MI model

The mouse MI model has been used extensively to study the role of the RAS in cardiac remodelling and dysfunction post-MI and its therapeutic potential, with the role of the angiotensin receptors being particularly well investigated (Harada et al., 1999; Yang et al., 2002a). The role of the AT_1R in remodelling post-MI was demonstrated using global AT_1R knock-out mice (Harada et al., 1999). AT_1R KO mice have been shown to have increased survival rate, decreased expression of foetal, collagen and TGFß-1 genes, attenuation of HF (as measured *via* activity levels and right ventricular to body weight ratio) and decreased left ventricular dilation and increased fractional shortening (as measured using echocardiography following infarction). This demonstrated that the AT_1R is a major contributor to cardiac remodelling and progression to heart failure following MI (Harada et al., 1999). Conversely, transgenic mice which over-express the AT_2R specifically in the heart have significantly decreased end systolic volume indices and preserved EF as determined *via* MRI versus wild type groups, highlighting the dramatically converse effects of Ang II signalling *via* its different receptors (Yang et al., 2002b). The use of AT_2R knock-out mice has also demonstrated that the cardio-protective effects seen by valsartan (an AT1R antagonist)-mediated AT_1R blockade are in part mediated by the AT_2R. Decreases in left ventricular dimensions and decreased lung to body-weight ratio was observed in wild-type mice treated with valsartan post-MI. This attenuation was not observed in the AT_2R knock-out animals when administered with valsartan (Oishi et al., 2006). Despite the positive results observed in transgenic

animals with regards to the therapeutic potential of the AT_2R, the mouse MI model has also been used to show that a synthetic small molecule agonist (compound 21; C21) of the AT_2R does not have the same effect as AT_2R over-expression (Jehle et al., 2012). C21 administered *via* minipump, or the AT_1R antagonist candesartan, delivered *via* drinking water, was given to mice following MI. Cardiac function was assessed at 28 days using CMR and only the candesartan group had preserved left ventricular EF, showing that direct stimulation of the AT_2R does not have the same beneficial effects as AT_1R blockade or AT_2R over-expression following MI (Jehle et al., 2012).

The effects and mechanisms of ACE inhibition have also been well studied in the model. ACEi administered 1 month after MI in wild-type mice has been shown to have a beneficial effect on cardiac structural and functional remodelling, with echocardiography measurements showing decreased LVDD, increased LV EF and increased FS, and histological analysis showing reduced cardiac hypertrophy and fibrosis (Liu et al., 2002). These beneficial effects were found to be mediated by eNOS which was increased due to the inhibition of Ang II synthesis as a result of ACEi. The effects seen as a result of ACEi were absent or reduced in eNOS knock-out animals following MI (Liu et al., 2002). The model has also been used to demonstrate that ACE inhibition using enalapril or AT_1R blockade using Losartan have equivalent effects on reducing cardiac hypertrophy and ANP and collagen type I gene expression following MI (Patten et al., 2003).

The therapeutic potential of the counter-regulatory RAS has been less well studied in the mouse MI model, however it has been demonstrated that subcutaneous injection of Ang-(1-7) following MI increased left ventricular pressure measured *via* LV catheter, reduced LV and RV hypertrophy and decreases BNP and collagen type I expression. These effects were associated with an increase in VEGF and c-kit positive cells in the infarcted hearts, suggesting Ang-(1-7) may enhance cardiac recovery post-MI through stimulation of bone-marrow derived progenitor cells which migrate to the myocardium (Wang et al., 2010a).

These findings highlight the utility of the MI model for studying the therapeutic potential of the RAS and unravelling some of the mechanisms underlying the effects seen.

3.2 Aims

The aims of this chapter were to:

- Learn how to surgically induce MI in the mouse.

- Characterise the mouse MI model for functional, haemodynamic, histological and gene expression parameters, particularly with respect to the RAS.

3.3 Results

3.3.1 MI surgery mortality

MI-associated incidence and cause of mortality was monitored for an 8-wk period following MI in male C57BL/6 mice (Figure 3.1). Kaplan-Meier survival curves plotting mortality rates of all MI-animals successfully recovered from procedure demonstrated a significant reduction in survival of MI animals *vs*. sham (n= 53 and 46, respectively, P<0.01) over an 8 wk period, with 15 % of MI animals dying within the first wk following surgery (Figure 3.1 A). The main cause of death for animals which survived the MI procedure was cardiac rupture, accounting for 33.3 % of all procedure-related mortality, with 4.2 % dying of an unknown cause post-operatively which could not be determined by post-mortem analysis. The remainder of deaths were associated with intra-operative complications (Figure 3.1 B). A change in mortality was associated with gaining experience in the MI procedure, with an inverse relationship observed between the number of MI procedures performed and the number of deaths resulting from procedural complications, increasing overall survival rates from 30 % at its lowest to 67 % at its highest (Figure 3.1 C).

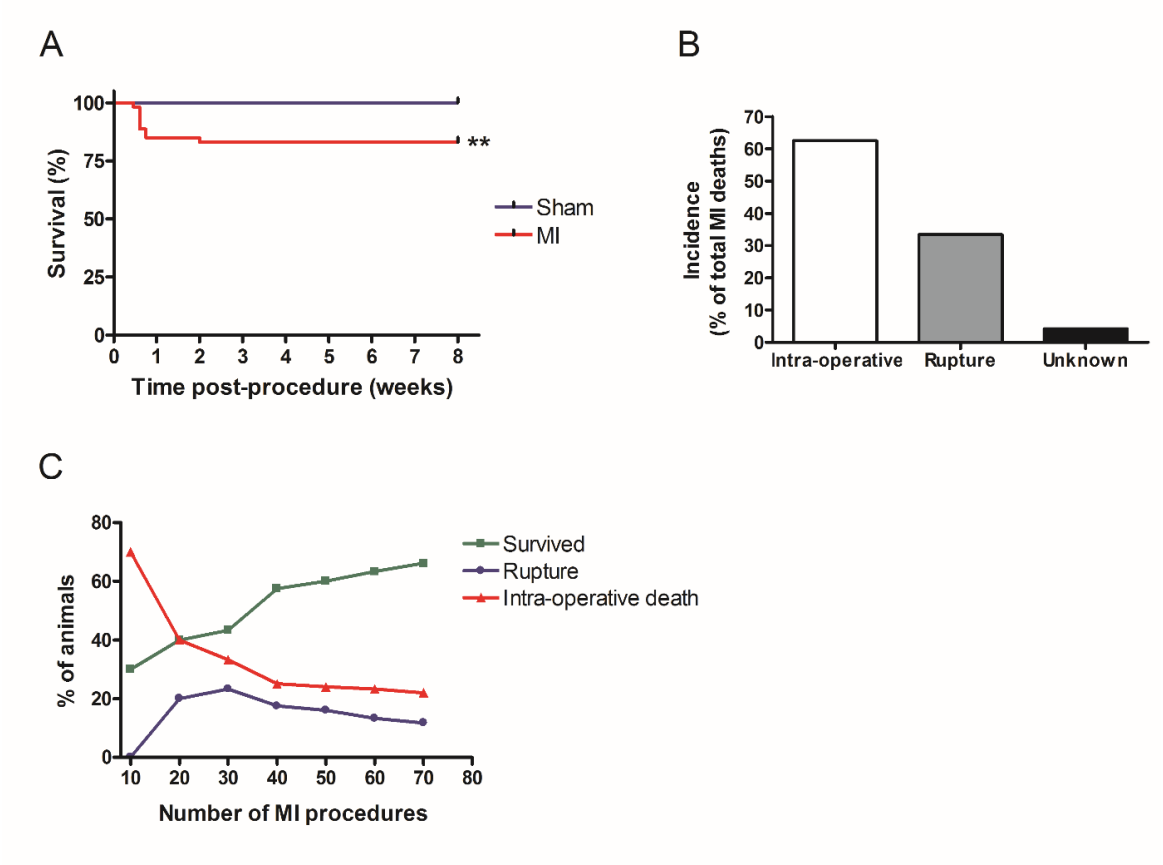

Figure 3.1 MI-surgery related mortality.
(A) Kaplan-Meier plot of MI *vs*. sham mortality following recovery from procedure over an 8 wk period. **= $P<0.01$, $n= 53$ and 46 for MI and sham, respectively. (B) Cause of MI-mortality, both intra-operatively and post-recovery. (C) Relationship of intra-operative associated death, cardiac rupture rates and overall survival to the number of procedures performed.

3.3.2 Haemodynamic and functional measurements in the MI model

3.3.2.1 Echocardiography

Serial echocardiography measurements were performed on sham and MI animals on a weekly basis for 4 wks. A separate cohort of animals were taken to 8 wks post-MI for comparison (Figure 3.2).

At 1 wk post-MI there was a significant drop in FS in MI animals compared to sham (49.9± 0.2 *vs*. 30.4± 0.3 %, 1 wk sham (*n*= 12) *vs*. 1 wk MI (*n*= 12); *P*<0.001; Figure 3.2 A-ii). The significant reduction in the MI group was maintained at all time-points, with a gradual further reduction in FS from 1 wk to 8 wks post-MI by 15.2 % (30.4± 0.3 *vs*. 25.8± 0.9 %, 1 wk MI (*n*= 12) *vs*. 8 wk MI (*n*= 6); *P*<0.05). FS was unchanged throughout the 8 wk period in the sham group (Figure 3.2 A-ii). The reduction observed in FS was associated with increases in both LVEDD and LVESD in the MI group compared to sham animals and gradually increased from 1 wk to 8 wk post-MI. At 1 wk, LVEDD in MI was significantly increased to 120.6 % of sham animals (4.1± 0.03 *vs*. 3.4± 0.02 mm, 1 wk MI (*n*= 12) *vs*. 1 wk sham (*n*= 12); *P*<0.00; Figure 3.2 A-iii). LVEDD gradually increased throughout the study, with a significant increase in the 8 wk MI group to 140.1 % of sham animals (4.6± 0.2 *vs*. 3.3± 0.04 mm, 8 wk MI (*n*= 6) *vs*. 8 wk sham (*n*= 6); *P*<0.001), however LVEDD in 1 wk animals was not significantly different at 8 wks post-MI (Figure 3.2 A-ii). A similar pattern was seen in LVESD with a significant increase at 1 wk post MI of 164.0 % of sham (1.7± 0.02 *vs*. 2.8± 0.02 %, 1 wk sham (*n*= 12) *vs*. 1 wk MI (*n*= 12); *P*< 0.001; Figure 3.2 A-iv) which gradually increased until 8 wks, reaching 200 % of sham animals (*P*<0.001). LVESD significantly increased between 1 and 8 wks post MI, with a further expansion at 8 wks to 121.4 % of 1 wk post-MI animals (2.8± 0.2 *vs*. 3.4± 0.1 mm, 1 wk MI (*n*= 12) *vs*. 8 wk MI (*n*= 6); *P*<0.05; Figure 3.2 A-iii). Sham LVESD and LVEDD were unchanged throughout the 8 wks. LV posterior wall thickness was unchanged between sham and MI at all time-points (Figure 3.2 A-v & vi).

E/A wave ratios were determined using mitral valve Doppler measurements (Figure 3.2 B). E/A wave showed no significant difference between sham and MI animals at 4 and 8 wks following procedure or between 4 and 8 wk post-MI animals (Figure 3.2 B-ii).

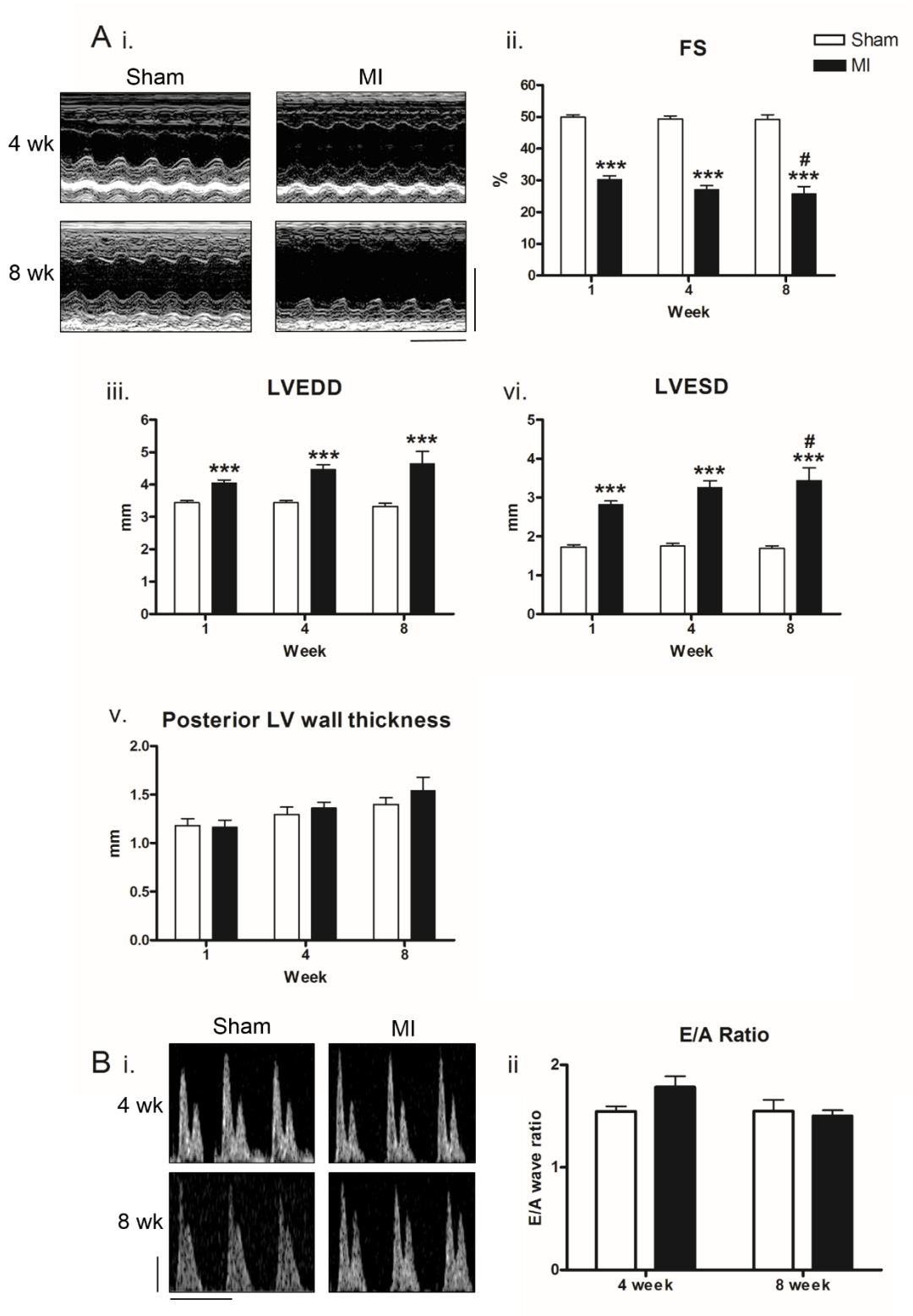

Figure 3.2 Effect of MI on FS, LV wall-thickness and E/A ratio assessed by echocardiography.
(A-i.) Example M-mode images for 4 wk and 8 wk sham and MI animals. Scale bars= 5 mm and 1 second. Serial FS (ii.), LVEDD (iii.), LVESD (vi.) and posterior LV wall thickness measurements from M-mode echocardiography images for MI and sham groups from 1 to 8 wks post-MI. ***= $P<0.05$ *vs*. sham, #= $P<0.05$ vs. 1 wk MI. (B-i.) Example E/A wave Doppler measurements for 4 wk and 8 wk sham and MI animals. Scale= 0.2 m/s and 20 mm. (ii.) Average E/A ratio measurements for the mitral valve determined using echocardiography Doppler for 4 and 8 wk sham and MI animals. *n*= 12 and 6 for 4 and 8 wk data sets, respectively. Data presented as mean± SEM. FS= fractional shortening, LVEDD= left-ventricular end-diastolic dimension, LVESD= left-ventricular end-systolic dimension, E= early wave and A= after wave.

3.3.2.2 PV-loop

The effects of MI on LV haemodynamic indices were assessed using closed chest PV-loop measurements in 4 and 8 wk MI and sham animals (Figure 3.3 & Table 3.1). It was shown that MI had a significant effect on a range of systolic, diastolic and volume indices at both 4 and 8 wks following MI.

Systolic measurements demonstrated a significant reduction in ESP between sham and MI groups at each time point, with MI ESP reduced to 76.2 % and 81.7 % of time-matched shams for 4 and 8 wk groups, respectively (P<0.001; Table 3.1). There was no significant difference between 4 and 8 wk MI ESP (Figure 3.3 A & B-i). Similarly, dP/dt_{max} was significantly reduced in MI animals compared to sham at each time point, with a reduction to 53.2 % and 67.0 % of sham for 4 and 8 wk MI, respectively (P<0.001). There were no differences between MI groups at any time-point (Figure 3.3 B-ii). EF was also significantly reduced in MI to 62.8 % and 57.5 % of sham animals at the 4 and 8 wk time-points, respectively (P<0.01 at 4 wks; P<0.001 at 8 wks). Although there was no significant difference in EF between 4 and 8 wk MI, there was a trend towards a reduction at the 8 wk time point (Figure 3.3 B-iii). CO was shown to be unchanged between all 4 groups (Figure 3.3 B-iv).

Diastolic measurements showed no significant change in EDP between sham and MI groups at either time-point (Figure 3.3 C-i). However, dP/dt_{min} was significantly reduced in MI groups at both time points to 54.8 % (P<0.01) and 66.1 % (P<0.001) of sham for 4 and 8 wk groups, respectively (Figure 3.3 C-ii). Tau was also significantly increased in the MI groups at both time-points, with increases to 154.2 % at 4 wks (P<0.001) and 140.0 % at 8 wks (P<0.05) of sham (Figure 3.3 C-iii). EDPVR measurements were not significantly different between sham and MI at the 4 wk time-point. At 8 wks there was a significant difference between sham and MI groups, with MI animals having a EDPVR 3 times greater than that of sham animals (P<0.001; Figure 3.3 B-iv).

Volume parameters demonstrated a significant difference in EDV in 4 wk MI animals, increasing to 228.7 % of sham animals (P<0.01) (Figure 3.3 D-i). This was also the case at 8 wks, where MI EDV was significantly increased to 203.0 % of sham animals (P<0.05). The same pattern was seen in ESV, with significant

increases in MI animals of 345.6 % (P<0.01) and 292.7 % (P<0.01) for 4 and 8 wk groups, respectively (Figure 3.3 D-ii).

Table 3.1 Effect of MI on haemodynamic LV PV-loop indices.

	4 wk		8 wk	
	Sham	**MI**	**Sham**	**MI**
HR (bpm)	600.9 ± 15.0	581.1 ± 6.0	604.3 ± 8.5	571.5 ± 7.5
ESP (mmHg)	104.7 ± 3.1	79.6 ± 3.6 ***	103.5 ± 1.6	84.7 ± 2.7 ***
EDP (mmHg)	7.7 ± 1.8	12.7 ± 1.1	6.3 ± 1.3	7.2 ± 1.2
Developed pressure (mmHg)	96.92 ± 2.3	66.7 ± 5.3 ***	97.3 ± 0.4	77.5 ± 2.5 ***
dp/dt_{max} (mmHg/min)	10920.8 ± 450.0	5761.1 ± 376.8 ***	10719.9 ± 732.6	7219.5 ± 443.8 ***
dp/dt_{min} (mmHg/min)	8664.2 ± 717.6	4749.6 ± 314.7 ***	8343.1 ± 669.3	5517.5 ± 409.1 **
Tau (ms)	5.9 ± 0.5	9.1 ± 0.3 ***	5.5 ± 0.3	7.7 ± 0.7 **
EDPVR	0.03 ± 0.02	0.08 ± 0.01	0.03 ± 0.00	0.11 ± 0.01 **
ESV (µL)	12.3 ± 2.3	42.5 ± 8.5 **	16.5 ± 0.5	48.3 ± 7.1 **
EDV (µL)	28.2 ± 3.4	64.5 ± 8.2 ***	33.4 ± 1.2	67.8 ± 9.4 *
CO (µL/min)	9948.0 ± 1095.4	12722.8 ± 610.6	10190.9 ± 475.3	10880.9 ± 1550.5
EF (%)	58.1 ± 3.7	36.5 ± 4.0 **	50.4 ± 0.9	29.0 ± 1.7 ***

HR= heart rate, ESP= end systolic pressure, EDP= end diastolic pressure, dp/dt_{max}= maximal rate of rise of pressure, $-dp/dt_{min}$= maximum rate of fall in pressure, Tau= time relaxation constant, EDPVR= end diastolic pressure-volume relationship stiffness constant, ESV= end systolic volume, EDV= end diastolic volume, CO= cardiac output, EF= ejection fraction. *= $P<0.05$, **= $P<0.01$, ***= $P<0.001$ *vs*. time-matched sham.

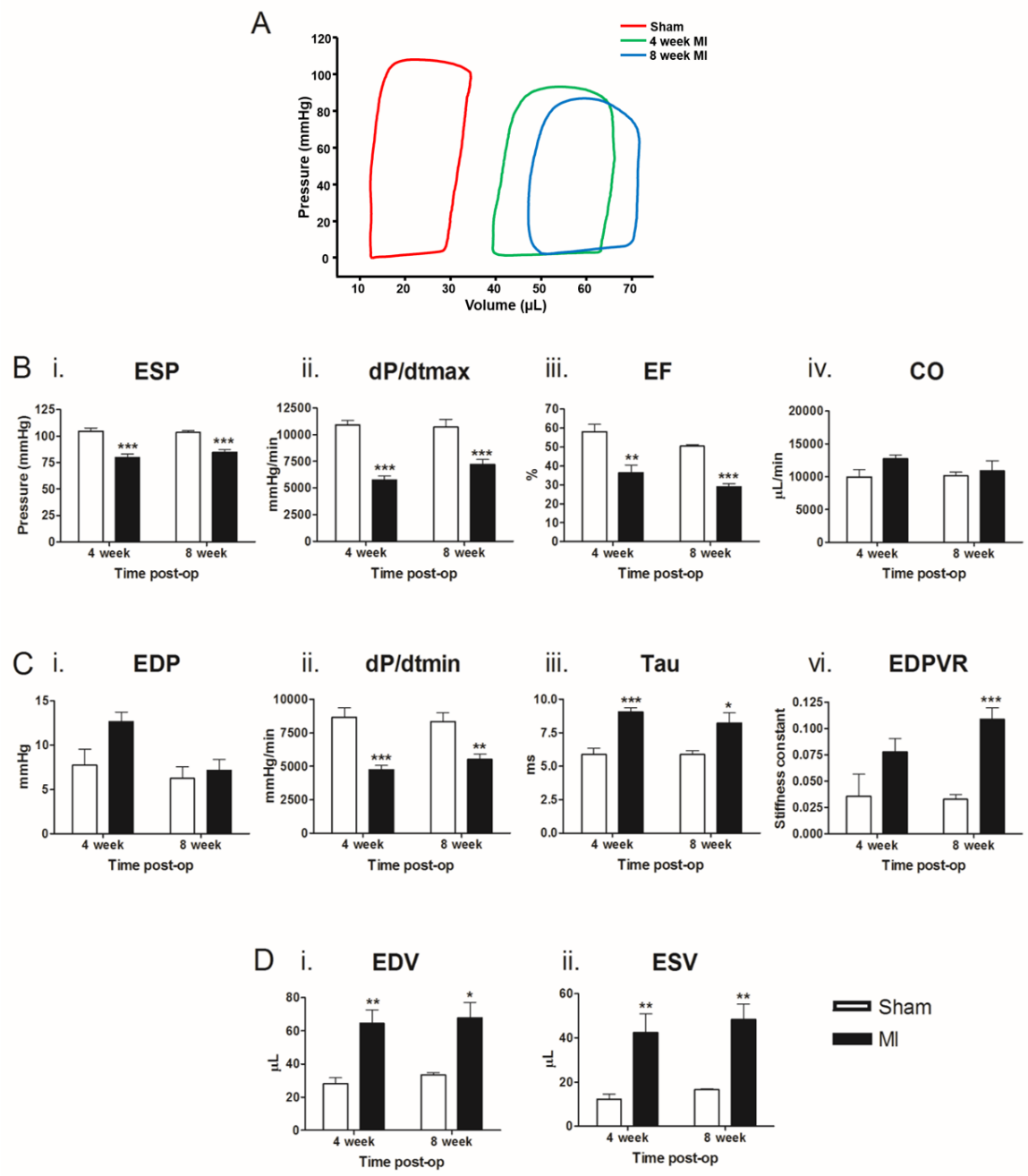

Figure 3.3 Effect of MI on LV haemodynamic indices as determined by PV-loop measurements.
LV haemodynamic measurements for 4 and 8 wk sham and MI animals determined using the ADVantage PV-loop system with true blood volume calculated using Wei's equation (A) Example PV-loop relationships for sham, 4 wk MI and 8 wk MI animals. (B) Systolic functional indices of ESP (i.), dP/dt_{max} (ii.), EF (iii.) and CO (vi.); (C) Diastolic functional indices of EDP (i.), dP/dt_{min} (ii.), Tau (iii.) and EDPVR (vi.); and (D) Volume indices of EDV (i.) and ESV (ii.). *= P<0.05, **= P<0.01, ***=P<0.001 *vs*. time-matched sham. n= 7, 6, 5 and 9 for 4 wk sham and MI and 8 wk sham and MI, respectively. Data presented as mean± SEM.

3.3.3 Post-mortem and Histological Analysis

3.3.3.1 Organ weights

Examination of excised hearts during post-mortem analysis demonstrated progressive scar thinning and increase in heart size in MI animals compared to sham at each time point (Figure 3.4 A). No significant change in HW: TL is evident between sham and MI groups at 3 days, 1 wk and 4 wks following surgical procedure (Figure 3.4 B). However, at 8 wks post-MI HW:TL in the MI group was significantly increased to 125 % of sham (8.8± 0.6 *vs*.10.9± 0.4, 8 wk sham (*n*= 6) *vs*. 8 wk MI (*n*= 6); $P<0.05$; Figure 3.4 B). No significant difference in LuW:TL and LiW:TL was evident between sham and MI groups at any of the time points studied (Figure 3.4 C and D).

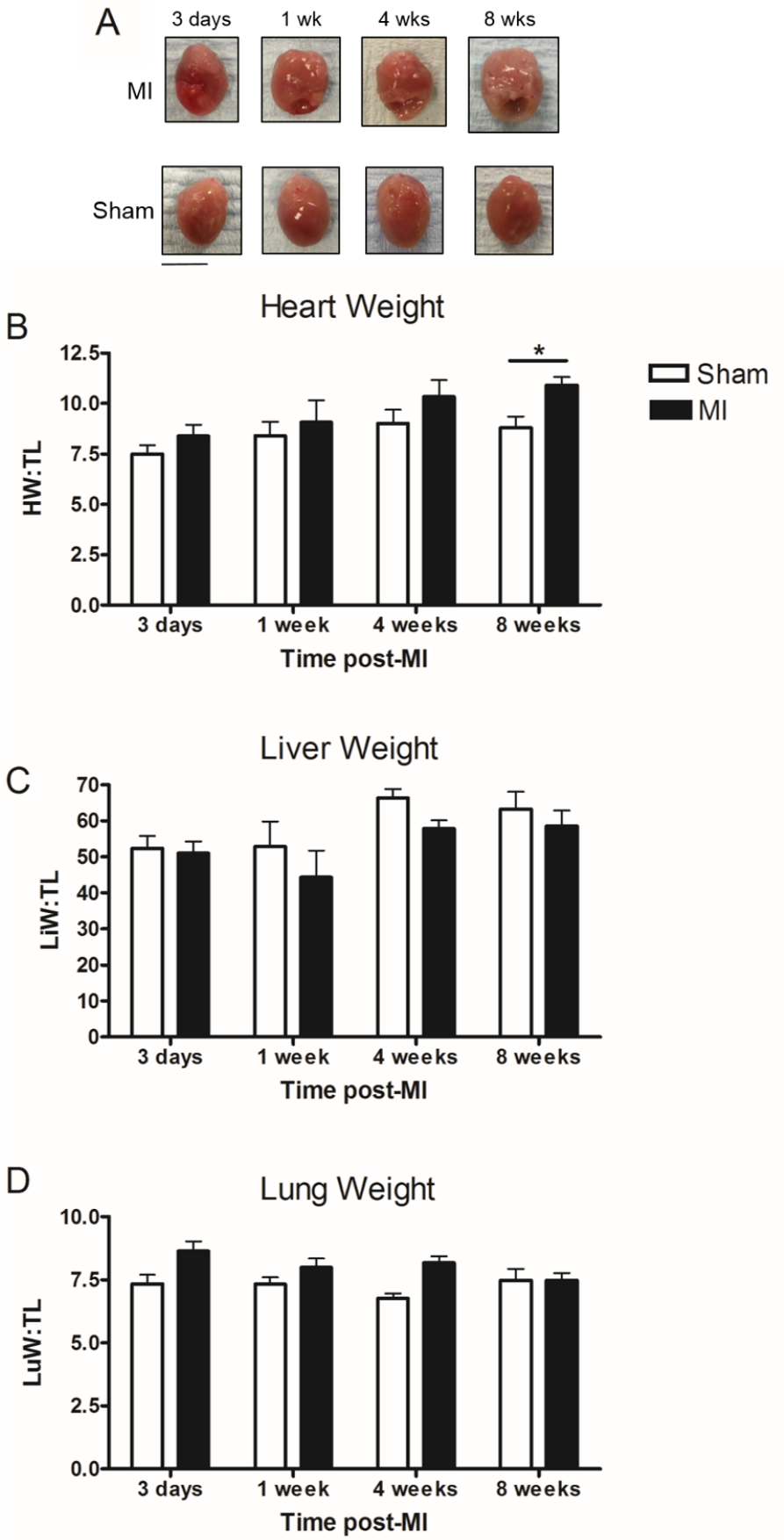

Figure 3.4 Effect of MI on post-mortem organ weights.
(A) Example images of MI and sham hearts for each of the studied time points. HW:TL (B), LiW:TL (C) and LuW:TL (D) ratios for sham and MI animals at 3 days, 1, 4, and 8 wks following surgical procedure *= $P<0.05$. n= 6, 5, 7 and 6 for 3 day, 1, 4 and 8 wk groups, respectively. Data is presented as mean± SEM. Scale bar= 5 mm. TL= tibia length, HW= heart weight, LuW= lung weight and LiW= liver weight.

3.3.3.2 Cardiomyocyte sizing

WGA staining of heart sections from 4 and 8 wk sham and MI animals was used to quantify average cardiomyocyte cell length and diameter as a measure of cardiomyocyte hypertrophy. Exclusion criteria were applied to cells below a minimum threshold length of 70 μm (Figure 3.6 A).

Average cell diameter was shown to be significantly increased in both MI groups compared to the corresponding time-matched sham group (15.0± 0.3 *vs*. 18.2± 0.4 μm, 4 wk sham (*n*= 9) *vs*. 4 wk MI (*n*= 9); *P*<0.01; 15.1± 0.3 *vs*. 20.2± 0.5 μm, 8 wk sham (*n*= 10) *vs*. 8 wk MI (*n*= 10); *P*<0.001; Figure 3.5 A-i & ii). Cell diameter was also significantly increased between 4 and 8 wk MI groups (*P*<0.001; Figure 3.5 A-ii). Average cell length was shown to be unchanged between sham and MI animals across both time points (Figure 3.5 B-i & ii).

When mean cell length was correlated to dilation as measured *via* PV-loop for MI animals, a significant relationship between increasing cell length and EDV was observed (*P*<0.01; Figure 3.6 B).

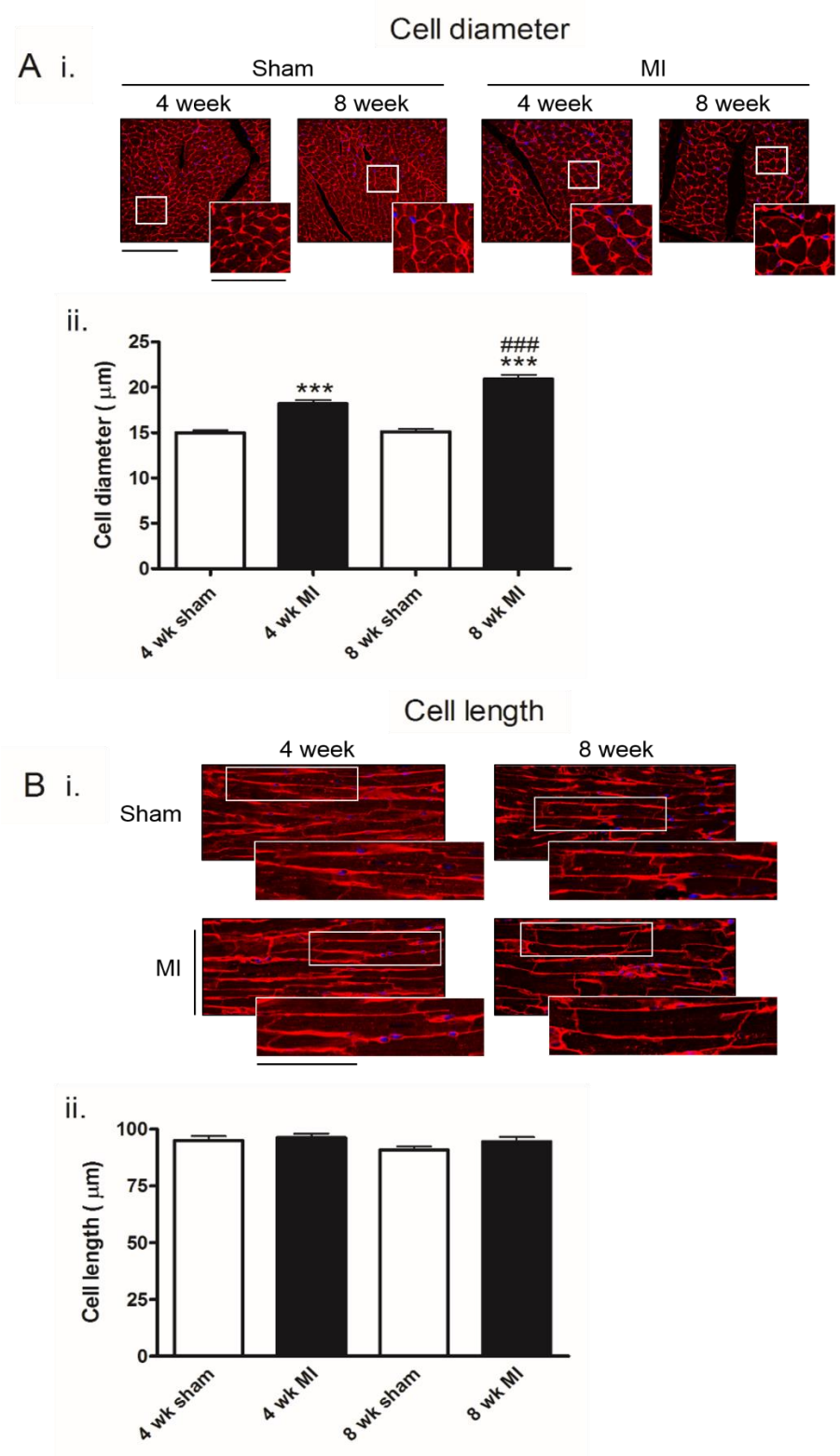

Figure 3.5 Quantification of cardiomyocyte size post-MI.
Example images of cellular cross-sections in both transverse (A-i.) and longitudinal (B-i.) axis are shown for 4 and 8 wk sham and MI animals, with cellular membranes stained red and cellular nuclei in blue. Magnification= 25x, scale= 100 µm. B-i zoom image insert scale= 50 µm. Determination of left-ventricular cardiomyocyte diameter (A-ii. *n*= 126, 126, 144 and 139 cells for 4 wk sham and MI and 8 wk sham and MI groups, respectively) and length (B-ii. *n*= 105, 92, 99 and 89 cells for 4 wk sham and MI and 8 wk sham and MI groups, respectively) in the hearts of 4 and 8 wk sham and MI animals using WGA staining. ***= *P*<0.001 *vs* time-matched sham, ###= *P*<0.001 vs.4 wk MI. *n*= 9 and 10 animals for 4 and 8 wk groups, respectively. Data presented as mean± SEM with the average cell-size for each animal taken as the average of a group of cells evenly distributed across the left ventricle.

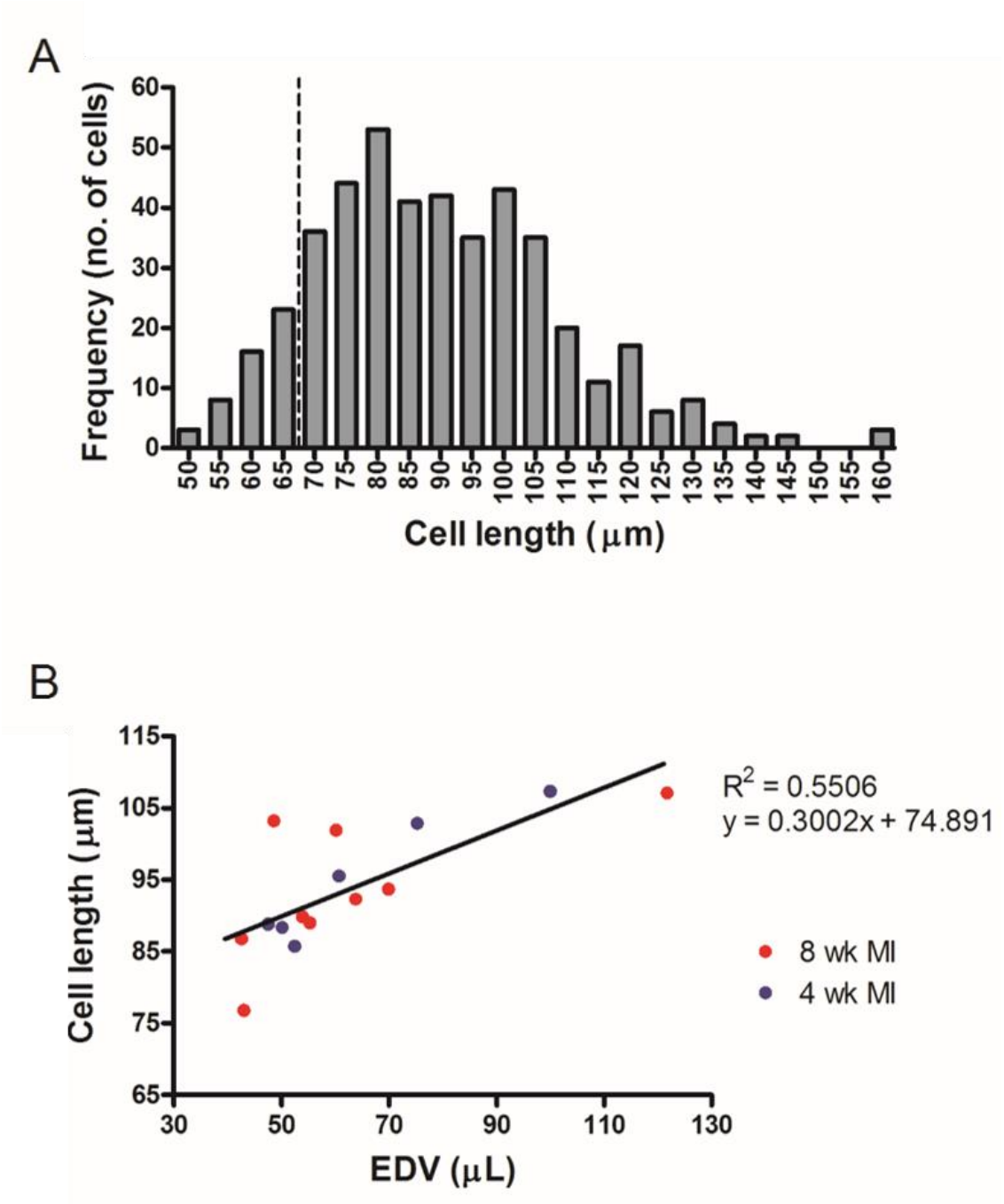

Figure 3.6 Cell length histogram and EDV vs. cardiomyocyte length relationship.
(A) Cell length frequency histogram showing 70 μm minimum threshold indicated by dashed line. (B)Cardiomyocyte length *vs.* EDV from PV-loop measurements for 4 and 8 wk MI animals. Each point indicates one animal. EDV= end diastolic volume.

3.3.3.3 Regional fibrosis, collagen expression and scar size

At 4 wks, % fibrosis as measured by picrosirius red staining in the scar region of MI animals was significantly increased compared to sham (2.6± 0.5 *vs*. 72.4± 5 %, 4 wk sham (*n*= 9) *vs*. 4 wk MI (*n*= 9); *P*<0.001; Figure 3.7 B-i). This was predominantly due to deposition of collagen I, which was also significantly increased in 4 wk MI scars (14.9± 1.48 *vs*. 31.7± 7.6 %, 4 wk sham (*n*= 9) *vs*. 4 wk MI (*n*= 9); *P*<0.05; Figure 3.8 B-i), with no change in collagen III expression (Figure 3.9 B-i). By 8 wks total fibrosis had increased further to 88.2± 2.7 % of the myocardium, and was significantly increased compared to both 8 wk sham (*P*<0.001) and 4 wk MI animals (*P*<0.01; Figure 3.7 B-i), however there was no change in collagen I or III expression. In the left ventricle, total fibrosis was significantly increased in the MI groups at both the 4 wk and 8 wk time points in comparison to time-matched sham groups (8.5± 1.2 *vs*. 1.1± 0.4 %, 4 wk MI (*n*= 9) *vs*. 4 wk sham (*n*= 9); *P*<0.001; 7.5± 0.5 *vs*. 1.8± 0.5 %, 8 wk MI (*n*= 10) *vs*. 8 wk sham (*n*= 10); *P*<0.001; Figure 3.7 B-ii). However, there was no significant difference between LV fibrosis between 4 and 8 wk MI groups (*P*>0.05; Figure 3.7 B-ii). There was no change in collagen I or III expression in the LV at either time-point. In the septum, MI fibrosis was significantly increased at 4 and 8 wks compared to time-matched sham groups (*P*<0.01; Figure 3.7 B-iii). Fibrosis was also significantly increased at 8 wks post-MI compared to the 4 wk time-point (4 wk MI= 4.6± 0.8, 4 wk sham= 0.7±0.2, 8 wk MI= 23.2± 5.9 and 8 wk sham= 2± 0.4 %; *P*<0.01; Figure 3.7 B-iii). The increased fibrosis at 8 wks was due to significant increases in collagen I only compared to sham (3.9± 1.6 *vs*. 15.7± 4.2 %, 8 wk sham (*n*= 10) *vs*. 8 wk MI (*n*= 10); *P*<0.05; Figure 3.8 B-iii) and 4 wk MI groups (4 wk MI= 3.9± 1.3 %; *P*<0.05; Figure 3.8 B-iii). Fibrosis % of the right ventricle was significantly increased in MI groups *vs*. the corresponding sham group at both time points (*P*<0.01), with a significant increase at 8 wks compared to 4 wks post-MI (4 wk MI= 3.2± 0.6, 4 wk sham= 1±0.3, 8 wk MI= 10.4± 2.6 and 8 wk sham= 0.7± 0.1 %; *P*<0.05; Figure 3.7 B-iv). At 8 weeks, collagen I was significantly increased in the RV region compared to sham (10.0± 2.0 *vs*. 35.9± 4.5 %, 8 wk sham (*n*= 10) *vs*. 8 wk MI (*n*= 10); *P*<0.001; Figure 3.8 B-vi) and 4 wk MI groups (4 wk MI= 12.2± 3.3 %; *P*<0.001; Figure 3.8 B-vi). Collagen III was also significantly increased in 8 wk MI RV compared to both sham (2.2± 1.1 *vs*. 7.7± 1.7 %, 8 wk sham (*n*= 10) *vs*. 8 wk MI (*n*= 10); *P*<0.05; Figure 3.9 B-vi) and 4 wk MI groups (4 wk MI= 1.2± 0.5 %; *P*<0.01; Figure 3.9 B-vi).

Scar sizes, determined as a % of the LV, were shown to be unchanged between 4 wk and 8 wk MI groups (Figure 3.7 C-i). There was also no significant difference in scar thickness between 4 and 8 wk MI groups (Figure 3.7 C-ii).

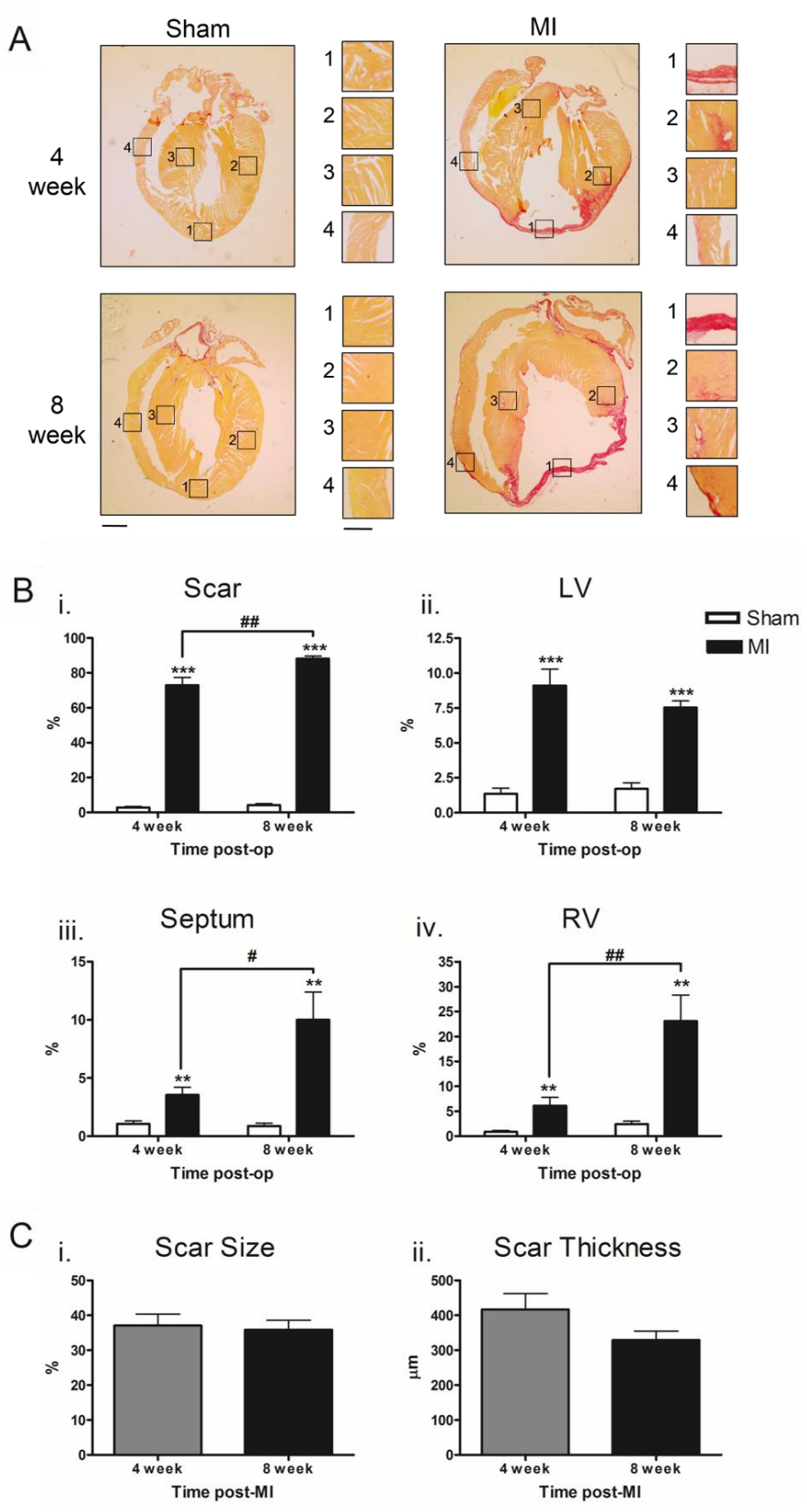

Figure 3.7 Cardiac regional fibrosis quantification and scar sizing following MI.
(A) Example images of picrosirius red staining of 4 and 8 wk sham and MI heart sections. (B) Quantification of total cardiac fibrosis of the scar (i.), left ventricle (ii.), right ventricle (iii.) and septum (iv.) regions of 4 and 8 wk sham and MI animals. **= *P*<0.01, ***= *P*<0.001 *vs* time-matched sham, #= *P*<0.05, ##= *P*<0.01 for 4 wk *vs*. 8 wk MI. (C) Scar size (i) and thickness (ii) comparison of 4 and 8 wk MI animals. Scar size was determined as a % of the total myocardial area. *n*= 9 and 10 for 4 and 8 wk groups, respectively. Data presented as mean± SEM. Magnification= 1.25x, scale= 1 mm.

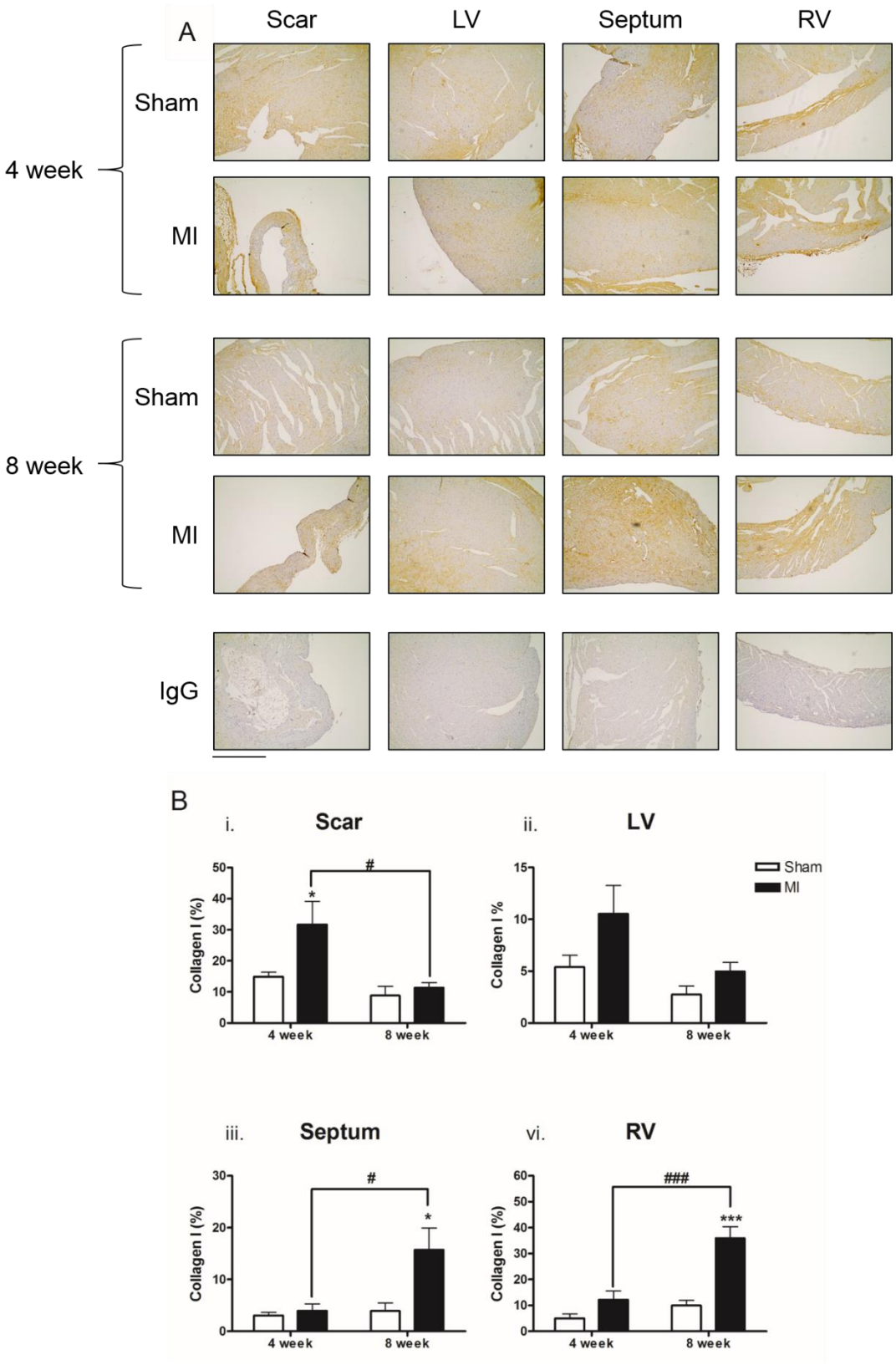

Figure 3.8 Cardiac regional collagen I quantification following MI.
(A) Representative images of heart regions showing distribution of DAB staining for collagen I expression in 4 and 8 wk sham and MI animals. Negative IgG used as a control for antibody specificity. Magnification= 10x, scale bar= 500 µm. (B) Quantification of DAB staining for positive collagen I expression in cardiac regions of scar (i.), LV (ii.), septum (iii.) and RV (iv.) as a percentage of the total region for 4 and 8 wk sham and MI animals. *= P<0.05, ***P<0.001 *vs*. time-matched sham, #=P<0.05, ###P<0.001 for 4 wk MI *vs*. 8 wk MI, n= 9 and 10 for 4 and 8 wk groups, respectively. Data presented as mean± SEM.

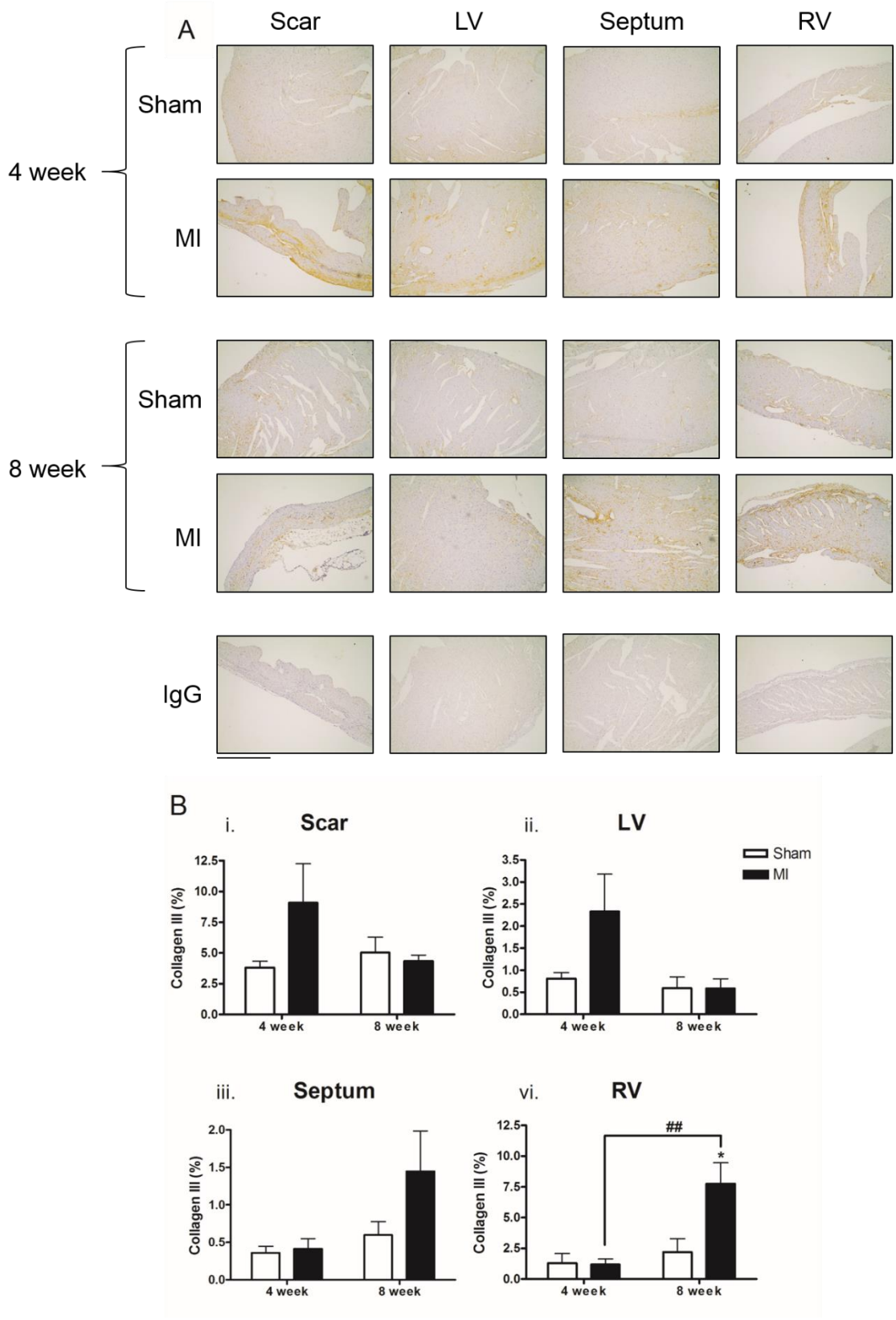

Figure 3.9 Cardiac regional collagen III quantification following MI.
(A) Representative images of heart regions showing distribution of DAB staining for collagen III expression in 4 and 8 wk sham and MI animals. Negative IgG used as a control for antibody specificity. Magnification= 10x, scale bar= 500 µm. (B) Quantification of DAB staining for positive collagen III expression in cardiac regions of scar (i.), LV (ii.), septum (iii.) and RV (iv.) as a percentage of the total region for 4 and 8 wk sham and MI animals. *= P<0.05 *vs*. time-matched sham, ##P<0.01 for 4 wk MI *vs*. 8 wk MI, n= 9 and 10 for 4 and 8 wk groups, respectively. Data presented as mean± SEM.

3.3.3.4 Perivascular fibrosis and collagen expression

At the 4 wk time point there was no significant difference in perivascular fibrosis between MI and sham groups (Figure 3.10 B). However, the 8 wk MI group demonstrated a significant increase in perivascular fibrosis compared to both the 8 wk sham group (15.8± 1.1 *vs*. 23.7± 1.9 %, 8 wk sham (*n*= 10) *vs*. 8 wk MI (*n*= 10); *P*<0.01; Figure 3.10 B) and 4 wk MI group (4 wk MI=15.8± 1.6 %; *P*<0.01; Figure 3.10 B). This was due to significant increases in perivascular collagen I expression compared to sham (5.8± 0.4 *vs*. 9.4± 1.0, 8 wk sham (*n*= 10) *vs*. 8 wk MI (*n*= 10); *P*<0.01; Figure 3.11 B) and 4 wk MI groups (4 wk MI= 6.4± 1.0 %; *P*<0.05; Figure 3.11 B), as well as a significant increase in perivascular collagen III expression compared to sham (4.3± 0.7 *vs*. 8.05± 0.6 %, 8 wk sham (*n*= 9) *vs*. 8 wk MI (*n*= 9); *P*<0.01; Figure 3.12 B) and 4 wk MI groups (4 wk MI= 4.2± 0.6 %; *P*<0.001; Figure 3.12 B).

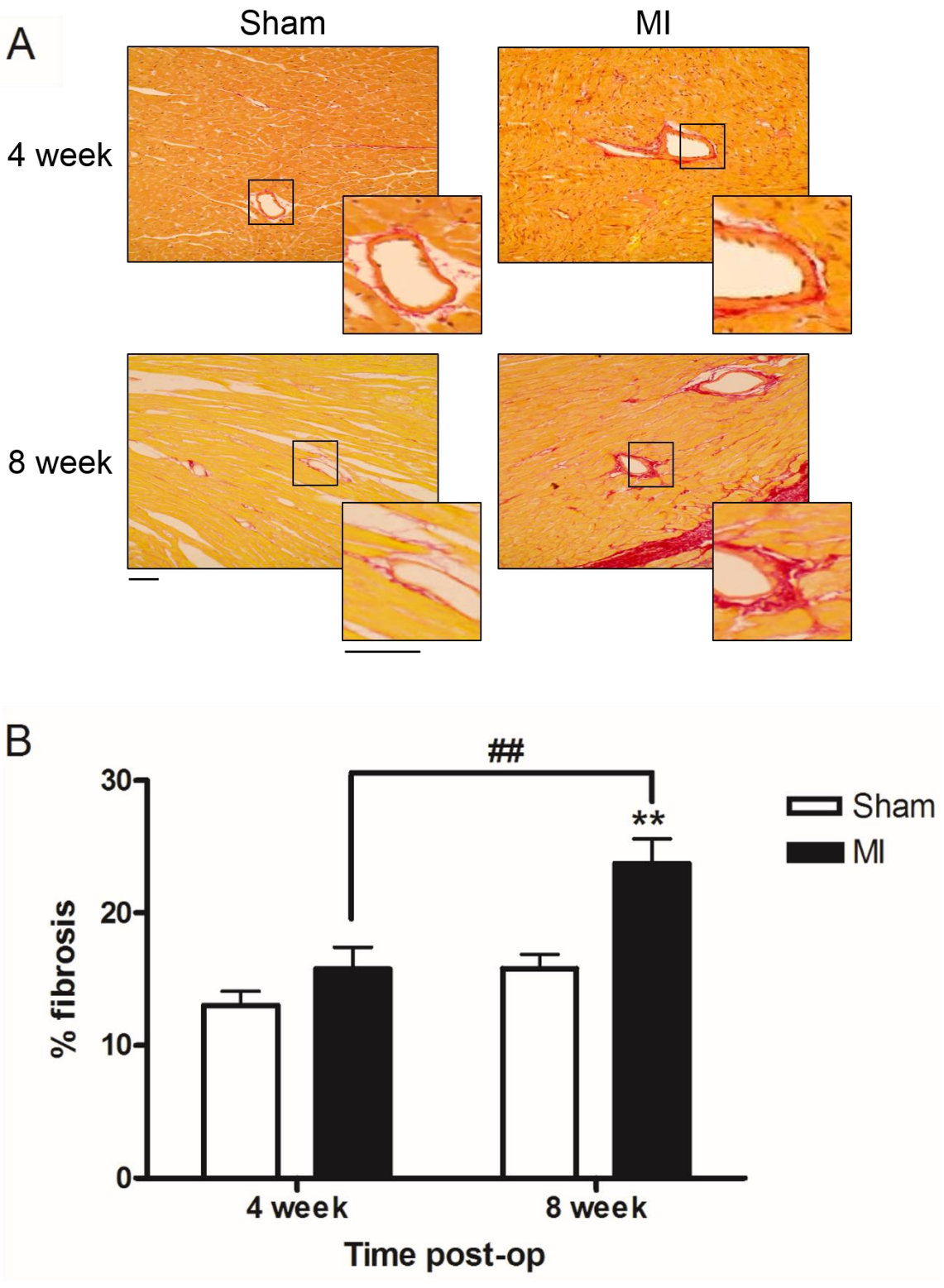

Figure 3.10 Cardiac perivascular fibrosis quantification following MI.
(A) Representative images of left-ventricular localised vessels and associated picrosirius red staining for 4 and 8 wk sham and MI heart sections. Magnification= 20x, scale= 100 µm. (B) Total perivascular cardiac fibrosis quantification of 4 and 8 wk sham and MI animals. **= *P*<0.01 *vs*. time-matched sham, ##= *P*<0.01 for 4 wk *vs*. 8 wk MI. *n*= 9 and 10 for 4 and 8 wk groups, respectively. Data presented as mean± SEM.

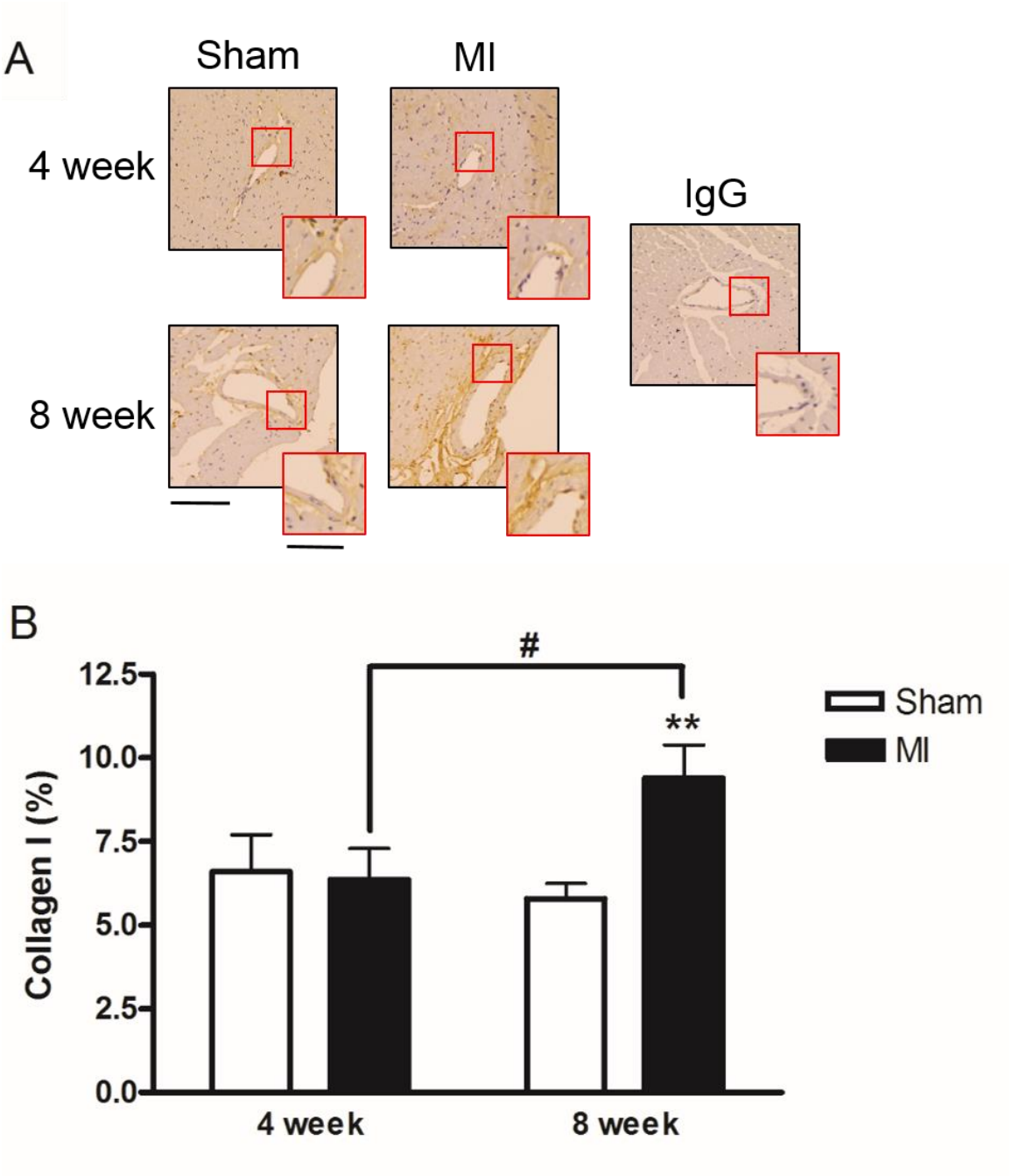

Figure 3.11 Cardiac perivascular collagen I quantification following MI.
(A) Representative images of cardiac vessels and associated DAB staining for collagen I expression for 4 and 8 wk sham and MI heart sections. Negative IgG used as a control for antibody specificity. Magnification= 20x, scale= 200 µm. Insert zoom image scale= 100 µm. (B) Quantification of DAB staining for perivascular collagen I expression in heart sections of 4 and 8 wk sham and MI animals. **= P<0.01 *vs* time-matched sham, #= P<0.05 for 4 wk *vs*. 8 wk MI. n= 7 and 10 for 4 wk and 8 wk groups, respectively. Data presented as mean± SEM.

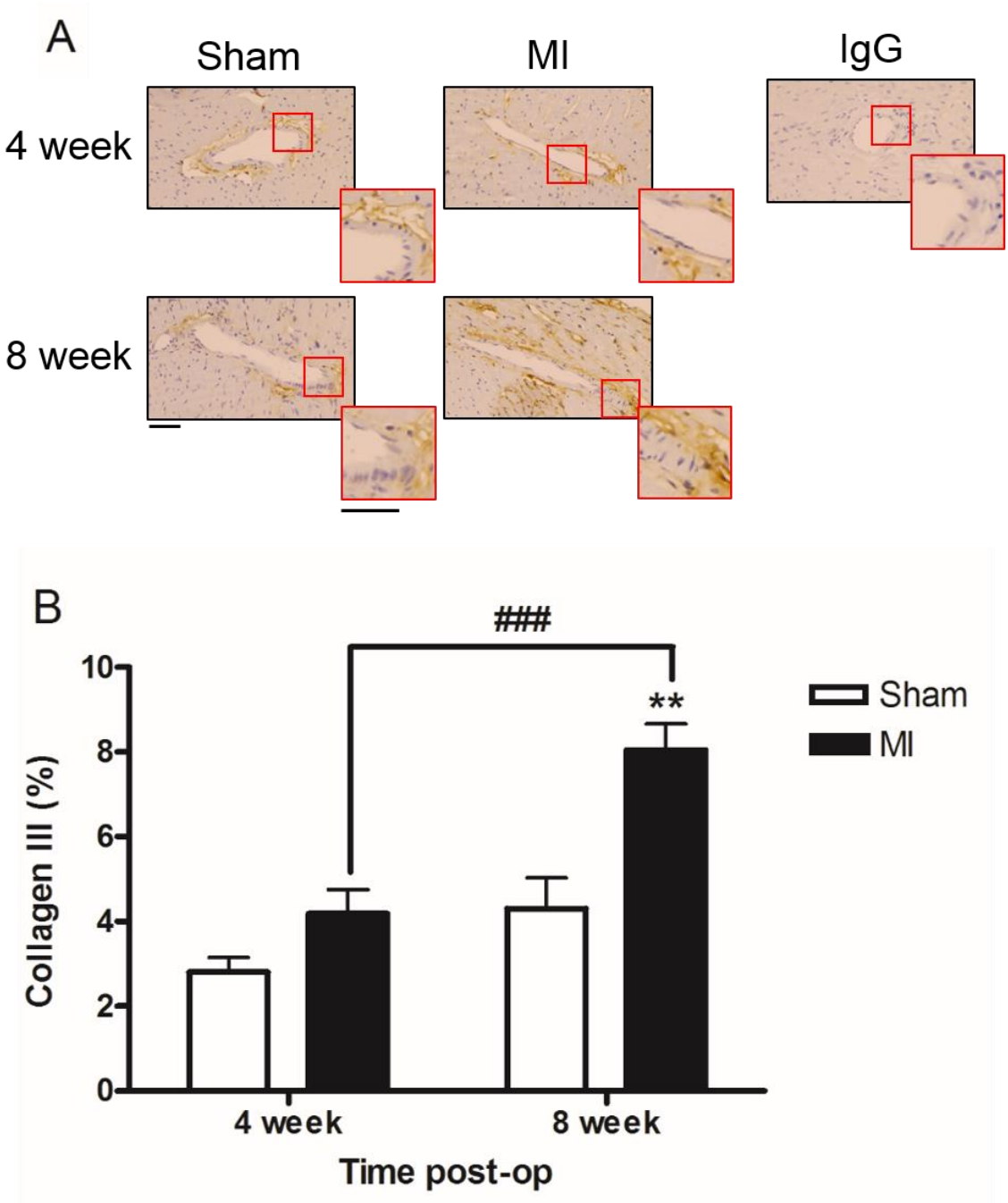

Figure 3.12 Cardiac perivascular collagen III quantification following MI.
(A) Representative images of cardiac vessels and associated DAB staining for collagen III expression for 4 and 8 wk sham and MI heart sections. Negative IgG used as a control for antibody specificity. Magnification= 20x, scale= 200 µm. (B). Quantification of perivascular DAB staining for collagen III expression in heart sections of 4 and 8 wk sham and MI animals. **= $P<0.01$ *vs* time-matched sham, ###= $P<0.001$ for 4 wk *vs*. 8 wk MI. $n= 9$ for each group. Data presented as mean± SEM.

3.3.4 Gene expression analysis

3.3.4.1 Selection of a stable housekeeping gene for normalisation

In order to identify a suitable housekeeping gene for use in gene expression analysis in mouse MI tissue, qRT-PCR was performed for 3 housekeeping genes (GAPDH, 18s and B2m) (Figure 3.13). With only 0.3 Ct difference between average MI and sham values, GAPDH was the most stable between the two groups, therefore GAPDH was used as the housekeeping control gene for normalisation of data in all other gene expression analysis.

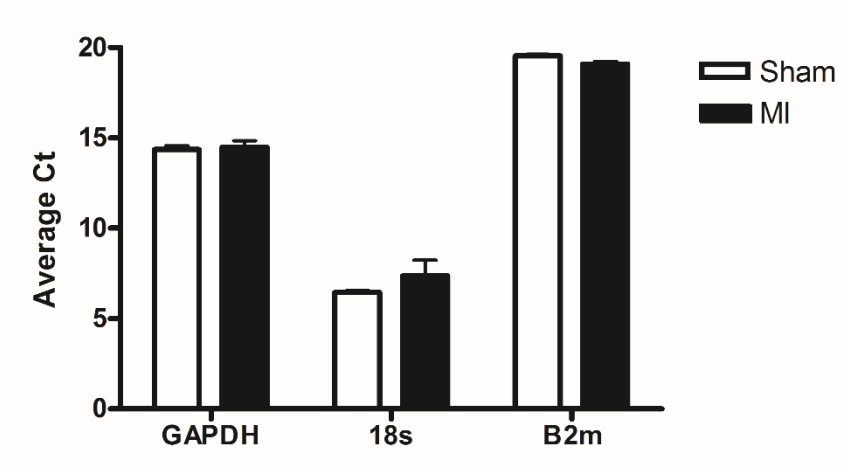

Figure 3.13 Stability of house-keeping genes for use in qRT-PCR in sham and MI heart tissue.
Global gene expression of 3 common house-keeping genes (GAPDH, 18s and B2m) in the cardiac tissue of 8 wk sham and MI animals as determined by qRT-PCR. *n*= 4 per group. Data presented as mean Ct± SEM. Ct= cycle threshold.

3.3.4.2 RAS Receptor Gene Expression

Regional expression of the main RAS receptors, AT_1R, AT_2R and Mas, was determined using qRT-PCR in sham and MI heart tissue at 3 days, 1, 4 and 8 wks post-MI (Figure 3.14). Gene expression was normalised to GAPDH and MI expression relative to the corresponding time- and region-matched sham expression. Hearts were separated into 4 regions; scar, border, remote LV and RV, with a proximal apical region of sham hearts taken as the scar region.

AT_1R expression was significantly reduced following MI at all time-points except the 1 wk post-MI time-point. At 3 days post-MI, expression was significantly reduced in all MI regions ($P<0.05$), with the most pronounced reduction in expression evident in the scar region, with a 6.6-fold reduction in expression corresponding to a doubling of the normalised Ct value (3.6± 0.01 *vs*. 6.4± 0.2 Ct, 3 day sham scar ($n= 3$) *vs*. 3 day MI scar ($n= 3$); $P<0.05$). At 4 wks there was a trend towards reduced expression in the scar and remote-LV regions, and a significant reduction in the border region ($P<0.05$). At 8 wks post-MI, expression in all regions was significantly reduced by 2-4 fold in each region compared to sham ($P<0.05$; Figure 3.14 A). AT_2R expression was significantly up-regulated specifically in the scar region but this gradually reduced to sham levels as the time post-MI increased (Figure 3.14 B). At 3-days post-MI, expression in the scar region was increased approximately 17-fold compared to the corresponding sham region (RQ= 16.7± 0.6, $P<0.001$). Expression was increased 7-fold in the scar region one week post MI compared to sham (RQ= 6.9± 2.2, $P<0.05$). At 4-wks post-MI, there was a 20-fold increase in AT_2R expression in the scar region. At 8-wks post-MI there was still a small but significant increase in AT_2R expression in the scar region (RQ= 3.9± 0.03, $P<0.001$; Figure 3.14 B). Mas receptor expression was unchanged in all regions at all time-points post-MI in comparison to corresponding sham animal regions and time-points (Figure 3.14 C).

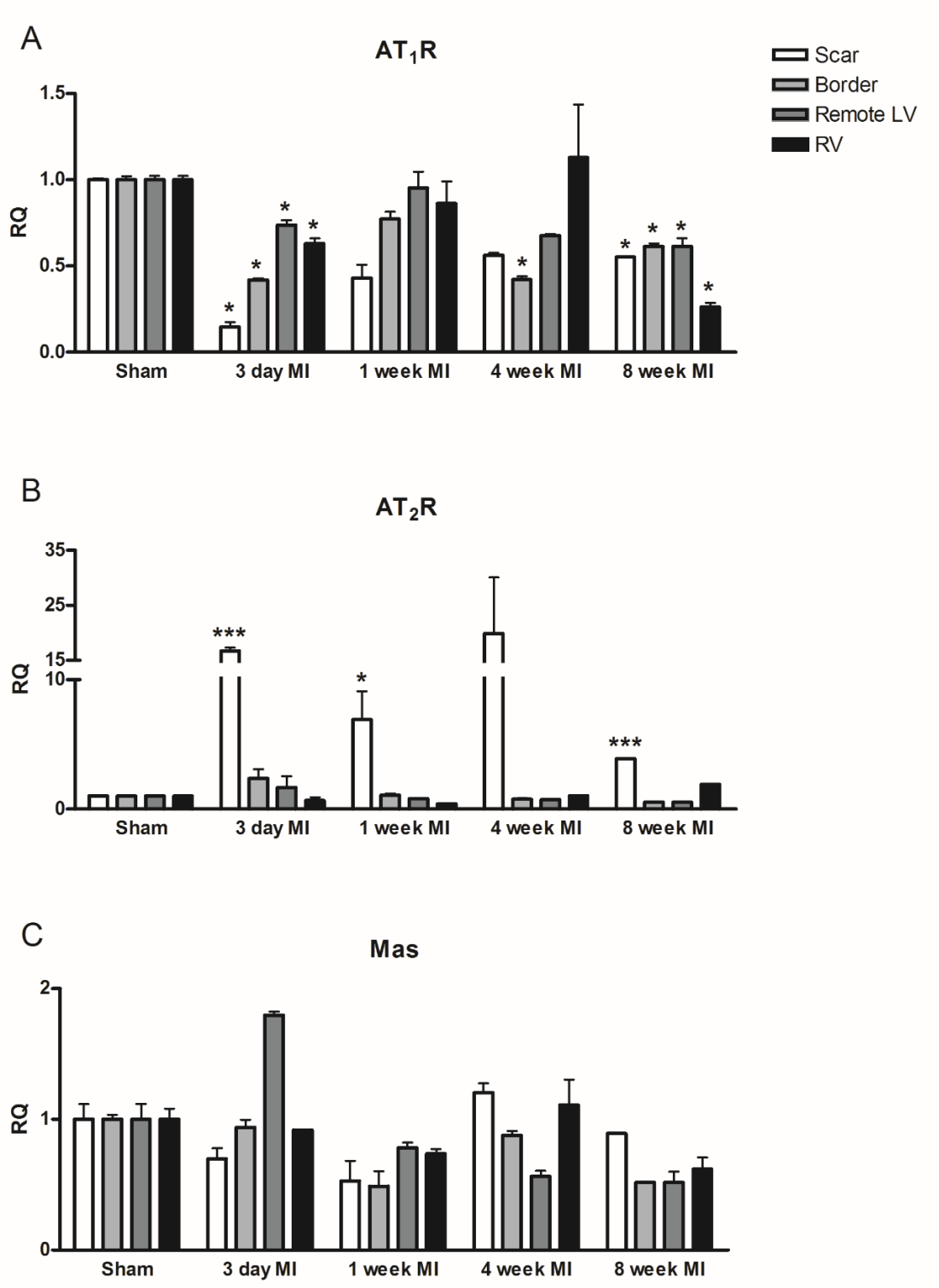

Figure 3.14 RAS-receptor regional cardiac gene expression in MI and sham animals. qRT-PCR-determined gene expression quantification of AT_1R (A), AT_2R (B) and Mas (C) receptors in the scar, border, remote-LV and RV regions of 3 day, 1, 4 and 8 wk sham and MI hearts. *= $P<0.05$, **= $P<0.01$, ***= $P<0.001$ *vs*. time-matched sham region. n= 3 per time-point. Data presented as RQ± rq_{max}. Normalisation of expression to a housekeeper (GAPDH) was performed for all samples. MI gene expression was normalised to equivalent time-matched sham region expression, therefore sham expression was arbitrarily set at a RQ= 1. RQ= relative quantification, LV= left ventricle, RV= right ventricle.

3.3.4.3 ACE and ACE2 Expression

Next, regional expression of ACE and ACE2 was determined (Figure 3.15). ACE expression showed a region-specific expression pattern, with significant up-regulation in the scar region of MI animals at all time-points with the exception of 3 days post-MI. Expression levels were increased in the MI scar region from 1 wk post-MI onwards, with levels increased 4.2± 0.3 (P<0.01), 4.6± 0.2 (P<0.01) and 4.2± 0.9 (P<0.05) fold compared to sham scar for 1, 4 and 8 wk MI respectively (Figure 3.15 A). Conversely, ACE2 expression was down-regulated, but in a region-specific manner, primarily at acute time-points following MI. The most pronounced change was observed 3 days post-MI, with a significant decrease in expression in the scar and border regions (RQ= 0.29± 0.05 and 0.66± 0.04, respectively; P<0.05). A significant reduction was also seen in the border region 4 wks post-MI (RQ= 0.7± 0.03, P<0.05). At 8 following MI, ACE2 expression had normalised to sham levels (Figure 3.15 B).

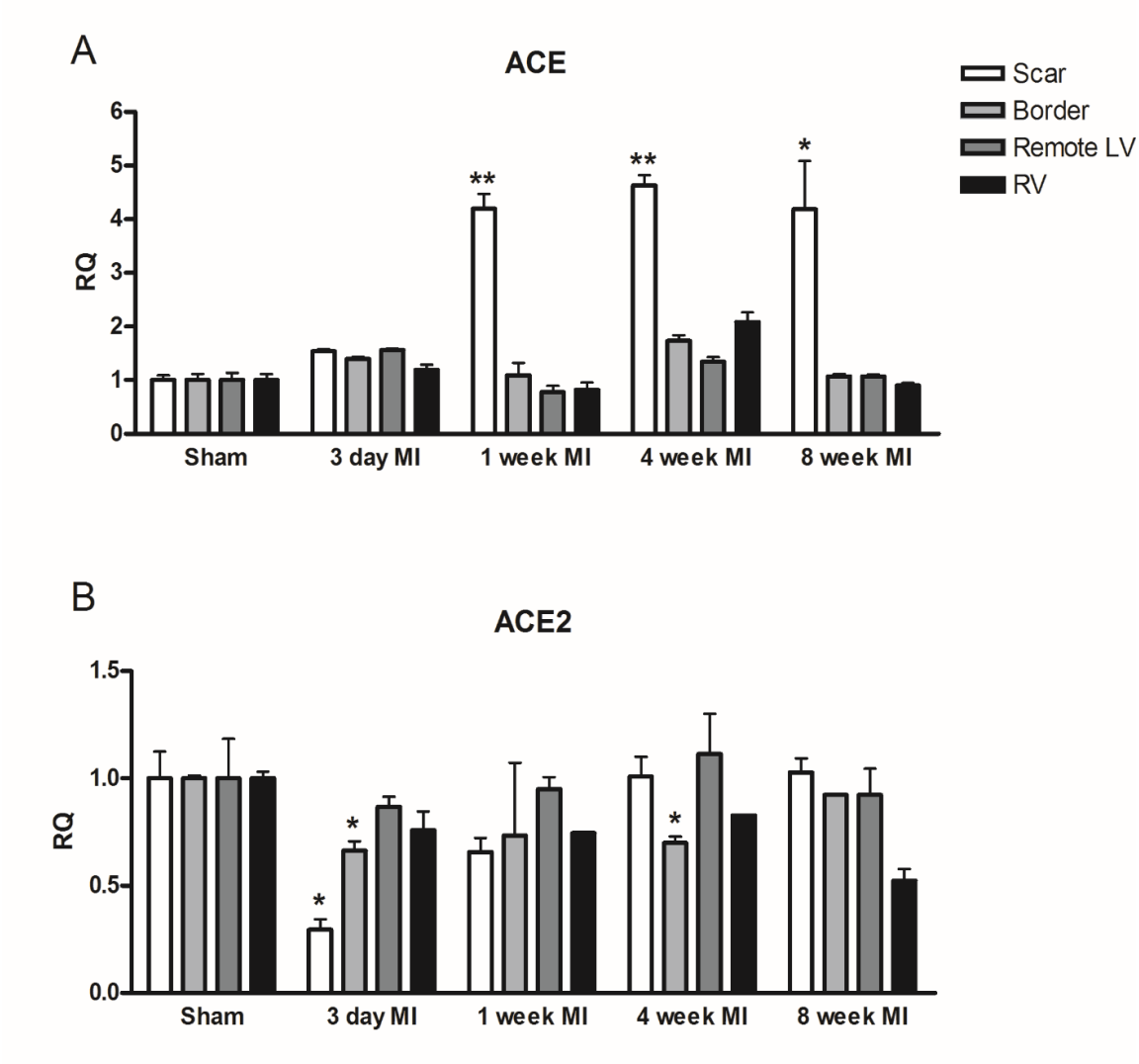

Figure 3.15 ACE and ACE2 regional cardiac gene expression in MI and sham animals. qRT-PCR-determined gene expression quantification of ACE (A) and ACE2 (B) enzymes in the scar, border, remote-LV and RV regions of 3 day, 1, 4 and 8 wk sham and MI hearts. *= $P<0.05$, **= $P<0.01$ *vs*. time-matched sham region. n= 3 per time-point. Data presented as RQ± rq_{max}. Normalisation of expression to a housekeeper (GAPDH) was performed for all samples. MI gene expression was normalised to equivalent time-matched sham region expression, therefore sham expression was arbitrarily set at a RQ= 1. RQ= relative quantification, LV= left ventricle, RV= right ventricle.

3.4 Discussion

Here, the permanent CAL mouse MI model was characterised for both functional, structural and gene expression parameters, primarily at 4 and 8 wk post-MI time-points, to assess its suitability as a model of cardiac dysfunction and remodelling. The data demonstrated adverse changes to both cardiac function and structure following MI, including reduced LV systolic indices and increased fibrosis and hypertrophy, which were associated with changes to RAS receptor and enzyme expression.

It is well established that the mouse LAD permanent ligation model is associated with high incidence of mortality (Gehrmann et al., 2001; Lutgens et al., 1999; Patten et al., 1998), consistent with what was observed here, where the main cause of reduced survival, other than procedural-associated mortality, was cardiac rupture, which occurred within the first week following recovery. Cardiac rupture has been shown to occur primarily between a few hours up to 6 days following procedure, and found to be accountable for between 12.5-26.4 % of total published mortality (Barandon et al., 2003; Gehrmann et al., 2001; Patten et al., 1998). Cardiac rupture can occur in 10 % of human patients who have suffered a transmural MI, accounting for approximately a third of total MI patients (Kumar and Cannon, 2009; Oliva et al., 1993). The mouse MI model is thought to be the only experimental animal model to mimic this (Gao et al., 2010). In the present study only a small number of deaths occurred outside the rupture-risk time frame (≤ 7 days post-MI) in the MI group. Sudden death at later time-points have also been reported elsewhere in the model, with mortalities recorded from 2 wks up to 6 months following MI (Patten et al., 1998; Yang et al., 2002a). Both rupture-related and later sudden deaths have been reported to be potentially associated with large infarcts incorporating >48 % of the left ventricle (Patten et al., 1998). This is due to greater collagen degradation during the scar healing phases leading to enhanced wall-thinning and increased wall stress being exerted on the surviving myocardium and more severe ventricular remodelling and progression to HF (Patten et al., 1998).

Echocardiography in MI animals demonstrated an acute and progressive reduction in cardiac contractility following MI. Using echocardiography, it has been demonstrated that significant LV dilation and reduced wall movement

leads to a significantly reduced FS in MI as early as 1 wk following infarction (Gao et al., 2000; Gehrmann et al., 2001; Patten et al., 1998), consistent with observations here. Early LV dilation is a result of acute scar expansion in the infarcted region, with expansion of the non-infarcted LV occurring in the more chronic remodelling phase (Trueblood et al., 2001). Trans-mitral Doppler analysis using echocardiography allows assessment of diastolic filling patterns as a measurement of diastolic dysfunction and ventricular compliance (Hoit and Walsh, 1997). Here, no difference was observed between sham and MI E/A wave isoform ratios at either 4 or 8 wks following MI. In failing MI hearts, an increased E/A ratio is normally evident due to impairment of LV relaxation (Krishnamurthy et al., 2006; Liu et al., 2010b). However, it was previously reported that to identify parameters to distinguish HF and non-failing mouse MI hearts at 2 weeks post-MI a significant decrease in mitral valve Doppler velocity was only detectable in mice with large infarcts (>40 %) (Finsen et al., 2005). Therefore the results observed here may be as a result of smaller infarct sizes. Moreover, no significant alteration in E/A ratio in mouse MI animals up to 90 days post-MI, despite obvious fibrotic tissue accumulation and evidence of reduced myocardial performance, has also been observed (Benavides-Vallve et al., 2012).

LV hypertrophy was not evident in MI animals from echocardiography measurements, however cardiac hypertrophy was identified from post-mortem heart weight and histological analysis. It is possible that hypertrophy was not evident in M-mode images due to limited spatial resolution when used on the rapidly beating mouse heart as a result of the low transducer frequency available here (Doevendans et al., 1998; Hoit and Walsh, 1997). WGA staining demonstrated that the LV hypertrophy in MI animals was due to concentric hypertrophy, or cell thickening, rather than eccentric hypertrophy, or cell lengthening, at both time-points. This increase in cross-sectional area is consistent with that observed by Yang *et al.*, (2002) where myocyte cross-sectional area of the non-infarcted region of mouse MI hearts was assessed at various time-points, with a significant increase evident from as early as 1 wk post-MI, with progressive increases until 6 months post-MI (Yang et al., 2002a). Concentric hypertrophy has been shown to be more commonly associated with cardiac functional compensation, with a transition to eccentric hypertrophy being associated with decline of cardiac function and progression to heart failure

(Francis and Chu, 1995; Gerdes, 1997; Lemmens et al., 2007; Scherrer-Crosbie et al., 2001). This is another indication that the MI hearts at 4 and 8 weeks are still well compensated. Although concentric hypertrophy is beneficial for LV dilation and systolic function, it can still be associated with diastolic dysfunction (Jain et al., 2002). However, the presence of ventricular dilation, as evidenced by PV-loop measurements at both 4 and 8 wks post-MI, in the absence of non-infarcted wall thinning suggests there may also be eccentric hypertrophy occurring. In fact, when EDV was plotted against cell length for MI animals here there was a significant relationship between increasing cell length and EDV, suggested greater cell lengthening in a small sub-set of MI animals with more advanced dilation. It has been demonstrated that both eccentric and concentric hypertrophy occurs following MI as a result of the combined increase in volume and pressure load on non-infarcted myocardium (Force and Molkentin, 2006; Opie et al., 2006; Runge and Patterson, 2007).

PV loop measurements demonstrated the development of systolic and diastolic dysfunction in the mouse MI model. Systolic dysfunction combined with ventricular dilation resulted in a significantly reduced EF, with a tendency to be more severe at 8 wks. EDPVR measurements, which assess ventricular compliance independent of load, demonstrated a significant increase at 8 wks post-MI, but not at 4 wks, suggesting increasing ventricular stiffness over time. However, between 4 and 8 wks post-MI, haemodynamic parameters did not change significantly, with equivalent levels of dysfunction at each time-point in the MI group. This is consistent with previous observations in this model (Shioura et al., 2007). Using the mouse MI model a comparison of closed-chest haemodynamic properties in mice 2, 4, 6 and 10 wks post-MI was performed and demonstrated an early decline in systolic function which declined gradually with increased time, with diastolic dysfunction declining gradually and only reaching significance by 10 wks. Hearts at 4 and 6 wks post-MI were found to be well compensated, thought to be as a result of hypertrophy and scar stabilisation, with decompensation evident at 10 wks post-MI (Shioura et al., 2007). In the study presented here the only notable difference between 4 and 8 wk post-MI animals was an increased EDPVR at the 8 wk time-point compared to 4 wks. Increased EDPVR indicates dysfunctional relaxation of the ventricle following

contraction due to stiffening, primarily as a result of interstitial fibrosis and collagen deposition (Tsuda et al., 2003).

This increased EDPVR at 8 wks post-MI was consistent with histology assessing total fibrosis and collagen deposition, which demonstrated a significant increase in total fibrosis of the scar, LV, septum and RV of 4 and 8 wk MI hearts, which was significantly worse at the 8 wk time point, as was perivascular fibrosis, suggesting the majority of fibrosis at 4 wks is interstitial with a mix of both interstitial and perivascular fibrosis at 8 wks. When looking specifically at different collagen isoform expression, there was no significant change in either collagen I or III expression in the LV of either MI group at either time-point. However, at 4 wks the scar region shows a significant increase in collagen I expression. This reduced to equivalent levels as sham animals by 8 wks. The increase in total fibrosis seen in the septum, RV and in the perivascular region of the 8 wk animals corresponded to an increase in both collagen I and collagen III isoforms in these regions. In general collagen I was more highly expressed than collagen III in all regions. The extent of interstitial and perivascular fibrosis and the enhanced collagen deposition in the non-infarcted myocardial regions is consistent with previous reports in the mouse MI model (Doevendans et al., 1998; Takeshita et al., 2004). ECM deposition and fibroblast proliferation is dynamically regulated by MMPs in response to myocardial injury and inflammation (Jugdutt, 2003; Shioura et al., 2007), with ECM proteins undergoing rapid synthesis and breakdown (Trueblood et al., 2001). The dynamic nature of collagen expression may account for the differences in collagen isoforms observed between 4 and 8 wks post-MI. Isoform expression has been identified to be time-specific following MI, with myofibroblast proliferation and collagen synthesis occurring while the scar is forming, which, once complete, triggers collagen expression to be down-regulated and stimulates apoptosis of most of the myofibroblasts (Sutton and Sharpe, 2000). The dynamic nature of collagen expression has been demonstrated in the rat MI model, where collagen I and III expression was dramatically altered in different heart regions at different times, with collagen III found to be associated with the more acute remodelling phase but being down-regulated at later time-points, while collagen I levels were elevated at 4 days post-MI and remained up-regulated at 90 days (Cleutjens et al., 1995a). This may help explain the reduction in collagen and the increase

in fibrotic area observed in the scar region at 8 wks. With collagen and myofibroblasts mainly being associated with necrotising myocytes (Sutton and Sharpe, 2000), it could be assumed that by 8 wks there are far fewer myocytes remaining in the infarcted area and the scar is fully formed, therefore collagen is down-regulated. Collagen I and collagen III isoforms are the two most common collagen isoforms found in the heart and have been shown to have different physical properties (Janicki et al., 1988). An increase in collagen I: collagen III ratio has been found in hearts from patients with CHF (Bishop et al., 1990) and it has also been shown that the collagen I: collagen III ratio is increased in both the LV and RV of the rat MI HF model, consistent with changes in haemodynamic measurements and the development of ventricular dysfunction (Wei et al., 1999). This is consistent with observations in the mouse MI model here.

The haemodynamic changes following MI suggests that although considerable LV remodelling had taken place, the hearts had not reached failure stage and cardiac function was still compensated. The rat MI model has previously been characterised to present with similar pathophysiological manifestations as human CHF patients, such as depressed CO and elevated left ventricular filling pressure (Pfeffer et al., 1979), and therefore is an accepted animal model of CHF. In contrast, CO has been shown to be preserved in this model even up to 12 months following MI (Pons et al., 2003). CHF is developed in the model providing a sufficiently large infarct is induced (>40 % of the LV) (Finsen et al., 2005; Kinugawa et al., 2000; Li et al., 2006b). Animals with infarcts above 50 % demonstrate a high mortality rate within the first 2 wks following surgery, while mice with infarcts of less than 30 % show very little adverse remodelling compared to sham animals (Bayat et al., 2002). However, large infarct also has the disadvantage of leading to an increased rupture rate (Patten et al., 1998). In the present study, infarct size was consistently <40 %; there was no alteration in E/A ratio; the hypertrophic response was found to be predominantly concentric; CO, SV and EDP was unaltered and there was no indication of pulmonary oedema, all of which suggest the mouse MI model in this setting was a model of compensated left-ventricular dysfunction rather than one of CHF.

Gene expression analysis of RAS components following MI have previously been reported primarily in the rat MI model (Savoia et al., 2011; Sun et al., 1998; Yang et al., 1998). The changes in AT_2R receptor levels in this study are

consistent with what has been reported in the rat, with it being shown that AT_2R expression levels are extremely low in the normal rodent heart (Schluter and Wenzel, 2008), but are found to be up-regulated in pathological conditions, including MI (Savoia et al., 2011). However, AT_1R levels have been demonstrated to be up-regulated in rat hearts immediately following global ischemia (Yang et al., 1998) and in the rat MI model (Sun et al., 1998). The discrepancy seen here may be the result of AT_1R regulation by Ang II. It has been shown that following acute Ang II up-regulation, AT_1R receptor expression increases in the associated tissue. However, upon chronic Ang II exposure, AT_1R will be down-regulated due to a negative feedback loop (Kim et al., 2005). Furthermore, the expression pattern of both the AT_1R and AT_2R seen here is similar to that seen in biopsies performed in hearts from patients with CHF, where AT_1R expression has been shown to be down-regulated in the atrial and LV tissue in comparison to the AT_2R (Tsutsumi et al., 1998).

ACE and ACE2 gene expression was shown in the present study to be dysregulated in a region-specific manner, with expression only changing within the scar and, in some instances, the border region. ACE levels were unchanged in the acute phase immediately following MI, however by 1 wk post-MI it was found to be significantly up-regulated in the scar region. This up-regulation then remained stable at the later time-points studied. Conversely, ACE2 was significantly down-regulated during the acute phase following MI, with this change evident in the scar at 3 days post-MI and in the scar and border regions 4 wks post-MI, with levels returning to that of sham at the more chronic 8 wk time-point. Again, any comparable data on ACE and ACE2 expression following MI has been performed in the rat. Two such studies have shown almost identical changes in ACE expression in the rat as seen here in the mouse, with up-regulation evident from 3 days- 1 wk post-MI and maintained up until at least 8 wks post-MI (Burrell et al., 2005; Ocaranza et al., 2006). However, the pattern of ACE2 expression reported does not match what has been observed here, with it reported as being up-regulated in the LV during the acute phase but down-regulated at later time points (Ocaranza et al., 2006). ACE2 has also been reported to be up-regulated in both infarcted and non-infarcted regions in both acute and chronic phases following MI (Burrell et al., 2005). Global cardiac ACE and ACE2 expression in the rat 4 wks following MI demonstrated no changes in

expression of either enzyme (Ishiyama et al., 2004). The discrepancies seen in these studies compared to this work could potentially be the result of species variation or the region of the heart in which expression was assessed. It is also likely that infarct size and resulting severity of remodelling, level of contractile compensation and region of expression are all key in affecting ACE and ACE2 expression levels, especially as they have been associated with decline and improved cardiac contractility, respectively (Crackower et al., 2002; Zhao et al., 2010).

In human heart disease, ACE and ACE2 are found up-regulated in the LV in cases of ischemic HF, with ACE found to be increased 3 fold compared to controls (Goulter et al., 2004; Studer et al., 1994; Zisman et al., 2003). Up-regulation of ACE2 in this setting has been proposed to be a compensatory mechanism for counter-acting chronic activation of the RAS through degradation of Ang II (Ferreira et al., 2010b; Wang et al., 2012). This increase in ACE expression in LV seen in human MI is consistent with the increased ACE expression seen here in the mouse scar region. Similarly, in advanced stages post-MI in human MI, LV AT_1R expression is found to be down-regulated while AT_2R expression remains unchanged following an initial increase during the acute post-MI phase (Haywood et al., 1997). A very similar pattern of expression is observed here in the MI model, with a global decrease in AT_1R expression associated with reduction of AT_2R expression by 8 weeks post-MI.

3.5 Summary

These data have demonstrated that the mouse MI model is a suitable model of compensated left-ventricular dysfunction that presents with measurable structural and functional cardiac remodelling changes comparable to that previously reported. Furthermore, the model shows changes in RAS component gene expression that are comparable to that seen in hearts of patients with cardiac dysfunction and which have previously not been demonstrated in the mouse MI model. Therefore, it is a suitable model in which to study the effects of a potential RAS-targeted therapeutic on these adverse remodelling changes.

Chapter 4: Assessment of the effects of Ad-mediated delivery of Ang-(1-9) in the mouse MI model

4.1 Introduction

4.1.1 Ad

Adenoviruses (Ad) are non-enveloped, medium-sized viruses carrying a linear, double stranded genome of 30-40 Kb in an icosahedral nucleocapsid between 70-100 nm in diameter (Graham and Prevec, 1991; Kennedy and Parks, 2009). They were first isolated from human adenoid tissue in 1953 (Rowe et al., 1953). Over 51 human Ad serotypes have since been identified, with human Ad5 the most extensively characterised (Russell, 2009). Serotyping was the original classification used on the basis of the virus's ability to be neutralised by specific animal antisera. They can be further classified into 6 species, A-F, based on their ability to agglutinate erythrocytes. Members of a particular species tend to show similarities in tissue tropism and clinical manifestations (Borriello et al., 2005). Human Ad infection is prevalent in the population, however it is generally not associated with severe disease. Species C, such as Ad5, cause mild respiratory infection when inhaled, with some serotypes (e.g. species F) associated with gastrointestinal infection (Duncan and Hutchison, 1961) and others with conjunctivitis (e.g. species B and D) when they come into contact with the eye (Lichtenstein and Wold, 2004). Ad4 and Ad14 have been identified as having the potential to induce acute respiratory distress (ARD) upon inhalation, although this occurs more commonly in immunocompromised individuals (Russell, 2009).

Different Ad serotypes are reasonably well conserved, however they do show differences in their host and tissue tropism (Kennedy and Parks, 2009). Determination of tissue tropism and host species of Ad5 vectors has been shown to be determined by fibre and penton base domains which dictate cell receptor interactions (Havenga et al., 2002). This has been elegantly demonstrated through the development of fibre chimeric Ad5 vectors which are engineered to express the fibre proteins of a different serotype, thus altering its tropism. For example, an Ad5 vector expressing an Ad16 fibre shows more efficient transduction of vascular endothelial and smooth muscle cells than Ad5 (Havenga et al., 2001). Due to the ubiquitous nature of coxsackie Ad receptor (CAR), tissue targeting of Ad vectors is problematic. Ad delivered systemically will disseminate throughout the body, potentially causing off-target effects. This can

be controlled through the route of administration, such as direct injection to target tissues rather than systemic delivery (Johnson et al., 2006), as well as through direct modification of viral fibre molecules, viral conjugation or chemical polymer modifications (Mizuguchi and Hayakawa, 2004). *Iv* delivery results in sequestration of the virus primarily to the liver through interaction with FX in the blood (Kalyuzhniy et al., 2008; Waddington et al., 2008).

4.1.1.1 Adenoviral structure, infection and DNA replication

The development of advanced X-ray crystallography and microscopy techniques enabled determination and assignment of the main Ad structural proteins (Saban et al., 2005; Stewart et al., 1993)(Figure 4.1). The basic capsid structure is composed of 240 homotrimeric hexon proteins composing the faces and edges of the capsid, and penton base proteins which are located on the 12 apices of the capsid and are attached to the fibres which are composed of 3 distinct regions; the tail, shaft and knob (Russell, 2009). There are also several minor proteins (IIIa, VI, VIII and IX) associated with the capsid and thought to be required for capsid stabilisation (Smith et al., 2010; Vellinga et al., 2005). In the virus core there are 6 other proteins, 5 of which are associated with the genome [V, VII, Mu, IVa2 and the terminal protein (TP)], with the sixth being the virion protease, which is essential in the assembly of new viral particles (Russell, 2009).

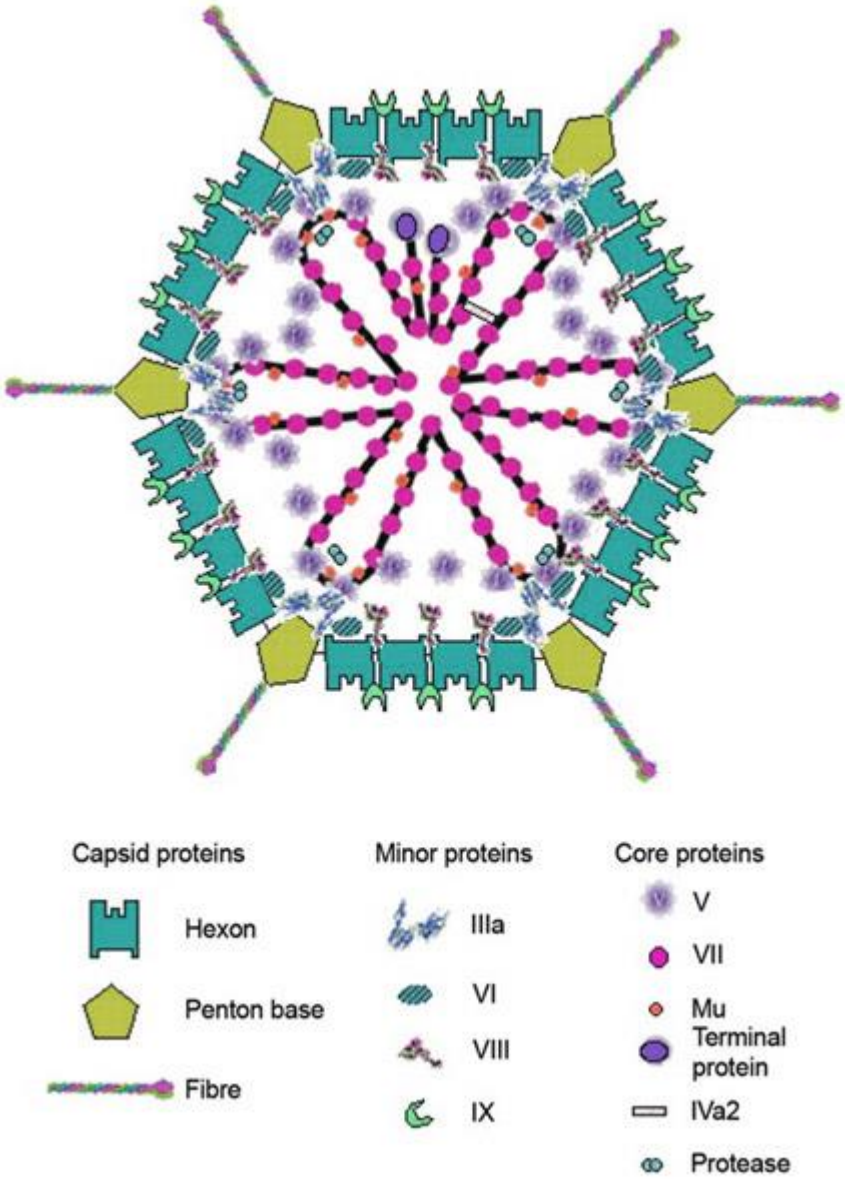

Figure 4.1 Ad capsid and core structure.
Schematic of an Ad capsid cross-section identifying the location of the major and minor capsid and core proteins (Russell, 2009).

Upon infection the first stage of virus internalisation into the cell has been found to be through receptor binding of the fibre knob (Zhang and Bergelson, 2005). Species C Ad5 is the best characterised with it identified *in vitro* and during local infection in many tissues to utilises the immunoglobulin coxsackie Ad receptor (CAR) for cell entry, which is found on many different cell types (Bergelson et al., 1997; Noutsias et al., 2001). Other species have been shown to utilise other receptors, e.g. some members of the species D family utilise sialic acid (Arnberg et al., 2002), whereas most of the species B serotypes bind to CD46 (Gaggar et al., 2005; Marttila et al., 2005). Following receptor attachment, entry into the cell is facilitated by the interaction of the RGD motif located on the penton base with cellular α_V integrins, which triggers viral internalisation *via* endocytosis into an endosome through clathrin-coated pit formation and rearrangement of the cytoskeleton (Mathias et al., 1994). Once internalised, a step-wise disassembly of the viral capsid begins with release of the fibre proteins and dissociation of the penton bases. The core and minor capsid proteins are then shed or degraded (Greber et al., 1993). Endosome membrane disruption is then brought about by the activity of the endosomalytic protein VI (Wiethoff et al., 2005), releasing the partially un-coated capsid into the cytoplasm where it translocates *via* microtubules towards the nucleus into which it releases its genome by docking at a nuclear pore (Russell, 2009).

Once the genome has entered the nucleus Ad replication occurs (Figure 4.2). This can be separated into two main phases; the early stage and DNA replication, and the late stage (Paul Thomas and Mathews, 1980). Each stage involves expression of particular genes; the early genes (E1A, E1B, E2B, E3 and E4) and late genes (L1-L5) which encode for functions specific to each stage. Host cell proteins are also utilised by the virus for successful replication (Cann, 2001; Davison et al., 2003; Hay, 1985; Van der Vliet, 1995).

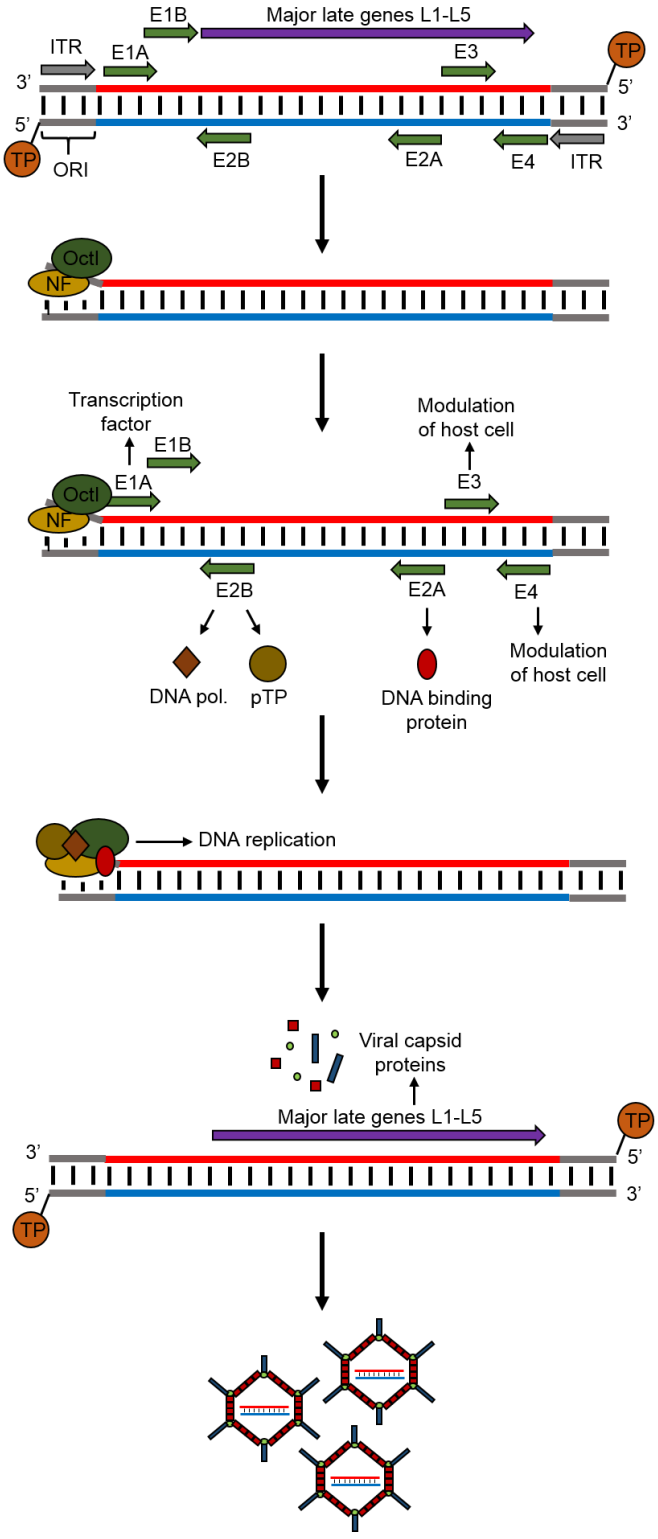

Figure 4.2 Ad DNA replication
Schematic showing the process of Ad DNA replication following host cell invasion. ITR= inverted terminal repeat, ORI= origin of replication, TP= terminal protein, E= early, L= late, TP= terminal protein, pTP= pre-cursor terminal protein, NFI= nuclear factor I, OctI/NFIII= nuclear factor III.

4.1.2 Ad as a gene therapy vector

Human Ad5 is currently the most commonly used vector for clinical gene therapy applications (Dormond et al., 2009). Its relative ease of construction, ability to infect post-mitotic cells, be produced in high titres in complementing cell lines (Kamen and Henry, 2004), and its high transduction rates in a variety of cells *in vitro* and *in vivo* (Schiedner et al., 1998) make them ideal vectors for gene therapy research. The late 1990's saw a dramatic increase in research surrounding the clinical application of Ad gene therapy vectors, however this suffered a severe blow in 1999 when 18 year old Jesse Gelsinger tragically died as a result of taking part in an Ad5 gene therapy trial for ornithine transcarbamylase (OTC) deficiency as a result of fatal systemic inflammatory response syndrome in response to transduction with the virus (Raper et al., 2003).

Modification of the Ad genome for gene therapy application initially saw the generation of replication-deficient vectors through the deletion of E1A and E1B regions of the genome, inhibiting viral replication but allowing propagation in cell lines, such as 293 cells, which encode the E1 genes *in trans* necessary for Ad5 replication (Kozarsky and Wilson, 1993). However, first generation rAd vectors, with only E1 deletions, retain a high level of cytotoxicity and have a cloning capacity of only 5.2 kb (Graham et al., 1977), making them unsuitable for many gene therapy uses (Benihoud et al., 1999). Second generation rAds have multiple deletions in the viral genome, with the E1 deletion combined with either E2, E3 or E4 deletions, which further improves their safety profile, reduces the host inflammatory response and increases transgene capacity (Rauschhuber et al., 2012). Second generation vectors superceded by third generation rAd vectors are also termed gutless vectors, in that all viral genes have been removed excluding the ITRs and viral packaging signal. They therefore require helper viruses for replication *in vitro* (Benihoud et al., 1999). These vectors have the added benefits of being able to carry a transgene up to 36 kb in size, and further improved safety profile due to the absence of the viral genes and, as they do not express viral antigens, they do not elicit a host immune response (Parks et al., 1996; Rauschhuber et al., 2012). The production of a large quantity of clinical grade rAd vectors is extremely important for their pre-clinical and clinical use (Kamen and Henry, 2004). This has driven the

development of new methods for virus quantitation, complementary cell line cultivation and viral purification, with a move from traditional small-scale CsCl gradient purification to more efficient chromatography methods, making production of first generation rAds on an industrial scale feasible (Kamen and Henry, 2004).

The use of first generation rAds in a clinical setting is made problematic mainly due to the onset of host immunity limiting the time-frame of transgene expression and preventing the further vector administration, as well as the prevalence of pre-existing immunity in the population to the predominantly utilised human serotype 5 virus (Chirmule et al., 1999). Host immunity is thought to be an important determinant of clinical outcome when using Ad as a gene therapy vector (Hedman et al., 2003), with expression of the viral transgene only being transient due to clearance of the virus between 2-4 wks and administration of a second dose usually ineffective (Laitinen et al., 1997). This has been demonstrated in the rat heart, where Ad expression was detectable up until 21 days post-delivery. However, animals that had been previously exposed to the virus showed a dramatic drop in expression after 48 hr and complete clearance by 6 days post-delivery due to immune mediated clearance (Gilgenkrantz et al., 1995). High proportions of most populations already have pre-existing immunity to Ad5 vectors due to natural exposure, mainly through an antibody response to the capsid hexon antigens (Barouch et al., 2004; Sumida et al., 2005). In one study, a cohort of patients being screened for Ad5 immunity found all subjects possessed Ig for Ad5, 55 % of which were neutralising (Chirmule et al., 1999). In order to circumvent this, research into the safe use of alternative serotypes that are rarer in humans has been pursued along with the development of chimeric Ad5 vectors carrying hexon antigens from other serotypes. For example, Ad35 has shown to be effective in the presence of pre-existing Ad5 immunity, making it a candidate as an alternative vector (Barouch et al., 2004). Similarly, synthesis of chimeric Ad5 vectors which have had the immunogenic hexon epitopes replaced by those of Ad48 have also been shown not to be repressed by pre-existing Ad5 immunity (Roberts et al., 2006).

4.2 Aims

Despite the drawbacks of Ad use, they remain powerful tools for gene-based research and therapy. In the present study they have been used to investigate the therapeutic potential of Ang-(1-9) in an animal model of cardiac dysfunction. The aims of this chapter were to:

- Optimise Ad-mediated gene delivery to the mouse myocardium *in vivo* and demonstrate efficient transduction in sham and MI animals.

- Utilise intra-cardiac delivery of an Ad serotype 5 vector expressing Ang-(1-9) in order to assess its effect on structural and functional cardiac remodelling in the mouse model of MI.

4.3 Results

4.3.1 Ad titration

Batches of RAdAng-(1-9), RAd60 and a ß-galactosidase expressing vectors (RAdß-gal) were prepared and titered using both limiting dilution assay on 293 cells to determine infectious plaque forming units per mL titre (pfu/mL) and micro-BCA assay to determine total viral particles per mL titre (VP/mL) (Table 4.1).

Table 4.1 Ad preparation plaque-forming unit titres.

Virus	Batch	Titre (Plaque forming units/ml)	Titre (VP/mL)	Ratio pfu:VP
RAd-ß-gal	1	1.88×10^{10}	9.79×10^{11}	1 : 52.0
	2	2.95×10^{11}	8.66×10^{12}	1 : 29.4
RAd60	1	5.176×10^{11}	7.59×10^{12}	1 : 15.1
RAd-Ang-(1-9)	1	1.11×10^{11}	2.90×10^{12}	1 : 26.1

4.3.2 RAd-Ang-(1-9) generation

The design of the transgene inserted into the Ad5 vector utilised in this study to over-express Ang-(1-9) was first described by Methot et al., in 2001 (Methot et al., 2001). It is a fusion protein sequence encoding for a biological peptide pump that enables the synthetic production of Angiotensin peptides without the need for the peptide precursors of the RAS system (Figure 4.3 A). The protein core is composed of four regions; a signal peptide from human pro-renin, the mouse heavy chain constant of IgG2B, a portion of human pro-renin pro-segment and Ang-(1-9). The signal peptide targets the protein to the endoplasmic reticulum of the cell to ensure eventual peptide secretion, while the mouse IgG segment provides sufficient molecular weight to ensure efficient production of the protein. The pro-renin pro-segment contains a protease cleavage site at its carboxyl terminus which has been modified so that it is cleaved by furin- a protease located in the Golgi network of the secretory pathway in a broad range of cell types (Methot et al., 2001). Following cleavage, the active Ang-(1-9) peptide is released and secreted from the cell.

Successful expression of the fusion protein from the Ad vector was confirmed *in vitro* by transduction of HeLa cells of either the Ang-(1-9) expressing recombinant adenoviral vectors [RAdAng-(1-9)] or an empty control Ad5 vector (RAd60) for 48 hr by western immunoblotting for the mouse IgG2B region of the fusion protein revealing an un-cleaved fusion protein band visible in RAdAng-(1-9) transduced cells only at approximately 32 KDa (Figure 4.3 B).

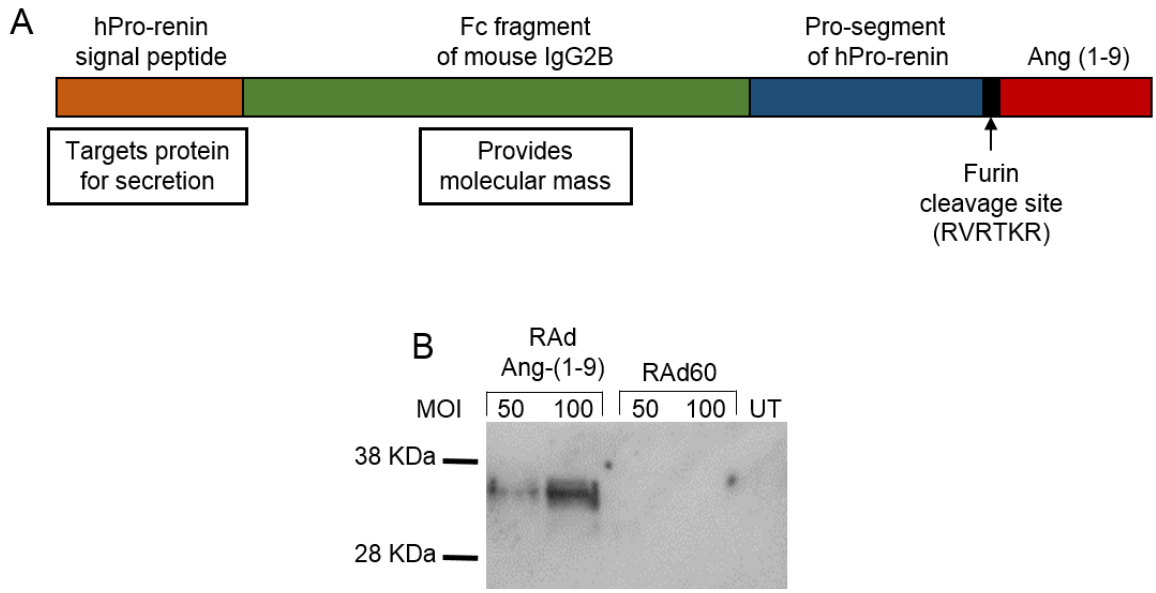

Figure 4.3 Ang-(1-9) Ad expression cassette structure and expression.
(A) Schematic showing the structure of the Ang-(1-9) fusion peptide expressed from the RAdAng-(1-9) encoded expression cassette. (B) Western blot of HeLa cell lysates transduced with RAdAng-(1-9) or RAd60 MOI 50 and 100 or untransduced and probed for the mouse Fc IgG2B fragment.

4.3.3 Optimisation of *in vivo* Ad delivery

4.3.3.1 Ad delivery to the mouse myocardium

Prior to use of the RAdAng-(1-9) in the mouse MI model, optimisation experiments to ensure sufficient transgene expression would be achieved *in vivo* were performed using RAd-ß-gal delivered in non-infarcted mouse hearts *via* direct intra-cardiac injection. A range of viral doses were assessed and expression determined at 5 days post-vector delivery (Figure 4.4). Increasing viral dose from 1 x 10^9 through to 5 x 10^9 produced increasing cardiomyocyte transduction measured by X-Gal staining (Figure 4.4 A i-iii) and immunostaining for ß-gal (Figure 4.4 B i-iv).

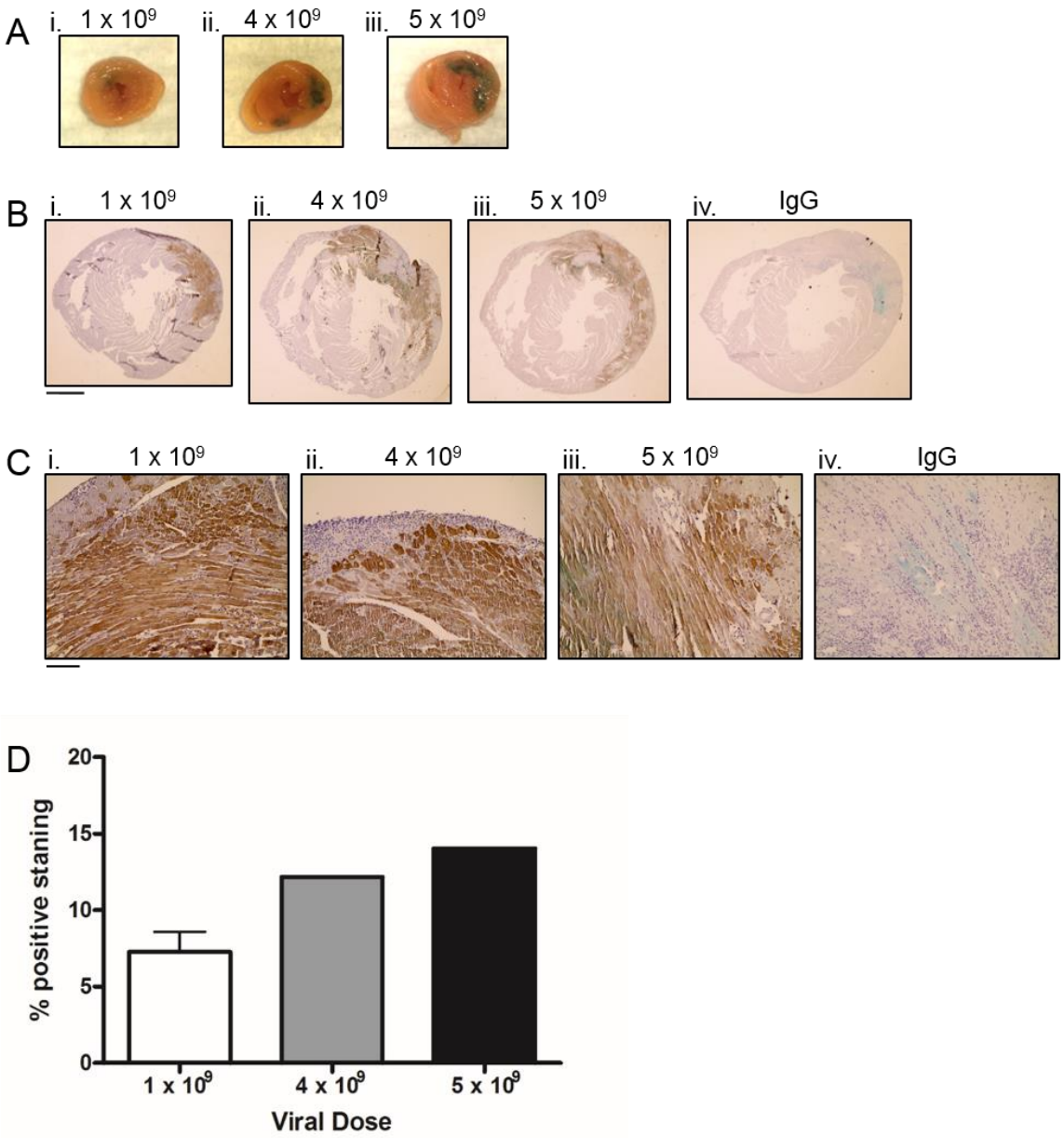

Figure 4.4 Ad transduction of the mouse heart.
Transduction of the mouse heart by RAd-β-gal following intramyocardial delivery of 1 (i.), 4 (ii.) and 5 x 10^9 pfu (iii.) of virus per heart. (A) Gross fixed hearts stained using X-gal, identifying regions of virus expression as blue. (B) & (C) DAB staining for β-Gal expression on sections from wax embedded hearts. Negative IgG was used as a control for antibody specificity. (D) Quantification of DAB staining as a % of the total myocardial area. *n*= 3 for 1 x 10^9 pfu, *n*= 2 for 4 and 5 x 10^9 pfu. Data presented as mean (± SEM where *n*>2). Magnification= 1.25 x and 20 x, scale= 1 mm and 10 µm, respectively.

4.3.3.2 Ad delivery in MI

Following successful transduction of non-infarcted mouse hearts, transduction of infarcted mouse hearts was assessed using viral injection in the border zone region immediately following infarction. Transduction was assessed at 5 days post-virus delivery of either the high (5 x 10^9 pfu) or low (1 x 10^9 pfu) viral dose (Figure 4.5). Blue X-gal staining or ß-gal immunopositivity was evident in both hearts at both doses just above the site of ligation but not in the scar, as indicated by the white arrows (Figure 4.5 A-i & ii). As the 1 x 10^9 pfu dose produced efficient transgene expression it was selected for further studies.

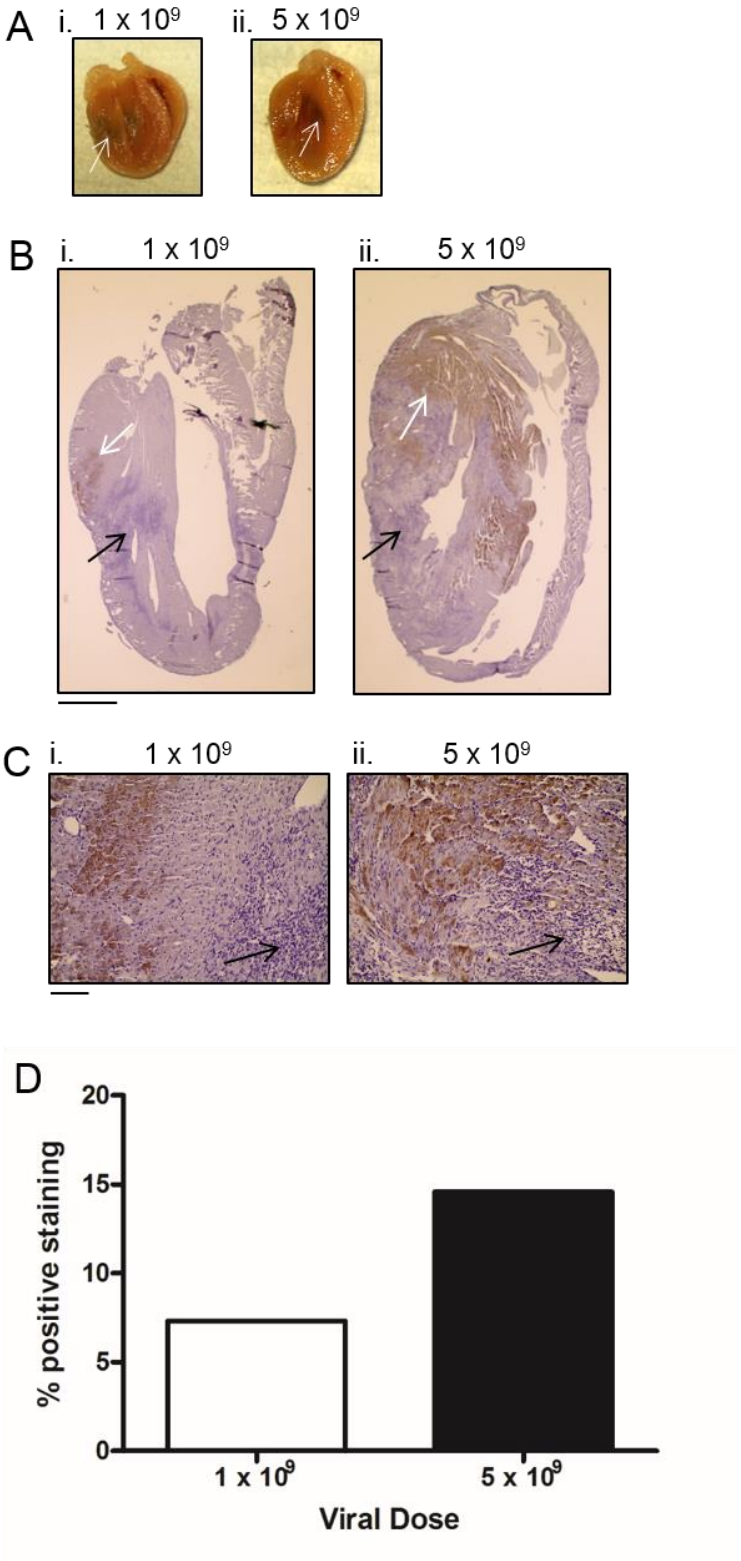

Figure 4.5 Ad transduction of the infarcted mouse heart.
Transduction of the infarcted mouse heart by RAd-β-gal following intramyocardial delivery of 1 (i.) and 5 x 10^9 pfu (ii.) of virus post-infarction in the infarct border region. (A) Gross fixed hearts stained using X-gal, identifying regions of virus expression as blue. White arrows indicate areas of positive X-gal staining. (B) & (C) DAB staining for β-Gal expression on sections from wax embedded hearts. Black arrows indicate areas of infarct tissue, white arrows indicate areas of positive staining. (C) Quantification of DAB staining as a % of the total myocardial area. *n*= 2 for each dose. Data presented as mean values. Magnification= 1.25 x and 20 x, scale= 1 mm and 10 µm, respectively.

4.3.4 Study design and mortality rates

Following confirmation of sufficient viral transduction of the myocardium, therapeutic gene transfer was assessed in 4 groups [sham, MI, MI+RAd60 and MI+RAdAng-(1-9)] (Figure 4.6 A).

A Kaplan-Meier survival plot for mortality of all animals recovered from procedure in each group demonstrated that no deaths occurred in the sham group. Each of the MI groups demonstrated a high incidence of mortality following the MI procedure (MI= 50, MI+RAd60= 55.56, MI+RAdAng-(1-9)= 35.7 %; Figure 4.6 B & C). Within the first 7 days following surgery all deaths were due to cardiac rupture. In the MI and MI+RAd60 groups there were a small number of deaths from unknown causes out with the first 7 days following procedure. This accounted for 22.2 % and 11.1 % of total mortality in MI and MI+RAd60 groups, respectively (Figure 4.6 C). Overall, the MI+RAdAng-(1-9) group demonstrated the lowest overall mortality rate of the MI groups at 4 wk post-procedure, with no significant difference compared to sham animals and no deaths recorded past 7 days post-surgery. MI and MI+RAd60 group mortality was significantly increased compared to the sham group ($P<0.05$; Figure 4.6 B & C).

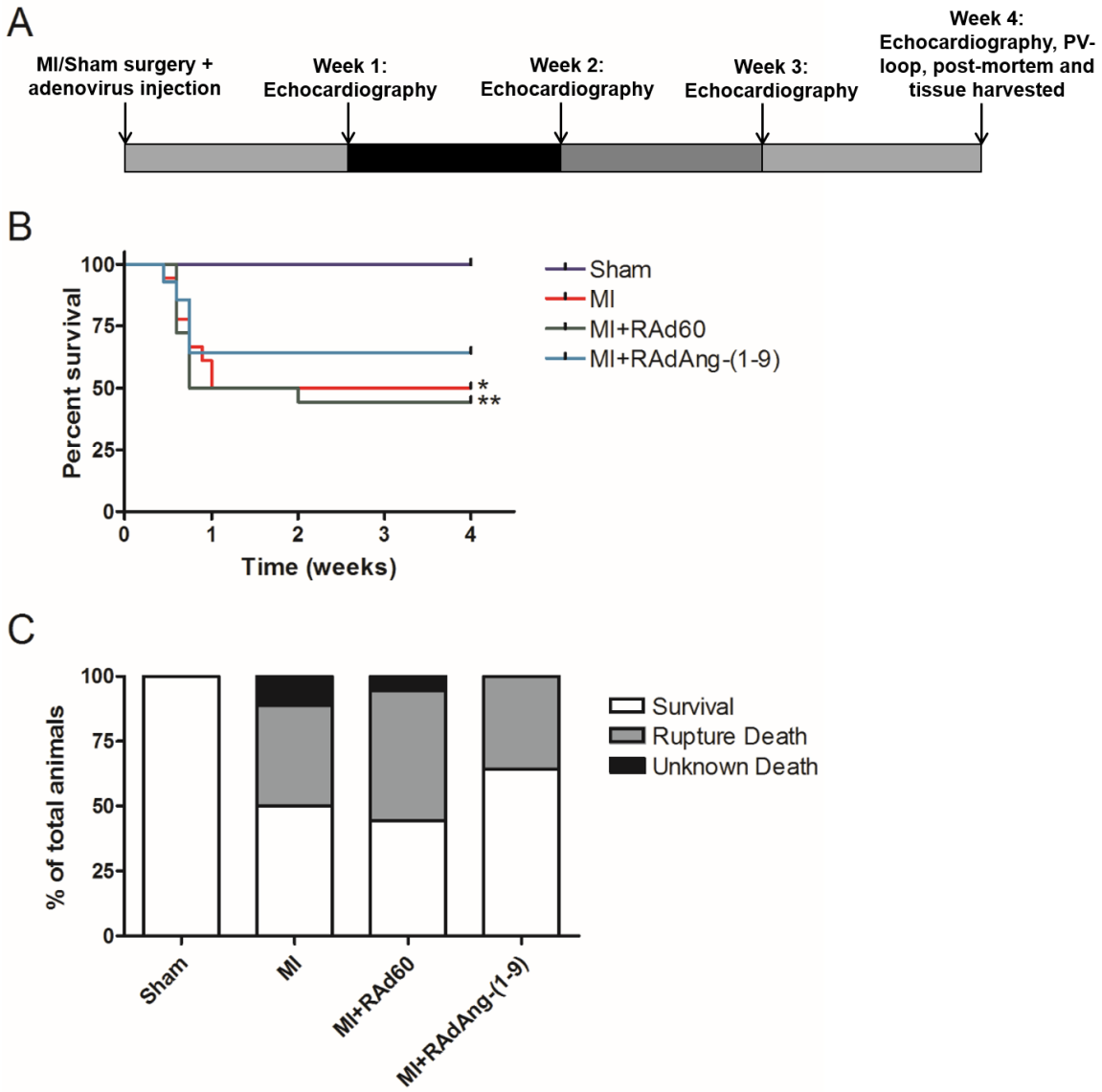

Figure 4.6 Study design and procedure-associated mortality.
(A) Study design showing time-frame of measurements over the 4 wk study period. (B) Kaplan-Meier plot of mortality following recovery from procedure for each animal group (sham, MI, MI+RAd60, MI+RAdAng-(1-9)) over the 4 wk study period. *= $P<0.05$, **= $P<0.01$ *vs.* sham. n= 9, 18, 18 and 14 for sham, MI, MI+RAd60 and M+RAdAng-(1-9), respectively. (C) % survival and cause of mortality for each animal group following recovery from procedure.

4.3.5 Haemodynamic and functional measurements

4.3.5.1 Echocardiography

Serial echocardiography measurements were used in order to perform functional and structural cardiac measurements. E/A wave ratios were determined using mitral valve Doppler measurements. At 1 wk post-MI there is was significant reduction in FS in MI animals compared to sham, with the significant decrease maintained at each time-point and progressively declining from 1 to 4 wks (Figure 4.7 A-ii). This was associated with a significant increase in LVEDD and LVESD at all time-points (Figure 4.7 A-iii & iv), with no changes in sham FS, LVEDD or LVESD across the 4 wk period. The changes in FS observed in the RAd60 group was almost identical to that observed in the MI group, being significantly reduced compared to sham at 1 wk post-MI (52± 0.6 *vs*. 28.7± 0.9 %, 1 wk sham (*n*= 6) *vs*. 1 wk MI+RAd60 (*n*= 6); *P*<0.05), with FS progressively declining from 1 to 4 wks post-MI, with a 10.1 % reduction in FS at 4 wks compared to 1 wk post-MI (Figure 4.7 A-ii). Again, this was associated with a significant increase in LVEDD and LVESD compared to sham at all time-points. By 4 wks post-MI, LVEDD had significantly increased to 136 % of sham (3.4± 0.1 *vs*. 4.6± 0.3 mm, 4 wk sham (*n*= 6) *vs*. 4 wk MI+RAd60 (*n*= 6); *P*<0.05) and LVESD had significantly increased to 207 % of sham (1.7± 0.1 *vs*. 3.4± 0.3 mm, 4 wk sham (*n*= 6) *vs*. 4 wk MI+RAd60 (*n*= 6); *P*<0.05; Figure 4.7 A-iii & iv). In the MI+RAdAng-(1-9) group, a significant attenuation in the reduction in FS was observed at 1 wk post-MI compared to that of MI and MI+RAd60 groups, with FS increased to approximately 141 % of MI and MI+RAd60 groups (MI+RAdAng-(1-9)= 40.1± 0.9; *P*<0.05). This significant attenuation was maintained from 1 to 4 wks, with the MI+RAdAng-(1-9) group having a FS of approximately 145.6 % of MI and MI+RAd60 at 4 wks post-MI (MI= 24.6± 1.7, MI+RAd60= 25.8± 1.7, MI+RAdAng-(1-9)= 36.4± 2.1; *P*<0.05; Figure 4.7 A-ii). There was no significant difference in LVEDD in any of the MI groups at any time-point, however at 1 and 4 wks post-MI, LVESD in the MI+RAdAng-(1-9) group was significantly reduced compared to that of MI and MI+RAd60 groups (Figure 4.7 A-iii & iv). There was no significant difference in posterior LV wall thickness between any of the groups at any time-point (Figure 4.7 A-v & vi). E/A wave ratios for each group demonstrated no significant difference between any of the groups at 4 wks post-procedure (*P*>0.05; Figure 4.7 B-i & ii).

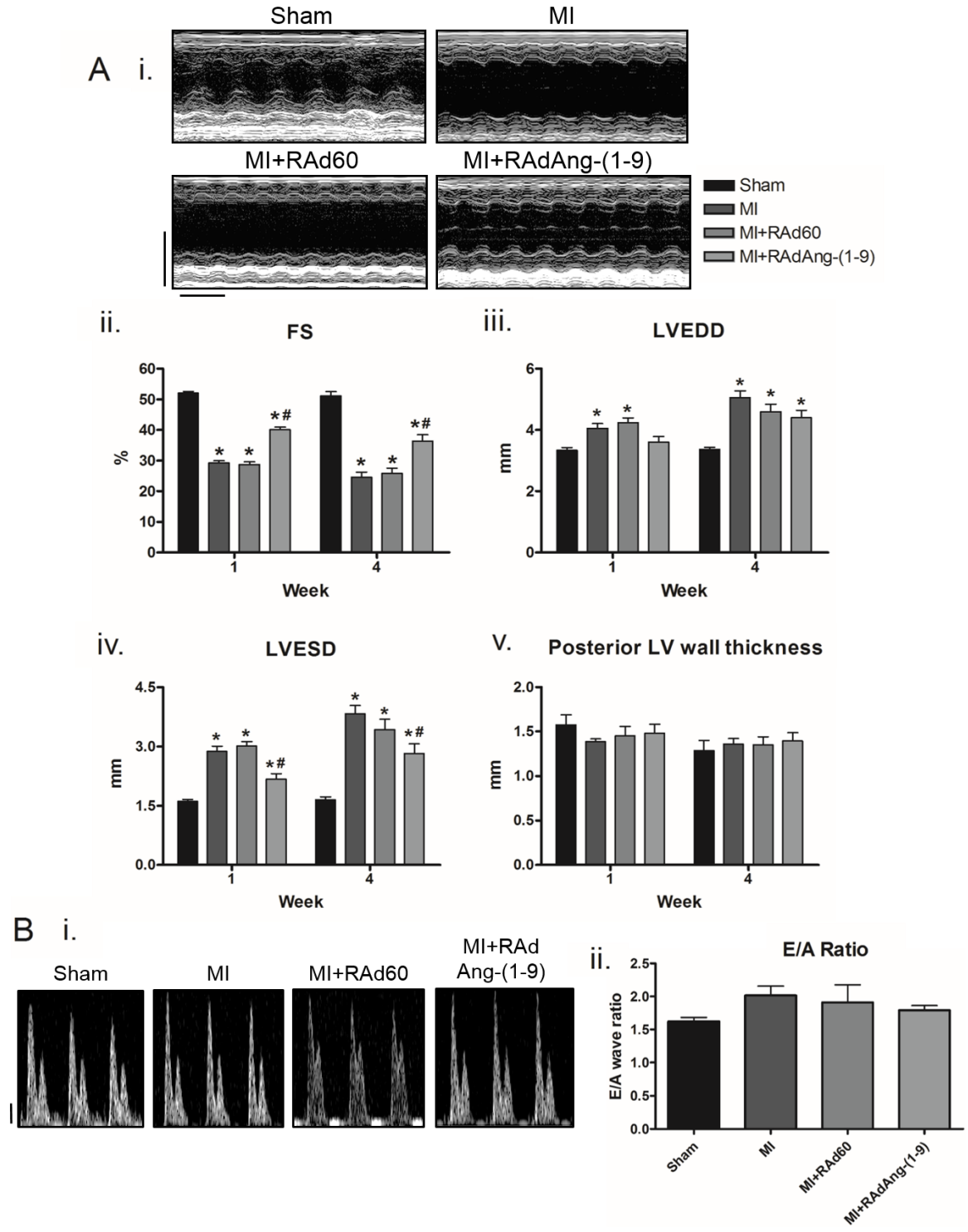

Figure 4.7 Effect of RAdAng-(1-9) on FS, wall thickness and E/A ratio in MI as assessed by echocardiography.
(A-i.) Example M-mode images for each animal cohort at 4 wks. Scale= 0.2 m/s and 20 mm. Serial FS (ii.), LVEDD (iii.), LVESD (iv.) and posterior LV wall thickness (v.) measurements from M-mode echocardiography images for sham, MI, MI+RAd60 and MI+RAdAng-(1-9) animal cohorts from 1 to 4 wks post-procedure. (B-i.) Example E/A wave Doppler measurements for each animal group at 4 wks post-procedure. Scale= 5 mm and 1 second. (ii.) Average E/A ratio measurements for the mitral valve determined using echocardiography Doppler for sham, MI, MI+RAd60 and MI+RAdAng-(1-9) animal groups. *n*=6 for each group. Data presented as mean± SEM FS= fractional shortening, LVEDD= left-ventricular end-diastolic dimension, LVESD= left-ventricular end-systolic dimension, E= early wave, A= after wave.*= *P*<0.05 *vs*. sham; #= *P*<0.05 *vs*. MI and MI+RAd60.

4.3.5.2 PV loop measurements

The effect of RAdAng-(1-9) on LV haemodynamics following MI was assessed *via* closed-chest PV loop measurements (Table 4.2). Similarly to the echocardiography data, the MI+RAd60 group demonstrated almost identical changes in haemodynamic parameters as the MI group in comparison to sham (Figure 4.8). Systolic parameters in the MI+RAd60 animal groups were decreased significantly to 75.0, 64.2 and 63.2 % of sham for ESP, dP/dt_{max} and EF, respectively (P<0.05; Figure 4.8 B i-iii). CO in the MI+RAd60 was not significantly changed compared to sham (Figure 4.8 B iv). Diastolic differences in the MI+RAd60 groups showed a significant decrease in dP/dt_{min} to 58.4 % of sham (P<0.01) and a significant increase in Tau to 152.5 % of sham (P<0.01). No significant difference was evident between any of the groups for EDP and EDPVR (Figure 4.8 C i-iv). Volume parameters showed a significant increase in both EDV and ESV to 239.4 and 370.7 % of sham, respectively (P<0.05; Figure 4.8 D i-iii), however SV remained unchanged.

In the MI+RAdAng-(1-9) group, the reductions in ESP, dP/dt_{max} and EF seen in the MI and MI+RAd60 groups were significantly attenuated. ESP and EF were significantly increased to 122.8 and 148.1 % of both MI and MI+RAd60 groups, respectively (P<0.05). The EF of the MI+RAdAng-(1-9) was essential normalised to sham levels. Dp/dt_{max} was still significantly reduced to 75.3 % of sham, however this was a significant increase in comparison to the MI group. CO in the MI+RAdAng-(1-9) group was significantly increased to 139.3 % of sham (P<0.05; Figure 4.8 B-i-iv).

The diastolic parameters dP/dt_{min} and Tau in the MI+RAdAng-(1-9) animals remained unchanged compared to the other two MI groups, with EDP and EDPVR remained unchanged compared to sham (Figure 4.8 C i.-vi.). SV, ESV and EDV values for the MI+RAdAng-(1-9) group were not significantly different from either the sham group or the MI and MI+RAd60 groups (P>0.05; Figure 4.8 D-i-iii).

Table 4.2 Effect of RAdAng-(1-9) on haemodynamic LV PV-loop indices in MI.

		MI		
	Sham	**MI only**	**+RAd60**	**+RAdAng-(1-9)**
HR (bpm)	600.9 ± 15.0	583.1 ± 5.3	577.6 ± 12.7	586.1 ± 12.3
ESP (mmHg)	104.7 ± 3.1	79.6 ± 3.6 ***	79.0 ± 5.1 ***	97.1 ± 2.5 ##
EDP (mmHg)	7.7 ± 1.8	12.7 ± 1.1	12.5 ± 1.2	12.3 ± 0.8
Developed pressure (mmHg)	96.92 ± 2.3	66.7 ± 5.3 **	66.6 ± 6.1 **	85.9 ± 2.6
dp/dt_{max} (mmHg/min)	10920.8 ± 450.0	5761.1 ± 376.8 ***	7014 ± 430.6 ***	8222.5 ± 314.9 *** ~~
dp/dt_{min} (mmHg/min)	8664.2 ± 717.6	4749.6 ± 314.7 ***	5062.4 ± 774.2 **	5505.6 ± 325.5 **
Tau (ms)	5.9 ± 0.5	9.1 ± 0.3 **	9.0 ± 1.0 **	9.2 ± 0.5 **
EDPVR	0.03 ± 0.02	0.08 ± 0.01	0.07 ± 0.01	0.06 ± 0.01
ESV (µL)	12.3 ± 2.3	42.5 ± 8.5 *	45.6 ± 11.6 *	25.9 ± 4.7
EDV (µL)	28.2 ± 3.4	64.5 ± 8.2 **	67.5 ± 10.5 **	45.4 ± 4.6
SV (µL)	15.9 ± 1.5	22 ± 1.0	22.0 ± 1.8	23.5 ± 1.7
CO (µL/min)	9948.0 ± 1095.4	12722.8 ± 610.6	12208.0 ± 1018.1	13857.5 ± 1192.8 *
EF (%)	58.1 ± 3.7	36.5 ± 4.0 *	36.7 ± 7.2 *	54.2 ± 5.4 #

HR= heart rate, ESP= end systolic pressure, EDP= end diastolic pressure, dp/dt_{max}= maximum rate of rise of pressure, $-dp/dt_{min}$= maximum rate of fall in pressure, Tau= time relaxation constant, EDPVR= end diastolic pressure-volume relationship stiffness constant, ESV= end systolic volume, EDV= end diastolic volume, SV= stroke volume, CO= cardiac output, EF= ejection fraction. *= $P<0.05$, **= $P<0.01$, ***= $P<0.001$ *vs*. sham; #= $P<0.05$, ##= $P<0.01$ *vs*. MI and MI+RAd60; ~~= $P<0.01$ *vs*. MI only.

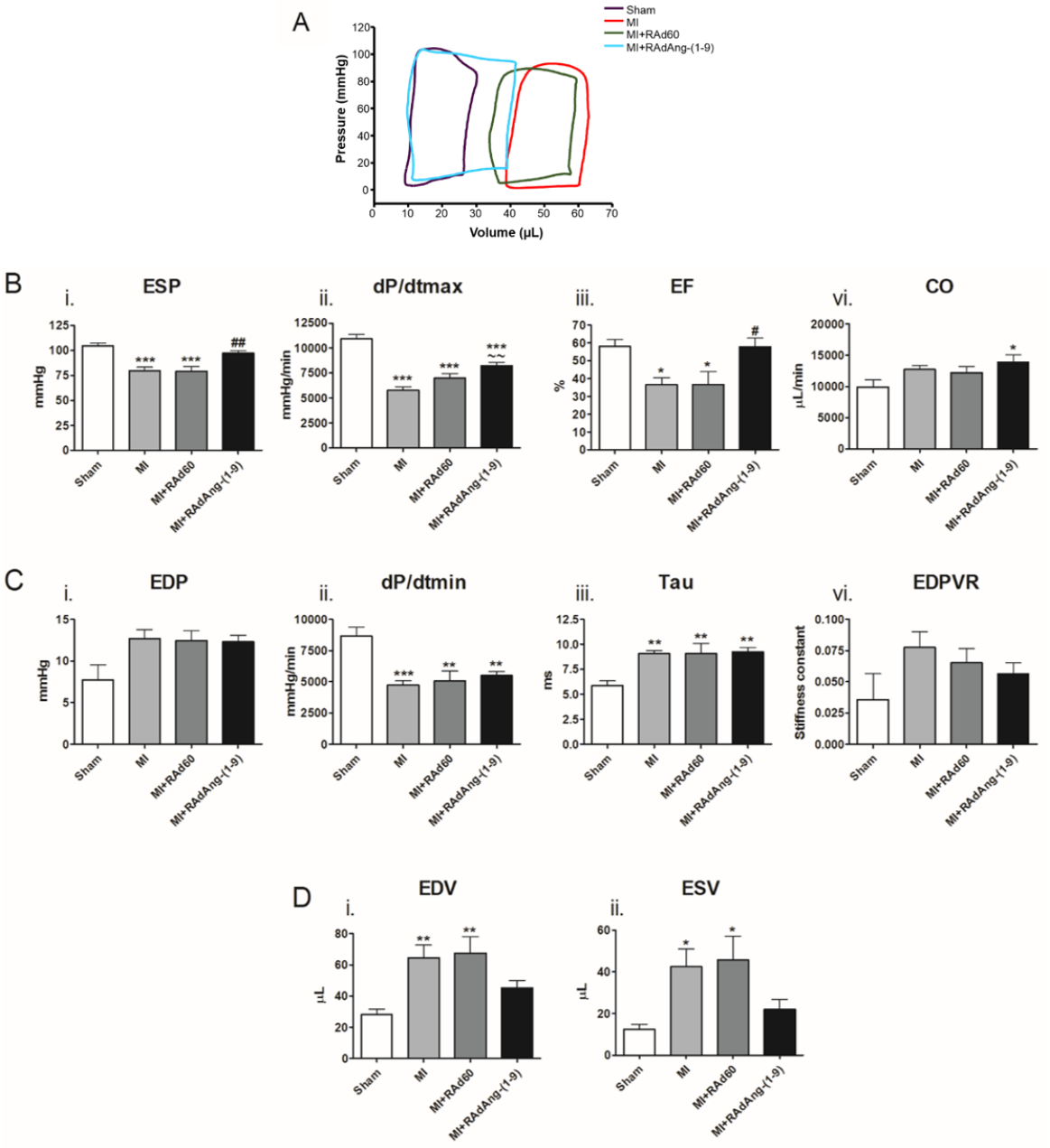

Figure 4.8 Effect of RAdAng-(1-9) on LV haemodynamic indices in MI as determined by PV-loop measurements.
LV haemodynamic measurements for sham, MI, MI+RAd60 and MI+RAdAng-(1-9) animals 4 wks post-procedure determined using the ADVantage PV-loop system with true blood volume calculated using Wei's equation. (A) Example PV-loop relationships for each animal group at 4 wks. (B) Systolic functional indices of ESP (i.), dP/dt_{max} (ii.), EF (iii.) and CO (iv.); (C) Diastolic functional indices of EDP (i.), dP/dt_{min} (ii.), Tau (iii.) and EDPVR (iv.); and (D) Volume indices of SV (i.), EDV (ii.) and ESV (iii.). *= P<0.05, **= P<0.01, ***= P<0.001 *vs*. sham; #= P<0.05, ##= P<0.01 *vs*. MI and MI+RAd60; ~~= P<0.01 *vs*. MI only. n= 7, 6, 5 and 7 for, sham, MI, MI+RAd60 and MI+RAdAng-(1-9), respectively. Data presented as mean± SEM.

4.3.6 Post-mortem and histological analysis

4.3.6.1 Organ weights

Analysis of organ weights found an increase in HW:TL ratio of the MI+RAd60 group equivalent to that of the MI group, both of which were significantly increased to approximately 125.6 % of sham (sham= 7.8± 0.2, MI=9.9± 0.6, MI+RAd60= 9.8± 0.4; $P<0.01$). HW:TL ratio for the MI+RAdAng-(1-9) group was not significantly different to that of the other 3 groups (Figure 4.9 B). There was no significant difference between LuW:TL and LiW:TL ratios between any of the 4 groups (Figure 4.9 C & D).

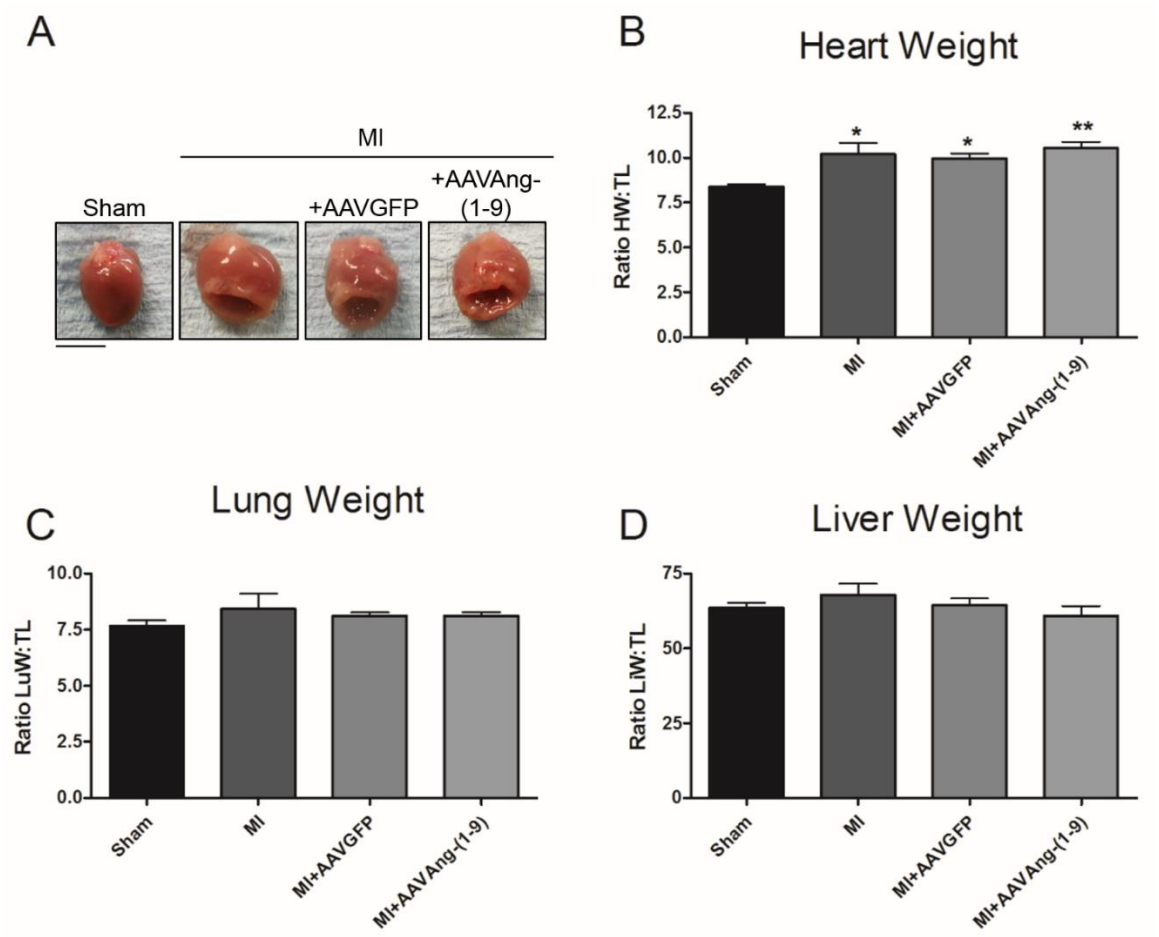

Figure 4.9 Effect of RAdAng-(1-9) on post-mortem organ weights in MI.
(A) Example images of hearts for each animal group at 4 wks. *n*= 7, 6, 5 and 7 for, sham, MI, MI+RAd60 and MI+RAdAng-(1-9), respectively. HW:TL (B), LuW:TL (C) and LiW:TL (D) ratios for sham, MI, MI+RAd60 and MI+RAdAng-(1-9) groups at 4 wks post-surgery. **= *P*<0.01 *vs*. sham. Data presented as mean± SEM. Scale bar= 5 mm. TL= tibia length, HW= heart weight, LuW= lung weight and LiW= liver weight.

4.3.6.2 Cardiomyocyte sizing

Average cell diameter, assessed using WGA staining, was significantly increased in MI and MI+RAd60 groups compared to sham (sham= 15.0± 0.3, MI= 18.2± 0.4, MI+RAd60= 18.7± 0.4 μm; $P<0.001$; Figure 4.10 A-ii). However, average cell diameter of the MI+RAdAng-(1-9) group was significantly reduced compared to the 2 control MI groups (MI+RAdAng-(1-9)= 16.0± 0.3 μm; $P<0.001$; Figure 4.10 A-ii). Cell length was not significantly altered across any of the animal groups (Figure 4.10 B-ii).

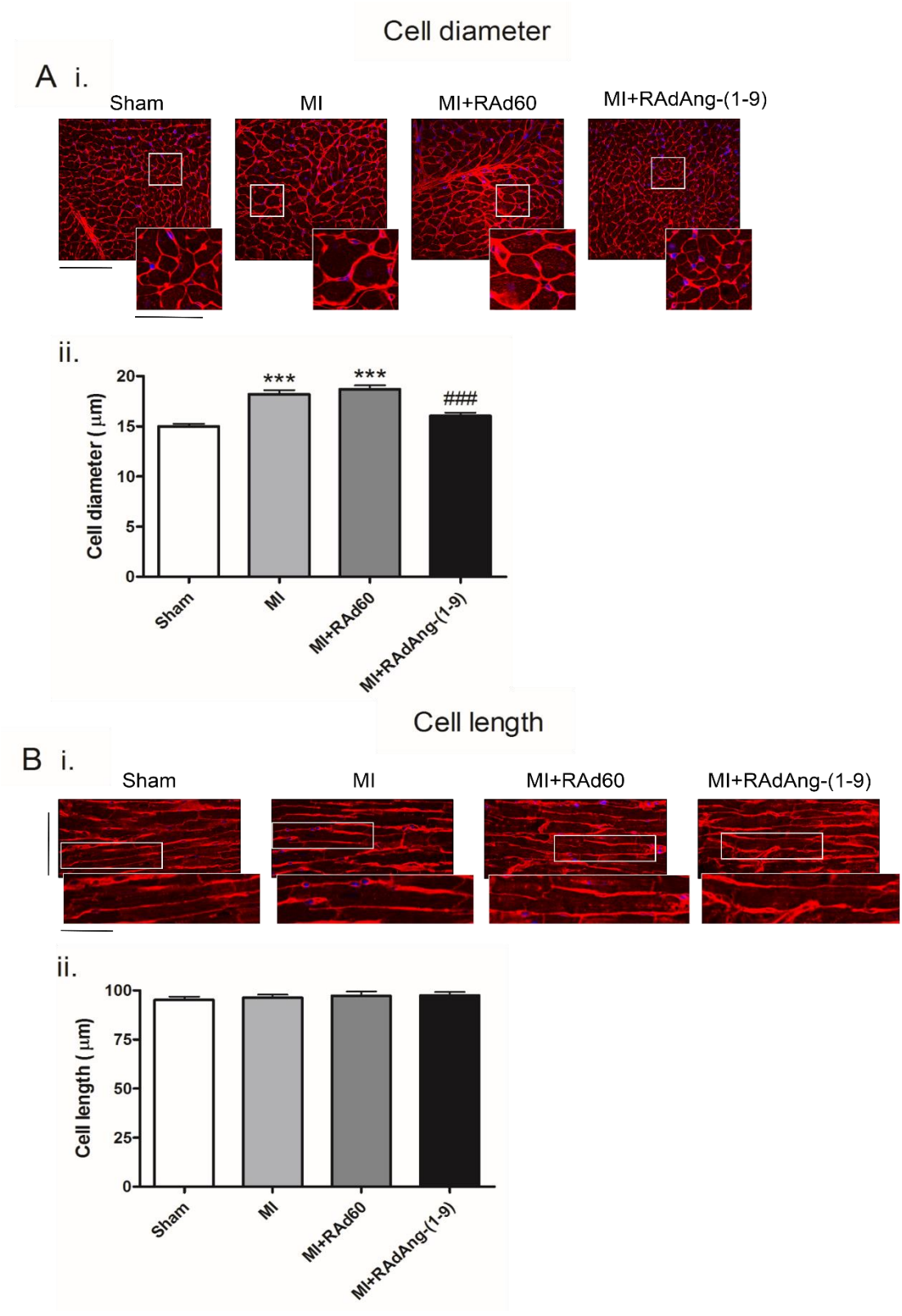

Figure 4.10 Effect of RAdAng-(1-9) on cardiomyocyte size following MI.
Example images of cellular cross-sections in both transverse (A-i.) and longitudinal (B-i.) axis are shown for each animal group, with cellular membranes stained red and cellular nuclei blue. Main image magnification= 25x, scale= 50 µm and 100 µm, inset zoom image scale= 25 µm and 50 µm for A-i. and B-i., respectively. Determination of left-ventricular cardiomyocyte diamater (A-ii. *n*= 126, 126, 109 and 124 cells for sham, MI, MI+RAd60 and MI+RAdAng-(1-9), respectively) and length (B-ii. *n*= 105, 92, 78 and 84 cells for sham, MI, MI+RAd60 and MI+RAdAng-(1-9), respectively) in the hearts of sham, MI, MI+RAd60 and MI+RAdAng-(1-9) animals using WGA staining. ***= *P*<0.001 *vs* sham, ###= *P*<0.001 vs. MI and MI+RAd60. *n*= 9, 9, 8 and 9 animals for sham, MI, MI+RAd60 and MI+RAdAng-(1-9), respectively. Data presented as mean± SEM with the average cell-size for each animal taken as the average of a group of cells evenly distributed across the LV.

4.3.6.3 Regional fibrosis, collagen expression and scar sizing

The scar region of all 3 MI groups was found to be the most fibrotic region within the MI hearts, with positive fibrosis staining significantly increased to approximately 268 % of sham in the MI and MI+RAd60 groups (sham= 2.7± 0.5, MI= 72.9± 4.5, MI+RAd60= 72.0± 5.1 %; *P*<0.001; Figure 4.11) and to 239 % of sham in the MI+RAdAng-(1-9) group (2.7± 0.5 *vs*. 64.6± 4.9 %, sham (*n*= 9) *vs*. MI+RAdAng-(1-9) (*n*= 9); *P*<0.001; Figure 4.11), with no significant difference between the % of staining in the scar region between any of the 3 MI groups themselves. Collagen expression was not significantly different in MI animals compared to sham, however there was a non-significant increase in both collagen I and III in the scar region of all MI animals, with collagen I most abundant (Figure 4.12 and Figure 4.13). LV fibrosis quantification was significantly increased in the MI and MI+RAd60 groups compared to sham (sham= 1.34± 0.4, MI= 9.1± 1.2, MI+RAd60= 10.7± 1.5 %; *P*<0.001). However, LV fibrosis in the MI+RAdAng-(1-9) group was significantly reduced to approximately 54 % of MI and MI+RAd60 LV fibrosis (*P*<0.05) and unchanged compared to sham. Again, there were no significant changes in the expression of either collagen isoform in the LV, but a non-significant trend towards increase in both isoforms (Figure 4.12 and Figure 4.13). Quantification of fibrosis in the septum region only showed a significant increase in the % of staining in the MI group compared to sham (1.1± 0.3 % *vs*. 3.5± 0.7 %, sham (*n*= 9) *vs*. MI (*n*= 9); *P*<0.01), with no other differences between groups. This appeared to be predominantly a result of increased collagen I expression which was increased but not significantly altered (Figure 4.12). Collagen III expression remained unchanged (Figure 4.13). Quantification of the RV demonstrated a very similar change in fibrosis expression as seen in the LV, with MI and MI+RAd60 groups % fibrosis equivalent and increased significantly to approximately 800 % of sham (sham= 0.9± 0.2 %, MI= 6.1± 1.7 %, MI+RAd60= 6.7± 1.7 %; *P*<0.05). Again, collagen staining suggested this was predominantly a result of collagen I expression, which again was increased in MI and MI+RAd60 groups but not significantly different (Figure 4.12). Collagen III expression remained unchanged (Figure 4.13). MI+RAdAng-(1-9) RV fibrosis was not significantly different to any of the other 3 groups (Figure 4.11 B). Average scar size and scar thickness was not significantly different between the 3 MI groups (Figure 4.11 C & D).

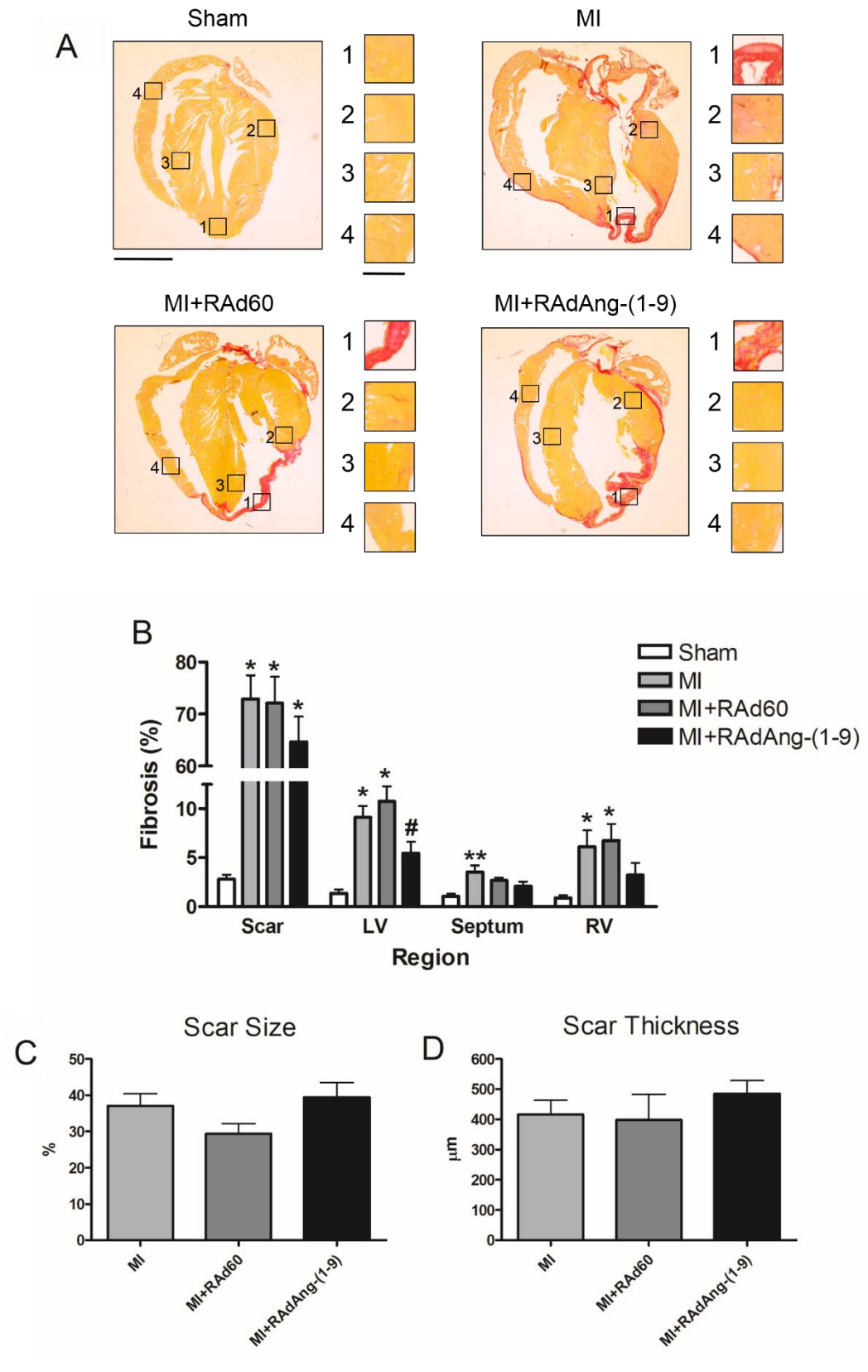

Figure 4.11 Effect of RAdAng-(1-9) on regional fibrosis and scar size following MI.
(A) Example images of picrosirius red staining of heart sections for each animal group. Data presented as mean± SEM. Magnification= 1.25x, scale= 2 mm. Zoom insert image scale= 0.5 mm. (B) Quantification of total cardiac fibrosis of the scar, left ventricle, right ventricle and septum regions of sham, MI, MI+RAd60 and MI+RAdAng-(1-9) hearts. *= $P<0.05$, **= $P<0.01$ *vs* sham region; #= $P<0.05$ *vs*. MI and MI+RAd60 region. (C) Scar size for each MI group, determined as a % of the total myocardial area. (D) Average scar thickness for each MI groups. n= 9, 9, 8 and 9 for sham, MI, MI+RAd60 and MI+RAdAng-(1-9), respectively.

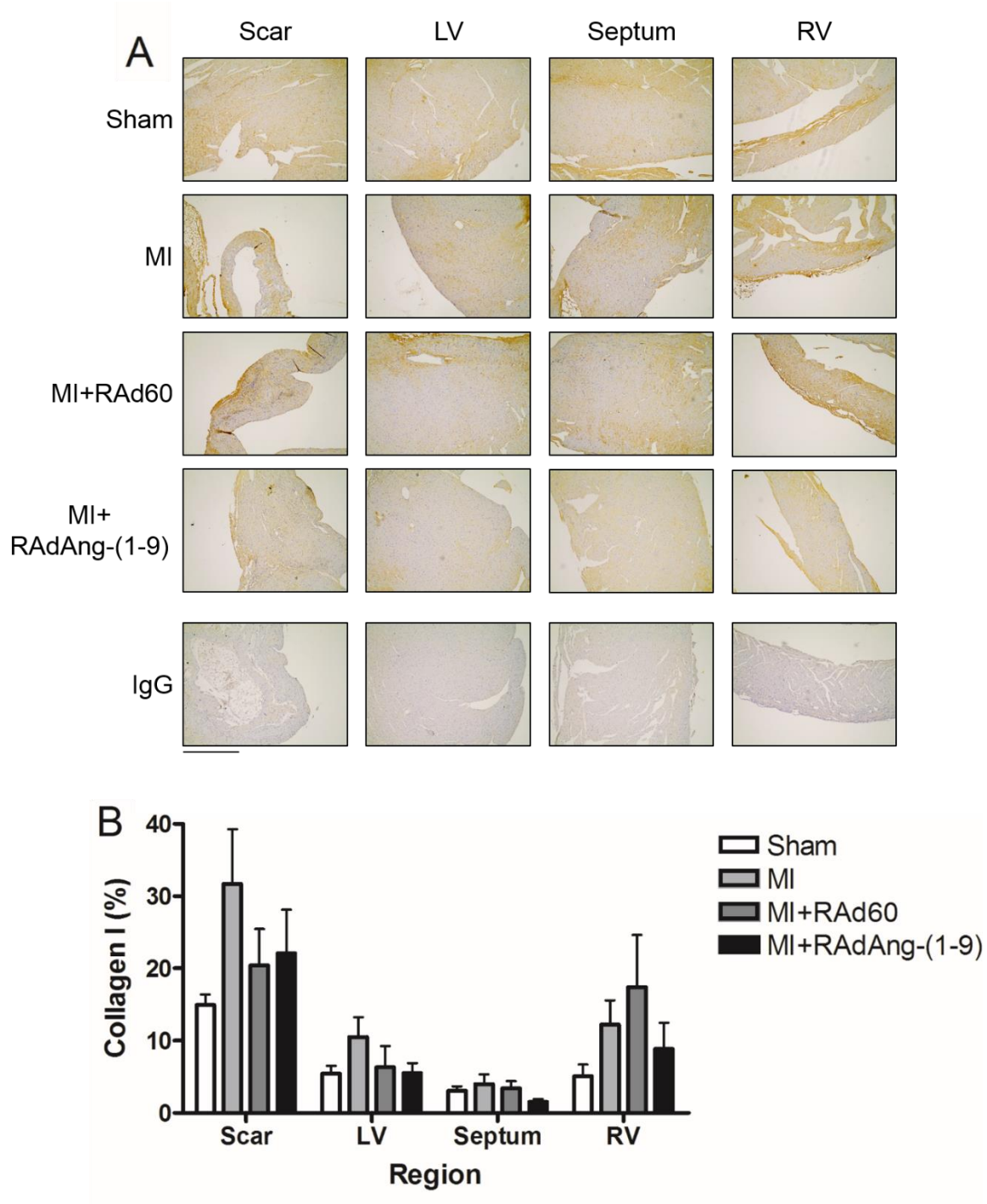

Figure 4.12 Effect of RAdAng-(1-9) on regional cardiac collagen I expression following MI. (A) Representative images of heart sections showing the distribution of DAB staining for collagen I expression in each of the animal groups. Negative IgG was used as a control for antibody specificity. Magnification= 10x, scale bar= 500 µm. (B) Quantification of DAB staining for positive collagen I expression in the cardiac regions of scar, LV, septum and RV as a percentage of the total region for sham, MI, MI+RAd60 and MI+RAdAng-(1-9) groups. *n*= 9, 9, 8 and 8 for sham, MI, MI+RAd60 and MI+RAdAng-(1-9) groups, respectively. Data presented as mean± SEM.

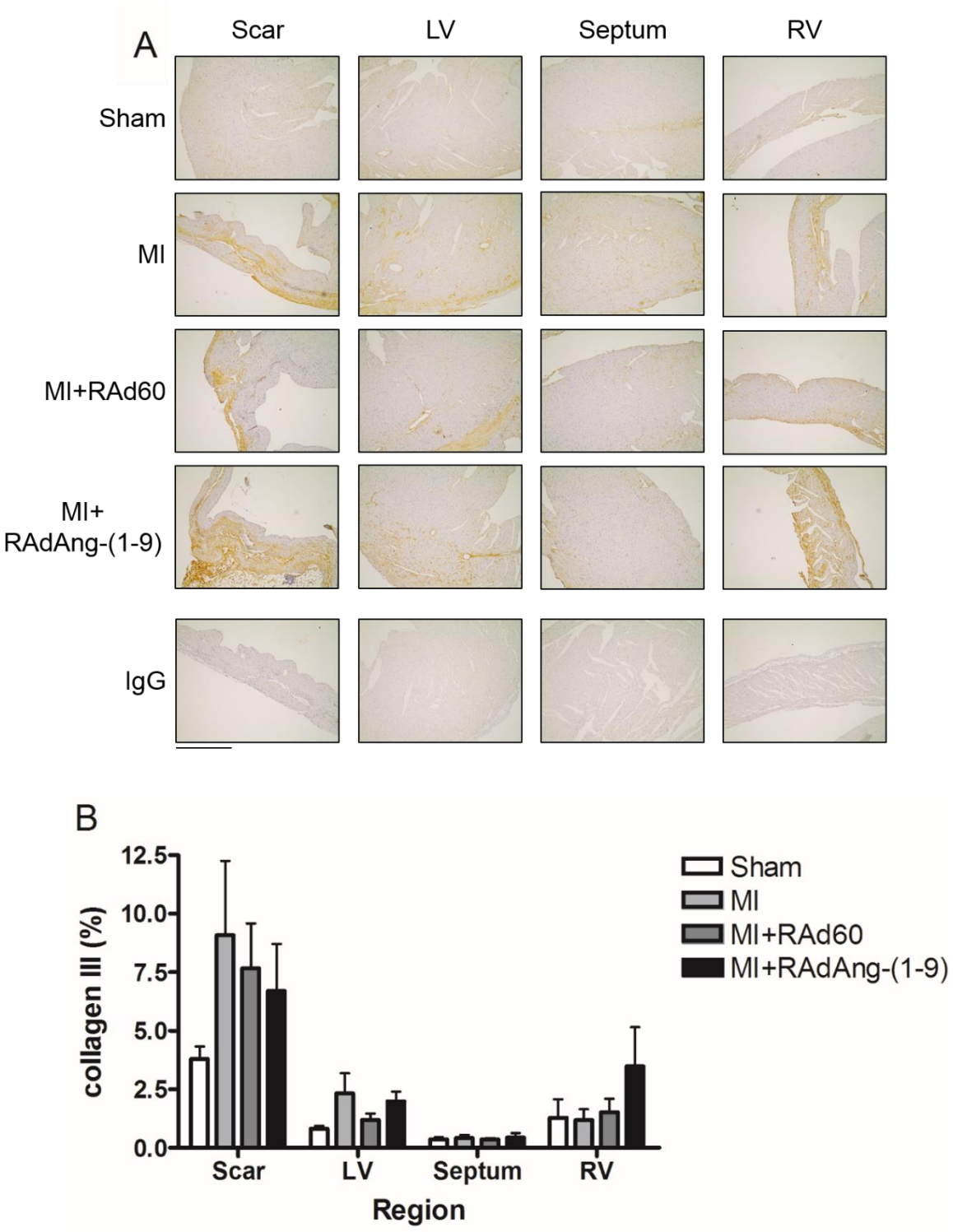

Figure 4.13 Effect of RAdAng-(1-9) on regional cardiac collagen III expression following MI. (A) Representative images of heart sections showing distribution of DAB staining for collagen III expression in each animal group. Negative IgG used as a control for antibody specificity. Magnification= 10x, scale bar= 500 µm. (B) Quantification of DAB staining for positive collagen III expression in the cardiac regions of scar, LV, septum and RV as a percentage of the total region for sham, MI, MI+RAd60 and MI+RAdAng-(1-9) animals. *n*= 9, 9, 8 and 9 for sham, MI, MI+RAd60 and MI+RAdAng-(1-9) groups, respectively. Data presented as mean± SEM.

4.3.6.4 Perivascular fibrosis and collagen expression

Quantification demonstrated no significant difference in the % of positive fibrosis staining associated with the cardiac vasculature between any of the animal groups (Figure 4.14). Perivascular collagen I levels were not significantly altered between sham, MI and MI+RAd60 groups (Figure 4.15). However, staining in the MI+RAdAng-(1-9) group was significantly reduced compared to the MI group (6.4± 0.9 % *vs*. 3.1± 0.5 %, MI *vs*. MI+RAdAng-(1-9), $P<0.05$; Figure 4.15). There was no significant difference in perivascular collagen III levels between all 4 groups (Figure 4.16).

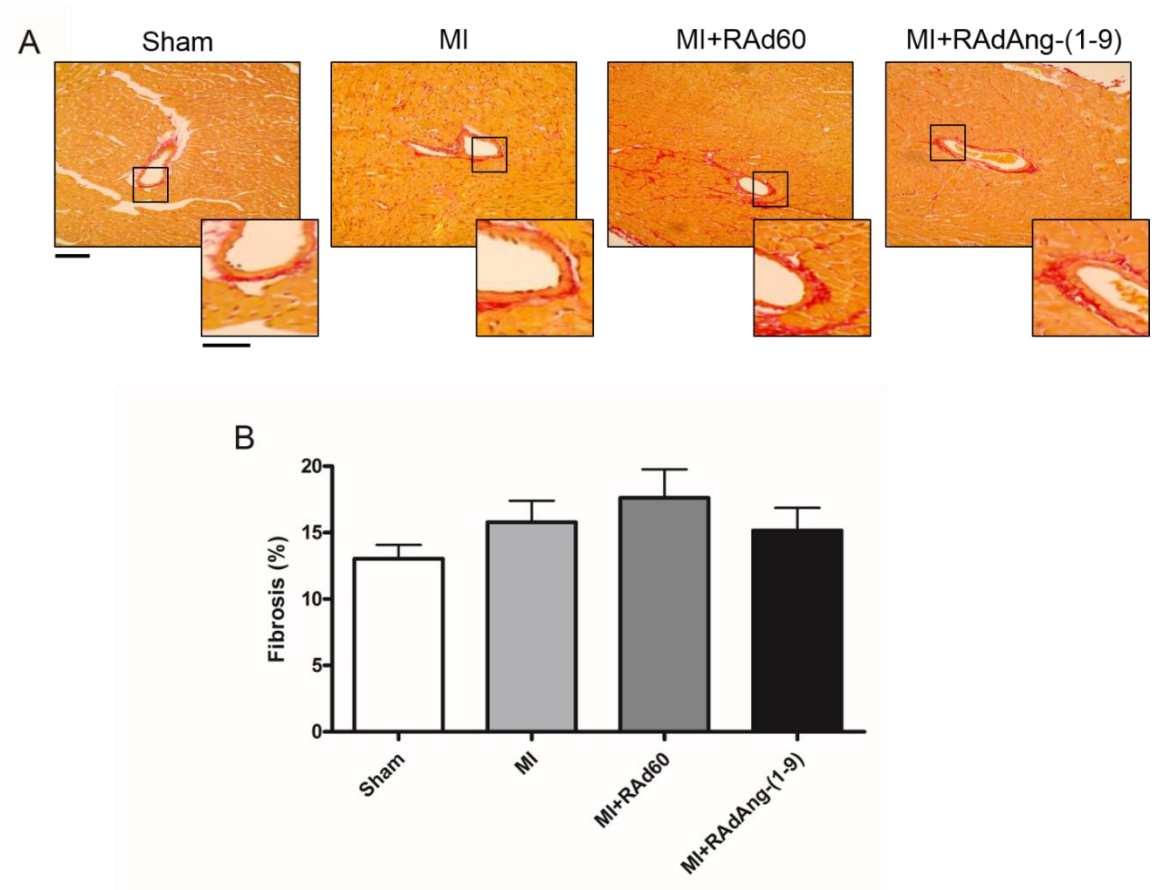

Figure 4.14 Effect of RAdAng-(1-9) on cardiac perivascular fibrosis following MI.
(A) Representative images of left-ventricular localised vessels and associated picrosirius red staining of heart sections for each animal group. Magnification= 20x, scale= 100 µm. Insert zoom image scale= 50 µm. (B) Total perivascular cardiac fibrosis quantification for sham, MI, MI+RAd60 and MI+RAdAng-(1-9) hearts. *n*= 9, 9, 8 and 9 for sham, MI, MI+RAd60 and MI+RAdAng-(1-9), respectively. Data presented as mean± SEM.

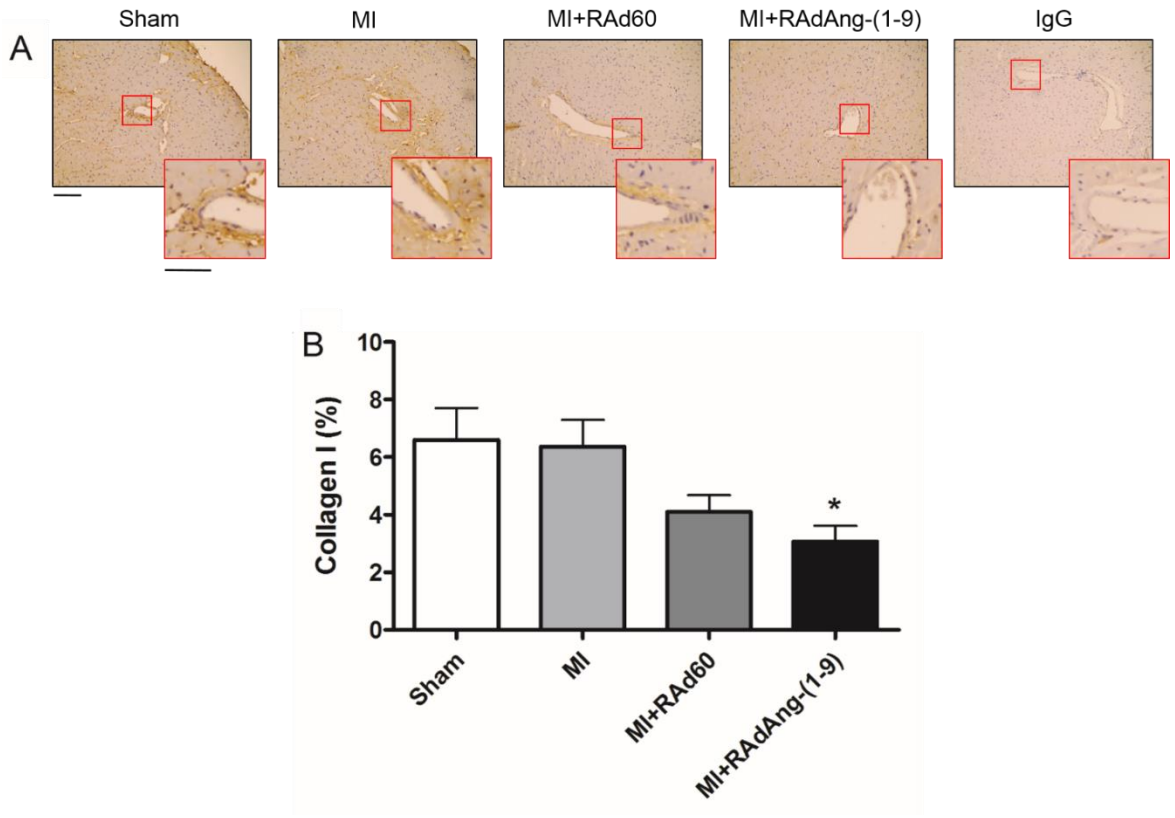

Figure 4.15 Effect of RAdAng-(1-9) on perivascular cardiac collagen I expression following MI.
(A) Representative images of cardiac vessels and associated DAB staining for collagen I expression for heart sections of each animal group. Negative IgG used as a control for antibody specificity. Magnification= 20x, scale= 200 µm. Insert zoom image scale= 100 µm. (B) Quantification of DAB staining for perivascular collagen I expression in heart sections of sham, MI, MI+RAd60 and MI+RAdAng-(1-9) animals. *= $P<0.05$ *vs* sham and MI. n= 7, 7, 6 and 8 for sham, MI, MI+RAd60 and MI+RAdAng-(1-9), respectively. Data presented as mean± SEM

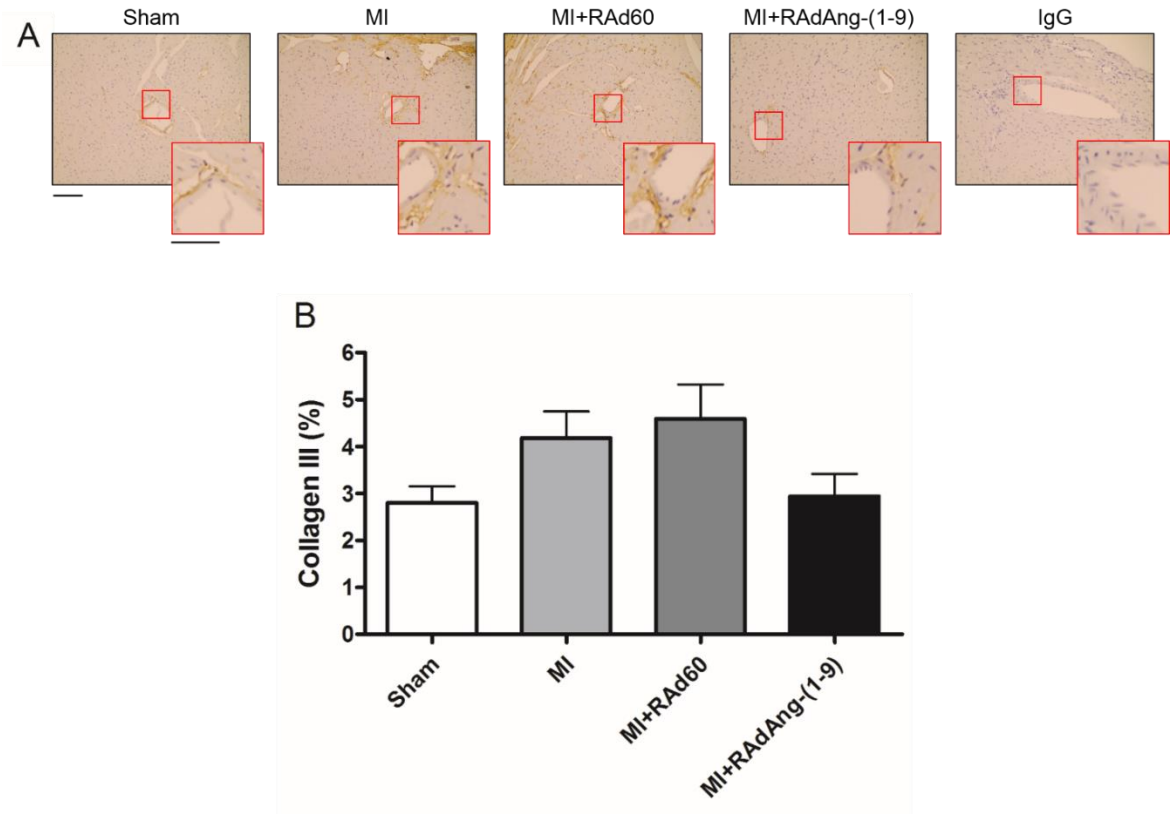

Figure 4.16 Effect of RAdAng-(1-9) on perivascular cardiac collagen III expression following MI.
(A) Representative images of cardiac vessels and associated DAB staining for collagen III expression in heart sections for each group. Negative IgG used as a control for antibody specificity. Magnification= 20x, scale= 200 µm. Insert zoom image scale= 100 µm. (B) Quantification of perivascular DAB staining for collagen III expression in heart sections of sham, MI, MI+RAd60 and MI+RAdAng-(1-9) animals. *n*= 9, 9, 8 and 9 for sham, MI, MI+RAd60 and MI+RAdAng-(1-9), respectively. Data presented as mean± SEM.

4.3.7 Gene expression analysis

qRT-PCR analysis revealed ACE expression was unchanged in the MI and MI+RAdAng-(1-9) groups compared to sham. However, expression was significantly increased in the MI+RAd60 group relative to sham (RQ= 2.0± 0.2, *P*<0.05; Figure 4.17 A). ACE2 expression was not significantly altered between any of the groups, nor was AT_1R gene expression (Figure 4.17 B & C). AT_2R gene expression was found to be significantly increased in all the MI groups. Expression was significantly increased 3-4 fold in the MI groups compared to sham (RQ= 4.5± 3.0, 3.4± 0.7 and 3.5± 0.2 for MI, MI+RAd60 and MI+RAdAng-(1-9), respectively; *P*<0.05; Figure 4.17 D). Mas receptor gene expression was unchanged in MI and MI+RAdAng-(1-9) groups, however it was significantly down-regulated in the MI+RAd60 group (RQ= 0.75± 0.04; *P*<0.05; Figure 4.17 E).

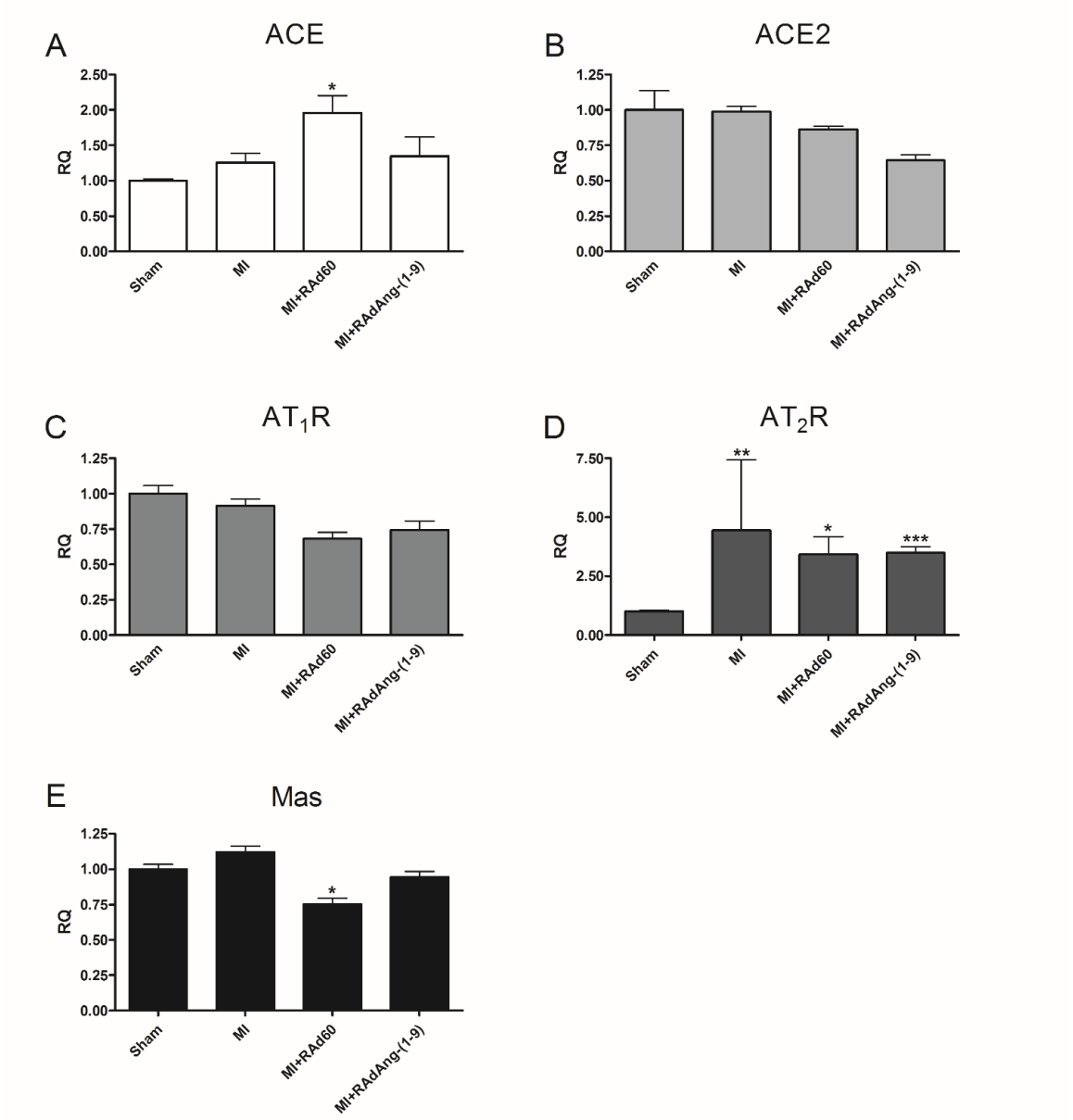

Figure 4.17 Effect of RAdAng-(1-9) on RAS receptor and enzyme gene expression following MI.

qRT-PCR-determined gene expression quantification of ACE (A), ACE2 (B), AT_1R (C), AT_2R (D) and Mas (E) in the hearts of sham, MI, MI+RAd60 and MI+RAdAng-(1-9) animals. *= $P<0.05$, **= $P<0.01$, ***= $P<0.001$ *vs*. sham. Data presented as RQ± rq_{max}. n= 3 per group. Normalisation of expression to a housekeeper (GAPDH) was performed for all samples. MI gene expression was normalised to sham expression, therefore sham expression was arbitrarily set at a RQ= 1. RQ= relative quantification.

4.4 Discussion

In this chapter, efficient transduction of the infarcted mouse heart has been demonstrated using direct injection of a rAd vector. When this approach was utilised in order to over-express Ang-(1-9), an attenuation in the depressed cardiac contractility observed following MI was demonstrated in response to Ang-(1-9), with improved FS and normalised EF. Moreover, a reduction in interstitial fibrosis and an anti-hypertrophic effect was observed following RAdAng-(1-9) delivery.

Efficient transduction of cardiomyocytes in infarcted and non-infarcted mouse myocardium was demonstrated using direct intramyocardial injection of Ad-ß-gal at doses of 1 and 5 x 10^9 pfu per animal. Direct injection as a means of transducing the myocardium with Ad has been previously reported as a safe and efficient method of achieving transient cardiomyocyte transgene expression in the rat and mouse heart (Guzman et al., 1993). The doses selected for testing were based on what has been reported elsewhere, with doses used for direct intramyocardial injection of the mouse heart in the literature ranging from 1 x 10^7 to 1 x 10^{10} pfu per animal, with transduction efficiencies ranging from 6 to 20 % of LV cardiomyocytes transduced (Agah et al., 1997; Chen et al., 2012; Ruixing et al., 2007; Toivonen et al., 2012; Vassalli et al., 2003). This is consistent with the transduction efficiencies seen here of between 7-15 % of the total myocardium transduced, depending on dose.

The post-operative rupture rate seen in the MI and MI+RAdAng-(1-9) groups of 38.9 % and 35.7 %, respectively, were consistent with the high mortality rate associated with the MI model as reported elsewhere and discussed previously (Gehrmann et al., 2001; Lutgens et al., 1999; Patten et al., 1998). However, the 50 % mortality seen in the MI+RAd60 group was much higher than what is generally reported. With the two main determinants of cardiac rupture in the murine model having been reported as infarct size and post-infarct inflammation (Gao et al., 2010), it is feasible that one of these determinants is responsible for the increased rate of rupture observed in this group. In the acute phase post-infarction, MMP levels and activity dramatically increases, (Fang et al., 2007; Matsumura et al., 2005), there is significant neutrophil and macrophage infiltration into the myocardium in order to clear away necrotic myocytes as

well as increased Toll-like receptor signalling, increased chemokine and cytokine expression and an increase in circulating inflammatory cells (Frangogiannis, 2012; Gao et al., 2010; Tao et al., 2004). This inflammatory response is thought to to promote scar formation and avoid adverse remodelling (Frangogiannis, 2012). Prolongation of the inflammatory response can be detrimental to cardiac healing, promoting further apoptosis of cardiomyocytes and preventing efficient collagen deposition, further reducing the tensile strength of the scar (Frangogiannis, 2012). This is potentially as a result of increased MMP activity, which has been shown to break down the fibrillary network and extracellular matrix molecules post-MI, weakening the scar (Fang et al., 2007), all of which can increase risk of rupture.

As Ad delivery is associated with an increase in inflammatory mediators and recruitment of inflammatory cells into transduced tissue (Liu and Muruve, 2003), including the rodent heart resulting in significant myocardial inflammation (Chu et al., 2003), it is possible the Ad delivery was responsible for this increased rupture rate, which was perhaps being attenuated to an extent by Ang-(1-9) in the RAdAng-(1-9) transduced hearts. As Ang II acting *via* the AT_1R is known to be pro-inflammatory in cardiovascular disease, with blockade *via* ACE-I and ARBs exerting anti-inflammatory effects, it is possible that activation of the counter-regulatory RAS *via* Ang-(1-9) could have similar anti-inflammatory effects (Ferrario and Strawn, 2006). In fact, activation of the Mas receptor *via* Ang-(1-7) has been shown to be anti-inflammatory in experimental models of arthritis (da Silveira et al., 2010). As scar size was slightly reduced in the RAd60 group, it is unlikely that large infarct sizes contributed to the increased rupture rate. Although increased or prolonged inflammation caused by Ad delivery is a potential explanation for the increased rupture rate, this remains to be clarified. As there is already extensive inflammation present post-MI (Frangogiannis, 2012), this may not necessarily be affected by a great degree by Ad administration. Determination of expression and duration of expression of various inflammatory mediators such as TNF-α, IL-1 and IL-6 in MI and MI+Ad hearts would help to resolve this (Nian et al., 2004). Deaths out with the rupture time-period in the mouse MI model is usually attributed to acute pump failure, ventricular arrhythmia or development of HF (Gao et al., 2000; Hattori et al., 2004). The absence of post-rupture phase deaths and lower overall deaths in the

MI+RAdAng-(1-9) groups may support its cardio-protective effects and may also indicate a possible anti-arrhythmogenic effect. However, as only a small number of animals died suddenly in the MI and MI+RAd60 groups after the rupture risk period this is not conclusive and requires further work.

This study has been the first to show a beneficial effect of Ang-(1-9) on cardiac function in the mouse MI model. Delivery of RAdAng-(1-9) directly to the non-infarcted myocardium in infarcted hearts demonstrated a completely normalised EF, as well as increased FS and improved LV systolic indices as measured by invasive PV loop measurements. No changes in diastolic parameters were observed. The improved function was associated with increased pressure generation and decreased volume indices in the RAdAng-(1-9) transduced hearts.

There is currently only one other study reported in the literature assessing the role of Ang-(1-9) on cardiac function post-MI in the rat model (Ocaranza et al., 2010). In this instance, systemic delivery of the peptide *via* minipump was used and cardiac function was assessed *via* echocardiography measurements. Echocardiography parameters demonstrated significantly reduced LV dimensions and volumes in Ang-(1-9)-infused animals compared to MI controls and revealed a reduction in wall-thickness, suggesting an anti-hypertrophic effect and reduced LV expansion, but no change was observed in functional parameters of EF and FS between infarcted rats being treated with Ang-(1-9) and controls (Ocaranza et al., 2010). There are many reasons why the results observed in this study are not necessarily consistent with what has been shown here. Previously echocardiography measurements did show alterations in volume and LV dimensional parameters, this was never corroborated using a more sensitive technique such as PV loops and did not translate into increased FS or EF (Ocaranza et al., 2010). The method of peptide delivery is the most likely explanation as here, the peptide has been expressed locally within the heart, most likely at high concentrations compared to previously where delivery *via* minipump involves its slow release into the blood where it is likely to reach the heart at far lower concentrations. Moreover, it has been suggested that the effects of a RAS component produced locally in a tissue may differ from those observed from the same RAS component present systemically. The local RAS involves the formation of RAS peptides within tissues and is independent from peptide formation within the circulation, with the local RAS thought to act

specifically in one cell or tissue in order to orchestrate tissue specific functions, whereas the systemic RAS is thought to facilitate more acute effects (Lee et al., 1993). These differential effects can be seen when comparing local Ang II production in the heart to systemic Ang II delivery, with acute cardiac remodelling only observed when the peptide is infused systemically (Mercure et al., 2008; van Kats et al., 2001), however the exact mechanisms underlying these differences remain to be clarified. It is therefore possible that systemic delivery of Ang-(1-9) *via* minipump may not exert the same effect on the heart as production of that peptide from the myocytes themselves as a result of viral gene delivery. Examples of this have also been seen with regards to the study of Ang-(1-7) and its effects on cardiac function and remodelling. A study comparing the effect of circulating and cardiomyocyte-produced Ang-(1-7) on cardiac function in the rat MI model found that only circulating Ang-(1-7) appeared to exert a beneficial effect on cardiac function 3 wks post-MI, with no effect observed where Ang-(1-7) was locally produced in the heart (Wang et al., 2010a). This is consistent with an earlier study which utilised transgenic rats which over-expressed Ang-(1-7) specifically in the heart. They found that the over-expression of Ang-(1-7) had no effect on functional cardiac parameters or BP in response to Ang II infusion, although seemed to have anti-hypertrophic and anti-fibrotic effects (Mercure et al., 2008). Comparatively, when delivered systemically *via* minipump infusion in the rat MI model, Ang-(1-7) appears to exert beneficial effects on cardiac function, restoring ventricular pressure and preventing progression to HF (Loot et al., 2002a). Moreover, this perhaps suggests that effects external to the myocardium, such as in the vasculature, are required for the beneficial effects of Ang-(1-7) which are only exerted when it is delivered systemically. An exception to this was illustrated in a study where lentiviral delivery of Ang-(1-7) was utilised in the rat model of MI. The viral vectors were delivered directly to the left ventricle resulting in over-expression of Ang-(1-7) specifically in the heart. In this instance, a beneficial effect was seen on cardiac function (Qi et al., 2011). This conflicting evidence suggests that method of delivery as well as location of expression of RAS peptides can have dramatic opposing effects on the outcome with regards to its effects on cardiac function and remodelling, and also supports independent activity of Ang-(1-7) and Ang-(1-9).

In vitro and *in vivo* evidence has suggested Ang-(1-9) signals *via* the AT_2R (Flores-Muñoz et al., 2012; Flores-Muñoz et al., 2011; Flores-Munoz et al., 2012; Ocaranza et al., 2014), and although direct stimulation of the AT_2R by Ang-(1-9) has not been associated with improved cardiac function to date, the receptor itself has been implicated in functional improvements. It is therefore possible that Ang-(1-9) may be exerting its effects *via* the AT_2R in this setting, thereby counter-acting Ang II-induced cardiac remodelling. Although Ang-(1-9) has not been directly implicated in improved cardiac function post-MI prior to this study, there is evidence suggesting that the counter-regulatory RAS is a promising therapeutic target for maintenance of cardiac function post-MI, specifically the ACE2-Ang-(1-7)-Mas axis (Santos et al., 2008). Ang-(1-7) acting *via* Mas has been shown to exert beneficial effects on Ang II induced remodelling (Grobe et al., 2006) and to exert beneficial effects on LV haemodynamic parameters when infused or delivered lentiviral vectors following MI in the rat (Loot et al., 2002a; Qi et al., 2011). ACE2 has also been demonstrated to be crucial in cardiac remodelling post-MI, with ACE2 deficient mouse hearts demonstrating exacerbated remodelling post-MI, with increased MMP activation, inflammation and ROS production, all of which are accompanied with increased circulating Ang II and decreased Ang-(1-7) (Kassiri et al., 2009). Further cardioprotective effects of ACE2 were demonstrated using an ACE2 inhibitor, C16, in the rat MI model, where FS was decreased and scar size increased in animals treated with the inhibitor (Kim et al., 2010). Although there is enough evidence to suggest Ang-(1-9) exerts independent biological effects, there is a possibility that when produced locally *in vivo* Ang-(1-9) undergoes conversion to Ang-(1-7) *via* ACE activity, which has been shown here to be elevated in MI hearts, and could then act *via* Mas, exerting further beneficial effects. Synergistic therapeutic effects of both Ang-(1-9) and locally produced Ang-(1-7) may therefore provide dual benefit in MI, however this remains to be assessed.

Histological analysis of MI hearts revealed scar size of between 30-40 %. Despite similar scar sizes, RAdAng-(1-9) transduced hearts demonstrated reduced total fibrosis in the LV region of the heart, which appeared to be primarily interstitial. Anti-fibrotic effects of Ang-(1-9) have previously been demonstrated *in vivo* in the SHRSP *via* AT_2R signalling (Flores-Munoz et al., 2012). The AT_2R again has been associated with anti-fibrotic effects in models of cardiac dysfunction, with

direct stimulation using C21 shown to reduced cardiac fibrosis and collagen deposition again through MMP regulation (Lauer et al., 2014; Rehman et al., 2012). There is also a well-established role for Ang-(1-7) and the Mas axis in exerting anti-fibrotic effects on the myocardium with ACE2 over-expression and Ang-(1-7) signalling both inhibiting collagen deposition and fibroblast proliferation (Grines et al., 2003; Grobe et al., 2007; Iwata et al., 2005; McCollum et al., 2012). This suggest Ang-(1-9) could be exerting this anti-fibrotic effect through direct signalling *via* the AT_2R and/or through conversion to Ang-(1-7).

A trend towards an anti-hypertrophic effect was seen in MI hearts transduced by RAdAng-(1-9) through both heart weight and direct cell sizing measurements. This is consistent with the anti-hypertrophic effects already reported for Ang-(1-9) in *in vitro* and *in vivo* models of Ang II induced hypertrophy and in the rat MI model (Flores-Muñoz et al., 2012; Flores-Muñoz et al., 2011; Ocaranza et al., 2010). Although initially adaptive, chronic cardiac hypertrophy has been demonstrated to be maladaptive following MI, eventually leading to the depression of cardiac contractility, increased LV dilation and increased cardiac fibrosis (Pfeffer and Braunwald, 1990). Similarly to cardiac fibrosis, cardiomyocyte hypertrophy is also associated with increased ROS production and MMP activity (Miura et al., 2003; Murdoch et al., 2006; Takimoto and Kass, 2007), with AT_2R over-expression or stimulation also being associated with reduced wall thickening and reduced expression of pro-hypertrophic genes (Rehman et al., 2012; Yang et al., 2002b). As Ang-(1-7) acting *via* Mas has also been demonstrated to be anti-hypertrophic (Keidar et al., 2007; Loot et al., 2002a; Tallant et al., 2005), this again suggests an AT_2R and/or conversion to Ang-(1-7) mediated anti-hypertrophic effect of Ang-(1-9) in this setting.

In the previous chapter, regional changes in RAS receptor and enzyme gene expression was demonstrated at 4 wks post-MI in relation to sham. Some of those changes were evident when whole heart gene expression was analysed in this study, such as the increase in AT_2R expression, which is consistent with what has been reported in the rat MI model elsewhere (Savoia et al., 2011). However, other changes in MI hearts discussed previously, such as decreased ACE2 and AT_1R gene expression and increased ACE, have not been seen here, although there were small trends towards these changes. This is most likely due to the

regional nature of these changes shown previously. There were also no obvious changes in gene expression in the RAdAng-(1-9) transduced hearts. This again may be the result of the changes being region specific and therefore undetectable in whole heart lysates or alternatively due to the transient nature of Ad-mediated transgene expression. As the Ad would have been cleared from the animals by 4 wks following administration (Laitinen et al., 1997), it is possible that there were changes in RAS gene expression during peak expression of the virus transgene that were lost upon clearance.

The primary finding of this chapter was the protective functional effects exerted by RAdAng-(1-9) delivery, which was shown to completely normalise cardiac EF. This suggests an effect on inotropy of the heart is being exerted in order to maintain force of contraction. One possible hypothesis is that Ang-(1-9) is able to exert direct effects on cardiomyocyte Ca^{2+}-handling, increasing cardiomyocyte contractility. This is explored further in a later chapter.

4.5 Summary

Efficient transduction of the myocardium in both sham and MI animals can be achieved using direct intra-myocardial delivery of an Ad vector. When this approach was used to deliver an Ad vector expressing an Ang-(1-9) fusion protein in the mouse MI model, the peptide was found to confer both structural and functional cardio-protective effects compared to control Ad, including improved LV systolic indices and contractility, decreased total cardiac fibrosis and decreased cardiomyocyte hypertrophy. These findings provide proof of concept for the utility of Ang-(1-9) therapeutic delivery in the heart *via* gene transfer.

Chapter 5: Assessing the effects of adeno-associated virus serotype 9-mediated Ang-(1-9) delivery in the mouse MI model

5.1 Introduction

5.1.1 Adeno-associated virus

Adeno-associated virus (AAV) was first discovered in 1965 when it was identified as a contaminant in a simian adenovirus preparation (Atchison et al., 1965). AAV were described as small, DNA-containing particles that behaved as 'defective viruses' (Atchison et al., 1965). At approximately 260 Å in diameter, the AAV family are very small, non-enveloped viral particles with an icosahedral capsid which carries a 4.7-4.9 Kb single-stranded DNA (ssDNA) genome (Agbandje-McKenna and Kleinschmidt, 2011; Day et al., 2014; DiMattia et al., 2012). As of 2014, 12 AAV serotypes (AAV1 to AAV12) had been isolated from humans and non-human primates (Chahal et al., 2014; DiMattia et al., 2012), with AAV2 perhaps the most well characterised and the serotype most often utilised in clinical trials to date (Kotterman et al., 2015). Initially, different AAV serotypes were distinguished based on their susceptibility to serological neutralisation and the absence of cross-reactivity indicating no shared antigens on the viral surface. These antigenic differences also dramatically affect the vector tropism and interaction with the host immune system (Gao et al., 2004). However, as more serotypes have been discovered, genome similarities and antigenic cross-reactivity of certain serotypes has allowed them to be sub-divided into 8 different clades or classes, A-F, with AAV4 and AAV5 existing currently as clonal isolates (Agbandje-McKenna and Kleinschmidt, 2011). For example, AAV1 and AAV6 both belong to clade A, with members of each clade sharing between 60-99 % genome identity, with AAV4 and AAV5 being the most genetically different from each other and all other serotypes (Agbandje-McKenna and Kleinschmidt, 2011).

Unlike Ad, AAV infection of humans is not associated with any known pathology (Day et al., 2014). Despite this, infection with AAVs in the population is common, therefore so is the presence of neutralising antibodies, with antibodies to AAV2 being the most commonly occurring, followed closely by AAV1 (Calcedo et al., 2009). The 'defective virus' property of AAV is due to the dependency of AAV on co-infection with a helper virus, such as Ad or herpes simplex virus (HSV), in order to replicate (Day et al., 2014).

5.1.1.1 AAV structure and genome

The AAV genome is comparatively simple compared to that of Ad, containing only 3 distinct open reading frames (ORFs); *rep*, *cap* and a nested alternative reading frame within the *cap* gene. The 3 ORFs are flanked by ITRs (145 bp for AAV2) at either end of the genome which form tight T-shaped hairpin structures essential for viral packaging (Day et al., 2014). It is the *cap* gene which encodes for the 3 structural proteins which compose the viral capsid; VP1, VP2 and VP3, through alternative splicing of the *cap* mRNA (Agbandje-McKenna and Kleinschmidt, 2011). The full length mRNA encodes for the largest protein VP1 (87 KDa). Encoding from an alternative start codon produces the mRNA for VP2 (73 KDa), and VP3 (61 KDa) is encoded from a downstream ATG sequence (Agbandje-McKenna and Kleinschmidt, 2011). The *rep* ORF encodes for the 4 genes required for viral replication (Rep40, Rep52, Rep68 and Rep72), with the third nested ORF within the *cap* gene encoding for a chaperone protein required for localisation of capsid proteins during viral assembly, which will be discussed later (Sonntag et al., 2010).

The AAV capsid is composed of 60 copies of the VP proteins arranged with *T*= 1 icosahedral symmetry, the structure of which has been determined to 3 Å resolution using X-ray crystallography (Xie et al., 2002). The VP proteins exist in a predicted ratio of 1:1:10 for VP1, VP2 and VP3, respectively, with VP3 accounting for 90 % of the capsids protein content and being the most well-conserved protein across the AAV serotypes (Agbandje-McKenna and Kleinschmidt, 2011; DiMattia et al., 2012). Each VP has a core composed of an 8-strand β-barrel motif and an α-helix, which is conserved throughout the serotypes. Nine surface-exposed variable regions (VRs) are located on the loops connecting the β-strands (Walters et al., 2004). It is these VRs that are responsible for the variation in tissue tropism and immunogenicity among the different serotypes (DiMattia et al., 2012).

5.1.1.2 AAV cell transduction and replication

AAV cellular transduction bares many similarities to that already discussed for Ad, requiring the same basic steps of cell surface receptor binding, internalisation, virus trafficking through an endosomal compartment, endosomal

escape, trafficking to the nucleus, viral uncoating and replication (Ding et al., 2005). Many cell surface receptors have been identified for AAV cell entry (Johnson and Dudleenamjil, 2012). For AAV2 its primary receptor has been identified as heparan sulfate proteoglycan (HSPG) (Summerford and Samulski, 1998) which it binds using specific arginine residues located in its capsid VRs (Opie et al., 2003). It is also thought to bind other co-receptors including $\alpha_V\beta_5$ integrin (Summerford et al., 1999), human fibroblast growth factor receptor 1 (FGFR-1) (Qing et al., 1999) and hepatocyte growth factor receptor (c-Met) (Kashiwakura et al., 2005), which are thought to stabilise viral attachment and facilitate internalisation. Other receptors and co-receptors identified for other serotypes include various glycoprotein sialic acid residues for AAV1, AAV4, AAV5, AAV6 and AAV12 (Kaludov et al., 2001; Schmidt et al., 2008; Walters et al., 2001; Wu et al., 2006), platelet-derived growth factor receptor for AAV5 (Di Pasquale et al., 2003), FGFR-1 for AAV3 (Blackburn et al., 2006) and the 37/67 KDa laminin receptor for AAV2, AAV3, AAV8 and AAV9 (Akache et al., 2006).

Cell transduction of AAVs has been most extensively studied for AAV2. Upon receptor binding, AAV2 particles are taken up into an endosome through dynamin-dependent, clathrin-mediated endocytosis (Bartlett et al., 2000). This requires activation of Rac1, which in turn activates the phosphatidylinositol-3 kinase pathway required for subsequent trafficking of the AAV to the nucleus *via* the cellular microtubules (Sanlioglu et al., 2000). AAV escape from the endosome is thought to be triggered by the acidification of the endosome during maturation and potentially facilitated by phospholipase A2 (PLA_2) activity seen at the N-terminus of VP1 of AAV2 after transduction of HeLa cells (Girod et al., 2002). However, this cell entry and release process appears to vary between cell types, with high transduction efficiency in cells such as skeletal muscle, neurons and hepatocytes, but very limited transduction efficacy in vascular endothelial cells (Denby et al., 2005). This is thought to be attributed to two factors; sequestration of the virus to the ECM due to high expression of the AAV2 HSPG receptor competing for virus binding thus inhibiting cell entry (Pajusola et al., 2002) and impaired intracellular processing of internalised viral particles resulting in targeting of the viral proteasome for degradation (Nicklin et al., 2001; Yan et al., 2004). Following escape, the viral particles translocate to the nucleus and enter the nuclear pore. This process is thought to be facilitated by

putative nuclear translocation signals located at the N-terminus of VP2 (Johnson et al., 2010). Both the PLA_2 and nuclear translocation motifs are found to be highly conserved between AAV serotypes. Moreover, they are located on the interior of the capsid structure during assembly and are inaccessible to antibodies, but appear to be translocated to the capsid exterior during the infection process as a result of a conformational change (Sonntag et al., 2006). During the infection process viral un-coating occurs. Whether this occurs primarily outside or inside the nucleus is unknown (Xiao et al., 2002), however it has been demonstrated that intact capsids can enter the nucleus (Johnson and Samulski, 2009). Following un-coating and entry into the nucleus, the ssDNA genome is converted into a double-stranded molecule (Thomas et al., 2004).

AAV vectors have a bi-phasic life-cycle. Following cell transduction, either the lytic or lysogenic life-cycle will progress depending on whether a helper virus is present or absent. In cells co-infected with either an Ad or HSV, AAV will follow its lytic life-cycle of viral replication. If it infects alone however, it will follow its lysogenic life-cycle, whereby its gene expression is repressed and latency is established by integration of its own genome into that of the host cell (Goncalves, 2005). Latency occurs through preferential integration into a specific site on human chromosome 19, 19q13.3q-ter, known as AAVS1, mediated by Rep78 and Rep68 (Kotin et al., 1991). A variety of helper functions have been identified as being required for the completion of AAV replication, as well as functions provided by the host DNA replication machinery (Janik et al., 1981; Weindler and Heilbronn, 1991), including transcriptional activation, mRNA maturation, translational enhancement, modulation of the host cell cycle and roles in DNA replication (Ferrari et al., 1996; Ward and Kerr, 2005; Weindler and Heilbronn, 1991). Following successful DNA replication and translation of the VP structural proteins, AAV assembly occurs in the nucleus, with new capsids first detectable in the nucleoli. Assembly only requires the *cap* genes *via* expression of the chaperone virus assembly protein, which targets newly synthesised VP proteins to the nucleolus (Sonntag et al., 2011; Sonntag et al., 2010).

5.1.2 AAV as a gene therapy vector

The use of recombinant AAV vectors (rAAV) for gene therapy applications was first explored in 1980 with the development of infectious molecular clones of

AAV2 (Carter, 2004), with this leading to the development of the first rAAV vectors some years later (Hermonat and Muzyczka, 1984; Tratschin et al., 1985). Refinement of rAAV design and of the *trans*-complementation system over the following two decades has resulted in an explosion in the interest of AAV as a gene therapy vector for a variety of target diseases (Carter, 2004).

The production of rAAV vectors involves the deletion of the full *rep* and *cap* ORFs, leaving only the flanking inverted terminal repeat (ITR) regions intact, allowing a possible transgene insert size of up to approximately 5 Kb (Dong et al., 1996). This is possible as the ITRs are the only *cis*-acting regions required for AAV genome rescue, replication and packaging (Carter, 2004; Schwartz et al., 2009). Even with the removal of the majority of AAV genes, the small viral particle size of AAV restricts the packaging capacity thus precluding the modification of the vector for diseases requiring larger genes, especially compared to that of rAds which have a packaging capacity of between 8-40 Kb, compared to only 4.7 Kb for AAV (Duan et al., 2001). Production of rAAV vectors requires the use of a producer cell line, co-transfected with a plasmid carrying the rAAV genome, composed of the transgene flanked by the ITRs under the control of a promotor, and a second helper plasmid expressing Ad helper function genes as well as the AAV viral *rep* and *cap* genes in *trans* (Lai et al., 2002). The presence of the viral replication genes and the Ad helper functions subject the rAAV genome to the wild-type lytic cycle by rescuing it from the plasmid backbone, replicating then packaging it into pre-formed AAV viral capsids (Goncalves, 2005). The development of rAAVs has mainly utilised AAV2, however any transgene expression cassette flanked by the 145 bp ITR regions of AAV2 can be packaged into any of the other serotype capsids (Nonnenmacher and Weber, 2012). The absence of the *rep* genes in the rAAV vector genome means integration into the AAVS1 site of the host genome does not occur as it does for wild-type AAV (Goncalves, 2005).

The use of rAAVs as a gene therapy vector has several advantages over the use of rAds. They exhibit sustained transgene expression with no associated pathologies and the various serotypes exhibit a variety of tropisms allowing for efficient tissue specificity. The sustained transgene expression exhibited by rAAV vectors is perhaps one of the qualities which makes them such an attractive prospect as a gene therapy vector, with rAAV particles found to still be detectable in retinal

cells 6 years after the initial delivery (Stieger et al., 2008). As mentioned, rAAVs do not site-specifically integrate into the host cell genome. Experiments performed in mice *in vivo* demonstrated that only approximately 10 % of transduced viruses integrating at random sites into the host cell chromosomes (Nakai et al., 2001). It is now accepted that the majority of rAAV DNA persists in an extrachromosomal capacity as episomal circular genomes (Yang et al., 1999) from which the majority of transgene expression occurs (Nakai et al., 2001). This is thought to explain the stability of rAAV genomes in cells such as hepatocytes, myofibers, cardiomyocytes and neurons, which have a low or absent mitotic activity (Alexander et al., 2008).

The induction of a strong cell-mediated immune response to a vector is extremely disadvantageous with regards to gene therapy, such as occurs with Ad vectors, as it limits the duration of transgene expression by clearance of virally transduced cells (Brockstedt et al., 1999; Daya and Berns, 2008). However, due to the absence of all viral genes in rAAV vectors, there is a very limited innate immune response by the host as the transgene and capsid remain the only antigens (Lai et al., 2002; Nayak and Herzog, 2009), with it demonstrated in mice that intramuscular delivery does not elicit a cellular-mediated immune response at all (Brockstedt et al., 1999). However, this lack of response tends to be route of administration and transgene-specific, with a cytotoxic T-cell response to viral capsid proteins evident in mice where rAAV was administered *iv* and *ip* (Brockstedt et al., 1999). The extent of this response also appears to be serotype-specific, with recent clinical trials utilising AAV8 vectors for treatment of haemophilia resulting in the production of AAV8-capsid-specific peripheral T-cells and increased liver enzymes requiring glucocorticoid treatment to avoid complete clearance of virally transduced cells (Nathwani et al., 2011; Tuddenham, 2012). However, where a chemokine and cellular immune response is triggered, this has been demonstrated to be to a far lesser extent than that induced by an Ad vector as AAV interacts with TLR-9, which induces only transient cytokine production and cell infiltration (Zaiss et al., 2002; Zhu et al., 2009). Ad delivery has also been demonstrated to induce a strong type I interferon response, which is absent upon AAV delivery (McCaffrey et al., 2008). The main host immune response to AAV is humoral as its interaction with the complement system is primarily through the classical pathway and is antibody-

dependent (Nayak and Herzog, 2009), resulting in the production of neutralising antibodies (Sun et al., 2003). Again, the magnitude of this response tends to be route of administration dependent, with neutralising antibodies produced when the virus is delivered *im* or *iv*, but not when administered intranasally in non-human primate models (Hernandez et al., 1999). Other factors affecting the extent of response include virus serotype, target organ and the transgene being expressed (Nayak and Herzog, 2009). Neutralising antibodies to the common serotypes AAV1 and AAV2 have been reported in up to 80 % of the population, with antibodies to the less common serotypes such as AAV4, AAV7 and AAV8 being far lower (Blacklow et al., 1968; Calcedo et al., 2009). Avoiding pre-existing immunity may be possible by utilising the less common serotypes in vector design and considering the route of administration carefully (Nayak and Herzog, 2009).

Of the identified AAV serotypes, AAV1-AAV9 have been evaluated for *in vivo* transduction and have been demonstrated to show distinct tissue tropisms (Table 5.1) (Zincarelli et al., 2008). Therefore, selective use of certain serotypes can help target gene therapies more specifically to tissues (Lai et al., 2002). As well as this innate tropism, rAAV tissue transduction can be further modified to expand or reduce tissue specificity. Cross-packaging approaches can be utilised in order to expand the tissue tropism of AAV. For example, an AAV2 genome packaged into an AAV5 capsid (AAV2/5) will transduce both photoreceptors and retinal pigment epithelial (RPE) cells of the eye, whereas AAV2 alone will only transduce the photoreceptor cells (Auricchio et al., 2001).

One limitation of the use of rAAV as a gene therapy vector compared to rAd is its unique pattern of transgene expression. Whereas rAd transgene expression will be detectable within 24 hr, it has been demonstrated that expression following rAAV delivery increases gradually following transduction with the vector, requiring approximately 2-6 wks before a plateau is reached, depending on the serotype (Zincarelli et al., 2008). This has been attributed to 2 rate-limiting steps; inefficient AAV trafficking in certain tissues (Hauck et al., 2004) and second strand synthesis of the ssDNA genome (Ferrari et al., 1996).

Table 5.1 AAV serotype tissue tropism.

Virus	Tissue Tropism
AAV1	SM, CNS, retina, pancreas, heart
AAV2	VSMC, SM, CNS, liver, kidney
AAV3	Hepatocarcinoma, SM
AAV4	CNS, retina
AAV5	SM, CNS, lung, retina
AAV6	SM, heart, lung
AAV7	SM, retina, CNS
AAV8	Liver, SM, CNS, retina, pancreas, heart
AAV9	Liver, heart, brain, SM, lungs, pancreas, kidney

SM= smooth muscle, CNS= central nervous system, VSMC= vascular smooth muscle cells. Modified from (Nonnenmacher and Weber, 2012).

5.1.2.1 AAV serotype 9

AAV9 is a novel serotype first isolated from primate tissue using a PCR-based molecular rescue method (Gao et al., 2002). It was isolated from human tissue 2 years later and was found to be serologically distinct from all other known serotypes at that time allowing it to be grouped into its own clade, clade F (Gao et al., 2004). It has received particular attention as a potential gene therapy vector since its identification as it has the potential to be used as a global gene delivery vector, disseminating into all tissues of the body with a single *iv* dose (Bostick et al., 2007). In particular it has been shown to have an affinity for lung, skeletal muscle and heart when delivered intravenously (Ghosh et al., 2007; Inagaki et al., 2006; Pacak et al., 2006). In fact, it has been demonstrated that a low dose of 1 x 10^{11} vp of AAV9 delivered *iv* in the mouse will transduce over 80 % of cardiomyocytes within the heart, with 100 % transduction possible when the dose is increased (Inagaki et al., 2006). Moreover, it has been shown that transduction efficiency is un-altered when the vector is delivered directly into the myocardium *via* direct injection (Bostick et al., 2007). Not only does AAV9 have the strongest tropism towards the heart of all known cardio-tropic AAV serotypes in mice (Bish et al., 2008), it has also been determined to be part of the 'high-expression' and 'rapid-onset' AAV groups. It has the most varied tissue transduction capability and highest transgene protein expression levels out of serotypes 1-9 and its transgene expression is detectable in mice just 7 days following *iv* delivery, whereas other serotypes such as AAV2 and AAV3 may not have detectable expression levels until 4 wks post-delivery (Zincarelli et al., 2008). More recently, mutagenesis of the AAV9 capsid surface VRs has allowed the generation of liver-detargeted vectors, allowing more specific targeting to the heart and skeletal muscle (Pulicherla et al., 2011). AAV9s ability to cross the blood-brain barrier also makes it an ideal vector for targeting the brain and CNS (Forsayeth and Bankiewicz, 2011; Manfredsson et al., 2009). The unique properties of AAV9 therefore make it an ideal candidate vector for gene therapy applications, especially for the targeting of cardiac disease. Here, AAV9 has been utilised to study the potential therapeutic properties of Ang-(1-9) for cardiac remodelling in the mouse MI model.

5.2 Aims

The aims of this chapter were to:

- Clone an expression cassette into an AAV shuttle vector for the production of AAV9 vectors expressing the Ang-(1-9) fusion protein and demonstrate successful transgene expression from the cassette.

- Optimise AAV9 delivery in the mouse MI model using systemic tail vein delivery and show successful myocardial transduction.

- Utilise systemic delivery of the Ang-(1-9) expressing AAV9 vector in order to assess its effect on structural and functional cardiac remodelling in the mouse model of MI.

5.3 Results

5.3.1 Cloning of the AAV expression cassette

5.3.1.1 Plasmid maps, ligation and recombination

The pBluescript SK+ parental plasmid encoding the Ang-(1-9) fusion protein transgene sequence, as described in Chapter 4, had been previously been cloned into the MCS of the plasmid using *Hin*DIII and *Eco*RI restriction sites (Figure 5.1 A-i). In order to produce an AAV9 vector expressing this fusion protein, the full transgene sequence was excised from the pBluescript SK+ plasmid at *Cla*I and *Bam*HI sites and inserted at the corresponding sites into the plasmid pAAV-MCS (Figure 5.1 A-ii). This inserted the sequence between the CMV promotor and poly-A sequences, flanked by the AAV2 ITR sequences.

*Cla*I and *Bam*HI restriction endonuclease digests were performed on both plasmids and the Ang-(1-9) encoding insert band at 1 Kb and the pAAV-MCS backbone at 4.6 Kb were excised from the gel and the DNA purified (Figure 5.1B-i). A ligation reaction was performed and subsequently transformed into competent *E.coli* and resultant colonies screened for the successfully ligated pAAV-MCS containing the inserted Ang-(1-9) DNA sequence (Figure 5.1 B-ii, positive colonies indicated by the black arrows).

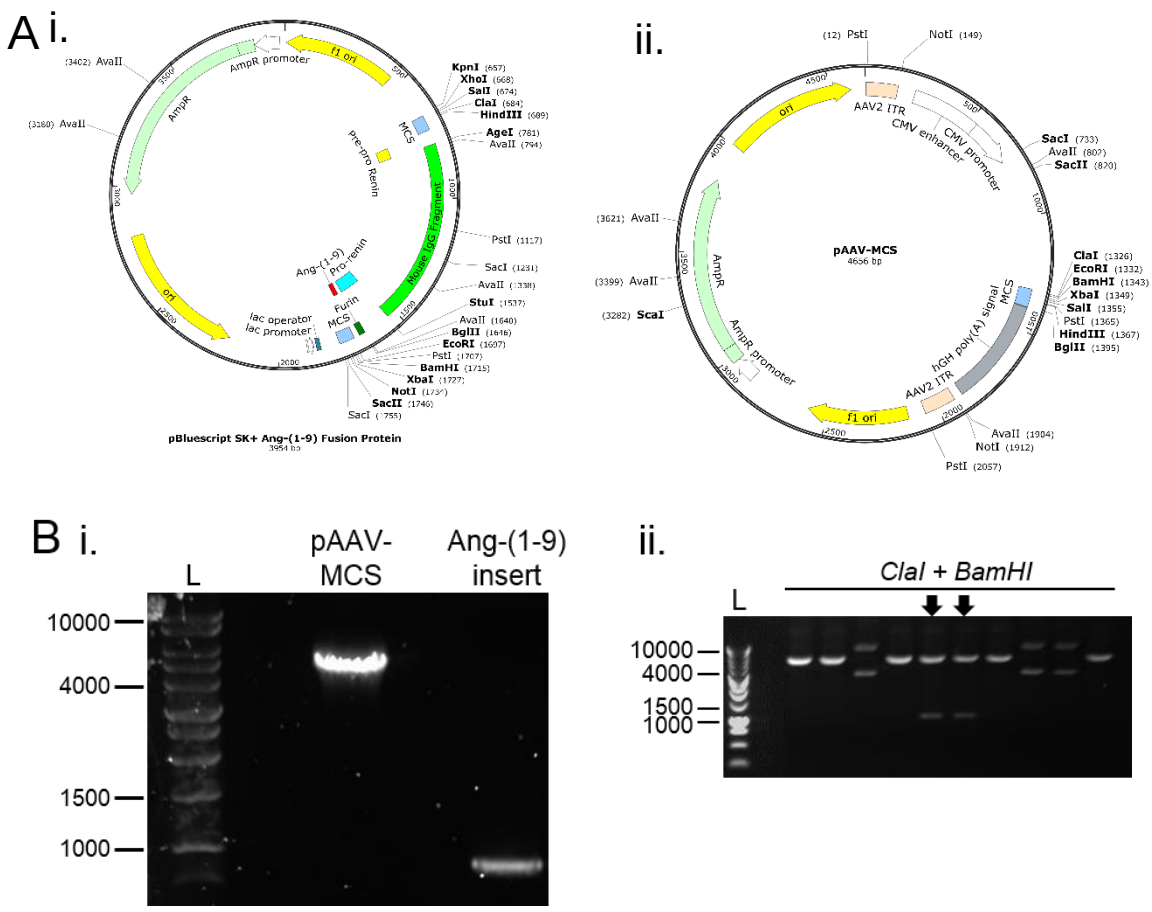

Figure 5.1 Ang-(1-9) expression cassette plasmid maps, purification of vector and insert DNA and clone screening.
(A-i.) pBluescript parental plasmid carrying the original Ang-(1-9) fusion protein sequence in the MCS. (ii.) The empty pAAV-MCS AAV shuttle plasmid, into the MCS of which the Ang-(1-9) fusion protein sequence was to be inserted. MCS= multiple cloning site. (B-i.) Ethidium bromide agarose gel showing separation of DNA fragments from the double *Cla*I and *Bam*HI digests of the pBluescript and pAAV-MCS plasmids following gel purification of the desired vector and insert fragments. (ii.) Ethidium bromide agarose gel of clone screening using double *Cla*I and *Bam*HI digests following ligation of insert and vector DNA. Positive clones are indicated by the black arrows and show the excised insert. L= 1 Kb ladder.

5.3.1.2 Expression of the Ang-(1-9) fusion protein from the AAV expression cassette

Expression of the transgene was confirmed *in vitro via* RT-PCR following transfection into H9c2 cells. Following electrophoresis a band present at 710 bp indicated successful mRNA expression from the transgene (Figure 5.2 A-i & ii).

Following confirmation of successful transgene mRNA expression, protein expression was confirmed *via* western immunoblotting with probing for the mouse heavy chain IgG2B fragment of the fusion protein in transfected HeLa cell lysates performed, revealing a band at approximately 32 KDa confirming successful expression of the protein (Figure 5.2 B).

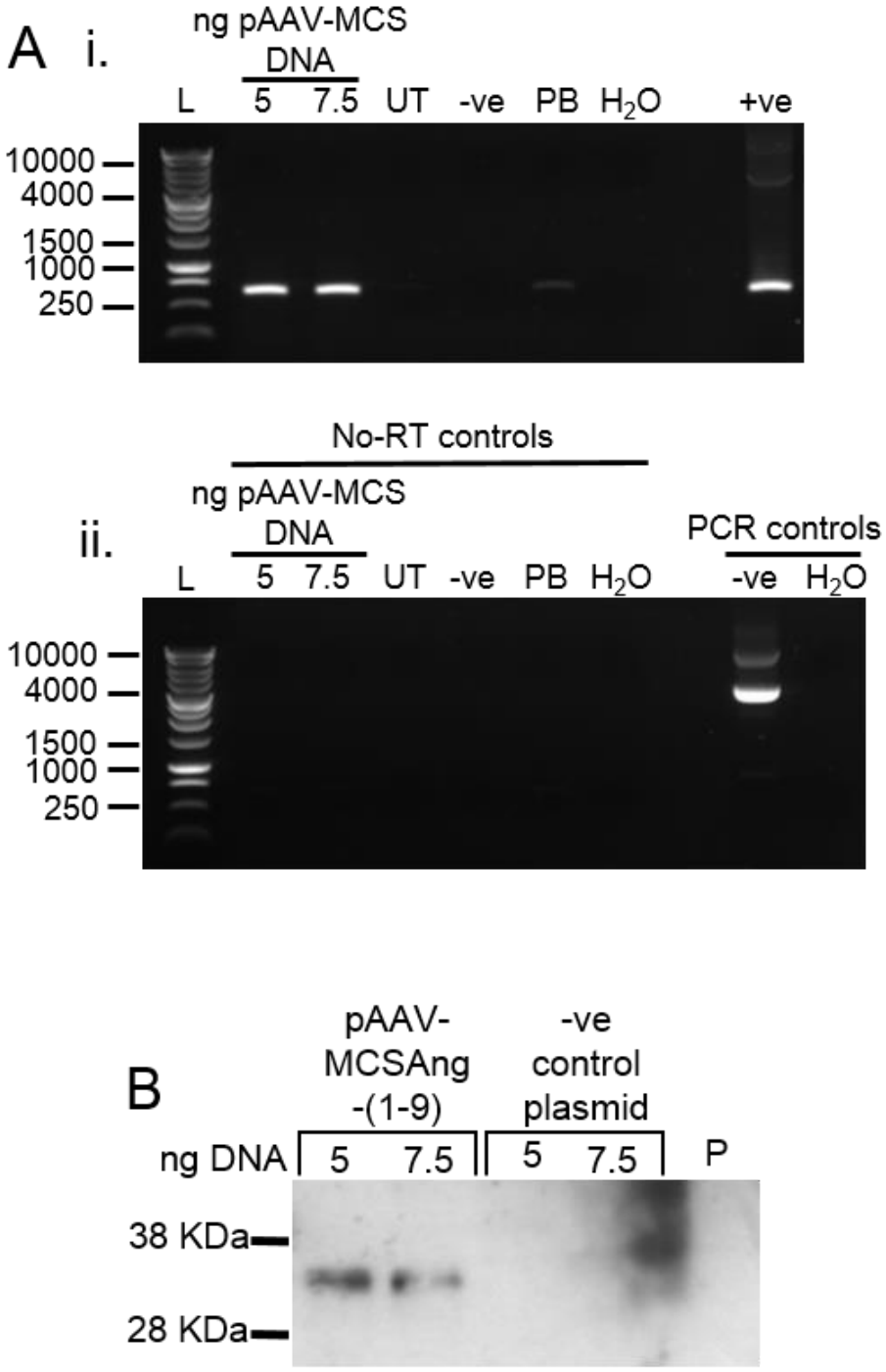

Figure 5.2 Confirmation of fusion protein transcription and protein expression from the pAAV-MCS expression cassette.
(A-i.) Ethidium bromide agarose gel showing separation of DNA fragments from a PCR reaction carried out on cDNA synthesised from RNA extracted from H9c2 cells transduced with 5 or 7.5 ng of pAAV-MCS plasmid DNA or control DNA. (ii.) Ethidium bromide agarose gel loaded with no-RT control wells of the PCR reactions to control for DNA contamination and negative PCR control reactions to check for primer specificity. L= 1 Kb ladder, UT= untransfected cells, -ve= negative control plasmid DNA transduced, PB= pBluescript parental plasmid transduced, +ve= positive control plasmid for PCR reaction. (B) Western blot carried out on HeLa cell lysates transfected with 5 or 7.5 ng of pAAV-MCS or negative control plasmid DNA and probed for the mouse Fc IgG2B fragment. P= polymer transfection control.

5.3.2 Optimisation of AAV *in vivo* delivery

5.3.2.1 AAV transgene expression in MI

Transduction of infarcted myocardium was first assessed using AAVGFP to optimise transgene expression. Following infarction but prior to recovery, 1 x 10^{11} vg were delivered intravenously *via* tail vein. Hearts were harvested at 1, 2 and 8 wks following viral delivery. (Figure 5.3). GFP expression was detectable at 1 wk post-delivery in the infarcted mouse heart. This was shown to increase between wks 1 and 2 by approximately 5-fold, with higher expression maintained up until the 8 wk time-point (Figure 5.3 A).

Via IHC, GFP expression was evident in the cardiomyocytes of the AAVGFP transduced infarcted hearts at 1, 2 and 8 wks post-virus delivery. GFP expression was visibly more extensive at the 2 and 8 wk post-delivery time-points, consistent with the GFP assay results and demonstrating efficient global transduction of the heart by the AAV9 vector (Figure 5.3 B).

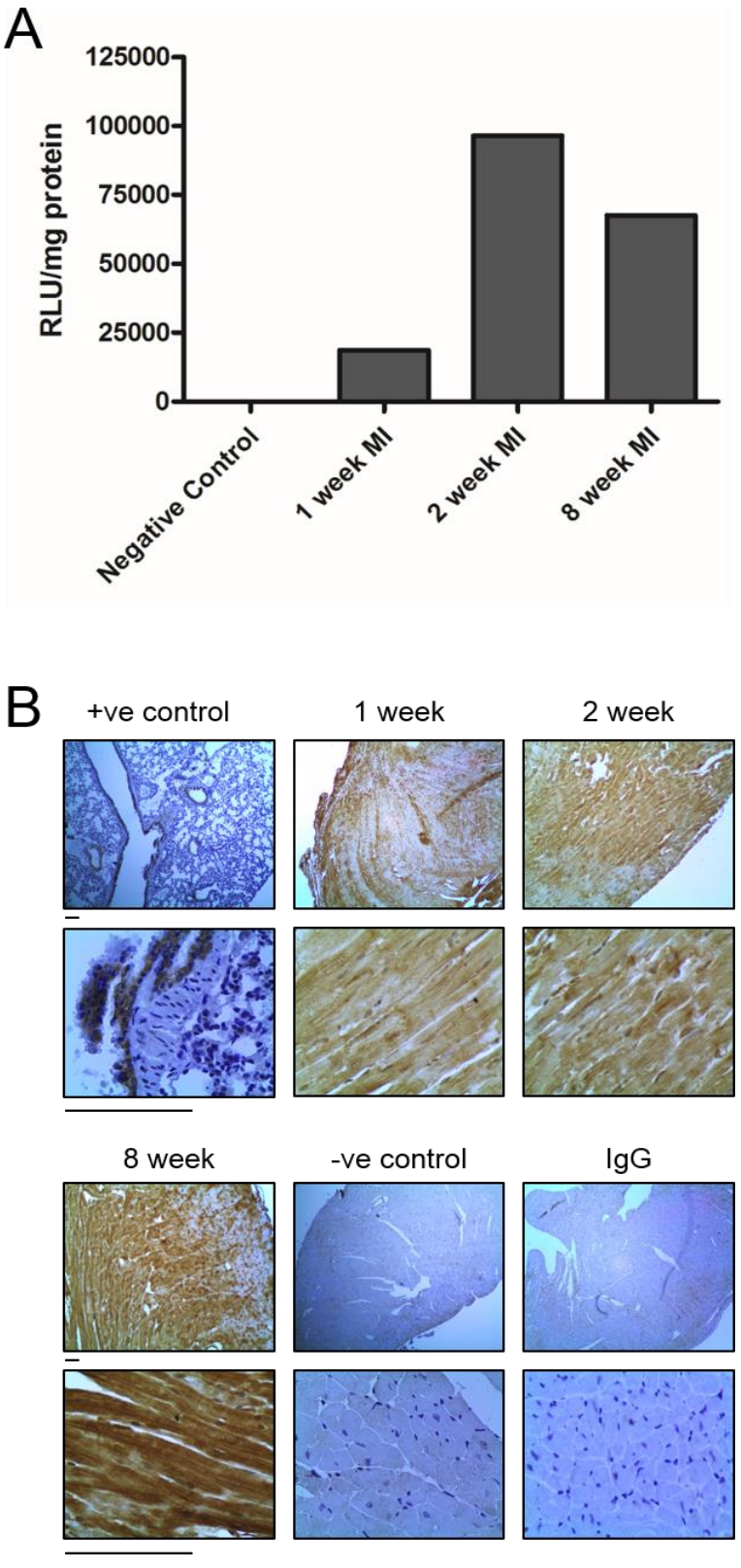

Figure 5.3 AAV9 transduction of the infarcted mouse heart.
Transduction of the infarcted mouse heart by AAVGFP following tail vein delivery of 1 x 10^{11} vg per animal post-infarction. Expression was assessed at 1, 2 and 8 wks following virus delivery (A) Quantification of GFP expression in transduced mouse heart lysates using a GFP assay. Fluorescence was normalised to both negative control heart tissue basal fluorescence and protein concentration of the lysate. *n*= 2 per time-point. Data presented as mean values. (B) DAB staining for GFP expression in sections from wax-embedded hearts transduced with AAV-GFP for 1, 2 and 8 wks. GFP -positive lung tissue, GFP-negative heart tissue and IgG were used to confirm antibody specificity. *n*= 2. Magnification= 4x and 40x, scale= 100 µm.

5.3.3 Mortality

Following confirmation of successful AAV-mediated transduction of the myocardium in the mouse MI model, the effect of AAVAng-(1-9) on structural and functional remodelling post-MI was assessed. Four animal groups were utilised; sham, MI, MI+AAVGFP and MI+AAVAng-(1-9) (Figure 5.4 A).

A Kaplan-Meier plot of mortality for all animals recovered from procedure demonstrated that total mortality in each of the 3 MI groups occurred within the first 7 days following procedure due to rupture. The % mortality was approximately equivalent in the MI and MI+AAVGFP groups, however only MI+AAVGFP mortality was significantly increased compared to sham animals (MI+AAVGFP= 33.3 %; $P<0.05$). Mortality was reduced in the MI+AAVAng-(1-9) group and was not significantly different to sham animals (sham= 100, MI= 26.7, and MI+AAVAng-(1-9)= 9.1 %; $P>0.05$; Figure 5.4 B). 100 % of these deaths were attributable to cardiac rupture as determined by post-mortem analysis (Figure 5.4 C). The sham group demonstrated a 100 % survival rate.

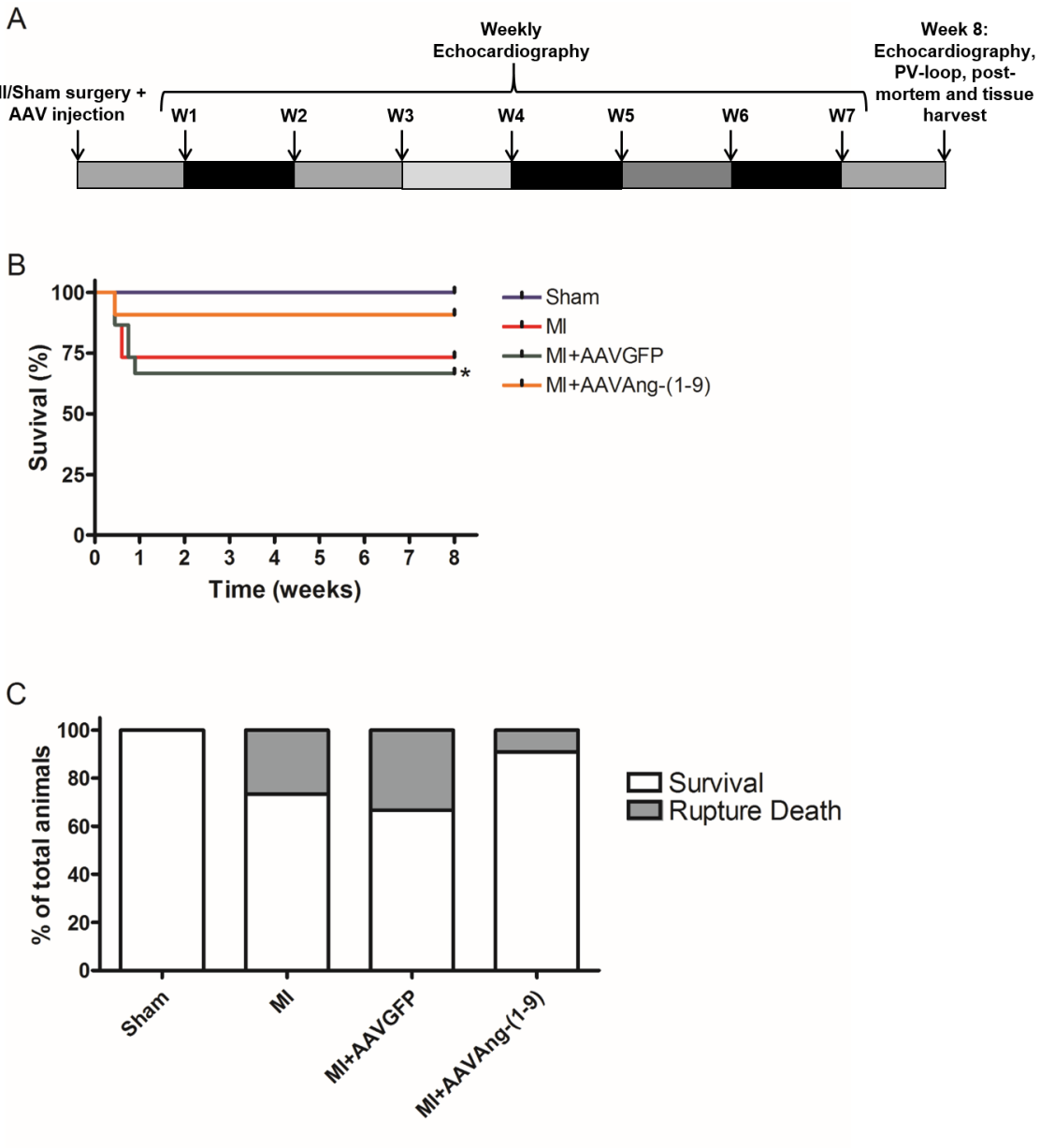

Figure 5.4 Study-design and procedure-associated mortality.
(A) Study design showing time-frame of measurements over the 8 wk study period. (B) Kaplan-Meier plot of mortality following recovery from procedure for each animal group (sham, MI, MI+AAVGFP, MI+AAVAng-(1-9)) over the 8 wk study period. *= $P<0.05$ *vs.* sham. n= 10, 15, 15 and 11 for sham, MI, MI+AAVGFP and M+AAVAng-(1-9), respectively. (C) % of survival and cause of mortality for each animal group following recovery from procedure.

5.3.4 Haemodynamic and functional measurements

5.3.4.1 Echocardiography

A significant reduction in FS was seen from 1 wk post-MI onwards in the MI and MI+AAVGFP groups, with a progressive decrease in FS with time from 1 to 8 wks post-MI (Figure 5.5 A-i & ii). This was associated with increases in LVESD in both groups at all time-points and a trend towards increase in LVEDD at each time-point (Figure 5.5 A-iii & iv). Delivery of AAVAng-(1-9) resulted in a significant attenuation of this reduced FS at all time-points. At the 8 wk time-point, MI+AAVAng-(1-9) FS, although significantly reduced to 78.4 % of sham (49.1± 1.6 *vs.* 38.5± 1.9 %, sham (n= 6) *vs.* MI+AAVAng-(1-9) (*n*= 6); $P<0.05$), was significantly increased compared to both the MI and MI+AAVGFP groups (MI= 25.8± 2.2, MI+AAVGFP= 26.6± 0.7 %; $P<0.05$ *vs.* MI+AAVAng-(1-9)). Overall, FS in the MI+AAVAng-(1-9) FS remained stable from 1 wk onwards, with no progressive decline as seen in the other 2 MI groups (Figure 5.5 A-ii). There was no difference in LVEDD in the MI+AAVAng-(1-9) group compared to the MI and MI+AAVGFP groups (Figure 5.5 A-iii). There was also no significant difference in LVESD, except at the 1 wk time-point where MI+AAVAng-(1-9) LVESD was significantly reduced compared to MI+AAVGFP only (2.5± 0.1 *vs.* 3.0± 0.1 mm, MI+AAVAng-(1-9) (*n*= 6) *vs.* MI+AAVGFP (*n*= 6); $P<0.05$). For the remaining time-points, there was a trend towards a decrease in LVESD in the MI+AAVAng-(1-9) group compared to the other 2 MI groups (Figure 5.5 A-iv). No significant changes in posterior LV wall thickness was detectable between groups at any time-points (Figure 5.5 A-v & iv). E/A wave ratio measurements demonstrated no significant changes between animal groups (Figure 5.5 B i & ii).

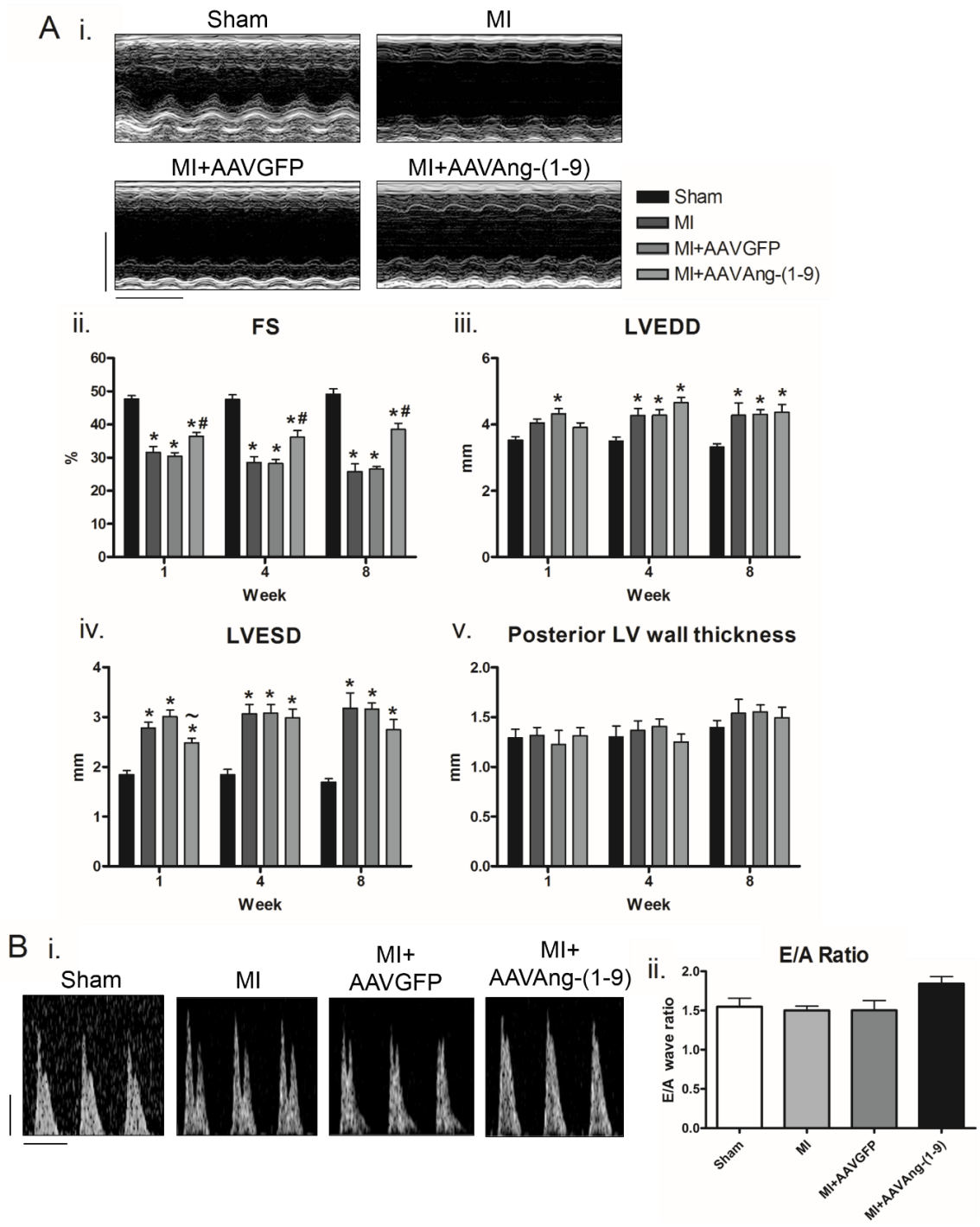

Figure 5.5 Effect of AAVAng-(1-9) on FS, wall thickness and E/A ratio in MI as assessed by echocardiography.
(A-i.) Example M-mode images for each animal cohort at 8 wks Scale= 5 mm and 1 second. Serial FS (ii.), LVEDD (iii.), LVESD (iv.) and posterior LV wall thickness (v.) measurements from M-mode echocardiography images for sham, MI, MI+AAVGFP and MI+AAVAng-(1-9) animal cohorts from 1 to 8 wks post-procedure. *= $P<0.05$ *vs.* sham; #= $P<0.05$ *vs.* MI and MI+AAVGFP; ~= $P<0.05$ *vs.* MI+AAVGFP only. (B-i.) Example E/A wave Doppler measurements for each animal group at 8 wks post-procedure. Scale= 0.2 m/s and 20 mm. (B-ii.) Average E/A ratio measurements for the mitral valve determined using echocardiography Doppler for sham, MI, MI+AAVGFP and MI+AAVAng-(1-9) animal groups at 8 wks post-procedure. *n*= 6 per group. Data presented as mean± SEM. FS= fractional shortening, LVEDD= left-ventricular end-diastolic dimension, LVESD= left-ventricular end-systolic dimension E= early wave and A= after wave.

5.3.4.2 PV loops

In the MI+AAVAng-(1-9) group, a significant attenuation in the changes to the systolic indices seen in the MI and MI+AAVGFP groups following PV loop measurements was evident (Table 5.2 & Figure 5.6). There were significant increases in ESP (P<0.001), EF (P<0.001) and CO (P<0.05) to approximately 113, 163 and 178 % of both MI and MI+AAVGFP groups, respectively. Moreover, EF was normalised to that of the sham group, with CO significantly increase when compared to sham levels (P<0.05). DP/dt_{max} was still significantly reduced to 78.5 % of sham (P<0.001), which was not significantly altered compared to the other 2 MI groups (Figure 5.6 B-i-iv).

AAVAng-(1-9) delivery appeared to have no significant effect on LV diastolic parameters (Figure 5.6 C). EDP was not significantly changed across any groups. DP/dt_{min} was significantly decreased in the MI+AAVAng-(1-9) group to 79.6 % of sham, with Tau increased significantly to 138.2 % of sham (P<0.05). This was similar to what was observed in the MI and MI+AAVGFP groups (Figure 5.6 C-i-iii). However, where EDPVR in the MI and MI+AAVGFP groups was significantly increased to 363.3 % and 400 % of sham, respectively, MI+AAVAng-(1-9) EDPVR remained unchanged compared to sham (P<0.05).

MI and MI+AAVGFP EDV was significantly increased compared to sham. MI+AAVAng-(1-9) EDV was also increased, however this was not significant compared to sham (Figure 5.6 D-i). ESV was significantly increased to approximately 282 % of sham in the MI and MI+AAVGFP groups (P<0.01). ESV for the MI+AAVAng-(1-9) group was not significantly different of that of sham and was reduced compared to the 2 MI groups (Figure 5.6 D-ii). SV was significantly increased in the MI+AAVAng-(1-9) group to approximately 188 % of sham and 160 % of the other 2 MI groups (P<0.05; Figure 5.6 D-iii).

Table 5.2 Effect of AAVAng-(1-9) on haemodynamic LV PV-loop indices in MI.

		MI		
	Sham	**MI only**	**+AAVGFP**	**+AAVAng-(1-9)**
HR (bpm)	604.3 ± 8.5	571.5 ± 7.5	558.0 ± 4.6	583.1 ± 13.5
ESP (mmHg)	103.5 ± 1.6	84.7 ± 2.7 ***	85.1 ± 2.0 ***	95.9 ± 1.4 * ##
EDP (mmHg)	6.3 ± 1.3	7.2 ± 1.2	6.1 ± 0.7	6.9 ± 1.8
Developed pressure (mmHg)	97.3 ± 0.4	77.5 ± 2.5 ***	78.9 ± 2.1	89.0 ± 1.8
dp/dt_{max} (mmHg/min)	10719.9 ± 732.6	7219.5 ± 443.8 ***	7144.8 ± 340.8 ***	8415.3 ± 471.0 ***
dp/dt_{min} (mmHg/min)	8343.1 ± 669.3	5517.5 ± 409.1 ***	5635.8 ± 276.4 ***	6637.2 ± 546.8 **
Tau (ms)	5.5 ± 0.3	7.7 ± 0.7 *	7.3 ± 0.2	7.6 ± 0.6 *
EDPVR	0.03 ± 0.00	0.109 ± 0.01 **	0.12 ± 0.01 **	0.07 ± 0.01 ~
ESV (µL)	16.5 ± 0.5	48.3 ± 7.1 **	45.3 ± 3.6 **	32.9 ± 5.2
EDV (µL)	33.4 ± 1.2	67.8 ± 9.4 *	65.5 ± 3.5 *	64.8 ± 10.8
SV (µL)	16.9 ± 0.8	19.5 ± 2.6	20.2 ± 1.0	31.9 ± 5.7 *#
CO (µL/min)	10190.9 ± 475.3	10880.9 ± 1550.5	10869.2 ± 578.1	19335.7 ± 3859.6 *#
EF (%)	50.4 ± 0.9	29.0 ± 1.7 ***	31.5 ± 2.2 ***	48.8 ± 1.4 ###

HR= heart rate, ESP= end systolic pressure, EDP= end diastolic pressure, dp/dt max= maximal rate of rise of pressure, -dp/dt min= maximum rate of fall in pressure, Tau= time relaxation constant, EDPVR= end diastolic pressure-volume relationship stiffness constant, ESV= end systolic volume, EDV= end diastolic volume, SV= stroke volume, CO= cardiac output, EF= ejection fraction. *= $P<0.05$, **= $P<0.01$, ***= $P<0.001$ *vs.* sham; #= $P<0.05$, ##= $P<0.01$, ###= $P<0.001$ *vs.* MI and MI+AAVGFP; ~= $P<0.05$ *vs.* MI+AAVGFP only. n= 9, 9, 9 and 8 for, sham, MI, MI+AAVGFP and MI+AAVAng-(1-9), respectively.

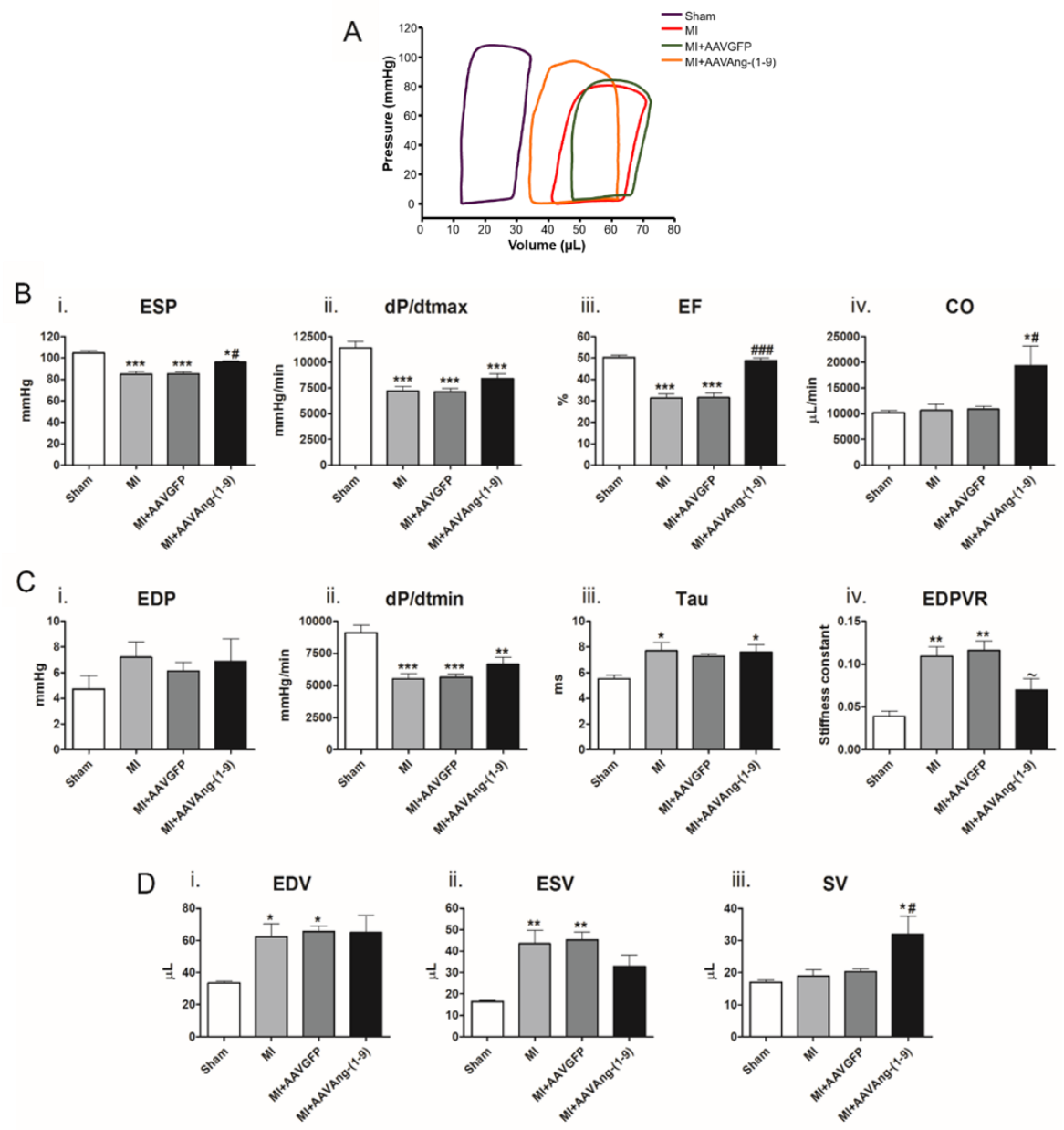

Figure 5.6 Effect of AAVAng-(1-9) on LV haemodynamic indices in MI as determined by PV-loop measurements.
LV haemodynamic measurements for sham, MI, MI+AAVGFP and MI+AAVAng-(1-9) animals 8 wks post-procedure determined using the ADVantage PV-loop system with true blood volume calculated using Wei's equation. (A) Example PV-loop relationships for each animal group at 8 wks. (B) Systolic functional indices of ESP (i.), dP/dt_{max} (ii.), EF (iii.) and CO (iv.); (C) Diastolic functional indices of EDP (i.), dP/dt_{min} (ii.), Tau (iii.) and EDPVR (iv.); and (D) Volume indices of EDV (i.), ESV (ii.) and SV (iii.). *= P<0.05, **= P<0.01, ***= P<0.001 *vs.* sham; #= P<0.05, ##= P<0.01, ###= P<0.001 *vs.* MI and MI+AAVGFP; ~= P<0.05 *vs.* MI+AAVGFP only. n= 9, 9, 9 and 8 for, sham, MI, MI+AAVGFP and MI+AAVAng-(1-9), respectively. Data presented as mean± SEM.

5.3.5 Post-mortem and histological analysis

5.3.5.1 Organ weights

HW:TL ratio was significantly increased in all MI groups to 121, 118 and 125 % of sham for MI, MI+AAVGFP ($P<0.05$) and MI+AAVAng-(1-9) ($P<0.01$) groups, respectively (Figure 5.7 A & B). LuW:TL and LiW:TL ratios remained unchanged across all 4 groups (Figure 5.7 C & D).

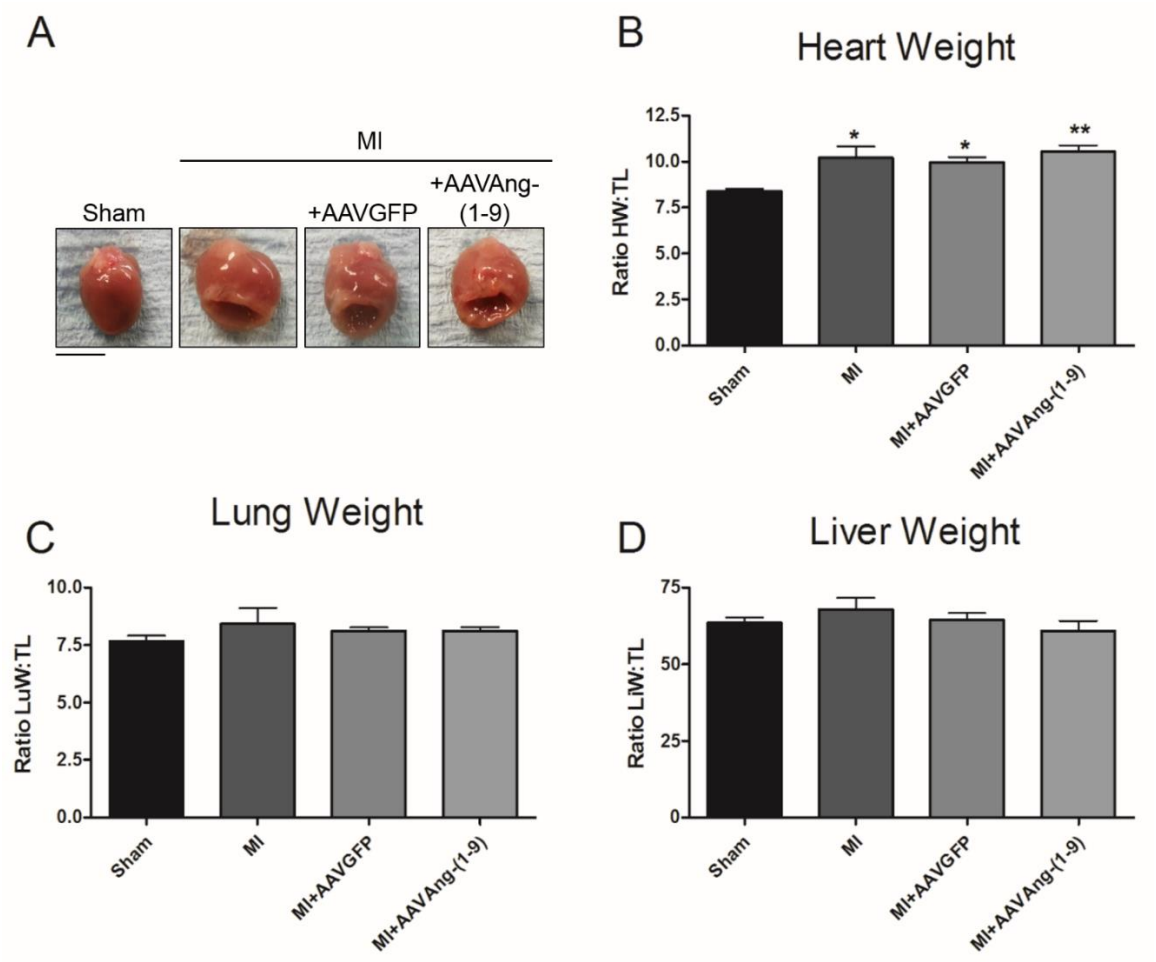

Figure 5.7 Effect of AAVAng-(1-9) on post-mortem organ weights in MI.
(A) Example images of hearts for each animal group at 8 wks. Scale bar= 5 mm. TL= tibia length, HW= heart weight, LuW= lung weight and LiW= liver weight.HW:TL (B), LuW:TL (C) and LiW:TL (D) ratios for sham, MI, MI+AAVGFP and MI+AAVAng-(1-9) groups at 8 wks post-procedure. *= $P<0.05$, **= $P<0.01$ *vs.* sham. n= 10, 10, 9 and 8 for, sham, MI, MI+AAVGFP and MI+AAVAng-(1-9), respectively. Data presented as mean± SEM.

5.3.5.2 Cardiomyocyte sizing

Cell diameter was significantly increased in all 3 MI groups to 128.2, 119.0 and 123.9 % of sham for MI, MI+AAVGFP and MI+AAVAng-(1-9) animal groups, respectively (sham= 15.1± 0.3, MI=20.9± 0.9, MI+AAVGFP= 19.4± 0.4, MI+AAVAng-(1-9)= 20.1± 0.4 μm; P<0.001; Figure 5.8 A-ii). There was no significant difference in cell length between any groups (Figure 5.8 B-ii).

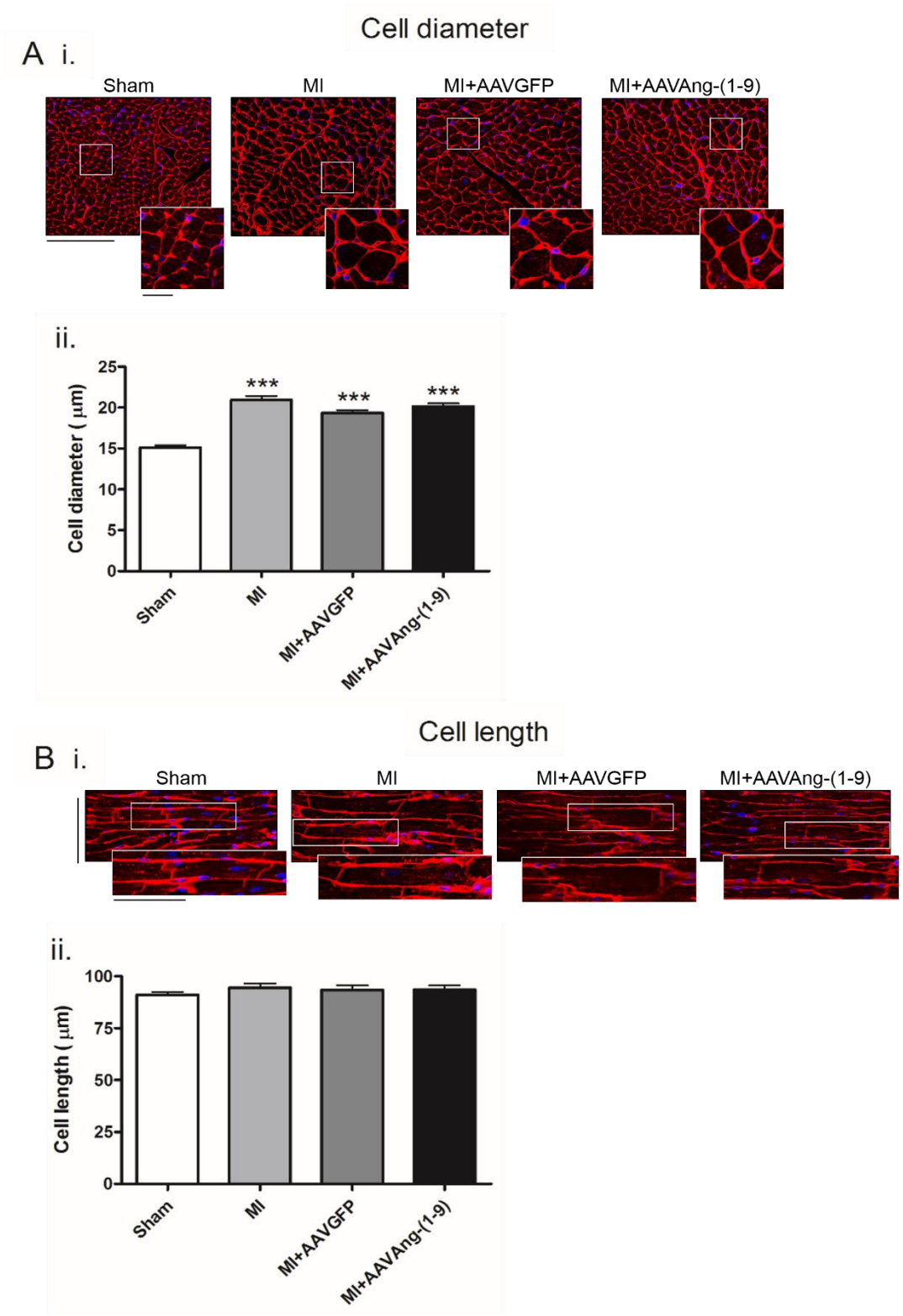

Figure 5.8 Effect of AAVAng-(1-9) on cardiomyocyte size following MI.
Example images of cellular cross-sections in both transverse (A-i) and longitudinal (B-i) axis are shown for each animal group, with cellular membranes stained red and cellular nuclei blue. Main image magnification= 25x, scale= 50 µm. Inset zoom image scale= 12.5 µm for A-i., 50 µm for B-i. Determination of left-ventricular cardiomyocyte diameter (A-ii. *n*= 144, 139, 127 and 112 cells for sham, MI, MI+AAVGFP and MI+AAVAng-(1-9), respectively) and length (B-ii. *n*= 99, 89, 69 and 66 for sham, MI, MI+AAVGFP and MI+AAVAng-(1-9), respectively) in the hearts of sham, MI, MI+AAVGFP and MI+AAVAng-(1-9) animals using WGA staining. ***= *P*<0.001 *vs* sham. *n*= 10, 10, 9 and 8 animals for sham, MI, MI+AAVGFP and MI+AAVAng-(1-9), respectively. Data presented as mean± SEM with the average cell-size for each animal taken as the average of a group of cells evenly distributed across the LV.

5.3.5.3 Regional fibrosis and collagen expression

The scar regions of all 3 MI groups were significantly more fibrotic in comparison to proximal sham apical tissue, with over 80 % of the area positive for fibrosis. However fibrosis in the scar area of the MI+AAVAng-(1-9) group was significantly reduced compared to the corresponding region in the MI+AAVGFP group (86.9± 1.0 *vs.* 92.4± 1.0 %, MI+AAVAng-(1-9) (*n*= 10) *vs.* MI+AAVGFP (*n=9)*; *P*<0.01). Fibrosis in the LV region was significantly increased in all 3 MI groups compared to sham (*P*<0.01). Fibrosis was significantly increased in the septum in the MI and MI+AAVGFP groups compared to sham, however it was significantly reduced in the MI+AAVAng-(1-9) group (MI= 10± 2.4 , MI+AAVGFP= 6.3± 0.4 , MI+AAVAng-(1-9)= 3.4± 0.6 %; *P*<0.01). Similarly in the RV, fibrosis was significantly increased in MI and MI+AAVGFP (*P*<0.01), however it was not significantly different to any other group in MI+AAVAng-(1-9) animals (Figure 5.9 A & B).

Scar size was consistent between all 3 MI groups (MI= 35.9± 2.8, MI+AAVGFP= 35.2± 2.1, MI+AAVAng-(1-9)= 36.9± 2.5 %; Figure 5.9 C). MI and MI+AAVGFP scar thickness was found to be 329± 25 µm and 276± 3.9 µm, respectively. MI+AAVAng-(1-9) group scar thickness was 383± 14 µm, significantly increased compared to the MI+AAVGFP group (*P*<0.05), however not compared to the MI group (Figure 5.12 D).

There were no significant differences in the extent of collagen I in the scar or LV regions across any groups. However, in the septum collagen I levels in the MI group only was significantly increased compared to sham (3.9± 1.6 *vs.* 15.7± 4.2 %, sham (*n*= 10) *vs.* MI (*n*= 10), *P*<0.001). The MI+AAVAng-(1-9) group had significantly less collagen I than the MI septum region (MI+AAVAng-(1-9)= 3.4± 1.0 %; *P*<0.05 *vs.* MI). In the RV, collagen I in the MI group was significantly increased compared to sham (10.0± 2.0 *vs.* 35.9± 4.5 %, sham (*n*= 10) *vs.* MI (*n*= 10); *P*<0.001). While the MI+AAVGFP RV region showed no significant difference compared to other groups, MI+AAVAng-(1-9) collagen I levels were significantly reduced to 37 % of MI (*P*<0.001) (Figure 5.10 A & B). There were no significant differences in collagen III expression in any of the regions between any groups (Figure 5.11 A & B).

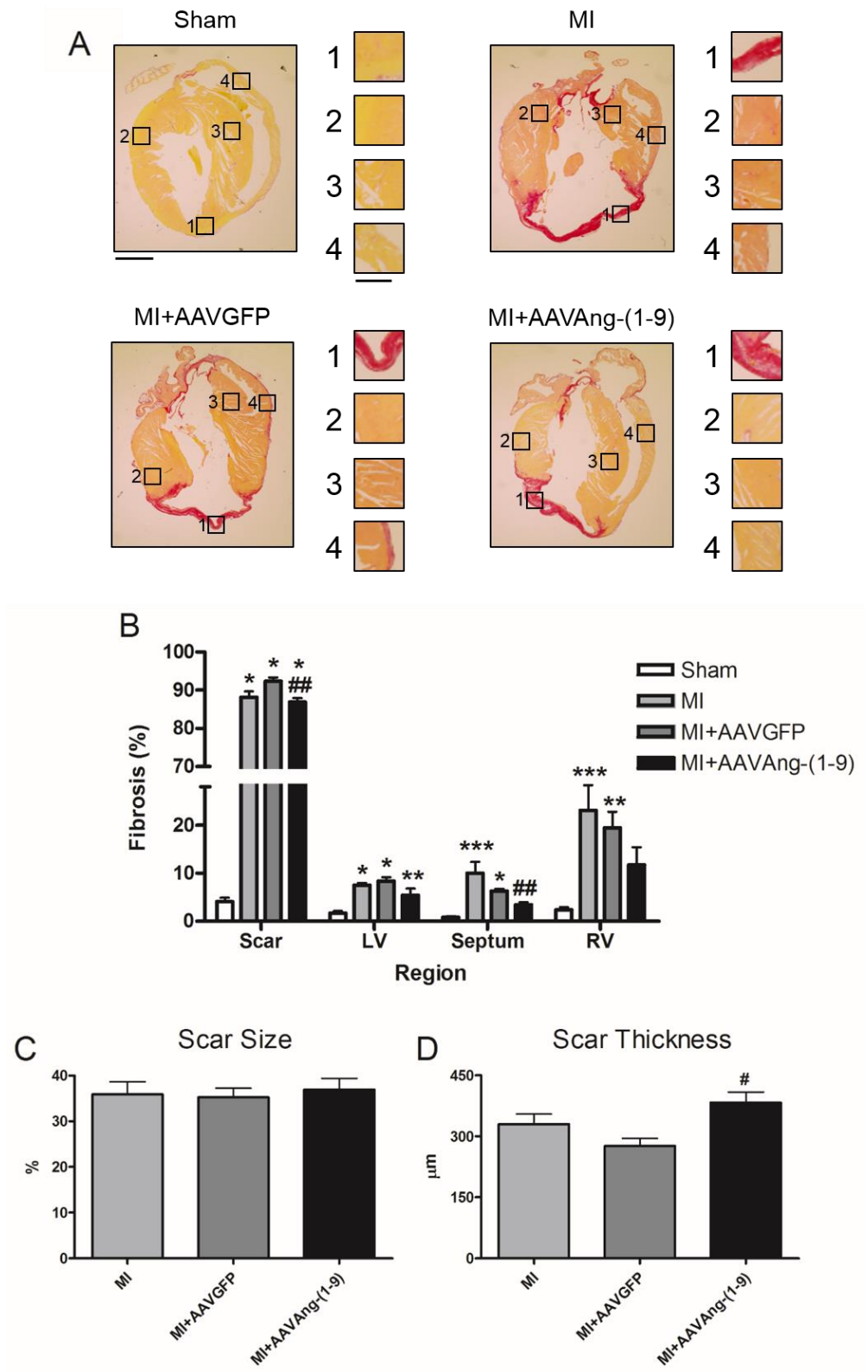

Figure 5.9 Effect of AAVAng-(1-9) on regional fibrosis and scar size following MI.
(A) Example images of picrosirius red staining of heart sections for each animal group. Data presented as mean± SEM. Magnification= 1.25x, scale= 1 mm. Zoom inset image scale= 0.5 mm. (B) Quantification of total cardiac fibrosis of the scar, left ventricle, right ventricle and septum regions of sham, MI, MI+AAVGFP and MI+AAVAng-(1-9) hearts. *= P<0.05, **= P<0.01, ***= P<0.001 *vs* sham region; #= P<0.05, ##= P<0.01 *vs.* MI and MI+AAVGFP region. (C) Scar size for each MI group, determined as a % of the total myocardial area. (D) Average scar thickness for each MI groups. n= 10, 10, 9 and 8 for sham, MI, MI+AAVGFP and MI+AAVAng-(1-9), respectively.

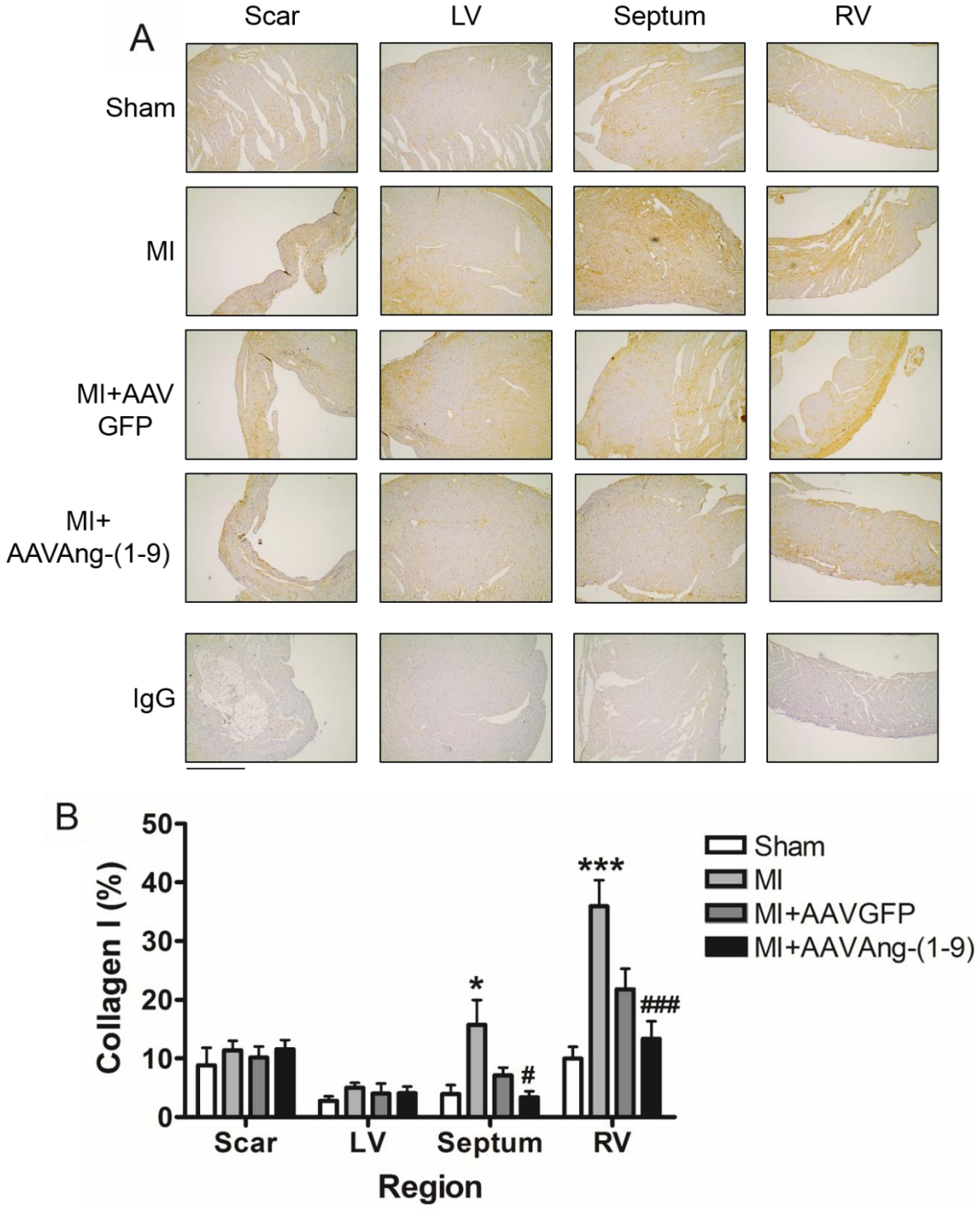

Figure 5.10 Effect of AAVAng-(1-9) on regional cardiac collagen I expression following MI. (A) Representative images of heart sections showing the distribution of DAB staining for collagen I expression in each of the animal groups. Negative IgG was used as a control for antibody specificity. Magnification= 10x, scale bar= 500 µm. (B) Quantification of DAB staining for positive collagen I expression in the cardiac regions of scar, LV, septum and RV as a percentage of the total region for sham, MI, MI+AAVGFP and MI+AAVAng-(1-9) groups.*= P<0.05, ***= P<0.001 *vs.* sham; #= P<0.05, ###= P<0.001 *vs.* MI. n= 10, 10, 9 and 8 for sham, MI, MI+AAVGFP and MI+AAVAng-(1-9) groups, respectively. Data presented as mean± SEM.

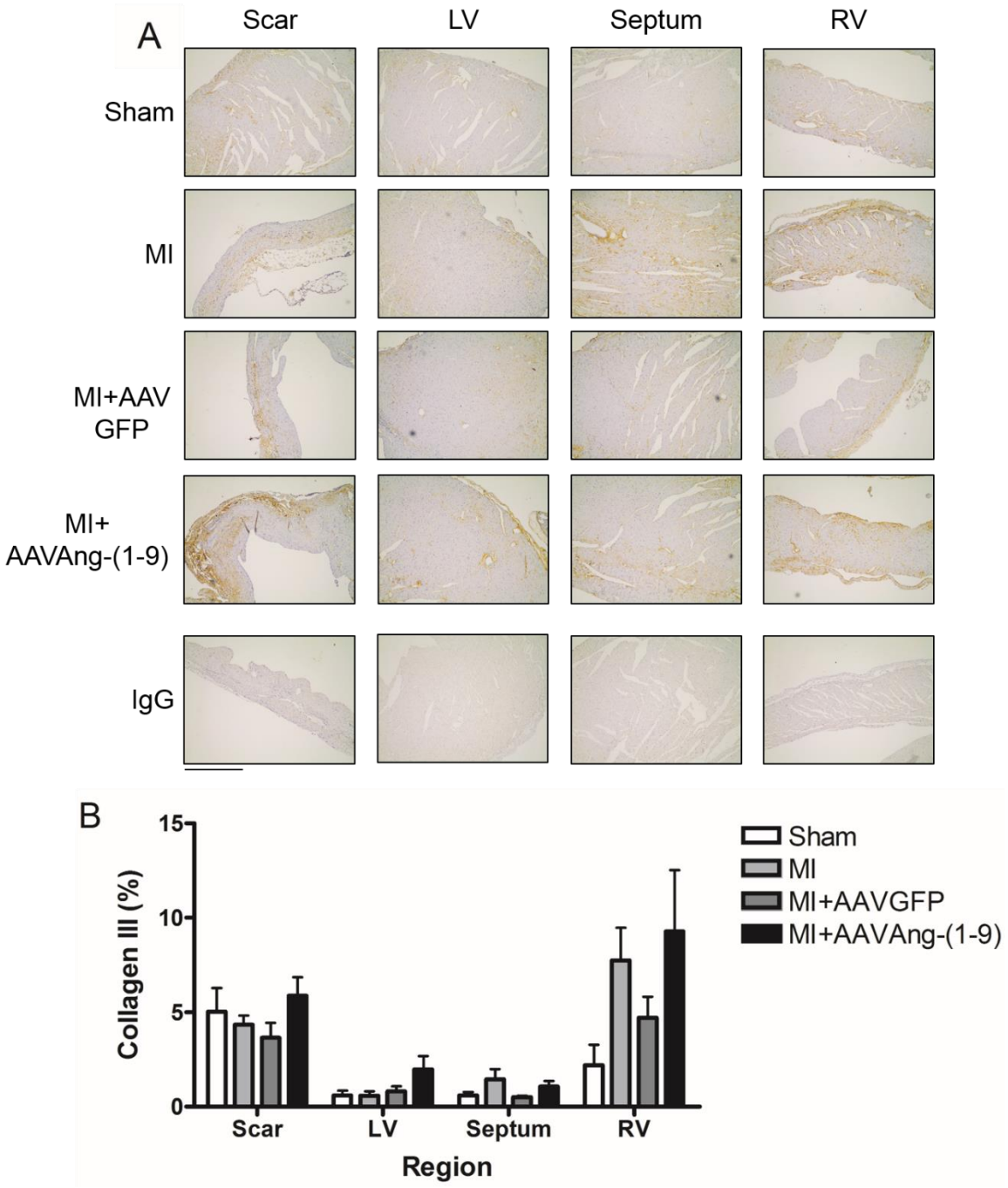

Figure 5.11 Effect of AAVAng-(1-9) on regional cardiac collagen III expression following MI. (A) Representative images of heart sections showing distribution of DAB staining for collagen III expression in each animal group. Negative IgG used as a control for antibody specificity. Magnification= 10x, scale bar= 500 µm. (B) Quantification of DAB staining for positive collagen III expression in the cardiac regions of scar, LV, septum and RV as a percentage of the total region for sham, MI, MI+AAVGFP and MI+AAVAng-(1-9) animals. *n*= 10, 10, 9 and 8 for sham, MI, MI+AAVGFP and MI+AAVAng-(1-9) groups, respectively. Data presented as mean± SEM.

5.3.5.4 Perivascular fibrosis and collagen expression

Total perivascular fibrosis in the MI and MI+AAVGFP groups was significantly increased to approximately 152 % of sham (P<0.01). This increase was significantly attenuated in the MI+AAVAng-(1-9) group (MI= 23.7± 1.9, MI+AAVGFP= 24.7± 2.3, MI+AAVAng-(1-9)= 18.1± 1.3 %; P<0.05; Figure 5.12 A & B). Perivascular collagen I expression was only significantly increased in the MI group compared to sham (5.8± 0.4 *vs.* 9.4± 1.0 %, sham (n= 10) *vs.* MI (n= 10); P<0.05; Figure 5.13 A & B), whereas perivascular collagen III expression was significantly increased in the MI+AAVGFP group only compared to sham (4.3± 0.7 *vs.* 8.6± 1.4 %, sham (n= 10) *vs.* MI+AAVGFP (n= 8); P<0.05; Figure 5.14 A & B).

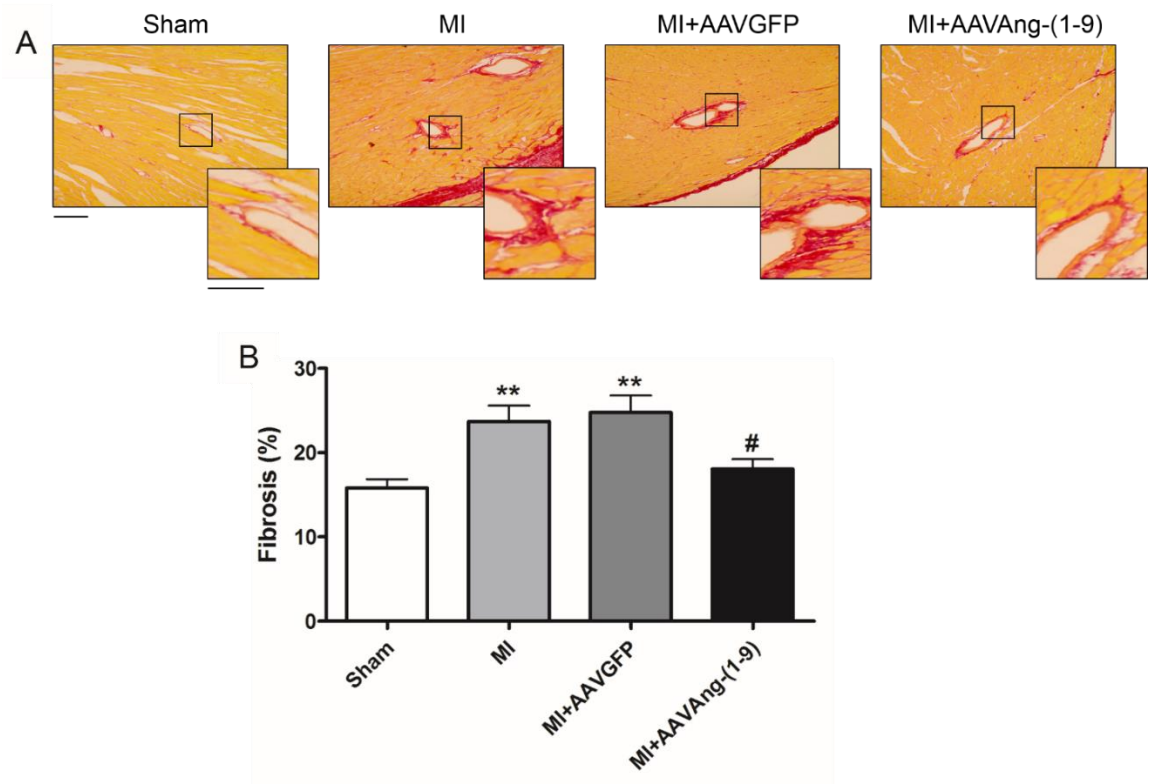

Figure 5.12 Effect of AAVAng-(1-9) on cardiac perivascular fibrosis following MI.
(A) Representative images of left-ventricular localised vessels and associated picrosirius red staining of heart sections for each animal group. Magnification= 20x, scale= 200 µm. Zoom inset images scale= 100 µm. (B) Total perivascular cardiac fibrosis quantification for sham, MI, MI+AAVGFP and MI+AAVAng-(1-9) hearts. **= P<0.01 *vs.* sham; #= P<0.05 *vs.* MI and MI+AAVGFP. n= 10, 10, 9 and 8 for sham, MI, MI+AAVGFP and MI+AAVAng-(1-9), respectively. Data presented as mean± SEM.

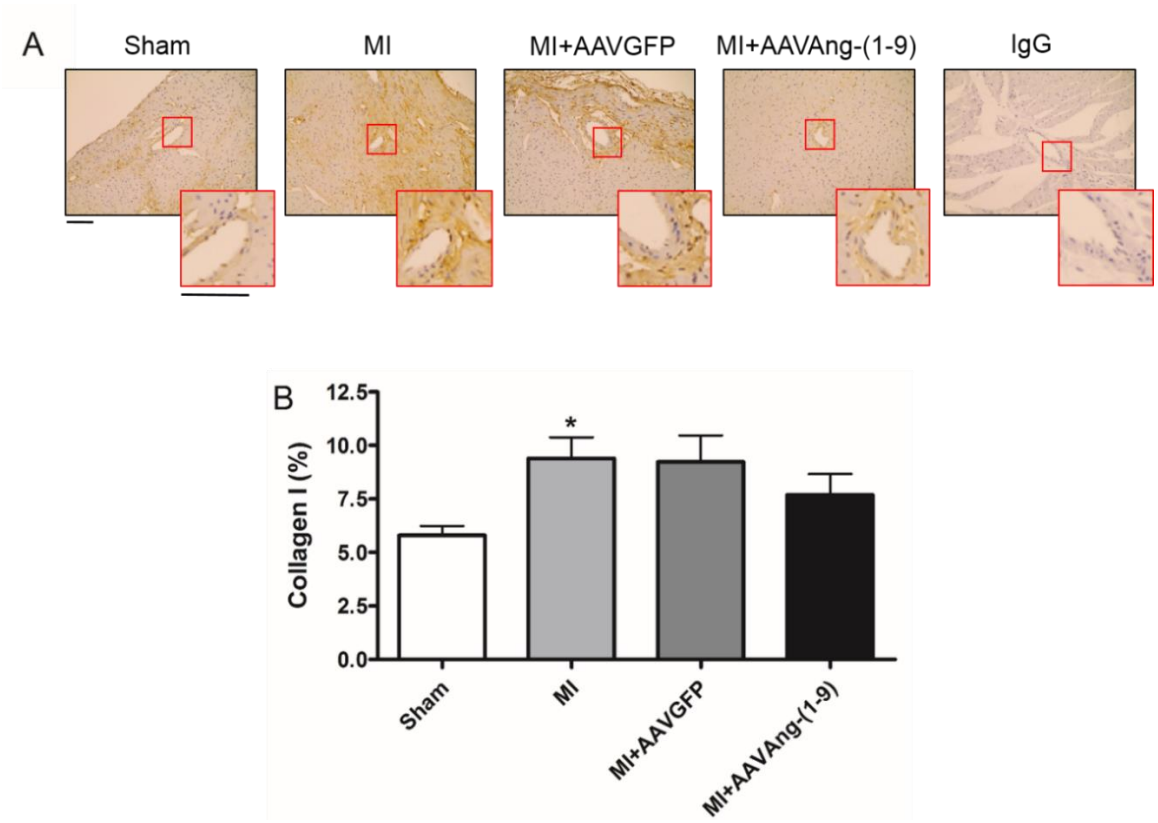

Figure 5.13 Effect of AAVAng-(1-9) on perivascular cardiac collagen I expression following MI.
(A) Representative images of cardiac vessels and associated DAB staining for collagen I expression for heart sections of each animal group. Negative IgG used as a control for antibody specificity. Magnification= 20x, scale= 200 µm. (B) Quantification of DAB staining for perivascular collagen I expression in heart sections of sham, MI, MI+AAVGFP and MI+AAVAng-(1-9) animals. *= P<0.05 *vs* sham. n= 10, 10, 9 and 8 for sham, MI, MI+AAVGFP and MI+AAVAng-(1-9), respectively. Data presented as mean± SEM.

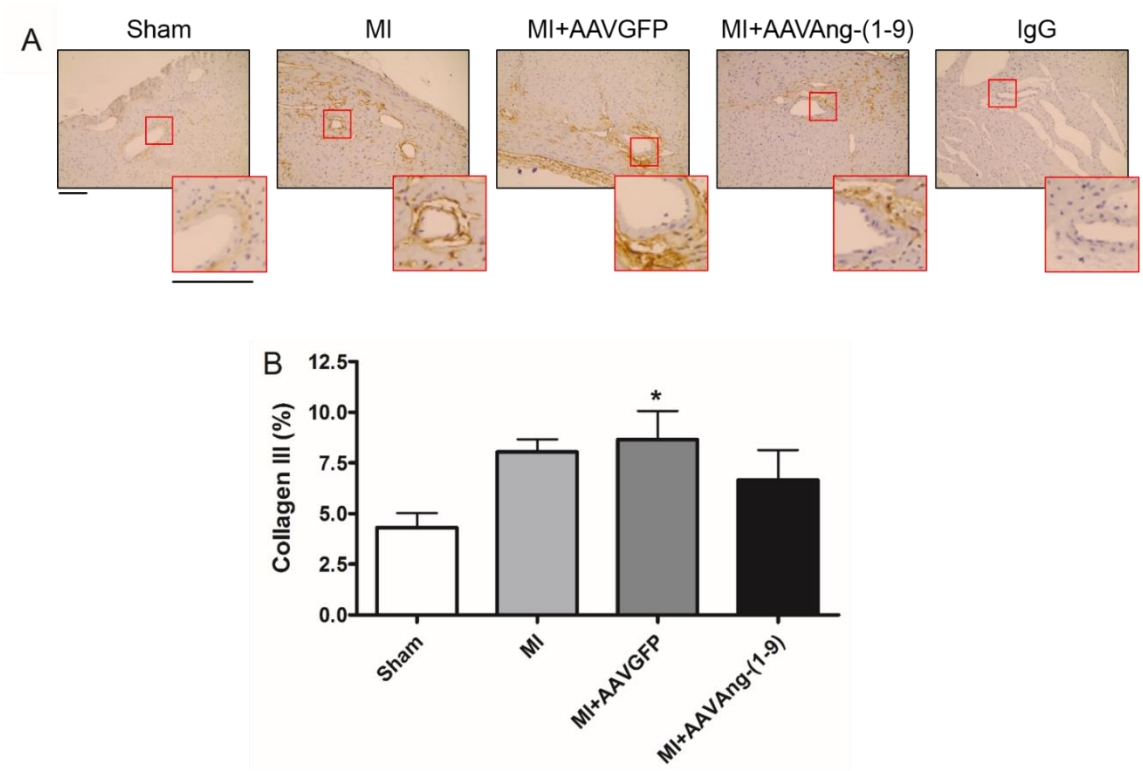

Figure 5.14 Effect of AAVAng-(1-9) on perivascular cardiac collagen III expression following MI.
(A) Representative images of cardiac vessels and associated DAB staining for collagen III expression in heart sections for each group. Negative IgG used as a control for antibody specificity. Magnification= 20x, scale= 200 µm. (B) Quantification of perivascular DAB staining for collagen III expression in heart sections of sham, MI, MI+AAVGFP and MI+AAVAng-(1-9) animals. *= $P<0.05$ *vs.* sham. n= 10, 10, 9 and 8 for sham, MI, MI+AAVGFP and MI+AAVAng-(1-9), respectively. Data presented as mean± SEM.

5.3.6 Gene expression analysis

Cardiac gene expression of the main RAS components following MI was determined using qRT-PCR (Figure 5.15). ACE expression was significantly increased in all 3 MI groups relative to sham, with a 1.5-2 fold increase in expression (RQ= 1.9± 0.1, 1.3± 0.02 and 1.4± 0.04 for MI, MI+AAVGFP and MI+AAVAng-(1-9), respectively; $P<0.05$; Figure 5.15 A). ACE2 expression remained unchanged across the groups (Figure 5.15 B). AT_1R expression was significantly decreased in all 3 MI groups relative to sham by approximately 1.5 fold (RQ= 0.7± 0.01, 0.7± 0.03 and 0.6± 0.02 for MI, MI+AAVGFP and MI+AAVAng-(1-9), respectively; $P<0.05$; Figure 5.15 C). There was no significant difference in AT_2R expression in MI and MI+AAVGFP groups relative to sham, however expression in the MI+AAVAng-(1-9) group was significantly increased 4 fold in comparison to both sham and the 2 MI groups (RQ= 1.4± 0.1, 1.2± 0.1 and 4.5± 1.0 for MI, MI+AAVGFP and MI+AAVAng-(1-9), respectively; $P<0.05$; Figure 5.15 D). Similarly, Mas levels remained unchanged in MI and MI+AAVGFP groups relative to sham, however were significantly decreased 1.4 fold in the MI+AAVAng-(1-9) group compared to sham and MI only (RQ= 1.0± 0.02 and 0.6± 0.03 for MI and MI+AAVAng-(1-9), respectively; $P<0.05$; Figure 5.15 E).

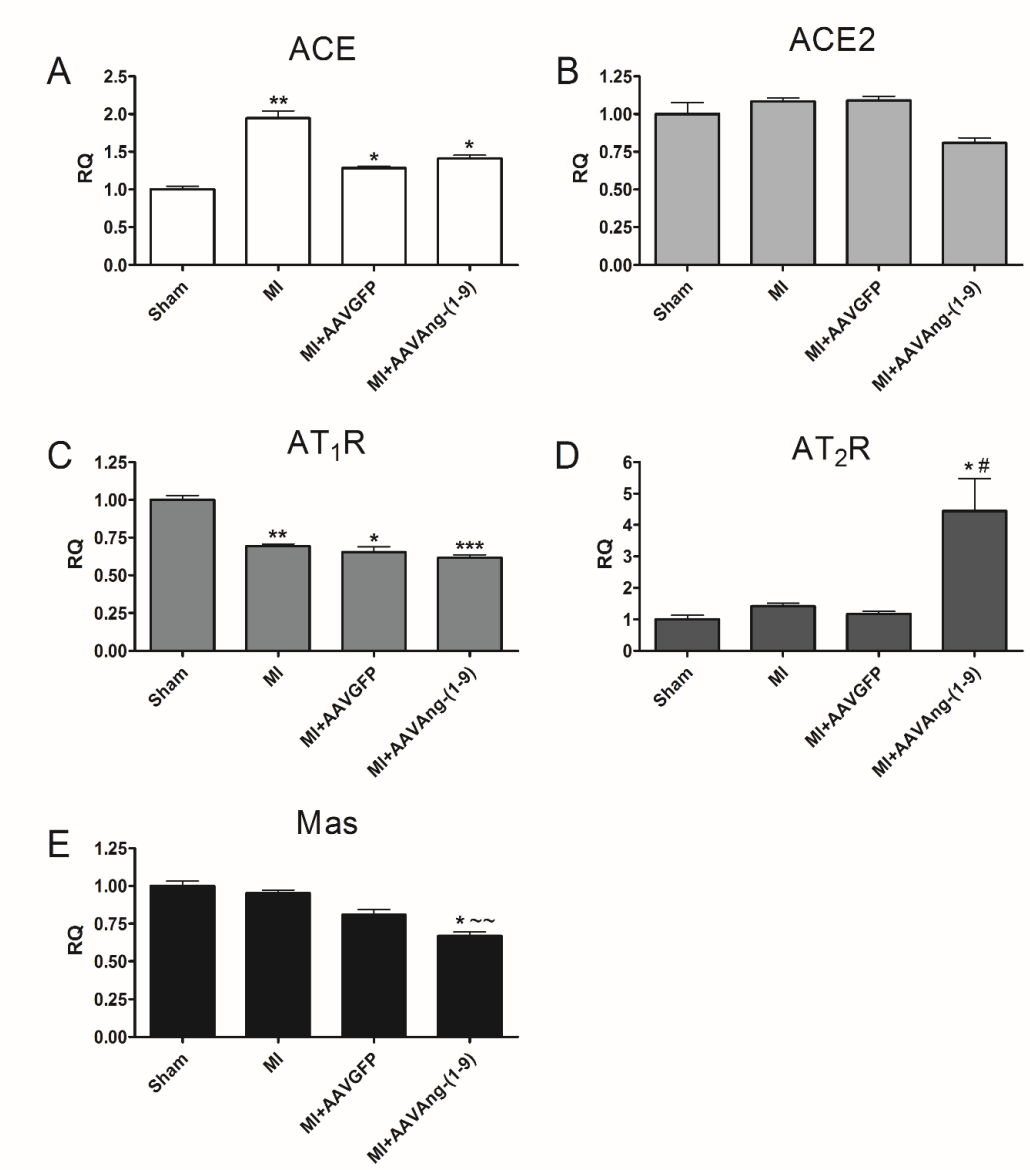

Figure 5.15 Effect of AAVAng-(1-9) on RAS receptor and enzyme gene expression following MI.
qRT-PCR-determined gene expression quantification of ACE (A), ACE2 (B), AT_1R (C), AT_2R (D) and Mas (E) in the hearts of sham, MI, MI+AAVGFP and MI+AAVAng-(1-9) animals. *= $P<0.05$, **= $P<0.01$, ***= $P<0.001$ *vs.* sham, #= $P<0.05$ *vs* MI and MI+AAVGFP, ~~= $P<0.01$ *vs.* MI only. $n= 3$ per group. Data presented as RQ± rqmax. Normalisation of expression to a housekeeper (GAPDH) was performed for all samples. MI gene expression was normalised to sham expression, therefore sham expression was arbitrarily set at a RQ= 1. RQ= relative quantification.

5.4 Discussion

In this chapter, AAV9 demonstrated efficient transduction of the infarcted mouse myocardium using *iv* systemic delivery. AAVAng-(1-9) was shown to mediated cardio-protective effects following MI in the mouse, with improvements observed in cardiac contractility and EF, reduced ventricular stiffness and reduced fibrosis, all of which occurred in parallel with increased cardiac AT_2R expression.

AAV transduction and transgene expression in the mouse infarcted myocardium was demonstrated to be efficient and homogeneous with AAVGFP when delivered systemically at a dose of 1×10^{11} vg. Transgene expression was detectable at 7 days post-delivery, with maximal expression detected by 2 wks. The pattern of expression observed is consistent with that reported previously (Zincarelli et al., 2008). AAV9 is reported to have strong tropism for the heart when delivered *iv* in the mouse (Ghosh et al., 2007; Pacak et al., 2006), with as high as 80 % transduction of cardiomyocytes observed (Inagaki et al., 2006). Detectable expression as early as 1 wk post-delivery has also been demonstrated, with AAV9 classed as having 'rapid-onset' of expression compared to other AAV vectors, e.g. AAV2 and AAV3 where expression may not be detectable until 4 wks post-delivery (Zincarelli et al., 2008). *Iv* delivery was selected over direct myocardial injection as non-invasive delivery is a more attractive translational approach as it minimises physical damage to the myocardium. Furthermore, direct injection of AAV9 to the myocardium has been shown to provide no further benefit in transduction efficiency over *iv* delivery (Inagaki et al., 2006).

Rupture rates in MI and MI+AAVGFP groups were found to be consistent with previous reports, however MI rupture rate was less in the MI+AAVGFP and not significantly different to sham (Gehrmann et al., 2001; Lutgens et al., 1999; Patten et al., 1998). The rupture rate in the MI+AAVAng-(1-9) group was lower than the other 2 MI groups and out with the reported 12.6-26.4 % mortality that would be expected in this model (Gehrmann et al., 2001), despite scar sizes being consistent between groups. The overall rupture rate in MI animals was far lower in the present study compared to the previous chapter, therefore it is difficult to directly compare the effects of Ad *vs.* AAV delivery on rupture rate. The decreased rupture rate in MI+AAVAng-(1-9) animals was reduced compared

to the MI+AAVGFP group, providing further indication that Ang-(1-9) expression may prevent cardiac rupture, potentially by promoting thicker scar formation, or alternatively through modulation of the inflammatory response. As discussed in the previous chapter, a prolongation of the inflammatory response post-MI can increase the risk of rupture by reducing the tensile strength of the scar (Frangogiannis, 2012). AAV vectors are reported to invoke negligible cell-mediated immune responses, although this can depend on tissue and serotype utilised (Lai et al., 2002; Nayak and Herzog, 2009; Nicklin et al., 2001). In fact, direct comparison of AAV and Ad in rat heart demonstrated significant inflammatory cell infiltrate into the myocardium in response to Ad transduction, which is completely absent in AAV transduction (Chu et al., 2003). Therefore, if Ang-(1-9) exerts an anti-inflammatory effect it may reduce the inflammatory response post-MI and reduce the rupture rate. However, as the transgene expression levels from AAV9 within the rupture time-frame is unknown and the mortality rate differences were not significant, the reduced rupture rate in the MI+AAVAng-(1-9) group needs to be explored further in future studies.

AAVAng-(1-9) transduced hearts demonstrated improvements in cardiac contractility and systolic LV hemodynamic indices which are consistent with the effects seen following Ad-mediated delivery. Ang-(1-9) also reduced LV stiffness at the 8 wk post-MI time-point. The potential pathways associated with this improved function are discussed in detail in the previous chapter. However, differences in echocardiography and PV-loop measurements between the 2 studies were evident. In the previous study, there was strong evidence for a reduction in LVESD following Ang-(1-9) delivery, indicating increased contraction, however this effect was less pronounced following AAV-Ang-(1-9) delivery. Increased LV dilation was also evident in the AAVAng-(1-9) group, reflected by the increased EDV found using PV loop measurements. However, regardless of dilation, the MI+AAVAng-(1-9) hearts consistently had greater contraction and blood ejection, as reflected in the dramatically increased CO and SV and normalised EF, showing that regardless of the extent of dilation, function was maintained. The exact mechanism by which Ang-(1-9) is promoting this increased contraction is unclear. One possibility is modulation of cardiomyocyte inotropy which is explored further in the next chapter.

Total fibrosis in the RV and septum regions in the AAVAng-(1-9) transduced hearts was found to be significantly reduced compared to that of the other two MI groups, with this appearing to be primarily as a result of a decrease in collagen I expression, but not collagen III, with greater collagen I expression in the control MI groups. This is consistent with findings that in the rat MI model, elevated collagen III expression is commonly associated with the acute phase following MI, with down-regulation at later time-points, whereas collagen I levels stay elevated (Cleutjens et al., 1995a). An increase in collagen I: collagen III ratio in the heart, as seen in control MI animals here, is found in human patients with CHF and in the rat HF model, and is associated in the rat with changes to haemodynamic properties of the ventricle and the development of severe LV dysfunction such as elevated LVEDP (Bishop et al., 1990; Wei et al., 1999). The different properties of the two collagen isoforms accounts for the different effects they exert on the heart. Collagen I forms thick, rigid fibre bundles which significantly contribute to ventricle stiffening, whereas collagen III forms thin isolated fibres with a much greater extent of laxity (Friedman et al., 1993), therefore reduced expression of collagen I in the AAVAng-(1-9) transduced hearts may help account for the improved haemodynamic properties observed and the reduced stiffness coefficient demonstrated from the PV loop measurements. This is not the first study to demonstrate effects of Ang-(1-9) on cardiac collagen expression, with the effects seen here consistent with what has been seen in the SHRSP, where minipump infusion of Ang-(1-9) demonstrated a significant decrease in cardiac collagen I deposition with no change in collagen III, thus decreasing the collagen I: collagen III ratio in an AT_2R dependent manner (Flores-Munoz et al., 2012). The anti-fibrotic effects evident in this study contrast with that observed following Ad-mediated delivery of Ang-(1-9) where the anti-fibrotic effects were focussed in the LV. Here, a more global effect was seen, primarily in the RV and septum. This could perhaps be attributed to the differential fibrosis seen here between the 4 and 8 wk time-points post-MI, where there was less fibrosis at 4 wks therefore an effect was not detectable, or alternatively as a result of the distribution of the viral vectors. As discussed, *iv* delivery of AAV9 provides global cardiac transduction, compared to direct Ad injection which transduces smaller regions proximal to injection sites. AAV9-Ang-(1-9) may therefore have a more potent effect than Ad gene transfer in regions other than the LV.

Due to the more advanced time-point post-MI compared to the previous study, total perivascular fibrosis was increased in MI and MI+AAVGFP groups, which appeared to be as a result of a combination of both collagen I and collagen III deposition. This appeared to be attenuated in AAVAng-(1-9) transduced hearts which showed significantly reduced total perivascular fibrosis and no significant increase in collagen I or collagen III perivascular deposition. Unlike fibrosis as part of the scar healing process, which occurs in response to cell loss, perivascular fibrosis occurs in response to inflammation (Swynghedauw, 1999), with adventitial fibroblast proliferation shown to be mediated by Ang II- AT_1R interaction (McEwan et al., 1998). This also has the additional effects of inhibiting MMP-1 and thus preventing collagen break-down (Brilla et al., 1994). As discussed, maladaptive ventricular fibrosis and collagen deposition contributes to ventricular stiffening and progression to HF (Kania et al., 2009). The use of low-dose anti-inflammatory drugs post-MI in the rat has demonstrated attenuation of perivascular fibrosis, however this was not associated with improvements in diastolic function of the heart, whereas inhibition of combined interstitial and perivascular fibrosis was (Van Kerckhoven et al., 2000). This is similar to what has been found here, where despite an anti-fibrotic effect, diastolic LV haemodynamic indices appear largely unchanged, with only some small, non-significant trends towards improvement.

Activation of the counter-regulatory RAS has also been shown to exert anti-fibrotic effects, with Ang-(1-7) attenuating cardiac perivascular fibrosis in the rat DOCA-salt model of hypertension (Grobe et al., 2006) and Ang-(1-9) acting *via* the AT_2R being associated with reduced cardiac fibrosis in the SHRSP and inhibition of fibroblast proliferation *in vitro* (Flores-Munoz et al., 2012). Moreover, the effects of Ang-(1-9) in the study by Flores-Munoz *et al.*, (2012) were thought to be in part mediated by increased NO bioavailability and Nox-4 expression in endothelial cells (Flores-Munoz et al., 2012). As AT_2R signalling is associated with regulation of MMPs and decreased ROS production (Dandapat et al., 2008; Namsolleck et al., 2014), which in turn is associated with decreased expression of inflammatory mediators due to the reduced activity of NADPH oxidase, it is possible that modulation of these pathways is a potential mechanism for the effects seen in the present study and which could be investigated in future.

Unlike in the previous study, there were no anti-hypertrophic effects evident in the AAVAng-(1-9) transduced hearts. This may also be explained by the differences in viral vectors used. When assessed *in vitro*, the anti-hypertrophic effects seen by Ang-(1-9) peptide are dose-dependent (Flores-Muñoz et al., 2011). As AAV-mediated transgene expression is lower than Ad (Wright et al., 2001) and as angiotensin peptides have very short half-lives (circa 2 min in the circulation) *in vivo* (Chappell et al., 1998) it is possible AAV-mediated Ang-(1-9) delivery does not reach a high enough concentration to have the same effect as seen when expressed by Ad. However, without determination of the exact concentration of Ang-(1-9) being produced by each vector *in vivo,* the reason for this disparity between the two studies still remains unclear. Alternatively, it could be attributed to the later time-point at which hypertrophy was assessed (8 wks compared to 4 wks) however this also remains to be assessed.

Increased ACE and decreased AT_1R expression were observed *via* qRT-PCR at 8 weeks. In Chapter 3 it was demonstrated that AT_2R expression was increased acutely following MI, but reduced to sham levels by 8 wks post-MI. This has been reported in other models of MI (Savoia et al., 2011; Schluter and Wenzel, 2008). However, here Ang-(1-9) delivery maintained elevated AT_2R expression to 8 wks. As the AT_2R is associated with a variety of cardio-protective effects, including reduced remodelling and improved function post-MI (Kaschina et al., 2008; Kaschina et al., 2014; Namsolleck et al., 2014; Oishi et al., 2003; Yang et al., 2002b) and the regulation of MMPs and resulting anti-fibrotic effects in the heart (Kaschina et al., 2008; Lauer et al., 2014), increased AT_2R expression may mediate these cardioprotective effects. The decrease in Mas expression observed in AAVAng-(1-9) transduced hearts is relatively difficult to explain. Mas receptor expression is usually associated with ACE2 activity, with increased ACE2 producing increased Ang-(1-7) levels and in turn increased Mas expression (Zhang et al., 2014). The reverse is also true, where decreased ACE2 and increased ACE activity decreases Ang-(1-7) levels, thus decreasing Mas expression (Lakshmanan et al., 2011). Therefore more detailed analysis of protein levels and receptor function is required.

5.5 Summary

Iv delivery of AAV9 in the mouse MI model is an efficient method of globally transducing the mouse myocardium. AAV9 mediated delivery of Ang-(1-9) in the mouse MI model conferred cardio-protective effects. These effects included increased LV systolic indices, EF and CO, decreased LV stiffness and decreased total fibrosis and collagen I expression. This was also associated with an increase in AT_2R gene expression. These results suggest Ang-(1-9) may be a promising therapeutic target for functional and structural remodelling post-MI.

Chapter 6: The effect of renin-angiotensin system peptide hormones on mouse cardiomyocyte Ca^{2+}-handling

6.1 Introduction

6.1.1 The use of isolated cardiomyocytes in understanding ECC

The use of isolated, single adult cardiomyocytes has proved an invaluable tool in the study and understanding of electrophysiological properties of the heart and the role of the electrical and contractile dysregulation of individual cardiomyocytes on overall heart function (Roth et al., 2014). The use of isolated cardiomyocytes has the advantage over whole organs of allowing selection of cardiomyocytes from a particular area of the heart, ease of visualisation of internal cellular structures, suitability for immunohistochemical applications and ease of imaging (Louch et al., 2011). Moreover, it provides the opportunity to study the mechanisms underlying cardiomyocyte contractility and Ca^{2+}-handling in the single cell and how this is affected by different pharmacological interventions as well as changes that occur in health and disease (Despa et al., 2012; Helmes et al., 2003; Touchberry et al., 2013). The successful isolation of adult rat cardiomyocytes using enzyme digestion was first described in 1969 (Kono, 1969), with enzyme digestion using retrograde Langendorff perfusion *via* aortic cannulation described a year later (Berry et al., 1970). Prior to this, only embryonic and neonatal cardiomyocytes had been isolated with any success (Farmer et al., 1983). However, neonatal cardiomyocytes differ considerably in their morphological and Ca^{2+}-handling properties (Kato et al., 1996; Katsube et al., 1996; Smolich et al., 1989; Wetzel et al., 1993), as do immortalised cardiomyocyte cell lines such as HL-1, which lack many of the structural and physiological properties associated with freshly isolated cells (Claycomb and Palazzo, 1980). Moreover, culturing of adult cardiomyocytes results in cell transformation in order to adapt to the culture conditions, with cell rounding and shortening (Leach et al., 2005), loss of T-tubule density (Pavlović et al., 2010), prolongation of the cellular AP (Schackow et al., 1995), decrease in systolic peak Ca^{2+} (Banyasz et al., 2008) and the loss of synchronous SR Ca^{2+} release (Mitcheson et al., 1996). Therefore, for electrophysiological and Ca^{2+}-handling measurement purposes, acutely isolated adult cardiomyocytes are the most physiologically relevant to the living organism (Louch et al., 2011).

Compared to rat, mouse cardiomyocyte isolation has proved more problematic, with direct application of methods that proved successful in other species failing

to produce high quality cells when applied to mouse hearts (O'Connell et al., 2007). This is thought to be due to an increased susceptibility to hypercontracture compared to other species (Li et al., 2014). Successful protocols developed for mouse isolation require particular attention to be paid to timing of digestion protocols, appropriate collagenase enzyme batch selection, water quality and to ensure that all perfusion solutions remain nominally Ca^{2+} free (O'Connell et al., 2003; O'Connell et al., 2007; Wolska and Solaro, 1996).

6.1.1.1 Ca^{2+} paradox

Early isolation of adult rat cardiomyocytes encountered the issue of the Ca^{2+} paradox; that is the 'rounding up' or hypercontracture of cardiomyocytes isolated using Ca^{2+}-free solutions upon exposure to physiological Ca^{2+} concentrations (Farmer et al., 1983; Powell and Twist, 1976). This results from a large Ca^{2+} overload of the cells following a period in Ca^{2+}-free conditions, resulting in continuous cellular contraction, disruption of the sarcolemma, loss of mechanical and electrical activity, depletion of phosphate stores and release of the intracellular contents and enzymes (Liu et al., 2006; Piper, 2000). This phenomenon is similar to the processes observed in I/R injury of whole hearts, where reperfusion of ischemic myocardium results in further irreversible myocardial damage as a result of reintroduction of physiological Ca^{2+} concentrations (Zimmerman and Hülsmann, 1966). In mouse ventricular cardiomyocytes, Ca^{2+} entry following Ca^{2+} restoration is thought to be primarily through the transient receptor potential canonical (TRPC) channels, which mediate signals in response to PLC-coupled receptors and are activated as a result of SR Ca^{2+} depletion during the period in Ca^{2+}-free conditions (Kojima et al., 2010; Soboloff et al., 2007). Other causal mechanisms of Ca^{2+}-overload which have been suggested include disruption of sarcolemmal mechanical stability making it permeable to Ca^{2+} and activation of reverse-mode NCX due to Na^{+} overload (Piper, 2000). It is thought that Na^{+} overload is a result of depletion of both Ca^{2+} and Mg^{+} during the Ca^{2+}-free period resulting in permeability of the L-type Ca^{2+} channel to Na^{+} (Ashraf, 1979; Chapman et al., 1984; Rodrigo and Chapman, 1991). Upon restoration of physiological Ca^{2+}, reverse-mode NCX is activated and there is an influx of Ca^{2+}. However, this is not thought to be the

case in all instances of Ca^{2+} overload (Jansen et al., 1998; Van Echteld et al., 1998).

6.1.2 Ca^{2+} imaging

Ca^{2+} is crucial in the regulation of cardiomyocyte ECC (Bers, 2002), hypertrophy (Hunton et al., 2002) and apoptosis (Atsma et al., 1995), therefore its homeostasis is of vital importance for cardiomyocyte function. The development of methods to allow Ca^{2+} imaging in single cardiomyocytes has played a vital role in the study of electrophysiological properties of the heart and the study of ECC for decades. It was this technique which was used to discover CICR as the precise mechanism behind ECC (Fabiato and Fabiato, 1979), and since the development of ratiometric Ca^{2+} sensitive dyes and epifluorescent Ca^{2+} imaging techniques in the 1980's (Bright et al., 1989; Grynkiewicz et al., 1985), it has been utilised for a variety of mechanistic studies into the dysregulation of ECC and Ca^{2+} handling in disease (Gomez et al., 1997).

Ca^{2+} handling measurements indirectly assess the function of the various Ca^{2+} handling proteins during ECC (Bers, 2001). Measuring the average Ca^{2+} transient amplitude assesses SR-mediated Ca^{2+} release (the culmination of L-type Ca^{2+} channel activity, sensitivity of the RyR to Ca^{2+} and SR Ca^{2+} content). The Tau of the transient, defined as the time required for the transient to decay by 1/e (i.e. 36.8 %), allows assessment of the main Ca^{2+} extrusion mechanisms, the NCX and SERCA. Finally, the use of a rapidly applied bolus of high concentration caffeine as a means of emptying the SR Ca^{2+} store allows an estimation of SR Ca^{2+} content, and the Tau of the caffeine-induced Ca^{2+}-transient allows an estimation of NCX activity only (Bers, 2002).

6.1.2.1 Myofilament sensitivity

Ca^{2+} homeostasis is not the only regulator of cardiomyocyte contractile force as modification of myofilament Ca^{2+} sensitivity is an alternative mechanism. This is determined through the minimum threshold Ca^{2+} concentration required for activation of contraction (Stoehr et al., 2014). Modification of myofilament sensitivity occurs *via* ß-adrenergic stimulation, where the myofilaments become desensitized in order to accelerate relaxation (Janssen, 2010). Increased

sensitivity and force generation can be brought about by the use of Ca^{2+}-sensitising drugs and myosin activators (Janssen, 2010). Therefore, an increased Ca^{2+}-transient may not always be sufficient for increased contractility. The opposite is also true, with a positive inotropic effect may be induced without the presence of a change in Ca^{2+}-handling, making it important that cell shortening measurements are also performed.

6.1.3 The effects of RAS peptides on cardiomyocyte Ca^{2+}-handling

6.1.3.1 Ang II

The effect of Ang II on cardiomyocyte Ca^{2+}-handling and contractility has been extensively studied. There have been various studies identifying a positive ionotropic effect of Ang II on cardiomyocytes, however the mechanism of this has, too, been conflicting. In rabbit cardiomyocytes, a positive AT_1R-mediated ionotropic effect has been demonstrated in response to Ang II, with increase myofibrillar sensitivity thought to be a potential mechanism (Fujita and Endoh, 1999; Ikenouchi et al., 1994). However, although these two studies demonstrated similar effects on cardiomyocyte contractility, one demonstrated no change to the Ca^{2+}-transient or L-type current, suggesting only a change to myofibrillar Ca^{2+} sensitivity occurred in response to Ang II (Ikenouchi et al., 1994). The second study demonstrated an increased Ca^{2+}-transient and an increase in NCX and reverse mode NCX activity, suggesting alterations to Ca^{2+}-handling also had a role in the positive ionotropic effects being exerted. The increase in the Ca^{2+}-transient observed in this study was proposed to be due to activation and modulation of the NCX as well as sensitization of the myofilaments to Ca^{2+} as a result of AT_1R-stimulation (Fujita and Endoh, 1999). Reverse-mode NCX facilitates influx of extracellular Ca^{2+} into the cytoplasm as opposed to forward mode NCX which facilitates Ca^{2+} extrusion following CICR (O'Rourke, 2008). The mode in which the NCX acts is dependent on Ca^{2+} and Na^{+} sarcolemma gradients (O'Rourke, 2008). Studies on isolated cat cardiomyocytes have also identified a positive ionotropic effect of Ang II, with increased Ca^{2+}-transient amplitude and an increase in L-type Ca^{2+} current (Petroff et al., 2000; Salas et al., 2001). A negative lusitropic effect was also associated with a decrease in NCX, mediated by PKC signalling, with increased intracellular Ca^{2+} as

a result of reduced extrusion *via* the NCX and prolongation of the AP (Salas et al., 2001). A later study, also in isolated cat cardiomyocytes, again identified an increased Ca^{2+}-transient and positive ionotropic effect of Ang II, mediated by AT_1R signalling. However, in contrast, NCX activity was found to be increased and reverse mode NCX activated. This was found to be due to an Ang II-dependent increase in ET-1 signalling which stimulated ROS production thus activating the NCX (Cingolani et al., 2006). Ang II, *via* the AT_1R, also has a positive iontropic effect on isolated dog ventricular cardiomyocytes. Interestingly, in cells isolated from dogs with pacing-induced CHF, Ang II elicited a negative inotropic effect, with cells exhibiting depressed contraction (Cheng et al., 1996). A mechanism proposed for these varying effects was activation of IP_3 and PKC by Ang II, resulting in modulation of Ca^{2+}-handling, changes to myofilament Ca^{2+}-sensitivity and activation of NCX, producing a positive inotropic response in healthy cardiomyocytes. In CHF cardiomyocytes, activation of the same pathways may exacerbate the existing dysfunctional Ca^{2+}-handling (Cheng et al., 1996)

Other studies have also found Ang II to exert a negative inotropic effect on isolated cardiomyocytes. In cells isolated from normal and hypertrophied rat myocardium, Ang II resulted in reduced cellular contractility which was accompanied by reduced peak systolic Ca^{2+} (Meissner et al., 1998), although a later study also in rat cardiomyocytes found that the negative ionotropic effect they observed was not associated with a change in the Ca^{2+}-transient, but was rather a result of reduced myofilament sensitivity which was thought to be modulated by PKC activation of p38 MAPK (Palomeque et al., 2006). In mouse ventricular cardiomyocytes a similar effect was observed in response to Ang II, with a PKC-mediated reduction in cellular contractility observed in the absence of a change in the Ca^{2+}-transient (Sakurai et al., 2002). PKC/p38 MAPK can modulate contractility either through modulation of intracellular pH or through direct phosphorylation of the contractile apparatus such as TnI, with modulation of phosphorylation proposed to be the mechanism of action of Ang II in both of these studies (Palomeque et al., 2006; Sakurai et al., 2002). As well as this conflicting evidence, it has also been demonstrated in cardiomyocytes isolated from rat, guinea pig, humans and infarcted rat myocardium that Ang II in a

concentration range of 1 nM to 10 μM has no effect on inotropy or Ca^{2+}-handling (Lefroy et al., 1996; Touyz et al., 1996).

6.1.3.2 Ang-(1-7)

There is limited evidence for a direct effect of Ang-(1-7) on isolated cardiomyocyte inotropy and Ca^{2+}-handling. A single study looking at the direct application of 10 nM Ang-(1-7) on isolated WT mouse cardiomyocytes demonstrated no effect of the peptide on Ca^{2+}-handling parameters (Dias-Peixoto et al., 2008), which was confirmed in ventricular cardiomyocytes isolated from transgenic rats overexpressing circulating Ang-(1-7) (Gomes et al., 2010). However, both of these studies had interesting caveats. In the former, Ca^{2+}-handling was also assessed in cardiomyocytes isolated from Mas receptor knock-out mice, which were demonstrated to have slower Ca^{2+}-transients, reduced peak systolic Ca^{2+} and reduced SERCA expression (Dias-Peixoto et al., 2008). As these animals have been demonstrated to have reduced cardiac function *in vivo*, this altered Ca^{2+}-handling was proposed as a potential mechanism (Santos et al., 2006). In the second study, although the cardiomyocytes isolated from the transgenic rats overexpressing Ang-(1-7) did not show any altered Ca^{2+}-handling parameters, they were found to be resistant to the decrease in Ca^{2+}-transient amplitude induced by Ang II in a potential NO/guanosine 3',5'-cyclic monophosphate–dependent pathway (Gomes et al., 2010). Interestingly, ventricular cardiomyocytes isolated from transgenic rats with cardiac over-expression of an Ang-(1-7) fusion protein demonstrated an increase in Ca^{2+}-transient amplitude, faster transient kinetics and increased SERCA2a protein expression, which the authors stated was consistent with the improved cardiac function observed in these animals in response to isoproterenol *in vivo* (Ferreira et al., 2010a).

To date, no studies have been reported on the assessment of the effects of Ang-(1-9) on single cardiomyocyte Ca^{2+}-handling properties. In the present study, the effects of the RAS peptides Ang-(1-7), Ang-(1-9) and Ang II, on isolated mouse cardiomyocyte Ca^{2+}-handling and inotropy was assessed using epifluorescent microscopy and cell shortening measurements.

6.2 Aims

The aims of this chapter were to:

- Optimise the Langendorff single mouse cardiomyocyte isolation protocol.
- Assess the effects of the peptides Ang II, Ang-(1-7) and Ang-(1-9) on inotropy and Ca^{2+}-handling in isolated mouse cardiomyocytes using epifluorescent microscopy and cell shortening measurements.
- Investigate the mechanism of action of the peptides in this setting using RAS receptor antagonists.

6.3 Results

6.3.1 Mouse cardiomyocyte isolation optimisation and study design

6.3.1.1 Collagenase I enzyme batch selection

Prior to the isolation of single mouse cardiomyocytes for study purposes, a suitable collagenase I enzyme to yield good-quality, Ca^{2+}-tolerant cells suitable for experimental procedure was required to be identified. The total yield of cells from each enzyme batch at 0 mM Ca^{2+} was not significantly altered between enzyme batches, and as expected was not changed upon increasing the Ca^{2+} concentration, with a consistent yield of approximately 1.5-2 million cells per heart from LV and septum tissue (Figure 6.1 A). However, there were noticeable differences in the % of surviving rod-shaped cardiomyocytes between the enzyme batches. At 0 mM Ca^{2+}, the 275 U/mg batch preparations contained a far greater % of rod-shaped cardiomyocytes compared to both the 370 and 390 U/mg enzymes (270 U/mg= 14.2± 9.6 %, 270 U/mg= 7.3± 4.5 %, 390 U/mg= 5.5± 0.8 %). Overall the cells isolated using each enzyme were Ca^{2+}-tolerant, with only a small loss in the % of rod-shaped cells (Figure 6.1 B).

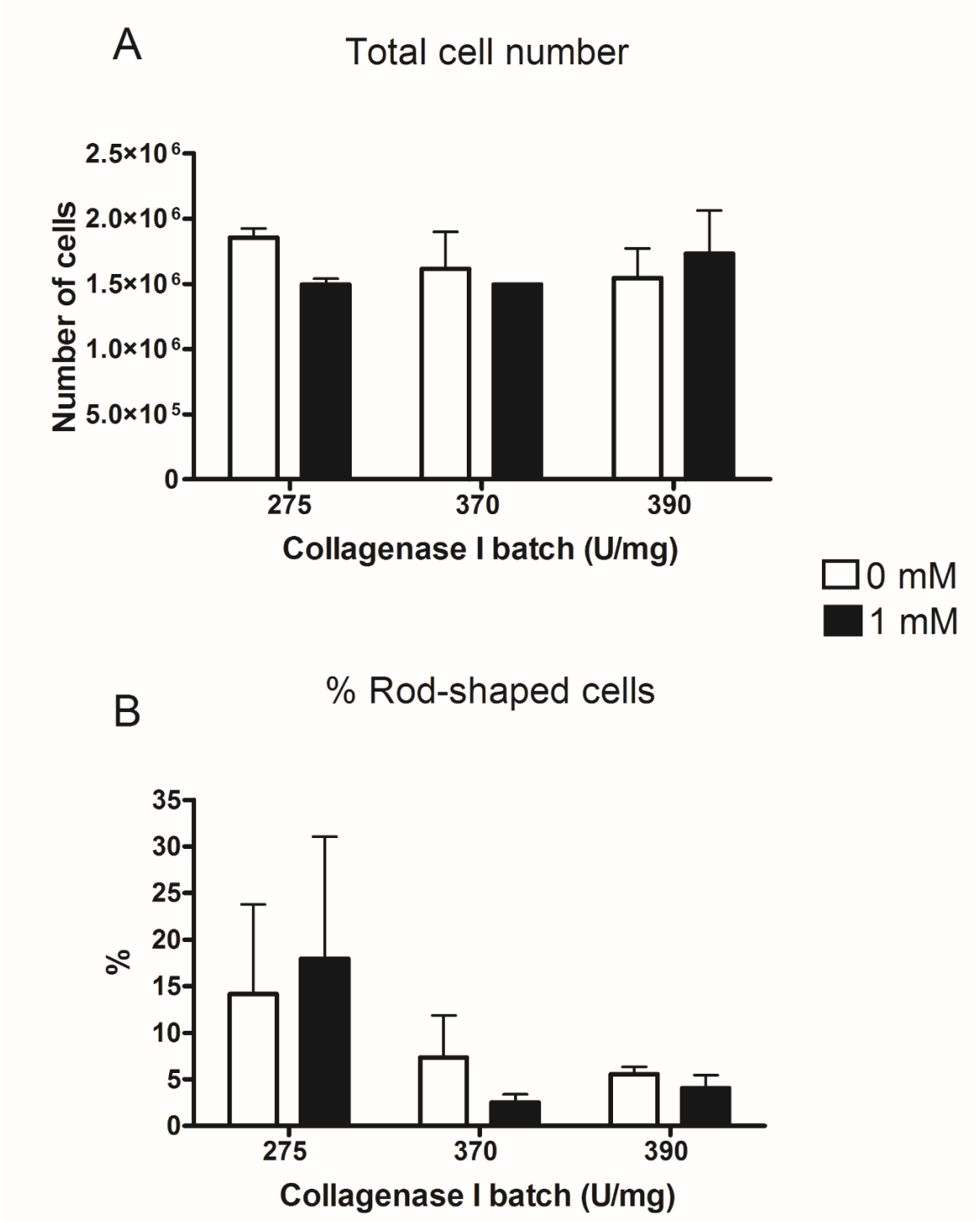

Figure 6.1 Collagenase I enzyme batch selection.
(A) Total cell number counts from mouse cardiomyocyte isolations performed using different collagenase I enzyme batches in 0 and 1 mM Ca^{2+} solutions. (B) Rod-shaped cardiomyocyte counts represented as a % of the total cardiomyocytes in each isolation performed using different collagenase I batches in 0 and 1 mM Ca^{2+} solutions. *n*= 3 per batch. Data presented as mean± SEM.

6.3.1.2 Experimental design and cardiomyocyte isolation

Due to its better rod yield, the 275 u/mg batch was selected to take forward for experiments. Once digestion times and conditions had been optimised with this enzyme batch, the average total cell yield per isolation was approximately 2 million, with approximately 30 % of these being rod-shaped at 1 mM Ca^{2+} (Figure 6.2).

In order to investigate the effects of RAS peptides on cardiomyocyte Ca^{2+} handling, 4 different protocols were employed (Figure 6.3):

- Peptide pre-treatment: Cells were incubated with 1 μM of Ang-(1-7), Ang-(1-9) or Ang II for 15 min prior to 2 min stimulation at 1 Hz. Perfusate was supplemented with 1 μM of appropriate peptide, with water used as a control (Figure 6.3 A).

- Peptide pre-treatment + double caffeine: For estimation of L-type Ca^{2+} channel activity the peptide pre-treatment protocol was combined with a 10 mM caffeine bolus prior to initiating stimulation. The amplitude of the first transient produced, referred to the L-type Ca^{2+}-transient hence-forth, was used to estimate Ca^{2+} entry *via* the L-type Ca^{2+} channel (Eisner et al., 2000; Elliott et al., 2013) (Figure 6.3 B).

- Peptide perfusion: A 2 min steady-state cell stimulation was recorded for control solution. The solution was then switched to either a second control solution or a 100 or 500 nM solution of either Ang-(1-9) or Ang II for a further 1 min (Figure 6.3 C).

- Antagonist pre-treatment + peptide perfusion: The peptide perfusion approach was combined with pre-treatment of cells for 15 min prior to stimulation with either 1 μM Losartan (AT_1R antagonist) or 500 nm PD123319 (AT_2R antagonist) in order to investigate the actions of the peptides. Perfusate was supplemented with the appropriate antagonist throughout (Figure 6.3 D).

A 10 mM caffeine bolus was applied simultaneously with the cessation of stimulation at the end of each protocol in order to assess SR Ca^{2+} content. Cell shortening measurements were recorded simultaneously with Ca^{2+}-transient measurements.

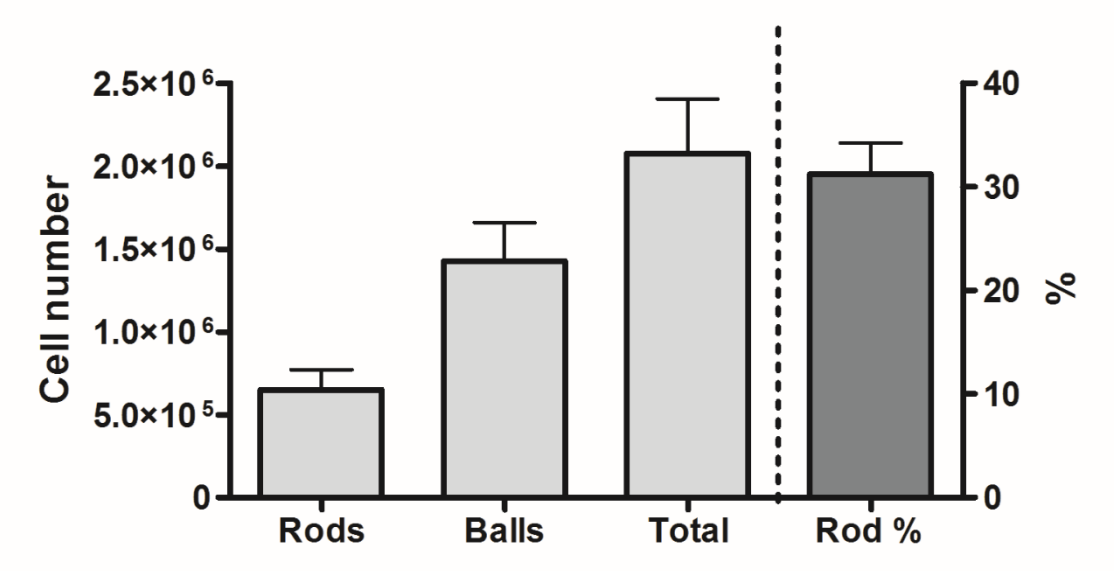

Figure 6.2 Experimental cardiomyocyte isolation cell yields.
Average cell yields and rod % from cardiomyocyte isolations performed for experimental work using the 275 u/mg batch of collagenase I enzyme. Count performed at 1 mM Ca^{2+}, *n*= 7. Data presented as mean± SEM.

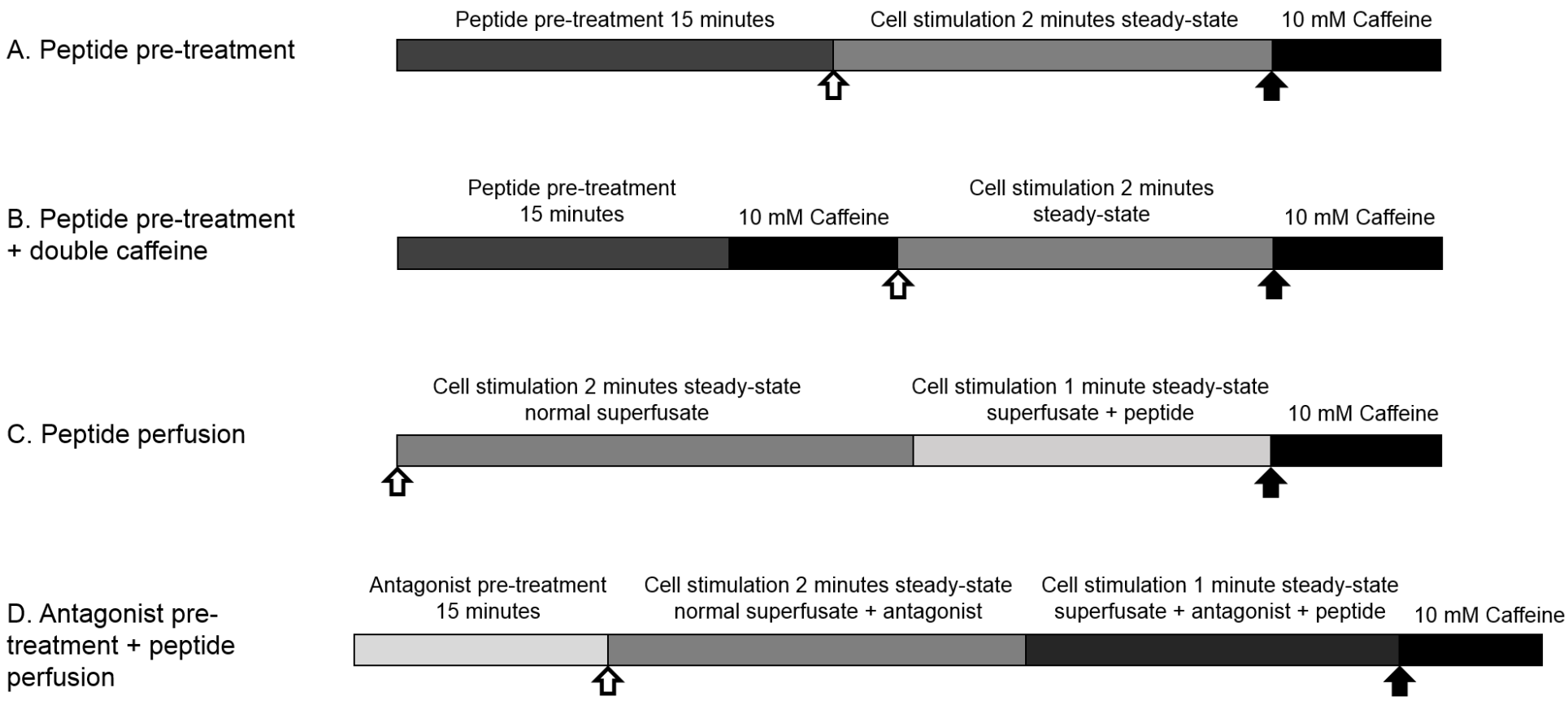

Figure 6.3 Ca^{2+} imaging experimental protocols.
Schematics showing the various protocols employed to study the effects of the RAS peptides Ang II, Ang-(1-7) and Ang-(1-9) on Ca^{2+}-handling protein activity and to investigate the mechanisms of action of these peptides. The white arrow indicates the start of stimulation and the black arrow the end.

6.3.2 Peptide pre-treatment

6.3.2.1 Ca^{2+}-transient analysis

Using protocol A (Figure 6.3), the effect of pre-treatment of mouse cardiomyocytes with 1 μM of either Ang-(1-7), Ang-(1-9) or Ang II (Fukuta et al., 1996; Fukuta et al., 1998; Gunasegaram et al., 1999) on Ca^{2+}-transient amplitude and Tau was determined (Figure 6.4). Ca^{2+}-transient amplitude was found to be unaltered between control and Ang-(1-7) treated cells (Figure 6.4 B-i). However, the average amplitude of Ang-(1-9) treated cells was significantly increased to 177 % of control cells (549.3± 71.5 *vs*. 972.0± 100.6 nM, control (*n*= 31) *vs*. Ang-(1-9) (*n*= 34); *P*<0.05; Figure 6.4 B-ii). The amplitude of Ang II treated cells was also significantly increased to 174.7 % of control cells (549.3± 71.5 *vs*. 959.3± 146.1 nM, control (*n*= 31) *vs*. Ang II (*n*= 24); *P*<0.05; Figure 6.4 B-iii). Tau of the Ca^{2+}-transient was not significantly altered across all the treatment groups (Figure 6.4 C-i-iii).

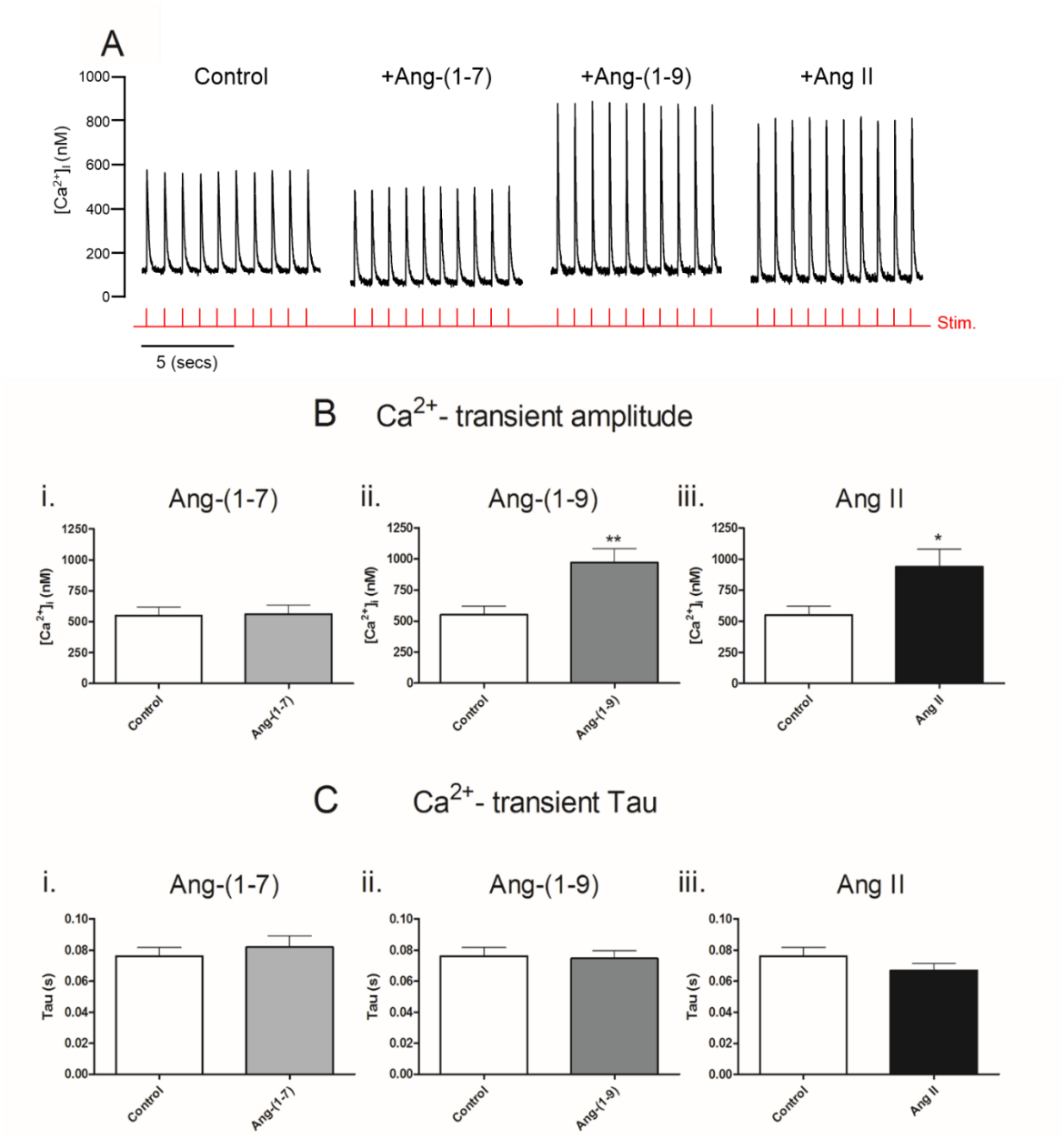

Figure 6.4 The effects of 1 μM of RAS peptides on mouse cardiomyocyte Ca^{2+}-transient amplitude and tau.
(A) Example Ca^{2+}-transient traces for each cell treatment group. Red trace indicates 1 Hz stimulation. Average Ca^{2+}-transient amplitude (B) and Tau (C) for isolated mouse cardiomyocytes untreated or pre-treated with 1 μM of Ang-(1-7) (i.), Ang-(1-9) (ii.) or Ang II (iii.). *= P<0.05 *vs.* control. n= 31, 26, 34 and 24 for control, Ang-(1-7), Ang-(1-9) and Ang II, respectively. Data presented as mean± SEM.

6.3.2.2 L-type Ca^{2+}-transient analysis

Using protocol B (Figure 6.3), the effect of the peptides on the L-type Ca^{2+} transient was assessed. Average amplitudes of the L-type Ca^{2+}-transient was unchanged in Ang-(1-7) and Ang II treated cells compared to control (Figure 6.5 B-i & iii). However, Ang-(1-9) treated cells showed a significantly increase L-type Ca^{2+}-transient amplitude, which was increased to 250 % of control (70.8± 15.9 *vs.* 187.1± 23.5, control (*n*= 11) *vs.* Ang-(1-9) (*n*= 14); *P*<0.01; Figure 6.5 B-ii).

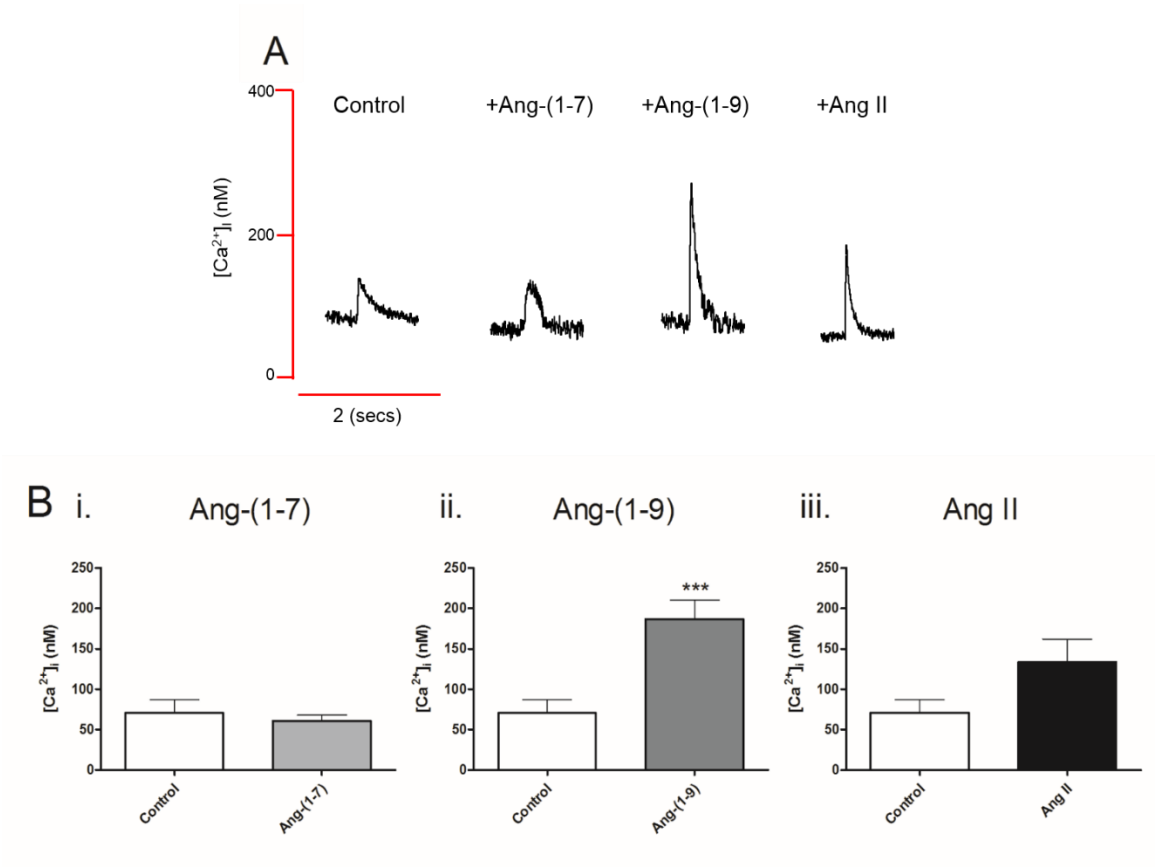

Figure 6.5 The effects of 1 µM of RAS peptides on mouse cardiomyocyte L-type Ca^{2+}-transient amplitude.
(A) Example L-type Ca^{2+}-transient traces for each cell treatment group. (B) Average L-type Ca^{2+}-transient amplitude for isolated mouse cardiomyocytes untreated or pre-treated with 1 µM of Ang-(1-7) (i.), Ang-(1-9) (ii.) or Ang II (iii.). ***= *P*<0.001 *vs.* control. *n*= 11, 12, 14 and 10 for control, Ang-(1-7), Ang-(1-9) and Ang II, respectively. Data presented as mean± SEM.

6.3.2.3 Caffeine-induced Ca^{2+}-transient analysis

The effects of 1 μM of Ang-(1-7), Ang-(1-9) and Ang II on SR Ca^{2+} content and extrusion of Ca^{2+} *via* the NCX was assessed using a 10 mM caffeine bolus applied following stimulation, with resulting transient correlating to release of Ca^{2+} *via* the RyR. Caffeine-induced Ca^{2+}-transient amplitude was unchanged compared to control cells in cells treated with Ang-(1-7) and Ang II (Figure 6.6 B-i & iii). However, caffeine-induced Ca^{2+}-transient amplitude was significantly increased in Ang-(1-9) treated cells to 160 % of control cells (1076.1± 132.1 *vs.* 1792.6± 288.9, control (*n*= 28) *vs.* Ang-(1-9) (*n*= 30); $P<0.05$; Figure 6.6 B-ii). Caffeine-induced Ca^{2+}-transient Tau was unaltered in all treatment groups (Figure 6.6 C-i-iii).

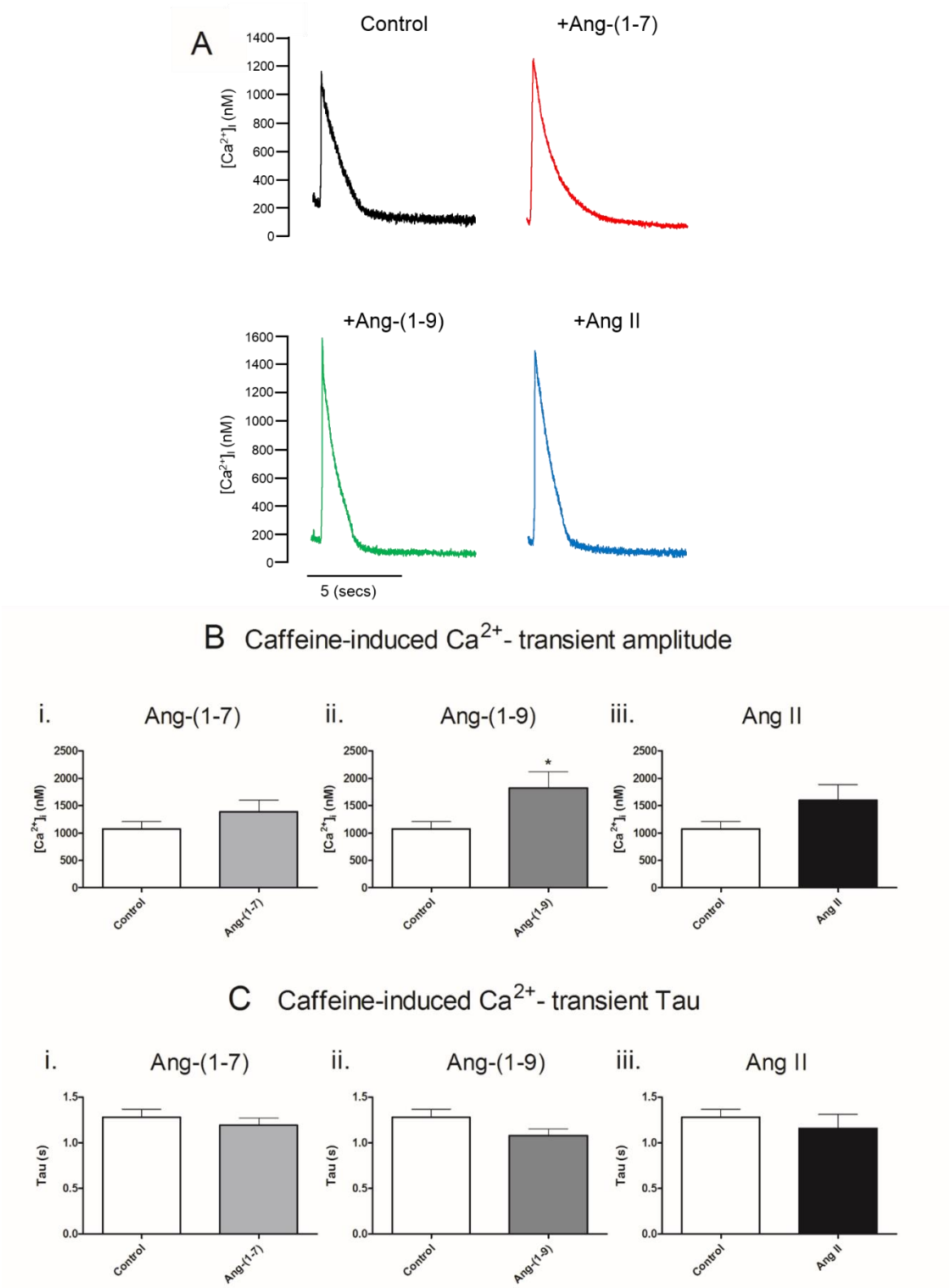

Figure 6.6 The effects of 1 μM of RAS peptides on mouse cardiomyocyte caffeine-induced Ca^{2+}-transient amplitude and tau.
(A) Example caffeine-induced Ca^{2+}-transients for each cell treatment group. Average caffeine-induced Ca^{2+}-transient amplitude (B) and Tau (C) for isolated mouse cardiomyocytes untreated or pre-treated with 1 μM of Ang-(1-7) (i.), Ang-(1-9) (ii.) or Ang II (iii.).*= $P<0.05$ *vs.* control. n= 28, 23, 30 and 20 for control, Ang-(1-7), Ang-(1-9) and Ang II, respectively. Data presented as mean± SEM.

6.3.2.4 Cell shortening measurements

The effect of 1 μM of Ang-(1-7), Ang-(1-9) or Ang II on cell shortening was measured simultaneously with Ca^{2+}-handling measurements. Shortening was presented as the average % reduction in diastolic cell length during contraction. Resting cell length was shown to be consistent across all treatment groups at approximately 150 μm (Figure 6.7 B-i-iii). Cell shortening was not significantly altered compared to control in Ang-(1-7) and Ang II treated groups (Figure 6.7 C-i & iii). However, cell shortening measurements were significantly increased in Ang-(1-9) treated cells to 166.9 % of control (6.8± 0.9 *vs.* 10.2± 1.1 %, control (*n*= 17) *vs.* Ang-(1-9) (*n*= 22); $P<0.05$; Figure 6.7 C-ii).

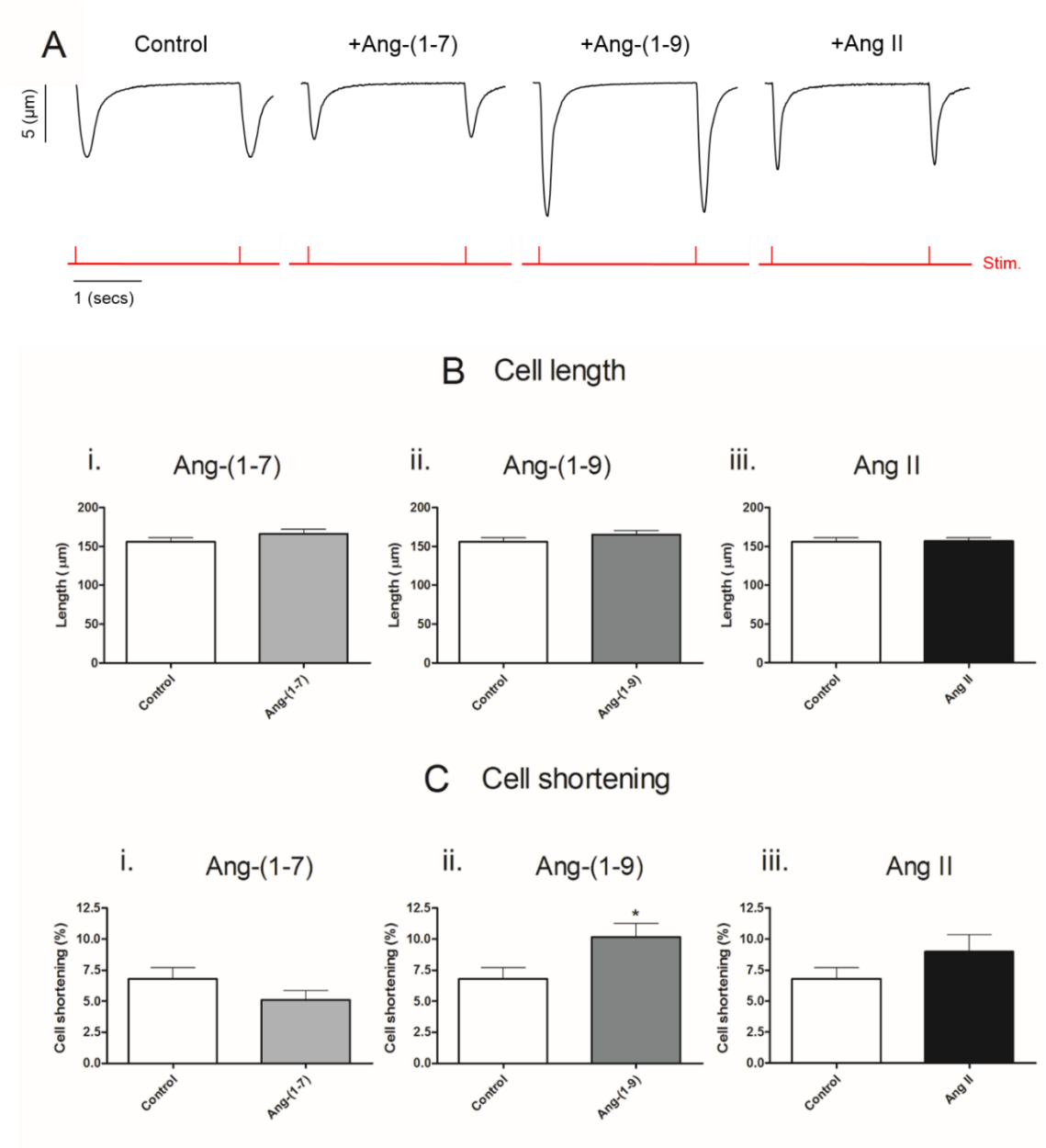

Figure 6.7 The effects of 1 µM of RAS peptides on mouse cardiomyocyte length and FS. (A) Example cell shortening traces for each cell group. Red trace indicates 1 Hz stimulation Average cell length (B) and cell shortening (C) measurements for isolated mouse cardiomyocytes untreated or pre-treated with 1 µM of Ang-(1-7) (i.), Ang-(1-9) (ii.) or Ang II (iii.). *= $P<0.05$ *vs.* control. n= 17, 19, 22 and 16 for control, Ang-(1-7), Ang-(1-9) and Ang II, respectively. Data presented as mean± SEM.

6.3.2.5 Spontaneous rises in intracellular Ca^{2+}

The effect of Ang-(1-7), Ang-(1-9) and Ang II on spontaneous rises in intracellular Ca^{2+} compared to un-treated cells during the 2 min stimulation period was determined by counting the number of spontaneous Ca^{2+} releases throughout the trace and expressing the value as spontaneous rises in intracellular Ca^{2+} per second. Example Ca^{2+}-transient traces from Ang II treated cells showed the presence of spontaneous Ca^{2+} release as anomalies in the trace, independent of cell stimulation (Figure 6.8 A). Only Ang II treatment was shown to significantly increase the frequency spontaneous Ca^{2+} release compared to control cells reaching 400 % of control (0.02± 0.01 *vs.* 0.08± 0.02 Ca^{2+} release/s, control (*n*= 31) *vs.* Ang II (*n*= 26); *P*<0.01; Figure 6.8 B-iii). Neither Ang-(1-7) nor Ang-(1-9) produced a significant increase in spontaneous Ca^{2+}-rise frequency compared to control cells (Figure 6.8 B–i & ii).

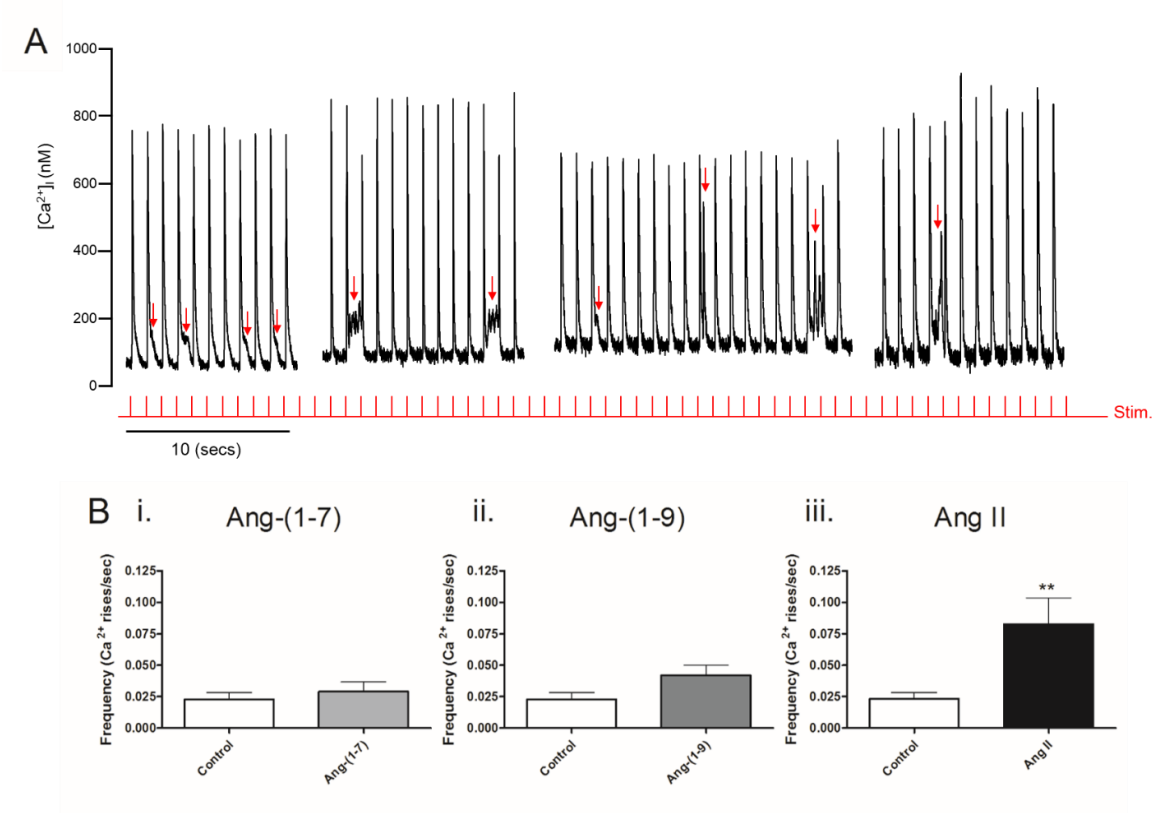

Figure 6.8 The effects of 1 μM of RAS peptides on mouse cardiomyocyte spontaneous rise in intracellular Ca^{2+} frequency.
(A) Example of Ca^{2+}-transient traces from an Ang II-treated cells. Spontaneous Ca^{2+} release is indicated by the red arrows. Red trace indicates 1 Hz stimulation. (B) Average spontaneous Ca^{2+} release frequency for isolated mouse cardiomyocytes untreated or pre-treated with 1 μM of Ang-(1-7) (i.), Ang-(1-9) (ii.) or Ang II (iii.). **= P<0.01 *vs.* control. n= 31, 26, 34 and 26 for control, Ang-(1-7), Ang-(1-9) and Ang II, respectively. Data presented as mean± SEM.

6.3.3 Peptide perfusion

6.3.3.1 Ca^{2+}-transient analysis

Following demonstration of the modulating effects on Ca^{2+}-handling properties using 1 μM of Ang-(1-9) and Ang II incubated on cells, both peptides were further investigated for their effects using lower concentrations (100 and 500 nM) on separate cohorts of cells to determine if the response observed was dose-dependent or whether other differences between the actions of the peptides became apparent. For this, protocol C (Figure 6.3) was utilised. Data was presented as the % increase in transient amplitude and % decrease in Tau within the same cell between control solution and peptide. Control cells were also subjected to a solution change mid-stimulation, however in this case there was no peptide present. Application of 100 or 500 nM of Ang-(1-9) or Ang II produced a significant increase in the Ca^{2+}-amplitude by 17-25 % (P<0.001; Figure 6.9 A). A similar trend was observed with the Tau changes where all peptide concentrations produced a significant decrease in Tau by 7-12 % (P<0.05; Figure 6.9 B).

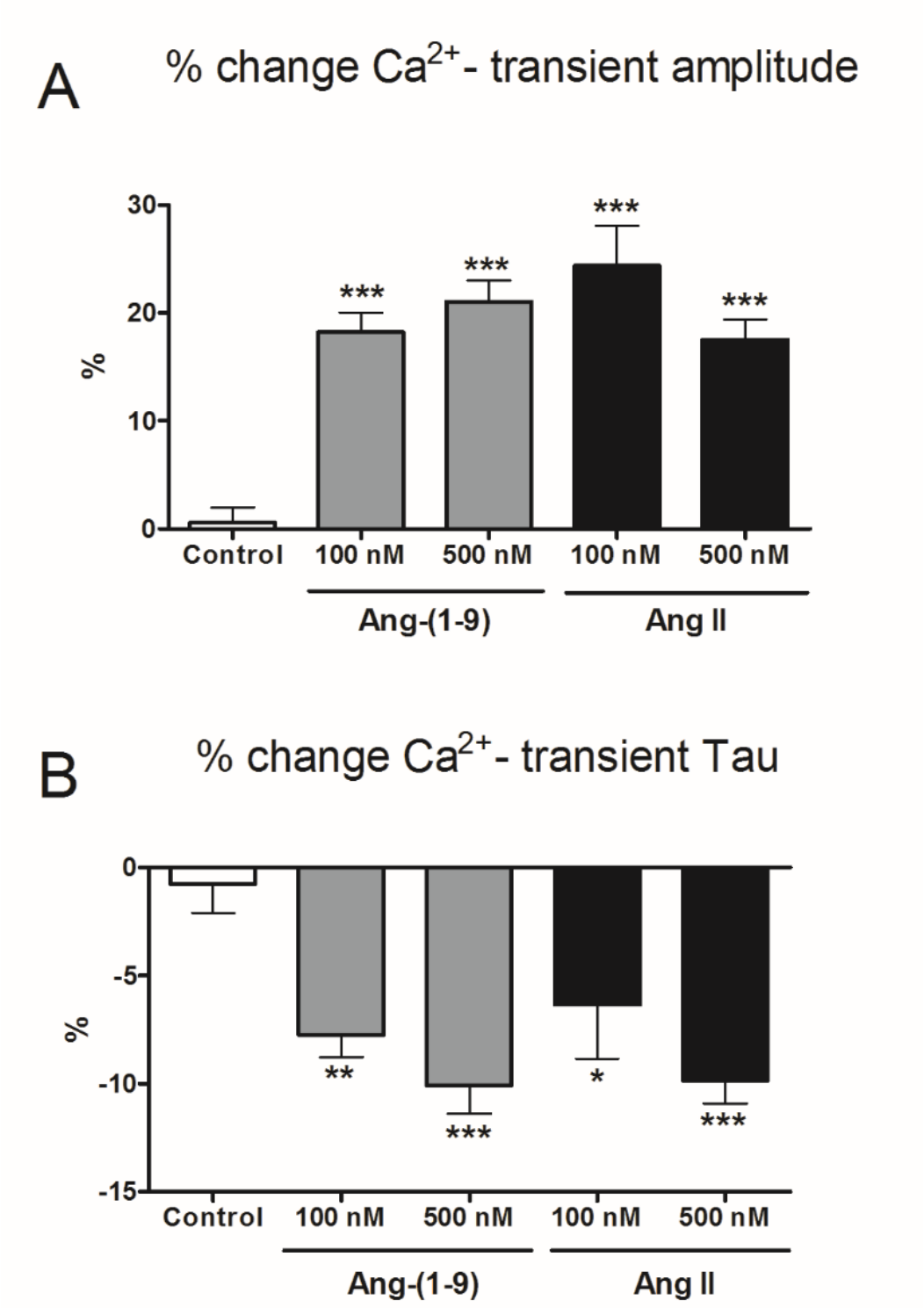

Figure 6.9 The effects of RAS peptide perfusion on mouse cardiomyocyte Ca^{2+}-transient amplitude and Tau.
Average % change in Ca^{2+} transient amplitude (A) and Tau (B) for isolated mouse cardiomyocytes perfused with control solution followed by further perfusion with a second control solution or with 100 or 500 nM of an Ang-(1-9) or Ang II solution. *=*P*<0.05, **=*P*<0.01, ***= *P*<0.001 *vs.* control. *n*= 11, 8, 20, 9 and 11 for control, Ang-(1-9) 100 nM, Ang-(1-9) 500 nM, Ang II 100 nM and Ang II 500 nM, respectively. Data presented as mean % change± SEM.

6.3.3.2 Caffeine-induced Ca^{2+}-transient analysis

Next, the effect of Ang-(1-9) and Ang II on SR Ca^{2+} content and NCX-mediated Ca^{2+} extrusion was assessed using 10 mM caffeine as described previously. There was no significant difference in either caffeine-induced Ca^{2+}-transient amplitude or Tau any of the treatment groups (Figure 6.10 A & B).

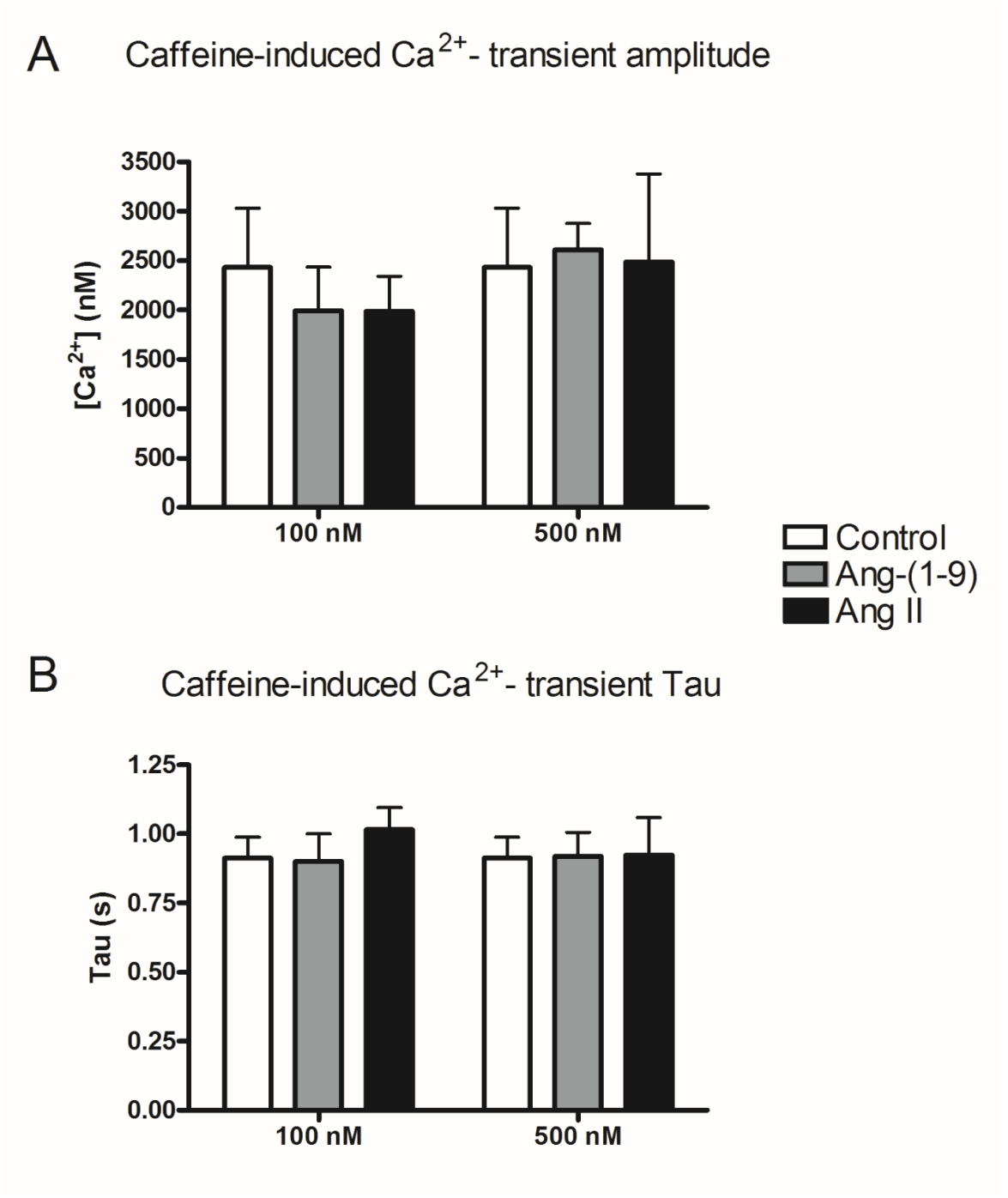

Figure 6.10 The effects of 100 and 500 nM of RAS peptides on mouse cardiomyocyte caffeine-induced Ca^{2+}-transient amplitude and tau.
Average caffeine-induced Ca^{2+}-transient amplitude (A) and Tau (B) for cells perfused with 100 or 500 nM of Ang-(1-9) or Ang II or control solution. *n*= 5, 7, 7, 14 and 4 for control, 100 nM Ang-(1-9), 100 nM Ang II, 500 nM Ang-(1-9) and 500 nM Ang II, respectively. Data presented as mean± SEM.

6.3.3.3 Cell shortening measurements and spontaneous rises in intracellular Ca^{2+} frequency analysis

Both the 100 and 500 nM Ang-(1-9) produced a significant increase in cell shortening compared to control solution. When 100 or 500 nM of Ang-(1-9) was applied cell shortening was increased by 33.0± 5.7 % and 32.5± 7.8 %, respectively (P<0.05). A similar trend was seen with application of a 100 or 500 nM Ang II producing an increase in cell shortening by 54.1± 16.6 % and 33.7± 10.4 %, respectively (P<0.05; Figure 6.11 A). The frequency of spontaneous rises in intracellular Ca^{2+} was unaffected by switching between control solutions. Application of either concentration of Ang-(1-9) or Ang II also had no significant effect. However application of either concentration of Ang II produced a trend towards an increase in the frequency of spontaneous Ca^{2+} release during stimulation (Figure 6.11 B).

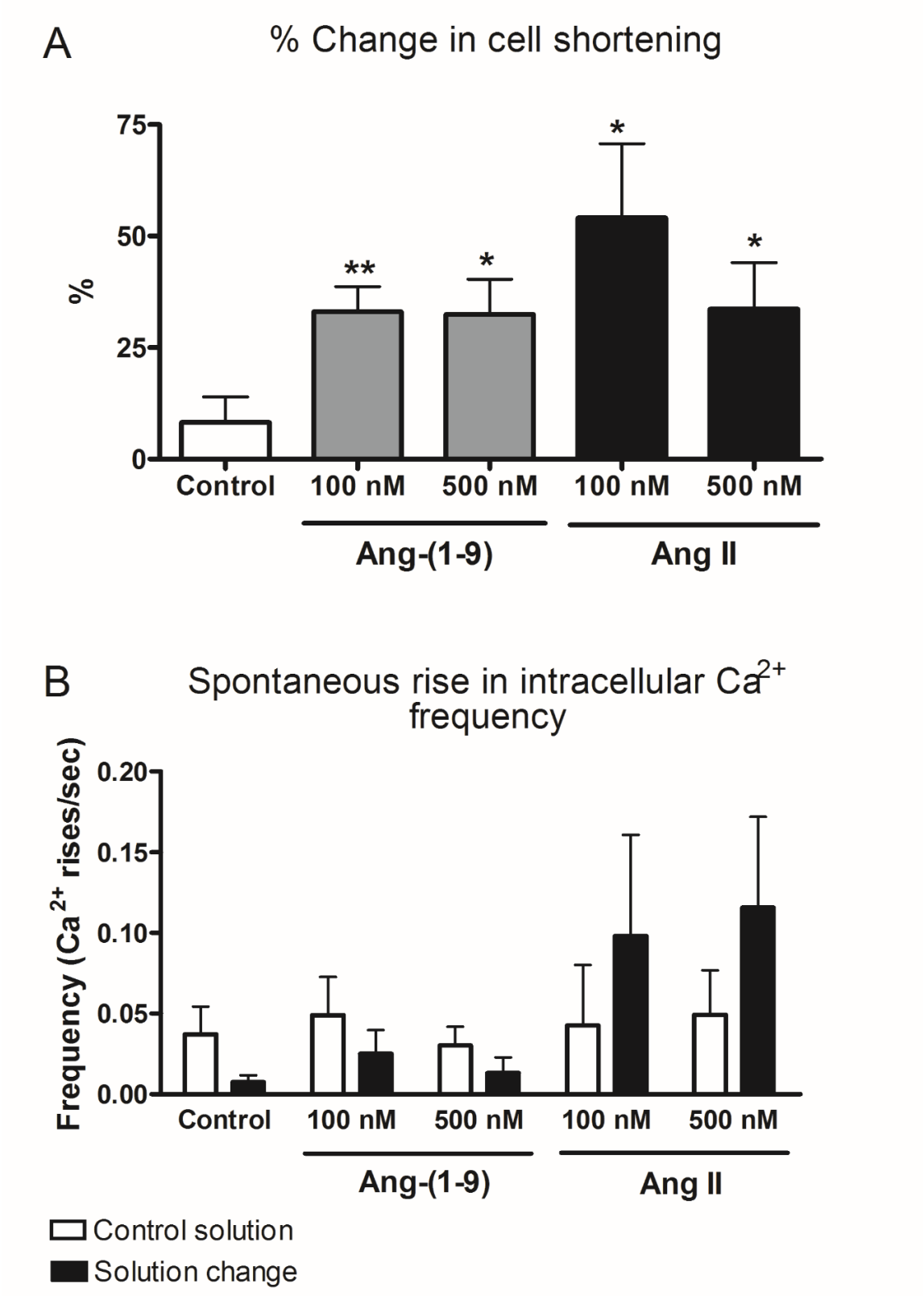

Figure 6.11 The effects of 100 and 500 nM of RAS peptides on mouse cardiomyocyte cell shortening and spontaneous rises in intracellular Ca^{2+} frequency.
Average % change in cell shortening (A) and spontaneous Ca^{2+} release frequency pre and post-peptide perfusion (B) for cells perfused with 100 or 500 nM of Ang-(1-9) or Ang II or control solution. *= P<0.05, **= P<0.01 *vs.* control. n= 5, 7, 7, 14 and 4 for control, 100 nM Ang-(1-9), 100 nM Ang II, 500 nM Ang-(1-9) and 500 nM Ang II, respectively. Data presented as mean± SEM.

6.3.4 Peptide inhibitor studies

6.3.4.1 Ca^{2+}-transient analysis

In order to establish whether the effects Ang-(1-9) and Ang II were dependent on the AT_1R or AT_2R, incubation and perfusion of the mouse cardiomyocytes with the AT_1R antagonist Losartan and/or the AT_2R antagonist PD123319 was performed in combination with perfusion of the peptides as per protocol D (Figure 6.3).

For Ang-(1-9), the change in Ca^{2+}-transient amplitude seen previously was unaltered in the presence of either antagonist, with both Ang-(1-9) concentrations inducing a significant increase in Ca^{2+}-transient amplitude by 21-29 % after peptide application, regardless of antagonist (Figure 6.12 A-i; $P<0.05$). An almost identical change was seen in Tau, with Ang-(1-9) application significantly decreasing Tau by 8-10 % ($P<0.05$; Figure 6.12 A-ii).

For Ang II, the low dose of 100 nM was assessed with either Losartan, PD123319 or a combination of both. In this instance, the change in amplitude seen in the cells treated with Losartan or Losartan and PD123319, which was increased by approximately 12 %, was found to be significantly reduced compared to the 37 % increase seen in the cells treated with PD123319 only ($P<0.05$; Figure 6.12 B-i). The % decrease in Tau observed followed similar pattern. The Losartan and Losartan/PD123319 combination groups Tau was significantly decreased by 8.6± 1.7 % and 10.7± 2.0 % for Losartan and Losartan + PD123319 combination, respectively ($P<0.05$). The decrease in Tau by 13.1± 6.4 % in the PD123319 group was larger, however this was not significantly different to control cells (Figure 6.12 B-ii).

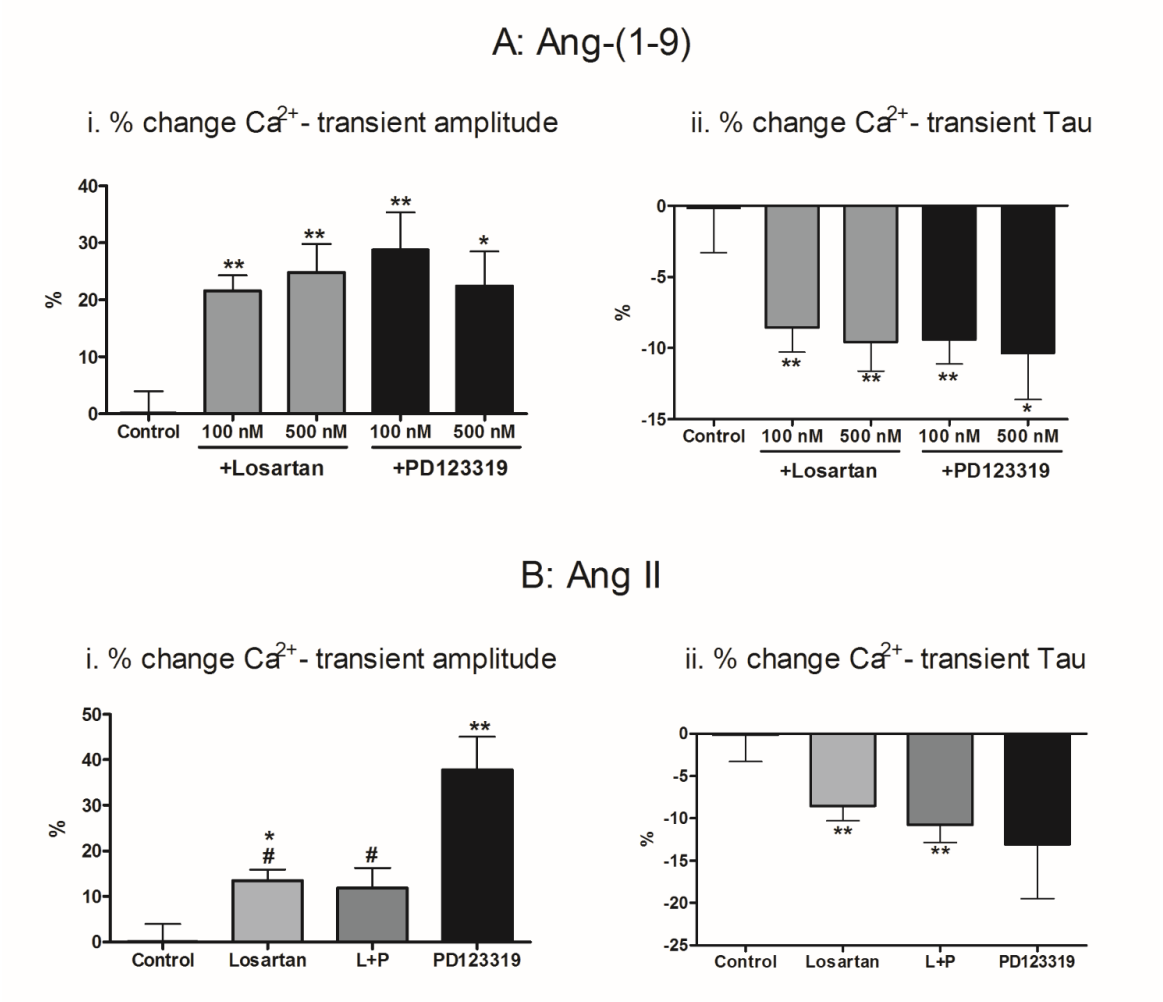

Figure 6.12 The effects of RAS inhibitors on Ang-(1-9) and Ang II- induced Ca^{2+}-transient amplitude and Tau changes in mouse cardiomyocytes.
(A) Average % change in Ca^{2+}-transient amplitude (i.) and rate of decline (ii.) for isolated mouse cardiomyocytes pre-treated with 1 µM of Losartan or 500 nM of PD123319 and perfused with control solution followed by further perfusion with control or with 100 or 500 nM of an Ang-(1-9) solution. *=*P*<0.05, **=*P*<0.01 *vs.* control. *n*= 4, 12, 7, 5 and 8 for control, 100 nM + Losartan, 500 nM + Losartan, 100 nM + PD123319 and 500 nM + PD123319, respectively. Data presented as mean % change± SEM. (B) Average % change in Ca^{2+}-transient amplitude (i.) and rate of decline (ii.) for isolated mouse cardiomyocytes pre-treated with 1 µM of Losartan, 500 nM of PD123319 or a combination of both and perfused with control solution followed by further perfusion with control or with 100 nM of an Ang II solution. **P*<0.05, ***=*P*<0.01 *vs.* control; #=*P* <0.05 *vs.* Ang II+ PD123319. *n*= 4, 14, 5 and 6 for control, +Losartan, + Losartan and PD123319 and + PD123319, respectively. Data presented as mean % change± SEM.

6.3.4.2 Caffeine-induced Ca^{2+}-transient analysis

The effect of the combined peptide and antagonist treatment on SR Ca^{2+} content and NCX mediated Ca^{2+} extrusion *via* NCX was assessed using 10 mM caffeine. No experimental condition appeared to have a significant effect on caffeine-induced Ca^{2+}-transient amplitude or Tau compared to the control cell group (Figure 6.13 A-i & ii & B-i & ii).

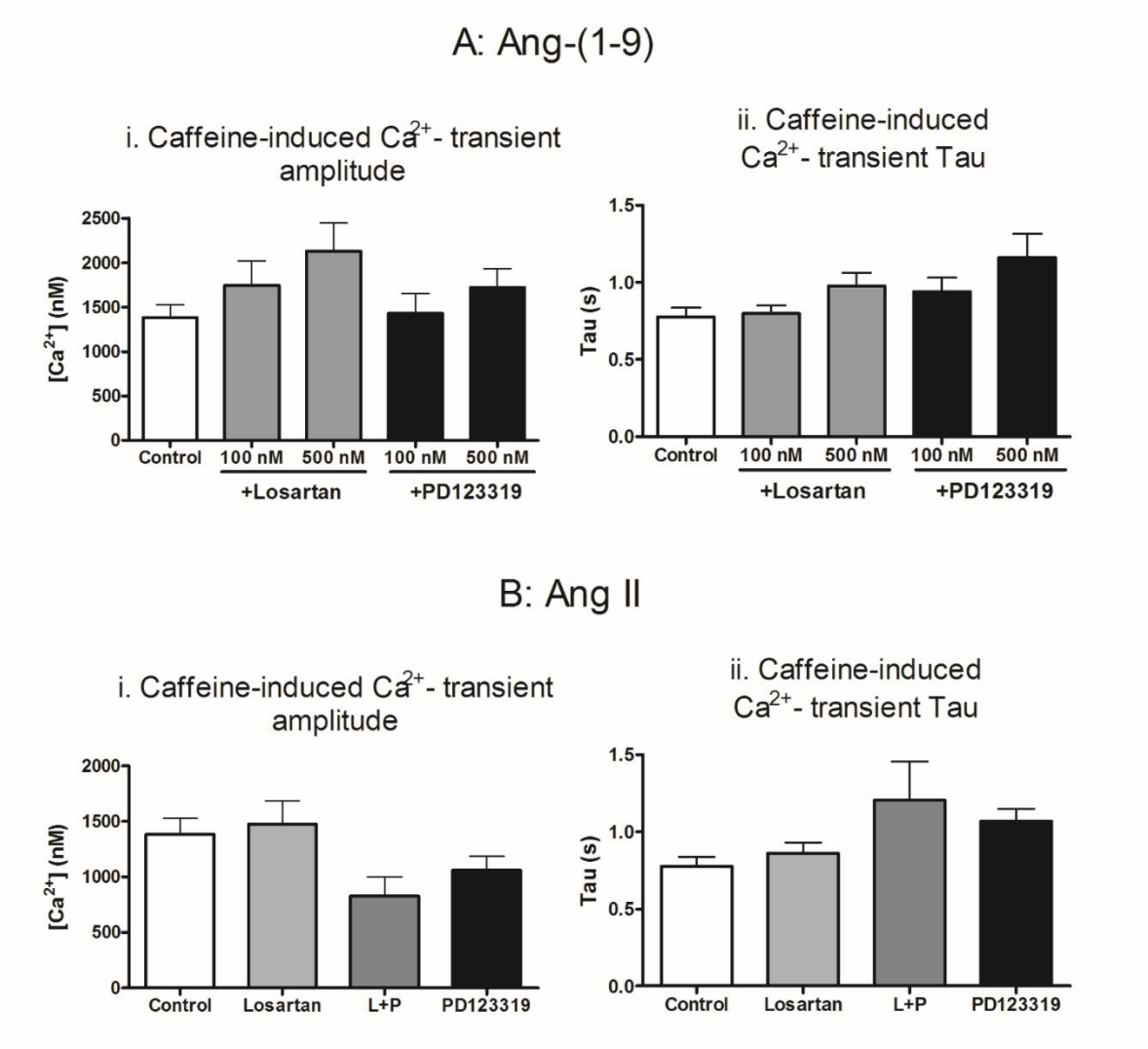

Figure 6.13 The effects of RAS inhibitors on Ang-(1-9) and Ang II- induced caffeine-induced Ca^{2+}-transient amplitude and Tau changes in mouse cardiomyocytes.
(A) Average caffeine-induced Ca^{2+}-transient amplitude (i.) and Tau (ii.) for isolated mouse cardiomyocytes pre-treated with 1 µM of Losartan or 500 nM of PD123319 and perfused with 100 or 500 nM of an Ang-(1-9) solution. *n*= 4, 12, 7, 5 and 8 for control, 100 nM + Losartan, 500 nM + Losartan, 100 nM + PD123319 and 500 nM + PD123319, respectively. Data presented as mean± SEM. (B) Average Ca^{2+}-transient amplitude (i.) and Tau (ii.) for isolated mouse cardiomyocytes pre-treated with 1 µM of Losartan, 500 nM of PD123319 or a combination of both and perfused with 100 nM of an Ang II solution. *n*= 4, 14, 5 and 6 for control, +Losartan, + Losartan and PD123319 and + PD123319, respectively. Data presented as mean± SEM.

6.3.4.3 Cell shortening measurements and spontaneous rise in intracellular Ca^{2+} frequency analysis

Next, the effects of combined peptide and antagonist treatment on cell shortening and spontaneous Ca^{2+} release was assessed. The pre-treatment of cells with either Losartan or PD123319 produced no effect on the changes observed upon application of 500 or 100 nM of Ang-(1-9), with a significant increase in cell shortening produced following Ang-(1-9) application by 33.6± 3.8 %, 51.0± 3.8 %, 80.9± 27.1 % and 74.7± 35.9 % for 500 and 100 nM Ang-(1-9) + Losartan and 500 and 100 nM Ang-(1-9) + PD123319, respectively (Figure 6.14 A-i). Again, there were no changes observed in the frequency of spontaneous rises in intracellular Ca^{2+} in response to Ang-(1-9) application and this was not altered by pre-treatment with the receptor antagonists (Figure 6.14 A-ii).

The pre-treatment of cells with Losartan or a combination of Losartan and PD123319 reduced the increase in cell shortening response previously seen in response to 100 nM of Ang II (AngII+Losartan= 20.3± 8.0 %, AngII+Losartan+PD123319= 24.3± 13.7 %), which was significantly reduced compared to cells pre-treated with PD123319 only, which showed a significant increase in cell shortening of 69.5± 23.7 % of control solution (P<0.05) (Figure 6.14 B-i). Again, there was no significant difference in the frequency of spontaneous intracellular rises in Ca^{2+} between control solution and upon application of 100 nM of Ang II, however there was a trend towards an increase in frequency in cells pre-treated with PD123319 only (Figure 6.14 B-ii).

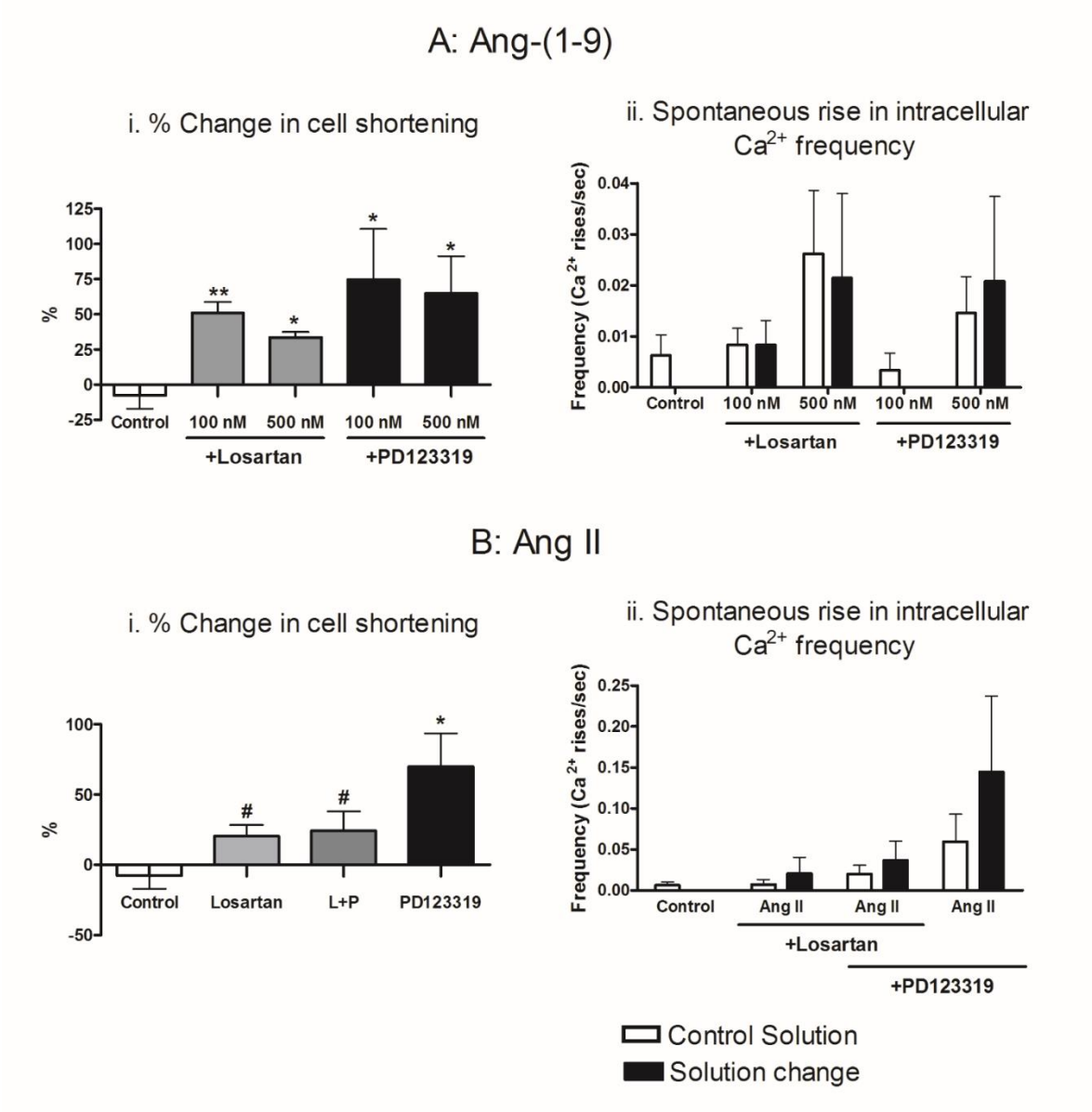

Figure 6.14 The effects of RAS inhibitors on Ang-(1-9) and Ang II- induced cell shortening and spontaneous rises in intracellular Ca^{2+} frequency changes in mouse cardiomyocytes. (A) Average % change in cell shortening (i.) and average spontaneous Ca^{2+} release frequency pre and post-peptide perfusion (ii.) for isolated mouse cardiomyocytes pre-treated with 1 µM of Losartan or 500 nM of PD123319 and perfused with 100 or 500 nM of an Ang-(1-9) solution. *= P<0.05, **= P<0.01 *vs.* control. n= 4, 12, 7, 5 and 8 for control, 100 nM + Losartan, 500 nM + Losartan, 100 nM + PD123319 and 500 nM + PD123319, respectively. Data presented as mean± SEM. (B) Average % change in cell shortening (i.) and average spontaneous Ca^{2+} release frequency pre and post-peptide perfusion (ii.) for isolated mouse cardiomyocytes pre-treated with 1 µM of Losartan, 500 nM of PD123319 or a combination of both and perfused with 100 nM of an Ang II solution. *= P<0.05 *vs.* control; #= P<0.05 *vs.* PD123319. n= 4, 14, 5 and 6 for control, +Losartan, + Losartan and PD123319 and + PD123319, respectively. Data presented as mean± SEM.

6.4 Discussion

The present study assessed the effects of Ang-(1-7), Ang-(1-9) and Ang II on single mouse cardiomyocyte Ca^{2+}-handling and dissected their mechanisms of action. No effect on any Ca^{2+}-handling parameters was detected using Ang-(1-7), however both Ang-(1-9) and Ang II exerted a positive inotropic effect on mouse cardiomyocytes, increasing Ca^{2+}-transient amplitude and cell contractility at 1 μM, 500 nM and 100 nM. The response was instantaneous upon exposure of the cells to the peptide. NCX and SERCA activity appeared to be not significantly altered in response to pre-treatment of cells with 1 μM of both Ang-(1-9) and Ang II, however incubation of cells with Ang-(1-9) appeared to increase SR Ca^{2+}-content and suggested a role for increased L-type Ca^{2+} channel activity, which was absent in cells treated with Ang II. Ang II also resulted in an increased frequency of diastolic Ca^{2+} waves which was absent in cells treated with Ang-(1-9). The effects of Ang II were found to be mediated by the AT_1R, however the actions of Ang-(1-9) on the Ca^{2+}-transient appeared to be AT_2R-independent.

This is the first study to show a direct effect of Ang-(1-9) on mouse cardiomyocyte Ca^{2+}-handling. The lack of effect seen here through Ang-(1-7) treatment, however, is consistent with previous reports (Dias-Peixoto et al., 2008) (Gomes et al., 2010). Despite this, there is some evidence for Ang-(1-7) to have a protective effect on Ca^{2+}-handling properties in cells which have undergone treatment to modify Ca^{2+}-handling parameters, such as isoproterenol (Ferreira et al., 2010a) or Ang II stimulation (Gomes et al., 2010), suggesting it may be beneficial in cells isolated from remodelled hearts. As the cardiomyocytes used here were isolated from healthy, WT mouse hearts and were used without prior stimulus or treatment the data agree with previous findings.

In the present study, a positive inotropic effect was observed for Ang II. The results seen here in response to Ang II treatment has shown an increased Ca^{2+}-transient amplitude when incubated on cells at a concentration of 1 μM, consistent with several other studies which have reported a similar effect (De Mello and Monterrubio, 2004; Petroff et al., 2000; Salas et al., 2001). In the majority of these studies the primary receptor thought to be mediating the effects of Ang II was the AT_1R, which was identified through the use of the AT_1R

antagonist Losartan used in similar doses ranges to what was utilised here (Cheng et al., 1996; Cingolani et al., 2006; Fujita and Endoh, 1999). However, in these previous studies a complete inhibition of the effects of Ang II was seen when used in combination with Losartan, in contrast to what was observed here in the present study. Here the use of Losartan in combination with Ang II brought about a trend towards normalisation back to control levels for Ca^{2+}-transient amplitude and cell shortening, but not a complete inhibition of the effects. This suggests the effects seen here are at least in part mediated by the AT_1R, with potential incomplete blocking of the receptor being the most reasonable explanation for the partial reversal. As there was no effect of PD123319 and an equivalent effect of combined Losartan and PD123319 to Losartan only, this suggests no role for the AT_2R in the effects seen.

Previous data exploring the mechanisms of action of Ang-(1-9) has identified the AT_2R as the mediator of its effects using the AT_2R antagonist PD123319 in similar concentrations utilised here (Flores-Muñoz et al., 2012; Flores-Muñoz et al., 2011; Flores-Munoz et al., 2012; Ocaranza et al., 2010). However, in the present study neither Losartan or PD123319 appeared to abrogate the positive inotropic effects observed in response to Ang-(1-9) on the mouse cardiomyocytes. This suggests that Ang-(1-9) is possibly eliciting its effects *via* an alternative mechanism to Ang II and *via* an unidentified receptor. Alternatively, it is possible the AT_2R receptor was not completely inhibited by PD123319. Moreover, although PD123319 is a very commonly used AT_2R antagonist, recently there have been some concerns identified with its selectivity (Henrion, 2012).

The main differences observed between the effects seen in response to 1 μM Ang II and Ang-(1-9) incubation was the increased SR Ca^{2+}-content and L-type Ca^{2+} channel observed in cells pre-treated with Ang-(1-9) and the increased incidence of spontaneous rises in intracellular Ca^{2+} seen in Ca^{2+}-transient traces from cells exposed to Ang II. The increase in SR Ca^{2+} content combined with the increased L-type current seen in cells pre-treated with Ang-(1-9) suggests that the increased Ca^{2+}-influx is resulting in loading of the SR. This increased SR content may be sensitising the RyR, allowing for more Ca^{2+} to be released during CICR, thus leading to the increased transient. The absence of this increase in Ang II pre-treated cells may be due to the absence of increased Ca^{2+} entry *via* the L-type, with the increased transient potentially primarily a result of increased RyR

sensitivity. The increased frequency of spontaneous rises in intracellular Ca^{2+} seen in response to Ang II incubation is similar to the effects reported for Ang II treatment in human atrial cells, where it was found to significantly increase spontaneous Ca^{2+} spark frequency in an AT_1R-depdendent manner. *In vivo*, spontaneous Ca^{2+} release, or Ca^{2+}-leak from the RyR is common in patients with HF and can lead to fatal ventricular arrhythmia (Farr and Basson, 2004; Venetucci et al., 2008). In fact, early positive inotropic agents such as catecholamines and PDE-I's investigated for the potential treatment of HF enhanced this problem by increasing cytosolic Ca^{2+} concentration, thus increasing the propensity for spontaneous Ca^{2+} release (Du Toit et al., 1999). There are several potential mechanism by which Ang II could be exerting this effect. As mentioned, Ang II could potentially be modifying RyR sensitivity. Moreover, the increased spontaneous Ca^{2+} release and lack of increased SR Ca^{2+} content in the Ang II pre-treated cells may be associated as diastolic Ca^{2+} leak from the SR is not only known to be a cause of arrhythmia, but is also associated with depleted SR Ca^{2+} (Bers et al., 2003).

The spontaneous rises in intracellular Ca^{2+} observed in Ang II treated cells occurred as early-after depolarisations (EADs) rather than delayed after depolarisations (DADs), both of which have distinct mechanisms (Levy and Wiseman, 1991). DADs occur in instances of Ca^{2+} overload as a result of the generation of a transient inward current, attributed to NCX, which can lead to a second depolarisation of the cell (Sipido et al., 2007). EADs occur when the AP is prolonged, allowing time for Ca^{2+} entry *via* reactivation of the L-type Ca^{2+} which reverses repolarization (Qu et al., 2013). DADs occur late into or after full repolarization of the cell, whereas EADs occur during plateau or at the beginning of repolarization (Levy and Wiseman, 1991). Both can trigger propagation impulses *via* spontaneous CICR from the SR, as was observed in some instances in Ang II treated cells (Levy and Wiseman, 1991). This suggests that the mechanisms for the increased spontaneous Ca^{2+} release observed in response to Ang II involves the modulation of the AP and/or L-type Ca^{2+} function, however this requires further investigation.

The positive inotropic effect induced by Ang-(1-9) was associated with increased L-type Ca^{2+}-transient amplitude and an increase in SR Ca^{2+} content when cells were pre-treated with 1 μM of the peptide. The increase in L-type Ca^{2+}-transient

observed suggests a possible increase in L-type Ca^{2+}-channel activity or expression and may account for the overall increased Ca^{2+}-transient amplitude, with more Ca^{2+} entering the cell during each AP (Berridge et al., 2003). The L-type Ca^{2+} channel has been demonstrated to be regulated by PKC- and PKA-mediated pathways, with multiple G-protein coupled receptors in the heart acting through cAMP/PKA pathways (Kamp and Hell, 2000), therefore it is possible Ang-(1-9) is acting through a similar pathway in this setting. Increased SR Ca^{2+} content can also increase Ca^{2+} release during CICR by increasing the luminal sensitisation of the RyR (Bers, 2002), which is consistent with the increased SR Ca^{2+}-content seen in cells pre-treated with Ang-(1-9) here. The increased Ca^{2+}-transient amplitude resulted in the increased cell shortening observed.

There were a number of differences found between peptide incubation and perfusion experiments. Transient amplitude and FS were the only parameters found to be equivalently altered upon both pre-incubation and perfusion of Ang-(1-9) and Ang II. Ca^{2+}-transient Tau was unaltered in pre-incubation experiments but was found to be significantly reduced in perfusion experiments. This may be explained by the more sensitive nature of the perfusion experiments, where changes were being detected within one cell, allowing smaller changes to be more easily identified. Increased SR Ca^{2+} content was observed in cells pre-treated with Ang-(1-9) but not in perfusion experiments. This perhaps indicates that an extended period of Ang-(1-9) exposure is required to allow sufficient time to load the SR. The increase in spontaneous rises in intracellular Ca^{2+} were only observed in cells pre-treated with Ang II and not in perfusion experiments. Again, this may be to do with the time of exposure to the peptide. The different concentrations of the peptide may also explain some of these differences however this required further investigation. L-type Ca^{2+}-transient was not measured in the perfusion experiments and it is therefore unclear as to its activity in these conditions.

The exact receptor interactions and mechanisms underlying the actions of the peptides in this setting still remain to be clarified. Larger *n*-numbers for the lower dose groups would be advantageous in detecting more subtle changes to Ca^{2+}-handling due to the variation in parameters from cell to cell. More direct methods of measuring the L-type Ca^{2+} channel, such as patch clamping, could

also be employed and the effect of the peptides on the cell AP may also provide further information on the mechanism.

6.5 Summary

Retrograde Langendorff perfusion of a collagenase I enzyme is an efficient way of isolating single, Ca^{2+}-tolerant mouse cardiomyocytes. The peptides Ang-(1-7), Ang-(1-9) and Ang II have varying effects on single mouse cardiomyocyte Ca^{2+}-handling properties and inotropy as assessed using epifluorescence microscopy and cell shortening measurements. Ang-(1-7) exerted no measurable effects. Ang-(1-9) and Ang II exerted positive inotropic effects associated with increased Ca^{2+}-transient amplitude and increased cell shortening. Ang II only was associated with an increase in spontaneous SR-mediated Ca^{2+} release events. Ang-(1-9) was associated with an increase in L-type Ca^{2+} transient amplitude and an increase in SR Ca^{2+} content when pre-treated with a 1 μM dose, suggesting a possible mechanism of action. The effects seen in response to Ang II were mediated, in part, by the AT_1R. The receptor interaction for Ang-(1-9) remains to be determined. This is the first time Ang-(1-9) has been associated with a positive inotropic effect in isolated mouse cardiomyocytes.

Chapter 7: General discussion

7.1 Overall summary

Activation of the RAS hormonal cascade following infarction contributes significantly to the pathophysiological changes which drive the decline in cardiac function post-MI, contributing to eventual HF (Carey and Siragy, 2003). Targeting of the counter-regulatory axis of the RAS is emerging as a potential novel therapeutic strategy to attenuate adverse cardiac remodelling and preserve cardiac function (McKinney et al., 2014). Therefore, the primary aim of this thesis was to assess the potential therapeutic effects of the counter-regulatory RAS peptide Ang-(1-9) in MI using a viral-mediated gene transfer approach.

Firstly, the mouse MI model, selected as a suitable animal model for cardiac remodelling and dysfunction, was characterised for structural, functional and gene expression changes. Following MI at both 4 and 8 weeks, it was demonstrated that there was a significant expansion of the LV and decline in cardiac contractility. Changes to the cardiac structure were also evident, with the development of cardiomyocyte hypertrophy and the deposition of collagen I and collagen III in interstitial and perivascular areas, which was more enhanced at 8 weeks post-MI, and as such hearts at 8 weeks post-MI also demonstrated significantly increased ventricular stiffening. Gene expression changes in RAS components were also evident, with increased ACE and AT_2R expression, and decreased AT_1R and ACE2. The structural and functional changes that occurred in this animal model resemble the main pathophysiological changes which occur in human hearts following MI (Sutton and Sharpe, 2000), and therefore made it suitable for assessment of the therapeutic potential of Ang-(1-9).

Next, optimisation of a viral-vector mediated delivery of Ang-(1-9) was performed. Initially, a rAd5 vector was utilised for delivery. Successful transduction of 7-14 % of the myocardium was achieved using direct myocardial injection using a ß-gal expressing rAd and assessing myocardial transduction at 5 days post-delivery. A second study was also carried out utilising a rAAV9 vector. Efficient transduction across approximately 80 % of the myocardium was achieved using a single *iv* injection of rAAV9, which was assessed using an eGFP expressing vector. Both candidate therapeutic viral vectors expressed identical Ang-(1-9) fusion proteins to facilitate the successful expression and cellular secretion of the peptide (Methot et al., 2001).

The first of the two *in vivo* studies utilised rAd gene transfer and assessed the effects of Ang-(1-9) on cardiac remodelling over a 4 week period. It was found that Ang-(1-9) successfully preserved cardiac function following MI, with enhanced contractility, EF and ESP compared to control groups. Cardio-protective effects were evident in cardiac structure, with a small decrease in hypertrophy and regional interstitial fibrosis observed. Moreover, this demonstrated that with expression of a potent secreted transgene product significant, whole-heart effects were observed even when only a small proportion of cardiomyocytes (approximately 7-14 % of the myocardium) had been transduced. Clinical trials have utilised Ad vectors to express pro-angiogenic factors in ischaemic hearts for this reason, with increased protein levels detectable in areas of the myocardium remote from the original rAd injection site observed in animals models (Grines et al., 2002; Grines et al., 2003; Hedman et al., 2003; Mack et al., 1998; Magovern et al., 1996; Stewart et al., 2006). Therefore it could be anticipated a similar effect occurred in the current study, however this remains to be demonstrated. The second study utilising the rAAV9 vector allowed assessment of the effects of Ang-(1-9) at a later time-point due to the longevity of transgene expression. The rAAV9 vector also targets a greater proportion of cardiomyocytes and therefore achieves enhanced homogeneous delivery compared to rAd, making it the preferred choice for clinical gene therapy applications (Bajgelman et al., 2015; Byrne et al., 2008; Hajjar et al., 2008; Jaski et al., 2009; Kawase et al., 2011; Kawase et al., 2008; Zsebo et al., 2014). Similarly to the first study, cardiac function in MI animals was preserved by Ang-(1-9) from 1 week post-MI, which was unexpected due to the delay in transgene expression onset displayed by AAV vectors (Zincarelli et al., 2008). However, further investigation demonstrated that rAAV9 transgene expression was detectable in the mouse heart as soon as 1 wk following delivery. Similarly to the rAd study, Ang-(1-9) when delivered by rAAV9 demonstrated improved contractility, normalised EF and increased ESP. The advancement of the time-point from 4 to 8 wk resulted in increased ventricular stiffening and dilation in the MI model, however Ang-(1-9) reduced ventricular stiffness and produced a significantly increased CO even compared to sham due to the increased dilation but maintained EF. The more advanced interstitial and perivascular fibrosis at 8 weeks was also significantly attenuated by Ang-(1-9), primarily through decreased deposition of collagen I, the isoform associated with

development of severe LV dysfunction (Wei et al., 1999). These cardioprotective effects were also associated with significantly increased AT_2R expression. Unlike in the previous study, there was no obvious anti-hypertrophic effect seen at 8 weeks using AAV9-mediated delivery. The reason for this has not been determined in this study, however it is possible that LV hypertrophy is inherent at this stage in the model and cannot be overcome, although there is a stabilisation of remodelling in the adaptive phase where improved cardiac function is maintained. This stabilisation may be advantageous as it may prevent progression to maladaptive remodelling and HF, however this remains to be investigated in longer-term studies.

An accompanying study was performed in order to try and elucidate the mechanisms by which Ang-(1-9) acts in cardiomyocytes utilising Ca^{2+}-handling measurements on isolated mouse cardiomyocytes. Ca^{2+}-handling is impaired in hearts post-MI, with this thought to contribute to a decline in cardiac function (Gwathmey et al., 1987). Therefore, it was proposed that the beneficial effects exerted by Ang-(1-9) in the mouse MI model perhaps involved the direct modulation of cardiomyocyte Ca^{2+}-handling. The effect of the application of endogenous Ang-(1-9) peptide on isolated mouse cardiomyocyte Ca^{2+}-handling was compared to that of Ang-(1-7) and Ang II using epifluorecence microscopy. It was found that both Ang-(1-9) and Ang II exerted a positive inotropic effect on mouse cardiomyocytes, with increased Ca^{2+}-transient amplitude and increased cell shortening. Ang-(1-7) had no effect. The effects mediated by Ang-(1-9) were found to potentially be mediated by increased L-type Ca^{2+} channel activity and increased SR Ca^{2+} content. Moreover, Ang II treatment was associated with an increased propensity for spontaneous rises in intracellular Ca^{2+}, whereas this was not observed with Ang-(1-9). Identification of the receptor through which each peptide was exerting its effects was investigated using the AT_1R and AT_2R receptor antagonists Losartan and PD123319. It was found that the effects of Ang II were at least in part being mediated by the AT_1R, however the Ang-(1-9) mediated effects appeared AT_2R-independent under these experimental conditions. Further studies are required to clarify if indeed this is the case.

7.2 Future perspectives

This study is the first to demonstrate a functional cardioprotective effect of Ang-(1-9) post-MI using gene transfer. One other previous study has reported a beneficial functional effect of Ang-(1-9) on the heart in a model of dilated cardiomyopathy and also demonstrated using the Mas receptor antagonist A-779 that the effects observed were completely independent of conversion to Ang-(1-7) (Zheng et al., 2015). However, the present study has not used receptor antagonists in order to investigate the *in vivo* receptor by which Ang-(1-9) is exerting its effects. There are now a multitude of studies which have demonstrated the independent biological activity of Ang-(1-9) *via* the AT_2R (Flores-Muñoz et al., 2012; Flores-Muñoz et al., 2011; Flores-Munoz et al., 2012; Zheng et al., 2015), therefore the assumption could be made that in the current studies Ang-(1-9) is mediating its effects *via* the AT_2R. However, in the complex *in vivo* environment, and especially following MI where cardiac ACE expression is elevated, the partial or complete conversion of Ang-(1-9) to Ang-(1-7) is highly likely. This however may be advantageous as the beneficial effects of Ang-(1-9) signalling *via* the AT_2R may be further enhanced by conversion to Ang-(1-7) and subsequent signalling *via* the Mas receptor, which is well established to exert cardioprotective effects in models of MI and HF (Loot et al., 2002b; Marques et al., 2012; Patel et al., 2012; Qi et al., 2011; Wang et al., 2010a; Zhao et al., 2013). What is unclear in this study is the extent this possible conversion is contributing to the effects seen. In order to address this, subsequent studies could utilise minipump infusion of A-779, Losartan or combination into viral vector transduced MI animals in order to identify the contribution of each peptide to the effects seen in this setting. Peptide levels could also be measured directly from cardiac lysates using techniques able to differentiate between the similar peptide structures, such as mass-spectrometry, high-performance liquid chromatography and enzyme-linked immunosorbent assays.

The mouse MI model has previously been demonstrated to be a suitable model for severe cardiac remodelling (Klocke et al., 2007; Zolotareva and Kogan, 1978). However, this remodelling, consistent with what has been observed here, generally remains in the compensated LV dysfunction phase for an extended period of time following MI without a further decline in cardiac function, with preserved CO observed up to 12 months following infarction (Pons et al., 2003).

Therefore in the current study the cardioprotective capacity of Ang-(1-9) treatment has been assessed only in the compensatory phase of remodelling and not in the more severe de-compensatory phase leading to HF. Therefore in the future the therapeutic potential of Ang-(1-9) could be assessed in a more severe cardiac dysfunction model, such as the rat CHF model which develops similar pathophysiological manifestations as human HF patients including depressed CO and elevated LV filling pressure (Pfeffer et al., 1979) or a large-infarct mouse MI group (Finsen et al., 2005; Kinugawa et al., 2000). Moreover, the AAV-vector mediated delivery approach used here would be particularly well suited for a long-term study into the effects of Ang-(1-9) on HF due to the extended transgene expression potential (Stieger et al., 2008), allowing for a time-course of the protective effects of Ang-(1-9) to be determined without requiring re-administration of the vector. As well as the development of the biological pump described here which enables the peptides to be utilised using a gene therapy approach (Methot et al., 2001), oral formulation of RAS peptides, including Ang-(1-7) and Alamandine, have already been developed and efficacy demonstrated. Although these oral formulations demonstrate short half-lives following absorption they still demonstrate that promising advances are being made to take RAS peptides closer to be utilised therapeutically in a clinical setting (Lautner et al., 2013; Marques et al., 2012). Similarly, the oral agonist of the AT_2R, C21, has demonstrated promising pre-clinical therapeutic effects in MI and stroke (Joseph et al., 2014; Kaschina et al., 2008). Moreover, Ang-(1-7) is currently being utilised clinically for a variety of purposes. Ongoing clinical trials include the use of the active peptide analogue NorLeu-A(1-7) which has been shown to clinically accelerate diabetic wound healing when applied topically through modulation of cellular proliferation, angiogenesis, and dermal repair (Balingit et al., 2012; Rodgers et al., 2011; Rodgers et al., 2003) and in cancer therapy, delivery of Ang-(1-7) following chemotherapy promotes reconstitution of the haematopoietic system by promoting proliferation of bone marrow progenitor cells (Ellefson et al., 2004; Heringer-Walther et al., 2009; Rodgers and Xiong, 2003; Rodgers and Oliver, 2006).

Following the identification of a beneficial functional effect of Ang-(1-9) peptide *in vivo* a potential mechanism by which this occurred was explored *in vitro* using Ca^{2+}-handling studies as abnormal cardiomyocyte Ca^{2+}-handling is known to be a

contributing factor to the decline in cardiac function post-MI (Gwathmey et al., 1987). The present study has identified for the first time that Ang-(1-9) is able to enhance the contraction of mouse cardiomyocytes by increasing the cellular Ca^{2+}-transient, possible in a L-type Ca^{2+} channel-dependent manner. However, as Ca^{2+}-handling measurements only indirectly assess the function of the main Ca^{2+}-handling proteins, more direct measurements are required to confirm what has been observed (Bers, 2001). Whole cell patch clamp is a technique which allows the study of a single ion channel species on a cell membrane and could be used to directly measure any changes in L-type Ca^{2+} channel activity in response to Ang-(1-9) (Sakmann and Neher, 1984). Changes to expression levels of the ion channel could also be assessed using qRT-PCR and western blot approaches, although large changes in expression would be unexpected within a short incubation period. Moreover, there is no evidence in the present study to suggest alterations in Ca^{2+}-handling are contributing to the improved cardiac function observed *in vivo*. Further studies could be undertaken to investigate this further and potentially establish a link between what has been seen in the *in vivo* and *in vitro* studies. By performing the Ca^{2+}-handling measurements on cells isolated from MI animals transduced with either an Ang-(1-9) expressing vector or control vector, any differences in Ca^{2+}-handling could be identified and directly correlated with the improved cardiac function observed. In the present study the effects of Ang-(1-9) on Ca^{2+}-handling were only assessed in healthy cardiomyocytes, an interesting study would be to assess its effects on cells with dysfunctional Ca^{2+}-handling, such as those subjected to hypoxia (Kang et al., 2006; Saini and Dhalla, 2005). Moreover, as rodent ECC differs from that of humans with regards to the AP and the extrusion of Ca^{2+} (Bers, 2002; Hove-Madsen and Bers, 1993) studies could also be performed in cardiomyocytes isolated from a species with more similar ECC properties to humans, such as rabbit. Additionally, a receptor through which Ang-(1-9) was exerting the positive inotropic effect observed *in vitro* was not identified. To date, the primary receptor through which Ang-(1-9) has been reported to interact has been the AT_2R (Flores-Muñoz et al., 2011). This work has primarily been done through using the antagonist PD123319, also utilised here in these studies, but however failed to block the effects of Ang-(1-9). However, there have been concerns raised over the selectivity of PD123319, with off-target effects being a possibility (Henrion, 2012). Therefore, the AT_2R-deficient transgenic mouse

(Ichiki et al., 1995) would provide the ideal way to investigate and clarify the involvement of the AT_2R for Ang-(1-9) function.

Interestingly, when compared to Ang II, Ang-(1-9) failed to elicit an increase in spontaneous rises in intracellular Ca^{2+} to the same degree. This perhaps warrants further investigation into the possible anti-arrhythmogenic effects of the peptide. This could be performed in a variety of ways. *In vivo* arrhythmogenesis could be continuously monitored post-MI using telemetry probe implantation and continuous ECG recording, with differences between Ang-(1-9) treated and untreated animals assessed (Stilli et al., 2001). Whole-heart Langendorff ECG recording could also be utilised to assess its potential anti-arrhythmogenic effects in a different pro-arrhythmogenic model, such as I/R injury, with the effects on Ang-(1-9) infusion assessed on the incidence to reperfusion arrhythmias. A similar approach has previously been utilised for Ang-(1-7), where there is already evidence that it exerts anti-arrhythmogenic effects (De Mello, 2004; Ferreira et al., 2001; Ferreira et al., 2010b; Santos et al., 2004). Therefore it is possible that Ang-(1-9) acts in a similar way or that *in vivo* its possible conversion to Ang-(1-7) also mediates anti-arrhythmogenic effects, however this remains to be clarified. The whole-heart approach would also allow measurements of pressure changes in response to Ang-(1-9), providing further information on its positive inotropic effects at the whole-organ level (Skrzypiec-Spring et al., 2007).

There are a variety of other potential effects Ang-(1-9) exerts on the heart following MI that have not been explored here. One interesting aspect to assess would be any change in the inflammatory response brought about by Ang-(1-9) following MI. In both *in vivo* studies there was a trend towards a reduced rupture rate in Ang-(1-9) treated animals, although this did not reach significance. As a prolonged or severe post-MI inflammatory response can be detrimental to post-infarct myocardial healing, resulting in reduced tensile strength of the scar and promotion of cardiac rupture (Frangogiannis, 2012), it is possible Ang-(1-9) was exerting an anti-inflammatory effect. This is a possibility as not only is stimulation of the AT_2R associated with anti-inflammatory effects post-MI (Kaschina et al., 2008), but in a recent study Ang-(1-9) infusion in the rat STZ model of dilated cardiomyopathy was shown to reduce expression of the pro-inflammatory mediators TNF-α and IL-1ß within the myocardium (Zheng et al.,

2015). Other aspects which could be investigated are the effects of Ang-(1-9) on angiogenesis and apoptosis. In both *in vivo* studies there was again a trend towards increased scar thickness, potentially indicating 2 things; improved scar healing and collagen deposition or improved survival of the myocardium within the infarct area. If the latter were true it is possible that enhanced angiogenesis within the infarct or reduced cardiomyocyte apoptosis occurred. There is currently no evidence to suggest Ang-(1-9) affects either of these parameters within the heart, however Ang-(1-7) signalling *via* Mas has been demonstrated to be essential for angiogenesis during the infarct healing process post-MI in the rat through increasing expression of VEGF-D and MMP-9 (Zhao et al., 2013). Therefore it is possible that over-expression of Ang-(1-9) enhanced angiogenesis in MI hearts through conversion to Ang-(1-7) or independently through other mechanisms. Cardiomyocyte apoptosis is thought to be mediated by activation of the AT_1R, with Ang II induced activation of the Ras/Raf/MAPK pathway found to induce apoptosis (Bucher et al., 2001; Cigola et al., 1997; Kajstura et al., 1997). As AT_2R stimulation is generally thought to counter-act the effects of Ang II and is associated with the expression of phosphatases that inhibit the MAPK signalling pathway (Kaschina and Unger, 2003), it is possible that if Ang-(1-9) is signalling *via* the AT_2R in this setting that it may have exerted an anti-apoptotic effect, however this requires further investigation. A disparity observed in the present studies to what has been reported previously about Ang-(1-9) is the lack of a potent anti-hypertrophic response, with only a small effect seen with rAd treatment and no effect seen with rAAV. Previous studies, including Ang-(1-9) infusion in the rat MI model, have reported reduced HW and pro-hypertrophic marker expression, including ANP, BNP, ß-MHC and MLC, both *in vivo* and *in vitro* in response to Ang-(1-9) (Flores-Muñoz et al., 2011; Ocaranza et al., 2010). In the present studies, hypertrophy was assessed only using HW measurements and WGA staining. In order to more accurately establish whether a hypertrophic response in present or not, hypertrophic marker expression analysis could be performed. As mentioned, the differences observed here and in the rat MI model may be attributed to the difference in peptide administration (circulatory *vs.* tissue-derived).

The present study has not investigated any specific signalling pathways involved in the effects exerted by Ang-(1-9), however there are several pathways which

could be investigated in future studies. One such pathway which warrants further investigation is the ROS signalling pathway. As discussed previously, Ang II raises ROS levels in the heart through increased expression of NADPH oxidase and H_2O_2 generation (Garrido and Griendling, 2009; Li et al., 2006a). This has the effect of modulating Ca^{2+}-handling protein channels through redox modification, activating the PKC and MAPK pathways and increasing NF-κB expression, which increases expression of NO-synthase and promotes increased production of ROS, and through direct modulation of ion channel expression (Akki et al., 2009; Palomeque et al., 2006; Shang et al., 2008). Recent studies have identified an anti-oxidative effect of Ang-(1-9), with it found to depress NADPH oxidase expression thus reducing ROS in the heart in hypertensive and cardiomyopathy models (Ocaranza et al., 2014; Zheng et al., 2015). Moreover, Ang-(1-9) also appears to inhibit the Ang II-induced increase in NF-κB expression, subsequently leading to decreased CTGF, collagen I, fibronectin and MMP-2 expression in the heart, thus attenuating fibrosis development (Johar et al., 2006; Thakur et al., 2014; Zheng et al., 2015). Through modulation of the ROS signalling pathway, Ang-(1-9) could be inducing the anti-fibrotic and improved contractile properties of the heart as observed here *in vivo* as well as modulating Ca^{2+}-handling protein activity as observed *in vitro* and therefore this warrants further investigation.

7.3 Conclusion

In summary, the data from this thesis have demonstrated for the first time that gene delivery of Ang-(1-9) can confer functional cardio-protective effects in a mouse model of MI, combined with an attenuation in adverse myocardial fibrosis and ventricular stiffening. Moreover, accompanying studies have identified a potential novel role of Ang-(1-9) in exerting a positive inotropic effect on isolated cardiomyocytes through an increased Ca^{2+}-transient amplitude. Overall, this study highlights the potential of Ang-(1-9) as a therapeutic agent for adverse structural and functional cardiac remodelling post-MI and provides impetus for further future development of Ang-(1-9) as a potential therapy in this setting.

List of references

Abadir, P.M., Periasamy, A., Carey, R.M., and Siragy, H.M. (2006). Angiotensin II type 2 receptor–bradykinin B2 receptor functional heterodimerization. Hypertension *48*, 316-322.

AbdAlla, S., Lother, H., Abdel-tawab, A.M., and Quitterer, U. (2001). The Angiotensin II AT2 receptor is an AT1 receptor antagonist. Journal of Biological Chemistry *276*, 39721-39726.

Agah, R., Kirshenbaum, L.A., Abdellatif, M., Truong, L.D., Chakraborty, S., Michael, L.H., and Schneider, M.D. (1997). Adenoviral delivery of E2F-1 directs cell cycle reentry and p53-independent apoptosis in postmitotic adult myocardium *in vivo*. Journal of Clinical Investigation *100*, 2722.

Agbandje-McKenna, M., and Kleinschmidt, J. (2011). AAV capsid structure and cell interactions. Adeno-Associated Virus (Springer), pp. 47-92.

Ahmad, S., Wei, C.-C., Tallaj, J., Dell'Italia, L.J., Moniwa, N., Varagic, J., and Ferrario, C.M. (2013). Chymase mediates angiotensin-(1-12) metabolism in normal human hearts. Journal of the American Society of Hypertension *7*, 128-136.

Akache, B., Grimm, D., Pandey, K., Yant, S.R., Xu, H., and Kay, M.A. (2006). The 37/67-kilodalton laminin receptor is a receptor for adeno-associated virus serotypes 8, 2, 3, and 9. Journal of virology *80*, 9831-9836.

Akishita, M., Iwai, M., Wu, L., Zhang, L., Ouchi, Y., Dzau, V.J., and Horiuchi, M. (2000). Inhibitory effect of angiotensin II type 2 receptor on coronary arterial remodeling after aortic banding in mice. Circulation *102*, 1684-1689.

Akki, A., Zhang, M., Murdoch, C., Brewer, A., and Shah, A.M. (2009). NADPH oxidase signaling and cardiac myocyte function. Journal of molecular and cellular cardiology *47*, 15-22.

Al-Maghrebi, M., Benter, I.F., and Diz, D.I. (2009). Endogenous angiotensin-(1-7) reduces cardiac ischemia-induced dysfunction in diabetic hypertensive rats. Pharmacological Research *59*, 263-268.

Alba, R., Baker, A.H., and Nicklin, S.A. (2012). Vector systems for prenatal gene therapy: principles of adenovirus design and production. Prenatal Gene Therapy (Springer), pp. 55-84.

Alexander, I., Cunningham, S., Logan, G., and Christodoulou, J. (2008). Potential of AAV vectors in the treatment of metabolic disease. Gene therapy *15*, 831-839.

Anzai, T., Yoshikawa, T., Shiraki, H., Asakura, Y., Akaishi, M., Mitamura, H., and Ogawa, S. (1997). C-reactive protein as a predictor of infarct expansion and cardiac rupture after a first Q-wave acute myocardial infarction. Circulation *96*, 778-784.

Arnberg, N., Kidd, A.H., Edlund, K., Nilsson, J., Pring-Åkerblom, P., and Wadell, G. (2002). Adenovirus type 37 binds to cell surface sialic acid through a charge-dependent interaction. Virology *302*, 33-43.

Asakura, M., Kitakaze, M., Takashima, S., Liao, Y., Ishikura, F., Yoshinaka, T., Ohmoto, H., Node, K., Yoshino, K., and Ishiguro, H. (2002). Cardiac hypertrophy is inhibited by antagonism of ADAM12 processing of HB-EGF: metalloproteinase inhibitors as a new therapy. Nature medicine *8*, 35-40.

Ashraf, M. (1979). Correlative studies on sarcolemmal ultrastructure, permeability, and loss of intracellular enzymes in the isolated heart perfused with Ca^{2+}-free medium. The American Journal of Pathology *97*, 411.

Atchison, R.W., Casto, B.C., and Hammon, W.M. (1965). Adenovirus-associated defective virus particles. Science *149*, 754-755.

Atlas, S.A. (2007). The renin-angiotensin aldosterone system: pathophysiological role and pharmacologic inhibition. Journal of Managed Care Pharmacy *13*, S9.

Atlas, S.A., Case, D.B., Yu, Z.Y., and Laragh, J.H. (1984). Hormonal and metabolic effects of angiotensin converting enzyme inhibitors: possible differences between enalapril and captopril. The American Journal of Medicine *77*, 13-17.

Atsma, D.E., Bastiaanse, E.L., Jerzewski, A., Van der Valk, L.J., and Van der Laarse, A. (1995). Role of Ca^{2+}-activated neutral protease (calpain) in cell death in cultured neonatal rat cardiomyocytes during metabolic inhibition. Circulation Research *76*, 1071-1078.

Auricchio, A., Kobinger, G., Anand, V., Hildinger, M., O'Connor, E., Maguire, A.M., Wilson, J.M., and Bennett, J. (2001). Exchange of surface proteins impacts on viral vector cellular specificity and transduction characteristics: the retina as a model. Human Molecular Genetics *10*, 3075-3081.

Avila, M.D., Morgan, J.P., and Yan, X. (2011). Genetically modified mouse models used for studying the role of the AT 2 receptor in cardiac hypertrophy and heart failure. BioMed Research International *2011*.

Bai, J., Zhang, N., Hua, Y., Wang, B., Ling, L., Ferro, A., and Xu, B. (2013). Metformin inhibits angiotensin II-induced differentiation of cardiac fibroblasts into myofibroblasts. PloS one *8*, e72120.

Bajgelman, M.C., dos Santos, L., Silva, G.J., Nakamuta, J., Sirvente, R.A., Chaves, M., Krieger, J.E., and Strauss, B.E. (2015). Preservation of cardiac function in left ventricle cardiac hypertrophy using an AAV vector which provides VEGF-A expression in response to p53. Virology *476*, 106-114.

Balingit, P.P., Armstrong, D.G., Reyzelman, A.M., Bolton, L., Verco, S.J., Rodgers, K.E., Nigh, K.A., and diZerega, G.S. (2012). NorLeu3-A (1–7) stimulation of diabetic foot ulcer healing: Results of a randomized, parallel-group, double-blind, placebo-controlled phase 2 clinical trial. Wound Repair and Regeneration *20*, 482-490.

Banyasz, T., Lozinskiy, I., Payne, C.E., Edelmann, S., Norton, B., Chen, B., Chen-Izu, Y., Izu, L.T., and Balke, C.W. (2008). Transformation of adult rat cardiac myocytes in primary culture. Experimental Physiology *93*, 370-382.

Barandon, L., Couffinhal, T., Ezan, J., Dufourcq, P., Costet, P., Alzieu, P., Leroux, L., Moreau, C., Dare, D., and Duplàa, C. (2003). Reduction of infarct size and prevention of cardiac rupture in transgenic mice overexpressing FrzA. Circulation *108*, 2282-2289.

Barouch, D.H., Pau, M.G., Custers, J.H., Koudstaal, W., Kostense, S., Havenga, M.J., Truitt, D.M., Sumida, S.M., Kishko, M.G., and Arthur, J.C. (2004). Immunogenicity of recombinant adenovirus serotype 35 vaccine in the presence of pre-existing anti-Ad5 immunity. The Journal of Immunology *172*, 6290-6297.

Bartlett, J.S., Wilcher, R., and Samulski, R.J. (2000). Infectious entry pathway of adeno-associated virus and adeno-associated virus vectors. Journal of Virology *74*, 2777-2785.

Bayat, H., Swaney, J.S., Ander, A.N., Dalton, N., Kennedy, B.P., Hammond, H.K., and Roth, D.M. (2002). Progressive heart failure after myocardial infarction in mice. Basic Research in Cardiology *97*, 206-213.

Bedecs, K., Elbaz, N., Sutren, M., Masson, M., Susini, C., Strosberg, A., and Nahmias, C. (1997). Angiotensin II type 2 receptors mediate inhibition of mitogen-activated protein kinase cascade and functional activation of SHP-1 tyrosine phosphatase. Biochem J *325*, 449-454.

Benavides-Vallve, C., Corbacho, D., Iglesias-Garcia, O., Pelacho, B., Albiasu, E., Castaño, S., Muñoz-Barrutia, A., Prosper, F., and Ortiz-de-Solorzano, C. (2012). New strategies for echocardiographic evaluation of left ventricular function in a mouse model of long-term myocardial infarction. PloS one *7*, e41691.

Benihoud, K., Yeh, P., and Perricaudet, M. (1999). Adenovirus vectors for gene delivery. Current Opinion in Biotechnology *10*, 440-447.

Bergelson, J.M., Cunningham, J.A., Droguett, G., Kurt-Jones, E.A., Krithivas, A., Hong, J.S., Horwitz, M.S., Crowell, R.L., and Finberg, R.W. (1997). Isolation of a common receptor for Coxsackie B viruses and adenoviruses 2 and 5. Science *275*, 1320-1323.

Berridge, M.J., Bootman, M.D., and Roderick, H.L. (2003). Ca^{2+} signalling: dynamics, homeostasis and remodelling. Nature Reviews Molecular Cell Biology *4*, 517-529.

Berry, M.N., Friend, D.S., and Scheuer, J. (1970). Morphology and metabolism of intact muscle cells isolated from adult rat heart. Circulation Research *26*, 679-687.

Bers, D. (2001). Excitation-contraction coupling and cardiac contractile force, Vol 237 (Springer).

Bers, D.M. (2002). Cardiac excitation–contraction coupling. Nature *415*, 198-205.

Bers, D.M., Eisner, D.A., and Valdivia, H.H. (2003). Sarcoplasmic reticulum Ca^{2+} and heart failure roles of diastolic leak and Ca^{2+} transport. Circulation Research *93*, 487-490.

Beuckelmann, D., Näbauer, M., and Erdmann, E. (1992). Intracellular Ca^{2+} handling in isolated ventricular myocytes from patients with terminal heart failure. Circulation *85*, 1046-1055.

Beuckelmann, D.J., Näbauer, M., Krüger, C., and Erdmann, E. (1995). Altered diastolic $[Ca^{2+}]_i$ handling in human ventricular myocytes from patients with terminal heart failure. American Heart Journal *129*, 684-689.

Bish, L.T., Morine, K., Sleeper, M.M., Sanmiguel, J., Wu, D., Gao, G., Wilson, J.M., and Sweeney, H.L. (2008). Adeno-associated virus (AAV) serotype 9 provides global cardiac gene transfer superior to AAV1, AAV6, AAV7, and AAV8 in the mouse and rat. Human Gene Therapy *19*, 1359-1368.

Bishop, J.E., Greenbaum, R., Gibson, D.G., Yacoub, M., and Laurent, G.J. (1990). Enhanced deposition of predominantly type I collagen in myocardial disease. Journal of Molecular and Cellular Cardiology *22*, 1157-1165.

Blackburn, S., Steadman, R., and Johnson, F. (2006). Attachment of adeno-associated virus type 3H to fibroblast growth factor receptor 1. Archives of Virology *151*, 617-623.

Blacklow, N.R., Hoggan, M.D., and Rowe, W.P. (1968). Serologic evidence for human infection with adenovirus-associated viruses. Journal of the National Cancer Institute *40*, 319-327.

Borriello, S.P., Murray, P.R., Funke, G., Topley, W.W.C., and Wilson, G. (2005). Topley and Wilson's Microbiology and Microbial Infections: Bacteriology (Hodder Arnold).

Bostick, B., Ghosh, A., Yue, Y., Long, C., and Duan, D. (2007). Systemic AAV-9 transduction in mice is influenced by animal age but not by the route of administration. Gene Therapy *14*, 1605-1609.

Braun-Menendez, E., Fasciolo, J., Leloir, L., and Munoz, J. (1940). The substance causing renal hypertension. The Journal of Physiology *98*, 283-298.

Braunwald, E. (2012). The treatment of acute myocardial infarction: the past, the present, and the future. European Heart Journal: Acute Cardiovascular Care *1*, 9-12.

Braunwald, E., and Kloner, R.A. (1985). Myocardial reperfusion: a double-edged sword? Journal of Clinical Investigation *76*, 1713.

Bright, G., Fisher, G., Rogowska, J., and Taylor, D. (1989). Fluorescence ratio imaging microscopy. Methods Cell Biol *30*, 157-192.

Brilla, C.G., Zhou, G., Matsubara, L., and Weber, K.T. (1994). Collagen metabolism in cultured adult rat cardiac fibroblasts: response to angiotensin II and aldosterone. Journal of Molecular and Cellular Cardiology *26*, 809-820.

Brittsan, A.G., and Kranias, E.G. (2000). Phospholamban and cardiac contractile function. Journal of Molecular and Cellular Cardiology *32*, 2131-2139.

Brockstedt, D.G., Podsakoff, G.M., Fong, L., Kurtzman, G., Mueller-Ruchholtz, W., and Engleman, E.G. (1999). Induction of immunity to antigens expressed by recombinant adeno-associated virus depends on the route of administration. Clinical Immunology *92*, 67-75.

Brown, B., and Hall, A.S. (2005). Renin-angiotensin system modulation: the weight of evidence. American journal of hypertension *18*, 127-133.

Brown, R.D., Ambler, S.K., Mitchell, M.D., and Long, C.S. (2005). The cardiac fibroblast: therapeutic target in myocardial remodeling and failure. Annu Rev Pharmacol Toxicol *45*, 657-687.

Bruneval, P., Hinglais, N., Alhenc-Gelas, F., Tricottet, V., Corvol, P., Menard, J., Camilleri, J., and Bariety, J. (1986). Angiotensin I converting enzyme in human intestine and kidney. Histochemistry *85*, 73-80.

Bucher, M., Ittner, K.-P., Hobbhahn, J., Taeger, K., and Kurtz, A. (2001). Downregulation of angiotensin II type 1 receptors during sepsis. Hypertension *38*, 177-182.

Buisson, B., Laflamme, L., Bottari, S.P., de Gasparo, M., Gallo-Payet, N., and Payet, M.D. (1995). AG protein is involved in the Angiotensin AT receptor inhibition of the T-Type Ca^{2+} current in non-differentiated NG10815 cells. Journal of Biological Chemistry *270*, 1670-1674.

Bumpus, F. (1991). Angiotensin I and II. Some early observations made at the Cleveland Clinic Foundation and recent discoveries relative to angiotensin II formation in human heart. Hypertension *18*, III122.

Bumpus, F.M., Green, A.A., and Page, I.H. (1954). Purification of angiotonin. Journal of Biological Chemistry *210*, 287-294.

Burkhoff, D., Mirsky, I., and Suga, H. (2005). Assessment of systolic and diastolic ventricular properties via pressure-volume analysis: a guide for clinical, translational, and basic researchers. American Journal of Physiology-Heart and Circulatory Physiology *289*, H501-H512.

Burrell, L.M., Johnston, C.I., Tikellis, C., and Cooper, M.E. (2004). ACE2, a new regulator of the renin–angiotensin system. Trends in Endocrinology & Metabolism *15*, 166-169.

Burrell, L.M., Risvanis, J., Kubota, E., Dean, R.G., MacDonald, P.S., Lu, S., Tikellis, C., Grant, S.L., Lew, R.A., and Smith, A.I. (2005). Myocardial infarction increases ACE2 expression in rat and humans. European Heart Journal *26*, 369-375.

Busche, S., Gallinat, S., Bohle, R.-M., Reinecke, A., Seebeck, J., Franke, F., Fink, L., Zhu, M., Sumners, C., and Unger, T. (2000). Expression of angiotensin AT 1 and AT 2 receptors in adult rat cardiomyocytes after myocardial infarction: a single-cell reverse transcriptase-polymerase chain reaction study. The American Journal of Pathology *157*, 605-611.

Byrne, M., Power, J., Preovolos, A., Mariani, J., Hajjar, R., and Kaye, D. (2008). Recirculating cardiac delivery of AAV2/1SERCA2a improves myocardial function in an experimental model of heart failure in large animals. Gene Therapy *15*, 1550–1557.

Caballero, R., Gómez, R., Moreno, I., Nuñez, L., González, T., Arias, C., Guizy, M., Valenzuela, C., Tamargo, J., and Delpón, E. (2004). Interaction of angiotensin II with the angiotensin type 2 receptor inhibits the cardiac transient outward potassium current. Cardiovascular Research *62*, 86-95.

Calcedo, R., Vandenberghe, L.H., Gao, G., Lin, J., and Wilson, J.M. (2009). Worldwide epidemiology of neutralizing antibodies to adeno-associated viruses. Journal of Infectious Diseases *199*, 381-390.

Campagnole-Santos, M.J., Diz, D.I., Santos, R., Khosla, M.C., Brosnihan, K.B., and Ferrario, C.M. (1989). Cardiovascular effects of angiotensin-(1-7) injected

into the dorsal medulla of rats. American Journal of Physiology-Heart and Circulatory Physiology *257*, H324-H329.

Campbell, D.J., Kladis, A., and Duncan, A.M. (1993). Nephrectomy, converting enzyme inhibition, and angiotensin peptides. Hypertension *22*, 513-522.

Campbell, D.J., Lawrence, A.C., Towrie, A., Kladis, A., and Valentijn, A.J. (1991). Differential regulation of angiotensin peptide levels in plasma and kidney of the rat. Hypertension *18*, 763-773.

Cann, A. (2001). Principles of molecular virology, Vol 1 (Academic Press).

Carabello, B.A. (2002). Concentric versus eccentric remodeling. Journal of Cardiac Failure *8*, S258-S263.

Carey, R.M., and Siragy, H.M. (2003). Newly recognized components of the renin-angiotensin system: potential roles in cardiovascular and renal regulation. Endocrine Reviews *24*, 261-271.

Carter, B.J. (2004). Adeno-associated virus and the development of adeno-associated virus vectors: a historical perspective. Molecular Therapy *10*, 981-989.

Castro, C.H., Santos, R.A., Ferreira, A.J., Bader, M., Alenina, N., and Almeida, A.P. (2006). Effects of genetic deletion of angiotensin-(1–7) receptor Mas on cardiac function during ischemia/reperfusion in the isolated perfused mouse heart. Life Sciences *80*, 264-268.

Celladon (2015). Celladon reports negative results for CUPID2 trial of Mydicar in advanced heart failure. [press release http://ir.celladon.com/releasedetail.cfm?releaseid=908592].

Cha, S.A., Park, B.M., Gao, S., and Kim, S.H. (2013). Stimulation of ANP by angiotensin-(1-9) via the angiotensin type 2 receptor. Life Sciences *93*, 934-940.

Chahal, P.S., Schulze, E., Tran, R., Montes, J., and Kamen, A.A. (2014). Production of adeno-associated virus (AAV) serotypes by transient transfection of

HEK293 cell suspension cultures for gene delivery. Journal of Virological Methods *196*, 163-173.

Chapman, R., Rodrigo, G., Tunstall, J., Yates, R., and Busselen, P. (1984). Ca^{2+} paradox of the heart: a role for intracellular sodium ions. American Journal of Physiology-Heart and Circulatory Physiology *247*, H874-H879.

Chapman, R., and Tunstall, J. (1987). The calcium paradox of the heart. Progress in Biophysics and Molecular Biology *50*, 67-96.

Chappell, M., Tallant, E., Brosnihan, K., and Ferrario, C. (1994). Conversion of angiotensin I to angiotensin-(1-7) by thimet oligopeptidase (EC 3.4. 24.15) in vascular smooth muscle cells. Journal of Vascular Medicine and Biology *5*, 129-129.

Chappell, M.C. (2012). The non-classical renin-angiotensin system and renal function. Comprehensive Physiology *2*, 2733-2752. PMC.

Chappell, M.C., Brosnihan, K.B., Diz, D.I., and Ferrario, C.M. (1989). Identification of angiotensin-(1-7) in rat brain. Evidence for differential processing of angiotensin peptides. Journal of Biological Chemistry *264*, 16518-16523.

Chappell, M.C., Pirro, N.T., Sykes, A., and Ferrario, C.M. (1998). Metabolism of angiotensin-(1–7) by angiotensin-converting enzyme. Hypertension *31*, 362-367.

Chazov, E., Matveeva, L., Mazaev, A., Sargin, K., Sadovskaia, G., and Ruda, M. (1976). Intracoronary administration of fibrinolysin in acute myocardial infarct. Terapevticheskiĭ Arkhiv *48*, 8.

Chen, J.-X., Zeng, H., Reese, J., Aschner, J.L., and Meyrick, B. (2012). Overexpression of angiopoietin-2 impairs myocardial angiogenesis and exacerbates cardiac fibrosis in the diabetic db/db mouse model. American Journal of Physiology-Heart and Circulatory Physiology *302*, H1003-H1012.

Chen, J., and Mehta, J.L. (2006). Angiotensin II-mediated oxidative stress and procollagen-1 expression in cardiac fibroblasts: blockade by pravastatin and pioglitazone. American Journal of Physiology-Heart and Circulatory Physiology *291*, H1738-H1745.

Chen, W., Wasserstrom, J.A., and Shiferaw, Y. (2009). Role of coupled gating between cardiac ryanodine receptors in the genesis of triggered arrhythmias. American Journal of Physiology-Heart and Circulatory Physiology *297*, H171-H180.

Chen, Y., Escoubet, B., Prunier, F., Amour, J., Simonides, W.S., Vivien, B., Lenoir, C., Heimburger, M., Choqueux, C., and Gellen, B. (2004). Constitutive cardiac overexpression of sarcoplasmic/endoplasmic reticulum Ca^{2+}-ATPase delays myocardial failure after myocardial infarction in rats at a cost of increased acute arrhythmias. Circulation *109*, 1898-1903.

Chen, Z., Tan, F., Erdös, E.G., and Deddish, P.A. (2005). Hydrolysis of angiotensin peptides by human Angiotensin I–converting enzyme and the resensitization of B2 kinin receptors. Hypertension *46*, 1368-1373.

Cheng, C.-P., Suzuki, M., Ohte, N., Ohno, M., Wang, Z.-M., and Little, W.C. (1996). Altered ventricular and myocyte response to angiotensin II in pacing-induced heart failure. Circulation Research *78*, 880-892.

Chiariello, M., and Perrone-Filardi, P. (1998). Pathophysiology of heart failure. Mineral and electrolyte metabolism *25*, 6-10.

Chirmule, N., Propert, K., Magosin, S., Qian, Y., Qian, R., and Wilson, J. (1999). Immune responses to adenovirus and adeno-associated virus in humans. Gene Therapy *6*, 1574-1583.

Chu, D., Sullivan, C.C., Weitzman, M.D., Du, L., Wolf, P.L., Jamieson, S.W., and Thistlethwaite, P.A. (2003). Direct comparison of efficiency and stability of gene transfer into the mammalian heart using adeno-associated virus versus adenovirus vectors. The Journal of Thoracic and Cardiovascular Surgery *126*, 671-679.

Cigola, E., Kajstura, J., Li, B., Meggs, L.G., and Anversa, P. (1997). Angiotensin II activates programmed myocyte cell death *in vitro*. Experimental Cell Research *231*, 363-371.

Cingolani, H.E., Villa-Abrille, M.C., Cornelli, M., Nolly, A., Ennis, I.L., Garciarena, C., Suburo, A.M., Torbidoni, V., Correa, M.V., and Hurtado, M.C.C. (2006). The positive inotropic effect of angiotensin II role of endothelin-1 and reactive oxygen species. Hypertension *47*, 727-734.

Claycomb, W.C., and Palazzo, M.C. (1980). Culture of the terminally differentiated adult cardiac muscle cell: a light and scanning electron microscope study. Developmental Biology *80*, 466-482.

Cleutjens, J., Verluyten, M., Smiths, J., and Daemen, M. (1995a). Collagen remodeling after myocardial infarction in the rat heart. The american journal of pathology *147*, 325.

Cleutjens, J.P., Blankesteijn, W.M., Daemen, M.J., and Smits, J.F. (1999). The infarcted myocardium: simply dead tissue, or a lively target for therapeutic interventions. Cardiovascular Research *44*, 232-241.

Cleutjens, J.P., Kandala, J.C., Guarda, E., Guntaka, R.V., and Weber, K.T. (1995b). Regulation of collagen degradation in the rat myocardium after infarction. Journal of Molecular and Cellular Cardiology *27*, 1281-1292.

Coutinho, D.C., Foureaux, G., Rodrigues, K.D., Salles, R.L., Moraes, P.L., Murça, T.M., De Maria, M.L., Gomes, E.R., Santos, R.A., and Guatimosim, S. (2014). Cardiovascular effects of angiotensin A: A novel peptide of the renin–angiotensin system. Journal of Renin-Angiotensin-Aldosterone System *15*, 480-486.

Covell, J. (1990). Factors influencing diastolic function. Possible role of the extracellular matrix. Circulation *81*, III155-158.

Crackower, M.A., Sarao, R., Oudit, G.Y., Yagil, C., Kozieradzki, I., Scanga, S.E., Oliveira-dos-Santos, A.J., da Costa, J., Zhang, L., and Pei, Y. (2002).

Angiotensin-converting enzyme 2 is an essential regulator of heart function. Nature *417*, 822-828.

Curiel, D.T., and Douglas, J.T. (2002). Adenoviral vectors for gene therapy (Academic Press).

D'Amore, A., Black, M.J., and Thomas, W.G. (2005). The angiotensin II type 2 receptor causes constitutive growth of cardiomyocytes and does not antagonize angiotensin II type 1 receptor–mediated hypertrophy. Hypertension *46*, 1347-1354.

da Silveira, K.D., Coelho, F.M., Vieira, A.T., Sachs, D., Barroso, L.C., Costa, V.V., Bretas, T.L.B., Bader, M., de Sousa, L.P., and da Silva, T.A. (2010). Anti-inflammatory effects of the activation of the angiotensin-(1–7) receptor, MAS, in experimental models of arthritis. The Journal of Immunology *185*, 5569-5576.

Dahlöf, B., Devereux, R.B., Kjeldsen, S.E., Julius, S., Beevers, G., de Faire, U., Fyhrquist, F., Ibsen, H., Kristiansson, K., and Lederballe-Pedersen, O. (2002). Cardiovascular morbidity and mortality in the Losartan Intervention For Endpoint reduction in hypertension study (LIFE): a randomised trial against atenolol. The Lancet *359*, 995-1003.

Dandapat, A., Hu, C.P., Chen, J., Liu, Y., Khan, J.A., Remeo, F., Carey, R.M., Hermonat, P.L., and Mehta, J.L. (2008). Over-expression of angiotensin II type 2 receptor (agtr2) decreases collagen accumulation in atherosclerotic plaque. Biochemical and Biophysical Research Communications *366*, 871-877.

Danser, A.J., van Kesteren, C.A., Bax, W.A., Tavenier, M., Derkx, F.H., Saxena, P.R., and Schalekamp, M.A. (1997). Prorenin, renin, angiotensinogen, and angiotensin-converting enzyme in normal and failing human hearts evidence for renin binding. Circulation *96*, 220-226.

Davison, A.J., Benkő, M., and Harrach, B. (2003). Genetic content and evolution of adenoviruses. Journal of General Virology *84*, 2895-2908.

Day, T.P., Byrne, L.C., Schaffer, D.V., and Flannery, J.G. (2014). Advances in AAV vector development for gene therapy in the retina. In Retinal Degenerative Diseases (Springer), pp. 687-693.

Daya, S., and Berns, K.I. (2008). Gene therapy using adeno-associated virus vectors. Clinical Microbiology Reviews *21*, 583-593.

de Boer, R.A., Pinto, Y.M., Suurmeijer, A.J., Pokharel, S., Scholtens, E., Humler, M., Saavedra, J.M., Boomsma, F., van Gilst, W.H., and van Veldhuisen, D.J. (2003). Increased expression of cardiac angiotensin II type 1 (AT1) receptors decreases myocardial microvessel density after experimental myocardial infarction. Cardiovascular Research *57*, 434-442.

De Mello, W., and Altieri, P. (1992). The role of the renin-angiotensin system in the control of cell communication in the heart: effects of enalapril and angiotensin II. Journal of Cardiovascular Pharmacology *20*, 643-651.

De Mello, W.C. (1996). Renin-angiotensin system and cell communication in the failing heart. Hypertension *27*, 1267-1272.

De Mello, W.C. (2004). Angiotensin (1-7) re-establishes impulse conduction in cardiac muscle during ischaemia-reperfusion. The role of the sodium pump. Journal of Renin-Angiotensin-Aldosterone System *5*, 203-208.

De Mello, W.C. (2014). Angiotensin (1–7) re-establishes heart cell communication previously impaired by cell swelling: Implications for myocardial ischemia. Experimental Cell Research *323*, 359-365.

De Mello, W.C., and Monterrubio, J. (2004). Intracellular and extracellular angiotensin II enhance the L-type calcium current in the failing heart. Hypertension *44*, 360-364.

del Monte, F., Williams, E., Lebeche, D., Schmidt, U., Rosenzweig, A., Gwathmey, J.K., Lewandowski, E.D., and Hajjar, R.J. (2001). Improvement in survival and cardiac metabolism after gene transfer of sarcoplasmic reticulum Ca^{2+}-ATPase in a rat model of heart failure. Circulation *104*, 1424-1429.

Dell'Italia, L.J., and Ferrario, C.M. (2013). The never-ending story of angiotensin peptides beyond angiotensin I and II. Circulation Research *112*, 1086-1087.

Denby, L., Nicklin, S., and Baker, A. (2005). Adeno-associated virus (AAV)-7 and-8 poorly transduce vascular endothelial cells and are sensitive to proteasomal degradation. Gene Therapy *12*, 1534-1538.

Denegri, M., Bongianino, R., Lodola, F., Boncompagni, S., De Giusti, V.C., Avelino-Cruz, J.E., Liu, N., Persampieri, S., Curcio, A., and Esposito, F. (2014). A single delivery of an adeno-associated viral construct to transfer the CASQ2 gene to knock-in mice affected by catecholaminergic polymorphic ventricular tachycardia is able to cure the disease from birth to advanced age. Circulation, 113.006901.

Der Sarkissian, S., Grobe, J.L., Yuan, L., Narielwala, D.R., Walter, G.A., Katovich, M.J., and Raizada, M.K. (2008). Cardiac overexpression of angiotensin converting enzyme 2 protects the heart from ischemia-induced pathophysiology. Hypertension *51*, 712-718.

Despa, S., Lingrel, J.B., and Bers, D.M. (2012). Na^+/K^+-ATPase α2-isoform preferentially modulates Ca^{2+} transients and sarcoplasmic reticulum Ca^{2+} release in cardiac myocytes. Cardiovascular Research *95*, 480-486.

Di Pasquale, G., Davidson, B.L., Stein, C.S., Martins, I., Scudiero, D., Monks, A., and Chiorini, J.A. (2003). Identification of PDGFR as a receptor for AAV-5 transduction. Nature Medicine *9*, 1306-1312.

Dias-Peixoto, M.F., Santos, R.A., Gomes, E.R., Alves, M.N., Almeida, P.W., Greco, L., Rosa, M., Fauler, B., Bader, M., and Alenina, N. (2008). Molecular mechanisms involved in the angiotensin-(1-7)/Mas signaling pathway in cardiomyocytes. Hypertension *52*, 542-548.

Dickstein, K., Kjekshus, J., Committee, O.S., and Group, O.S. (2002). Effects of losartan and captopril on mortality and morbidity in high-risk patients after acute myocardial infarction: the OPTIMAAL randomised trial. The Lancet *360*, 752-760.

Díez-Freire, C., Vázquez, J., de Adjounian, M.F.C., Ferrari, M.F.R., Yuan, L., Silver, X., Torres, R., and Raizada, M.K. (2006). ACE2 gene transfer attenuates hypertension-linked pathophysiological changes in the SHR. Physiological Genomics *27*, 12-19.

DiGiorgi, P.L., Reel, M.S., Thornton, B., Burton, E., Naka, Y., and Oz, M.C. (2005). Heart transplant and left ventricular assist device costs. The Journal of Heart and Lung Transplantation *24*, 200-204.

DiMattia, M.A., Nam, H.-J., Van Vliet, K., Mitchell, M., Bennett, A., Gurda, B.L., McKenna, R., Olson, N.H., Sinkovits, R.S., and Potter, M. (2012). Structural insight into the unique properties of adeno-associated virus serotype 9. Journal of Virology *86*, 6947-6958.

Dimmeler, S., Rippmann, V., Weiland, U., Haendeler, J., and Zeiher, A.M. (1997). Angiotensin II induces apoptosis of human endothelial cells. Protective effect of nitric oxide. Circulation Research *81*, 970-976.

Ding, W., Zhang, L., Yan, Z., and Engelhardt, J. (2005). Intracellular trafficking of adeno-associated viral vectors. Gene Therapy *12*, 873-880.

Doevendans, P.A., Daemen, M.J., de Muinck, E.D., and Smits, J.F. (1998). Cardiovascular phenotyping in mice. Cardiovascular Research *39*, 34-49.

Dong, B., Yu, Q.T., Dai, H.Y., Gao, Y.Y., Zhou, Z.L., Zhang, L., Jiang, H., Gao, F., Li, S.Y., and Zhang, Y.H. (2012). Angiotensin-converting enzyme-2 overexpression improves left ventricular remodeling and function in a rat model of diabetic cardiomyopathy. Journal of the American College of Cardiology *59*, 739-747.

Dong, J.-Y., Fan, P.-D., and Frizzell, R.A. (1996). Quantitative analysis of the packaging capacity of recombinant adeno-associated virus. Human Gene Therapy *7*, 2101-2112.

Donoghue, M., Hsieh, F., Baronas, E., Godbout, K., Gosselin, M., Stagliano, N., Donovan, M., Woolf, B., Robison, K., and Jeyaseelan, R. (2000). A novel

angiotensin-converting enzyme–related carboxypeptidase (ACE2) converts angiotensin I to angiotensin 1-9. Circulation Research *87*, e1-e9.

Donoghue, M., Wakimoto, H., Maguire, C.T., Acton, S., Hales, P., Stagliano, N., Fairchild-Huntress, V., Xu, J., Lorenz, J.N., and Kadambi, V. (2003). Heart block, ventricular tachycardia, and sudden death in ACE2 transgenic mice with downregulated connexins. Journal of Molecular and Cellular Cardiology *35*, 1043-1053.

Dormond, E., Perrier, M., and Kamen, A. (2009). From the first to the third generation adenoviral vector: what parameters are governing the production yield? Biotechnology Advances *27*, 133-144.

Downey, J.M. (2003). Electrical activity of the heart. Essential Medical Physiology, 175. Academic Press.

Drumme, O.H., Kourtis, S., and Johnson, H. (1988). Formation of angiotensin II and other angiotensin peptides from des-leu 10-angiotensin I in rat lung and kidney. Biochemical Pharmacology *37*, 4327-4333.

Du, G., Huang, P., Liang, B.T., and Frohman, M.A. (2004). Phospholipase D2 localizes to the plasma membrane and regulates angiotensin II receptor endocytosis. Molecular Biology of the Cell *15*, 1024-1030.

Du Toit, E., Muller, C., McCarthy, J., and Opie, L. (1999). Levosimendan: effects of a Ca^{2+} sensitizer on function and arrhythmias and cyclic nucleotide levels during ischemia/reperfusion in the Langendorff-perfused guinea pig heart. Journal of Pharmacology and Experimental Therapeutics *290*, 505-514.

Duan, D., Yue, Y., and Engelhardt, J.F. (2001). Expanding AAV packaging capacity with trans-splicing or overlapping vectors: a quantitative comparison. Molecular Therapy *4*, 383.

Dulin, N.O., Alexander, L.D., Harwalkar, S., Falck, J.R., and Douglas, J.G. (1998). Phospholipase A2-mediated activation of mitogen-activated protein

kinase by angiotensin II. Proceedings of the National Academy of Sciences *95*, 8098-8102.

Duncan, I., and Hutchison, J. (1961). Type-3 adenovirus infection with gastrointestinal symptoms. The Lancet *277*, 530-532.

Efimov, I.R. (2006). Connections, connections, connexins: towards systems biology paradigm of cardiac arrhythmia. Journal of Molecular and Cellular Cardiology *41*, 949-951.

Eguchi, S., Dempsey, P.J., Frank, G.D., Motley, E.D., and Inagami, T. (2001). Activation of MAPKs by angiotensin II in vascular smooth muscle cells metalloprotease-dependent EGF receptor activation is required for activation of ERK and p38 MAPK but not for JNK. Journal of Biological Chemistry *276*, 7957-7962.

Eisner, D., Choi, H., Diaz, M., O'Neill, S., and Trafford, A. (2000). Integrative analysis of Ca^{2+} cycling in cardiac muscle. Circulation Research *87*, 1087-1094.

Ellefson, D.D., Espinoza, T., Roda, N., Maldonado, S., and Rodgers, K.E. (2004). Synergistic effects of co-administration of angiotensin 1–7 and neupogen on hematopoietic recovery in mice. Cancer Chemotherapy and Pharmacology *53*, 15-24.

Elliott, E.B., McCarroll, D., Hasumi, H., Welsh, C.E., Panissidi, A.A., Jones, N.G., Rossor, C.L., Tait, A., Smith, G.L., and Mottram, J.C. (2013). Trypanosoma brucei cathepsin-L increases arrhythmogenic sarcoplasmic reticulum-mediated Ca^{2+} release in rat cardiomyocytes. Cardiovascular Research *100* (2), 325-335.

Erdös, E.G., Jackman, H.L., Brovkovych, V., Tan, F., and Deddish, P.A. (2002). Products of angiotensin I hydrolysis by human cardiac enzymes potentiate bradykinin. Journal of Molecular and Cellular Cardiology *34*, 1569-1576.

Erlebacher, J.A., Weiss, J.L., Weisfeldt, M.L., and Bulkley, B.H. (1984). Early dilation of the infarcted segment in acute transmural myocardial infarction: role

of infarct expansion in acute left ventricular enlargement. Journal of the American College of Cardiology *4*, 201-208.

Ertl, G., and Frantz, S. (2005). Healing after myocardial infarction. Cardiovascular Research *66*, 22-32.

Fabiato, A. (1983). Ca^{2+}-induced release of Ca^{2+} from the cardiac sarcoplasmic reticulum. American Journal of Physiology-Cell Physiology *245*, C1-C14.

Fabiato, A., and Fabiato, F. (1979). Use of chlorotetracycline fluorescence to demonstrate Ca^{2+}-induced release of Ca^{2+} from the sarcoplasmic reticulum of skinned cardiac cells.

Falcón, B.L., Stewart, J.M., Bourassa, E., Katovich, M.J., Walter, G., Speth, R.C., Sumners, C., and Raizada, M.K. (2004). Angiotensin II type 2 receptor gene transfer elicits cardioprotective effects in an angiotensin II infusion rat model of hypertension. Physiological genomics *19*, 255-261.

Falkenhahn, M., Franke, F., Bohle, R.M., Zhu, Y.-C., Stauss, H.M., Bachmann, S., Danilov, S., and Unger, T. (1995). Cellular distribution of angiotensin-converting enzyme after myocardial infarction. Hypertension *25*, 219-226.

Fang, L., Gao, X.-M., Moore, X.-L., Kiriazis, H., Su, Y., Ming, Z., Lim, Y.L., Dart, A.M., and Du, X.-J. (2007). Differences in inflammation, MMP activation and collagen damage account for gender difference in murine cardiac rupture following myocardial infarction. Journal of molecular and cellular cardiology *43*, 535-544.

Farmer, B.B., Mancina, M., Williams, E.S., and Watanabe, A.M. (1983). Isolation of Ca^{2+} tolerant myocytes from adult rat hearts: review of the literature and description of a method. Life Sciences *33*, 1-18.

Farr, M.A., and Basson, C.T. (2004). Sparking the failing heart. New England Journal of Medicine *351*, 185-187.

Ferrari, F.K., Samulski, T., Shenk, T., and Samulski, R.J. (1996). Second-strand synthesis is a rate-limiting step for efficient transduction by recombinant adeno-associated virus vectors. Journal of Virology *70*, 3227-3234.

Ferrario, C.M. (2006). Role of angiotensin II in cardiovascular disease—therapeutic implications of more than a century of research. Journal of Renin-Angiotensin-Aldosterone System *7*, 3-14.

Ferrario, C.M., and Strawn, W.B. (2006). Role of the renin-angiotensin-aldosterone system and proinflammatory mediators in cardiovascular disease. The American Journal of Cardiology *98*, 121-128.

Ferreira, A.J., Bader, M., and Santos, R.A. (2012). Therapeutic targeting of the angiotensin-converting enzyme 2/Angiotensin-(1-7)/Mas cascade in the renin-angiotensin system: a patent review. Expert Opinion on Therapeutic Patents *22*, 567-574.

Ferreira, A.J., Castro, C.H., Guatimosim, S., Almeida, P.W., Gomes, E.R., Dias-Peixoto, M.F., Alves, M.N., Fagundes-Moura, C.R., Rentzsch, B., and Gava, E. (2010a). Attenuation of isoproterenol-induced cardiac fibrosis in transgenic rats harboring an angiotensin-(1-7)-producing fusion protein in the heart. Therapeutic Advances in Cardiovascular Disease 1-14.

Ferreira, A.J., Santos, R.A., and Almeida, A.P. (2001). Angiotensin-(1-7): cardioprotective effect in myocardial ischemia/reperfusion. Hypertension *38*, 665-668.

Ferreira, A.J., Santos, R.A., Bradford, C.N., Mecca, A.P., Sumners, C., Katovich, M.J., and Raizada, M.K. (2010b). Therapeutic implications of the vasoprotective axis of the renin-angiotensin system in cardiovascular diseases. Hypertension *55*, 207-213.

Ferreira, P.M., Souza dos Santos, R.A., and Campagnole-Santos, M.J. (2007). Angiotensin-(3–7) pressor effect at the rostral ventrolateral medulla. Regulatory Peptides *141*, 168-174.

Finsen, A.V., Christensen, G., and Sjaastad, I. (2005). Echocardiographic parameters discriminating myocardial infarction with pulmonary congestion from myocardial infarction without congestion in the mouse. Journal of Applied Physiology *98*, 680-689.

Fischer, J.W., Stoll, M., Hahn, A.W., and Unger, T. (2001). Differential regulation of thrombospondin-1 and fibronectin by angiotensin II receptor subtypes in cultured endothelial cells. Cardiovascular Research *51*, 784-791.

Fischer, R., Dechend, R., Gapelyuk, A., Shagdarsuren, E., Gruner, K., Gruner, A., Gratze, P., Qadri, F., Wellner, M., and Fiebeler, A. (2007). Angiotensin II-induced sudden arrhythmic death and electrical remodeling. American Journal of Physiology-Heart and Circulatory Physiology *293*, H1242-H1253.

Flores-Muñoz, M., Godinho, B.M., Almalik, A., and Nicklin, S.A. (2012). Adenoviral delivery of angiotensin-(1-7) or angiotensin-(1-9) inhibits cardiomyocyte hypertrophy via the mas or angiotensin type 2 receptor. PloS one *7*, e45564.

Flores-Muñoz, M., Smith, N.J., Haggerty, C., Milligan, G., and Nicklin, S.A. (2011). Angiotensin1-9 antagonises pro-hypertrophic signalling in cardiomyocytes via the angiotensin type 2 receptor. The Journal of Physiology *589*, 939-951.

Flores-Munoz, M., Work, L.M., Douglas, K., Denby, L., Dominiczak, A.F., Graham, D., and Nicklin, S.A. (2012). Angiotensin-(1-9) attenuates cardiac fibrosis in the stroke-prone spontaneously hypertensive rat via the angiotensin type 2 receptor. Hypertension *59*, 300-307.

Fontes, M., Silva, L., Campagnole-Santos, M., Khosla, M., Guertzenstein, P., and Santos, R. (1994). Evidence that angiotensin-(1–7) plays a role in the central control of blood pressure at the ventro-lateral medulla acting through specific receptors. Brain Research *665*, 175-180.

Force, T., and Molkentin, J.D. (2006). Cardiac hypertrophy. In Principles of Molecular Medicine (Springer), pp. 146-156.

Forsayeth, J.R., and Bankiewicz, K.S. (2011). AAV9: over the fence and into the woods. Molecular Therapy *19*, 1006.

Francis, G., and Chu, C. (1995). Post-infarction myocardial remodelling: why does it happen? European Heart Journal *16*, 31-36.

Frangogiannis, N.G. (2012). Regulation of the inflammatory response in cardiac repair. Circulation Research *110*, 159-173.

Frank, K., Bölck, B., Bavendiek, U., and Schwinger, R. (1998). Frequency dependent force generation correlates with sarcoplasmic Ca^{2+} ATPase activity in human myocardium. Basic Research in Cardiology *93*, 405-411.

Frank, K.F., Bölck, B., Brixius, K., Kranias, E.G., and Schwinger, R.H. (2002). Modulation of SERCA: implications for the failing human heart. Basic Research in Cardiology *97*, I72-I78.

Frey, N., Katus, H.A., Olson, E.N., and Hill, J.A. (2004). Hypertrophy of the heart a new therapeutic target? Circulation *109*, 1580-1589.

Friedman, D.W., Boyd, C.D., Norton, P., Greco, R.S., Boyarsky, A.H., Mackenzie, J.W., and Deak, S.B. (1993). Increases in type III collagen gene expression and protein synthesis in patients with inguinal hernias. Annals of Surgery *218*, 754.

Fujita, S., and Endoh, M. (1999). Influence of a Na^{+}-H^{+} exchange inhibitor ethylisopropylamiloride, a Na^{+}-Ca^{2+} exchange inhibitor KB-R7943 and their combination on the increases in contractility and Ca^{2+} transient induced by angiotensin II in isolated adult rabbit ventricular myocytes. Naunyn-Schmiedeberg's Archives of Pharmacology *360*, 575-584.

Fukuta, Y., Yoshizumi, M., Kitagawa, T., Hori, T., Chikugo, F., Kawahito, T., Katoh, I., Houchi, H., and Oka, M. (1996). Angiotensin II as a stimulator of Na^{+}-dependent Ca^{2+} efflux from freshly isolated adult rat cardiomyocytes. Neuroscience Letters *213*, 95-98.

Fukuta, Y., Yoshizumi, M., Kitagawa, T., Hori, T., Katoh, I., Houchi, H., and Tamaki, T. (1998). Effect of angiotensin II on Ca^{2+} efflux from freshly isolated adult rat cardiomyces: Possible involvement of Na^{+}-Ca^{2+} exchanger. Biochemical Pharmacology *55*, 481-487.

Gaggar, A., Shayakhmetov, D.M., Liszewski, M.K., Atkinson, J.P., and Lieber, A. (2005). Localization of regions in CD46 that interact with adenovirus. Journal of Virology *79*, 7503-7513.

Ganz, W. (1985). The thrombolysis in myocardial infarction (TIMI) trial. The New England Journal of Medicine *313*, 1018.

Gao, G.-P., Alvira, M.R., Wang, L., Calcedo, R., Johnston, J., and Wilson, J.M. (2002). Novel adeno-associated viruses from rhesus monkeys as vectors for human gene therapy. Proceedings of the National Academy of Sciences *99*, 11854-11859.

Gao, G., Vandenberghe, L.H., Alvira, M.R., Lu, Y., Calcedo, R., Zhou, X., and Wilson, J.M. (2004). Clades of adeno-associated viruses are widely disseminated in human tissues. Journal of Virology *78*, 6381-6388.

Gao, X.-M., Dart, A.M., Dewar, E., Jennings, G., and Du, X.-J. (2000). Serial echocardiographic assessment of left ventricular dimensions and function after myocardial infarction in mice. Cardiovascular Research *45*, 330-338.

Gao, X.-M., Ming, Z., Su, Y., Fang, L., Kiriazis, H., Xu, Q., Dart, A.M., and Du, X.-J. (2010). Infarct size and post-infarct inflammation determine the risk of cardiac rupture in mice. International Journal of Cardiology *143*, 20-28.

Garrido, A.M., and Griendling, K.K. (2009). NADPH oxidases and angiotensin II receptor signaling. Molecular and Cellular Endocrinology *302*, 148-158.

Garza, M.A., Wason, E.A., and Zhang, J.Q. (2015). Cardiac remodeling and physical training post myocardial infarction. World Journal of Cardiology *7*, 62-54.

Gehrmann, J., Frantz, S., Maguire, C.T., Vargas, M., Ducharme, A., Wakimoto, H., Lee, R.T., and Berul, C.I. (2001). Electrophysiological characterization of murine myocardial ischemia and infarction. Basic Research in Cardiology *96*, 237-250.

Gerdes, A.M. (1997). A reliable, efficient, and comprehensive approach to assess myocyte remodeling in cardiac hypertrophy and failure. Journal of Cardiac Failure *3*, 63-68.

Ghosh, A., Yue, Y., Long, C., Bostick, B., and Duan, D. (2007). Efficient whole-body transduction with trans-splicing adeno-associated viral vectors. Molecular Therapy *15*, 750-755.

Giani, J.F., Gironacci, M.M., Muñoz, M.C., Peña, C., Turyn, D., and Dominici, F.P. (2007). Angiotensin-(1–7) stimulates the phosphorylation of JAK2, IRS-1 and Akt in rat heart *in vivo*: role of the AT1 and Mas receptors. American Journal of Physiology *293*, 1154-1163.

Giani, J.F., Gironacci, M.M., Muñoz, M.C., Turyn, D., and Dominici, F.P. (2008). Angiotensin-(1–7) has a dual role on growth-promoting signalling pathways in rat heart *in vivo* by stimulating STAT3 and STAT5a/b phosphorylation and inhibiting angiotensin II-stimulated ERK1/2 and Rho kinase activity. Experimental Physiology *93*, 570-578.

Gilgenkrantz, H., Duboc, D., Juillard, V., Couton, D., Pavirani, A., Guillet, J., Briand, P., and Kahn, A. (1995). Transient expression of genes transferred *in vivo* into heart using first-generation adenoviral vectors: role of the immune response. Human Gene Therapy *6*, 1265-1274.

Gilmour, R.F., and Moïse, S. (1996). Triggered activity as a mechanism for inherited ventricular arrhythmias in German shepherd dogs. Journal of the American College of Cardiology *27*, 1526-1533.

Girod, A., Wobus, C.E., Zádori, Z., Ried, M., Leike, K., Tijssen, P., Kleinschmidt, J.A., and Hallek, M. (2002). The VP1 capsid protein of adeno-associated virus

type 2 is carrying a phospholipase A2 domain required for virus infectivity. Journal of General Virology *83*, 973-978.

Gohlke, P., Pees, C., and Unger, T. (1998). AT2 receptor stimulation increases aortic cyclic GMP in SHRSP by a kinin-dependent mechanism. Hypertension *31*, 349-355.

Gomes, E.R., Lara, A.A., Almeida, P.W., Guimarães, D., Resende, R.R., Campagnole-Santos, M.J., Bader, M., Santos, R.A., and Guatimosim, S. (2010). Angiotensin-(1-7) prevents cardiomyocyte pathological remodeling through a nitric oxide/guanosine 3′, 5′-cyclic monophosphate–dependent pathway. Hypertension *55*, 153-160.

Gomez, A., Guatimosim, S., Dilly, K., Vassort, G., and Lederer, W. (2001). Heart failure after myocardial infarction altered excitation-contraction coupling. Circulation *104*, 688-693.

Gomez, A., Valdivia, H., Cheng, H., Lederer, M.R., Santana, L., Cannell, M., McCune, S., Altschuld, R., and Lederer, W. (1997). Defective excitation-contraction coupling in experimental cardiac hypertrophy and heart failure. Science *276*, 800-806.

Goncalves, M. (2005). Adeno-associated virus: from defective virus to effective vector. Virol J *2*, 517-534.

Gotzmann, M., Lindstaedt, M., and Mügge, A. (2012). From pressure overload to volume overload: aortic regurgitation after transcatheter aortic valve implantation. American Heart Journal *163*, 903-911.

Goulter, A.B., Goddard, M.J., Allen, J.C., and Clark, K.L. (2004). ACE2 gene expression is up-regulated in the human failing heart. BMC Medicine *2*, 19.

Graham, F., Smiley, J., Russell, W., and Nairn, R. (1977). Characteristics of a human cell line transformed by DNA from human adenovirus type 5. Journal of General Virology *36*, 59-72.

Graham, F.L., and Prevec, L. (1991). Manipulation of adenovirus vectors. Gene Transfer and Expression Protocols (Springer), pp. 109-128.

Gray, M.O., Long, C.S., Kalinyak, J.E., Li, H.-T., and Karliner, J.S. (1998). Angiotensin II stimulates cardiac myocyte hypertrophy via paracrine release of TGF-β1 and endothelin-1 from fibroblasts. Cardiovascular Research *40*, 352-363.

Greber, U.F., Willetts, M., Webster, P., and Helenius, A. (1993). Stepwise dismantling of adenovirus 2 during entry into cells. Cell *75*, 477-486.

Greene, L.J., Spadaro, A., Martins, A.R., De Jesus, W.P., and Camargo, A. (1982). Brain endo-oligopeptidase B: a post-proline cleaving enzyme that inactivates angiotensin I and II. Hypertension *4*, 178-184.

Griendling, K., Delafontaine, P., Rittenhouse, S., Gimbrone, M., and Alexander, R. (1987). Correlation of receptor sequestration with sustained diacylglycerol accumulation in angiotensin II-stimulated cultured vascular smooth muscle cells. Journal of Biological Chemistry *262*, 14555-14562.

Griendling, K.K., Sorescu, D., and Ushio-Fukai, M. (2000). NAD (P) H oxidase role in cardiovascular biology and disease. Circulation Research *86*, 494-501.

Grines, C.L., Watkins, M.W., Helmer, G., Penny, W., Brinker, J., Marmur, J.D., West, A., Rade, J.J., Marrott, P., and Hammond, H.K. (2002). Angiogenic Gene Therapy (AGENT) trial in patients with stable angina pectoris. Circulation *105*, 1291-1297.

Grines, C.L., Watkins, M.W., Mahmarian, J.J., Iskandrian, A.E., Rade, J.J., Marrott, P., Pratt, C., and Kleiman, N. (2003). A randomized, double-blind, placebo-controlled trial of Ad5FGF-4 gene therapy and its effect on myocardial perfusion in patients with stable angina. Journal of the American College of Cardiology *42*, 1339-1347.

Grobe, J., Der Sarkissian, S., Stewart, J., Meszaros, J., Raizada, M., and Katovich, M. (2007). ACE2 overexpression inhibits hypoxia-induced collagen production by cardiac fibroblasts. Clinical Science *113*, 357-364.

Grobe, J.L., Mecca, A.P., Mao, H., and Katovich, M.J. (2006). Chronic angiotensin-(1–7) prevents cardiac fibrosis in DOCA-salt model of hypertension. American Journal of Physiology-Heart and Circulatory Physiology *290*, H2417-H2423.

Grynkiewicz, G., Poenie, M., and Tsien, R.Y. (1985). A new generation of Ca^{2+} indicators with greatly improved fluorescence properties. Journal of Biological Chemistry *260*, 3440-3450.

Gunasegaram, S., Haworth, R.S., Hearse, D.J., and Avkiran, M. (1999). Regulation of sarcolemmal Na+/H+ exchanger activity by angiotensin II in adult rat ventricular myocytes opposing actions via AT1 versus AT2 receptors. Circulation Research *85*, 919-930.

Guzman, R.J., Lemarchand, P., Crystal, R.G., Epstein, S.E., and Finkel, T. (1993). Efficient gene transfer into myocardium by direct injection of adenovirus vectors. Circulation Research *73*, 1202-1207.

Gwathmey, J., Slawsky, M., Hajjar, R., Briggs, G., and Morgan, J. (1990). Role of intracellular Ca^{2+} handling in force-interval relationships of human ventricular myocardium. Journal of Clinical Investigation *85*, 1599.

Gwathmey, J.K., Copelas, L., MacKinnon, R., Schoen, F.J., Feldman, M.D., Grossman, W., and Morgan, J.P. (1987). Abnormal intracellular Ca^{2+} handling in myocardium from patients with end-stage heart failure. Circulation Research *61*, 70-76.

Habiyakare, B., Alsaadon, H., Mathai, M.L., Hayes, A., and Zulli, A. (2014). Reduction of angiotensin A and alamandine vasoactivity in the rabbit model of atherogenesis: differential effects of alamandine and Ang (1-7). International Journal of Experimental Pathology *95*, 290-295.

Hahn, A.W., Resink, T.J., Kern, F., and Bühler, F.R. (1993). Peptide vasoconstrictors, vessel structure, and vascular smooth-muscle proliferation. Journal of Cardiovascular Pharmacology *22*, 37-43.

Haithcock, D., Jiao, H., Cui, X.-L., Hopfer, U., and Douglas, J.G. (1999). Renal proximal tubular AT2 receptor: signaling and transport. Journal of the American Society of Nephrology: JASN *10*, S69-74.

Hajjar, R.J., Zsebo, K., Deckelbaum, L., Thompson, C., Rudy, J., Yaroshinsky, A., Ly, H., Kawase, Y., Wagner, K., and Borow, K. (2008). Design of a phase 1/2 trial of intracoronary administration of AAV1/SERCA2a in patients with heart failure. Journal of Cardiac Failure *14*, 355-367.

Hall, J. (1986). Control of sodium excretion by angiotensin II: intrarenal mechanisms and blood pressure regulation. American Journal of Physiology-Regulatory, Integrative and Comparative Physiology *250*, R960-R972.

Handa, R.K. (2000). Metabolism alters the selectivity of angiotensin-(1-7) receptor ligands for angiotensin receptors. Journal of the American Society of Nephrology *11*, 1377-1386.

Harada, K., Sugaya, T., Murakami, K., Yazaki, Y., and Komuro, I. (1999). Angiotensin II type 1A receptor knockout mice display less left ventricular remodeling and improved survival after myocardial infarction. Circulation *100*, 2093-2099.

Harmer, D., Gilbert, M., Borman, R., and Clark, K.L. (2002). Quantitative mRNA expression profiling of ACE 2, a novel homologue of angiotensin converting enzyme. FEBS Letters *532*, 107-110.

Hasenfuss, G. (1998). Alterations of calcium-regulatory proteins in heart failure. Cardiovascular Research *37*, 279-289.

Hasenfuss, G., Reinecke, H., Studer, R., Meyer, M., Pieske, B., Holtz, J., Holubarsch, C., Posival, H., Just, H., and Drexler, H. (1994). Relation between myocardial function and expression of sarcoplasmic reticulum Ca^{2+}-ATPase in failing and nonfailing human myocardium. Circulation Research *75*, 434-442.

Hattori, T., Shimokawa, H., Higashi, M., Hiroki, J., Mukai, Y., Tsutsui, H., Kaibuchi, K., and Takeshita, A. (2004). Long-term inhibition of Rho-kinase

suppresses left ventricular remodeling after myocardial infarction in mice. Circulation *109*, 2234-2239.

Hauck, B., Zhao, W., High, K., and Xiao, W. (2004). Intracellular viral processing, not single-stranded DNA accumulation, is crucial for recombinant adeno-associated virus transduction. Journal of Virology *78*, 13678-13686.

Havenga, M., Lemckert, A., Grimbergen, J., Vogels, R., Huisman, L., Valerio, D., Bout, A., and Quax, P. (2001). Improved adenovirus vectors for infection of cardiovascular tissues. Journal of Virology *75*, 3335-3342.

Havenga, M., Lemckert, A., Ophorst, O., Van Meijer, M., Germeraad, W., Grimbergen, J., van Den Doel, M., Vogels, R., Van Deutekom, J., and Janson, A. (2002). Exploiting the natural diversity in adenovirus tropism for therapy and prevention of disease. Journal of Virology *76*, 4612-4620.

Hay, R.T. (1985). Origin of adenovirus DNA replication: Role of the nuclear factor I binding site *in vivo*. Journal of Molecular Biology *186*, 129-136.

Haywood, G.A., Gullestad, L., Katsuya, T., Hutchinson, H.G., Pratt, R.E., Horiuchi, M., and Fowler, M.B. (1997). AT1 and AT2 angiotensin receptor gene expression in human heart failure. Circulation *95*, 1201-1206.

Hedman, M., Hartikainen, J., Syvänne, M., Stjernvall, J., Hedman, A., Kivelä, A., Vanninen, E., Mussalo, H., Kauppila, E., and Simula, S. (2003). Safety and feasibility of catheter-based local intracoronary vascular endothelial growth factor gene transfer in the prevention of postangioplasty and in-stent restenosis and in the treatment of chronic myocardial ischemia phase II results of the Kuopio Angiogenesis Trial (KAT). Circulation *107*, 2677-2683.

Helmes, M., Lim, C.C., Liao, R., Bharti, A., Cui, L., and Sawyer, D.B. (2003). Titin determines the Frank-Starling relation in early diastole. The Journal of General Physiology *121*, 97-110.

Henrion, D. (2012). Why do we need a selective angiotensin II type 2 receptor agonist? Hypertension *60*, 616-617.

Heringer-Walther, S., Eckert, K., Schumacher, S.-M., Uharek, L., Wulf-Goldenberg, A., Gembardt, F., Fichtner, I., Schultheiss, H.-P., Rodgers, K., and Walther, T. (2009). Angiotensin-(1–7) stimulates hematopoietic progenitor cells *in vitro* and *in vivo*. Haematologica *94*, 857-860.

Hermonat, P.L., and Muzyczka, N. (1984). Use of adeno-associated virus as a mammalian DNA cloning vector: transduction of neomycin resistance into mammalian tissue culture cells. Proceedings of the National Academy of Sciences *81*, 6466-6470.

Hernandez-Hernandez, R., Sosa-Canache, B., Velasco, M., Armas-Hernandez, M., Armas-Padilla, M., and Cammarata, R. (2002). Angiotensin II receptor antagonists role in arterial hypertension. Journal of Human Hypertension *16*, S93-99.

Hernandez, Y.J., Wang, J., Kearns, W.G., Loiler, S., Poirier, A., and Flotte, T.R. (1999). Latent adeno-associated virus infection elicits humoral but not cell-mediated immune responses in a nonhuman primate model. Journal of Virology *73*, 8549-8558.

Hingtgen, S.D., Tian, X., Yang, J., Dunlay, S.M., Peek, A.S., Wu, Y., Sharma, R.V., Engelhardt, J.F., and Davisson, R.L. (2006). Nox2-containing NADPH oxidase and Akt activation play a key role in angiotensin II-induced cardiomyocyte hypertrophy. Physiological Genomics *26*, 180-191.

Ho, K., Anderson, K.M., Kannel, W.B., Grossman, W., and Levy, D. (1993). Survival after the onset of congestive heart failure in Framingham Heart Study subjects. Circulation *88*, 107-115.

Hobai, I.A., and O'Rourke, B. (2001). Decreased sarcoplasmic reticulum calcium content is responsible for defective excitation-contraction coupling in canine heart failure. Circulation *103*, 1577-1584.

Hodsman, G., Kohzuki, M., Howes, L., Sumithran, E., Tsunoda, K., and Johnston, C. (1988). Neurohumoral responses to chronic myocardial infarction in rats. Circulation *78*, 376-381.

Hoit, B.D., and Walsh, R.A. (1997). *In vivo* echocardiographic assessment of left ventricular function in transgenic and gene-targeted mice. Trends in Cardiovascular Medicine *7*, 129-134.

Hood, W.B., McCarthy, B., and Lown, B. (1967). Myocardial infarction following coronary ligation in dogs hemodynamic effects of isoproterenol and acetylstrophanthidin. Circulation Research *21*, 191-200.

Horiuchi, M., Hayashida, W., Kambe, T., Yamada, T., and Dzau, V.J. (1997). Angiotensin type 2 receptor dephosphorylates Bcl-2 by activating mitogen-activated protein kinase phosphatase-1 and induces apoptosis. Journal of Biological Chemistry *272*, 19022-19026.

Houser, S.R., Piacentino III, V., and Weisser, J. (2000). Abnormalities of calcium cycling in the hypertrophied and failing heart. Journal of Molecular and Cellular Cardiology *32*, 1595-1607.

Hove-Madsen, L., and Bers, D.M. (1993). Sarcoplasmic reticulum Ca^{2+} uptake and thapsigargin sensitivity in permeabilized rabbit and rat ventricular myocytes. Circulation Research *73*, 820-828.

Huang, B., Wang, S., Qin, D., Boutjdir, M., and El-Sherif, N. (1999). Diminished basal phosphorylation level of phospholamban in the postinfarction remodeled rat ventricle role of ß-adrenergic pathway, Gi protein, phosphodiesterase, and phosphatases. Circulation Research *85*, 848-855.

Huang, D., Wang, Y., Yang, C., Liao, Y., and Huang, K. (2009). Angiotensin II promotes poly (ADP-ribosyl) ation of c-Jun/c-Fos in cardiac fibroblasts. Journal of Molecular and Cellular Cardiology *46*, 25-32.

Huentelman, M.J., Grobe, J.L., Vazquez, J., Stewart, J.M., Mecca, A.P., Katovich, M.J., Ferrario, C.M., and Raizada, M.K. (2005). Protection from angiotensin II-induced cardiac hypertrophy and fibrosis by systemic lentiviral delivery of ACE2 in rats. Experimental Physiology *90*, 783-790.

Hunton, D.L., Lucchesi, P.A., Pang, Y., Cheng, X., Dell'Italia, L.J., and Marchase, R.B. (2002). Capacitative calcium entry contributes to nuclear factor of activated T-cells nuclear translocation and hypertrophy in cardiomyocytes. Journal of Biological Chemistry *277*, 14266-14273.

Ibrahim, M.M. (2006). RAS inhibition in hypertension. Journal of Human Hypertension *20*, 101-108.

Ichihara, S., Senbonmatsu, T., Price, E., Ichiki, T., Gaffney, F.A., and Inagami, T. (2001). Angiotensin II type 2 receptor is essential for left ventricular hypertrophy and cardiac fibrosis in chronic angiotensin II–induced hypertension. Circulation *104*, 346-351.

Ichiki, T., Labosky, P.A., Shiota, C., Okuyama, S., Imagawa, Y., Fogo, A., Niimura, F., Ichikawa, I., and Hogan, B.L. (1995). Effects on blood pressure and exploratory behaviour of mice lacking angiotensin II type-2 receptor.

Ihara, M., Urata, H., Kinoshita, A., Suzumiya, J., Sasaguri, M., Kikuchi, M., Ideishi, M., and Arakawa, K. (1999). Increased chymase-dependent angiotensin II formation in human atherosclerotic aorta. Hypertension *33*, 1399-1405.

Ikenouchi, H., Barry, W.H., Bridge, J., Weinberg, E.O., Apstein, C.S., and Lorell, B.H. (1994). Effects of angiotensin II on intracellular Ca^{2+} and pH in isolated beating rabbit hearts and myocytes loaded with the indicator indo-1. The Journal of Physiology *480*, 203-215.

Inagaki, K., Fuess, S., Storm, T.A., Gibson, G.A., Mctiernan, C.F., Kay, M.A., and Nakai, H. (2006). Robust systemic transduction with AAV9 vectors in mice: efficient global cardiac gene transfer superior to that of AAV8. Molecular Therapy *14*, 45-53.

The E.T.o.R.o.C.E.w.P.i.S.C.A.D Investigators (2003). Efficacy of perindopril in reduction of cardiovascular events among patients with stable coronary artery disease: randomised, double-blind, placebo-controlled, multicentre trial (the EUROPA study). The Lancet *362*, 782-788.

Irani, K. (2000). Oxidant signaling in vascular cell growth, death, and survival a review of the roles of reactive oxygen species in smooth muscle and endothelial cell mitogenic and apoptotic signaling. Circulation Research *87*, 179-183.

Iravanian, S., and Dudley, S.C. (2008). The renin-angiotensin-aldosterone system (RAAS) and cardiac arrhythmias. Heart Rhythm *5*, S12-S17.

Ishiyama, Y., Gallagher, P.E., Averill, D.B., Tallant, E., Brosnihan, K.B., and Ferrario, C.M. (2004). Upregulation of angiotensin-converting enzyme 2 after myocardial infarction by blockade of angiotensin II receptors. Hypertension *43*, 970-976.

Ito, H., Hirata, Y., Adachi, S., Tanaka, M., Tsujino, M., Koike, A., Nogami, A., Murumo, F., and Hiroe, M. (1993). Endothelin-1 is an autocrine/paracrine factor in the mechanism of angiotensin II-induced hypertrophy in cultured rat cardiomyocytes. Journal of Clinical Investigation *92*, 398.

Ito, M., Oliverio, M.I., Mannon, P.J., Best, C.F., Maeda, N., Smithies, O., and Coffman, T.M. (1995). Regulation of blood pressure by the type 1A angiotensin II receptor gene. Proceedings of the National Academy of Sciences *92*, 3521-3525.

Iwanaga, K., Takano, H., Ohtsuka, M., Hasegawa, H., Zou, Y., Qin, Y., Odaka, K., Hiroshima, K., Tadokoro, H., and Komuro, I. (2004). Effects of G-CSF on cardiac remodeling after acute myocardial infarction in swine. Biochemical and Biophysical Research Communications *325*, 1353-1359.

Iwata, M., Cowling, R.T., Gurantz, D., Moore, C., Zhang, S., Yuan, J.X.-J., and Greenberg, B.H. (2005). Angiotensin-(1–7) binds to specific receptors on cardiac fibroblasts to initiate antifibrotic and antitrophic effects. American Journal of Physiology-Heart and Circulatory Physiology *289*, H2356-H2363.

Jackman, H.L., Massad, M.G., Sekosan, M., Tan, F., Brovkovych, V., Marcic, B.M., and Erdös, E.G. (2002). Angiotensin 1-9 and 1-7 release in human heart role of cathepsin A. Hypertension *39*, 976-981.

Jain, M., Liao, R., Podesser, B.K., Ngoy, S., Apstein, C.S., and Eberli, F.R. (2002). Influence of gender on the response to hemodynamic overload after myocardial infarction. American Journal of Physiology-Heart and Circulatory Physiology *283*, H2544-H2550.

Janicki, J., Shroff, S., Pick, R., Chen, R., and Bashey, R. (1988). Collagen remodeling of the pressure-overloaded, hypertrophied non-human primate myocardium. Circ Res *62*, 757.

Janik, J.E., Huston, M.M., and Rose, J.A. (1981). Locations of adenovirus genes required for the replication of adenovirus-associated virus. Proceedings of the National Academy of Sciences *78*, 1925-1929.

Jankowski, V., Vanholder, R., van der Giet, M., Tölle, M., Karadogan, S., Gobom, J., Furkert, J., Oksche, A., Krause, E., and Tran, T.N.A. (2007). Mass-spectrometric identification of a novel angiotensin peptide in human plasma. Arteriosclerosis, Thrombosis, and Vascular Biology *27*, 297-302.

Jansen, M., Van Echteld, C., and Ruigrok, T. (1998). Na^+/Ca^{2+} exchange during Ca^{2+} repletion is not a prerequisite for the Ca^{2+} paradox in isolated rat hearts. Pflügers Archiv *436*, 515-520.

Janssen, P.M. (2010). Kinetics of cardiac muscle contraction and relaxation are linked and determined by properties of the cardiac sarcomere. American Journal of Physiology-Heart and Circulatory Physiology *299*, H1092-H1099.

Janssens, S., Pokreisz, P., Schoonjans, L., Pellens, M., Vermeersch, P., Tjwa, M., Jans, P., Scherrer-Crosbie, M., Picard, M.H., and Szelid, Z. (2004). Cardiomyocyte-specific overexpression of nitric oxide synthase 3 improves left ventricular performance and reduces compensatory hypertrophy after myocardial infarction. Circulation Research *94*, 1256-1262.

Jaski, B.E., Jessup, M.L., Mancini, D.M., Cappola, T.P., Pauly, D.F., Greenberg, B., Borow, K., Dittrich, H., Zsebo, K.M., and Hajjar, R.J. (2009). Calcium upregulation by percutaneous administration of gene therapy in cardiac disease

(CUPID Trial), a first-in-human phase 1/2 clinical trial. Journal of Cardiac Failure *15*, 171-181.

Jehle, A.B., Xu, Y., DiMaria, J.M., French, B.A., Epstein, F.H., Berr, S.S., Roy, R.J., Kemp, B.A., Carey, R.M., and Kramer, C.M. (2012). A non-peptide angiotensin II type 2 receptor agonist does not attenuate post-myocardial infarction left ventricular remodeling in mice. Journal of Cardiovascular Pharmacology *59*, 363.

Jessup, M., Greenberg, B., Mancini, D., Cappola, T., Pauly, D.F., Jaski, B., Yaroshinsky, A., Zsebo, K.M., Dittrich, H., and Hajjar, R.J. (2011). Calcium Upregulation by Percutaneous Administration of Gene Therapy in Cardiac Disease (CUPID) A phase 2 trial of intracoronary gene therapy of sarcoplasmic reticulum Ca^{2+}-ATPase in patients with advanced heart failure. Circulation *124*, 304-313.

Johar, S., Cave, A.C., Narayanapanicker, A., Grieve, D.J., and Shah, A.M. (2006). Aldosterone mediates angiotensin II-induced interstitial cardiac fibrosis via a Nox2-containing NADPH oxidase. The FASEB Journal *20*, 1546-1548.

Johnson, F.B., and Dudleenamjil, E. (2012). Clathrin-associated endocytosis as a route of entry into cells for parvoviruses. Biochemistry, Genetics and Molecular Biology: molecular regulation of endocytosis. InTech, DOI 10.5772/48510.

Johnson, H., Kourtis, S., Waters, J., and Drummer, O.H. (1989). Radioimmunoassay for immunoreactive [des-Leu10]-angiotensin I. Peptides *10*, 489-492.

Johnson, J.S., Li, C., DiPrimio, N., Weinberg, M.S., McCown, T.J., and Samulski, R.J. (2010). Mutagenesis of adeno-associated virus type 2 capsid protein VP1 uncovers new roles for basic amino acids in trafficking and cell-specific transduction. Journal of Virology *84*, 8888-8902.

Johnson, J.S., and Samulski, R.J. (2009). Enhancement of adeno-associated virus infection by mobilizing capsids into and out of the nucleolus. Journal of Virology *83*, 2632-2644.

Johnson, M., Huyn, S., Burton, J., Sato, M., and Wu, L. (2006). Differential biodistribution of adenoviral vector *in vivo* as monitored by bioluminescence imaging and quantitative polymerase chain reaction. Human Gene Therapy *17*, 1262-1269.

Jones, E.S., Vinh, A., McCarthy, C.A., Gaspari, T.A., and Widdop, R.E. (2008). AT 2 receptors: functional relevance in cardiovascular disease. Pharmacology & Therapeutics *120*, 292-316.

Joseph, J.P., Mecca, A.P., Regenhardt, R.W., Bennion, D.M., Rodríguez, V., Desland, F., Patel, N.A., Pioquinto, D.J., Unger, T., and Katovich, M.J. (2014). The angiotensin type 2 receptor agonist Compound 21 elicits cerebroprotection in endothelin-1 induced ischemic stroke. Neuropharmacology *81*, 134-141.

Ju, H., Zhao, S., Tappia, P.S., Panagia, V., and Dixon, I.M. (1998). Expression of Gqα and PLC-β in scar and border tissue in heart failure due to myocardial infarction. Circulation *97*, 892-899.

Jugdutt, B.I. (2003). Ventricular remodeling after infarction and the extracellular collagen matrix when is enough enough? Circulation *108*, 1395-1403.

Kadambi, V.J., Ponniah, S., Harrer, J.M., Hoit, B.D., Dorn 2nd, G., Walsh, R.A., and Kranias, E.G. (1996). Cardiac-specific overexpression of phospholamban alters calcium kinetics and resultant cardiomyocyte mechanics in transgenic mice. Journal of Clinical Investigation *97*, 533.

Kaibara, M., Mitarai, S., Yano, K., and Kameyama, M. (1994). Involvement of Na^+-H^+ antiporter in regulation of L-type Ca^{2+} channel current by angiotensin II in rabbit ventricular myocytes. Circulation Research *75*, 1121-1125.

Kajstura, J., Cigola, E., Malhotra, A., Li, P., Cheng, W., Meggs, L.G., and Anversa, P. (1997). Angiotensin II induces apoptosis of adult ventricular myocytesin vitro. Journal of molecular and cellular cardiology *29*, 859-870.

Kaludov, N., Brown, K.E., Walters, R.W., Zabner, J., and Chiorini, J.A. (2001). Adeno-associated virus serotype 4 (AAV4) and AAV5 both require sialic acid binding for hemagglutination and efficient transduction but differ in sialic acid linkage specificity. Journal of Virology *75*, 6884-6893.

Kalyuzhniy, O., Di Paolo, N., Silvestry, M., Hofherr, S., Barry, M., Stewart, P., and Shayakhmetov, D. (2008). Adenovirus serotype 5 hexon is critical for virus infection of hepatocytes *in vivo*. Proceedings of the National Academy of Sciences *105*, 5483-5488.

Kamen, A., and Henry, O. (2004). Development and optimization of an adenovirus production process. The Journal of Gene Medicine *6*, S184-S192.

Kamp, T.J., and Hell, J.W. (2000). Regulation of cardiac L-type calcium channels by protein kinase A and protein kinase C. Circulation Research *87*, 1095-1102.

Kang, S.-M., Lim, S., Song, H., Chang, W., Lee, S., Bae, S.-m., Chung, J.H., Lee, H., Kim, H.-G., and Yoon, D.-H. (2006). Allopurinol modulates reactive oxygen species generation and Ca^{2+} overload in ischemia-reperfused heart and hypoxia-reoxygenated cardiomyocytes. European Journal of Pharmacology *535*, 212-219.

Kania, G., Blyszczuk, P., and Eriksson, U. (2009). Mechanisms of cardiac fibrosis in inflammatory heart disease. Trends in Cardiovascular Medicine *19*, 247-252.

Kannel, W.B., and Belanger, A.J. (1991). Epidemiology of heart failure. American Heart Journal *121*, 951-957.

Kaschina, E., Grzesiak, A., Li, J., Foryst-Ludwig, A., Timm, M., Rompe, F., Sommerfeld, M., Kemnitz, U.R., Curato, C., and Namsolleck, P. (2008). Angiotensin II type 2 receptor stimulation a novel option of therapeutic interference with the renin-angiotensin system in myocardial infarction? Circulation *118*, 2523-2532.

Kaschina, E., Lauer, D., Schmerler, P., Unger, T., and Steckelings, U.M. (2014). AT2 receptors targeting cardiac protection post-myocardial infarction. Current Hypertension Reports *16*, 1-9.

Kaschina, E., and Unger, T. (2003). Angiotensin AT1/AT2 receptors: regulation, signalling and function. Blood Pressure *12*, 70-88.

Kashiwakura, Y., Tamayose, K., Iwabuchi, K., Hirai, Y., Shimada, T., Matsumoto, K., Nakamura, T., Watanabe, M., Oshimi, K., and Daida, H. (2005). Hepatocyte growth factor receptor is a coreceptor for adeno-associated virus type 2 infection. Journal of Virology *79*, 609-614.

Kasi, V.S., Xiao, H.D., Shang, L.L., Iravanian, S., Langberg, J., Witham, E.A., Jiao, Z., Gallego, C.J., Bernstein, K.E., and Dudley, S.C. (2007). Cardiac-restricted angiotensin-converting enzyme overexpression causes conduction defects and connexin dysregulation. American Journal of Physiology-Heart and Circulatory Physiology *293*, H182-H192.

Kassiri, Z., Zhong, J., Guo, D., Basu, R., Wang, X., Liu, P.P., Scholey, J.W., Penninger, J.M., and Oudit, G.Y. (2009). Loss of ACE2 accelerates maladaptive left ventricular remodeling in response to myocardial infarction. Circulation: Heart Failure, 108.840124.

Kato, Y., Masumiya, H., Agata, N., Tanaka, H., and Shigenobu, K. (1996). Developmental changes in action potential and membrane currents in fetal, neonatal and adult guinea-pig ventricular myocytes. Journal of Molecular and Cellular Cardiology *28*, 1515-1522.

Katsube, Y., Yokoshiki, H., Nguyen, L., and Sperelakis, N. (1996). Differences in isoproterenol stimulation of Ca^{2+} current of rat ventricular myocytes in neonatal compared to adult. European Journal of Pharmacology *317*, 391-400.

Katz, A.M. (2010). Physiology of the heart (Lippincott Williams & Wilkins).

Kawase, Y., Ladage, D., and Hajjar, R.J. (2011). Rescuing the failing heart by targeted gene transfer. Journal of the American College of Cardiology *57*, 1169-1180.

Kawase, Y., Ly, H.Q., Prunier, F., Lebeche, D., Shi, Y., Jin, H., Hadri, L., Yoneyama, R., Hoshino, K., and Takewa, Y. (2008). Reversal of cardiac

dysfunction after long-term expression of SERCA2a by gene transfer in a pre-clinical model of heart failure. Journal of the American College of Cardiology *51*, 1112-1119.

Keeley, E.C., Boura, J.A., and Grines, C.L. (2003). Primary angioplasty versus intravenous thrombolytic therapy for acute myocardial infarction: a quantitative review of 23 randomised trials. The Lancet *361*, 13-20.

Kehat, I., Davis, J., Tiburcy, M., Accornero, F., Saba-El-Leil, M.K., Maillet, M., York, A.J., Lorenz, J.N., Zimmermann, W.H., and Meloche, S. (2011). Extracellular signal-regulated kinases 1 and 2 regulate the balance between eccentric and concentric cardiac growth. Circulation Research *108*, 176-183.

Keidar, S., Kaplan, M., and Gamliel-Lazarovich, A. (2007). ACE2 of the heart: from angiotensin I to angiotensin (1–7). Cardiovascular Research *73*, 463-469.

Kennedy, M.A., and Parks, R.J. (2009). Adenovirus virion stability and the viral genome: size matters. Molecular therapy: the Journal of the American Society of Gene Therapy *17*, 1664.

Kijima, K., Matsubara, H., Murasawa, S., Maruyama, K., Ohkubo, N., Mori, Y., and Inada, M. (1996). Regulation of angiotensin II type 2 receptor gene by the protein kinase C–calcium pathway. Hypertension *27*, 529-534.

Kim, J., Ahn, S., Ren, X.-R., Whalen, E.J., Reiter, E., Wei, H., and Lefkowitz, R.J. (2005). Functional antagonism of different G protein-coupled receptor kinases for ß-arrestin-mediated angiotensin II receptor signaling. Proceedings of the National Academy of Sciences of the United States of America *102*, 1442-1447.

Kim, M.-A., Yang, D., Kida, K., Molotkova, N., Yeo, S.J., Varki, N., Iwata, M., Dalton, N.D., Peterson, K.L., and Siems, W.-E. (2010). Effects of ACE2 inhibition in the post-myocardial infarction heart. Journal of Cardiac Failure *16*, 777-785.

Kinugawa, S., Tsutsui, H., Hayashidani, S., Ide, T., Suematsu, N., Satoh, S., Utsumi, H., and Takeshita, A. (2000). Treatment with dimethylthiourea prevents

left ventricular remodeling and failure after experimental myocardial infarction in mice role of oxidative stress. Circulation Research *87*, 392-398.

Klabunde, R. (2011). Cardiovascular physiology concepts (Lippincott Williams & Wilkins).

Klocke, R., Tian, W., Kuhlmann, M.T., and Nikol, S. (2007). Surgical animal models of heart failure related to coronary heart disease. Cardiovascular Research *74*, 29-38.

Koh, K.K., Ahn, J.Y., Han, S.H., Kim, D.S., Jin, D.K., Kim, H.S., Shin, M.-S., Ahn, T.H., Choi, I.S., and Shin, E.K. (2003). Pleiotropic effects of angiotensin II receptor blocker in hypertensive patients. Journal of the American College of Cardiology *42*, 905-910.

Kohout, T.A., and Rogers, T.B. (1995). Angiotensin II activates the Na+/HCO3− symport through a phosphoinositide-independent mechanism in cardiac cells. Journal of Biological Chemistry *270*, 20432-20438.

Kojima, A., Kitagawa, H., Omatsu-Kanbe, M., Matsuura, H., and Nosaka, S. (2010). Ca^{2+} paradox injury mediated through TRPC channels in mouse ventricular myocytes. British Journal of Pharmacology *161*, 1734-1750.

Kokkonen, J.O., Saarinen, J., and Kovanen, P.T. (1997). Regulation of local angiotensin II formation in the human heart in the presence of interstitial fluid inhibition of chymase by protease inhibitors of interstitial fluid and of angiotensin-converting enzyme by Ang-(1-9) formed by heart carboxypeptidase A–Like activity. Circulation *95*, 1455-1463.

Kono, T. (1969). Roles of collagenases and other proteolytic enzymes in the dispersal of animal tissues. Biochimica et Biophysica Acta (BBA)-Enzymology *178*, 397-400.

Kotin, R.M., Menninger, J.C., Ward, D.C., and Berns, K.I. (1991). Mapping and direct visualization of a region-specific viral DNA integration site on chromosome 19q13-qter. Genomics *10*, 831-834.

Kotterman, M.A., Koerber, J.T., Nam, J.-s., Cho, Y.-h., Kim, S.-h., Jang, J.-h., and Lim, K.-i. (2015). Enhanced cellular secretion of AAV2 by expression of foreign viral envelope proteins. Biochemical Engineering Journal *93*, 108-114.

Kozarsky, K.F., and Wilson, J.M. (1993). Gene therapy: adenovirus vectors. Current Opinion in Genetics & Development *3*, 499-503.

Kramkowski, K., Mogielnicki, A., Leszczynska, A., and Buczko, W. (2010). Angiotensin-(1-9), the product of angiotensin I conversion in platelets, enhances arterial thrombosis in rats. Journal of Physiology and Pharmacology *61*, 317.

Krishnamurthy, P., Subramanian, V., Singh, M., and Singh, K. (2006). Deficiency of ß1 integrins results in increased myocardial dysfunction after myocardial infarction. Heart *92*, 1309-1315.

Kudoh, S., Komuro, I., Mizuno, T., Yamazaki, T., Zou, Y., Shiojima, I., Takekoshi, N., and Yazaki, Y. (1997). Angiotensin II stimulates c-Jun NH2-terminal kinase in cultured cardiac myocytes of neonatal rats. Circulation Research *80*, 139-146.

Kuhlmann, M.T., Kirchhof, P., Klocke, R., Hasib, L., Stypmann, J., Fabritz, L., Stelljes, M., Tian, W., Zwiener, M., and Mueller, M. (2006). G-CSF/SCF reduces inducible arrhythmias in the infarcted heart potentially via increased connexin43 expression and arteriogenesis. The Journal of Experimental Medicine *203*, 87-97.

Kumar, A., and Cannon, C.P. (2009). Acute Coronary Syndromes: Diagnosis and Management, Part I. Mayo Clinic Proceedings *84*, 917-938.

Lai, C.M., Lai, Y.K., and Rakoczy, P.E. (2002). Adenovirus and adeno-associated virus vectors. DNA and Cell Biology *21*, 895-913.

Laitinen, M., Pakkanen, T., Donetti, E., Baetta, R., Luoma, J., Lehtolainen, P., Viita, H., Agrawal, R., Miyanohara, A., and Friedmann, T. (1997). Gene transfer into the carotid artery using an adventitial collar: comparison of the effectiveness of the plasmid-liposome complexes, retroviruses, pseudotyped retroviruses, and adenoviruses. Human Gene Therapy *8*, 1645-1650.

Lakshmanan, A.P., Watanabe, K., Thandavarayan, R.A., Sari, F.R., Harima, M., Giridharan, V.V., Soetikno, V., Kodama, M., and Aizawa, Y. (2011). Telmisartan attenuates oxidative stress and renal fibrosis in streptozotocin induced diabetic mice with the alteration of angiotensin-(1-7) mas receptor expression associated with its PPAR-γ agonist action. Free Radical Research *45*, 575-584.

Lassegue, B., Alexander, R.W., Nickenig, G., Clark, M., Murphy, T., and Griendling, K.K. (1995). Angiotensin II down-regulates the vascular smooth muscle AT1 receptor by transcriptional and post-transcriptional mechanisms: evidence for homologous and heterologous regulation. Molecular Pharmacology *48*, 601-609.

Lassègue, B., Sorescu, D., Szöcs, K., Yin, Q., Akers, M., Zhang, Y., Grant, S.L., Lambeth, J.D., and Griendling, K.K. (2001). Novel gp91phox homologues in vascular smooth muscle cells nox1 mediates angiotensin II–induced superoxide formation and redox-sensitive signaling pathways. Circulation Research *88*, 888-894.

Lauer, D., Slavic, S., Sommerfeld, M., Thöne-Reineke, C., Sharkovska, Y., Hallberg, A., Dahlöf, B., Kintscher, U., Unger, T., and Steckelings, U.M. (2014). Angiotensin type 2 receptor stimulation ameliorates left ventricular fibrosis and dysfunction via regulation of tissue inhibitor of matrix metalloproteinase 1/matrix metalloproteinase 9 axis and transforming growth factor ß1 in the rat heart. Hypertension *63*, e60-e67.

Lautner, R.Q., Villela, D.C., Fraga-Silva, R.A., Silva, N., Verano-Braga, T., Costa-Fraga, F., Jankowski, J., Jankowski, V., Sousa, F., and Alzamora, A. (2013). Discovery and Characterization of Alamandine A Novel Component of the Renin–Angiotensin System. Circulation Research *112*, 1104-1111.

Leach, R., Desai, J., and Orchard, C. (2005). Effect of cytoskeleton disruptors on L-type Ca^{2+} channel distribution in rat ventricular myocytes. Cell Calcium *38*, 515-526.

Lee, A.A., Dillmann, W.H., McCulloch, A.D., and Villarreal, F.J. (1995). Angiotensin II stimulates the autocrine production of transforming growth factor-

ß1 in adult rat cardiac fibroblasts. Journal of molecular and cellular cardiology *27*, 2347-2357.

Lee, M.A., Böhm, M., Paul, M., and Ganten, D. (1993). Tissue renin-angiotensin systems. Their role in cardiovascular disease. Circulation *87*, IV7-13.

Lee, Y.-M., Peng, Y.-Y., Ding, Y.-A., and Yen, M.-H. (1997). Losartan attenuates myocardial ischemia-induced ventricular arrhythmias and reperfusion injury in spontaneously hypertensive rats. American Journal of Hypertension *10*, 852-858.

Lefroy, D., Crake, T., Del Monte, F., Vescovo, G., Dalla Libera, L., Harding, S., and Poole-Wilson, P. (1996). Angiotensin II and contraction of isolated myocytes from human, guinea pig, and infarcted rat hearts. American Journal of Physiology-Heart and Circulatory Physiology *270*, H2060-H2069.

Lehnart, S.E., Terrenoire, C., Reiken, S., Wehrens, X.H., Song, L.-S., Tillman, E.J., Mancarella, S., Coromilas, J., Lederer, W., and Kass, R.S. (2006). Stabilization of cardiac ryanodine receptor prevents intracellular calcium leak and arrhythmias. Proceedings of the National Academy of Sciences *103*, 7906-7910.

Lemmens, K., Segers, V.F., Demolder, M., Michiels, M., Van Cauwelaert, P., and De Keulenaer, G.W. (2007). Endogenous inhibitors of hypertrophy in concentric versus eccentric hypertrophy. European Journal of Heart Failure *9*, 352-356.

Levitsky, D., De La Bastie, D., Schwartz, K., and Lompré, A.-M. (1991). Ca^{2+}-ATPase and function of sarcoplasmic reticulum during cardiac hypertrophy. Am J Physiol *261*, 23-26.

Levy, M.N., and Wiseman, M.N. (1991). Electrophysiologic mechanisms for ventricular arrhythmias in left ventricular dysfunction: electrolytes, catecholamines and drugs. The Journal of Clinical Pharmacology *31*, 1053-1060.

Li, D., Wu, J., Bai, Y., Zhao, X., and Liu, L. (2014). Isolation and culture of adult mouse cardiomyocytes for cell signaling and in vitro cardiac hypertrophy. JoVE (Journal of Visualized Experiments), e51357-e51357.

Li, S.-Y., Yang, X., Ceylan-Isik, A., Du, M., Sreejayan, N., and Ren, J. (2006a). Cardiac contractile dysfunction in Lep/Lep obesity is accompanied by NADPH oxidase activation, oxidative modification of sarco (endo) plasmic reticulum Ca^{2+}-ATPase and myosin heavy chain isozyme switch. Diabetologia *49*, 1434-1446.

Li, W., Ye, Y., Fu, B., Wang, J., Yu, L., Ichiki, T., Inagami, T., Ichikawa, I., and Chen, X. (1998). Genetic deletion of AT2 receptor antagonizes angiotensin II-induced apoptosis in fibroblasts of the mouse embryo. Biochemical and Biophysical Research Communications *250*, 72-76.

Li, Y., Takemura, G., Okada, H., Miyata, S., Maruyama, R., Li, L., Higuchi, M., Minatoguchi, S., Fujiwara, T., and Fujiwara, H. (2006b). Reduction of inflammatory cytokine expression and oxidative damage by erythropoietin in chronic heart failure. Cardiovascular Research *71*, 684-694.

Libby, P., and Theroux, P. (2005). Pathophysiology of coronary artery disease. Circulation *111*, 3481-3488.

Lichtenstein, D.L., and Wold, W.S. (2004). Experimental infections of humans with wild-type adenoviruses and with replication-competent adenovirus vectors: replication, safety, and transmission. Cancer Gene Therapy *11*, 819-829.

Lijnen, P., and Petrov, V. (1999). Renin-angiotensin system, hypertrophy and gene expression in cardiac myocytes. Journal of Molecular and Cellular Cardiology *31*, 949-970.

Lijnen, P., Petrov, V., and Fagard, R. (2000). Induction of cardiac fibrosis by angiotensin II. Methods Find Exp Clin Pharmacol *22*, 709-723.

Litwin, S.E., Zhang, D., and Bridge, J.H. (2000). Dyssynchronous Ca^{2+} sparks in myocytes from infarcted hearts. Circulation Research *87*, 1040-1047.

Liu, E., Yang, S., Xu, Z., Li, J., Yang, W., and Li, G. (2010a). Angiotensin-(1–7) prevents atrial fibrosis and atrial fibrillation in long-term atrial tachycardia dogs. Regulatory Peptides *162*, 73-78.

Liu, J., Pang, Y., Chang, T., Bounelis, P., Chatham, J.C., and Marchase, R.B. (2006). Increased hexosamine biosynthesis and protein O-GlcNAc levels associated with myocardial protection against calcium paradox and ischemia. Journal of Molecular and Cellular Cardiology *40*, 303-312.

Liu, Q., Anderson, C., Broyde, A., Polizzi, C., Fernandez, R., Baron, A., and Parkes, D.G. (2010b). Glucagon-like peptide-1 and the exenatide analogue AC3174 improve cardiac function, cardiac remodeling, and survival in rats with chronic heart failure. Cardiovasc Diabetol *9*, 76.

Liu, Q., and Muruve, D. (2003). Molecular basis of the inflammatory response to adenovirus vectors. Gene Therapy *10*, 935-940.

Liu, Y.-H., Xu, J., Yang, X.-P., Yang, F., Shesely, E., and Carretero, O.A. (2002). Effect of ACE inhibitors and angiotensin II type 1 receptor antagonists on endothelial NO synthase knockout mice with heart failure. Hypertension *39*, 375-381.

Liu, Y.-H., Yang, X.-P., Sharov, V.G., Nass, O., Sabbah, H.N., Peterson, E., and Carretero, O.A. (1997). Effects of angiotensin-converting enzyme inhibitors and angiotensin II type 1 receptor antagonists in rats with heart failure. Role of kinins and angiotensin II type 2 receptors. Journal of Clinical Investigation *99*, 1926.

Lloyd-Jones, D., Adams, R., Carnethon, M., De Simone, G., Ferguson, T.B., Flegal, K., Ford, E., Furie, K., Go, A., and Greenlund, K. (2009). Heart disease and stroke statistics—2009 update a report from the American Heart Association Statistics Committee and Stroke Statistics Subcommittee. Circulation *119*, e21-e181.

Longacre, L.S., Kloner, R.A., Arai, A.E., Baines, C.P., Bolli, R., Braunwald, E., Downey, J., Gibbons, R.J., Gottlieb, R.A., and Heusch, G. (2011). New horizons in cardioprotection recommendations from the 2010 national heart, lung, and blood institute workshop. Circulation *124*, 1172-1179.

Loot, A.E., Roks, A.J., Henning, R.H., Tio, R.A., Suurmeijer, A.J., Boomsma, F., and van Gilst, W.H. (2002a). Angiotensin-(1–7) attenuates the development of heart failure after myocardial infarction in rats. Circulation *105*, 1548-1550.

Loot, A.E., Roks, A.J.M., Henning, R.H., Tio, R.A., Suurmeijer, A.J.H., Boomsma, F., and van Gilst, W.H. (2002b). Angiotensin-(1–7) attenuates the development of heart failure after myocardial infarction in rats. Circulation *105*, 1548-1550.

Lopez-Sendon, J., Swedberg, K., McMurray, J., Tamargo, J., Maggioni, A.P., Dargie, H., Tendera, M., Waagstein, F., Kjekshus, J., and Lechat, P. (2004). Expert consensus document on angiotensin converting enzyme inhibitors in cardiovascular disease The Task Force on ACE-inhibitors of the European Society of Cardiology. European Heart Journal *25*, 1454-1470.

Louch, W.E., Sheehan, K.A., and Wolska, B.M. (2011). Methods in cardiomyocyte isolation, culture, and gene transfer. Journal of Molecular and Cellular cardiology *51*, 288-298.

Ludwig, M., Steinhoff, G., and Li, J. (2012). The regenerative potential of angiotensin AT2 receptor in cardiac repair. Canadian Journal of Physiology and Pharmacology *90*, 287-293.

Lutgens, E., Daemen, M.J., de Muinck, E.D., Debets, J., Leenders, P., and Smits, J.F. (1999). Chronic myocardial infarction in the mouse: cardiac structural and functional change. Cardiovascular Research *41*, 586-593.

Ma, F., Li, Y., Jia, L., Han, Y., Cheng, J., Li, H., Qi, Y., and Du, J. (2012). Macrophage-stimulated cardiac fibroblast production of IL-6 is essential for TGF ß/Smad activation and cardiac fibrosis induced by angiotensin II. PloS one *7*, e35144.

Mack, C.A., Magovern, C.J., Budenbender, K.T., Patel, S.R., Schwarz, E.A., Zanzonico, P., Ferris, B., Sanborn, T., Isom, P., Ferris, B., *et al.* (1998). Salvage angiogenesis induced by adenovirus-mediated gene transfer of vascular

endothelial growth factor protects against ischemic vascular occlusion. Journal of Vascular Surgery *27*, 699-709.

MacLennan, D.H., and Kranias, E.G. (2003). Phospholamban: a crucial regulator of cardiac contractility. Nature reviews Molecular cell biology *4*, 566-577.

Maggioni, A.P., Anand, I., Gottlieb, S.O., Latini, R., Tognoni, G., and Cohn, J.N. (2002). Effects of valsartan on morbidity and mortality in patients with heart failure not receiving angiotensin-converting enzyme inhibitors. Journal of the American College of Cardiology *40*, 1414-1421.

Magovern, C.J., Mack, C.A., Zhang, J., Hahn, R.T., Ko, W., Isom, O.W., Crystal, R.G., and Rosengart, T.K. (1996). Direct *in vivo* gene transfer to canine myocardium using a replication-deficient adenovirus vector. The Annals of Thoracic Surgery *62*, 425-433; discussion 433-424.

Mahmood, T., and Yang, P.-C. (2012). Western blot: technique, theory, and trouble shooting. North American Journal of Medical Sciences *4*, 429.

Maier, L.S., and Bers, D.M. (2007). Role of Ca^{2+}/calmodulin-dependent protein kinase (CaMK) in excitation–contraction coupling in the heart. Cardiovascular Research *73*, 631-640.

Mancina, R., Susini, T., Renzetti, A., Forti, G., Razzoli, E., Serio, M., and Maggi, M. (1996). Sex steroid modulation of AT2 receptors in human myometrium. The Journal of Clinical Endocrinology & Metabolism *81*, 1753-1757.

Manfredsson, F.P., Rising, A.C., and Mandel, R.J. (2009). AAV9: a potential blood-brain barrier buster. Molecular Therapy: the Journal of the American Society of Gene Therapy *17*, 403.

Mann, D.L., and Spinale, F.G. (1998). Activation of matrix metalloproteinases in the failing human heart breaking the tie that binds. Circulation *98*, 1699-1702.

Markis, J.E., Malagold, M., Parker, J.A., Silverman, K.J., Barry, W.H., Als, A.V., Paulin, S., Grossman, W., and Braunwald, E. (1981). Myocardial salvage after

intracoronary thrombolysis with streptokinase in acute myocardial infarction: assessment by intracoronary thallium-201. New England Journal of Medicine *305*, 777-782.

Marques, F.D., Melo, M.B., Souza, L.E., Irigoyen, M.C.C., Sinisterra, R.D., de Sousa, F.B., Savergnini, S.Q., Braga, V.B.A., Ferreira, A.J., and Santos, R.A.S. (2012). Beneficial effects of long-term administration of an oral formulation of angiotensin-(1–7) in infarcted rats. International Journal of Hypertension *2012*, 795452.

Marttila, M., Persson, D., Gustafsson, D., Liszewski, M.K., Atkinson, J.P., Wadell, G., and Arnberg, N. (2005). CD46 is a cellular receptor for all species B adenoviruses except types 3 and 7. Journal of Virology *79*, 14429-14436.

Masaki, H., Kurihara, T., Yamaki, A., Inomata, N., Nozawa, Y., Mori, Y., Murasawa, S., Kizima, K., Maruyama, K., and Horiuchi, M. (1998). Cardiac-specific overexpression of angiotensin II AT2 receptor causes attenuated response to AT1 receptor-mediated pressor and chronotropic effects. Journal of Clinical Investigation *101*, 527.

Mascareno, E., and Siddiqui, M. (2000). The role of Jak/STAT signaling in heart tissue renin-angiotensin system. Molecular and Cellular Biochemistry *212*, 171-175.

Mathias, P., Wickham, T., Moore, M., and Nemerow, G. (1994). Multiple adenovirus serotypes use alpha v integrins for infection. Journal of Virology *68*, 6811-6814.

Matsubara, H., and Inada, M. (1998). Molecular insights into angiotensin II type 1 and type 2 receptors: expression, signaling and physiological function and clinical application of its antagonists. Endocrine Journal Tokyo *45*, 137-150.

Matsumura, S.-i., Iwanaga, S., Mochizuki, S., Okamoto, H., Ogawa, S., and Okada, Y. (2005). Targeted deletion or pharmacological inhibition of MMP-2 prevents cardiac rupture after myocardial infarction in mice. Journal of Clinical Investigation *115*, 599-609.

McCaffrey, A.P., Fawcett, P., Nakai, H., McCaffrey, R.L., Ehrhardt, A., Pham, T.-T.T., Pandey, K., Xu, H., Feuss, S., and Storm, T.A. (2008). The host response to adenovirus, helper-dependent adenovirus, and adeno-associated virus in mouse liver. Molecular Therapy *16*, 931-941.

McCollum, L.T., Gallagher, P.E., and Tallant, E.A. (2012). Angiotensin-(1–7) abrogates mitogen-stimulated proliferation of cardiac fibroblasts. Peptides *34*, 380-388.

McEwan, P.E., Gray, G.A., Sherry, L., Webb, D.J., and Kenyon, C.J. (1998). Differential effects of angiotensin II on cardiac cell proliferation and intramyocardial perivascular fibrosis *in vivo*. Circulation *98*, 2765-2773.

McKinney, C.A., Fattah, C., Loughrey, C.M., Milligan, G., and Nicklin, S.A. (2014). Angiotensin-(1-7) and angiotensin-(1-9): function in cardiac and vascular remodelling. Clinical Science *126*, 815-827.

Meffert, S., Stoll, M., Steckelings, U.M., Bottari, S.P., and Unger, T. (1996). The angiotensin II AT 2 receptor inhibits proliferation and promotes differentiation in PC12W cells. Molecular and Cellular Endocrinology *122*, 59-67.

Mehta, P.K., and Griendling, K.K. (2007). Angiotensin II cell signaling: physiological and pathological effects in the cardiovascular system. American Journal of Physiology-Cell Physiology *292*, C82-C97.

Meissner, A., Min, J.-Y., and Simon, R. (1998). Effects of angiotensin II on inotropy and intracellular Ca^{2+} handling in normal and hypertrophied rat myocardium. Journal of Molecular and Cellular Cardiology *30*, 2507-2518.

Mercure, C., Yogi, A., Callera, G.E., Aranha, A.B., Bader, M., Ferreira, A.J., Santos, R.A., Walther, T., Touyz, R.M., and Reudelhuber, T.L. (2008). Angiotensin (1-7) blunts hypertensive cardiac remodeling by a direct effect on the heart. Circulation Research *103*, 1319-1326.

Methot, D., Lochard, N., Tremblay, F., Silversides, D.W., and Reudelhuber, T.L. (2001). Development and application of a biological peptide pump for the study

of the *in vivo* actions of angiotensin peptides. American Journal of Hypertension *14*, 38S-43S.

Min, L., Sim, M.K., and Xu, X.G. (2000). Effects of des-aspartate-angiotensin I on angiotensin II-induced incorporation of phenylalanine and thymidine in cultured rat cardiomyocytes and aortic smooth muscle cells. Regulatory Peptides *95*, 93-97.

Mitcheson, J.S., Hancox, J.C., and Levi, A.J. (1996). Action potentials, ion channel currents and transverse tubule density in adult rabbit ventricular myocytes maintained for 6 days in cell culture. Pflügers Archiv *431*, 814-827.

Miura, S., Ohno, I., Suzuki, J., Suzuki, K., Okada, S., Okuyama, A., Nawata, J., Ikeda, J., and Shirato, K. (2003). Inhibition of matrix metalloproteinases prevents cardiac hypertrophy induced by ß-adrenergic stimulation in rats. Journal of Cardiovascular Pharmacology *42*, 174-181.

Miura, S.i., and Karnik, S.S. (2000). Ligand-independent signals from angiotensin II type 2 receptor induce apoptosis. The EMBO Journal *19*, 4026-4035.

Miyamoto, M.I., Del Monte, F., Schmidt, U., DiSalvo, T.S., Kang, Z.B., Matsui, T., Guerrero, J.L., Gwathmey, J.K., Rosenzweig, A., and Hajjar, R.J. (2000). Adenoviral gene transfer of SERCA2a improves left-ventricular function in aortic-banded rats in transition to heart failure. Proceedings of the National Academy of Sciences *97*, 793-798.

Mizuguchi, H., and Hayakawa, T. (2004). Targeted adenovirus vectors. Human Gene Therapy *15*, 1034-1044.

Mogielnicki, A., Kramkowski, K., Hermanowicz, J., Leszczynska, A., Przyborowski, K., and Buczko, W. (2013). Angiotensin-(1–9) enhances stasis-induced venous thrombosis in the rat because of the impairment of fibrinolysis. Journal of Renin-Angiotensin-Aldosterone System, 1470320313498631.

Moilanen, A.-M., Rysä, J., Mustonen, E., Serpi, R., Aro, J., Tokola, H., Leskinen, H., Manninen, A., Levijoki, J., and Vuolteenaho, O. (2011). Intramyocardial BNP

gene delivery improves cardiac function through distinct context-dependent mechanisms. Circulation: Heart Failure *4*, 483-495.

Morgan, L., Pipkin, F.B., and Kalsheker, N. (1996). Angiotensinogen: molecular biology, biochemistry and physiology. The International Journal of Biochemistry & Cell Biology *28*, 1211-1222.

Morita, H., Kimura, J., and Endoh, M. (1995). Angiotensin II activation of a chloride current in rabbit cardiac myocytes. The Journal of physiology *483*, 119-130.

Mukoyama, M., Nakajima, M., Horiuchi, M., Sasamura, H., Pratt, R.E., and Dzau, V. (1993). Expression cloning of type 2 angiotensin II receptor reveals a unique class of seven-transmembrane receptors. Journal of Biological Chemistry *268*, 24539-24542.

Müller, O.J., Katus, H.A., and Bekeredjian, R. (2007). Targeting the heart with gene therapy-optimized gene delivery methods. Cardiovascular Research *73*, 453-462.

Muñoz, M.C., Giani, J.F., and Dominici, F.P. (2010). Angiotensin-(1-7) stimulates the phosphorylation of Akt in rat extracardiac tissues *in vivo* via receptor Mas. Regulatory Peptides *161*, 1-7.

Munzenmaier, D.H., and Greene, A.S. (1996). Opposing actions of angiotensin II on microvascular growth and arterial blood pressure. Hypertension *27*, 760-765.

Murdoch, C.E., Zhang, M., Cave, A.C., and Shah, A.M. (2006). NADPH oxidase-dependent redox signalling in cardiac hypertrophy, remodelling and failure. Cardiovascular Research *71*, 208-215.

Mustafa, M.R., Dharmani, M., Kunheen, N.K., and Sim, M.K. (2004). Effects of des-aspartate-angiotensin I on the actions of angiotensin III in the renal and mesenteric vasculature of normo- and hypertensive rats. Regulatory Peptides *120*, 15-22.

Nagata, S., Kato, J., Kuwasako, K., and Kitamura, K. (2010). Plasma and tissue levels of proangiotensin-12 and components of the renin–angiotensin system (RAS) following low- or high-salt feeding in rats. Peptides *31*, 889-892.

Nahmias, C., and Strosberg, A.D. (1995). The angiotensin AT 2 receptor: searching for signal-transduction pathways and physiological function. Trends in Pharmacological Sciences *16*, 223-225.

Nakai, H., Yant, S.R., Storm, T.A., Fuess, S., Meuse, L., and Kay, M.A. (2001). Extrachromosomal recombinant adeno-associated virus vector genomes are primarily responsible for stable liver transduction *in vivo*. Journal of Virology *75*, 6969-6976.

Namsolleck, P., Recarti, C., Foulquier, S., Steckelings, U.M., and Unger, T. (2014). AT2 receptor and tissue injury: therapeutic implications. Current Hypertension Reports *16*, 1-10.

Nathwani, A.C., Tuddenham, E.G., Rangarajan, S., Rosales, C., McIntosh, J., Linch, D.C., Chowdary, P., Riddell, A., Pie, A.J., and Harrington, C. (2011). Adenovirus-associated virus vector–mediated gene transfer in hemophilia B. New England Journal of Medicine *365*, 2357-2365.

Navalkar, S., Parthasarathy, S., Santanam, N., and Khan, B.V. (2001). Irbesartan, an angiotensin type 1 receptor inhibitor, regulates markers of inflammation in patients with premature atherosclerosis. Journal of the American College of Cardiology *37*, 440-444.

Navar, L.G. (2014). Intrarenal renin-angiotensin system in regulation of glomerular function. Current Opinion in Nephrology and Hypertension *23*, 38.

Nayak, S., and Herzog, R.W. (2009). Progress and prospects: immune responses to viral vectors. Gene Therapy *17*, 295-304.

Nian, M., Lee, P., Khaper, N., and Liu, P. (2004). Inflammatory cytokines and postmyocardial infarction remodeling. Circulation Research *94*, 1543-1553.

Nicklin, S.A., and Baker, A.H. (1999). Simple methods for preparing recombinant adenoviruses for high-efficiency transduction of vascular cells. In Vascular Disease (Springer), pp. 271-283.

Nicklin, S.A., Buening, H., Dishart, K.L., de Alwis, M., Girod, A., Hacker, U., Thrasher, A.J., Ali, R.R., Hallek, M., and Baker, A.H. (2001). Efficient and selective AAV2-mediated gene transfer directed to human vascular endothelial cells. Molecular Therapy *4*, 174-181.

Nio, Y., Matsubara, H., Murasawa, S., Kanasaki, M., and Inada, M. (1995). Regulation of gene transcription of angiotensin II receptor subtypes in myocardial infarction. Journal of Clinical Investigation *95*, 46.

Nonnenmacher, M., and Weber, T. (2012). Intracellular transport of recombinant adeno-associated virus vectors. Gene Therapy *19*, 649-658.

Nouet, S., and Nahmias, C. (2000). Signal transduction from the angiotensin II AT 2 receptor. Trends in Endocrinology & Metabolism *11*, 1-6.

Noutsias, M., Fechner, H., de Jonge, H., Wang, X., Dekkers, D., Houtsmuller, A., Pauschinger, M., Bergelson, J., Warraich, R., and Yacoub, M. (2001). Human coxsackie-adenovirus receptor is colocalized with integrins αvß3 and αvß5 on the cardiomyocyte sarcolemma and upregulated in dilated cardiomyopathy implications for cardiotropic viral infections. Circulation *104*, 275-280.

O'Rourke, B. (2008). The ins and outs of calcium in heart failure. Circulation Research *102*, 1301-1303.

O'Connell, T.D., Ni, Y.G., Lin, K.-M., Han, H., and Yan, Z. (2003). Isolation and culture of adult mouse cardiac myocytes for signaling studies. AfCS Research Reports *1*, 1-9.

O'Connell, T.D., Rodrigo, M.C., and Simpson, P.C. (2007). Isolation and culture of adult mouse cardiac myocytes. In Cardiovascular Proteomics (Springer), pp. 271-296.

O'Rourke, B., Kass, D.A., Tomaselli, G.F., Kääb, S., Tunin, R., and Marbán, E. (1999). Mechanisms of altered excitation-contraction coupling in canine tachycardia-induced heart failure, I experimental studies. Circulation Research *84*, 562-570.

Ocaranza, M.P., Godoy, I., Jalil, J.E., Varas, M., Collantes, P., Pinto, M., Roman, M., Ramirez, C., Copaja, M., and Diaz-Araya, G. (2006). Enalapril attenuates downregulation of angiotensin-converting enzyme 2 in the late phase of ventricular dysfunction in myocardial infarcted rat. Hypertension *48*, 572-578.

Ocaranza, M.P., and Jalil, J.E. (2012). Protective role of the ACE2/Ang-(1–9) axis in cardiovascular remodeling. International Journal of Hypertension *2012*.

Ocaranza, M.P., Lavandero, S., Jalil, J.E., Moya, J., Pinto, M., Novoa, U., Apablaza, F., González, L., Hernández, C., and Varas, M. (2010). Angiotensin-(1-9) regulates cardiac hypertrophy *in vivo* and *in vitro*. Journal of Hypertension *28*, 1054.

Ocaranza, M.P., Moya, J., Barrientos, V., Alzamora, R., Hevia, D., Morales, C., Pinto, M., Escudero, N., García, L., and Novoa, U. (2014). Angiotensin-(1–9) reverses experimental hypertension and cardiovascular damage by inhibition of the angiotensin converting enzyme/Ang II axis. Journal of Hypertension *32*, 771-783.

Ocaranza, M.P., Rivera, P., Novoa, U., Pinto, M., Gonzalez, L., Chiong, M., Lavandero, S., and Jalil, J.E. (2011). Rho kinase inhibition activates the homologous angiotensin-converting enzyme-angiotensin-(1–9) axis in experimental hypertension. Journal of Hypertension *29*, 706-715.

Ohyama, K., Yamano, Y., Sano, T., Nakagomi, Y., Hamakubo, T., Morishima, I., and Inagami, T. (1995). Disulfide bridges in extracellular domains of angiotensin II receptor type I A. Regulatory Peptides *57*, 141-147.

Oishi, Y., Ozono, R., Yano, Y., Teranishi, Y., Akishita, M., Horiuchi, M., Oshima, T., and Kambe, M. (2003). Cardioprotective role of AT2 receptor in postinfarction left ventricular remodeling. Hypertension *41*, 814-818.

Oishi, Y., Ozono, R., Yoshizumi, M., Akishita, M., Horiuchi, M., and Oshima, T. (2006). AT2 receptor mediates the cardioprotective effects of AT1 receptor antagonist in post-myocardial infarction remodeling. Life Sciences *80*, 82-88.

Oliva, P.B., Hammill, S.C., and Edwards, W.D. (1993). Cardiac rupture, a clinically predictable complication of acute myocardial infarction: Report of 70 cases with clinicopathologic correlation. Journal of the American College of Cardiology *22*, 720-726.

Olson, E.R., Naugle, J.E., Zhang, X., Bomser, J.A., and Meszaros, J.G. (2005). Inhibition of cardiac fibroblast proliferation and myofibroblast differentiation by resveratrol. American Journal of Physiology-Heart and Circulatory Physiology *288*, H1131-H1138.

Omura, T., Yoshiyama, M., Ishikura, F., Kobayashi, H., Takeuchi, K., Beppu, S., and Yoshikawa, J. (2001). Myocardial ischemia activates the JAK–STAT pathway through angiotensin II signaling in *in vivo* myocardium of rats. Journal of Molecular and Cellular Cardiology *33*, 307-316.

Opie, L.H., Commerford, P.J., Gersh, B.J., and Pfeffer, M.A. (2006). Controversies in ventricular remodelling. The Lancet *367*, 356-367.

Opie, L.H., and Sack, M.N. (2001). Enhanced angiotensin II activity in heart failure: reevaluation of the counterregulatory hypothesis of receptor subtypes. Circ Res *88*, 654-658.

Opie, S.R., Warrington Jr, K.H., Agbandje-McKenna, M., Zolotukhin, S., and Muzyczka, N. (2003). Identification of amino acid residues in the capsid proteins of adeno-associated virus type 2 that contribute to heparan sulfate proteoglycan binding. Journal of Virology *77*, 6995-7006.

Pacak, C.A., Mah, C.S., Thattaliyath, B.D., Conlon, T.J., Lewis, M.A., Cloutier, D.E., Zolotukhin, I., Tarantal, A.F., and Byrne, B.J. (2006). Recombinant adeno-associated virus serotype 9 leads to preferential cardiac transduction *in vivo*. Circulation Research *99*, e3-e9.

Pacher, P., Nagayama, T., Mukhopadhyay, P., Bátkai, S., and Kass, D.A. (2008). Measurement of cardiac function using pressure–volume conductance catheter technique in mice and rats. Nature Protocols *3*, 1422-1434.

Pajusola, K., Gruchala, M., Joch, H., Lüscher, T.F., Ylä-Herttuala, S., and Büeler, H. (2002). Cell-type-specific characteristics modulate the transduction efficiency of adeno-associated virus type 2 and restrain infection of endothelial cells. Journal of Virology *76*, 11530-11540.

Palomeque, J., Sapia, L., Hajjar, R.J., Mattiazzi, A., and Petroff, M.V. (2006). Angiotensin II-induced negative inotropy in rat ventricular myocytes: role of reactive oxygen species and p38 MAPK. American Journal of Physiology-Heart and Circulatory Physiology *290*, H96-H106.

Pang, P.S., and Levy, P. (2010). Pathophysiology of volume overload in acute heart failure syndromes. Congestive Heart Failure *16*, S1-S6.

Papaiahgari, S., Zhang, Q., Kleeberger, S.R., Cho, H.-Y., and Reddy, S.P. (2006). Hyperoxia stimulates an Nrf2-ARE transcriptional response via ROS-EGFR-PI3K-Akt/ERK MAP kinase signaling in pulmonary epithelial cells. Antioxidants & Redox Signaling *8*, 43-52.

Parks, R.J., Chen, L., Anton, M., Sankar, U., Rudnicki, M.A., and Graham, F.L. (1996). A helper-dependent adenovirus vector system: removal of helper virus by Cre-mediated excision of the viral packaging signal. Proceedings of the National Academy of Sciences *93*, 13565-13570.

Passier, R., Smits, J., Verluyten, M., and Daemen, M. (1996). Expression and localization of renin and angiotensinogen in rat heart after myocardial infarction. American Journal of Physiology-Heart and Circulatory Physiology *271*, H1040-H1048.

Patel, V.B., Bodiga, S., Fan, D., Das, S.K., Wang, Z., Wang, W., Basu, R., Zhong, J., Kassiri, Z., and Oudit, G.Y. (2012). Cardioprotective Effects Mediated by Angiotensin II Type 1 Receptor Blockade and Enhancing Angiotensin 1-7 in

Experimental Heart Failure in Angiotensin-Converting Enzyme 2–Null Mice. Hypertension *59*, 1195-1203.

Patten, R.D., Aronovitz, M.J., Deras-Mejia, L., Pandian, N.G., Hanak, G.G., Smith, J.J., Mendelsohn, M.E., and Konstam, M.A. (1998). Ventricular remodeling in a mouse model of myocardial infarction. American Journal of Physiology-Heart and Circulatory Physiology *274*, H1812-H1820.

Patten, R.D., Aronovitz, M.J., Einstein, M., Lambert, M., Pandian, N.G., Mendelsohn, M.E., and Konstam, M.A. (2003). Effects of angiotensin II receptor blockade versus angiotensin-converting-enzyme inhibition on ventricular remodelling following myocardial infarction in the mouse. Clinical Science *104*, 109-118.

Paul, M., Mehr, A.P., and Kreutz, R. (2006). Physiology of local renin-angiotensin systems. Physiological Reviews *86*, 747-803.

Paul Thomas, G., and Mathews, M.B. (1980). DNA replication and the early to late transition in adenovirus infection. Cell *22*, 523-533.

Pavlović, D., McLatchie, L.M., and Shattock, M.J. (2010). The rate of loss of T-tubules in cultured adult ventricular myocytes is species dependent. Experimental Physiology *95*, 518-527.

Persson, P.B. (2003). Renin: origin, secretion and synthesis. The Journal of Physiology *552*, 667-671.

Peterson, K.L. (2002). Pressure overload hypertrophy and congestive heart failure*: Where is the “Achilles’ heel”? Journal of the American College of Cardiology *39*, 672-675.

Petroff, M.G.V., Aiello, E.A., Palomeque, J., Salas, M.A., and Mattiazzi, A. (2000). Subcellular mechanisms of the positive inotropic effect of angiotensin II in cat myocardium. The Journal of Physiology *529*, 189-203.

Pfeffer, J.M., Pfeffer, M.A., Fletcher, P.J., and Braunwald, E. (1991). Progressive ventricular remodeling in rat with myocardial infarction. American Journal of Physiology-Heart and Circulatory Physiology *260*, H1406-H1414.

Pfeffer, M.A., and Braunwald, E. (1990). Ventricular remodeling after myocardial infarction. Experimental observations and clinical implications. Circulation *81*, 1161-1172.

Pfeffer, M.A., Pfeffer, J.M., Fishbein, M.C., Fletcher, P.J., Spadaro, J., Kloner, R.A., and Braunwald, E. (1979). Myocardial infarct size and ventricular function in rats. Circulation Research *44*, 503-512.

Pfeffer, M.A., Swedberg, K., Granger, C.B., Held, P., McMurray, J.J., Michelson, E.L., Olofsson, B., Östergren, J., Yusuf, S., Investigators, C., *et al.* (2003). Effects of candesartan on mortality and morbidity in patients with chronic heart failure: the CHARM-Overall programme. The Lancet *362*, 759-766.

Phillips, M.I., Speakman, E.A., and Kimura, B. (1993). Levels of angiotensin and molecular biology of the tissue renin angiotensin systems. Regulatory Peptides *43*, 1-20.

Piacentino, V., Weber, C.R., Chen, X., Weisser-Thomas, J., Margulies, K.B., Bers, D.M., and Houser, S.R. (2003). Cellular basis of abnormal calcium transients of failing human ventricular myocytes. Circulation Research *92*, 651-658.

Pieruzzi, F., Abassi, Z.A., and Keiser, H.R. (1995). Expression of renin-angiotensin system components in the heart, kidneys, and lungs of rats with experimental heart failure. Circulation *92*, 3105-3112.

Piper, H. (2000). The calcium paradox revisited An artefact of great heuristic value. Cardiovascular Research *45*, 123-127.

Pleger, S.T., Shan, C., Ksienzyk, J., Bekeredjian, R., Boekstegers, P., Hinkel, R., Schinkel, S., Leuchs, B., Ludwig, J., and Qiu, G. (2011). Cardiac AAV9-S100A1

gene therapy rescues post-ischemic heart failure in a preclinical large animal model. Science Translational Medicine *3*, 92ra64-92ra64.

Pogwizd, S.M., and Bers, D.M. (2002). Calcium cycling in heart failure: the arrhythmia connection. Journal of Cardiovascular Electrophysiology *13*, 88-91.

Pons, S., Fornes, P., Hagege, A., Heudes, D., Giudicelli, J.F., and Richer, C. (2003). Survival, haemodynamics and cardiac remodelling follow up in mice after myocardial infarction. Clinical and Experimental Pharmacology and Physiology *30*, 25-31.

Porrello, E.R., Delbridge, L., and Thomas, W.G. (2008). The angiotensin II type 2 (AT2) receptor: an enigmatic seven transmembrane receptor. Frontiers in Bioscience (Landmark edition) *14*, 958-972.

Porter, K.E., and Turner, N.A. (2009). Cardiac fibroblasts: at the heart of myocardial remodeling. Pharmacology & Therapeutics *123*, 255-278.

Porterfield, J.E., Kottam, A.T., Raghavan, K., Escobedo, D., Jenkins, J.T., Larson, E.R., Treviño, R.J., Valvano, J.W., Pearce, J.A., and Feldman, M.D. (2009). Dynamic correction for parallel conductance, GP, and gain factor, α, in invasive murine left ventricular volume measurements. Journal of Applied Physiology *107*, 1693-1703.

Powell, T., and Twist, V. (1976). A rapid technique for the isolation and purification of adult cardiac muscle cells having respiratory control and a tolerance to calcium. Biochemical and Biophysical Research Communications *72*, 327-333.

Pueyo, M.E., Gonzalez, W., Nicoletti, A., Savoie, F., Arnal, J.-F., and Michel, J.-B. (2000). Angiotensin II stimulates endothelial vascular cell adhesion molecule-1 via nuclear factor-κB activation induced by intracellular oxidative stress. Arteriosclerosis, Thrombosis, and Vascular Biology *20*, 645-651.

Pulicherla, N., Shen, S., Yadav, S., Debbink, K., Govindasamy, L., Agbandje-McKenna, M., and Asokan, A. (2011). Engineering liver-detargeted AAV9 vectors for cardiac and musculoskeletal gene transfer. Molecular Therapy *19*, 1070-1078.

Qi, Y.F., Shenoy, V., Wong, F., Li, H., Afzal, A., Mocco, J., Sumners, C., Raizada, M.K., and Katovich, M.J. (2011). Lentivirus-mediated overexpression of angiotensin-(1–7) attenuated ischaemia-induced cardiac pathophysiology. Experimental Physiology *96*, 863.

Qing, K., Mah, C., Hansen, J., Zhou, S., Dwarki, V., and Srivastava, A. (1999). Human fibroblast growth factor receptor 1 is a co-receptor for infection by adeno-associated virus 2. Nature Medicine *5*, 71-77.

Qu, Z., Xie, L.-H., Olcese, R., Karagueuzian, H.S., Chen, P.-S., Garfinkel, A., and Weiss, J.N. (2013). Early afterdepolarizations in cardiac myocytes: beyond reduced repolarization reserve. Cardiovascular Research *99*, 6-15.

Raghavan, K., Porterfield, J.E., Kottam, A.T., Feldman, M.D., Escobedo, D., Valvano, J.W., and Pearce, J.A. (2009). Electrical conductivity and permittivity of murine myocardium. Biomedical Engineering, IEEE Transactions on *56*, 2044-2053.

Raper, S.E., Chirmule, N., Lee, F.S., Wivel, N.A., Bagg, A., Gao, G.-p., Wilson, J.M., and Batshaw, M.L. (2003). Fatal systemic inflammatory response syndrome in a ornithine transcarbamylase deficient patient following adenoviral gene transfer. Molecular Genetics and Metabolism *80*, 148-158.

Rauschhuber, C., Noske, N., and Ehrhardt, A. (2012). New insights into stability of recombinant adenovirus vector genomes in mammalian cells. European Journal of Cell Biology *91*, 2-9.

Rehman, A., Leibowitz, A., Yamamoto, N., Rautureau, Y., Paradis, P., and Schiffrin, E.L. (2012). Angiotensin type 2 receptor agonist compound 21 reduces vascular injury and myocardial fibrosis in stroke-prone spontaneously hypertensive rats. Hypertension *59*, 291-299.

Ren, Z., Raucci, F.J., Browe, D.M., and Baumgarten, C.M. (2008). Regulation of swelling-activated Cl− current by angiotensin II signalling and NADPH oxidase in rabbit ventricle. Cardiovascular Research *77*, 73-80.

Reudelhuber, T.L. (2005). The renin–angiotensin system: peptides and enzymes beyond angiotensin II. Current Opinion in Nephrology and Hypertension *14*, 155-159.

Rice, G.I., Thomas, D.A., Grant, P.J., Turner, A.J., and Hooper, N.M. (2004). Evaluation of angiotensin-converting enzyme (ACE), its homologue ACE2 and neprilysin in angiotensin peptide metabolism. The Biochemical Journal *383*, 45-51.

Roberts, D.M., Nanda, A., Havenga, M.J., Abbink, P., Lynch, D.M., Ewald, B.A., Liu, J., Thorner, A.R., Swanson, P.E., and Gorgone, D.A. (2006). Hexon-chimaeric adenovirus serotype 5 vectors circumvent pre-existing anti-vector immunity. Nature *441*, 239-243.

Rodgers, K., Verco, S., Bolton, L., and diZerega, G. (2011). Accelerated healing of diabetic wounds by NorLeu3-angiotensin (1-7). Expert Opinion on Investigational Drugs *20*, 1575-1581.

Rodgers, K., and Xiong, S. (2003). Effect of angiotensin II and angiotensin (1–7) on hematopoietic recovery after intravenous chemotherapy. Cancer Chemotherapy and Pharmacology *51*, 97-106.

Rodgers, K.E., Espinoza, T., Felix, J., Roda, N., Maldonado, S., and dizerega, G. (2003). Acceleration of healing, reduction of fibrotic scar, and normalization of tissue architecture by an angiotensin analogue, NorLeu3-A (1-7). Plastic and Reconstructive Surgery *111*, 1195-1206.

Rodgers, K.E., and Oliver, J. (2006). Phase I/II dose escalation study of angiotensin 1-7 [A (1-7)] administered before and after chemotherapy in patients with newly diagnosed breast cancer. Cancer Chemotherapy and Pharmacology *57*, 559-568.

Rodrigo, G., and Chapman, R. (1991). The calcium paradox in isolated guinea-pig ventricular myocytes: effects of membrane potential and intracellular sodium. The Journal of Physiology *434*, 627-645.

Roger, V.L., Go, A.S., Lloyd-Jones, D.M., Benjamin, E.J., Berry, J.D., Borden, W.B., Bravata, D.M., Dai, S., Ford, E.S., and Fox, C.S. (2012). Heart disease and stroke statistics—2012 update a report from the American heart association. Circulation *125*, e2-e220.

Rosenthal, N., and Brown, S. (2007). The mouse ascending: perspectives for human-disease models. Nature Cell Biology *9*, 993-999.

Roth, G.M., Bader, D.M., and Pfaltzgraff, E.R. (2014). Isolation and physiological analysis of mouse cardiomyocytes. JoVE (Journal of Visualized Experiments), e51109-e51109.

Rowe, W.P., Huebner, R.J., Gilmore, L.K., Parrott, R.H., and Ward, T.G. (1953). Isolation of a cytopathogenic agent from human adenoids undergoing spontaneous degeneration in tissue culture. Experimental Biology and Medicine *84*, 570-573.

Ruf, S., Piper, H., and Schlüter, K.-D. (2002). Specific role for the extracellular signal-regulated kinase pathway in angiotensin II-but not phenylephrine-induced cardiac hypertrophy in vitro. Pflügers Archiv *443*, 483-490.

Ruixing, Y., Jinzhen, W., Dezhai, Y., and Jiaquan, L. (2007). Cardioprotective role of cardiotrophin-1 gene transfer in a murine model of myocardial infarction. Growth Factors *25*, 286-294.

Runge, M.S., and Patterson, C. (2007). Principles of molecular medicine (Springer).

Russell, W. (2009). Adenoviruses: update on structure and function. Journal of General Virology *90*, 1-20.

Saban, S.D., Nepomuceno, R.R., Gritton, L.D., Nemerow, G.R., and Stewart, P.L. (2005). CryoEM structure at 9Å resolution of an adenovirus vector targeted to hematopoietic cells. Journal of Molecular Biology *349*, 526-537.

Sadoshima, J.-i., Jahn, L., Takahashi, T., Kulik, T., and Izumo, S. (1992). Molecular characterization of the stretch-induced adaptation of cultured cardiac cells. An in vitro model of load-induced cardiac hypertrophy. Journal of Biological Chemistry *267*, 10551-10560.

Sadoshima, J.-i., Xu, Y., Slayter, H.S., and Izumo, S. (1993). Autocrine release of angiotensin II mediates stretch-induced hypertrophy of cardiac myocytes in vitro. Cell *75*, 977-984.

Sadoshima, J.-l., and Izumo, S. (1993). Molecular characterization of angiotensin II--induced hypertrophy of cardiac myocytes and hyperplasia of cardiac fibroblasts. Critical role of the AT1 receptor subtype. Circulation Research *73*, 413-423.

Sah, R., Ramirez, R.J., Oudit, G.Y., Gidrewicz, D., Trivieri, M.G., Zobel, C., and Backx, P.H. (2003). Regulation of cardiac excitation–contraction coupling by action potential repolarization: role of the transient outward potassium current (Ito). The Journal of Physiology *546*, 5-18.

Saini, H.K., and Dhalla, N.S. (2005). Defective calcium handling in cardiomyocytes isolated from hearts subjected to ischemia-reperfusion. American Journal of Physiology-Heart and Circulatory Physiology *288*, H2260-H2270.

Saito, Y., and Berk, B.C. (2001). Transactivation: a novel signaling pathway from angiotensin II to tyrosine kinase receptors. Journal of Molecular and Cellular Cardiology *33*, 3-7.

Sakmann, B., and Neher, E. (1984). Patch clamp techniques for studying ionic channels in excitable membranes. Annual Review of Physiology *46*, 455-472.

Sakurai, K., Norota, I., Tanaka, H., Kubota, I., Tomoike, H., and Endoh, M. (2002). Negative inotropic effects of angiotensin II, endothelin-1 and phenylephrine in indo-1 loaded adult mouse ventricular myocytes. Life Sciences *70*, 1173-1184.

Salas, M.A., Palomeque, J., Aiello, E.A., and Mattiazzi, A. (2001). Positive inotropic and negative lusitropic effect of angiotensin II: intracellular mechanisms and second messengers. Journal of Molecular and Cellular Cardiology *33*, 1957-1971.

Sanlioglu, S., Benson, P.K., Yang, J., Atkinson, E.M., Reynolds, T., and Engelhardt, J.F. (2000). Endocytosis and nuclear trafficking of adeno-associated virus type 2 are controlled by rac1 and phosphatidylinositol-3 kinase activation. Journal of Virology *74*, 9184-9196.

Santos, R., and Almeida, A. (2002). Angiotensin-(1-7) improves the post-ischemic function in isolated perfused rat hearts. Braz J Med Biol Res *35*, 9.

Santos, R., Brosnihan, K.B., Chappell, M.C., Pesquero, J., Chernicky, C.L., Greene, L.J., and Ferrario, C.M. (1988). Converting enzyme activity and angiotensin metabolism in the dog brainstem. Hypertension *11*, I153.

Santos, R.A., Campagnole-Santos, M.J., Baracho, N.C., Fontes, M.A., Silva, L.C., Neves, L.A., Oliveira, D.R., Caligiorne, S.M., Rodrigues, A.R., and Gropen, C. (1994). Characterization of a new angiotensin antagonist selective for angiotensin-(1–7): evidence that the actions of angiotensin-(1–7) are mediated by specific angiotensin receptors. Brain Research Bulletin *35*, 293-298.

Santos, R.A., Castro, C.H., Gava, E., Pinheiro, S.V., Almeida, A.P., de Paula, R.D., Cruz, J.S., Ramos, A.S., Rosa, K.T., and Irigoyen, M.C. (2006). Impairment of *in vitro* and *in vivo* heart function in angiotensin-(1-7) receptor MAS knockout mice. Hypertension *47*, 996-1002.

Santos, R.A., e Silva, A.C.S., Maric, C., Silva, D.M., Machado, R.P., de Buhr, I., Heringer-Walther, S., Pinheiro, S.V.B., Lopes, M.T., and Bader, M. (2003).

Angiotensin-(1–7) is an endogenous ligand for the G protein-coupled receptor Mas. Proceedings of the National Academy of Sciences *100*, 8258-8263.

Santos, R.A., Ferreira, A.J., Nadu, A.P., Braga, A.N., de Almeida, A.P., Campagnole-Santos, M.J., Baltatu, O., Iliescu, R., Reudelhuber, T.L., and Bader, M. (2004). Expression of an angiotensin-(1–7)-producing fusion protein produces cardioprotective effects in rats. Physiological Genomics *17*, 292-299.

Santos, R.A., Ferreira, A.J., and Simões e Silva, A.C. (2008). Recent advances in the angiotensin-converting enzyme 2–angiotensin (1–7)–Mas axis. Experimental Physiology *93*, 519-527.

Sarkis, A., Lopez, B., and Roman, R.J. (2004). Role of 20-hydroxyeicosatetraenoic acid and epoxyeicosatrienoic acids in hypertension. Current opinion in nephrology and hypertension *13*, 205-214.

Sarmento-Leite, R., Krepsky, A.M., and Gottschall, C.A. (2001). Acute myocardial infarction: one century of history. Arquivos Brasileiros de Cardiologia *77*, 602-610.

Savoia, C., Burger, D., Nishigaki, N., Montezano, A., and Touyz, R.M. (2011). Angiotensin II and the vascular phenotype in hypertension. Expert Reviews in Molecular Medicine *13*.

Scisence PV Technical Note. How Wei's Equation Improves Volume Measurement Using Gamma Correction Factor. Accessed 10/03/2014: http://www.transonic.com/resources/research/how-to-post-calculate-admittance-volume-advol/

Schackow, T.E., Decker, R.S., and Ten Eick, R.E. (1995). Electrophysiology of adult cat cardiac ventricular myocytes: changes during primary culture. American Journal of Physiology-Cell Physiology *268*, C1002-C1017.

Scherrer-Crosbie, M., Ullrich, R., Bloch, K.D., Nakajima, H., Nasseri, B., Aretz, H.T., Lindsey, M.L., Vançon, A.-C., Huang, P.L., and Lee, R.T. (2001).

Endothelial nitric oxide synthase limits left ventricular remodeling after myocardial infarction in mice. Circulation *104*, 1286-1291.

Schiavone, M.T., Santos, R., Brosnihan, K.B., Khosla, M.C., and Ferrario, C.M. (1988). Release of vasopressin from the rat hypothalamo-neurohypophysial system by angiotensin-(1-7) heptapeptide. Proceedings of the National Academy of Sciences *85*, 4095-4098.

Schiedner, G., Morral, N., Parks, R.J., Wu, Y., Koopmans, S.C., Langston, C., Graham, F.L., Beaudet, A.L., and Kochanek, S. (1998). Genomic DNA transfer with a high-capacity adenovirus vector results in improved *in vivo* gene expression and decreased toxicity. Nature Genetics *18*, 180-183.

Schiller, M., Javelaud, D., and Mauviel, A. (2004). TGF-β-induced SMAD signaling and gene regulation: consequences for extracellular matrix remodeling and wound healing. Journal of Dermatological Science *35*, 83-92.

Schluter, K.D., and Wenzel, S. (2008). Angiotensin II: a hormone involved in and contributing to pro-hypertrophic cardiac networks and target of anti-hypertrophic cross-talks. Pharmacology & Therapeutics *119*, 311-325.

Schmidt, M., Voutetakis, A., Afione, S., Zheng, C., Mandikian, D., and Chiorini, J.A. (2008). Adeno-associated virus type 12 (AAV12): a novel AAV serotype with sialic acid-and heparan sulfate proteoglycan-independent transduction activity. Journal of Virology *82*, 1399-1406.

Schmidt, U., del Monte, F., Miyamoto, M.I., Matsui, T., Gwathmey, J.K., Rosenzweig, A., and Hajjar, R.J. (2000). Restoration of diastolic function in senescent rat hearts through adenoviral gene transfer of sarcoplasmic reticulum Ca^{2+}-ATPase. Circulation *101*, 790-796.

Schmittgen, T.D., and Livak, K.J. (2008). Analyzing real-time PCR data by the comparative CT method. Nature Protocols *3*, 1101-1108.

Schwartz, R.A., Carson, C.T., Schuberth, C., and Weitzman, M.D. (2009). Adeno-associated virus replication induces a DNA damage response coordinated by DNA-dependent protein kinase. Journal of Virology *83*, 6269-6278.

Schwinger, R.H., Böhm, M., Schmidt, U., Karczewski, P., Bavendiek, U., Flesch, M., Krause, E.-G., and Erdmann, E. (1995). Unchanged protein levels of SERCA II and phospholamban but reduced Ca^{2+} uptake and Ca^{2+}-ATPase activity of cardiac sarcoplasmic reticulum from dilated cardiomyopathy patients compared with patients with nonfailing hearts. Circulation *92*, 3220-3228.

Schwinger, R.H., Münch, G., Bölck, B., Karczewski, P., Krause, E.-G., and Erdmann, E. (1999). Reduced Ca^{2+}-Sensitivity of SERCA 2a in Failing Human Myocardium due to Reduced Serin-16 Phospholamban Phoshorylation. Journal of Molecular and Cellular Cardiology *31*, 479-491.

Senbonmatsu, T., Ichihara, S., Price Jr, E., Gaffney, F.A., and Inagami, T. (2000). Evidence for angiotensin II type 2 receptor–mediated cardiac myocyte enlargement during *in vivo* pressure overload. Journal of Clinical Investigation *106*, R25.

Seropian, I.M., Toldo, S., Van Tassell, B.W., and Abbate, A. (2014). Anti-inflammatory strategies for ventricular remodeling following ST-segment elevation acute myocardial infarction. Journal of the American College of Cardiology *63*, 1593-1603.

Serruys, P.W., Kutryk, M.J., and Ong, A.T. (2006). Coronary-artery stents. New England Journal of Medicine *354*, 483-495.

Shah, B.H., and Catt, K.J. (2003). A central role of EGF receptor transactivation in angiotensin II-induced cardiac hypertrophy. Trends in Pharmacological Sciences *24*, 239-244.

Shang, L.L., Sanyal, S., Pfahnl, A.E., Jiao, Z., Allen, J., Liu, H., and Dudley, S.C. (2008). NF-κB-dependent transcriptional regulation of the cardiac scn5a sodium channel by angiotensin II. American Journal of Physiology-Cell Physiology *294*, C372-C379.

Shanmugam, S., Corvol, P., and Gasc, J.-M. (1996). Angiotensin II type 2 receptor mRNA expression in the developing cardiopulmonary system of the rat. Hypertension *28*, 91-97.

Shanmugam, S., Lenkei, Z.G., Gasc, J.-M.R., Corvol, P.L., and Llorens-Cortes, C.M. (1995). Ontogeny of angiotensin II type (AT~ 2) receptor mRNA in the rat. Kidney International *47*, 1095-1095.

Shannon, T.R., Pogwizd, S.M., and Bers, D.M. (2003). Elevated sarcoplasmic reticulum Ca^{2+} leak in intact ventricular myocytes from rabbits in heart failure. Circulation Research *93*, 592-594.

Shao, Q., Ren, B., Elimban, V., Tappia, P.S., Takeda, N., and Dhalla, N.S. (2005). Modification of sarcolemmal Na^{+}-K^{+}-ATPase and Na^{+}/Ca^{2+} exchanger expression in heart failure by blockade of renin-angiotensin system. American Journal of Physiology-Heart and Circulatory Physiology *288*, H2637-H2646.

Shenoy, U.V., Richards, E.M., Huang, X.-C., and Sumners, C. (1999). Angiotensin II type 2 receptor-mediated apoptosis of cultured neurons from newborn rat brain 1. Endocrinology *140*, 500-509.

Shenoy, V., Ferreira, A.J., Qi, Y., Fraga-Silva, R.A., Díez-Freire, C., Dooies, A., Jun, J.Y., Sriramula, S., Mariappan, N., and Pourang, D. (2010). The angiotensin-converting enzyme 2/angiogenesis-(1–7)/Mas axis confers cardiopulmonary protection against lung fibrosis and pulmonary hypertension. American Journal of Respiratory and Critical Care Medicine *182*, 1065-1072.

Shimoni, Y., Hunt, D., Chuang, M., Chen, K., Kargacin, G., and Severson, D. (2005). Modulation of potassium currents by angiotensin and oxidative stress in cardiac cells from the diabetic rat. The Journal of Physiology *567*, 177-190.

Shioura, K.M., Geenen, D.L., and Goldspink, P.H. (2007). Assessment of cardiac function with the pressure-volume conductance system following myocardial infarction in mice. American Journal of Physiology-Heart and Circulatory Physiology *293*, H2870-H2877.

Sipido, K.R., Bito, V., Antoons, G., Volders, P.G., and Vos, M.A. (2007). Na^+/Ca^{2+} exchange and cardiac ventricular arrhythmias. Annals of the New York Academy of Sciences *1099*, 339-348.

Siragy, H.M., Jaffa, A.A., Margolius, H.S., and Carey, R.M. (1996). Renin-angiotensin system modulates renal bradykinin production. American Journal of Physiology-Regulatory, Integrative and Comparative Physiology *271*, R1090-R1095.

Skaletz-Rorowski, A., Pinkernell, K., Sindermann, J.R., Schriever, C., Müller, J.G., Eschert, H., and Breithardt, G. (2004). Angiotensin AT1 receptor upregulates expression of basic fibroblast growth factor, basic fibroblast growth factor receptor and coreceptor in human coronary smooth muscle cells. Basic Research in Cardiology *99*, 272-278.

Skrzypiec-Spring, M., Grotthus, B., Szeląg, A., and Schulz, R. (2007). Isolated heart perfusion according to Langendorff—still viable in the new millennium. Journal of Pharmacological and Toxicological Methods *55*, 113-126.

Smith, J.G., Silvestry, M., Lindert, S., Lu, W., Nemerow, G.R., and Stewart, P.L. (2010). Insight into the mechanisms of adenovirus capsid disassembly from studies of defensin neutralization. PLoS Pathogens *6*, e1000959.

Smolich, J.J., Walker, A.M., Campbell, G.R., and Adamson, T.M. (1989). Left and right ventricular myocardial morphometry in fetal, neonatal, and adult sheep. American Journal of Physiology-Heart and Circulatory Physiology *257*, H1-H9.

Soboloff, J., Spassova, M., Hewavitharana, T., He, L.-P., Luncsford, P., Xu, W., Venkatachalam, K., Van Rossum, D., Patterson, R., and Gill, D. (2007). TRPC channels: integrators of multiple cellular signals. Transient Receptor Potential (TRP) Channels (Springer), pp. 575-591.

Sonntag, F., Bleker, S., Leuchs, B., Fischer, R., and Kleinschmidt, J.A. (2006). Adeno-associated virus type 2 capsids with externalized VP1/VP2 trafficking domains are generated prior to passage through the cytoplasm and are

maintained until uncoating occurs in the nucleus. Journal of Virology *80*, 11040-11054.

Sonntag, F., Köther, K., Schmidt, K., Weghofer, M., Raupp, C., Nieto, K., Kuck, A., Gerlach, B., Böttcher, B., and Müller, O. (2011). The assembly-activating protein promotes capsid assembly of different adeno-associated virus serotypes. Journal of Virology *85*, 12686-12697.

Sonntag, F., Schmidt, K., and Kleinschmidt, J.A. (2010). A viral assembly factor promotes AAV2 capsid formation in the nucleolus. Proceedings of the National Academy of Sciences *107*, 10220-10225.

Stanton, A. (2003). Therapeutic potential of renin inhibitors in the management of cardiovascular disorders. American Journal of Cardiovascular Drugs *3*, 389-394.

Steckelings, U.M., Larhed, M., Hallberg, A., Widdop, R.E., Jones, E.S., Wallinder, C., Namsolleck, P., Dahlöf, B., and Unger, T. (2011). Non-peptide AT2-receptor agonists. Current Opinion in Pharmacology *11*, 187-192.

Stewart, D., Hilton, J., Arnold, J., Gregoire, J., Rivard, A., Archer, S., Charbonneau, F., Cohen, E., Curtis, M., and Buller, C. (2006). Angiogenic gene therapy in patients with nonrevascularizable ischemic heart disease: a phase 2 randomized, controlled trial of AdVEGF121 (AdVEGF121) versus maximum medical treatment. Gene Therapy *13*, 1503-1511.

Stewart, P.L., Fuller, S.D., and Burnett, R. (1993). Difference imaging of adenovirus: bridging the resolution gap between X-ray crystallography and electron microscopy. The EMBO Journal *12*, 2589.

Stieger, K., Schroeder, J., Provost, N., Mendes-Madeira, A., Belbellaa, B., Le Meur, G., Weber, M., Deschamps, J.-Y., Lorenz, B., and Moullier, P. (2008). Detection of intact rAAV particles up to 6 years after successful gene transfer in the retina of dogs and primates. Molecular Therapy *17*, 516-523.

Stilli, D., Sgoifo, A., Macchi, E., Zaniboni, M., De Iasio, S., Cerbai, E., Mugelli, A., Lagrasta, C., Olivetti, G., and Musso, E. (2001). Myocardial remodeling and arrhythmogenesis in moderate cardiac hypertrophy in rats. American Journal of Physiology-Heart and Circulatory Physiology *280*, H142-H150.

Stockand, J.D., and Meszaros, J.G. (2003). Aldosterone stimulates proliferation of cardiac fibroblasts by activating Ki-RasA and MAPK1/2 signaling. American Journal of Physiology-Heart and Circulatory Physiology *284*, H176-H184.

Stoehr, A., Neuber, C., Baldauf, C., Vollert, I., Friedrich, F.W., Flenner, F., Carrier, L., Eder, A., Schaaf, S., and Hirt, M.N. (2014). Automated analysis of contractile force and Ca^{2+} transients in engineered heart tissue. American Journal of Physiology-Heart and Circulatory Physiology *306*, H1353-H1363.

Studer, R., Reinecke, H., Müller, B., Holtz, J., Just, H., and Drexler, H. (1994). Increased angiotensin-I converting enzyme gene expression in the failing human heart. Quantification by competitive RNA polymerase chain reaction. Journal of Clinical Investigation *94*, 301.

Sumida, S.M., Truitt, D.M., Lemckert, A.A., Vogels, R., Custers, J.H., Addo, M.M., Lockman, S., Peter, T., Peyerl, F.W., and Kishko, M.G. (2005). Neutralizing antibodies to adenovirus serotype 5 vaccine vectors are directed primarily against the adenovirus hexon protein. The Journal of Immunology *174*, 7179-7185.

Summerford, C., Bartlett, J.S., and Samulski, R.J. (1999). αVß5 integrin: a co-receptor for adeno-associated virus type 2 infection. Nature Medicine *5*, 78-82.

Summerford, C., and Samulski, R.J. (1998). Membrane-associated heparan sulfate proteoglycan is a receptor for adeno-associated virus type 2 virions. Journal of Virology *72*, 1438-1445.

Sun, J., Anand-Jawa, V., Chatterjee, S., and Wong, K. (2003). Immune responses to adeno-associated virus and its recombinant vectors. Gene Therapy *10*, 964-976.

Sun, Y. (2010). Intracardiac renin–angiotensin system and myocardial repair/remodeling following infarction. Journal of Molecular and Cellular Cardiology *48*, 483-489.

Sun, Y., Kiani, M.F., Postlethwaite, A.E., and Weber, K.T. (2002). Infarct scar as living tissue. Basic Research in Cardiology *97*, 343-347.

Sun, Y., and Weber, K.T. (1996). Angiotensin converting enzyme and myofibroblasts during tissue repair in the rat heart. Journal of Molecular and Cellular Cardiology *28*, 851-858.

Sun, Y., Zhang, J.Q., Zhang, J., and Ramires, F.J.A. (1998). Angiotensin II, Transforming Growth Factor-[beta] 1and Repair in the Infarcted Heart. Journal of Molecular and Cellular Cardiology *30*, 1559-1569.

Sutton, M.G.S.J., and Sharpe, N. (2000). Left ventricular remodeling after myocardial infarction pathophysiology and therapy. Circulation *101*, 2981-2988.

Svilaas, T., Vlaar, P.J., van der Horst, I.C., Diercks, G.F., de Smet, B.J., van den Heuvel, A.F., Anthonio, R.L., Jessurun, G.A., Tan, E.-S., and Suurmeijer, A.J. (2008). Thrombus aspiration during primary percutaneous coronary intervention. New England Journal of Medicine *358*, 557-567.

Swynghedauw, B. (1999). Molecular mechanisms of myocardial remodeling. Physiological Reviews *79*, 215-262.

Takahashi, M., Suzuki, E., Takeda, R., Oba, S., Nishimatsu, H., Kimura, K., Nagano, T., Nagai, R., and Hirata, Y. (2008). Angiotensin II and tumor necrosis factor-α synergistically promote monocyte chemoattractant protein-1 expression: roles of NF-κB, p38, and reactive oxygen species. American Journal of Physiology-Heart and Circulatory Physiology *294*, H2879-H2888.

Takemura, G., Nakagawa, M., Kanamori, H., Minatoguchi, S., and Fujiwara, H. (2009). Benefits of reperfusion beyond infarct size limitation. Cardiovascular Research *83*, 269-276.

Takeshita, K., Hayashi, M., Iino, S., Kondo, T., Inden, Y., Iwase, M., Kojima, T., Hirai, M., Ito, M., and Loskutoff, D.J. (2004). Increased expression of plasminogen activator inhibitor-1 in cardiomyocytes contributes to cardiac fibrosis after myocardial infarction. The American Journal of Pathology *164*, 449-456.

Takimoto, E., and Kass, D.A. (2007). Role of oxidative stress in cardiac hypertrophy and remodeling. Hypertension *49*, 241-248.

Tallant, E.A., Ferrario, C.M., and Gallagher, P.E. (2005). Angiotensin-(1–7) inhibits growth of cardiac myocytes through activation of the mas receptor. American Journal of Physiology-Heart and Circulatory Physiology *289*, H1560-H1566.

Tao, Z.-Y., Cavasin, M.A., Yang, F., Liu, Y.-H., and Yang, X.-P. (2004). Temporal changes in matrix metalloproteinase expression and inflammatory response associated with cardiac rupture after myocardial infarction in mice. Life Sciences *74*, 1561-1572.

Thakur, S., Li, L., and Gupta, S. (2014). NF-κB-mediated integrin-linked kinase regulation in angiotensin II-induced pro-fibrotic process in cardiac fibroblasts. Life Sciences *107*, 68-75.

Thomas, C.E., Ehrhardt, A., and Kay, M.A. (2003). Progress and problems with the use of viral vectors for gene therapy. Nature Reviews Genetics *4*, 346-358.

Thomas, C.E., Storm, T.A., Huang, Z., and Kay, M.A. (2004). Rapid uncoating of vector genomes is the key to efficient liver transduction with pseudotyped adeno-associated virus vectors. Journal of Virology *78*, 3110-3122.

Thomas, W.G., Brandenburger, Y., Autelitano, D.J., Pham, T., Qian, H., and Hannan, R.D. (2002). Adenoviral-directed expression of the type 1A angiotensin receptor promotes cardiomyocyte hypertrophy via transactivation of the epidermal growth factor receptor. Circulation Research *90*, 135-142.

Tigerstedt, R., and Bergman, P. (1898). Kidney and circulation. Scand Arch Physiol *8*, 223-271.

Tipnis, S.R., Hooper, N.M., Hyde, R., Karran, E., Christie, G., and Turner, A.J. (2000). A human homolog of angiotensin-converting enzyme cloning and functional expression as a captopril-insensitive carboxypeptidase. Journal of Biological Chemistry *275*, 33238-33243.

Toivonen, R., Koskenvuo, J., Merentie, M., Söderström, M., Ylä-Herttuala, S., and Savontaus, M. (2012). Intracardiac injection of a capsid-modified Ad5/35 results in decreased heart toxicity when compared to standard Ad5. Virology Journal *9*, 296.

Toko, H., Zou, Y., Minamino, T., Sakamoto, M., Sano, M., Harada, M., Nagai, T., Sugaya, T., Terasaki, F., and Kitaura, Y. (2004). Angiotensin II type 1a receptor is involved in cell infiltration, cytokine production, and neovascularization in infarcted myocardium. Arteriosclerosis, Thrombosis, and Vascular Biology *24*, 664-670.

Tomasek, J.J., Gabbiani, G., Hinz, B., Chaponnier, C., and Brown, R.A. (2002). Myofibroblasts and mechano-regulation of connective tissue remodelling. Nature Reviews Molecular Cell Biology *3*, 349-363.

Touchberry, C.D., Green, T.M., Tchikrizov, V., Mannix, J.E., Mao, T.F., Carney, B.W., Girgis, M., Vincent, R.J., Wetmore, L.A., and Dawn, B. (2013). FGF23 is a novel regulator of intracellular calcium and cardiac contractility in addition to cardiac hypertrophy. American Journal of Physiology-Endocrinology and Metabolism *304*, E863-E873.

Touyz, R., Fareh, J., Thibault, G., Tolloczko, B., Lariviere, R., and Schiffrin, E. (1996). Modulation of Ca^{2+} transients in neonatal and adult rat cardiomyocytes by angiotensin II and endothelin-1. American Journal of Physiology-Heart and Circulatory Physiology *270*, H857-H868.

Touyz, R.M., and Schiffrin, E.L. (2000). Signal transduction mechanisms mediating the physiological and pathophysiological actions of angiotensin II in vascular smooth muscle cells. Pharmacological Reviews *52*, 639-672.

Tratschin, J.-D., Miller, I., Smith, M., and Carter, B. (1985). Adeno-associated virus vector for high-frequency integration, expression, and rescue of genes in mammalian cells. Molecular and Cellular Biology *5*, 3251-3260.

Trueblood, N.A., Xie, Z., Communal, C., Sam, F., Ngoy, S., Liaw, L., Jenkins, A.W., Wang, J., Sawyer, D.B., and Bing, O.H. (2001). Exaggerated left ventricular dilation and reduced collagen deposition after myocardial infarction in mice lacking osteopontin. Circulation Research *88*, 1080-1087.

Tsai, C.-T., Wang, D.L., Chen, W.-P., Hwang, J.-J., Hsieh, C.-S., Hsu, K.-L., Tseng, C.-D., Lai, L.-P., Tseng, Y.-Z., and Chiang, F.-T. (2007). Angiotensin II increases expression of α1C Subunit of L-Type Calcium Channel Through a Reactive Oxygen Species and cAMP response element–binding protein–dependent pathway in HL-1 myocytes. Circulation Research *100*, 1476-1485.

Tsuchiya, K., Horie, M., Watanuki, M., Albrecht, C.A., Obayashi, K., Fujiwara, H., and Sasayama, S. (1997). Functional compartmentalization of ATP is involved in angiotensin II–mediated closure of cardiac ATP-sensitive K+ channels. Circulation *96*, 3129-3135.

Tsuda, T., Gao, E., Evangelisti, L., Markova, D., Ma, X., and Chu, M.-L. (2003). Post-ischemic myocardial fibrosis occurs independent of hemodynamic changes. Cardiovascular Research *59*, 926-933.

Tsutsumi, Y., Matsubara, H., Ohkubo, N., Mori, Y., Nozawa, Y., Murasawa, S., Kijima, K., Maruyama, K., Masaki, H., and Moriguchi, Y. (1998). Angiotensin II type 2 receptor is upregulated in human heart with interstitial fibrosis, and cardiac fibroblasts are the major cell type for its expression. Circulation Research *83*, 1035-1046.

Tsuzuki, S., Eguchi, S., and Inagami, T. (1996). Inhibition of cell proliferation and activation of protein tyrosine phosphatase mediated by angiotensin II type 2

(AT 2) receptor in R3T3 cells. Biochemical and Biophysical Research Communications *228*, 825-830.

Tuddenham, E. (2012). Gene therapy for haemophilia B. Haemophilia *18*, 13-17.

Unger, T. (1999). Björn Fokow Award Lecture The angiotensin type 2 receptor: variations on an enigmatic theme. Journal of Hypertension *17*, 1775-1786.

Unger, T. (2000). Neurohormonal modulation in cardiovascular disease. American Heart Journal *139*, s2-s8.

Ushio-Fukai, M., Hilenski, L., Santanam, N., Becker, P.L., Ma, Y., Griendling, K.K., and Alexander, R.W. (2001). Cholesterol depletion inhibits epidermal growth factor receptor transactivation by Angiotensin II in vascular smooth muscle cells: role of cholesterol-rich microdomains and focal adhesions in angiotensin ii signaling. Journal of Biological Chemistry *276*, 48269-48275.

van den Borne, S.W., Diez, J., Blankesteijn, W.M., Verjans, J., Hofstra, L., and Narula, J. (2010). Myocardial remodeling after infarction: the role of myofibroblasts. Nature Reviews Cardiology *7*, 30-37.

Van der Vliet, P. (1995). Adenovirus DNA replication. The molecular repertoire of adenoviruses II (Springer), pp. 1-30.

Van Echteld, C.J., Van Emous, J.G., Jansen, M.A., Schreur, J.H., and Ruigrok, T.J. (1998). Manipulation of intracellular sodium by extracellular divalent cations: a 23 Na and 31 P NMR study on intact rat hearts. Journal of Molecular and Cellular Cardiology *30*, 119-126.

van Kats, J.P., de Lannoy, L.M., Danser, A.J., van Meegen, J.R., Verdouw, P.D., and Schalekamp, M.A. (1997). Angiotensin II Type 1 (AT1) receptor–mediated accumulation of angiotensin II in tissues and its intracellular half-life *in vivo*. Hypertension *30*, 42-49.

van Kats, J.P., Methot, D., Paradis, P., Silversides, D.W., and Reudelhuber, T.L. (2001). Use of a biological peptide pump to study chronic peptide hormone

action in transgenic mice. Direct and indirect effects of angiotensin ii on the heart. Journal of Biological Chemistry *276*, 44012-44017.

Van Kerckhoven, R., Kalkman, E.A., Saxena, P.R., and Schoemaker, R.G. (2000). Altered cardiac collagen and associated changes in diastolic function of infarcted rat hearts. Cardiovascular Research *46*, 316-323.

van Wamel, A.J., Ruwhof, C., van der Valk-Kokshoorn, L.E., Schriern, P.I., and van der Laarse, A. (2001). The role of angiotensin II, endothelin-1 and transforming growth factor-ß as autocrine/paracrine mediators of stretch-induced cardiomyocyte hypertrophy. Molecular and Cellular Biochemistry *218*, 113-124.

Vassalli, G., Büeler, H., Dudler, J., von Segesser, L.K., and Kappenberger, L. (2003). Adeno-associated virus (AAV) vectors achieve prolonged transgene expression in mouse myocardium and arteries *in vivo*: a comparative study with adenovirus vectors. International Journal of Cardiology *90*, 229-238.

Velez, J.C.Q., Ryan, K.J., Harbeson, C.E., Bland, A.M., Budisavljevic, M.N., Arthur, J.M., Fitzgibbon, W.R., Raymond, J.R., and Janech, M.G. (2009). Angiotensin I is largely converted to angiotensin (1-7) and angiotensin (2-10) by isolated rat glomeruli. Hypertension *53*, 790-797.

Vellinga, J., Van der Heijdt, S., and Hoeben, R.C. (2005). The adenovirus capsid: major progress in minor proteins. Journal of General Virology *86*, 1581-1588.

Venetucci, L.A., Trafford, A.W., O'Neill, S.C., and Eisner, D.A. (2008). The sarcoplasmic reticulum and arrhythmogenic calcium release. Cardiovascular Research *77*, 285-292.

Verrecchia, F., and Mauviel, A. (2002). Transforming growth factor-ß signaling through the smad pathway: Role in extracellular matrix gene expression and regulation. Journal of Investigative Dermatology *118*, 211-215.

Vickers, C., Hales, P., Kaushik, V., Dick, L., Gavin, J., Tang, J., Godbout, K., Parsons, T., Baronas, E., and Hsieh, F. (2002). Hydrolysis of biological peptides

by human angiotensin-converting enzyme-related carboxypeptidase. Journal of Biological Chemistry *277*, 14838-14843.

Waddington, S.N., McVey, J.H., Bhella, D., Parker, A.L., Barker, K., Atoda, H., Pink, R., Buckley, S.M., Greig, J.A., and Denby, L. (2008). Adenovirus serotype 5 hexon mediates liver gene transfer. Cell *132*, 397-409.

Wagner, S., Dantz, C., Flebbe, H., Azizian, A., Sag, C.M., Engels, S., Möllencamp, J., Dybkova, N., Islam, T., and Shah, A.M. (2014). NADPH oxidase 2 mediates angiotensin II-dependent cellular arrhythmias via PKA and CaMKII. Journal of Molecular and Cellular Cardiology *75*, 206-215.

Walters, R.W., Agbandje-McKenna, M., Bowman, V.D., Moninger, T.O., Olson, N.H., Seiler, M., Chiorini, J.A., Baker, T.S., and Zabner, J. (2004). Structure of adeno-associated virus serotype 5. Journal of Virology *78*, 3361-3371.

Walters, R.W., Yi, S.M.P., Keshavjee, S., Brown, K.E., Welsh, M.J., Chiorini, J.A., and Zabner, J. (2001). Binding of adeno-associated virus type 5 to 2, 3-linked sialic acid is required for gene transfer. Journal of Biological Chemistry *276*, 20610-20616.

Wang, D.H., Qiu, J., and Hu, Z. (1998). Differential regulation of angiotensin II receptor subtypes in the adrenal gland role of aldosterone. Hypertension *32*, 65-70.

Wang, L., Luo, D., Liao, X., He, J., Liu, C., Yang, C., and Ma, H. (2014a). Ang-(1–7) offers cytoprotection against ischemia–reperfusion injury by restoring intracellular calcium homeostasis. Journal of Cardiovascular Pharmacology *63*, 259-264.

Wang, R., Wang, Y., Lin, W.K., Zhang, Y., Liu, W., Huang, K., Terrar, D.A., Solaro, R.J., Wang, X., and Ke, Y. (2014b). Inhibition of angiotensin ii-induced cardiac hypertrophy and associated ventricular arrhythmias by a p21 activated kinase 1 bioactive peptide. PloS one *9*, e101974.

Wang, W., Bodiga, S., Das, S.K., Lo, J., Patel, V., and Oudit, G.Y. (2012). Role of ACE2 in diastolic and systolic heart failure. Heart Failure Reviews *17*, 683-691.

Wang, X., and Li, G. (2014). Angiotensin-(1–7) prevent atrial tachycardia induced sodium channel remodeling. Pacing and Clinical Electrophysiology *37*, 1349-1356.

Wang, Y., Qian, C., Roks, A.J., Westermann, D., Schumacher, S.-M., Escher, F., Schoemaker, R.G., Reudelhuber, T.L., van Gilst, W.H., and Schultheiss, H.-P. (2010a). Circulating rather than cardiac angiotensin-(1-7) stimulates cardioprotection after myocardial infarction. Circulation: Heart Failure *3*, 286-293.

Wang, Y., Qian, C., Roks, A.J.M., Westermann, D., Schumacher, S.M., Escher, F., Schoemaker, R.G., Reudelhuber, T.L., van Gilst, W.H., and Schultheiss, H.P. (2010b). Circulating rather than cardiac angiotensin-(1-7) stimulates cardioprotection after myocardial infarction. Circulation: Heart Failure *3*, 286-293.

Ward, P., and Kerr, J. (2005). Replication of adeno-associated virus DNA. Parvoviruses (Hodder Arnold, London, United Kingdom), 189-211.

Warren, S.E., Royal, H.D., Markis, J.E., Grossman, W., and McKay, R.G. (1988). Time course of left ventricular dilation after myocardial infarction: influence of infarct-related artery and success of coronary thrombolysis. Journal of the American College of Cardiology *11*, 12-19.

Wei, C.-L., Valvano, J.W., Feldman, M.D., and Pearce, J.A. (2005). Nonlinear conductance-volume relationship for murine conductance catheter measurement system. Biomedical Engineering, IEEE Transactions on *52*, 1654-1661.

Wei, S., Chow, L.T., Shum, I.O., Qin, L., and Sanderson, J.E. (1999). Left and right ventricular collagen type I/III ratios and remodeling post-myocardial infarction. Journal of Cardiac Failure *5*, 117-126.

Weindler, F.W., and Heilbronn, R. (1991). A subset of herpes simplex virus replication genes provides helper functions for productive adeno-associated virus replication. Journal of Virology *65*, 2476-2483.

Weisman, H.F., and Healy, B. (1987). Myocardial infarct expansion, infarct extension, and reinfarction: pathophysiologic concepts. Progress in Cardiovascular Diseases *30*, 73-110.

Welches, W.R., Santos, R.A.S., Chappell, M.C., Brosnihan, K.B., Greene, L.J., and Ferrario, C.M. (1991). Evidence that prolyl endopeptidase participates in the processing of brain angiotensin. Journal of Hypertension *9*, 631-638.

Wetzel, G.T., Chen, F., and Klitzner, T.S. (1993). Ca2+ channel kinetics in acutely isolated fetal, neonatal, and adult rabbit cardiac myocytes. Circulation Research *72*, 1065-1074.

White, M., Montezano, A.C., and Touyz, R.M. (2012). Angiotensin II signalling and calcineurin in cardiac fibroblasts: differential effects of calcineurin inhibitors FK506 and cyclosporine A. Therapeutic Advances in Cardiovascular Disease *6*, 5-14.

WHO (2015). Cardiovascular disease Fact Sheet. Accessed 02/04/2015: http://www.who.int/mediacentre/factsheets/fs317/en/

Wiethoff, C.M., Wodrich, H., Gerace, L., and Nemerow, G.R. (2005). Adenovirus protein VI mediates membrane disruption following capsid disassembly. Journal of Virology *79*, 1992-2000.

Willems, I., Havenith, M.G., De Mey, J., and Daemen, M. (1994). The alpha-smooth muscle actin-positive cells in healing human myocardial scars. The American journal of pathology *145*, 868.

Wokosin, D., Loughrey, C., and Smith, G. (2004). Characterization of a range of fura dyes with two-photon excitation. Biophysical Journal *86*, 1726-1738.

Wolf, G. (2000). Free radical production and angiotensin. Current Hypertension Reports *2*, 167-173.

Wollert, K.C., and Drexler, H. (1999). The renin–angiotensin system and experimental heart failure. Cardiovascular Research *43*, 838-849.

Wolska, B., and Solaro, R. (1996). Method for isolation of adult mouse cardiac myocytes for studies of contraction and microfluorimetry. American Journal of Physiology-Heart and Circulatory Physiology *271*, H1250-H1255.

Wong, J., Patel, R.A., and Kowey, P.R. (2004). The clinical use of angiotensin-converting enzyme inhibitors. Progress in Cardiovascular Diseases *47*, 116-130.

Wright, M.J., Wightman, L.M., Lilley, C., de Alwis, M., Hart, S.L., Miller, A., Coffin, R.S., Thrasher, A., Latchman, D.S., and Marber, M.S. (2001). *In vivo* myocardial gene transfer: optimization, evaluation and direct comparison of gene transfer vectors. Basic Research in Cardiology *96*, 227-236.

Wu, Z., Miller, E., Agbandje-McKenna, M., and Samulski, R.J. (2006). α2, 3 and α2, 6 N-linked sialic acids facilitate efficient binding and transduction by adeno-associated virus types 1 and 6. Journal of Virology *80*, 9093-9103.

Xiao, H.D., Fuchs, S., Campbell, D.J., Lewis, W., Dudley, S.C., Kasi, V.S., Hoit, B.D., Keshelava, G., Zhao, H., and Capecchi, M.R. (2004). Mice with cardiac-restricted angiotensin-converting enzyme (ACE) have atrial enlargement, cardiac arrhythmia, and sudden death. The American Journal of Pathology *165*, 1019-1032.

Xiao, W., Warrington, K.H., Hearing, P., Hughes, J., and Muzyczka, N. (2002). Adenovirus-facilitated nuclear translocation of adeno-associated virus type 2. Journal of Virology *76*, 11505-11517.

Xie, Q., Bu, W., Bhatia, S., Hare, J., Somasundaram, T., Azzi, A., and Chapman, M.S. (2002). The atomic structure of adeno-associated virus (AAV-2), a vector for human gene therapy. Proceedings of the National Academy of Sciences *99*, 10405-10410.

Yamagishi, H., Kim, S., Nishikimi, T., Takeuchi, K., and Takeda, T. (1993). Contribution of cardiac renin-angiotensin system to ventricular remodelling in myocardial-infarcted rats. Journal of Molecular and Cellular Cardiology *25*, 1369-1380.

Yamamoto, K., Chappell, M.C., Brosnihan, K.B., and Ferrario, C.M. (1992). *In vivo* metabolism of angiotensin I by neutral endopeptidase (EC 3.4. 24.11) in spontaneously hypertensive rats. Hypertension *19*, 692-696.

Yamamoto, K., Masuyama, T., Sakata, Y., Mano, T., Nishikawa, N., Kondo, H., Akehi, N., Kuzuya, T., Miwa, T., and Hori, M. (2000). Roles of renin–angiotensin and endothelin systems in development of diastolic heart failure in hypertensive hearts. Cardiovascular Research *47*, 274-283.

Yamamoto, K., Ohishi, M., Katsuya, T., Ito, N., Ikushima, M., Kaibe, M., Tatara, Y., Shiota, A., Sugano, S., and Takeda, S. (2006). Deletion of angiotensin-converting enzyme 2 accelerates pressure overload-induced cardiac dysfunction by increasing local angiotensin II. Hypertension *47*, 718-726.

Yamazaki, T., Komuro, I., Kudoh, S., Zou, Y., Shiojima, I., Hiroi, Y., Mizuno, T., Maemura, K., Kurihara, H., and Aikawa, R. (1996). Endothelin-1 is involved in mechanical stress-induced cardiomyocyte hypertrophy. Journal of Biological Chemistry *271*, 3221-3228.

Yamazaki, T., Komuro, I., Kudoh, S., Zou, Y., Shiojima, I., Mizuno, T., Takano, H., Hiroi, Y., Ueki, K., and Tobe, K. (1995). Angiotensin II partly mediates mechanical stress–induced cardiac hypertrophy. Circulation Research *77*, 258-265.

Yan, C., Kim, D., Aizawa, T., and Berk, B.C. (2003). Functional interplay between angiotensin II and nitric oxide cyclic GMP as a key mediator. Arteriosclerosis, Thrombosis, and Vascular Biology *23*, 26-36.

Yan, X., Schuldt, A.J., Price, R.L., Amende, I., Liu, F.-F., Okoshi, K., Ho, K.K., Pope, A.J., Borg, T.K., and Lorell, B.H. (2008). Pressure overload-induced hypertrophy in transgenic mice selectively overexpressing AT2 receptors in

ventricular myocytes. American Journal of Physiology-Heart and Circulatory Physiology *294*, H1274-H1281.

Yan, Z., Zak, R., Zhang, Y., Ding, W., Godwin, S., Munson, K., Peluso, R., and Engelhardt, J.F. (2004). Distinct classes of proteasome-modulating agents cooperatively augment recombinant adeno-associated virus type 2 and type 5-mediated transduction from the apical surfaces of human airway epithelia. Journal of Virology *78*, 2863-2874.

Yang, B., Phillips, M., Zhang, Y., Kimura, B., Shen, L., Mehta, P., and Mehta, J. (1998). Critical role of AT1 receptor expression after ischemia/reperfusion in isolated rat hearts beneficial effect of antisense oligodeoxynucleotides directed at AT1 receptor mRNA. Circulation Research *83*, 552-559.

Yang, F., Liu, Y.-H., Yang, X.-P., Xu, J., Kapke, A., and Carretero, O.A. (2002a). Myocardial infarction and cardiac remodelling in mice. Experimental Physiology *87*, 547-555.

Yang, J., Zhou, W., Zhang, Y., Zidon, T., Ritchie, T., and Engelhardt, J.F. (1999). Concatamerization of adeno-associated virus circular genomes occurs through intermolecular recombination. Journal of Virology *73*, 9468-9477.

Yang, R., Smolders, I., Vanderheyden, P., Demaegdt, H., Van Eeckhaut, A., Vauquelin, G., Lukaszuk, A., Tourwé, D., Chai, S.Y., and Albiston, A.L. (2011). Pressor and renal hemodynamic effects of the novel angiotensin A peptide are angiotensin II type 1A receptor dependent. Hypertension *57*, 956-964.

Yang, Z., Bove, C.M., French, B.A., Epstein, F.H., Berr, S.S., DiMaria, J.M., Gibson, J.J., Carey, R.M., and Kramer, C.M. (2002b). Angiotensin II type 2 receptor overexpression preserves left ventricular function after myocardial infarction. Circulation *106*, 106-111.

Yasunari, K., Kohno, M., Kano, H., Yokokawa, K., Minami, M., and Yoshikawa, J. (1999). Antioxidants improve impaired insulin-mediated glucose uptake and prevent migration and proliferation of cultured rabbit coronary smooth muscle cells induced by high glucose. Circulation *99*, 1370-1378.

Yayama, K., Hiyoshi, H., Imazu, D., and Okamoto, H. (2006). Angiotensin II stimulates endothelial NO synthase phosphorylation in thoracic aorta of mice with abdominal aortic banding via type 2 receptor. Hypertension *48*, 958-964.

Yellon, D.M., and Hausenloy, D.J. (2007). Myocardial reperfusion injury. New England Journal of Medicine *357*, 1121-1135.

Yu, H., Gao, J., Wang, H., Wymore, R., Steinberg, S., McKinnon, D., Rosen, M.R., and Cohen, I.S. (2000). Effects of the renin-angiotensin system on the current Ito in epicardial and endocardial ventricular myocytes from the canine heart. Circulation Research *86*, 1062-1068.

Yusuf, S., Sleight, P., Pogue, J., Bosch, J., Davies, R., and Dagenais, G. (2000). Effects of an angiotensin-converting-enzyme inhibitor, ramipril, on cardiovascular events in high-risk patients. The Heart Outcomes Prevention Evaluation Study Investigators. The New England Journal of Medicine *342*, 145-153.

Zaiss, A.-K., Liu, Q., Bowen, G.P., Wong, N.C., Bartlett, J.S., and Muruve, D.A. (2002). Differential activation of innate immune responses by adenovirus and adeno-associated virus vectors. Journal of Virology *76*, 4580-4590.

Zhang, Y., and Bergelson, J.M. (2005). Adenovirus receptors. Journal of Virology *79*, 12125-12131.

Zhang, Y., Li, B., Wang, B., Zhang, J., Wu, J., and Morgan, T. (2014). Alteration of cardiac ACE2/Mas expression and cardiac remodelling in rats with aortic constriction. The Chinese Journal of Physiology *57*, 335-342.

Zhao, W., Zhao, T., Chen, Y., and Sun, Y. (2013). Angiotensin 1-7 promotes cardiac angiogenesis following infarction. Current Vascular Pharmacology.

Zhao, Y.X., Yin, H.Q., Yu, Q.T., Qiao, Y., Dai, H.Y., Zhang, M.X., Zhang, L., Liu, Y.F., Wang, L.C., and Liu, D.S. (2010). ACE2 overexpression ameliorates left ventricular remodeling and dysfunction in a rat model of myocardial infarction. Human Gene Therapy *21*, 1545-1554.

Zheng, H., Pu, S.-Y., Fan, X.-F., Li, X.-S., Zhang, Y., Yuan, J., Zhang, Y.-F., and Yang, J.-L. (2015). Treatment with angiotensin-(1-9) alleviates the cardiomyopathy in streptozotocin-induced diabetic rats. Biochemical Pharmacology.

Zhou, C., Ziegler, C., Birder, L.A., Stewart, A.F., and Levitan, E.S. (2006). Angiotensin II and stretch activate NADPH oxidase to destabilize cardiac Kv4. 3 channel mRNA. Circulation Research *98*, 1040-1047.

Zhu, J., Huang, X., and Yang, Y. (2009). The TLR9-MyD88 pathway is critical for adaptive immune responses to adeno-associated virus gene therapy vectors in mice. The Journal of Clinical Investigation *119*, 2388-2398.

Zhu, M., Gelband, C.H., Moore, J.M., Posner, P., and Sumners, C. (1998). Angiotensin II type 2 receptor stimulation of neuronal delayed-rectifier potassium current involves phospholipase A2 and arachidonic acid. The Journal of Neuroscience *18*, 679-686.

Zhu, M.M., Feit, A., Chadow, H., Alam, M., Kwan, T., and Clark, L.T. (2001). Primary stent implantation compared with primary balloon angioplasty for acute myocardial infarction: a meta-analysis of randomized clinical trials. The American Journal of Cardiology *88*, 297-301.

Zhu, Y., Falkenhahn, M., Franke, F., Bohle, R., Stauss, H., Danilov, S., and Unger, T. (1999). Expression of cardiac angiotensin-converting enzyme after myocardial infarction. Acta Pharmacologica Sinica *20*, 97-102.

Zhu, Y.Z., Chimon, G.N., Zhu, Y., Lu, Q., Li, B., Hu, H.Z., Yap, E.H., Lee, H.S., and Wong, P.T.-H. (2000). Expression of angiotensin II AT2 receptor in the acute phase of stroke in rats. Neuroreport *11*, 1191-1194.

Zimmerman, A., and Hülsmann, W. (1966). Paradoxical influence of calcium ions on the permeability of the cell membranes of the isolated rat heart. Nature *211*, 646-647.

Zincarelli, C., Soltys, S., Rengo, G., and Rabinowitz, J.E. (2008). Analysis of AAV serotypes 1–9 mediated gene expression and tropism in mice after systemic injection. Molecular Therapy *16*, 1073-1080.

Zisman, L.S., Keller, R.S., Weaver, B., Lin, Q., Speth, R., Bristow, M.R., and Canver, C.C. (2003). Increased angiotensin-(1-7)–forming activity in failing human heart ventricles evidence for upregulation of the angiotensin-converting enzyme homologue ACE2. Circulation *108*, 1707-1712.

Zolotareva, A., and Kogan, M. (1978). Production of experimental occlusive myocardial infarction in mice. Cor et vasa *20*, 308-314.

Zou, Y., Komuro, I., Yamazaki, T., Aikawa, R., Kudoh, S., Shiojima, I., Hiroi, Y., Mizuno, T., and Yazaki, Y. (1996). Protein kinase C, but not tyrosine kinases or Ras, plays a critical role in angiotensin II-induced activation of Raf-1 kinase and extracellular signal-regulated protein kinases in cardiac myocytes. Journal of Biological Chemistry *271*, 33592-33597.

Zsebo, K., Yaroshinsky, A., Rudy, J.J., Wagner, K., Greenberg, B., Jessup, M., and Hajjar, R.J. (2014). Long-term effects of AAV1/SERCA2a gene transfer in patients with severe heart failure analysis of recurrent cardiovascular events and mortality. Circulation Research *114*, 101-108.